# Pleuromutilin and its Application Towards Bidentate Antibiotics: Triazoles, Linker Chemistry, and Serendipitous Discoveries

Logan Michael Breiner

Dissertation submitted to the faculty of the Virginia Polytechnic Institute and State University in partial fulfillment of the requirements for the degree of

Doctor of Philosophy

in

Chemistry

Andrew N. Lowell, Chair

Emily Mevers

Webster L. Santos

Michael D. Schulz

May 5th, 2025

Blacksburg, VA, USA

Keywords: Antibiotic, Antimicrobial Resistance, Natural Product Semi-synthesis, Ribosome, Hybrid Drugs

**Pleuromutilin and its Application Towards Bidentate Antibiotics: Triazoles, Linker Chemistry, and Serendipitous Discoveries**

Logan Michael Breiner

## Abstract

The world is facing a global antimicrobial-resistance (AMR) crisis. Classes of antibiotics continually face ineffectiveness as resistance mechanisms in microbes develop and propagate. The semi-synthetic derivatization of natural product antibiotics has provided many of our treatments, but new treatments are a constant necessity. The pleuromutilin antibiotics constitute a class of diterpenoid, ribosome-inhibiting antibiotics. Pleuromutilins have been developed into a number of veterinary antibiotics, as well as two FDA approved drugs, retapamulin and lefamulin. This class exhibits a low propensity to resistance development.

This dissertation reports progress in rational design, synthesis, and testing of pleuromutilin derived antibiotics. Among these new classes of pleuromutilins are the 20-triazolyl-12-*epi*-pleuromutilins, 22-S-oligoethylene glycol pleuromutilins, and two pleuromutilin based bidentate hybrid antibiotics: The pleuromutilin-blasticidins, and the pleuromutilin-azithromycins. Within these new classes, we found highly potent representatives which now serve as lead compounds for future structure activity relationship studies and development. Additionally, unexpected activity against *P. falciparum* has resulted in a new project pursuing pleuromutilin antimalarials.

**Pleuromutilin and its Application Towards Bidentate Antibiotics: Triazoles, Linker Chemistry, and Serendipitous Discoveries**

Logan Michael Breiner

GENERAL AUDIENCE ABSTRACT

We are rapidly approaching, and possibly already within, a post-antibiotic era where things as innocuous as a papercut can kill. The rapidity of antimicrobial resistance (AMR) arising is outpacing the creation of new antibiotics. One way of combatting this threat is the use of hybrid antibiotics, as they can have enhanced potency and lowered resistance development. Pleuromutilins are an attractive candidate for hybrid antibiotics, as they have low rates of spontaneous resistance development, and they have two positions which may be easily functionalized: The C22 hydroxyl and C20 vinyl. Additionally, two pleuromutilin based drugs are already on the market. Retapamulin is a topical antibiotic for skin infections, and lefamulin is a orally or intravenously delivered drug for community-acquired pneumonia.

The overarching aim of the Lowell lab is the created of hybrid *bidentate* antibiotics. Bidentate antibiotics are a continuation of the idea of hybrid antibiotics, but designed so that both antibiotics of the hybrid can bind simultaneously with their respective target sites. The beneficial effects of hybrid antibiotics will be retained, and potency may be increased in these bidentate antibiotics as their binding affinity increases. In this work, the sites of functionalization of pleuromutilin are explored to pave the way for their use as bidentate partners. Along the way, several serendipitous discoveries have been made, some of which leading to potent antibiotics in their own right. Finally, pleuromutilins are utilized as bidentate hybrid antibiotics with two other ribosome binding antibiotics: Blasticidin S and azithromycin.

**Acknowledgements**

I would like to thank my advisor, Prof. Andrew N. Lowell. Dr. Lowell has been not only an incredible mentor, but also a dear friend. More times than I can count, when my resolve for grad school was wavering, he was there to lend his support, no matter what decision I came to. He was always someone who I could come and talk to about any issue. Additionally, he is a great scientist, one who fosters a sense of independence in his students, but also one that is willing to admit errors in cognition. He is always willing to listen to new ideas, and if a student also brings forth a well-presented foundation for trying new experiments, he tells them to go for. His lab is not just teaching people how to be knowledgeable chemists, but also how to think and engage critically with scientific material. Lastly, he was incredibly understanding when it came to my family life and allowed me the time to commute to see my daughter frequently.

The Lowell Lab currently consists of graduate students Suzzudul Islam Shuvo and Toheeb Ajasa, and formerly Jacob Chappell, Harrison Miller, Austin Lowry, Dr. Cole Gannett, Dr. Zak Kohanov, Timilehin Adegboyega, Max Rivers, and postdoctoral researcher Dr. Jennifer McCord. These folks have become good friends and collaborators and have made many group meetings and group events solidly good affairs. We have developed many inside jokes over the years, and I get the feeling that onlookers from other labs may consider us a bit weird. However, these strangers never experienced the Oil Bath Fire of 2021, or the many times we accidentally flooded the Thornton lab (sorry Reilly and Matt, it's an old building), or the Box Tournament of Summer 2022 that lasted for several days over the course of a conference.

We have had many undergraduates come through our doors, but there are three in particular who I would like to thank: my mentee, Roman Slowinski, now at Purdue, Spencer Kearns and Noah Perotte. I could see in Roman the same obsessive interest in all things chemistry that I had

when I was an undergraduate. Combined with his innately inquisitive nature, motivation, and attention to detail, I am certain he will go on to do great things in the world of chemistry. Thank you for your challenging discussions and thank you for all your help! Noah and Spencer have been an invaluable asset to the undergraduate program in the Lowell Lab, and since Dr. Cole Gannett graduated have led the other undergraduates in their research. Many people claim that they have an open mind, but few demonstrate it in practice. Noah has the commendable ability to read dense and dry primary sources, even if they may contradict his currently held positions. Spencer has a deep curiosity about the underlying physical phenomena of chemical reactions. I have great hopes for both over their futures.

To my committee members (Profs. Mevers, Santos, Schulz, and formerly Carlier), thank you for all your help and insight. Dr. Mevers was always there to answer questions I had about purification techniques and structural issues concerning career goals. Dr. Santos was always willing to make time for chemistry discussions and was very supportive of my original research proposal (ORP) ideas. Dr. Schulz was a great collaborator to work with and I could always count on him (in committee meetings) to quietly observe and then come up with a handful of very precise and thought-provoking questions. Dr. Carlier I would like to thank for the use of his hood space and lab in the beginning of my grad school career, when we did not have the in the Lowell lab. Dr. Carlier was also instrumental in my ORP redesign, as he thought my original idea was too high risk. Because of this, however, I ended up going in a direction I hadn't previously imagined, expanding my breadth of knowledge and passing the ORP with flying colors.

The work performed by our collaborators has been instrumental in seeing my efforts come to fruition. To them I want to extend my deepest gratitude: Dr. Anne Brown and her students Tony Briganti, Micah Hoernig, and Marion LoPresti; Dr. Yuri Polikanov and his students Benjamin

Killam and Iza Kopec; Dr. Michael Klemba and his postdoctoral researcher Dr. Katherine Fike; Dr. Mohamed Seleem and his students Abdallah (Adam) Abdelsattar, Ahmed Abouelkhair, and Somaia Abdelmegeed; and Drs. Carla Slebodnick and Nancy J. Vogelaar.

I would like to thank Drs. John Morris and Alan Esker, the two graduate program directors during my years of graduate studies. They were always tremendously helpful and willing to answer my questions about the program. Joli Huynh, our graduate program coordinator without whom the department couldn't run, was always delightful to talk to and incredibly patient about programmatic requirements. I could always count on catching Sharelle Carbaugh at a busy time (I have terrible timing) but was always met with a smile and she would go above and beyond to help me find the things I needed. I would also like to thank Dr. James Tanko, who simultaneously taught the most challenging course I've ever taken (chemical kinetics) and was also one of my favorite instructors ever. I even took another course with him after the trauma of kinetics, but this time I audited it. Additionally, I was a TA for Dr. Tanko in the synthetic techniques laboratory, and that was the best time teaching I had during my time here.

I made several close friends in the department who deserve mention. Dr. Cole Gannett, Dr. Zak Kohanov, Jacob Chappell, Lindsay Sandusky, Kirsta Channell, Rose Campbell, and many others. These folks made getting through graduate school a less tedious and arduous process. In general, I have had great times with the many students of this department as we have shared the common struggle that is graduate level study.

My studies at the bachelor's level that led to my success as a chemist here had many influences. My PI and academic advisor Dr. Herman Holt Jr. was instrumental in my formation as chemist, and his patience and Socratic approach to questions were powerful in developing my chemical thought. You will never get a straight answer out of Dr. Holt, but what you will get is

more questions that will leave you with a deeper understanding of the material at hand. Dr. Holt's willingness to let me try things and his confidence in my chemistry abilities allowed me to blossom as a young chemist. My first chemistry instructor at UNC Asheville was Dr. Bert Holmes, for general chemistry and later for physical chemistry. I remember when I first came to UNCA and was meeting with a few professors and revealed that I wasn't that fond of math at that time. The other professors balked at that and said chemistry might not be for me, but Dr. Holmes came to my defense and said my record in his class demonstrated otherwise. Dr. Amanda Wolfe was my organic chemistry professor and an unofficial advisor in my research. She is an amazing instructor, and every day I looked forward to coming to her classes. Drs. Sally Wasileski and Jason Schmeltzer were also great instructors and were incredibly kind and hilarious respectively. Every single professor in the chemistry department of UNCA I thank for developing me as a chemist.

Finally, I would like to thank my friends and family back home. My entire family has always entertained my love of chemistry and pushed me in my studies. My parents Mike and Laurie Breiner were always supportive of my interest in chemistry. I knew I wanted to be a chemist from seven years old, and that solidified when I got my first chemistry set at nine. I remember waking my mother up early on Saturdays and asking her to take me to the hardware store to buy chemicals, copper wire, etc. and she always obliged. My father is a botanist, and science was always incredibly important in our household. I am thankful to him for helping pay for my undergraduate studies and allowing me to graduate without debt. My grandmother, Maree Krug Rankin, was immensely helpful during my time at UNCA, and helped take care of my daughter while I was in school or working. She also pushed me to never give up no matter how hard things got. My daughter's mother, Jenna Strickland, always supported my decision to come to graduate school, even relocating to be here with my daughter during the first few years. I am immensely

grateful for Jenna and her resolute support and resilience. My friends back home, you all know who you are, have given me tremendous support from afar. I love you all, and I am incredibly lucky to have so many close, long-lasting friendships. I also want to thank my extended family who have always shown interest in my research and lent encouragement. Last but most importantly, to my daughter Aurora Breiner, my biggest cheerleader and my best student. It has been so hard being away from you these past few years, and your pride in me and the promise of a better future for you were the only reasons I stuck with it. I love you with all my heart.

## Attribution

This consists of some chapters that were written with the help of several co-workers and collaborators. They are acknowledged below with their affiliations.

Dr. Jennifer P. McCord (Virginia Tech Department of Chemistry)

Moriah E. Heifetz (Virginia Tech Department of Chemistry)

Sophia Y. Philbrook. (Virginia Tech Department of Chemistry)

Dr. Carla Slebodnick (Virginia Tech Department of Chemistry)

Prof. Anne M. Brown (Virginia Tech Department of Biochemistry, Research and Informatics)

Anthony J. Briganti (Virginia Tech Department of Biochemistry)

Prof. Mohamed N. Seleem (Virginia Tech Department of Biomedical Sciences and Pathobiology, VA-MD College of Veterinary Medicine)

Roman P. Slowinski (Virginia Tech Department of Biochemistry, Department of Chemistry)

Dr. Nancy J. Vogelaar (Virginia Tech Department of Biochemistry, Department of Chemistry)

Abdallah (Adam) Abselsattar (Virginia Tech Department of Biomedical Sciences and Pathobiology, VA-MD College of Veterinary Medicine)

Ahmed Abouelkhair (Virginia Tech Department of Biomedical Sciences and Pathobiology, VA-MD College of Veterinary Medicine)

Prof. Yury S. Polikanov (University of Illinois at Chicago Department of Biological Sciences, Center for Biomolecular Sciences, Department of Pharmaceutical Sciences)

Benjamin Y. Killam (University of Illinois at Chicago Department of Biological Sciences)

Iza Kopec (University of Illinois at Chicago Department of Biological Sciences)

Micah Hoernig (Virginia Tech Department of Biochemistry)

Marion LoPresti (Virginia Tech Department of Biochemistry)

Dr. Katherine R. Fike (Virginia Tech Department of Biochemistry)

Prof. Michael Klemba (Virginia Tech Department of Biochemistry, College of Agriculture and Life Sciences)

Dr. Cole C. Gannett (Virginia Tech Department of Chemistry)

Somaia Abdelmegeed (Virginia Tech Department of Biomedical Sciences and Pathobiology, VA-MD College of Veterinary Medicine)

**Chapter 2** is a reprint of a manuscript published in *Tetrahedron Chem*. Dr. Andrew N. Lowell conceived and led the project. Logan M. Breiner and Dr. Andrew N. Lowell designed experiments. Logan M. Breiner performed compound synthesis, characterization, and microbial

testing. Dr. Jennifer P. McCord, Moriah E. Heifetz, and Sophia Y. Philbrook performed preliminary microbial testing. Dr. Carla Slebodnick performed X-ray crystallographic characterization. Dr. Anne M. Brown and Anthony J. Briganti performed docking studies and computational analysis. Logan M. Breiner, Dr. Andrew N. Lowell, Anthony J. Briganti and Dr. Anne M. Brown wrote the manuscript. All authors have approved the final manuscript.

**Chapter 3** is a manuscript submitted for peer review in a scientific journal. Dr. Andrew N. Lowell conceived and led the project. Logan M. Breiner and Dr. Andrew N. Lowell designed the synthetic experiments. Dr. Andrew N. Lowell and Dr. Mohamed N. Seleem led and supervised the anti-microbial testing. Logan M. Breiner performed compound synthesis (aided by Roman P. Slowinski), characterization, and partial antimicrobial testing (with design input from Nancy J. Vogelaar). Abdallah (Adam) Abselsattar and Ahmed Abouelkhair performed partial antimicrobial testing. Abdallah (Adam) Abselsattar performed cytotoxicity studies. Dr. Yury S. Polikanov supervised and led X-ray crystallographic and transcription translation experiments. Dr. Yury S. Polikanov, Benjamin Y. Killam, and Iza Kopec performed X-ray crystallographic and transcription translation experiments and determined the structures of ribosome-bound synthetic pleuromutilin compounds. Dr. Anne M. Brown designed and led the computation docking studies. Anthony J. Briganti, Micah Hoernig, and Marion LoPresti performed computational experiments. All authors interpreted the experimental results. Logan M. Breiner, Dr. Andrew Lowell, Anthony J. Briganti, Micah Hoernig, Marion Lopresit, Dr. Anne Brown, Abdallah (Adam) Abdelsattar, Benjamin Y. Killam, and Dr. Yury S. Polikanov wrote the manuscript. All authors have approved the final manuscript.

**Chapter 4** is work concerning pleuromutilin electrophiles. Logan M. Breiner and Dr. Andrew N. Lowell designed experiments. Logan M. Breiner performed compound synthesis,

characterization, and partial antimicrobial testing. Abdallah (Adam) Abselsattar and Ahmed Abouelkhair performed partial antimicrobial testing. Abdallah (Adam) Abselsattar performed cytotoxicity studies. Dr. Katherine R. Fike performed anti-malarial assays. Logan M. Breiner wrote the manuscript. Dr. Lowell aided with writing and editing.

**Chapter 5** is a reprint of a manuscript published in the *Journal of Organic Chemistry*. Dr. Andrew N. Lowell conceived and led the project. Logan M. Breiner and Dr. Andrew N. Lowell designed experiments. Logan M. Breiner performed compound synthesis (aided by Roman P. Slowinski), characterization, antimicrobial testing, and development of the solubility assay. Logan M. Breiner and Dr. Andrew N. Lowell wrote the manuscript. All authors have approved the final manuscript.

**Chapter 6** is work concerning pleuromutilin-blasticidin S and 12-*epi*-pleuromutilin hybrids. Logan M. Breiner and Dr. Andrew N. Lowell designed experiments. Logan M. Breiner performed compound synthesis, characterization, and partial antimicrobial testing. Dr. Cole C. Gannett performed purification of pleuromutilin-blasticidin S hybrids. Somaia Abdelmegeed performed partial antimicrobial testing. Dr. Katherine R. Fike performed anti-malarial assays. Logan M. Breiner wrote the manuscript. Dr. Lowell aided with writing and editing.

# Table of Contents

# Chapter 1. Overview

## 1.1 The antibiotic crisis

The rise of antibiotic-resistant microbes is a growing global crisis. By one estimate, the number of human deaths per year from resistant organisms could reach 10 million by 2050.[1] To put that in perspective, the global annual deaths directly attributable to antibiotic-resistant infections in 2019 was 1.27 million.[2] A total of 4.95 million deaths due to other causes were comorbid with antibiotic-resistant infections. We are at risk of continuing to lose this arms race against these insidious opponents because of the slow depletion of effective treatments due to the rise of AMR exacerbated by irresponsible use.[1] Since the 1980s, the number of new antibiotics approved by the FDA has declined drastically, with only one new class of antibiotic approved since 2000. Antibiotic resistance occurs rapidly once an antibiotic is introduced into commercial use, typically within a few years.[3] Thus, the world is in continual and dire need of new, effective drugs.

Between 1981 and 2006, 73% of the small-molecule, anti-infective, and anti-cancer drugs used clinically were either natural products or derivatizations thereof.[4] In comparison, natural product-based drugs comprised half of all drugs that were approved between 1994 and 2007.[5] Because the organisms that produce these natural products were often doing so as part of a defensive strategy to prevent the proliferation of other organisms competing for resources, these compounds did not arise to target human metabolic pathways.[6] Therefore, many of these compounds are naturally great leads for developing anti-infectives agents. Natural products can typically cross membranes to exert their action as well.[7] Combined with their evolutionary refinement to bind specific molecular targets, these inherently favorable pharmacokinetic properties makes them excellent leads for antibiotic and chemotherapeutic drug design.

In medicinal chemistry, a well-known and tested strategy in lead development is to take hit compounds of low activity and link them to generate higher potency leads. This process is called fragment-based lead discovery.[8] One outstanding example is the creation of an acetylcholinesterase inhibitor with potency on the femtomolar scale, by cyclizing alkyne-azide fragments in the enzyme. Two inhibitors with modest potency had the appropriate functionalities bound by varying chain lengths. Co-incubating these derivatives with the acetylcholinesterase enzyme led to highly potent compounds that were formed within the enzyme itself.[9, 10]

Fragment-based lead discovery as a concept can be taken even further and applied to leads or compounds that are drugs in their own right. Within the over-arching definition of covalently linked drugs, we can further subdivide them into various categories.[11] Hybrids and cleavage hybrids are pharmacophores or drugs bound by a linking moiety that is distinct from the compounds it is connecting. Cleavage hybrids can be hydrolyzed or degraded by other pathways in the body to release the two drugs, which may have separate mechanisms of action or targets. Fused hybrids may have no linker or a drastically reduced linker, which results in a compound where the two parent pharmacophores are intimately combined within the overall structure. Lastly, merged hybrids are connected by shared functional groups; in other words, the structures of the parent molecules are partially superimposable. Merged hybrids can be leads to be developed into drugs with shared pharmacophores and a simpler overall structure.[11] To focus on examples specific to the field of natural product-derived antibiotics, we seek to make a specific type of hybrid antibiotic called a bidentate antibiotic. The goal of a bidentate antibiotic is to covalently link two antibiotics in such a manner that they both engage their target sites simultaneously. We hypothesize the bidentate antibiotic will be more potent and better tolerate resistance mechanisms

relative to their co-administered parents. We will discuss this goal in the context of some pleuromutilin derivatives in Chapter 6.

### 1.2 Pleuromutilins

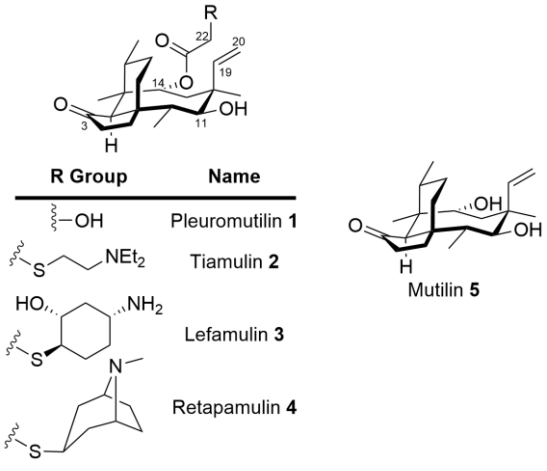


**Figure 1.** Pleuromutilin **1**, its semisynthetic derivatives **2-4**, and the mutilin core **5**.

Pleuromutilin (**1**, Figure 1), and its C22 thioether derivatives **2-4**, are antibiotics specific for Gram-positive bacteria, mycobacteria, and some fastidious Gram-negative strains,[12] that act upon the bacterial ribosome.[13] First isolated in 1951 from *Pleurotus mutilus* (renamed *Clitopilus scyphoides*),[14] pleuromutilin has been developed into a number of semi-synthetic derivatives that are used in veterinary medicine (tiamulin **2** and valnemulin) and recently as topical (retapamulin **4**) and systemic antibiotics (lefamulin **3)** for humans. Pleuromutilin itself is a glycolic ester of the mutilin core **5**. Structurally complex, yet with a dearth of functionality, pleuromutilin is an ideal target for total synthesis and semi-synthetic modification.

Currently, there are two veterinary and two clinical analogs of pleuromutilin. Tiamulin (**2**)[15] and Valnemulin[16] encompass the veterinary derivatives and are used mainly to combat animal borne mycoplasmas in agriculture. Retapamulin (**4**) is a topical antibiotic, approved in 2007, and is used

to treat skin structure infections in humans.[17] The design of retapamulin's C22 side chain enhances its already high lipophilicity, thus aiding its passage through skin but limiting the drug to this method of delivery. Lefamulin (**3**), approved in 2019,[18] is the first and only systemic pleuromutilin derivative approved for systemic human use, and can be administered intravenously or orally. Lefamulin is used to treat *Staphylococcus* infections[19] as well as community acquired bacterial pneumonia.[18]

### 1.2.1 Total syntheses of pleuromutilin

The first reported total synthesis of (±)-pleuromutilin was in 1982 by Gibbons (Figure 2). Staring with the kinetic enolate of cyclohexenone derivative **6** and a cyclopentene derivative, a sequential series of Michael additions gave tricycle **7**. A series of alkylations and oxidations generated the α,β-unsaturated ketone **8**, which was subsequently stereoselectively reduced to ketone **9**. An aldol reaction, followed by dehydrating and deprotecting conditions, produced the tetracyclic β,γ-unsaturated oxo-alcohol **10**. Subjection of **10** to Sharpless asymmetric epoxidation conditions furnished the epoxide **11**, the diastereomer being verified based on the vicinal coupling constant of 0 Hz in $^{1}$H NMR between the hydrogens of C10 and C11. Elimination conditions and selective protection provided vinylidene **12**, which, when subjected to an electrophilic bromine source, underwent ring-opening expansion resulting in the 8-membered ring species **13**, the first intermediate containing the tricyclic pleuromutilin core. A zinc reduction of the bromide and olefinic isomerization afforded vinylidene **14**. Reduction of both ketones, selective mesylation, and hydride displacement of the alcohol on C18 gave the monoalcohol. Reoxidation of the remaining alcohol, reduction to the preferred stereochemistry, and protection gave the di-MOM-de-oxo compound **15**. Ozonolysis under reducing conditions, followed by alkylation with a vinyl

lithium species and hydrolysis, generated an α,β-unsaturated aldehyde, which was reduced to the allyl

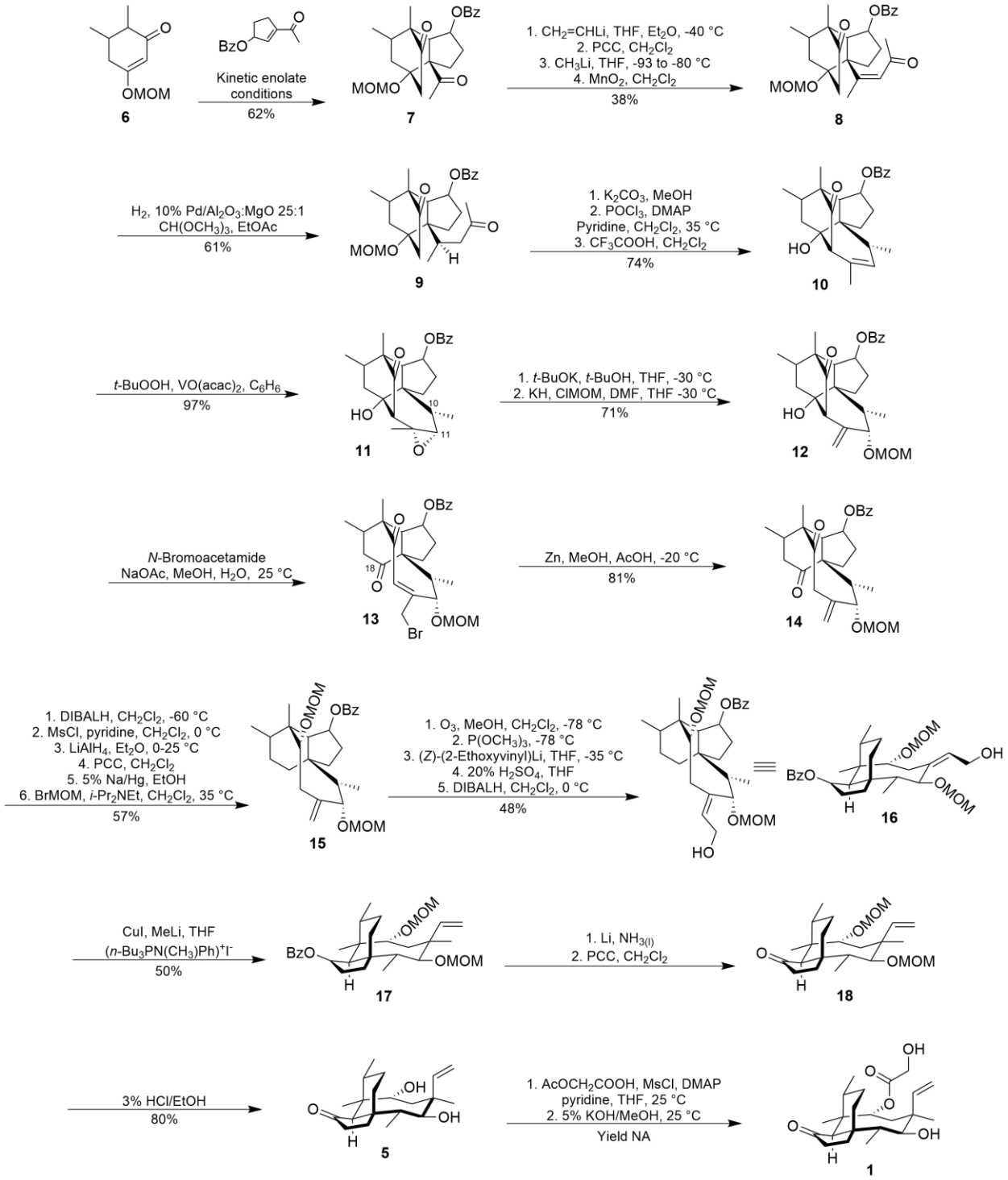

**Figure 2.** Total synthesis of pleuromutilin by Gibbons, 1982.

alcohol **16**. Alkylation with methyl lithium under Murahashi's conditions made the vinyl **17**. Debenzylation and oxidation gave the ketone **18**, which was deprotected by acidic hydrolysis revealing the oxo-diol **5**, also known as mutilin. Esterification followed by selective hydrolysis afforded pleuromutilin **1**. The entire synthesis was conducted in 30 steps, with a 0.6% overall yield.[20]

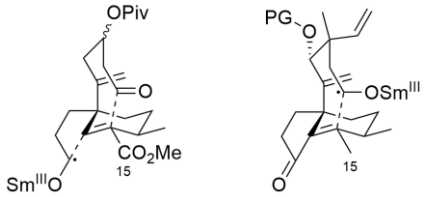


**Figure 3.** Two approaches to samarium catalyzed cycloaddition in the total synthesis of pleuromutilin. Left, Procter. Right, Reisman.

A recent total synthesis of (+)-pleuromutilin and (+)-*epi*-pleuromutilin was reported in 2018, which used 18 steps and had a 1.8 % overall yield.[21] Reisman et al. used a samarium catalyzed cyclization cascade to form the characteristic ring structure (**19**, Figure 3). Although previously Procter et. al had used a similar samarium catalyzed cyclization strategy (**20**), they used a ketyl radical to directly generate the ring structure. Although Procter's method elegantly resulted in two ring-forming bonds being generated as opposed to Reisman's one, Procter's use of a carboxylate at C15 required several additional steps to obtain the methyl, and thus loss of efficiency. While Procter's synthesis only gave a 0.9% yield over 35 steps, it was the first enantiospecific total synthesis of (+)-pleuromutilin and also provided the first efficient esterification of mutilin to pleuromutilin.[22]

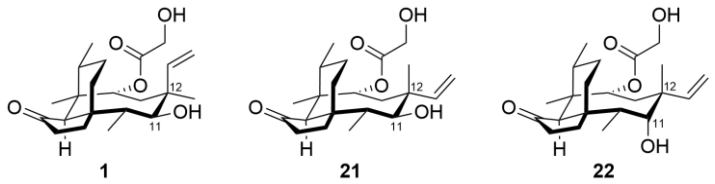


**Figure 4.** Herzon's diastereomers: (+)-Pleuromutilin **1**, (+)-12-*epi*-pleuromutilin **21**, and (+)-11,12-di-*epi*-pleuromutilin **22**.

In 2017, Herzon's group published an enantioselective total synthesis, which not only gave (+)-pleuromutilin **1**, but also (+)-12-*epi*-pleuromutilin **21** and (+)-11,12-di-*epi*-pleuromutilin **22** (Figure 4), all of which arise from their respective mutilin cores.[23] Of special interest is (+)-12-*epi*-pleuromutilin and its mutilin core. Previously work by Berner[24] demonstrated the ability to semi-synthetically convert native (+)-pleuromutilin to (+)-12-*epi*-pleuromutilin, with procedural streamlining performed by Thirring et al.[25] This pleuromutilin epimer, (+)-12-*epi*-pleuromutilin, was previously shown to be equipotent with pleuromutilin, demonstrating that the C12 position of pleuromutilin was amenable to manipulation of the non-polar functionality. Indeed, further derivatization of the vinyl group of (+)-12-*epi*-pleuromutilins produced derivatives which not only retained the antibiotic activity of the native epimer, but decreased the minimum inhibitory concentration (MIC) or expanded the range of activity to Gram-negative bacteria in some cases.[26] Due to the ease with which pleuromutilin derivatives could be semi-synthetically converted into (+)-12-*epi*-pleuromutilins, the number of derivatives that could be produced from vinyl group modification of pleuromutilin is effectively doubled. This approach is one we pursue and will be discussed in depth in later chapters of this thesis.

### 1.2.2 Biosynthesis

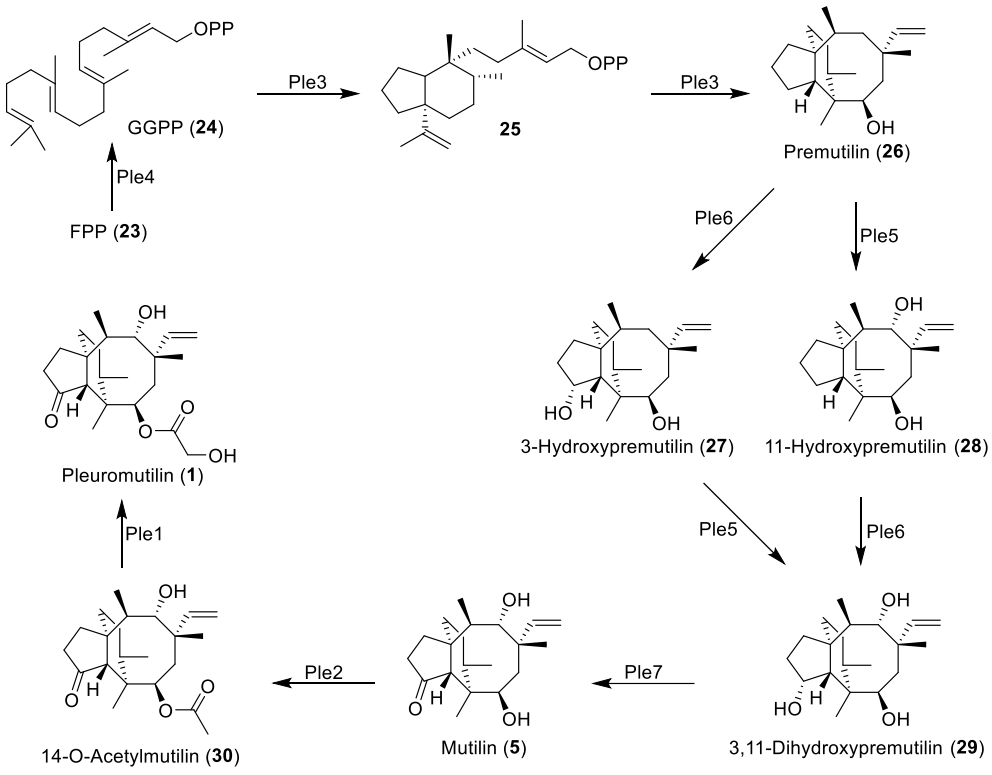


**Figure 5.** The biosynthetic pathway of pleuromutilin.

The full biosynthetic pathway of pleuromutilin was elucidated by Oikawa et al. (Figure 5). Using heterologously expressed genes of *Clitopilus pseudopinsitus* in *Aspergillus oryzae*, the group was able to synthesize and isolate pleuromutilin and two previously unknown intermediates, 3-hydroxypremutilin (**27**) and 3,11-dihydroxypremutilin (**29**), *in vivo*.[27] This study exemplifies a modern approach to piecing together natural product biosynthesis. By comparing enzymes of known function from other biosynthetic clusters to the target organism's genome, enzymes with high homologies can be identified. Subsequent expression or deactivation of those enzymes can be used to identify the biosynthetic intermediates, thus supporting or disproving a biosynthetic hypothesis.

### 1.2.3 Mechanism of action

Pleuromutilin's binding site is in the peptidyl transfer center (PTC) overlaying both the A- and P-site on the 50S ribosome. Specifically, the mutilin core fits into the tip of the A-site pocket, while the ester tail interacts with various residues in the P-site.[28, 29] This mechanism of action is unique to pleuromutilin and has the advantage of slow resistance development. Three mutations of *rplC*, encoding ribosomal protein L3, are required to confer resistance. Resistance follows a step-wise development, with minor resistance developing after the first two mutations and major resistance after the third.[30] Fortunately, the fitness of the organism is severely impacted in the final stage, and reversion to wild-type readily occurs. In practice, despite a long history of using pleuromutilin derivatives in veterinary medicine, resistance is still quite slow to appear. Resistance avoidance coupled with ease of derivatization make pleuromutilin an ideal scaffold for drug development.

#### 1.2.3.1 Resistance to resistance

What makes pleuromutilin particularly attractive for the development of future antibiotics is the low propensity for susceptible organisms to form resistances to it. Because of pleuromutilin's unique mechanism of action and binding site within the ribosome, it should lack cross-resistance with other classes of antibiotics that are commonly used.[31] However, even though the mechanism of action of pleuromutilin is distinct when compared with the chloramphenicols, the lincosamides, and the oxazolidinones,[28] some cross-resistance mechanisms can occur due to their partially overlapping binding sites. Cfr RNA methyltransferase can methylate A2503, which disrupts the binding of the phenicols, lincosamides, oxazolidinones, pleuromutilins, and streptogramin A ($PhLOPS_A$) antibiotics.[32]

In studies on various types of microorganisms including *Mycoplasma*,[33, 34] *Staphylococcus*,[35, 36] and *Streptococcus* spp.,[30, 35, 37] as well as *E. coli*,[36] the veterinary and clinical derivatives demonstrated low propensity for resistance development regardless of the composition

of the C22 side chain (on average $<10^{-9}$ spontaneous mutation frequency). Additionally, none of these cases were mutants with stable resistance able to be isolated at 4x to 8x MIC. In the case of multi-passage experiments, resistance mechanisms occurred slowly and required multiple mutations to confer high-level resistance. This resistance, however, came at a high fitness cost for the resulting mutants. Paukner and Riedl covered this topic in more detail in their 2017 review.[38] However, pleuromutilin based antibiotics are highly prone to efflux from Gram negative pathogens via the AcrB-TolC efflux pumps.[39] More work is necessary to generate derivatives of the pleuromutilin class that evade resistance via efflux.

### 1.2.4 Structure activity relationship

The preponderance of SAR studies with pleuromutilin derivatives focused on modification of the C14 sidechain. Due to sparse functionality on the molecule, activation of the primary alcohol on the α-hydroxy acetate with subsequent bimolecular nucleophilic substitution is a demonstrably viable strategy. Indeed, most work done on the C14 sidechain has utilized this strategy of substitution at C22 resulting in the thioether derivatives (**2**-**4**, Figure 1) currently in commercial use.

#### 1.2.4.1 C22 modification of pleuromutilin

In seminal work performed by Egger et al., the basis for the pharmacophore of pleuromutilin was laid out. Modification of the C11 alcohol or the ketone led to diminished activity. Hydrogenation of the vinyl group showed no decrease in activity.[40] However, derivatization of the C22 position led to a number of active derivatives, with C22 thioethers providing the most interesting activity. Indeed, the veterinary derivative tiamulin (Figure 1, **2**) was discovered among these initial derivatives. Of note, the C22 position was found to accommodate a wide range of substituents,

including linear chains, a finding that has been borne out by subsequent studies. For our purposes, this was a highly encouraging illumination, as conjugate antibiotics necessitate the use of flexible, linear linkers.

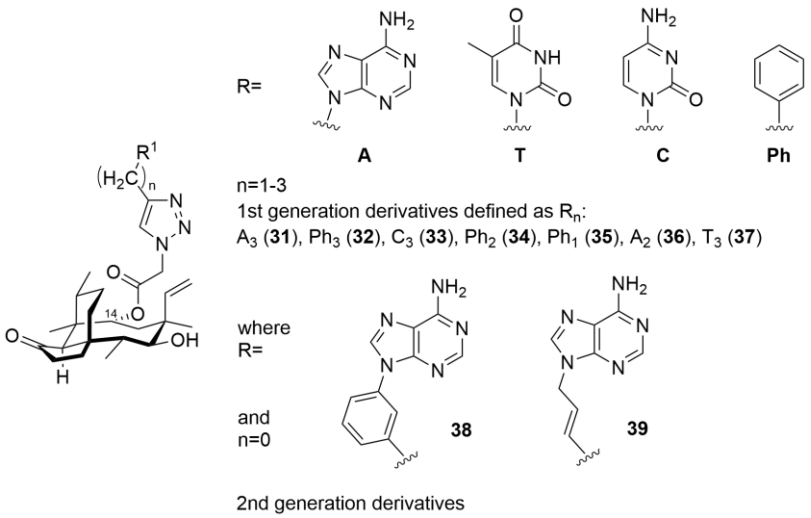


**Figure 6.** Nielsen's pleuromutilin nucleotide conjugates.

Nielsen et al. made a series of aromatic derivatives of pleuromutilin on the ester side chain (**31-39**, Figure 6). Starting by tosylating and then displacing the glycolic hydroxyl with azide, various alkynyl nucleotide derivatives and heterocycles were attached via copper catalyzed alkyne-azide cycloaddition. The goal of these modifications was to generate increased interaction with the ribosome nucleobase U2585 (*E. coli* numbering) near the mutilin binding pocket. Nielsen found that many of these compounds retained binding affinity when compared to pleuromutilin, while some showed enhanced binding affinity.[41] A further study by the same group continued with the trend of nucleotide conjugation, and generated eleven new compounds, seven of which showed increased binding affinity over pleuromutilin. Two of these compounds, **38** and **39** rivaled tiamulin (**2**) and valnemulin in MIC experiments with *E. coli*, *L. innocua*, and *B. subtilis*.[42] Modifications such as using oxygen in the linker chain decreased activity.[43] These studies demonstrate that the

binding site of pleuromutilin can handle large conjugates on the ester side-chain, and that these have the potential to increase desirable properties such as enhanced potency, higher water-solubility, and decreased toxicity.

### 1.2.4.2 C20 modification and C12 epimerization of pleuromutilin

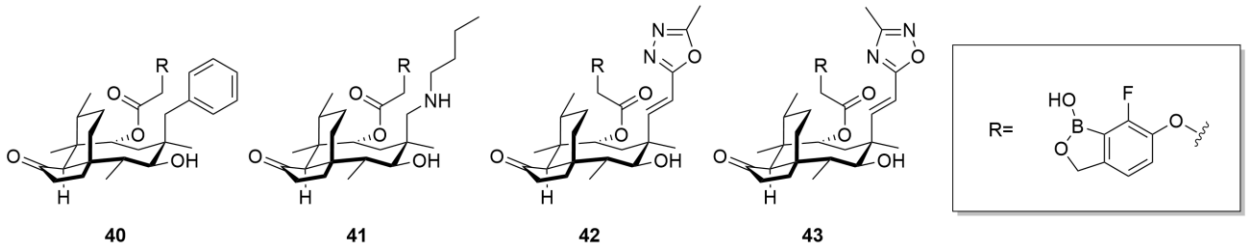


**Figure 7.** Selected examples demonstrating tolerated vinyl modifications in Xianfeng's work.

Based on previous findings of other groups and with the eventual goal of bidentate translation inhibitors in mind, we decided that an SAR study of pleuromutilin's vinyl moiety was necessary. This realm is underexplored and shows conflicting results.[44, 45] Research done by Xianfeng et al. demonstrated, using ozonolyzed intermediates, that various modifications to the vinyl side-chain could be tolerated, with either the same or minimally (<1 order of magnitude) decreased activity compared to pleuromutilin (**40**-**43**, Figure 7).[38, 45] These functionalities included linear chains and aromatic species. The vinyl group in these derivatives is not the only location of modification, with a boron-heterocycle derivatization (Figure 7 inset) replacing classic C22 thioether pleuromutilins, such as tiamulin and retapamulin, and showing similar activity. This precedent gives credence to the vinyl derivatization being a viable medicinal chemistry strategy.

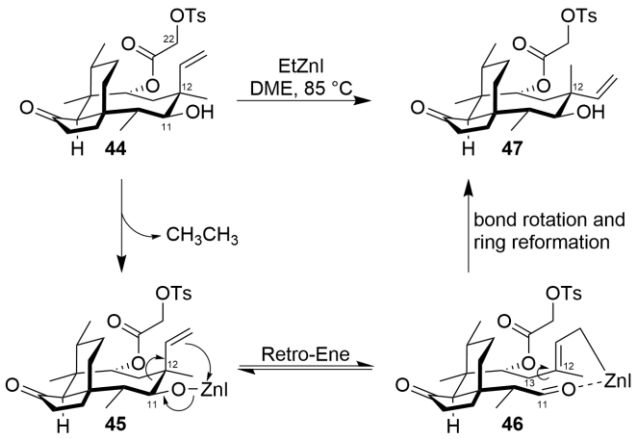


**Figure 8.** Berner's epimerization. **47** is achieved after protonation of the C11 alcohol during the quenching step. All steps after the deprotonation of the alcohol with the organozinc reagent (ethylzinc iodide in this case) and before the quench are reversible.

The work of Berner et al. provides arguably the most elegant transformation of pleuromutilin. Utilizing ethylzinc iodide with 22-*O*-tosylpleuromutilin **44**, a very interesting compound, 12-*epi*-22-*O*-tosylpleuromutilin **47** was afforded.[24] The reaction proceeds through a ring opening between C11 and C12 in a retro-ene cleavage (**45**). Rotation around the C12-C13 bond (**46**), followed by a reversal of the retro-ene reaction regenerates the 8-membered ring and furnishes the epimerized derivative **47** and the starting material **44** in an approximate 54:46 ratio and a yield of 37% for the isolated epimerized derivative. This ratio is constant, regardless of the organozinc reagent,[25, 26, 46] including in our hands as later described. These findings indicate that the ratio is the result of a thermodynamic equilibrium between the two reactive-intermediate epimers. The low isolated yield is attributable to this thermodynamic equilibrium, as well as the difficulty in separating two highly similar epimers which differ only in positioning of non-polar functionality via chromatographic means. The relevance of this epimerization to activity as highlighted by difference between the

work of Xianfeng and Nabriva and proved critical for our own development of pleuromutilin derivatives.

Nabriva Therapeutics also developed C19/C20 functionalized pleuromutilins (Figure 9). Nabriva is well known for its development of lefamulin (**3**) (brand name Xenleta) for systemic use, either through intravenous or oral delivery.[18, 47] With respect to epimerization, their work optimizing for production of 12-*epi*-22-*O*Ts-pleuromutilin, utilizing the reagent diethyl zinc[26] is more facile than Berner's[24] despite no yield being reported in their patent.

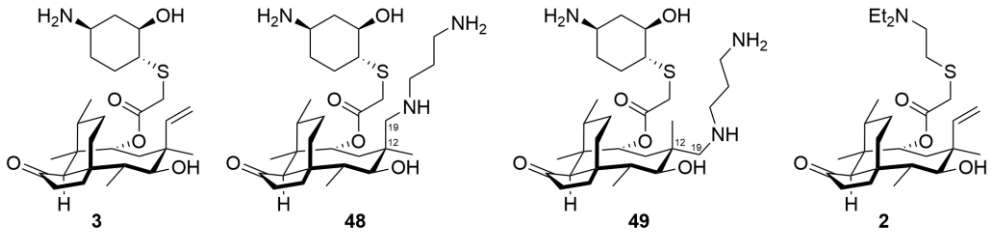


| Derivative | MIC µg/mL[a] *S. aureus* (ATCC 49951) | *E. coli* (ATCC 25922) |
|---|---|---|
| **48** | 16 | >32 |
| **49** | 0.25 | 4 |
| **2** | 0.5 | >32 |

[a]Determined via broth microdilution. Lefamulin not reported in this assay.

**Figure 9.** Lefamulin (**3**), tiamulin (**2**), and Nabriva's experimental derivatives **48** and **49**. Note the loss of activity of **48** in *S. aureus* and the gain of activity of **49**in *E. coli*.

To elaborate this drug class, Nabriva used their optimized epimerization method in the creation of 12-*epi*-pleuromutilin derivatives. After ozonolysis to activate the C19/C20 double bond and functionalization of the C22 position, installation of linear diamine chains via reductive amination at the C19 position afforded aminated derivatives (**48** and **49**, Figure 9). Epimeric derivative **49** retained similar activity to lefamulin against Gram-positive organisms, but also had enhanced Gram-negative activity.[26] This widened scope of anti-bacterial activity may be attributed to the polyamine character of the analogs.[48] Interestingly, in the analogous derivatives with no C12

epimerization (**48**), activity of the derivatives was lost completely. Calling back to Xianfeng's work,[45] a mystery is at hand. Activity of C19/C20 functionalized pleuromutilins appears to be highly dependent on not only the nature of the substituents at that position, but also of any functionalization of the C22 position. Thus, the exploration of C19/C20 derivatized pleuromutilins must be treated on a case-by-case basis, and no generalizations of these classes of compounds can currently be made.

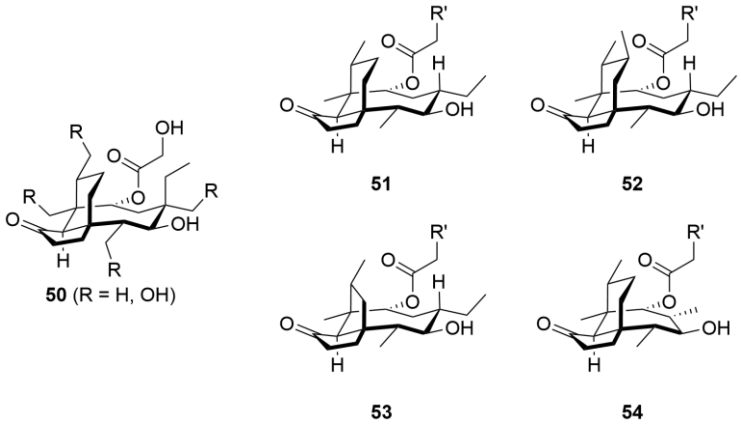


**Figure 10.** Representative structure of hydroxylated pleuromutilins (**50**) with R = H or OH, and representative core modified lefamulins (R' signifies a lefamulin chain). Nor-lefamulin (**51**) was the only compound to retain activity of these core modified structures. Additional methylation of the core (**52**), and ring contraction of the cyclohexane to a cyclopentane (**53**) or of the cyclooctane to a cycloheptane (**54**) resulted in loss of antibacterial activity.

Rounding out the discussion of pleuromutilin SAR studies is the work of Herzon's lab at Yale. Herzon, a veritable titan of pleuromutilin chemistry, has elaborated not only the core ring structures (Figure 10, **51**-**54**)[49] and provided total syntheses to pleuromutilin and two epimers (Figure 4),[23] his group has also created fascinating oxygenated derivatives (Figure 10, **50**).[50] By using hydroxyl-directed silylation followed by Tamao-Fleming oxidation, Herzon et al. installed

alcohols on various methyls of the pleuromutilin core. Their total syntheses are an important contribution, demonstrating the utility of late-stage diversification in total synthesis.

### 1.3 Ways to overcome antimicrobial resistance (AMR)

There are several methods by which antimicrobial resistance (AMR) can be overcome. Perhaps the most obvious is the introduction of new structural classes of antibiotics with unique mechanisms of action, thus avoiding resistance mechanisms which have developed to currently used antibiotics. Alternatively, drugs which have already seen widespread resistance development can be administered with an adjuvant — a compound which can neutralize the resistance mechanism itself — as seen with the combination therapy Augmentin, a combination of amoxicillin and the beta-lactamase inhibitor clavulanate potassium. The selective pressures which lead to the evolutionary development of resistance mechanisms in the first place could be avoided by using non-bactericidal antibiotics, targeting instead virulence or biofilm forming factors. However, the two methods most pertinent to the body of research discussed in this thesis are: 1. The semisynthetic modification of pre-existing antibiotics, and 2. The utilization of hybrid or conjugate antibiotics.

#### 1.3.1 Semisynthetic modification of pre-existing antibiotics

Perhaps the most well-known and widely used manner to combat emerging resistance mechanisms is modifying classes of antibiotics that are already used clinically to circumvent the resistance mechanism. There are numerous examples of this practice, from the beta-lactam class penicillins, to the tetracyclines, to the macrolides. This practice can seek to either mask reactive functionality and prevent the antibiotic's destruction via bacterial enzymes, enhance the binding of the antibiotic to the molecular target to overcome decreased binding affinity due to target site

modification by the bacteria, or to enhance uptake or avoid efflux. Semi-synthesis can be seen as a molecular arms race between medicinal chemists and nature, and side-stepping resistance in this manner is the most accepted and widely practiced method, with established results.

### 1.3.2 Hybrid and conjugate antibiotics

Hypothetically, a very attractive method of combatting AMR is the utilization of hybrid or conjugate antibiotics. To distinguish between the two, we will use the definitions of Klahn and Broenstrup: Hybrid antibiotics incorporate two or more antibiotics or their pharmacophores into one molecule, and conjugates attach an antibiotic to a compound which promotes uptake of the antibiotic or prevents its efflux, although this agent may have its own antibiotic effect.[51] These types of compounds have the potential benefit of combination therapies, where an organism has a very low incidence of spontaneous mutations resulting in resistance development to both compounds, but also because it is one single compound it should have consistent pharmacodynamic and kinetic properties. The Lowell lab is interested in a specific type of conjugate antibiotic, one which we term "bidentate" antibiotics. The theoretical basis for bidentate antibiotics will be discussed further in Chapter 6.

## 1.4 Precedent for 1,2,3-triazoles in medicinal chemistry

Compared to other functional groups, there is a dearth of 1,2,3-triazoles in FDA approved drugs, but this functional group is not unrepresented in medicinal chemistry.[52] The relative lack of FDA approved triazole drugs is surprising given their superior pharmacokinetic properties of metabolic stability, water solubility, and hydrogen bonding capability.[53] The triazole functional group as a pharmacophore can be a bioisostere for other functionalities, such as amides, esters, carboxylic acids, and other heterocycles.[54, 55] However, 1,2,3-triazole containing drugs are often still seen as

"long shot" candidates, despite the potential pros. Further, the ease of use of copper-catalyzed azide alkyne cycloadditions (CuAAC, click chemistry) could readily supply probes for testing and identifying lead compounds. Drug candidates could then be developed from these leads that replace the triazole pharmacophore with other established privileged structures if needed.

Previously, we discussed the work of Nielsen et al., where 1,4-disubstitued-1,2,3-triazoles were directly attached to the C22 position.[41-43, 56] It is worth mentioning the work performed by Zhang and Zhang et al. incorporating the triazole at various positions of chains substituted at the C22 position.[57, 58]In agreement with other work we have seen previously, where the C22 position can accommodate a wide range of functionality, we can see that the triazole ring is an acceptable modification in various positions. These results add to the evidence to support our hypothesis that the C22 position is amenable as a handle for linker attachment.

**1.5 Conclusion**

As we have seen, pleuromutilin provides a fantastic basis for semi-synthetic antibiotics. With a mainly hydrocarbon core, orthogonal reactions can be performed on it with ease. It has a well-established pharmacophore with two auxophores amenable to substitution. Resistance development to pleuromutilin derivatives as a class are slow, and there exists low cross-resistance to other drugs. Finally, several veterinary and clinical derivatives are in use and are well tolerated.

As has been demonstrated, the C22 position can tolerate a wide degree of functionality without loss of potency, from linear chains to rigid rings and large bulky groups, with a huge variance of polarity in between. The C20 position, while comparatively underexplored, also appears amenable to functionalization. For our purposes of generating conjugates, and ideally

bidentate, antibiotics, pleuromutilin is perhaps the best place to start. The compound meets all the criteria that we hypothesize makes a good bidentate candidate.

In this work, the process of turning pleuromutilin into a bidentate drug will be illuminated. Our original trials and tribulations of installing 1,2,3-triazoles at the C22 and C20 positions will be discussed (Chapter 2). The decision to switch to C12 epimerized derivatives will be explained in detail (Chapter 3). We will investigate the synthesis and activity of potentially covalently binding pleuromutilin electrophiles (Chapter 4). We will explore oligoethylene glycol linkers and the serendipitous discoveries achieved in that arena (Chapter 5). Finally, we will look at some experimental bidentates of pleuromutilin using blasticidin S and azithromycin, two other ribosome targeting antibiotics (Chapter 6), as well as some strange compounds which do not quite fit into other categories, before concluding (Chapter &) with a forward-looking analysis of pleuromutilins and antibiotic development.

### 1.6 References

1. *No time to wait: Securing the future from drug-resistant infections*; Interagency Coordination Group on Antimicrobial Resistance: 2019.
2. Murray, C. J.; Ikuta, K. S.; Sharara, F.; Swetschinski, L.; Robles Aguilar, G.; Gray, A.; Han, C.; Bisignano, C.; Rao, P.; Wool, E.; Johnson, S. C.; Browne, A. J.; Chipeta, M. G.; Fell, F.; Hackett, S.; Haines-Woodhouse, G.; Kashef Hamadani, B. H.; Kumaran, E. A. P.; McManigal, B.; Agarwal, R.; Akech, S.; Albertson, S.; Amuasi, J.; Andrews, J.; Aravkin, A.; Ashley, E.; Bailey, F.; Baker, S.; Basnyat, B.; Bekker, A.; Bender, R.; Bethou, A.; Bielicki, J.; Boonkasidecha, S.; Bukosia, J.; Carvalheiro, C.; Castañeda-Orjuela, C.; Chansamouth, V.; Chaurasia, S.; Chiurchiù, S.; Chowdhury, F.; Cook, A. J.; Cooper, B.; Cressey, T. R.; Criollo-Mora, E.; Cunningham, M.; Darboe, S.; Day, N. P. J.; De Luca, M.; Dokova, K.; Dramowski, A.; Dunachie, S. J.; Eckmanns, T.; Eibach, D.; Emami, A.; Feasey, N.; Fisher-Pearson, N.; Forrest, K.; Garrett, D.; Gastmeier, P.; Giref, A. Z.; Greer, R. C.; Gupta, V.; Haller, S.; Haselbeck, A.; Hay, S. I.; Holm, M.; Hopkins, S.; Iregbu, K. C.; Jacobs, J.; Jarovsky, D.; Javanmardi, F.; Khorana, M.; Kissoon, N.; Kobeissi, E.; Kostyanev, T.; Krapp, F.; Krumkamp, R.; Kumar, A.; Kyu, H. H.; Lim, C.; Limmathurotsakul, D.; Loftus, M. J.; Lunn, M.; Ma, J.; Mturi, N.; Munera-Huertas, T.; Musicha, P.; Mussi-Pinhata, M. M.; Nakamura, T.; Nanavati, R.; Nangia, S.; Newton, P.; Ngoun, C.; Novotney, A.; Nwakanma, D.; Obiero, C. W.; Olivas-Martinez, A.; Olliaro, P.; Ooko, E.; Ortiz-Brizuela, E.; Peleg, A. Y.; Perrone, C.; Plakkal, N.; Ponce-De-Leon, A.; Raad, M.; Ramdin, T.; Riddell, A.; Roberts, T.; Robotham, J. V.; Roca, A.; Rudd, K. E.; Russell, N.; Schnall, J.; Scott, J. A. G.; Shivamallappa, M.; Sifuentes-Osornio, J.; Steenkeste, N.; Stewardson, A. J.; Stoeva, T.; Tasak, N.;

Thaiprakong, A.; Thwaites, G.; Turner, C.; Turner, P.; Van Doorn, H. R.; Velaphi, S.; Vongpradith, A.; Vu, H.; Walsh, T.; Waner, S.; Wangrangsimakul, T.; Wozniak, T.; Zheng, P.; Sartorius, B.; Lopez, A. D.; Stergachis, A.; Moore, C.; Dolecek, C.; Naghavi, M., Global burden of bacterial antimicrobial resistance in 2019: a systematic analysis. *The Lancet* **2022,** *399* (10325), 629-655.
3. Ventola, C. L., The antibiotic resistance crisis: Part 1: Causes and threats. *P T* **2015,** *40* (4), 277-283.
4. Newman, D. J.; Cragg, G. M., Natural products as sources of new drugs over the last 25 years. *J. Nat. Prod.* **2007,** *70* (3), 461-477.
5. Harvey, A., Natural products in drug discovery. *Drug Discov. Today* **2008,** *13* (19-20), 894-901.
6. DančÍK, V.; Seiler, K. P.; Young, D. W.; Schreiber, S. L.; Clemons, P. A., Distinct biological network properties between the targets of natural products and disease genes. *J. Am. Chem. Soc.* **2010,** *132* (27), 9259-9261.
7. RoséN, J.; Gottfries, J.; Muresan, S.; Backlund, A.; Oprea, T. I., Novel chemical space exploration via natural products. *J. Med. Chem.* **2009,** *52* (7), 1953-1962.
8. Silverman, R. B.; Holladay, M. W., *The organic chemistry of drug design and drug action*. Academic press: 2014.
9. Lewis, W. G.; Green, L. G.; Grynszpan, F.; Radić, Z.; Carlier, P. R.; Taylor, P.; Finn, M.; Sharpless, K. B., Click chemistry in situ: Acetylcholinesterase as a reaction vessel for the selective assembly of a femtomolar inhibitor from an array of building blocks. *Angew. Chem.* **2002,** *114* (6), 1095-1099.
10. Manetsch, R.; Krasiński, A.; Radić, Z.; Raushel, J.; Taylor, P.; Sharpless, K. B.; Kolb, H. C., In situ click chemistry: Enzyme inhibitors made to their own specifications. *J. Am. Chem. Soc.* **2004,** *126* (40), 12809-12818.
11. Arsic, B.; Novak, P.; Kragol, G.; Barber, J.; Rimoli, M. G.; Sodano, F., *Macrolides: Properties, Synthesis and Applications*. Walter de Gruyter GmbH & Co KG: 2018.
12. Drews, J.; Georgopoulos, A.; Laber, G.; Schütze, E.; Unger, J., Antimicrobial activities of 81.723 hfu, a new pleuromutilin derivative. *Antimicrob. Agents Chemother.* **1975,** *7* (5), 507-516.
13. Hogenauer, G., The mode of action of pleuromutilin derivatives. Location and properties of the pleuromutilin binding site on *Escherichia coli* ribosomes. *Eur. J. Biochem.* **1975,** *52* (1), 93-98.
14. Kavanagh, F.; Hervey, A.; Robbins, W. J., Antibiotic substances from Basidiomycetes: VIII. *Pleurotus multilus* (Fr.) Sacc. and *Pleurotus passeckerianus* Pilat. *Proc. Natl. Acad. Sci. U. S. A.* **1951,** *37* (9), 570.
15. Czok, R.; Meingassner, J. G.; Mieth, H.; Schutze, E. Antibiotic compositions for treating coccidiosis. US patent 4,148,890, 1979.
16. Burch, D. G. S.; Ripley, P. H.; Zeisl, E. Veterinary use of a pleuromutilin derivative. US Patent 6,130,250, 2000.
17. Jacobs, M. R., Retapamulin: a semisynthetic pleuromutilin compound for topical treatment of skin infections in adults and children. *Future Microbiol.* **2007,** *2* (6), 591-600.
18. Hunt, A., FDA approves new antibiotic to treat community-acquired bacterial pneumonia. www.fda.gov/news-events/press-announcements, 2019.
19. Zeitlinger, M.; Schwameis, R.; Burian, A.; Burian, B.; Matzneller, P.; Müller, M.; Wicha, W. W.; Strickmann, D. B.; Prince, W., Simultaneous assessment of the pharmacokinetics of a pleuromutilin, lefamulin, in plasma, soft tissues and pulmonary epithelial lining fluid. *J. Antimicrob. Chemother.* **2016,** *71* (4), 1022-1026.
20. Gibbons, E. G., Total synthesis of (+-)-pleuromutilin. *J. Am. Chem. Soc.* **1982,** *104* (6), 1767-1769.
21. Farney, E. P.; Feng, S. S.; Schäfers, F.; Reisman, S. E., Total synthesis of (+)-pleuromutilin. *J. Am. Chem. Soc.* **2018,** *140* (4), 1267-1270.

22. Fazakerley, N. J.; Helm, M. D.; Procter, D. J., Total synthesis of (+)-pleuromutilin. *Chem. Eur. J.* **2013,** *19* (21), 6718-6723.
23. Murphy, S. K.; Zeng, M.; Herzon, S. B., A modular and enantioselective synthesis of the pleuromutilin antibiotics. *Science* **2017,** *356* (6341), 956-959.
24. Berner, H.; Vyplel, H.; Schulz, G.; Schneider, H., Chemie der Pleuromutiline, 11. Mitt.: Konfigurationsumkehr der Vinylgruppe am Kohlenstoff 12 durch reversible Retro-En-Spaltung. *Monatsh. Chem.* **1986,** *117* (8-9), 1073-1080.
25. Thirring, K.; Heilmayer, W.; Riedl, R.; Kollmann, H.; Ivezic-Schoenfeld, Z.; Wicha, W.; Paukner, S.; Strickmann, D. 12-epi pleuromutilins. 2017.
26. Thirring, K.; Heilmayer, W.; Riedl, R.; Kollmann, H.; Ivezic-Schoenfeld, Z.; Wicha, W.; Paukner, S.; Strickmann, D. Preparation of 12-epi-pleuromutilin derivatives as antimicrobial agents. WO2015110481A1, 2015.
27. Yamane, M.; Minami, A.; Liu, C.; Ozaki, T.; Takeuchi, I.; Tsukagoshi, T.; Tokiwano, T.; Gomi, K.; Oikawa, H., Biosynthetic machinery of diterpene pleuromutilin isolated from basidiomycete fungi. *ChemBioChem* **2017,** *18* (23), 2317-2322.
28. Schlünzen, F.; Pyetan, E.; Fucini, P.; Yonath, A.; Harms, J. M., Inhibition of peptide bond formation by pleuromutilins: the structure of the 50S ribosomal subunit from *Deinococcus radiodurans* in complex with tiamulin. *Mol. Microbiol.* **2004,** *54* (5), 1287-1294.
29. Davidovich, C.; Bashan, A.; Auerbach-Nevo, T.; Yaggie, R. D.; Gontarek, R. R.; Yonath, A., Induced-fit tightens pleuromutilins binding to ribosomes and remote interactions enable their selectivity. *Proc. Natl. Acad. Sci. U. S. A.* **2007,** *104* (11), 4291-4296.
30. Gentry, D. R.; Rittenhouse, S. F.; McCloskey, L.; Holmes, D. J., Stepwise exposure of *Staphylococcus aureus* to pleuromutilins Is associated with stepwise acquisition of mutations in rplC and minimally affects susceptibility to retapamulin. *Antimicrob. Agents Chemother.* **2007,** *51* (6), 2048-2052.
31. Yan, K.; Madden, L.; Choudhry, A. E.; Voigt, C. S.; Copeland, R. A.; Gontarek, R. R., Biochemical characterization of the interactions of the novel pleuromutilin derivative retapamulin with bacterial ribosomes. *Antimicrob. Agents Chemother.* **2006,** *50* (11), 3875-3881.
32. Long Katherine, S.; Poehlsgaard, J.; Kehrenberg, C.; Schwarz, S.; Vester, B., The Cfr rRNA methyltransferase confers resistance to phenicols, lincosamides, oxazolidinones, pleuromutilins, and streptogramin A antibiotics. *Antimicrob. Agents Chemother.* **2006,** *50* (7), 2500-2505.
33. Long, K. S.; Poehlsgaard, J.; Hansen, L. H.; Hobbie, S. N.; Böttger, E. C.; Vester, B., Single 23S rRNA mutations at the ribosomal peptidyl transferase centre confer resistance to valnemulin and other antibiotics in *Mycobacterium smegmatis* by perturbation of the drug binding pocket. *Mol. Microbiol.* **2009,** *71* (5), 1218-27.
34. Li, B.-B.; Shen, J.-Z.; Cao, X.-Y.; Wang, Y.; Dai, L.; Huang, S.-Y.; Wu, C.-M., Mutations in 23S rRNA gene associated with decreased susceptibility to tiamulin and valnemulin in Mycoplasma gallisepticum. *FEMS Microbiol. Lett.* **2010,** *308* (2), 144-149.
35. Kosowska-Shick, K.; Clark, C.; Credito, K.; McGhee, P.; Dewasse, B.; Bogdanovich, T.; Appelbaum, P. C., Single- and multistep resistance selection studies on the activity of retapamulin compared to other agents against *Staphylococcus aureus* and *Streptococcus pyogenes*. *Antimicrob. Agents Chemother.* **2006,** *50* (2), 765-9.
36. Miller, K.; Dunsmore, C. J.; Fishwick, C. W.; Chopra, I., Linezolid and tiamulin cross-resistance in Staphylococcus aureus mediated by point mutations in the peptidyl transferase center. *Antimicrob. Agents Chemother.* **2008,** *52* (5), 1737-42.
37. Paukner, S.; Clark, C.; Ivezic-Schoenfeld, Z.; Kosowska-Shick, K. In *Single-and multistep resistance selection with the pleuromutilin antibiotic BC-3781*, Fifty-second Interscience Conference on Antimicrobial Agents and Chemotherapy, San Francisco, CA, 2012.

38. Paukner, S.; Riedl, R., Pleuromutilins: Potent drugs for resistant bugs—Mode of action and resistance. *Cold Spring Harb. Perspect. Med.* **2017,** *7* (1), a027110.
39. Schuster, S.; Vavra, M.; Kern, W. V., Efflux-Mediated Resistance to New Oxazolidinones and Pleuromutilin Derivatives in Escherichia coli with Class Specificities in the Resistance-Nodulation-Cell Division-Type Drug Transport Pathways. *Antimicrob. Agents Chemother.* **2019,** *63* (9).
40. Egger, H.; Reinshagen, H., New pleuromutilin derivatives with enhanced antimicrobial activity. II. Structure-activity correlations. *J. Antibiot.* **1976,** *29* (9), 915-922.
41. Lolk, L.; Pøhlsgaard, J.; Jepsen, A. S.; Hansen, L. H.; Nielsen, H.; Steffansen, S. I.; Sparving, L.; Nielsen, A. B.; Vester, B.; Nielsen, P., A click chemistry approach to pleuromutilin conjugates with nucleosides or acyclic nucleoside derivatives and their binding to the bacterial ribosome. *J. Med. Chem.* **2008,** *51* (16), 4957-4967.
42. Dreier, I.; Kumar, S.; Søndergaard, H.; Rasmussen, M. L.; Hansen, L. H.; List, N. H.; Kongsted, J.; Vester, B.; Nielsen, P., A click chemistry approach to pleuromutilin derivatives, part 2: Conjugates with acyclic nucleosides and their ribosomal binding and antibacterial activity. *J. Med. Chem.* **2012,** *55* (5), 2067-2077.
43. Dreier, I.; Hansen, L. H.; Nielsen, P.; Vester, B., A click chemistry approach to pleuromutilin derivatives. Part 3: Extended footprinting analysis and excellent MRSA inhibition for a derivative with an adenine phenyl side chain. *Bioorg. Med. Chem. Lett.* **2014,** *24* (4), 1043-1046.
44. Bacque, E.; Pautrat, F.; Zard, S. Z., A flexible strategy for the divergent modification of pleuromutilin. *Chem. Commun.* **2002,** (20), 2312 - 2313.
45. Xianfeng, L.; Lunde, C. S.; Jacobs, R. T.; Yasheen, Z. Boron-containing small molecules. WO 2017/151492 A1, 2017.
46. Klaus Thirring, W. H., Rosemarie Riedl, Hermann Kollmann, Zrinka Ivezic-Schoenfeld, Wolfgang Wicha, Susanne Paukner, Dirk Strickmann 12-EPI PLEUROMUTILINS. 2016.
47. Paukner, S.; Sader Helio, S.; Ivezic-Schoenfeld, Z.; Jones Ronald, N., Antimicrobial Activity of the Pleuromutilin Antibiotic BC-3781 against Bacterial Pathogens Isolated in the SENTRY Antimicrobial Surveillance Program in 2010. *Antimicrob. Agents Chemother.* **2013,** *57* (9), 4489-4495.
48. Kwon, D. H.; Lu, C. D., Polyamine effects on antibiotic susceptibility in bacteria. *Antimicrob. Agents Chemother.* **2007,** *51* (6), 2070-7.
49. Goethe, O.; DiBello, M.; Herzon, S. B., Total synthesis of structurally diverse pleuromutilin antibiotics. *Nature Chemistry* **2022,** *14* (11), 1270-1277.
50. Ma, X.; Kucera, R.; Goethe, O. F.; Murphy, S. K.; Herzon, S. B., Directed C–H bond oxidation of (+)-pleuromutilin. *J. Org. Chem.* **2018,** *83* (13), 6843-6892.
51. Klahn, P.; Broenstrup, M., Bifunctional antimicrobial conjugates and hybrid antimicrobials. *Nat. Prod. Rep.* **2017,** *34* (7), 832-885.
52. Bozorov, K.; Zhao, J.; Aisa, H. A., 1,2,3-Triazole-containing hybrids as leads in medicinal chemistry: A recent overview. *Biorg. Med. Chem.* **2019,** *27* (16), 3511-3531.
53. Jain, A.; Piplani, P., Exploring the chemistry and therapeutic potential of triazoles: A comprehensive literature review. *Mini-Rev. Med. Chem.* **2019,** *19* (16), 1298-1368.
54. Agalave, S. G.; Maujan, S. R.; Pore, V. S., Click Chemistry: 1,2,3-Triazoles as Pharmacophores. *Chem. Asian J.* **2011,** *6* (10), 2696-2718.
55. Bonandi, E.; Christodoulou, M. S.; Fumagalli, G.; Perdicchia, D.; Rastelli, G.; Passarella, D., The 1,2,3-triazole ring as a bioisostere in medicinal chemistry. *Drug Discov. Today* **2017,** *22* (10), 1572-1581.
56. Heidtmann, C. V.; Voukia, F.; Hansen, L. N.; Soerensen, S. H.; Urlund, B.; Nielsen, S.; Pedersen, M.; Kelawi, N.; Andersen, B. N.; Pedersen, M.; Reinholdt, P.; Kongsted, J.; Nielsen, C. U.; Klitgaard, J. K.; Nielsen, P., Discovery of a potent adenine-benzyltriazolo-pleuromutilin conjugate with pronounced antibacterial activity against MRSA. *J. Med. Chem.* **2020,** *63* (24), 15693-15708.

57. Zhang, G.-Y.; Zhang, Z.; Li, K.; Liu, J.; Li, B.; Jin, Z.; Liu, Y.-H.; Tang, Y.-Z., Design, synthesis and biological evaluation of novel pleuromutilin derivatives containing piperazine and 1,2,3-triazole linker. *Bioorg. Chem.* **2020,** *105*, 104398.
58. Zhang, Z.; Li, K.; Zhang, G.-Y.; Tang, Y.-Z.; Jin, Z., Design, synthesis and biological activities of novel pleuromutilin derivatives with a substituted triazole moiety as potent antibacterial agents. *Eur. J. Med. Chem.* **2020,** *204*, 112604.

# Chapter 2. Synthesis, testing, and computational modeling of pleuromutilin 1,2,3-triazole derivatives in the ribosome

Logan M. Breiner[a,b], Anthony J. Briganti[c], Jennifer P. McCord[a], Moriah E. Heifetz[a], Sophia Y. Philbrook[a], Carla Slebodnick[a], Anne M. Brown[b,c,d], Andrew N. Lowell[a,b,e,*]

[a]Department of Chemistry, Virginia Polytechnic Institute and State University (Virginia Tech), Blacksburg, VA, 24061, United States

[b]Center for Emerging, Zoonotic, and Arthropod-borne Pathogens, Virginia Polytechnic Institute and State University (Virginia Tech), Blacksburg, VA, 24061, United States

[c]Department of Biochemistry, Virginia Polytechnic Institute and State University (Virginia Tech), Blacksburg, VA, 24061, United States

[d]Research & Informatics and Department of Biochemistry, Virginia Polytechnic Institute and State University (Virginia Tech), Blacksburg, VA, 24061, United States

[e]Faculty of Health Sciences, Virginia Polytechnic Institute and State University (Virginia Tech), Blacksburg, VA, 24061, United States

This study was published in *Tetrahedron Chem*:

Breiner, L. M.; Briganti, A. J.; McCord, J. P.; Heifetz, M. E.; Philbrook, S. Y.; Slebodnick, C.; Brown, A. M.; Lowell, A. N., Synthesis, testing, and computational modeling of pleuromutilin 1,2,3-triazole derivatives in the ribosome. *Tetrahedron Chem* **2022,** *4*.

## 2.1 Abstract

Pleuromutilin antimicrobials have given rise to the most recently FDA approved class of antibiotics for systemic human use. In this work, we describe a synthesis, assay, modeling approach to pleuromutilin development for the highly complex bacterial ribosome. Libraries of substituted 1,2,3-triazole derivatives were synthesized at the pleuromutilin C20 position by applying a recent anti-Markovnikov hydroazidation protocol to directly install an azido group, and at the C22 position through established methods. To learn about the interactions of these libraries with the ribosome and assess the potential for subsequent derivatization, an unbiased computational modeling method was used to biochemically rationalize binding modes of the C20 and C22 pleuromutilin derivatives. A pattern emerged where the triazole and its pendant chain, be it off the C20 or C22 position, moved to occupy the space vacated by the C22 sulfide group of clinical pleuromutilin compounds. Subsequent activity testing and comparative ranking of the computationally docked derivatives to the in vitro activity results showed a high predictability rating for the C22 substituted compounds. These combined investigations reveal potential restrictions and sites for expansion, paving the way for the development of future pleuromutilin derivates and other ribosome targeting antibiotics.

## 2.2 Introduction

Antimicrobial resistance (AMR) is a global health crisis, directly responsible for killing 1.27 million people in 2019,[1] with the number of people succumbing yearly to effects from antibiotic-resistant pathogens projected to increase to 10 million by 2050.[2] The number of antibiotics approved by the FDA has declined in recent decades,[3] making effective new treatments more urgently needed. Natural products are an incredibly rich source of pharmaceuticals, especially antibiotics,[4] and a strong focus on cultivating those that exhibit low rates of resistance is particularly relevant for the development of effective antimicrobials that help suppress AMR.

Pleuromutilin (**2**, **Figure 1**), a tricyclic diterpenoid antibiotic, was first isolated from *Pleurotus mutilus* (now *Clitopilus scyphoides*) in 1951.[5] Comprised of a mutilin core (**1**) with a glycolic ester side chain at the C14 position, pleuromutilin was shown to have activity against Gram-positive bacteria and mycoplasmas.[6] Mutilin drugs exert their effect by interfering with peptide bond formation in the peptidyl transfer center (PTC). The mutilin core binds in a hydrophobic pocket in the A-site of the 50S subunit of the ribosome[7] while the C14 sidechain interacts with nucleotides from the P-site.[7, 8] Early investigations showed that a wide range of functionality could be installed on the ester side chain.[6] Thus, semi-synthetic derivatization of pleuromutilin focused mainly on modification of the C22 position of the glycolic ester.[9, 10]

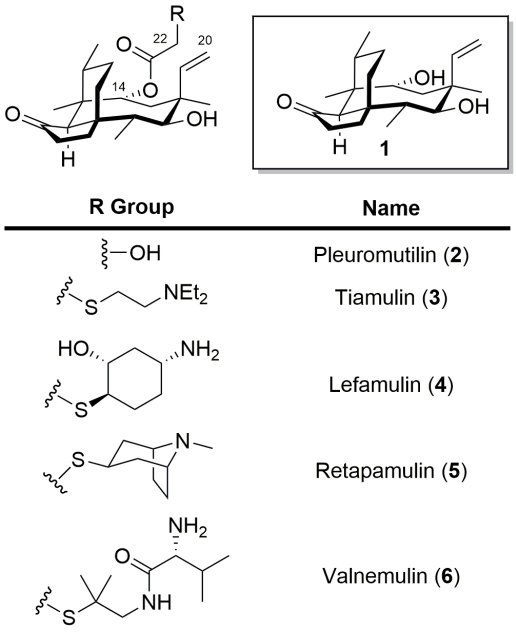


**Figure 1.** Pleuromutilin and its commercial derivatives.

Despite initial concerns about potentially unfavorable ADMET (absorption, distribution, metabolism, excretion, and toxicity) properties, empirical results demonstrated that the mutilin class could be optimized to avoid these issues.[11, 12] The first approved drug was the veterinary compound tiamulin (**3**)[13] with subsequent approvals including the veterinary drug valnemulin (**6**)[14] and the topical agent retapamulin (**5**).[15] Recent work by Nabriva Therapeutics generated lefamulin (**4**), which was approved by the Food and Drug Administration for systemic use in humans in 2019.[16] The mutilins are an attractive class for further improvement because of slow resistance development due to their unique binding site within the PTC, slow rates of spontaneous mutation,[2, 17-19] and a lack of shared resistance mechanisms from other antibiotic classes.[18]

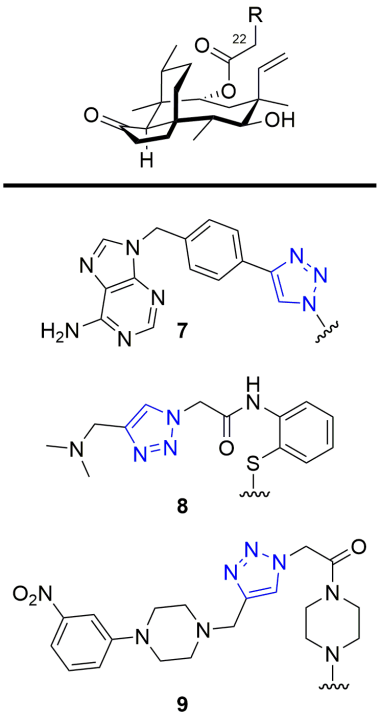


**Figure 2.** Triazole containing pleuromutilin derivatives.

Building on the success of first-generation pleuromutilin derivatives (Figure 1), several groups are undertaking a variety of improvement strategies focused on taking advantage of pi-stacking–type interactions with the ribosomal RNA nucleotides. One variation of this approach is the use of click-conjugates, especially triazoles via copper-catalyzed alkyne-azide cycloadditions (CuAAC), which is attractive because of its ease and the increased acceptance of 1,2,3-triazole–containing leads in medicinal chemistry.[20-22] Initial investigations in this area by Nielsen and coworkers[23-26] produced compounds that rivaled the activity of tiamulin (**3**) with additional, conformationally restricted analogs (such as **7**, Figure 2) surpassing it[24, 26] Other groups have likewise derivatized various spacers, such as 2-aminothiophenol (**8**)[27] or piperazine (**9**),[28] with CuAAC chemistry to generate novel triazole derivatives. Not only were these compounds more effective than tiamulin at reducing bacterial load and increasing survival in murine MRSA models,

but they had also only moderate inhibition against CYP3A4,[29] a metabolic enzyme responsible for the breakdown of common drugs.

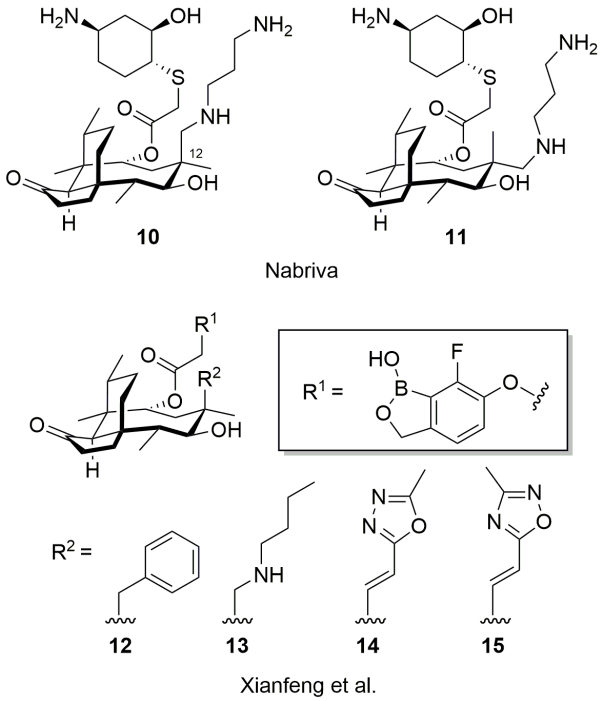


**Figure 3.** C20 modifications of pleuromutilin.

In contrast to C22 substitutions, derivatization of the C19-C20 vinyl group is just starting to be explored. Nabriva Therapeutics has functionalized the vinyl group through hydroboration-oxidation (not shown), or ozonolysis followed by reductive amination resulting in diamines (such as **10**, Figure 3), including C12 epimers (**11**)[30] Other work by Xianfeng and coworkers using C22-benzoxaboroles (*inset*) demonstrated that a pendant phenyl group (**12**), alkyl amines (**13**), and 5-membered heterocycles (**14** and **15**) were well tolerated in place of the vinyl group, increasing activity over the parent by an order of magnitude.[31]

Computational docking methods that can be applied to aid in the development of pleuromutilin derivatives, and for ribosome-targeting antibiotics generally, are lacking. The difficulty is in assessing the extraordinarily large ribosome (2.5 MDa) while also maintaining a sufficiently sensitive approach that enables analysis of the interaction of antibiotic ligands with the underlying nucleotide and protein structure of the ribosome. Beyond assisting in the specific development of new pleuromutilin or other antibiotic derivatives, the application of computational methods could also eventually be used to answer questions about the activity (or lack thereof) of previously reported compounds.

Thus, the opportunity to apply computational methodologies to the ribosome coupled with these synthetic findings spurred us to explore triazole derivatives of the glycolic ester and of the vinyl group. Established substitution conditions for the C22 alcohol would enable facile installation of an azide and subsequent CuAAC chemistry would enable access to a variety of flexible functionality capable of being further elaborated beyond the rotationally restricted aromatic and saturated rings that have been used previously. Activation of the C20 position, however, would require optimization of recent methodological breakthroughs. Accordingly, we sought to incorporate azide functionality at the C20 and C22 positions and subsequently derivatize them into a library of substituted triazoles. These compounds could then be tested for activity and used as a training set to assess computational approaches for analyzing ribosome-binding antibiotics.

## 2.3 Results and discussion

### 2.3.1 C22 Derivative synthesis by tosylation and direct displacement

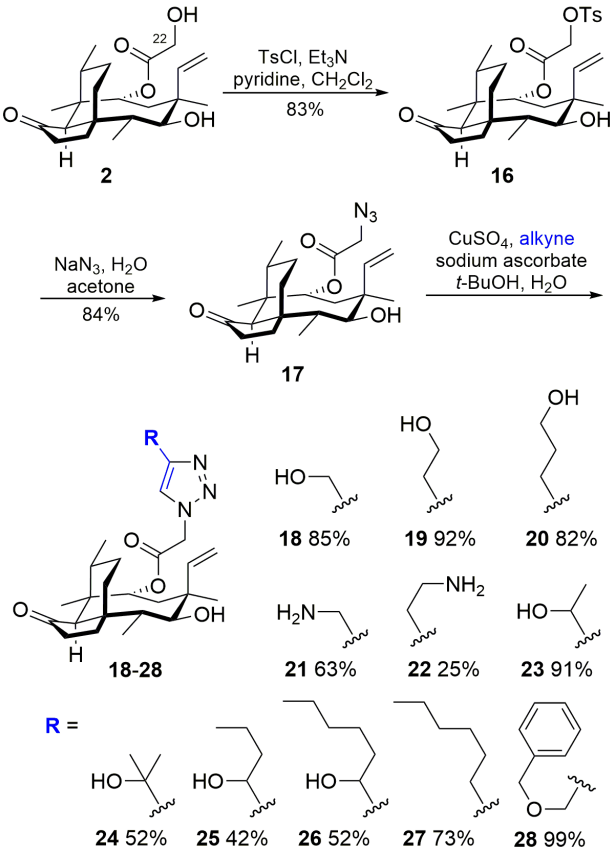


Figure 4. Synthesis of C22 triazoles.

In the first set of derivatives, the C22-triazoles (Figure 4) were synthesized via the well-known intermediate 22-*O*-tosylpleuromutilin (**16**).[31] This electrophile underwent conversion to the α-azidoester (**17**) via $S_N2$ displacement with sodium azide as previously described.[23] The triazoles (**18**-**28**) were produced using Sharpless's technique[32] with heating of **17** and the appropriate alkyne to approximately 70 °C. Most compounds were obtained in high yields but increased steric bulk near the alkyne reduced transformation efficacy (**24**-**26**).

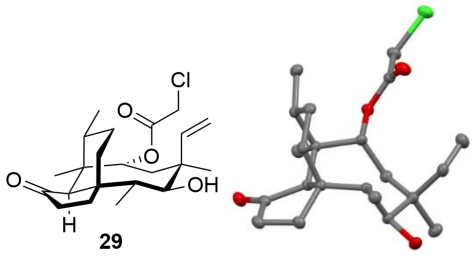


**Figure 5.** 22-Deoxy-22-chloropleuromutilin and its X-ray crystal structure.

During our preparation of 22-*O*-tosylpleuromutilin (**16**), we isolated and identified 22-deoxy-22-chloro-pleuromutilin (**29**, Figure 5), a material that has been intentionally generated,[33] but never to our knowledge reported as a byproduct of the tosylation reaction. In a procedure using 4-dimethylaminopyridine as a catalyst, we observed that the mother liquor from the recrystallization of **16** showed a non-trivial amount of mutilin-containing material. Chromatographic separation and characterization, including X-ray crystallography, confirmed this material to be **29**, which we isolated in a 20% yield. This material must arise from the nucleophilic displacement of the tosylate in **16** by the chloride anion formed during tosylation. The displacement of sulfonates by chloride during sulfonylation is known, especially with benzylic substrates.[34-36] As **16** is an intermediate in nearly all synthetic schemes that involve pleuromutilin modifications at C22, suppression of **29** or designing synthetic strategies that take advantage of its co-generation is an important consideration in the semisynthesis of pleuromutilin derivatives.

### 2.3.2 C20 Derivative synthesis using a modified anti-Markovnikov hydroazidation protocol

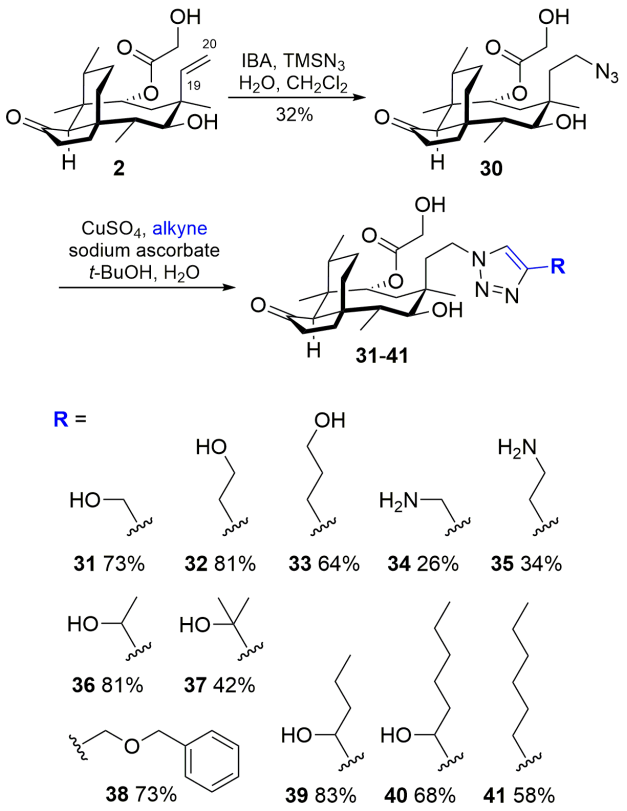


**Figure 6.** Synthesis of C20 triazoles.

Toward installation of a C20 azido component, we sought to modify the vinyl group into an azide directly instead of using a multi-step protocol. Previous studies describing the stoichiometric[37] or catalytic[38] hydroazidation of vinyl compounds suggested that this approach was achievable on pleuromutilin (**2**, Figure 6). The resulting novel intermediate (**30**) could then be decorated with diverse functionality through CuAAC chemistry.

Our initial trials focused on the catalytic hydroazidation of **2** using 2-iodosobenzoic acid (IBA), $TMSN_3$, trifluoroacetic acid (TFA), and water.[38] This approach created small amounts of **30**, but the acid and water present in the reaction mixture also hydrolyzed **2** to **1**. Removal of the acid from the reaction mixture eliminated hydrolysis, but yields were low and silylation of the primary and secondary alcohols was observed. Intentional silylation prior to hydroazidation

significantly reduced the yield of **30**, likely due to steric hinderance around the vinyl group. Further complicating a catalytic approach, the active catalyst species degraded over time, restricting conversion.

After experimenting with ratios of reagents, we determined that appreciable conversion of **2** to **30** could be achieved using a super-stoichiometric amount of IBA and $TMSN_3$ along with omission of the acid co-catalyst and inclusion of excess water. This combination afforded the highest yield of **30** without the production of silylated byproducts. Even under these optimized conditions, full conversion of the starting material was not observed without degradation of the catalyst. While the overall yield of **30** was modest (32%), this one-step protocol avoided a longer sequence of protection, hydroboration, activation, displacement, and deprotection.

Concerningly, the polarity of the desired hydroazide (**30**) prevented its separation from pleuromutilin (**2**) under standard chromatographic conditions (normal phase, $SiO_2$). However, the triazole achieved after CuAAC was easily separable from **2**, preserving this atom economic approach. Thus, a library of C20-triazoles were synthesized by reacting the resulting 80%/20% mixture of **30**/**2** with a variety of alkynes, giving **31-41** in 26-83% yield. As with the C22 derivatives, steric bulk near the alkyne generally decreased yields.

Azides are an increasingly popular functional group due to their ease of derivatization into triazoles[32] and the acceptance of triazoles in drugs.[39] However, azide chemistry can be hazardous because the presence of metals or halogenated solvents can cause an explosion and hydrazoic acid is both potentially explosive and toxic.[40] Of these potential dangers, the use of halogenated solvents and generation of hydrazoic acid are concerns for the current work. During the hydroazidation reaction (which is performed behind a blast shield), hydrazoic acid is generated transiently from TMS-azide and rapidly used up in the catalytic cycle. Excess hydrazoic acid

contributes to the breakdown of IBA, which liberates the acid as nitrogen gas.[38] Although the reaction is performed in dichloromethane, the neutral or acidic reaction conditions exclude the formation of azide anions needed to displace the chlorides and generate diazidomethane. The workup basifies any remaining hydrazoic acid, converting it to sodium azide that could potentially react with dichloromethane to form an explosive substance. However, the generated azide anions are only briefly exposed to a solution of dichloromethane during extraction. Formation of diazidomethane is slow, taking weeks at room temperature, even under concentrated conditions.[41] Thus, the risk of generating dangerously unstable or toxic azide species in this reaction is minimal, but care should be taken as outlined by the cautionary statements in the experimental.

### 2.3.3 Derivatization location impacts antibacterial activity

The minimum inhibitory concentration (MIC) of our libraries of C22 and C20 derivatives was measured against a series of Gram-positive and Gram-negative bacteria (Tables 1 and 2). Pleuromutilin was used as a positive control.

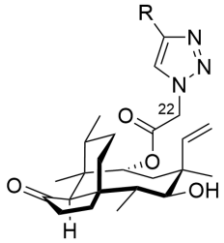

| Compound | R | *S. aureus* MRSA | *S. aureus* NorA | VRE | *E. coli* TolC |
|---|---|---|---|---|---|
| **18** | $CH_2OH$ | 8 | 8 | 32 | 32 |
| **19** | $(CH_2)_2OH$ | 8 | 8 | 16 | 16 |
| **20** | $(CH_2)_3OH$ | 8 | 8 | 16 | 64 |
| **21** | $CH_2NH_2$ | 16 | 8 | 64 | 16 |
| **22** | $(CH_2)_2NH_2$ | 16 | 8 | 32 | 16 |
| **23** | $CH(CH_3)OH$ | 32 | 8 | 32 | 16 |
| **24** | $C(CH_3)_2OH$ | 16 | 32 | 64 | 32 |
| **25** | $CH(OH)(CH_2)_2CH_3$ | 64 | 8 | 64 | 64 |
| **26** | $CH(OH)(CH_2)_4CH_3$ | 16 | 16 | 64 | 32 |
| **27** | $(CH_2)_5CH_3$ | 8 | 4 | 64 | >64 |
| **28** | $CH_2OCH_2C_6H_5$ | 8 | 8 | 32 | 32 |
| **2** | ---- | 4 | 4 | 16 | 4 |
| **17** | ---- | 2 | 1 | 8 | 4 |

**Table 1**. C22 Triazole derivatives. MICs are reported in µg/mL. Broth dilution assay performed in duplicate. NorA and TolC strains are efflux pump knockouts of their respective organisms. All tested compounds were inactive against *A. baumanii* at 64 µg/mL.

### 2.3.3.1 Antibacterial testing of C22 pleuromutilin derivatives

A portion of the C22-triazole derivatives (Table 1), namely the homologated alcohol series (**18-20**), the hexyl chain (**27**), and the benzyl ether (**28**), showed comparable activity to pleuromutilin in *Staphylococcus aureus*, both methicillin-resistant *S. aureus* (MRSA) and *S. aureus* with the NorA efflux pump removed (NorA).[42] The homologated alcohols were also comparable to pleuromutilin in vancomycin-resistant Enterococcus (VRE) growth inhibition. In addition, azido derivative **17** was comparable or slightly outperformed pleuromutilin against all species, showing broad spectrum activity corresponding to that reported by Reidl.[33] The homologated amines (**21** and **22**) showed diminished activity with all species, although their positive charge under physiological conditions likely resulted in their relative retention of activity against *Escherichia coli*. The other moderate-to-weakly active compounds against *E. coli* were methyl and ethyl alcohols **18** and **19**, branched alcohols **23** and **24**, and methyl benzyl ether **28**, suggesting that a polar atom close to the triazole makes critical contacts in the binding pocket.

However, the mixed results with alcohols with longer alkyl chains (**25** versus **26**) indicate the binding in this region is complicated. The activity of the other C22-triazole compounds was moderate to weak against *E. coli* TolC (the efflux pump knockout strain of *E. coli*[43]) and no compound had activity at 64 μg/mL against *Acinetobacter baumannii*, which may be an issue of permeability in this Gram negative pathogen or differences in its ribosome binding site.[44] However, there was no general correlation with the chemical property data (Tables S11 and S12) suggesting that all derivatives acted on the strains in the same basic way. While only **19** was active against *E. coli*, the entire series of short, homologated alcohols (**18**-**20**) were equally efficacious against the two *S. aureus* species and showed a slight increase in potency with increasing chain length against VRE, suggesting that the C22 triazole was accommodated by the binding site in all these species but subtler binding pocket difference beyond the triazole changed the activity due to differences in hydrogen bonding contacts. Despite having the same length as **18**, secondary and tertiary alcohols **23** and **24** were less active against MRSA and variable against the NorA knockout, indicating that a combination of binding site differences and efflux are responsible for the change in activity. Likewise, secondary alcohols attached to a longer alkyl chain (**25** and **26**) showed variable activity. With the butyl chain (**25**), efflux may be responsible for the differences in inhibition as activity was maintained against the NorA knockout but lost against MRSA. With the hexyl chain (**26**), activity between MRSA and the NorA knockout strain were identical suggesting that it is not prone to efflux. The alkyl derivative (**27**) showed similar potency to pleuromutilin against *S. aureus*, but lost efficacy against VRE and was inactive against *E. coli*. As the *E. coli* strain is efflux deficient, the change in activity is likely due to subtle differences between the *S. aureus* and *E. coli* binding sites. Lastly, the benzyl ether derivative (**28**) showed a marginal

reduction in activity for the Gram-positive strains compared to pleuromutilin and matched previously reported activity against *E. coli*.[24]

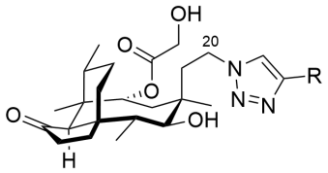


| Compound | R | *S. aureus* MRSA | *S. aureus* NorA | VRE | *E. coli* TolC |
|---|---|---|---|---|---|
| **31** | $CH_2OH$ | >64 | >64 | >64 | >64 |
| **32** | $(CH_2)_2OH$ | >64 | >64 | >64 | >64 |
| **33** | $(CH_2)_3OH$ | >64 | >64 | >64 | >64 |
| **34** | $CH_2NH_2$ | 32 | 64 | >64 | 64 |
| **35** | $(CH_2)_2NH_2$ | >64 | 64 | >64 | 64 |
| **36** | $CH(CH_3)OH$ | >64 | >64 | >64 | >64 |
| **37** | $C(CH_3)_2OH$ | >64 | >64 | >64 | >64 |
| **39** | $CH(OH)(CH_2)_2CH_3$ | >64 | >64 | >64 | >64 |
| **40** | $CH(OH)(CH_2)_4CH_3$ | >64 | 64 | >64 | >64 |
| **41** | $(CH_2)_5CH_3$ | >64 | >64 | >64 | 16 |
| **38** | $CH_2OCH_2C_6H_5$ | >64 | 64 | >64 | >64 |
| **2** | ---- | 4 | 4 | 16 | 4 |
| **30** | ---- | 32 | 32 | >64 | 16 |

**Table 2.** C20 Triazole derivatives. MICs are reported in µg/mL. Broth dilution assay performed in duplicate. All tested compounds were inactive against *A. baumanii* at 64 µg/mL.

### 2.3.3.2 Antibacterial testing of C20 pleuromutilin derivatives

Unexpectedly, and in contrast to previous results where heterocycles attached to the C20 position showed activity,[31] few of the C20-triazole derivatives demonstrated inhibition of the test organisms (Table 2). However, our results do align with the Nabriva findings, where C20 derivatives (such as **10**, Figure 3) lost activity compared to the parent compound *in vitro*.[30] One possible explanation is that without a C22 sidechain or an intact double bond at the C19-C20 position,[31] our C20 functionalized compounds did not bind or bound in an ineffective

configuration. Of the compounds tested, only two showed an appreciable level of activity, the hexyl derivative (**41**) against *E. coli* and the azide precursor (**30**) against everything except VRE. Compound **41** being active in contrast to its C22 partner **27**, which was inactive, indicates that uptake of alkyl-substituted pleuromutilins is probably not a critical issue; instead, this result suggests that subtle changes in the binding pocket among the different ribosomes influences binding and hence activity. This insight into binding site differences strongly supports the continued application and development of computational methods to help us learn about binding site differences in the ribosome and guide the development of future derivatives. Although these compounds were generally inactive in our assays, their synthesis demonstrates the synthetic utility of hydroazidating vinyl-containing natural products.

### 2.3.4 In-silico exploration of triazole derivative binding modes and efficacy predication

Predicting antibiotic derivative efficacy via computational methods is a growing area of research in rational antibiotic redesign;[45] however, determining protocols and acquiring training datasets are critical advancements for a large, complex cellular target, such as the bacterial ribosome. Historically, molecular docking programs have been optimized for small-molecule–protein interactions. With the continued emergence of nucleic acid polymers as therapeutic targets, these programs are finding new, more demanding applications. Evaluations of currently used docking programs to predict small molecule binding modes (poses) in structures partially or fully comprised of nucleic acids[46] suggests that AutoDock Vina[47] outperforms Schrödinger Glide[48] in predictive ability.[49] Accurate binding pose prediction was considered one of the most important criteria when selecting a molecule docking program for our exploration into prokaryotic ribosomal small molecule inhibitors. Accurate pose prediction gives invaluable insight on drug positioning within the ribosomal binding cavity, and therefore insight into drug repositioning through

modification, which then can be applied to future drug design. Thus, we worked to create a molecular docking protocol that could reliably dock antibiotics and novel derivatives into small or large ribosomal subunits while accurately ranking them as compared to MIC values.

Although inherently limited by their focus on the binding target (other important factors such as cellular penetration and efflux of drugs cannot be taken into account by docking), previous studies established that clipping the ribosomal binding cavity to a subset of relevant binding nucleotides and residues minimizes the effects of structural inaccuracies.[50] Within the 2.5 MDa ribosome complex, ribonucleoprotein elements within 3.5 Å of the co-crystalized ligand have the strongest interatomic contacts and are responsible for most direct binding interactions. Thus, all ribonucleoprotein elements that contained nucleotides or residues within 15 Å of the crystal structure ligand were considered relevant for antibiotic binding.

#### 2.3.4.1 Computational method design

In order to establish a robust protocol to apply computational design to ribosomal drug discovery, ribosome structures with antibiotics that target various regions were collected from the RCSB PDB (PDB IDs: 1FJG,[51] 4V56,[52] 5HL7,[53] 4V9Q,[54] 6CZR,[55] 4U56,[56] 6B4V,[57] 1KC8,[58] and 1XBP[7]) and overlayed. From these overlayed structures, we selected a receptor grid box that was large enough (30x30x30 Å) to accommodate all of the parent antibiotic binding sites in order to remove the variable of constantly changing box sizes, center coordinates, and relevant ribonucleoprotein elements. We then removed the various co-crystallized antibiotic from their crystal structures and redocked them using standard methods (Tables S1-S9, Figures S1-S9, SI Computation Methods pages S3-S4). Further, interactions between redocked antibiotics and nearby nucleotides were used as an additional metric to determine the ability to replicate co-crystal

antibiotic positioning, in addition to root-mean-square deviation (RMSD) calculations comparing atom coordinate overlap.

For these redocked antibiotics, AutoDock Vina[47] showed better consistency and accuracy than Schrödinger Glide[48] using an analogous protocol based on the same center and docking coordinate space (SI Computation Methods pages S3-S4) in terms of scoring interactions between the small molecule and nucleotides and by conformational ensemble quality. For example, redocking of tiamulin from 1XBP (Figure 7A) using Schrödinger Glide[48] did not generate a minimum of nine ligand poses, while AutoDock Vina did so reliably (Figure 7B). Further, those poses predicted by Schrödinger Glide were highly clustered into one area (Figure 7C), missing key ribosome interactions, while AutoDock Vina sampled more diversity throughout the antibiotic binding cavity space. Quantitatively, Schrödinger Glide resulted in RMSD values ranging between 5.17 Å to 5.52 Å (Figure 7D), a lack of sampling that indicated this docking program was not suitable for these systems. On the other hand, AutoDock Vina[47] consistently generated nine redocked poses (Tables S1-S9) with more diversity throughout the antibiotic binding cavity space as measured by RMSD values. A portion of these poses were lower than 2 Å for most of PDB structures tested during protocol development. Thus, the increased number of redocked poses produced by the AutoDock Vina[47] protocol allowed for more sampling of the binding cavity, conferring a conformational ensemble with a wider range of RMSD values including some sub-2 Å results that were sufficient for use in our study.

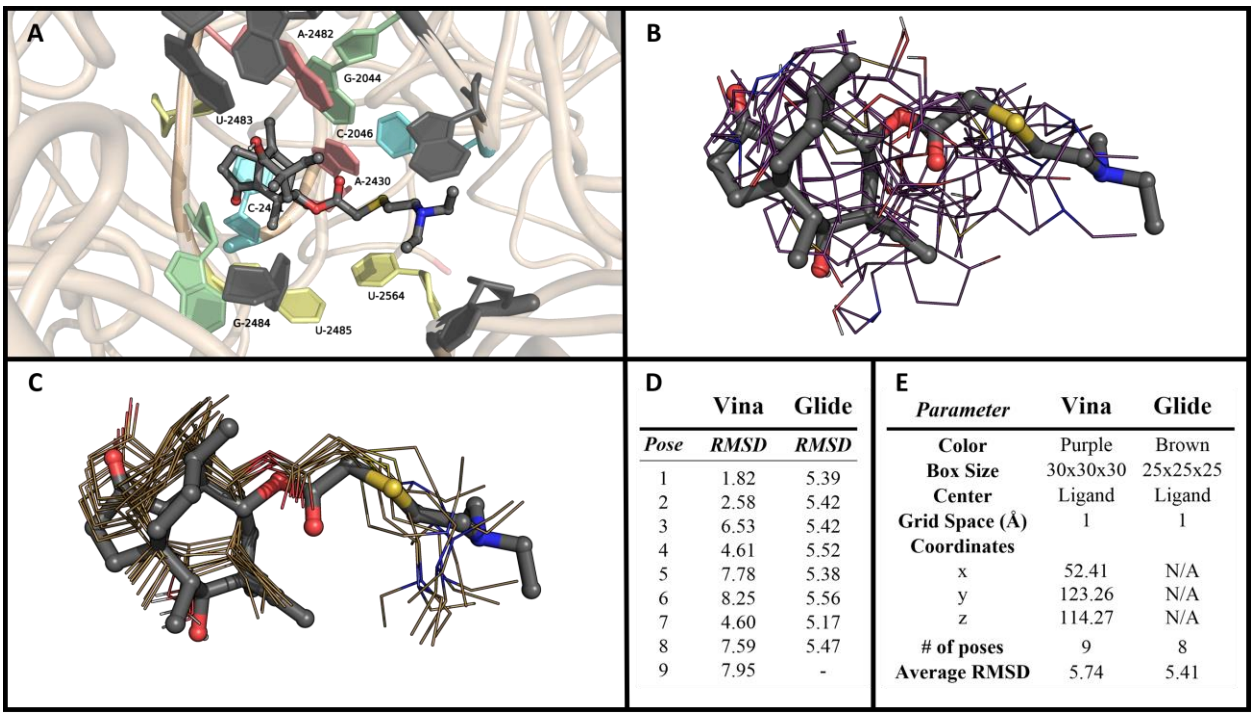


D

| | Vina | Glide |
|---|---|---|
| *Pose* | *RMSD* | *RMSD* |
| 1 | 1.82 | 5.39 |
| 2 | 2.58 | 5.42 |
| 3 | 6.53 | 5.42 |
| 4 | 4.61 | 5.52 |
| 5 | 7.78 | 5.38 |
| 6 | 8.25 | 5.56 |
| 7 | 4.60 | 5.17 |
| 8 | 7.59 | 5.47 |
| 9 | 7.95 | - |

E

| *Parameter* | Vina | Glide |
|---|---|---|
| **Color** | Purple | Brown |
| **Box Size** | 30x30x30 | 25x25x25 |
| **Center** | Ligand | Ligand |
| **Grid Space (Å)** | 1 | 1 |
| **Coordinates** | | |
| x | 52.41 | N/A |
| y | 123.26 | N/A |
| z | 114.27 | N/A |
| **# of poses** | 9 | 8 |
| **Average RMSD** | 5.74 | 5.41 |

**Figure 7.** (A) Tiamulin in PDB ID: 1XBP (grey, colored by element) with individual nucleotides of the binding pocket that contact (<3.5 Å) the redocked tiamulin and derivatives. Adenosines are shown in red, cytidines shown in blue, guanosines shown in yellow, and uridines shown in green. Low interactive nucleotides are greyed out. (B) The nine poses of redocked tiamulin (purple lines) overlayed with the native tiamulin ligand (grey sticks). (C) The eight poses of redocked tiamulin (purple lines) overlayed with the native tiamulin ligand (grey sticks). (D) RMSD values for the Autodock Vina and Schrödinger Glide poses shown in (B) and (C), respectively. Vina reliably furnished nine poses while Glide could only return a maximum of eight. While the average RMSD was approximately the same, the thorough sampling of the receptor grid box and broader range of RMSD values provided by Autodock Vina instilled confidence that it would provide better correlations. (E) Parameters for the two programs excerpted from the docking protocol (SI Computation Methods pages S3-S4).

Among the various antibiotic/ribosome complexes studied, the *average* RMSD values (obtained by averaging all nine poses produced by AutoDock Vina) ranged from 4.3 Å to 12.7 Å (Tables S1-S9, SI Computational Methods, pages S3-S4). These values are larger than traditionally observed for small molecule protein modeling,[50] but are critical to providing a baseline for establishing a widely applicable protocol to successfully model these highly complex systems.

**2.3.4.2. Method validation for pleuromutilin-containing co-crystal structures**

Among the co-crystal structures used to establish our docking method, the *Deinococcus radiodurans* (PDB ID: 1XBP[7]) and *Staphylococcus aureus* (PDB ID: 5HL7[53]) 50S ribosomal subunit structures co-crystallized with pleuromutilin derivatives tiamulin and lefamulin, respectively, offered the best potential platforms for the triazole derivatives under study. Redocking using the *S. aureus* and *D. radiodurans* 50S ribosomal subunits centered on the same coordinates and using the established 30x30x30 Å box size (Figure 7E) reliably produced binding poses with RMSDs of less than 2 Å (Tables S3 and S9). Lefamulin (Table S3, Figure S3) was successfully redocked into the *S. aureus* 50S ribosomal subunit with an RMSD of 1.5 Å for the lowest energy pose, but there were three major sub-pocket areas sampled during the redocking, resulting in an average RMSD for all poses of 12.7 Å. The affinity of lefamulin for these sub-pockets dramatically lowered the frequency of shared base pair interactions that the redocked poses shared with the co-crystalized ligand, conserving only five of the crystal structure/lefamulin interactions at ≥70% frequency. Tiamulin (Table S9, Figure S9) was successfully redocked into the *D. radiodurans* 50S ribosomal subunit with an RMSD of 1.8 Å for the lowest energy pose and an average RMSD of 5.7 Å for all poses. Redocking of tiamulin in the *D. radiodurans* PTC and lefamulin in the *S. aureus* PTC sampled the same volume of space, but the redocking of tiamulin produced a higher frequency of shared base pair interactions between

redocked poses and the co-crystalized ligand in the crystal structure, conserving all nine base pair interactions vital for coordination of the co-crystalized ligand at ≥70% frequency. Thus, redocking procedures based on *D. radiodurans* using tiamulin were selected over *S. aureus* with lefamulin because of their lower average RMSD and the observed high degree of alignment with the authentic tiamulin ligand from the co-crystal structure. Further, compounds **1**-**15**, which bear a variety of C20 and C22 substituents, could also be reliably docked to 1XBP (Figure S10 and Table S10). These successes gave us confidence that docking triazole derivatives to the PTC would be feasible.

#### 2.3.4.3. Application of computational methods to triazole pleuromutilin derivatives

C22-Functionalized triazole-pleuromutilin derivatives **18**-**28** (Figures S12-S39) and C20-functionalized derivatives **31**-**41** (Figures S40-S67) were docked using the tiamulin docking protocol (SI Computation Methods pages S3-S4) and parameters (Figure 7E). Each derivative's predicted lowest free energy pose (LFE, Tables 4 and 5) and average free energy of all poses (AFE) were calculated using AutoDock Vina.[47] Qikprop[59] was used to calculate ligand physicochemical properties including total heavy atoms, molecular weight, volume, logP of octanol/water, solvent accessible surface area, and human oral absorption (Table S11-S12). The predicted ranking of the triazole-pleuromutilin derivatives were based on each compound's ligand efficiency, defined as the free energy of binding divided by the number of non-hydrogen atoms in the ligand (heavy atom count, HAC). Ranks were assigned using the ligand efficiency for the lowest energy pose (LE-LP) in ascending order (most negative to least negative). Ranks from the ligand efficiency of all poses (LE-AP) gave a similar order. Top ranked derivatives showed the most consistent pose clustering and a high frequency of interaction with the nucleotides that contact tiamulin (Figures S12-S39) while lower ranks displayed poor clustering and a lower frequency of interaction with the proximal

nucleotides, results that support the modeling approach. The docked poses for all derivatives displayed a similar range of predicted free energies of binding (-10.7 kcal/mol to -9.1 kcal/mol). Overall, the C22 derivatives ranked better in predicted efficacy based on computational methods than the C20 derivatives.

**Table 4.** Docking results of the C22 triazoles.

| *ID* | *LFE* | *AFE* | *HAC* | *LE-LP* | *LE-AP* |
|---|---|---|---|---|---|
| **18** | -9.8 | -9.1 | 33 | -0.297 | -0.28 |
| **19** | -10.6 | -9.7 | 34 | -0.312 | -0.29 |
| **20** | -9.4 | -8.8 | 35 | -0.269 | -0.25 |
| **21** | -9.6 | -8.9 | 33 | -0.291 | -0.27 |
| **22** | -9.8 | -9.1 | 34 | -0.288 | -0.27 |
| **23R** | -10.0 | -9.6 | 34 | -0.294 | -0.28 |
| **23S** | -10.0 | -9.4 | | -0.294 | -0.28 |
| **24** | -10.2 | -9.4 | 35 | -0.291 | -0.27 |

**Table 5.** Docking results of the C20 triazoles.

| *ID* | *LFE* | *AFE* | *HAC* | *LE-LP* | *LE-AP* |
|---|---|---|---|---|---|
| **31** | -9.3 | -8.7 | 34 | -0.274 | -0.26 |
| **32** | -9.1 | -8.2 | 35 | -0.260 | -0.23 |
| **33** | -9.4 | -8.6 | 36 | -0.261 | -0.24 |
| **34** | -9.2 | -8.7 | 34 | -0.271 | -0.25 |
| **35** | -9.1 | -8.0 | 35 | -0.260 | -0.23 |
| **36R** | -9.5 | -8.9 | 35 | -0.271 | -0.25 |
| **36S** | -9.5 | -8.8 | | -0.271 | -0.25 |
| **37** | -9.6 | -8.9 | 36 | -0.267 | -0.25 |

Considering the computational analysis of the C22 and C20 groups separately, substitutions of short carbon chains terminated by an electronegative group, such as **18**, **21**, **31**, and **34** (Tables 4 and 5, Figures S12-S13, S18-S19, S40-S41, and S46-47), gave the most favorable predicted free energy of binding results. A main contributor to the more favorable binding modes of these compounds was their ability to interact favorably with G2044 (Figures S12-S67), the nucleotide that engages the ester on the thioether chain of tiamulin. Interaction with the G2044 nucleotide is essential for targeting derivatives to bind within the ribosomal PTC, showing interactions with over 70% of all docked derivative poses from both the C22 and C20 groups (Figure S12-S67). As the carbon chain-length off the triazole rings increased beyond an ethyl group, less favorable predicted free energies of binding and binding modes with poorer relative

fitness to the cavity (e.g., less similar position to tiamulin) were generally observed. This connection between longer chain length and worse predicted binding rank is illustrated by the difference between **19** and **20**. Compound **20**, with one additional carbon atom, did not perform as well as **19** with respect to predicted free energy of binding (Table 4, LFE and AFE), ligand efficiency measurements (LE-LP and LE-AP), and nucleotide interactions (Figure S15 and S17). This effect was accentuated in longer chain derivatives, such as **25**, **26**, **39**, and **40**. Compared to other long-chain derivatives, compounds **28** and **38** performed better, likely because of favorable pi-stacking interactions between the aromatic group and A2045 (Figures S39 and S67). Polar functional groups (alcohols and ethers) positioned closer to the triazole mitigated some of the negative effects of length by mimicking the interaction of the hydroxyl groups of the best-performing derivatives, **18** and **19**. Indeed, high (>70%) interaction levels between nucleotides A2430, C2431, U2483, and G2484 and the alcohols of derivatives **18** and **19** (as well as polar groups from other derivatives, Figures S12-S17) support the conclusion that polarity at the α- and b-carbon of the triazole chain plays a crucial role in coordinating triazole-derived pleuromutilins to the ribosome.

Comparing the predicted poses of C22 (Table 4) and C20 (Table 5) triazole derivatives with the same substituent from the other series showed that while they bound with similar energies, the C22 variants universally had lower predicted free energies of binding for the lowest energy pose and for the average energy of all poses. Energy minimizations of the C20 derivatives with Schrödinger Maestro[59] independent of docking showed no intramolecular interactions that would preclude successful docking. Pattern analysis of the binding modes for the two series were correlated to each other and to the tiamulin ligand by using fingerprint graphing (Figures S12-S67) of the docking simulations to quantify ligand-nucleotide interactions. The differences in

interactions were visualized using PyMOL 2.5.0[60] (Figures S12-S67). Nucleotide interactions placed the triazole ring of all derivatives in the same area, that which is normally occupied by the sulfide-containing chain of tiamulin.

**2.4 Unifying computational analysis and in vitro activity**

To rationalize these energetic and orientational differences revealed by the docking studies, close inspection of the two series was undertaken using PyMOL 2.5.0 and revealed that each grouped with separate orientations of the triazole ring. As the C22 triazole derivatives are substituted directly onto the C22 position, they and their pendant chains maximize contacts normally made by the sulfide ether chain while the mutilin core is easily accommodated within its binding pocket (Figure 8A, Figures S12-S39). In contrast, when the triazole ring derivatives are attached to the C20 position, they must rotate and bend inward to effectively contact the nucleotides that usually interact with the thioether substituent of tiamulin (Figure 8B, Figures S40-S67). Adding to the binding inadequacies the C20 triazole series, these derivatives still contain a C22 hydroxyl group; electron repulsion between it and the C20 triazole prevent either from assuming as favorable of a contact position. The resulting shift in orientation of the triazole in the C20 series also diminishes the contacts of the mutilin core to its binding pocket relative to those of the C22 series. Thus, we hypothesize that the C20 series cannot reach as far into the PTC while retaining the vital mutilin core interactions needed for effective inhibitory activity, while the C22-triazole derivatives can maintain these important contacts.

To compare the computational analysis to the MIC assay results, the averages of the MIC values for each triazole derivative were compared to the independently derived computational ranks of the C20 and C22 subgroups. A limitation of this computational/MIC comparison is that we are assuming that there is no difference in permeability or efflux of the derivatives, which range

in cLogP from -0.8 to 2.5 and solvent exposed surface area from 695–942 Å$^2$ (Tables S11 and S12). By averaging the MIC values among the various species tested, we sought to minimize organism-specific effects that would interfere with MIC/computational comparisons. Overall, high agreement between the MIC values and computational results was achieved by considering ligand efficiency for the active C22-substituted derivatives (Figure 8C, blue circles). For the inactive C20 subgroup, distinguishing the ranking agreement was hampered by low variance in the MIC assay results (Figure 8C, red diamonds). However, alignment for the general activity predictions comparing one series to the other by computational modeling and MIC assays were in accord: The C22 triazole series were more active than the C20 triazole series. The triazole group was tolerated as a viable substitution off the C22 position with shorter chains and polar functionality being more active. The C20 triazoles series lost activity compared to pleuromutilin likely due to the inability to maintain sufficient contacts of the mutilin core and the side chain simultaneously (Figure 8D).

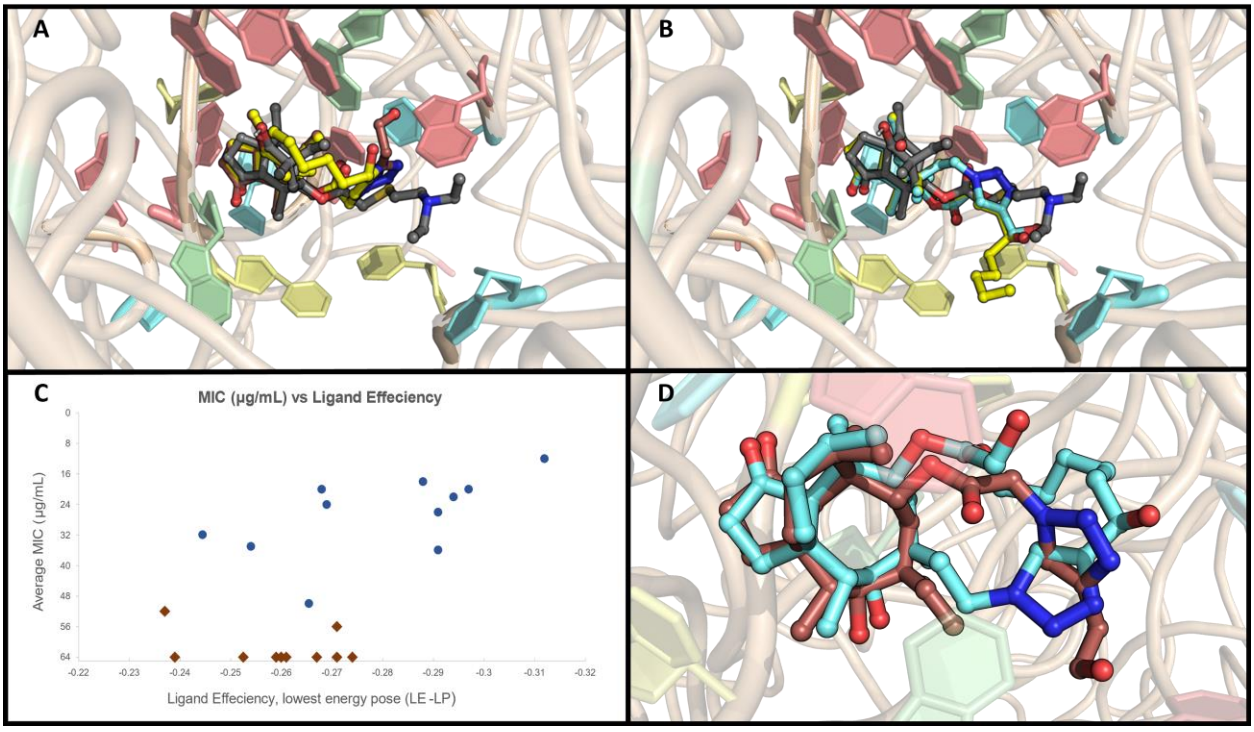

**Figure 8.** Comparison of docking poses and rank orders for the C20 and C22 pleuromutilin triazole derivatives. (A) The best poses of the highest (brown) and lowest (yellow) ranked C22 derivatives docked to the ribosome. Tiamulin (grey) is shown for reference. The triazoles make the same contacts as the tiamulin sulfide when not perturbing core mutilin contacts. (B) The best poses of the highest (light blue) and lowest (yellow) ranked C20 derivatives docked to the ribosome. Tiamulin (grey) is shown for reference. The triazole still makes contact with the same residues as the tiamulin sulfide, but must push the glycolic acid residue out of the way and perturb the mutilin binding position to do so. (C) Scatterplot comparing average MIC values (Tables 1 and 2) to ligand efficiency (LE-LP, Tables 4 and 5) for C22 derivatives (blue circles) and C20 derivatives (red diamonds). The activity of the C22 derivatives tracks well with the docking results while the lack of activity among the C20 derivatives prevents assessment of the docking fidelity. (D) Comparison overlay of C22 derivative **19** (brown) and C20 derivative **32** (light blue) highlighting the perturbation of the mutilin core (*left*) and overlay of the triazoles (*right*) with the site usually occupied by the tiamulin thioether.

### 2.5 Conclusions

We synthesized libraries of pleuromutilin derivatives containing triazoles at the C20 and C22 positions. To activate the vinyl as an azide, recently published hydroazidation techniques were used[37, 38] showing that a direct anti-Markovnikov hydroazidation can be performed on an unprotected, complex natural product. Subsequent CuAAC reactions on this C20 azido (**30**) and a traditionally prepared C22 azido intermediate (**17**) resulted in libraries of pleuromutilin-triazole derivatives that were tested against both Gram-positive and -negative strains, demonstrating that triazoles are well tolerated as a C22 sidechain modification and a viable pathway to rapidly create antibiotic derivative libraries. The underexplored C20 triazole derivatives did not show activity

against the tested organisms, but contribute additional data to an ongoing debate about whether this site is suitable for functionalization. Some reports suggest that pairing C20 heterocycles with more complex C22 sidechains produces active compounds[31] while others indicate that chain extension in place of the C20 vinyl position is deleterious to activity[30].

To gain further insight to the binding patterns responsible for the observed activity and to establish protocols for docking and developing antibiotic derivatives generally, we completed an unbiased computational docking study with of our libraries of compounds based on the tiamulin/*D. radiodurans* co-crystal ribosome structure (PDB ID: 1XBP[7]). The redocked ligand had a low RMSD and all derivatives were tightly clustered, indicating a high model validity. The computational ranks predicting derivative effectiveness based on *in silico* ligand efficiency measurements largely agreed with the ranks based on average minimum inhibitory concentration for the C22 derivatives. The poor activity of the C20 derivatives in the MIC assays prevented their differentiation, thus precluding a meaningful correlation to the computational results for this series. However, computational comparison between the C20 series and C22 series indicated that the latter should be more active, a result which was confirmed by the activity assay. Discrepancies in ranks could also be due to issues beyond the computationally assessed interactions, such as cellular penetration, an issue that will be addressed for future derivatives by using a cell-free transcription/translation assay to independently assess binding alongside the current MIC assay that determines actual efficacy. Overall, the C22 triazole-pleuromutilin derivates performed better in the activity assays and scored better computationally than the C20 derivatives, a result which we rationalize is caused by the inability of the latter to successfully bind to the underlying nucleotides with their substituted chain and mutilin core simultaneously.

This combined synthetic/assay/modeling approach serves as a basis for the continued development of pleuromutilin triazole derivatives and the guided evolution of ribosome-targeting antibiotics generally. The computational work establishes a critical starting point for the application of computational methods for analysis of antibiotic-ribosome binding, work that will help in unraveling the activity of functionalized C20 vinyl pleuromutilin derivatives, both with and without C12 epimerization. Further exploration of these derivatives is needed to understand the possibilities of substitution at the vinyl substituent, with or without C22 substitution. Future work will continue to use a combined computational/medicinal chemistry approach to guide development of additional potent pleuromutilin derivatives and for the development of other classes of antibiotics.

## 2.6 Experimental

### 2.6.1 Computational methods

The crystalized 50S ribosomal subunit from *Deinococcus radiodurans* in complex with tiamulin (PDB ID: 1XBP)[7] was retrieved from RCSB PDB.[61] The 22 triazole-pleuromutilin derivatives were converted from a CDX file into individual PDB files using Chem3D. The PDB files were further optimized in Schrödinger-Maestro 2021-2,[59] by running an OPLS4 energy minimization on the structures, and then docked using the following procedure. PyMOL 2.5.0[60] was used to clean the ribosomal subunit for molecular docking, with small molecules, waters, and ions removed before processing. The ribosomal subunit was clipped in size to be all structural elements within 15 Å of the tiamulin binding site. Additionally, ions, waters, and other small molecules present in the environment were removed. The co-crystalized tiamulin ligand within the *D. radiodurans* 50S ribosomal subunit was separated from the ribonucleoprotein complex, and both structures were exported from PyMOL 2.5.0[60] as PDB files with relative atom coordinates preserved. AutoDock Tools 1.5.6[62] was used to prepare the structure and ligand files by adding polar hydrogens, determining ligand torsion, computing Gasteiger partial charges, and assigning AD4 atom types. Molecular docking was performed with AutoDock Vina[47] using a box size of 30Å x 30Å x 30Å centered on the coordinates 52.564, 123.356, 114.265, which is based on the tiamulin ligand position in PDB ID: 1XBP[7]. The grid box size was determined by overlaying all ribosomes screened for redocking ability and is large enough to not bias binding cavity sampling based on ligand size. Compounds such as amicetin have also used this protocol in order to ensure size would not be a limitation. Redocking was performed to determine if experimental results could be replicated with a docking protocol. Tiamulin was redocked successfully into the clipped ribosomal subunit with a lowest energy pose of -8.9 kcal/mol and root-mean-square deviation

(RMSD) of 1.573 Å to the co-crystalized tiamulin position in the original crystal structure. All azido-pleuromutilin derivatives were processed and docked as outlined above. Coordinate files and docking configuration files are deposited on our Open Science Framework page (https://osf.io/82n73/).

Characterization of the docked derivatives poses was performed using Schrödinger-Maestro 2021-2.[59] Qikprop was used to calculate ligand physicochemical properties. Fingerprinting was used to determine any nucleotide or residue interactions within 3.5 Å.

To develop a ranking system of azido-pleuromutilin derivatives, output of predicted free energies of binding for ligand-ribosome interactions were calculated for both the lowest energy pose (LFE) and as an average of all nine poses (AFE). Ligand efficiency, defined as the free energy of binding divided by the heavy atom count (HAC, the number of non-hydrogen atoms in the ligand) was then calculated using Autodock Vina[47] for predicted free energies of binding and Qikprop[59] to calculate the HAC. Compounds were ranked with consideration to ligand efficiencies based on the ligand efficiency of the lowest energy pose of docked ligands (LE-LP).

### 2.6.2 Antimicrobial testing

Media components for microorganism growth were purchased from EMD Millipore, Sigma-Aldrich, Thermo Fisher Scientific, and Becton Dickinson and Company. Media and solutions were autoclaved or sterile filtered prior to use and manipulations were carried out in a laminar flow hood. Antibiotic testing was performed in polypropylene 96-well round bottom plates (Corning, Item #3365). The minimal inhibitory concentration of the derivatives against MRSA, *S. aureus* NorA, vancomycin-resistant *Enterococcus*, *E. coli* TolC, and *A. baumanii* was tested by broth dilution using pleuromutilin as a positive control. Stock solutions were prepared at 10.0

mg/mL in DMSO (molecular biology grade). Working solutions were prepared at 2.56 mg/mL by dilution of the stock solutions with DMSO, followed by 2-fold serial dilutions in DMSO, and application of 10 µL of each dilution to 96-well plates, in duplicate. Bacteria were grown overnight in LB broth solutions from individual colonies. The overnight cultures were diluted to an $OD_{600}$ of 0.04 for outgrowth in LB. When the cultures had reached an $OD_{600}$ of 0.4-0.6 (4-6 h), the bacteria were rediluted to an $OD_{600}$ of 0.004 and applied to the plates (190 µL per well). The plates were incubated at 37 °C for 18 hours. The MIC was recorded as the lowest concentration that visibly inhibited growth of the bacteria as assessed by percent transmittance.

### 2.6.3 X-ray crystallography

A colorless prism (0.12 × 0.24 × 0.28 $mm^3$) was centered on the goniometer of a Rigaku Oxford Diffraction Synergy-S diffractometer equipped with a HyPix6000HE detector and operating with CuKa radiation. The data collection routine, unit cell refinement, and data processing were carried out with the program CrysAlisPro.[63] The Laue symmetry and systematic absences were consistent with the monoclinic space groups $P2_1$ and $P2_1/m$. As the compound was known to be enantiomerically pure, the noncentrosymmetric space group $P2_1$ was chosen. The structure was solved using SHELXT[64] and refined using SHELXL[65] via Olex2.[66] The final refinement model involved anisotropic displacement parameters for non-hydrogen atoms. A riding model was used for the aromatic and alkyl hydrogens. The hydroxyl H-atom was located from the difference electron density map and the position and isotropic displacement parameter were refined independently. The absolute configuration was established from anomalous dispersion effects [Flack x = -0.023(7);[67] Hooft P2(true) = 1.000, P3(true) = 1.000, P3(rac-twin) = 0.000e+00; P3(false) = 0.000e+00, y = -0.014(5)].[66] The absolute stereochemistry at the chiral centers is assigned as C1 (R), C2 (R), C3 (R), C4 (S), C5 (R), C6 (S), C7 (S), C12 (R).

### 2.6.4 General synthetic

Unless otherwise noted, chemical reagents and solvents were purchased from EMD Millipore, Oakwood Chemical, Sigma-Aldrich, and Thermo Fisher Scientific. Unless otherwise specified, all non-aqueous reactions were carried out under an atmosphere of dry nitrogen in dried glassware. Commercially available starting materials and reagents were used as received or purified prior to use if necessary. Triethylamine was distilled from calcium hydride. Pleuromutilin was purchased as a commercial compound from TRC Canada. Analytical thin layer chromatography was performed using Supelco 0.25 mm silica gel 60 $F_{254}$ plates. Visualization was accomplished by irradiation with a 254 nm UV lamp or by staining with an aqueous solution of ceric ammonium molybdate, an acidified ethanolic solution of *p*-anisaldehyde, or a basified solution of potassium permanganate. Azides were visualized by developing plates in EtOAc/hexanes mixtures doped with 1% w/v $PPh_3$ and subsequently staining them with ninhydrin. Chromatography was performed using a forced flow of the indicated solvent system on SiliCycle SiliaFlash P60 silica gel (40-63 μm) or on prepacked RediSep Rf Gold high performance silica gel columns. Deionized water was obtained from the house deionized water system.

$^1$H NMR spectra were recorded on a Bruker Avance II 500 MHz spectrometer. Chemical shifts are reported in parts per million from tetramethylsilane (0 ppm) using the solvent resonance as an internal standard ($CDCl_3$ 7.26 ppm, $CD_3OD$ 3.31 ppm, DMSO-$d_6$ 2.50 ppm). Data are reported as follows: chemical shift, multiplicity (s=singlet, d=doublet, t=triplet, q=quartet, m=multiplet, br=broad), coupling constant, and number of proton. Proton decoupled $^{13}$C NMR were recorded on a Bruker Avance II 500 MHz (125 MHz) spectrometer. Chemical shifts are reported in ppm from tetramethylsilane (0 ppm) using the solvent resonance as an internal standard ($CDCl_3$ 77.2 ppm, $CD_3OD$ 49.0 ppm, DMSO-$d_6$ 39.5 ppm). High resolution mass spectra were obtained

on an Agilent Technologies 6220 TOF LC/MS or a Waters Synapt Q-TOF G2 in the Department of Chemistry and the VT-Mass Spectrometry Incubator at the Virginia Polytechnic Institute and State University. Specific rotations were obtained on a Jasco P-2000 polarimeter. All compounds used in biological testing were verified >95% pure via HPLC.

Compounds **16**[31] and **17**[23] were synthesized via known literature methods.

*Tosylation* **16** - The following reaction was carried out in an analogous manner to the published procedure.[31] To a stirring solution of pleuromutilin (1.14 g, 3.00 mmol) and TsCl (1.15 g, 6.02 mmol) in $CH_2Cl_2$ (8 mL) cooled in an ice bath was added triethylamine (1.00 mL, 7.19 mmol) and pyridine (0.080 mL, 1.0 mmol), generating a clear and colorless solution. After stirring for 20 h, a red precipitate was present in the clear, reddish solution. The mixture was diluted with $CH_2Cl_2$ (10 mL) and water (10 mL) causing the precipitate to dissolve. The pH was brought to ~2 with 1 N HCl. The layers were separated, and the organic layer was washed with water (10 mL), saturated $NaHCO_3$ solution (10 mL), water (10 mL), and brine (5 mL), dried over $Na_2SO_4$, and concentrated to afford a red oil, which solidified upon standing. The residue was purified using flash chromatography ($SiO_2$, 15% EtOAc/$CH_2Cl_2$) to give **16** (1.33 g, 83%) as a pink foam. Spectral data were in accord with those previously reported.[31]

*Alternative tosylation (**16**) and isolation of **29*** - To a stirring solution of pleuromutilin (3.78 g, 10.0 mmol) in $CH_2Cl_2$ (25 mL) cooled to 0 °C (ice bath) was added TsCl (2.88 g, 15.1 mmol), triethylamine (2.80 ml, 20.1 mmol), and 4-dimethylaminopyridine (0.303 g, 2.48 mmol). The mixture was allowed to slowly warm to room temperature and stirred for 28 h. The solution was partitioned with 1 M $KHSO_4$ (25 mL) and the organic layer was washed with saturated $NaHCO_3$ solution (25 mL). The organic layer was dried ($Na_2SO_4$) and concentrated to a translucent, red oil. This material was crystallized (EtOH/hexanes) to give **16** (2.08 39%) as an amorphous yellow

powder. Concentration of the mother liquor and flash chromatography ($SiO_2$, 40-60% EtOAc/Hexanes) gave additional **16** (650 mg, 12%) as an amorphous white powder and **29** (800 mg, 20 %) as an amorphous white powder. Spectral data were in accord with those previously reported.[31, 68]

*Azidation of C22* **17** - The following reaction was carried out in an analogous manner to the published procedure.[23] To a solution of **16** (548 mg, 1.03 mmol) in acetone (4 mL) was added a solution of $NaN_3$ (99.8 mg, 1.54 mmol) in DI $H_2O$ (1.5 mL). The mixture was heated to reflux, stirred for 4 h, cooled, and concentrated. CAUTION: Extractions containing halogenated solvents and azide anion should be completed expeditiously as extended exposure of basic azides to dichloromethane or chloroform can generate potentially explosive diazidomethane or azidoform. The residue was dissolved in $CHCl_3$ (10 mL), washed with water (10 mL), dried over $Na_2SO_4$, and concentrated to a white solid. This residue was purified via flash chromatography ($SiO_2$, 30% EtOAc/Hexanes) to give **17** (349 mg, 84%) as an amorphous white powder. Spectral data were in accord with those previously reported.[23]

*Anti-Markovnikov hydroazidation* **30** – CAUTION: Care should be taken when acidifying reaction mixtures containing inorganic or silyl azides. The reaction should be performed behind a blast shield, on a mmol scale, and quenched in basic solution. To a 2-dram vial containing a stir bar, 2-iodosobenzoic acid (527 mg, 2.00 mmol) and **2** (378 mg, 1.00 mmol) were added. The vessel was evacuated and backfilled with $N_2$ three times. Via syringe, $CH_2Cl_2$ (1.00 mL) and $TMSN_3$ (0.27 mL, 2.1 mmol) were added. The mixture was stirred for 50 h, with additions of water at 4 h (18 µL) and 30 h (18 µL). CAUTION: Extractions containing halogenated solvents and azide anion should be completed expeditiously as extended exposure of basic azides to dichloromethane or chloroform can generate potentially explosive diazidomethane or azidoform. The mixture was

quenched with saturated $NaHCO_3$ (15 mL) and extracted with $CH_2Cl_2$ (3x 5 mL). The combined organic layers were washed with saturated $NaHCO_3$ (5 mL), dried over $Na_2SO_4$, and concentrated to a yellow foam. The residue was purified via flash chromatography ($SiO_2$, 5% MeOH/$CHCl_3$) to give **30** (168 mg, 40% yield, comprised of 4:1 compounds **30**:**2** by NMR) as an amorphous, white powder. The material was carried on directly to the triazole syntheses with the limiting reagent computed based on NMR purity. A small amount of material was further purified for characterization purposes. $^1$H NMR ($CDCl_3$, 500 MHz): δ 5.66 (d, *J* = 8.3 Hz, 1H), 4.09 (dd, *J* = 5.1, 17.1 Hz, 1H), 4.02 (dd, *J* = 5.1, 17.1 Hz, 1H), 3.38 (t, *J* = 5.8 Hz, 1H), 3.29 (t, *J* = 7.6 Hz, 2H), 2.49 (t, *J* = 5.5 Hz, 1H), 2.40-2.31 (m, 1H), 2.28-2.18 (m, 2H), 2.07 (d, *J* = 2.4 Hz, 1H), 2.05-1.92 (m, 2H), 1.86 (dd, *J* = 8.3, 16.4 Hz, 1H), 1.82-1.74 (m, 2H), 1.71-1.63 (m, 1H), 1.65 (br s, 1H), 1.62-1.44 (m, 2H), 1.43-1.35 (m, 1H), 1.41 (s, 3H), 1.26 (d, *J* = 16.2 Hz, 1H), 1.13 (ddd, *J* = 4.5, 13.8, 14.1 Hz, 1H), 1.04 (s, 3H), 0.97 (d, *J* = 7.1 Hz, 3H), 0.69 (d, *J* = 7.0 Hz, 3H). $^{13}$C NMR ($CDCl_3$, 125 MHz): δ 216.5, 172.5, 75.9, 70.1, 61.3, 58.2, 48.1, 45.4, 43.3, 41.8, 40.3, 36.4, 34.7, 34.3, 30.1, 28.9, 26.8, 26.5, 24.9, 16.6, 14.7, 11.0. HR-MS (ESI): Calcd for $C_{22}H_{39}N_4O_5$ $[M+NH_4]^+$: 439.2915; Found: 439.2912. $[\alpha]_D^{24}$ = +20 (c = 0.89, $CHCl_3$).

*General Procedure for the Synthesis of Triazoles* (**18**-**28** and **31**-**41**) - To a 1-dram vial charged with a stirbar, **17** (0.050-0.075 mmol, 1.0 equiv.) or **30** (80% purity, 0.050-0.075 mmol, 1.0 equiv.) was added sodium ascorbate (0.3 equiv.), *t*-BuOH (0.30 mL), a $CuSO_4 \cdot 5H_2O_{(aq)}$ solution (0.30 mL, 11 mM), and alkyne (1.1 equiv.). The vessel was sealed with a cap and Teflon tape, placed behind a blast shield, and heated (70 °C, oil bath) for 20 h. The mixture was cooled, diluted with DI $H_2O$ (3 mL), and extracted with EtOAc (3x 3 mL). The combined organics were dried ($Na_2SO_4$) and concentrated to afford yellow-to-brown oils. The residues were purified using flash chromatography in EtOAc/hexanes or $CH_3OH/CHCl_3$ systems over $SiO_2$.

**(3a*R*,4*R*,5*S*,7*S*,8*S*,9*R*,9a*S*,12*R*)-8-Hydroxy-4,7,9,12-tetramethyl-3-oxo-7-vinyldecahydro-4,9a-propanocyclopenta[8]annulen-5-yl 2-(4-(hydroxymethyl)-1*H*-1,2,3-triazol-1-yl)acetate (18).** A white foam (30.3 mg, 85%): $^{1}$H NMR ($CDCl_3$, 500 MHz): δ 7.63 (s, 1H), 6.39 (dd, *J* = 11.1, 17.5 Hz, 1H), 5.80 (d, *J* = 8.5 Hz, 1H), 5.32 (d, *J* = 11.4 Hz, 1H), 5.20 (d, *J* = 17.5 Hz, 1H), 5.10 (d, *J* = 17.5 Hz, 1H), 5.02 (d, *J* = 17.5 Hz, 1H), 4.81 (s, 2H), 3.35 (d, *J* = 6.3 Hz, 1H), 2.31-2.13 (m, 3H), 2.24-2.00 (br s, 1H), 2.09 (dd, *J* = 8.6, 15.8 Hz, 1H), 2.07 (s, 1H), 2.05 (br s, 1H), 1.76 (dd, *J* = 3.0, 14.5 Hz, 1H), 1.71-1.59 (m, 2H), 1.55-1.41 (m, 2H), 1.40-1.35 (m, 1H), 1.34 (s, 3H), 1.31 (d, *J* = 15.8 Hz, 1H), 1.17 (s, 3H), 1.12 (dt, *J* = 4.4, 14.1 Hz, 1H), 0.86 (d, *J* = 7.0 Hz, 3H), 0.70 (d, *J* = 7.0 Hz, 3H). $^{13}$C NMR ($CDCl_3$, 125 MHz): δ 216.7, 165.2, 148.3, 138.7, 123.1, 117.8, 74.7, 71.2, 58.1, 56.7, 51.7, 45.5, 44.8, 44.1, 42.0, 36.7, 36.2, 34.5, 30.5, 26.9, 26.5, 24.9, 16.9, 14.8, 11.6. HR-MS (ESI): Calcd for $C_{25}H_{38}N_3O_5$ $[M+H]^+$: 460.2806; Found 460.2815. $[\alpha]_D^{23}$ = +25.4 (c = 1.42, $CHCl_3$).

**(3a*R*,4*R*,5*S*,7*S*,8*S*,9*R*,9a*S*,12*R*)-8-Hydroxy-4,7,9,12-tetramethyl-3-oxo-7-vinyldecahydro-4,9a-propanocyclopenta[8]annulen-5-yl 2-(4-(2-hydroxyethyl)-1*H*-1,2,3-triazol-1-yl)acetate (19).** An amorphous, white powder (42.6 mg, 96%): $^{1}$H NMR ($CDCl_3$, 500 MHz): δ 7.52 (s, 1H), 6.41 (dd, *J* = 10.9, 17.3 Hz, 1H), 5.81 (d, *J* = 8.5 Hz, 1H), 5.34 (d, *J* = 10.9 Hz, 1H), 5.21 (d, *J* = 17.3 Hz, 1H), 5.10 (d, *J* = 17.5 Hz, 1H), 5.02 (d, *J* = 17.6 Hz, 1H), 3.95 (t, *J* = 5.5 Hz, 2H), 3.36 (d, *J* = 6.4 Hz, 1H), 2.98 (t, *J* = 5.6 Hz, 2H), 2.32-2.15 (m, 3H), 2.13-2.06 (m, 2H), 1.77 (d, *J* = 14.5 Hz, 1H), 1.71-1.61 (m, 2H), 1.55-1.42 (m, 2H), 1.42-1.36 (m, 1H), 1.34 (s, 3H), 1.32 (d, *J* = 16.4 Hz, 1H), 1.18 (s, 3H) 1.12 (dt, *J* = 4.2, 14.4 Hz, 1H), 0.87 (d, *J* = 7.0 Hz, 3H), 0.70 (d, *J* = 7.0 Hz, 3H). $^{13}$C NMR ($CDCl_3$, 125 MHz): δ 216.9, 165.2, 146.0, 138.5, 123.0, 117.7, 74.5, 70.8, 61.6, 58.0, 51.5, 45.4, 44.6, 43.9, 41.8, 36.5, 36.0, 34.4, 30.30, 28.6, 26.7, 26.3, 24.8, 16.8, 14.6, 11.6.

HR-MS (ESI): Calcd for $C_{26}H_{40}N_3O_5$ $[M+H]^+$: 474.2973; Found, 474.2966. $[\alpha]_D^{23}$ = +30.6 (c = 2.09, $CHCl_3$).

**(3a*R*,4*R*,5*S*,7*S*,8*S*,9*R*,9a*S*,12*R*)-8-Hydroxy-4,7,9,12-tetramethyl-3-oxo-7-vinyldecahydro-4,9a-propanocyclopenta[8]annulen-5-yl 2-(4-(3-hydroxypropyl)-1*H*-1,2,3-triazol-1-yl)acetate (20).** A colorless glass (26.1 mg, 86%): $^1$H NMR ($CDCl_3$, 500 MHz): δ 7.39 (s, 1H), 6.40 (dd, *J* = 11.1, 17.4 Hz, 1H), 5.80 (d, *J* = 8.5 Hz, 1H), 5.32 (dd, *J* = 1.3, 11.1 Hz, 1H), 5.20 (dd, *J* = 1.3, 17.4 Hz, 1H), 5.06 (d, *J* = 17.6 Hz, 1H), 4.99 (d, *J* = 17.6 Hz, 1H), 3.70 (t, *J* = 5.8 Hz, 2H), 3.35 (dd, *J* = 6.6, 10.2 Hz, 1H), 2.85 (t, *J* = 7.4 Hz, 2H), 2.32-2.13 (m, 4H), 2.13-2.03 (m, 2H), 1.98-1.90 (m, 2H), 1.80-1.71 (m, 1H), 1.70-1.60 (m, 2H), 1.56-1.34 (m, 4H), 1.33-1.26 (m, 4H), 1.17 (s, 3H), 1.11 (dt, *J* = 4.5, 13.9 Hz, 1H), 0.86 (d, *J* = 7.0 Hz, 3H), 0.68 (d, 7.1 Hz, 3H). $^{13}$C NMR ($CDCl_3$, 125 MHz): δ 216.6, 165.2, 148.0, 138.6, 122.1, 117.5, 74.5, 70.8, 61.8, 58.0, 51.5, 45.4, 44.7, 44.0, 41.8, 36.5, 36.0, 34.4, 31.9, 30.3, 26.7, 26.3, 24.8, 22.0, 16.7, 14.6, 11.4. HR-MS (ESI): Calcd for $C_{27}H_{42}N_3O_5$ $[M+H]^+$: 488.3119; Found 488.3113. $[\alpha]_D^{23}$ = +25.6 (c = 1.30, $CHCl_3$).

**(3a*R*,4*R*,5*S*,7*S*,8*S*,9*R*,9a*S*,12*R*)-8-Hydroxy-4,7,9,12-tetramethyl-3-oxo-7-vinyldecahydro-4,9a-propanocyclopenta[8]annulen-5-yl 2-(4-(aminomethyl)-1*H*-1,2,3-triazol-1-yl)acetate (21).** An amorphous, yellow solid (22.3 mg, 63%): $^1$H NMR ($CD_3OD$, 500 MHz): δ 7.90 (s, 1H), 6.30 (dd, *J* = 11.3, 17.4 Hz, 1H), 5.79 (d, *J* = 8.4 Hz, 1H), 5.22-5.14 (m, 2H), 3.94 (s, 2H), 3.51 (d, *J* = 5.60 Hz, 1H), 2.39 (s, 1H), 2.28 (m, 2H), 2.16 (m, 2H), 1.82 (d, *J* = 14.0 Hz, 1H), 1.67 (m, 2H), 1.59-1.30 (m, 7H), 1.20-1.10 (m, 4H), 0.94 (d, *J* = 7.0 Hz, 3H), 0.75 (d, *J* = 7.0 Hz, 3H), expected α-methylene protons not observed due to deuterium exchange catalyzed by amine base. $^{13}$C NMR ($CD_3OD$, 125 MHz): δ 218.0, 165.6, 148.4, 139.6, 123.5, 115.3, 74.0, 71.0, 57.7, 50.9 (p, *J* = 21.4 Hz), 45.4, 44.3, 44.0, 41.8, 36.6, 36.4, 36.1, 33.8, 30.0, 26.9, 26.6, 24.4, 15.6, 13.7,

10.4. HR-MS (ESI): Calcd for $C_{25}H_{39}N_4O_4$ $[M+H]^+$: 459.2966; Found, 459.2972 $[\alpha]_D^{24}$ = +27.5 (c = 1.11, $CHCl_3$).

**(3a*R*,4*R*,5*S*,7*S*,8*S*,9*R*,9a*S*,12*R*)-8-Hydroxy-4,7,9,12-tetramethyl-3-oxo-7-vinyldecahydro-4,9a-propanocyclopenta[8]annulen-5-yl 2-(4-(2-aminoethyl)-1*H*-1,2,3-triazol-1-yl)acetate (22).** An amorphous, yellow powder (11.4 mg, 25%): $^1$H NMR ($CD_3OD$, 500 MHz): δ 7.81 (s, 1H), 6.28 (dd, *J* = 10.8, 17.4 Hz, 1H), 5.76 (d, *J* = 8.2 Hz, 1H), 5.20-5.12 (m, 2H), 3.48 (d, *J* = 6.0 Hz, 1H), 2.96 (t, *J* = 6.9 Hz, 2H), 2.88 (t, *J* = 6.9 Hz, 2H), 2.36 (s, 1H), 2.32-2.22 (m, 2H), 2.20-2.08 (m, 2H), 1.80 (d, *J* = 14.5 Hz, 1H), 1.73-1.56 (m, 2H), 1.56-1.38 (m, 3H), 1.36-1.27 (m, 1H), 1.30 (s, 3H), 1.16 (s, 3H), 1.14-1.09 (m, 1H), 0.92 (d, *J* = 7.0 Hz, 3H), 0.70 (d, *J* = 6.9 Hz, 3H), expected α-methylene protons not observed due to deuterium exchange catalyzed by amine base.[69] $^{13}$C NMR ($CD_3OD$, 125 MHz): δ 218.0, 165.6, 145.3, 139.6, 123.8, 115.3, 73.9, 71.0, 57.7, 50.7, (p, *J* = 23.0 Hz), 45.4, 44.3, 44.0, 41.8, 40.8, 36.6, 36.3, 33.8, 30.0, 27.9, 26.8, 26.6, 24.4, 15.6, 13.7, 10.4. HR-MS (ESI): Calcd for $C_{26}H_{41}N_4O_4$ $[M+H]^+$: 473.3122; Found 473.3119. $[\alpha]_D^{23}$ = +30 (c = 0.57, $CHCl_3$).

**(3a*R*,4*R*,5*S*,7*S*,8*S*,9*R*,9a*S*,12*R*)-8-Hydroxy-4,7,9,12-tetramethyl-3-oxo-7-vinyldecahydro-4,9a-propanocyclopenta[8]annulen-5-yl 2-(4-(1-hydroxyethyl)-1*H*-1,2,3-triazol-1-yl)acetate (23).** A white foam (41.6 mg, 91%): $^1$H NMR ($CDCl_3$, 500 MHz): δ 7.55 (s, 1H), 6.39 (dd, *J* = 11.0, 17.3 Hz, 1H), 5.79 (d, *J* = 8.4 Hz, 1H), 5.32 (dd, *J* = 1.3, 11.0 Hz, 1H), 5.20 (dd, *J* = 1.3, 17.3, 1H), 5.08 (m, 2H), 5.01 (dd, *J* = 5.0, 17.4 Hz, 1H), 3.34 (d, *J* = 6.5, 1H), 2.31-2.12 (m, 4H), 2.15 (br s, 1H), 2.13-2.02 (m, 2H), 1.75 (dd, *J* = 2.7, 14.9 Hz, 1H), 1.70-1.60 (m, 2H), 1.57 (d, *J* = 6.5 Hz, 3H), 1.53-1.40 (m, 2H), 1.39-1.33 (m, 1H), 1.33-1.25, (m, 4H), 1.16 (s, 3H), 1.11 (dt, *J* = 4.4, 13.9 Hz, 1H), 0.86 (d, *J* = 7.1 Hz, 3H), 0.68 (dd, *J* = 3.8, 7.3 Hz, 3H). $^{13}$C NMR ($CDCl_3$, 125 MHz): δ 216.7, 165.2, 153.0, 138.7, 121.5, 117.7, 74.6, 71.1, 63.2, 58.1, 51.7, 45.5, 44.8, 44.1,

42.0, 36.6, 36.2, 34.5, 30.4, 26.9, 26.5, 24.9, 23.3, 16.9, 14.7, 11.6. HR-MS (ESI): Calcd for $C_{26}H_{40}N_3O_5$ $[M+H]^+$: 474.2964; Found 474.2953. $[\alpha]_D^{23}$ = +27.6 (c = 2.06, $CHCl_3$).

**(3a*R*,4*R*,5*S*,7*S*,8*S*,9*R*,9a*S*,12*R*)-8-Hydroxy-4,7,9,12-tetramethyl-3-oxo-7-vinyldecahydro-4,9a-propanocyclopenta[8]annulen-5-yl 2-(4-(2-hydroxypropan-2-yl)-1*H*-1,2,3-triazol-1-yl)acetate (24).** A colorless glass (16.2 mg, 52%): $^1$H NMR ($CDCl_3$, 500 MHz): δ 7.52 (s, 1H), 6.41 (dd, *J* = 11.1, 17.4 Hz, 1H), 5.80 (d, *J* = 8.6 Hz, 1H), 5.34 (dd, *J* = 1.5, 11.1 Hz, 1H), 5.21 (dd, *J* = 1.5, 17.4 Hz, 1H), 5.08 (d, *J* = 17.4 Hz, 1H), 5.01 (d, *J* = 17.4 Hz, 1H), 3.34 (dd, *J* = 6.7, 10.7 Hz, 1H), 2.40 (s, 1H), 2.32-2.12 (m, 3H), 2.08 (dd, *J* = 8.7, 16.0 Hz, 1H), 2.07 (s, 1H), 1.76 (ddd, *J* = 3.1, 6.0, 14.4 Hz, 1H), 1.71-1.59 (m, 2H), 1.64 (s, 6H), 1.56-1.34 (m, 4H), 1.31 (s, 3H), 1.30 (d, 16.0 Hz, 1H), 1.17 (s, 3H), 1.12 (dt, 4.4, 13.6 Hz, 1H), 0.87 (d, 7.1 Hz, 3H), 0.68 (d, 7.1 Hz, 3H). $^{13}$C NMR ($CDCl_3$, 125 MHz): δ 216.5, 165.0, 156.1, 138.6, 120.4, 117.6, 74.5, 70.9, 68.6, 58.0, 51.5, 45.4, 44.7, 44.0, 41.8, 36.5, 36.0, 34.3, 30.5 (2C), 30.3, 26.7, 26.3, 24.8, 16.8, 14.6, 11.4. HR-MS (ESI): Calcd for $C_{27}H_{42}N_3O_5$ $[M+H]^+$: 488.3119; Found 488.3113. $[\alpha]_D^{23}$ = +24 (c = 0.81, $CHCl_3$).

**(3a*R*,4*R*,5*S*,7*S*,8*S*,9*R*,9a*S*,12*R*)-8-Hydroxy-4,7,9,12-tetramethyl-3-oxo-7-vinyldecahydro-4,9a-propanocyclopenta[8]annulen-5-yl 2-(4-(1-hydroxybutyl)-1*H*-1,2,3-triazol-1-yl)acetate (25).** A yellow glass (13.7 mg, 42%): $^1$H NMR ($CDCl_3$, 500 MHz): δ 7.56 (s, 1H), 6.40 (ddd, *J* = 0.9, 11.0, 17.3 Hz, 1H), 5.81 (d, *J* = 8.6 Hz, 1H), 5.34 (d, *J* = 11.0 Hz, 1H), 5.21 (dd, *J* = 1.3, 17.3 Hz, 1H), 5.09 (dd, *J* = 3.8, 17.5 Hz, 1H), 5.02 (dd, *J* = 3.5, 17.5 Hz, 1H), 4.94 (t, *J* = 5.8 Hz, 2H), 3.35 (d, *J* = 6.6 Hz, 1H), 2.31-2.14 (m, 3H), 2.08 (dd, *J* = 8.3, 16.1 Hz, 1H), 2.07 (s, 1H), 1.91-1.81 (m, 2H), 1.76 (dq, *J* = 2.7, 14.5 Hz, 1H), 1.71-1.60 (m, 2H), 1.55-1.35 (m, 6H), 1.33 (s, 3H), 1.30 (d, *J* = 16.1 Hz, 1H), 1.17 (s, 3H), 1.12 (dt, *J* = 4.6, 14.2 Hz, 1H), 0.96 (t, *J* = 7.4 Hz, 3H), 0.87 (d, *J* = 7.0 Hz, 3H), 0.69 (dd, *J* = 1.9, 7.1 Hz, 3H). $^{13}$C NMR ($CDCl_3$, 125 MHz): δ 216.8,

165.2, 152.7, 138.7, 121.9, 117.8, 74.7, 71.0, 67.0, 58.0, 51.7, 45.5, 44.8, 44.1, 42.0, 39.6, 36.7. 36.2, 34.5, 30.4, 26.9, 26.4, 24.9, 18.7, 16.9, 14.8, 14.0, 11.6. HR-MS (ESI): Calcd for $C_{28}H_{44}N_3O_5$ $[M+H]^+$: 502.3275; Found 502.3270. $[\alpha]_D^{25}$ = +25 (c = 0.68, $CHCl_3$).

**(3a*R*,4*R*,5*S*,7*S*,8*S*,9*R*,9a*S*,12*R*)-8-Hydroxy-4,7,9,12-tetramethyl-3-oxo-7-vinyldecahydro-4,9a-propanocyclopenta[8]annulen-5-yl 2-(4-(1-hydroxyhexyl)-1*H*-1,2,3-triazol-1-yl)acetate (26).** A yellow glass (15.9 mg, 52%): $^1$H NMR ($CDCl_3$, 500 MHz): δ 7.56 (s, 1H), 6.41 (ddd, *J* = 1.0, 11.0, 17.4 Hz, 1H), 5.81 (d, *J* = 8.6 Hz, 1H), 5.34 (d, *J* = 11.0 Hz, 1H), 5.21 (dd, *J* = 1.3, 17.4 Hz, 1H), 5.09 (dd, *J* = 3.2, 17.4 Hz, 1H), 5.02 (dd, *J* = 3.0, 17.5 Hz, 1H), 4.95-4.89 (m, 1H), 3.35 (d, *J* = 6.5 Hz, 1H), 2.31-2.14 (m, 3H), 2.08 (dd, *J* = 8.6, 16.1 Hz, 1H), 2.07 (s, 1H), 1.94-1.81 (m, 2H), 1.76 (dq, *J* = 2.8, 14.4 Hz, 1H), 1.71-1.59 (m, 2H), 1.55-1.42 (m, 3H), 1.41-1.35 (m, 2H), 1.34-1.28 (m, 8H), 1.17 (s, 3H), 1.12 (dt, *J* = 4.5, 14.2 Hz, 1H), 0.91-0.85 (m, 6H), 0.71-0.67 (dd, *J* = 1.9, 7.4 Hz, 3H). $^{13}$C NMR ($CDCl_3$, 125 MHz): δ 216.8, 165.2, 152.3, 138.7, 121.9, 117.8, 74.6, 71.0, 67.3, 58.1, 51.7, 45.5, 44.8, 44.1, 42.0, 37.5, 36.7, 36.2, 34.5, 31.7, 30.4, 26.9, 26.4, 25.2, 24.9, 22.7, 17.0, 14.8, 14.2, 11.62. HR-MS (ESI): Calcd for $C_{30}H_{48}N_3O_5$ $[M+H]^+$: 530.3588; Found 530.3578. $[\alpha]_D^{23}$ = +21 (c = 0.80, $CHCl_3$).

**(3a*R*,4*R*,5*S*,7*S*,8*S*,9*R*,9a*S*,12*R*)-8-Hydroxy-4,7,9,12-tetramethyl-3-oxo-7-vinyldecahydro-4,9a-propanocyclopenta[8]annulen-5-yl 2-(4-hexyl-1*H*-1,2,3-triazol-1-yl)acetate (27).** A colorless glass (22.3 mg, 73%): $^1$H NMR ($CDCl_3$, 500 MHz): δ 7.34 (s, 1H), 6.40 (dd, *J* = 11.0, 17.3 Hz, 1H), 5.80 (d, *J* = 8.50 Hz, 1H), 5.33 (dd, *J* = 1.1, 11.0 Hz, 1H), 5.20 (dd, *J* = 1.3, 17.3 Hz, 1H), 5.06 (d, *J* = 17.6 Hz, 1H), 5.00 (d, *J* = 17.6 Hz, 1H), 3.34 (d, *J* = 6.5 Hz, 1H), 2.72 (t, *J* = 7.7 Hz, 2H), 2.31-2.13 (m, 3H), 2.08 (dd, *J* = 9.0, 15.5 Hz, 1H), 2.07 (s, 1H), 1.75 (dq, *J* = 2.9, 14.4 Hz, 1H), 1.70-1.60 (m, 4H), 1.50 (dq, *J* = 3.5, 14.0 Hz, 1H), 1.44 (ddd, *J* = 2.7, 9.4, 12.9 Hz, 1H), 1.40-1.34 (m, 3H), 1.33-1.27 (m, 8H), 1.16 (s, 3H), 1.12 (dt, *J* = 4.7, 14.3 Hz, 1H), 0.90-0.84

(m, 6H), 0.68 (d, *J* = 7.0 Hz, 3H). $^{13}$C NMR ($CDCl_3$, 125 MHz): δ 216.8, 165.4, 149.1, 138.7, 122.0, 117.7, 74.6, 70.9, 58.1, 51.6, 45.5, 44.8, 44.1, 41.9, 36.7, 36.1, 34.5, 31.7, 30.4, 29.5, 29.0, 26.9, 26.4, 25.8, 24.9, 22.7, 16.9, 14.7, 14.2, 11.6. HR-MS (ESI): Calcd for $C_{30}H_{48}N_3O_4$ $[M+H]^+$: 514.3639; Found, 514.3631. $[\alpha]_D^{24}$ = +27.5 (c = 1.11, $CHCl_3$).

**(3a*R*,4*R*,5*S*,7*S*,8*S*,9*R*,9a*S*,12*R*)-8-Hydroxy-4,7,9,12-tetramethyl-3-oxo-7-vinyldecahydro-4,9a-propanocyclopenta[8]annulen-5-yl 2-(4-((benzyloxy)methyl)-1*H*-1,2,3-triazol-1-yl)acetate (28).** A colorless glass (41.8 mg, 99%): $^1$H NMR ($CDCl_3$, 500 MHz): δ 7.64 (s, 1H), 7.36-7.32 (m, 4H), 7.31-7.27 (m, 1H), 6.40 (dd, *J* = 11.0, 17.3 Hz, 1H), 5.80 (d, *J* = 8.6 Hz, 1H), 5.32 (dd, *J* = 1.2, 11.0 Hz, 1H), 5.20 (dd, *J* = 1.3, 17.4 Hz, 1H), 5.10 (d, *J* = 17.6 Hz, 1H), 5.02 (d, *J* = 17.6 Hz, 1H), 4.70 (s, 2H), 4.59 (s, 2H), 3.34 (d, *J* = 6.5 Hz, 1H), 2.30-2.13 (m, 3H), 2.08 (dd, *J* = 8.4, 24.7 Hz, 1H), 2.07 (s, 1H), 1.75 (dq, *J* = 2.9, 14.5 Hz, 1H), 1.70-1.58 (m, 2H), 1.49 (dq, *J* = 3.8, 14.0 Hz, 1H), 1.44 (ddd, *J* = 2.8, 9.4, 12.9 Hz, 1H), 1.37 (dq, *J* = 3.9, 14.2 Hz, 1H), 1.34 (s, 3H), 1.30 (d, *J* = 16.2 Hz, 1H), 1.16 (s, 3H), 1.11 (dt, *J* = 4.7, 14.2 Hz, 1H), 0.86 (d, *J* = 7.1 Hz, 3H,), 0.70 (d, *J* = 6.9 Hz, 3H). $^{13}$C NMR ($CDCl_3$, 125 MHz): δ 216.7, 165.2, 145.9, 138.6, 137.8, 128.6 (2C), 128.0 (2C), 127.9, 123.9, 117.7, 74.6, 72.6, 71.0, 63.6, 58.1, 51.6, 45.5, 44.8, 44.1, 41.9, 36.6, 36.1, 34.5, 30.4, 26.9, 26.4, 24.9, 16.9, 14.7, 11.6. HR-MS (ESI): Calcd for $C_{32}H_{44}N_3O_5$ $[M+H]^+$: 550.3275; Found, 550.3271. $[\alpha]_D^{23}$ = +23.2 (c = 2.09, $CHCl_3$).

**(3a*R*,4*R*,5*S*,7*R*,8*S*,9*R*,9a*S*,12*R*)-8-Hydroxy-7-(2-(4-(hydroxymethyl)-1*H*-1,2,3-triazol-1-yl)ethyl)-4,7,9,12-tetramethyl-3-oxodecahydro-4,9a-propanocyclopenta[8]annulen-5-yl 2-hydroxyacetate (31).** An amorphous, off-white powder (32.7mg, 73%): $^1$H NMR ($CD_3OD$, 500 MHz): δ 8.16 (s, 1H), 5.71 (d, *J* = 8.4 Hz, 1H), 4.69 (s, 2H), 4.47 (ddd, *J* = 6.2, 11.6, 13.1 Hz, 1H), 4.26 (ddd, *J* = 6.2, 11.6, 13.1 Hz, 1H), 4.14 (d, *J* = 17.1 Hz, 1H), 4.04 (d, *J* = 17.1 Hz, 1H), 3.48 (d, *J* = 6.1 Hz, 1H), 2.38 (s, 1H), 2.35-2.21 (m, 4H), 2.21-2.10 (m, 1H), 2.01 (dd, *J* = 8.3, 16.3 Hz,

1H), 1.80 (dd, *J* = 2.9, 14.6 Hz, 1H), 1.72-1.61 (m, 2H), 1.59-1.48 (m, 1H), 1.48-1.44 (m, 1H), 1.46 (s, 3H), 1.41 (d, *J* = 16.4 Hz, 1H), 1.46-1.35 (m, 1H), 1.15 (dt, *J* = 4.4, 14.4 Hz, 1H), 1.14 (s, 3H), 0.91 (d, *J* = 7.1 Hz, 3H), 0.74 (d, *J* = 7.0 Hz, 3H). $^{13}$C NMR ($CD_3OD$, 125 MHz): δ 218.0, 178.6, 147.4, 123.0, 74.6, 69.3, 60.5, 57.7, 55.1, 46.8, 45.4, 41.6, 41.5, 40.2, 36.6, 34.8, 33.9, 30.6, 30.0, 26.8, 25.8, 24.2, 15.9, 13.9, 10.3. HR-MS (ESI): Calcd for $C_{25}H_{40}N_3O_6$ $[M+H]^+$: 478.2912; Found: 478.2900. $[\alpha]_D^{23}$ = +51.7 (c = 1.64, $CHCl_3$).

**(3a*R*,4*R*,5*S*,7*R*,8*S*,9*R*,9a*S*,12*R*)-8-Hydroxy-7-(2-(4-(2-hydroxyethyl)-1*H*-1,2,3-triazol-1-yl)ethyl)-4,7,9,12-tetramethyl-3-oxodecahydro-4,9a-propanocyclopenta[8]annulen-5-yl 2-hydroxyacetate (32).** An amorphous, white powder (23.3 mg, 66%): $^1$H NMR ($CDCl_3$, 500 MHz): δ 7.72 (s, 1H), 5.62 (d, *J* = 8.3 Hz, 1H), 4.31 (dt, *J* = 5.8, 12.6 Hz, 1H), 4.22 (d, *J* = 17.3 Hz, 1H), 4.05 (d, *J* = 17.3 Hz, 1H), 4.04 (dt, *J* = 4.6, 12.5 Hz, 1H), 3.97-3.86 (m, 2H), 3.43 (d, *J* = 5.8 Hz, 1H), 2.95-2.86 (m, 2H), 2.32-2.12 (m, 5H), 2.09 (s, 1H), 1.90 (dd, *J* = 8.4, 16.3 Hz, 1H), 1.74 (d, *J* = 14.3 Hz, 1H), 1.69-1.62 (m, 1H), 1.61-1.52 (m, 1H), 1.50-1.43 (m, 2H), 1.42 (s, 3H), 1.39-1.32 (m, 2H), 1.15-1.06 (m, 1H), 1.12 (s, 3H), 0.91 (d, *J* = 6.9 Hz, 3H), 0.68 (d, *J* = 7.0 Hz, 3H). $^{13}$C NMR ($CDCl_3$, 125 MHz): δ 217.0, 173.3, 145.2, 122.7, 75.9, 69.7, 61.3, 61.2, 58.3, 46.7, 45.6, 41.9 (2C), 40.5, 36.6, 34.7, 34.5, 30.2, 29.9, 28.8, 27.0, 26.9, 25.0, 16.9, 14.9, 11.4. HR-MS (ESI): Calcd for $C_{26}H_{42}N_3O_6$ $[M+H]^+$: 492.3079; Found, 492.3076. $[\alpha]_D^{23}$ = +51.7 (c = 1.40, $CHCl_3$).

**(3a*R*,4*R*,5*S*,7*R*,8*S*,9*R*,9a*S*,12*R*)-8-Hydroxy-7-(2-(4-(3-hydroxypropyl)-1*H*-1,2,3-triazol-1-yl)ethyl)-4,7,9,12-tetramethyl-3-oxodecahydro-4,9a-propanocyclopenta[8]annulen-5-yl 2-hydroxyacetate (33).** An amorphous, white powder (14.3 mg, 64%): $^1$H NMR ($CD_3OD$, 500 MHz): δ 7.96 (s, 1H), 5.72 (d, *J* = 8.4 Hz, 1H), 4.44 (ddd, *J* = 7.4, 10.2, 13.2 Hz, 1H), 4.23 (ddd, *J* = 7.1, 10.1, 13.2 Hz, 1H), 4.14 (d, *J* = 17.1 Hz, 1H), 4.03 (d, *J* = 17.1 Hz, 1H), 3.62 (t, *J* = 6.4 Hz, 2H), 3.47 (d, *J* = 6.0 Hz, 1H), 2.79 (t, *J* = 7.5 Hz, 2H), 2.37 (s, 1H), 2.32-2.20 (m, 4H), 2.15

(m, 1H), 2.01 (dd, *J* = 8.5, 16.4 Hz, 1H), 1.95-1.88 (m, 2H), 1.81 (dd, *J* = 2.8, 14.4 Hz, 1H), 1.73-1.61 (m, 2H), 1.55 (ddd, *J* = 3.7, 13.6, 27.5 Hz, 1H), 1.48-1.44 (m, 1H), 1.46 (s, 3H), 1.44-1.35 (m, 1H), 1.40 (d, *J* = 16.5 Hz, 1H), 1.16 (dt, *J* = 4.5, 14.1 Hz, 1H), 1.13 (s, 3H), 0.92 (d, *J* = 7.0 Hz, 3H), 0.74 (d, *J* = 7.0 Hz, 3H). $^{13}$C NMR ($CD_3OD$, 125 MHz): δ 218.0, 172.6, 147.2, 122.1, 74.6, 69.2, 60.7, 60.5, 57.7, 46.7, 45.4, 41.6, 41.5, 40.2, 36.6, 34.9, 33.8, 31.9, 30.5, 30.0, 26.8, 25.8, 24.2, 21.4, 15.9, 13.9, 10.3. HR-MS (ESI): Calcd for $C_{27}H_{44}N_3O_6$ $[M+H]^+$: 506.3225; Found 506.3218. $[\alpha]_D^{24}$ = +48 (c = 0.72, $CHCl_3$).

**(3a*R*,4*R*,5*S*,7*R*,8*S*,9*R*,9a*S*,12*R*)-7-(2-(4-(Aminomethyl)-1*H*-1,2,3-triazol-1-yl)ethyl)-8-hydroxy-4,7,9,12-tetramethyl-3-oxodecahydro-4,9a-propanocyclopenta[8]annulen-5-yl 2-hydroxyacetate (34).** An amorphous, yellow solid (5.4 mg, 26%): $^1$H NMR ($CD_3OD$, 500 MHz): δ 8.12 (s, 1H), 5.72 (d, *J* = 8.6 Hz, 1H), 4.52-4.43 (m, 1H), 4.28-4.22 (m, 1H), 4.14 (d, *J* = 17.1 Hz, 1H), 4.04 (d, *J* = 17.1 Hz, 1H), 3.91 (s, 2H), 3.47 (d, *J* = 6.0 Hz, 1H), 2.38 (s, 1H), 2.34-2.10 (m, 5H), 2.01 (dd, *J* = 8.3, 16.3 Hz, 1H), 1.80 (dd, *J* = 2.9, 14.4 Hz, 1H), 1.67 (m, 2H), 1.60-1.30 (m, 7H), 1.20-1.09 (m, 4H), 0.91 (d, *J* = 7.4 Hz, 3H), 0.74 (d, *J* = 7.2 Hz, 3H). $^{13}$C NMR ($CD_3OD$, 125 MHz): δ 219.4, 174.1, 149.4, 123.7, 76.0, 70.7, 61.9, 59.1, 48.2, 46.8, 43.0, 42.8, 41.6, 38.0, 37.6, 36.3, 35.2, 31.9, 31.4, 28.2, 27.2, 25.6, 17.3, 15.2, 11.7. HR-MS (ESI): Calcd for $C_{25}H_{41}N_4O_5$ $[M+H]^+$: 477.3077; Found, 477.3082. $[\alpha]_D^{23}$ = +39 (c = 1.00, $(CH_3)_2SO$).

**(3a*R*,4*R*,5*S*,7*R*,8*S*,9*R*,9a*S*,12*R*)-7-(2-(4-(2-Aminoethyl)-1*H*-1,2,3-triazol-1-yl)ethyl)-8-hydroxy-4,7,9,12-tetramethyl-3-oxodecahydro-4,9a-propanocyclopenta[8]annulen-5-yl 2-hydroxyacetate (35).** An amorphous, yellow solid (7.1 mg, 34%): $^1$H NMR ($CD_3OD$, 500 MHz): δ 8.00 (s, 1H), 5.72 (d, *J* = 8.4 Hz, 1H), 4.49-4.41 (m, 1H), 4.28-4.20 (m, 1H), 4.14 (d, *J* = 17.5 Hz, 1H), 4.03 (d, *J* = 17.5 Hz, 1H), 3.47 (d, *J* = 5.9 Hz, 1H), 2.98 (t, *J* = 7.0 Hz, 2H), 2.88 (t, *J* = 6.9 Hz, 2H), 2.38 (s, 1H), 2.36-2.29 (m, 1H), 2.29-2.20 (m, 3H), 2.19-2.10 (m, 1H), 2.01 (dd, *J* =

8.2, 16.3 Hz, 1H), 1.80 (dd, *J* = 3.1, 14.4 Hz, 1H), 1.73-1.60 (m, 2H), 1.54 (dq, *J* = 3.1, 13.3 Hz, 1H), 1.48-1.43 (m, 1H), 1.46 (s, 3H), 1.43-1.35 (m, 2H), 1.19-1.10 (m, 1H), 1.14 (s, 3H), 0.92 (d, *J* = 7.1 Hz, 3H), 0.74 (d, *J* = 7.1 Hz, 3H). $^{13}$C NMR ($CD_3OD$, 125 MHz): δ 218.0, 172.6, 144.9, 122.6, 74.6, 69.2, 60.5, 57.7, 46.7, 45.4, 41.6, 41.5, 40.7, 40.2, 36.6, 34.9, 33.8, 30.5, 30.0, 27.9, 26.8, 25.8, 24.3, 15.9, 13.8, 10.3. HR-MS (ESI): Calcd for $C_{26}H_{43}N_4O_5$ $[M+H]^+$: 491.3228; Found 491.3223. $[\alpha]_D^{25}$ = +47 (c = 0.36, $CHCl_3$).

**(3a*R*,4*R*,5*S*,7*R*,8*S*,9*R*,9a*S*,12*R*)-8-Hydroxy-7-(2-(4-(1-hydroxyethyl)-1*H*-1,2,3-triazol-1-yl)ethyl)-4,7,9,12-tetramethyl-3-oxodecahydro-4,9a-propanocyclopenta[8]annulen-5-yl 2-hydroxyacetate (36).** An amorphous, pink solid (23.6 mg, 81%): $^1$H NMR ($CDCl_3$, 500 MHz): δ 7.77 (s, 2H), 5.64 (t, *J* = 7.6 Hz, 2H), 5.11-5.05 (m, 1H), 5.04-4.96 (m, 1H), 4.40-4.28 (m, 2H), 4.30-4.22 (m, 2H), 4.08 (d, *J* = 17.4 Hz, 2H), 4.05-3.99 (m, 1H), 3.99-3.91 (m, 1H), 3.43 (dd, *J* = 1.6, 5.7 Hz, 2H), 3.40 (br s, 4H), 2.34-2.04 (m, 12H), 1.90 (m, 2H), 1.76 (d, *J* = 14.40 Hz, 2H), 1.67 (br s, 2H), 1.62-1.38 (m, 16H), 1.44 (s, 6H), 1.35 (dd, *J* = 5.7, 16.3 Hz, 2H), 1.17-1.08 (m, 2H), 1.13 (s, 6H), 0.94-0.88 (m, 6H), 0.70 (dd, *J* = 1.8, 7.0 Hz, 6H). $^{13}$C NMR ($CDCl_3$, 125 MHz): δ 216.6 (2C), 173.26, 173.23 152.4, 151.8, 120.9, 120.7, 75.9 (2C), 69.8, 69.5, 62.8 (2C), 61.29, 61.25, 58.2 (2C), 46.65, 46.57, 45.4 (2C), 41.81 (2C), 41.76 (2C), 40.43, 40.40, 36.5 (2C), 34.6, 34.5, 34.4 (2C), 30.1 (2C), 29.9, 29.8, 26.9 (2C), 24.9 (2C), 23.1 (2C), 22.6 (2C), 16.8 (2C), 14.8 (2C), 11.11, 11.09. HR-MS (ESI): Calcd for $C_{26}H_{42}N_3O_6$ $[M+H]^+$: 491.2990; Found: 492.3062. $[\alpha]_D^{24}$ = +54.9 (c = 1.18, $CHCl_3$).

**(3a*R*,4*R*,5*S*,7*R*,8*S*,9*R*,9a*S*,12*R*)-8-Hydroxy-7-(2-(4-(2-hydroxypropan-2-yl)-1*H*-1,2,3-triazol-1-yl)ethyl)-4,7,9,12-tetramethyl-3-oxodecahydro-4,9a-propanocyclopenta[8]annulen-5-yl 2-hydroxyacetate (37).** An amorphous, white powder (9.6 mg, 42%): $^1$H NMR ($(CD_3)_2SO$, 500 MHz): δ 7.87 (s, 1H), 5.56 (d, *J* = 8.3 Hz, 1H), 5.33 (t, *J* = 6.5 Hz, 1H), 5.09 (s, 1H), 4.74 (d, *J* =

5.9 Hz, 1H), 4.30 (dt, *J* = 5.3, 12.8 Hz, 1H), 4.11 (dt, *J* = 4.8, 12.1 Hz, 1H), 4.01 (dd, *J* = 6.9, 17.0 Hz, 1H), 3.89 (dd, *J* = 6.8, 17.0 Hz, 1H), 3.42-3.38 (m, 1H), 2.24-2.03 (m, 4H), 2.02-1.92 (m, 2H), 1.71-1.58 (m, 2H), 1.55-1.20 (m, 6H), 1.47 (s, 3H), 1.45 (s, 3H), 1.37 (s, 3H), 1.07-0.97 (s, 4H), 0.82 (d, *J* = 7.1 Hz, 3H), 0.64 (d, *J* = 6.9 Hz, 3H). $^{13}$C NMR ($(CD_3)_2SO$, 125 MHz): δ 217.1, 172.3, 155.6, 120.3, 73.4, 68.1, 67.1, 60.4, 57.1, 46.3, 45.0, 41.7, 41.3, 40.4, 36.3, 34.7, 34.0, 31.0, 30.9, 30.7, 30.1, 26.8, 26.7, 24.3, 16.5, 14.6, 11.6. HR-MS (ESI): Calcd for $C_{27}H_{44}N_3O_6$ $[M+H]^+$: 506.3230; Found, 506.3220. $[\alpha]_D^{23}$ = +43 (c = 1.00, $(CH_3)_2SO$).

**(3a*R*,4*R*,5*S*,7*R*,8*S*,9*R*,9a*S*,12*R*)-7-(2-(4-((Benzyloxy)methyl)-1*H*-1,2,3-triazol-1-yl)ethyl)-8-hydroxy-4,7,9,12-tetramethyl-3-oxodecahydro-4,9a-propanocyclopenta[8]annulen-5-yl 2-hydroxyacetate (38).** An amorphous, white solid (16.1 mg, 73%): $^1$H NMR ($CDCl_3$, 500 MHz): δ 7.90 (s, 1H), 7.40-7.33 (m, 4H), 7.29 (tt, *J* = 1.6, 6.2 Hz, 1H), 5.65 (d, *J* = 8.4 Hz, 1H), 4.68 (d, *J* = 1.6 Hz, 2H), 4.62 (s, 2H), 4.44 (ddd, *J* = 6.2, 11.4, 13.0 Hz, 1H), 4.16 (d, *J* = 17.3 Hz, 1H), 4.16-4.10 (m, 1H), 4.05 (d, *J* = 17.3 Hz, 1H), 3.44 (d, *J* = 6.0 Hz, 1H), 2.70-2.15 (br s, 1H), 2.34-2.15 (m, 6H), 2.09 (s, 1H), 1.91 (dd, *J* = 8.5, 16.4 Hz, 1H), 1.76 (dd, *J* = 2.9, 14.6 Hz, 1H), 1.72-1.64 (m, 1H), 1.60-1.45 (m, 4H), 1.44 (s, 3H), 1.42-1.38 (m, 1H), 1.35 (d, *J* = 16.4 Hz, 1H), 1.17-1.09 (m, 4H), 1.13 (s, 3H), 0.93 (d, *J* = 7.1 Hz, 3H), 0.70 (d, *J* = 7.2 Hz, 3H). $^{13}$C NMR ($CDCl_3$, 125 MHz): δ 216.5, 173.0, 145.2, 138.0, 128.6 (2C), 128.1 (2C), 127.9, 123.0, 76.0, 72.8, 70.3, 63.9, 61.5, 58.3, 46.9, 45.6, 42.2, 41.0, 40.6, 36.6, 34.8, 34.5, 30.22, 30.18, 27.0, 26.9, 25.0, 16.9, 14.9, 11.2. HR-MS (ESI): Calcd for $C_{32}H_{46}N_3O_6$ $[M+H]^+$: 568.3381; Found: 568.3373. $[\alpha]_D^{24}$ = +41 (c = 0.80, $CHCl_3$).

**(3a*R*,4*R*,5*S*,7*R*,8*S*,9*R*,9a*S*,12*R*)-8-Hydroxy-7-(2-(4-(1-hydroxybutyl)-1*H*-1,2,3-triazol-1-yl)ethyl)-4,7,9,12-tetramethyl-3-oxodecahydro-4,9a-propanocyclopenta[8]annulen-5-yl 2-hydroxyacetate (39).** An amorphous, orange solid (18.8 mg, 83%): $^1$H NMR ($CD_3OD$, 500 MHz):

δ 8.13 (s, 1H), 8.10 (s, 1H), 5.73 (d, *J* = 8.4 Hz, 2H), 4.83 (m, 2H), 4.48 (m, 1H), 4.28 (m, 1H), 4.15 (dd, *J* = 1.0, 17.0 Hz, 2H), 4.06 (dd, *J* = 1.6, 17.1 Hz, 2H), 3.50 (d, *J* = 5.9 Hz, 2H), 2.39 (s, 2H), 2.37-2.13 (m, 10H), 2.03 (dd, *J* = 8.6, 16.4 Hz, 2H), 1.92-1.78 (m, 6H), 1.75-1.67 (m, 4H), 1.62-1.33 (m, 14H), 1.48 (s, 6H), 1.22-1.13 (m, 2H), 1.15 (s, 6H), 0.99 (dt, *J* = 2.9, 7.3 Hz, 6H), 0.93 (dd, *J* = 5.7, 7.0 Hz, 6H), 0.76 (d, *J* = 7.0 Hz, 6H). $^{13}$C NMR ($CD_3OD$, 125 MHz): δ 218.0 (2C), 172.63, 172.60, 151.5, 151.4, 121.80, 121.76, 74.63, 74.61, 69.28, 69.25, 66.1, 66.0, 60.5 (2C), 57.7 (2C), 46.8 (2C), 45.4 (2C), 41.6 (2C), 41.5, 41.4, 40.2 (2C), 39.2, 39.1, 36.6 (2C), 34.9, 34.8, 33.9 (2C), 30.51, 30.47, 30.0 (2C), 26.8 (2C), 25.8 (2C), 24.2 (2C), 18.43, 18.40, 15.9 (2C), 13.9 (2C), 12.8 (2C), 10.34, 10.31. HR-MS (ESI): Calcd for $C_{28}H_{46}N_3O_6$ $[M+H]^+$: 520.3381; Found 520.3371. $[\alpha]_D^{25}$ = +24 (c = 0.94, $CHCl_3$).

**(3a*R*,4*R*,5*S*,7*R*,8*S*,9*R*,9a*S*,12*R*)-8-Hydroxy-7-(2-(4-(1-hydroxyhexyl)-1*H*-1,2,3-triazol-1-yl)ethyl)-4,7,9,12-tetramethyl-3-oxodecahydro-4,9a-propanocyclopenta[8]annulen-5-yl 2-hydroxyacetate (40).** An amorphous, pink solid (16.0 mg, 68%): $^1$H NMR ($CDCl_3$, 500 MHz): δ 7.743 (s, 1H), 7.738 (s, 1H), 5.65 (d, *J* = 8.4 Hz, 1H), 5.63 (d, *J* = 8.4 Hz, 1H), 4.88 (dd, *J* = 5.7, 7.8 Hz, 1H), 4.78 (t, *J* = 6.9 Hz, 1H), 4.35 (dt, *J* = 5.3, 12.7 Hz, 1H), 4.29 (dt, *J* = 4.8, 12.2 Hz, 1H), 4.26 (d, *J* = 17.5 Hz, 1H), 4.24 (d, *J* = 17.4 Hz, 1H), 4.07 (d, *J* = 17.2 Hz, 1H), 4.06 (d, *J* = 17.4 Hz, 1H), 4.03 (dt, *J* = 4.7, 12.7 Hz, 1H), 3.94 (dt, *J* = 4.4, 12.7 Hz, 1H), 3.43 (d, *J* = 4.3 Hz, 2H), 2.34-2.03 (m, 10H), 2.08 (s, 2H), 1.94-1.81 (m, 6H), 1.77 (s, 1H), 1.74 (s, 1H), 1.67 (m, 2H), 1.60-1.45 (m, 8H), 1.44 (s, 3H), 1.43 (s, 3H), 1.41-1.28 (m, 14H), 1.15 (d, *J* = 4.4 Hz, 1H), 1.26 (s, 6H), 1.10 (d, *J* = 4.4 Hz, 1H), 0.92 (d, *J* = 6.9 Hz, 3H), 0.91 (d, *J* = 7.0 Hz, 3H), 0.87 (m, 6H), 0.70 (d, *J* = 7.1 Hz, 6H). $^{13}$C NMR ($CDCl_3$, 125 MHz): δ 216.70, 216.69, 173.4, 173.3, 152.0, 151.2, 121.2, 121.1, 76.04, 76.02, 69.9, 69.7, 67.0 (2C), 61.41, 61.37, 58.3 (2C), 46.8, 46.7, 45.6 (2C), 42.0 (2C), 41.9 (2C), 40.6, 40.5, 37.3 (2C), 36.9 (2C), 36.6 (2C), 34.70, 34.66, 34.5 (2C),

31.8, 31.7, 30.2 (2C), 30.0, 29.9, 27.03, 26.99, 25.5, 25.4, 25.0 (2C), 22.7 (2C), 16.9 (2C), 14.9 (2C), 14.2 (2C), 11.23, 11.20. HR-MS (ESI): Calcd for $C_{30}H_{50}N_3O_6$ $[M+H]^+$: 548.3694; Found 548.3692 $[\alpha]_D^{24}$ = +59 (c = 0.80, $CHCl_3$).

**(3a*R*,4*R*,5*S*,7*R*,8*S*,9*R*,9a*S*,12*R*)-7-(2-(4-Hexyl-1*H*-1,2,3-triazol-1-yl)ethyl)-8-hydroxy-4,7,9,12-tetramethyl-3-oxodecahydro-4,9a-propanocyclopenta[8]annulen-5-yl 2-hydroxyacetate (41).** A white foam (13.0 mg, 58%): $^1$H NMR ($CDCl_3$, 500 MHz): δ 7.55 (s, 1H), 5.68 (d, *J* = 8.3 Hz, 1H), 4.40-4.32 (m, 1H), 4.21 (d, *J* = 17.20 Hz, 1H), 4.10-4.03 (m, 1H), 4.06 (d, *J* = 17.20 Hz, 1H), 3.44 (d, *J* = 6.0 Hz, 1H), 3.40 (br s, 1H), 2.72-2.65 (m, 2H), 2.36-2.30 (m, 1H), 2.28-2.14 (m, 4H), 2.09 (s, 1H), 1.91 (dd, *J* = 8.3, 16.5 Hz, 1H), 1.76 (dd, *J* = 2.9, 14.5, 1H), 1.72-1.63 (m, 3H), 1.61-1.45 (m, 4H), 1.44 (s, 3H), 1.42-1.28 (m, 8H), 1.17-1.09 (m, 1H), 1.12 (s, 3H), 0.93 (d, *J* = 7.11 Hz, 3H), 0.88 (t, *J* = 6.9 Hz, 3H), 0.70 (d, *J* = 7.0 Hz, 3H). $^{13}$C NMR ($CDCl_3$, 125 MHz): δ 216.7, 173.1, 148.5, 120.9, 76.0, 70.0, 61.5, 58.4, 46.6, 45.6, 42.1, 42.0, 40.6, 36.6, 34.8, 34.5, 31.7, 30.2, 30.0, 29.6, 29.2, 27.03, 26.96, 25.9, 25.1, 22.7, 16.9, 14.9, 14.2, 11.3. HR-MS (ESI): Calcd for $C_{30}H_{50}N_3O_5$ $[M+H]^+$: 532.3745; Found 532.3737. $[\alpha]_D^{25}$ = +54 (c = 0.65, $CHCl_3$).

**Table S1.** Predicted free energy of binding and root-mean-square deviation (RMSD) of docked spectinomycin compared to co-crystal coordinates of spectinomycin in PDB ID: 1FJG. RMSD and predicted free energy of binding is provided for all poses.

| Pose | RMSD (Å) | Binding Affinity (kcal/mol) |
|---|---|---|
| 1 | **0.225** | -9.3 |
| 2 | 6.301 | -8.7 |
| 3 | 6.349 | -8.3 |
| 4 | 15.485 | -8.3 |
| 5 | 16.306 | -8.2 |
| 6 | 3.687 | -8.1 |
| 7 | 16.166 | -8.1 |
| 8 | 5.453 | -8.0 |
| 9 | 15.603 | -8.0 |
| AVG | 9.51 | -8.3 |

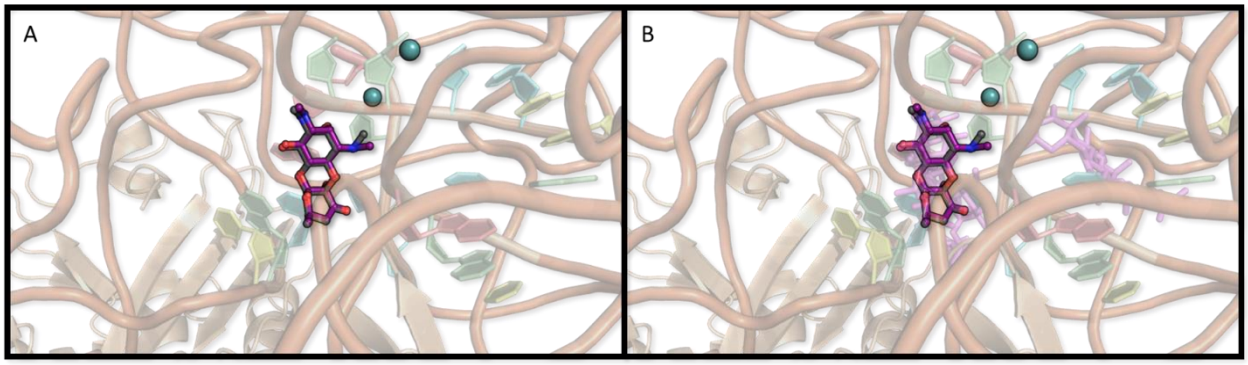


**Figure S1. Redocking of spectinomycin compared to co-crystal coordinates of spectinomycin in PDB ID: 1FJG.** (A) Co-crystalized spectinomycin in the *Thermus thermophilus* 30S ribosome subunit (PDB ID: 1FJG) is shown in grey sticks, colored by element. The lowest energy redocked pose of spectinomycin in the *T. thermophilus* 30S ribosome subunit is shown in purple sticks, colored by element (RMSD 0.225 Å). (B) All poses of docked spectinomycin (lines) overlaid with the lowest redocked pose of spectinomycin (purple, colored by element) and crystal structure (grey, colored by element) in the *T. thermophilus* 30S ribosome subunit.

**Table S2.** Predicted free energy of binding and RMSD of docked spectinomycin compared to co-crystal coordinates of spectinomycin in PDB ID: 4V56. RMSD and predicted free energy of binding is provided for all poses.

| **Pose** | **RMSD (Å)** | **Binding Affinity (kcal/mol)** |
|---|---|---|
| 1 | **0.393** | -9.7 |
| 2 | 6.412 | -9.1 |
| 3 | 4.348 | -8.5 |
| 4 | 15.974 | -8.5 |
| 5 | 6.181 | -8.2 |
| 6 | 5.459 | -8.2 |
| 7 | 6.530 | -8.2 |
| 8 | 15.057 | -8.0 |
| 9 | 13.898 | -8.0 |
| AVG | 8.25 | -8.5 |

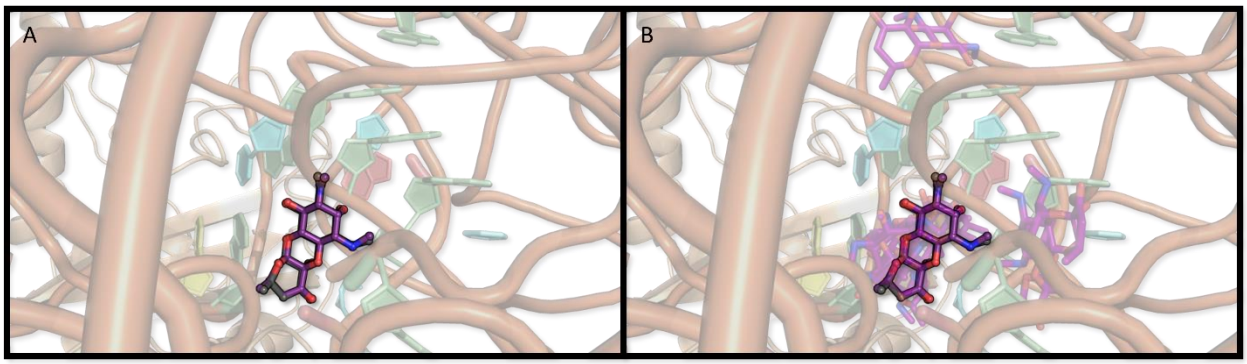


**Figure S2. Redocking of spectinomycin compared to co-crystal coordinates of spectinomycin in PDB ID: 4V56.** (A) Co-crystalized spectinomycin in the *Escherichia coli* 50S ribosome subunit (PDB ID: 4V56) is shown in grey sticks, colored by element. The lowest energy redocked pose of spectinomycin in the *E. coli* 50S ribosome subunit is shown in purple sticks, colored by element (RMSD 0.393 Å). (B) All poses of docked spectinomycin (lines) overlaid with the lowest redocked pose of spectinomycin (purple, colored by element) and crystal structure (grey, colored by element) in the *E. coli* 50S ribosome subunit.

**Table S3.** Predicted free energy of binding and RMSD of docked lefamulin compared to co-crystal coordinates of lefamulin in PDB ID: 5HL7. RMSD and predicted free energy of binding is provided for all poses.

| Pose | RMSD (Å) | Binding Affinity (kcal/mol) |
|---|---|---|
| 1 | **1.485** | -10.8 |
| 2 | 2.911 | -10.6 |
| 3 | 9.283 | -8.8 |
| 4 | 9.374 | -8.4 |
| 5 | 21.882 | -8.4 |
| 6 | 21.912 | -8.3 |
| 7 | 13.141 | -8.3 |
| 8 | 21.253 | -8.2 |
| 9 | 12.681 | -8.2 |
| AVG | 12.658 | -8.9 |

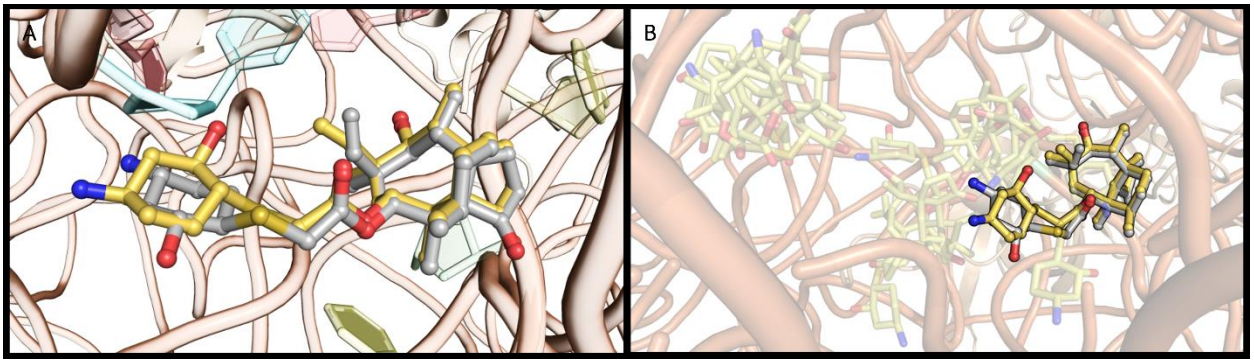


**Figure S3. Redocking of lefamulin compared to co-crystal coordinates of lefamulin in PDB ID: 5HL7.** (A) Co-crystalized lefamulin in the (PDB ID: 5HL7) is shown in grey sticks, colored by element. The lowest energy redocked pose of lefamulin in the *S. aureus* 50S ribosome subunit is shown in purple sticks, colored by element (RMSD 1.485 Å). (B) All poses of docked lefamulin (lines) overlaid with the lowest redocked pose of lefamulin (purple, colored by element) and crystal structure (grey, colored by element) in the *S. aureus* 50S ribosome subunit.

**Table S4.** Predicted free energy of binding and RMSD of docked blasticidin-S compared to co-crystal coordinates of blasticidin-S in PDB ID: 4V9Q. RMSD and predicted free energy of binding is provided for all poses**.**

| Pose | RMSD (Å) | Binding Affinity (kcal/mol) |
|---|---|---|
| 1 | 12.996 | -9.1 |
| 2 | **1.780** | -9.0 |
| 3 | 9.025 | -9.0 |
| 4 | 3.814 | -8.9 |
| 5 | 10.253 | -8.8 |
| 6 | 12.809 | -8.8 |
| 7 | 5.731 | -8.7 |
| 8 | 7.466 | -8.7 |
| 9 | 3.458 | -8.7 |
| AVG | 7.481 | -8.9 |

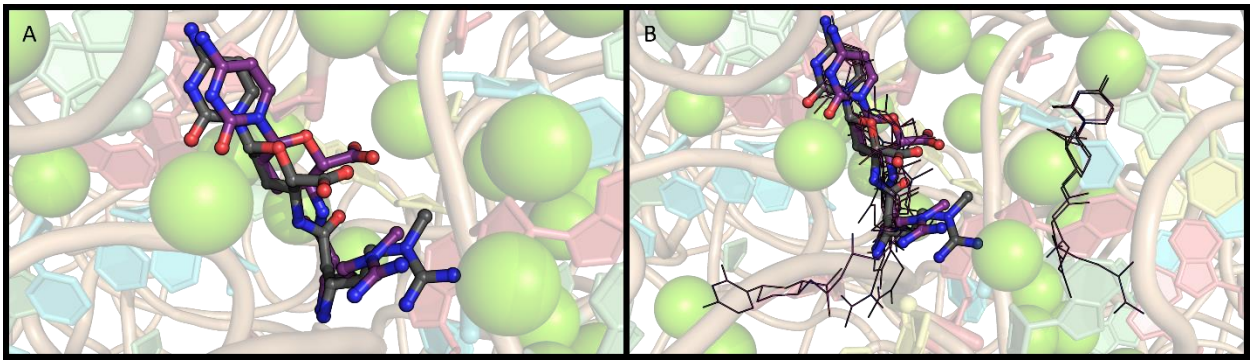


**Figure S4. Redocking of blasticidin-S compared to co-crystal coordinates of blasticidin-S in PDB ID: 4V9Q.** (A) Co-crystalized blasticidin-S in the *Thermus thermophilus* 50S ribosome subunit (PDB ID: 4V9Q) is shown in grey sticks, colored by element. The 2$^{nd}$ lowest RMSD redocked pose of blasticidin-S in the *T. thermophilus* 50S ribosome subunit is shown in purple sticks, colored by element (free binding energy -9.0kcal/mol, RMSD 1.780 Å). (B) All poses of docked blasticidin-S (lines) overlaid with the lowest redocked pose of blasticidin-S (purple, colored by element) and crystal structure (grey, colored by element) in the *T. thermophilus* 50S ribosome subunit.

**Table S5.** Predicted free energy of binding and RMSD of docked amicetin compared to co-crystal coordinates of amicetin in PDB ID: 6CZR. RMSD and predicted free energy of binding is provided for all poses.

| Pose | RMSD (Å) | Binding Affinity (kcal/mol) |
|---|---|---|
| 1 | 3.89 | -8.6 |
| 2 | 11.10 | -8.6 |
| 3 | 11.63 | -8.4 |
| 4 | 2.10 | -8.4 |
| 5 | 5.23 | -8.2 |
| 6 | 10.84 | -8.2 |
| 7 | 6.20 | -8.1 |
| 8 | 10.65 | -7.8 |
| 9 | 11.36 | -7.8 |
| AVG | 8.11 | -8.2 |

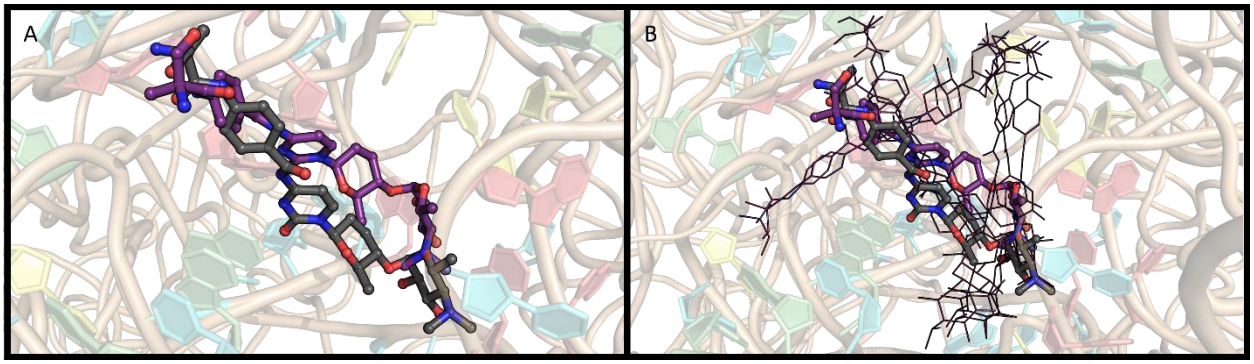


**Figure S5. Redocking of amicetin compared to co-crystal coordinates of amicetin in PDB ID: 6CZR.** (A) Co-crystalized amicetin in the *Thermus thermophilus* 50S ribosome subunit (PDB ID: 6CZR) is shown in grey sticks, colored by element. The lowest energy redocked pose of amicetin in the *T. thermophilus* 50S ribosome subunit is shown in purple sticks, colored by element (RMSD 3.89 Å). (B) All poses of docked amicetin (lines) overlaid with the lowest redocked pose of amicetin (purple, colored by element) and crystal structure (grey, colored by element) in the *T. thermophilus* 50S ribosome subunit.

**Table S6.** Predicted free energy of binding RMSD of docked blasticidin-S compared to co-crystal coordinates of blasticidin-S in PDB ID: 4U56. RMSD and predicted free energy of binding is provided for all poses.

| Pose | RMSD (Å) | Binding Affinity (kcal/mol) |
|---|---|---|
| 1 | 12.707 | -8.1 |
| 2 | 9.904 | -8.1 |
| 3 | 11.174 | -8.0 |
| 4 | 9.099 | -7.8 |
| 5 | 10.096 | -7.6 |
| 6 | 8.405 | -7.4 |
| 7 | 10.447 | -7.0 |
| 8 | 10.133 | -7.0 |
| 9 | 5.800 | -7.0 |
| AVG | 9.752 | -7.6 |

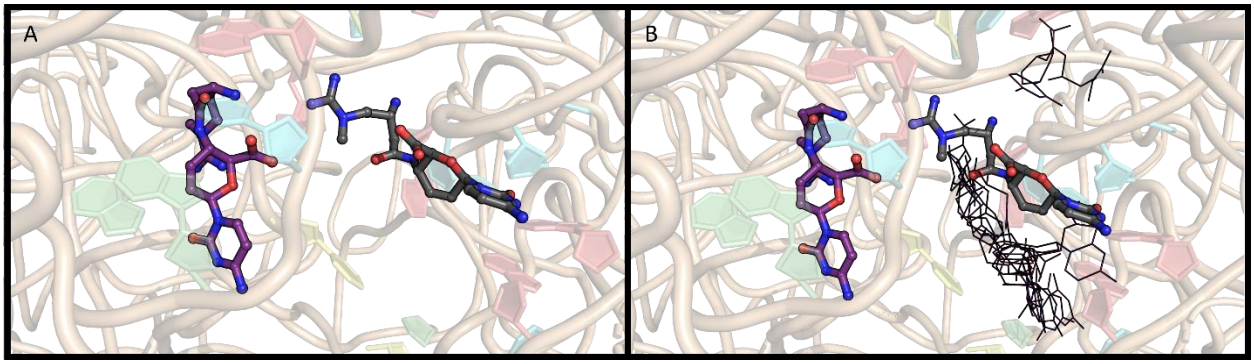


**Figure S6. Redocking of blasticidin-S compared to co-crystal coordinates of blasticidin-S in PDB ID: 4U56.** (A) Co-crystalized blasticidin-S in the *Saccharomyces cerevisiae* 60S/80S ribosome subunit (PDB ID: 4U56) is shown in grey sticks, colored by element. The lowest energy redocked pose of blasticidin-S in the *S. cerevisiae* oribosome subunit is shown in purple sticks, colored by element (RMSD 12.707 Å). (B) All poses of docked blasticidin-S (lines) overlaid with the lowest redocked pose of blasticidin-S (purple, colored by element) and crystal structure (grey, colored by element) in the *S. cerevisiae* 60S ribosome subunit.

**Table S7.** Predicted free energy of RMSD of docked blasticidin-S compared to co-crystal coordinates of blasticidin-S in PDB ID: 6B4V. RMSD and predicted free energy of binding is provided for all poses.

| Pose | RMSD (Å) | Binding Affinity (kcal/mol) |
|---|---|---|
| 1 | 4.093 | -9.6 |
| 2 | 3.307 | -9.3 |
| 3 | **1.319** | -9.1 |
| 4 | 2.538 | -8.9 |
| 5 | 3.808 | -8.5 |
| 6 | 8.382 | -8.4 |
| 7 | 8.130 | -8.3 |
| 8 | 3.576 | -8.3 |
| 9 | 3.466 | -8.1 |
| AVG | 4.291 | -8.7 |

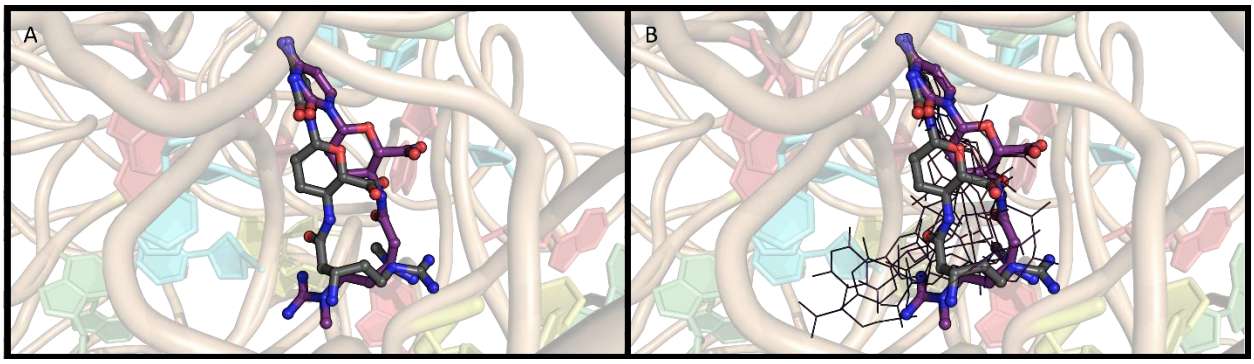


**Figure S7. Redocking of blasticidin-S compared to co-crystal coordinates of blasticidin-S in PDB ID: 6B4V.** (A) Co-crystalized blasticidin-S in the *Thermus thermophilus* 50S/70S ribosome subunit (PDB ID: 6B4V) is shown in grey sticks, colored by element. The 3$^{rd}$ lowest RMSD redocked pose of blasticidin-S in the *T. thermophilus* 50S ribosome subunit is shown in purple sticks, colored by element (Pose 3, Binding Affinity -9.1 kcal/mol, RMSD 1.319 Å). (B) All poses of docked blasticidin-S (lines) overlaid with the lowest redocked pose of blasticidin-S (purple, colored by element) and crystal structure (grey, colored by element) in the *T. thermophilus* 50S ribosome subunit.

**Table S8.** Predicted free energy of binding and RMSD of docked blasticidn-S compared to co-crystal coordinates of blasticidin-S in PDB ID: 1KC8. RMSD and predicted free energy of binding is provided for all poses.

| Pose | RMSD (Å) | Binding Affinity (kcal/mol) |
|---|---|---|
| 1 | 10.345 | -8.5 |
| 2 | 10.252 | -8.3 |
| 3 | 14.149 | -8.3 |
| 4 | 10.960 | -8.1 |
| 5 | 10.557 | -7.9 |
| 6 | 10.859 | -7.9 |
| 7 | 10.642 | -7.9 |
| 8 | 10.619 | -7.8 |
| 9 | 5.984 | -7.7 |
| AVG | 10.485 | -8.0 |

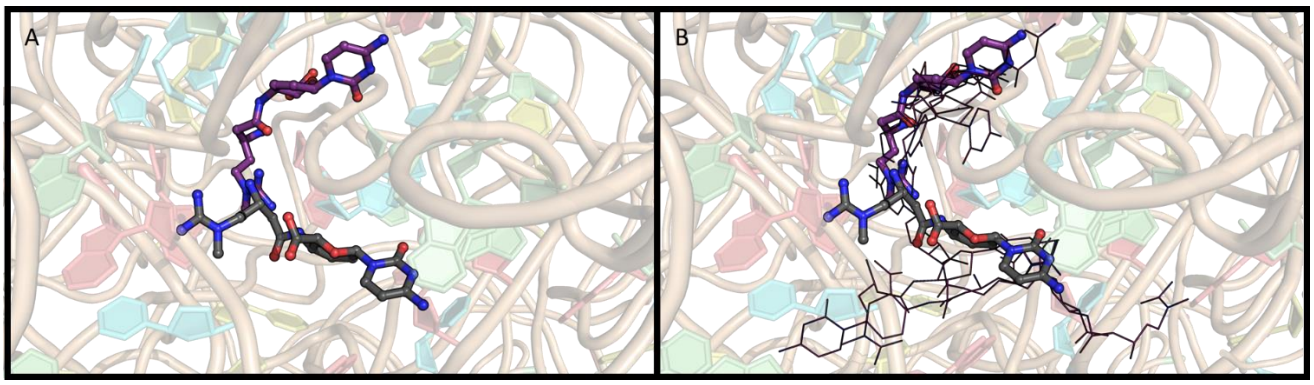


**Figure S8. Redocking of blasticidin-S compared to co-crystal coordinates of blasticidin-S in PDB ID: 1KC8.** (A) Co-crystalized blasticidin-S in the *Haloarcula marismortui* 50S ribosome subunit is shown in grey sticks, colored by element. The lowest energy redocked pose of blasticidin-S in the *H. marismortui* 50S ribosome subunit is shown in purple sticks, colored by element (RMSD 10.345 Å). (B) All poses of docked blasticidin-S (lines) overlaid with the lowest redocked pose of blasticidin-S (purple, colored by element) and crystal structure (grey, colored by element) in the *H. marismortui* 50S ribosome subunit.

**Table S9.** Predicted free energy of binding and RMSD of docked tiamulin compared to co-crystal coordinates of tiamulin in PDB ID: 1XBP. RMSD and predicted free energy of binding is provided for all poses.

| Pose | RMSD (Å) | Binding Affinity (kcal/mol) |
|---|---|---|
| 1 | **1.816** | -8.7 |
| 2 | 2.578 | -8.7 |
| 3 | 6.531 | -8.2 |
| 4 | 4.610 | -8.1 |
| 5 | 7.784 | -7.8 |
| 6 | 8.246 | -7.8 |
| 7 | 4.595 | -7.7 |
| 8 | 7.586 | -7.5 |
| 9 | 7.949 | -7.4 |
| AVG | 5.744 | -8.0 |

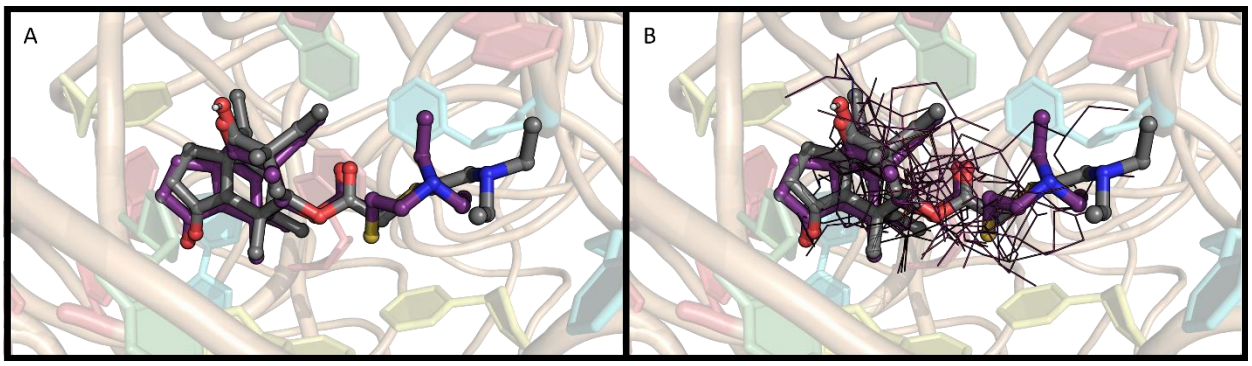


**Figure S9. Redocking of tiamulin compared to co-crystal coordinates of tiamulin in PDB ID: 1XBP.** (A) Co-crystalized tiamulin in the 1XBP ribosome subunit is shown in grey sticks, colored by element. The lowest energy redocked pose of tiamulin in the 1XBP ribosome subunit is shown in purple sticks, colored by element (RMSD 1.816 Å). (B) All poses of docked tiamulin (lines) overlaid with the lowest redocked pose of tiamulin (purple, colored by element) and crystal structure (grey, colored by element) in the 1XBP ribosome subunit.

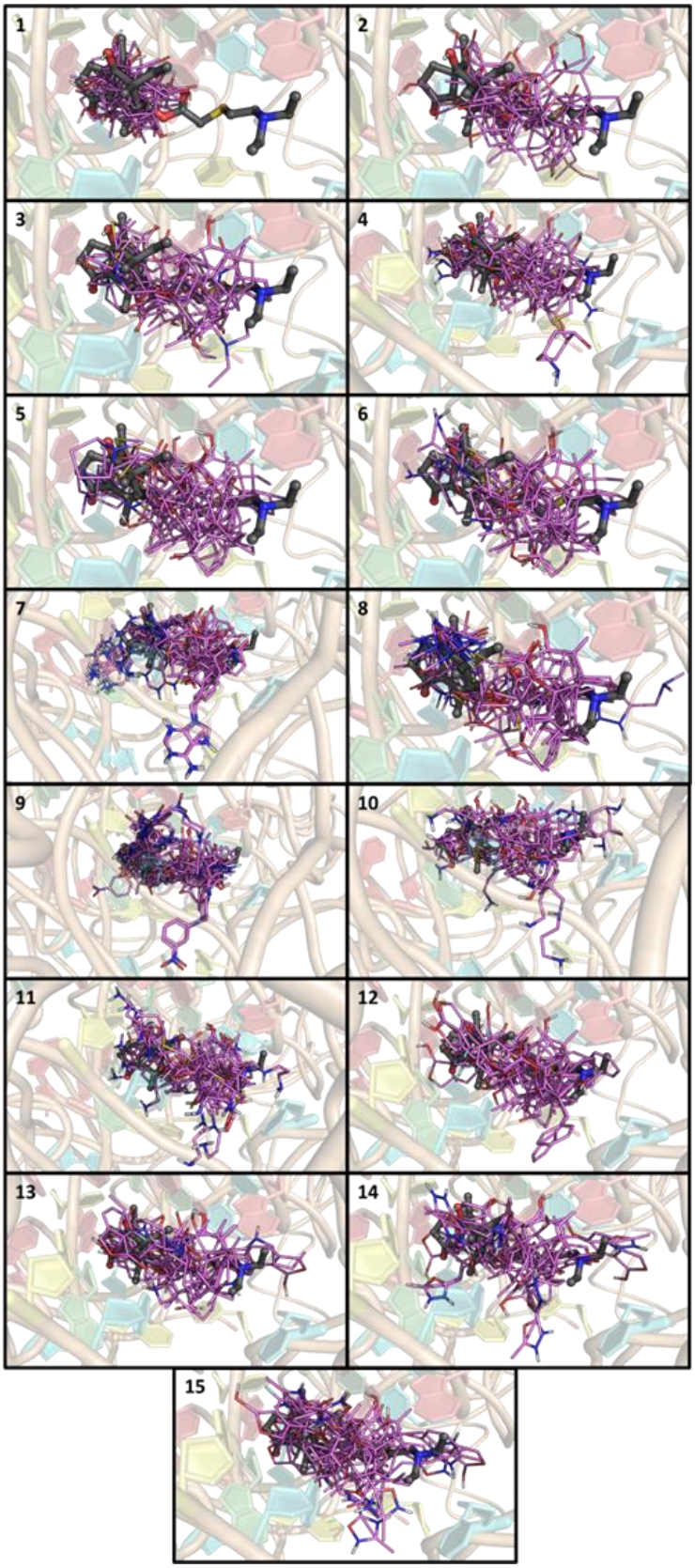
1
2
3
4
5
6
7
8
9
10
11
12
13
14
15

**Figure S10. Docked poses of pleuromutilin analogs 1-15.**

| | Compound Number | | | | | | | | | | | | | | |
|---|---|---|---|---|---|---|---|---|---|---|---|---|---|---|---|
| **Pose** | **1** | **2** | **3** | **4** | **5** | **6** | **7** | **8** | **9** | **10** | **11** | **12** | **13** | **14** | **15** |
| **1** | -8.7 | -8.3 | -8.7 | -10.0 | -10.4 | -9.3 | -13.0 | -10.4 | -12.3 | -9.3 | -9.5 | -11.6 | -10.3 | -12.3 | -12.3 |
| **2** | -8.7 | -8.1 | -8.7 | -9.4 | -10.0 | -9.3 | -12.6 | -10.3 | -12.1 | -9.1 | -9.4 | -11.6 | -10.1 | -11.8 | -12.1 |
| **3** | -8.6 | -8.1 | -8.2 | -9.2 | -9.8 | -9.1 | -12.6 | -10.2 | -11.9 | -8.8 | -9.3 | -11.6 | -9.8 | -11.8 | -12.0 |
| **4** | -8.6 | -7.9 | -8.1 | -9.2 | -9.7 | -8.7 | -12.3 | -10.2 | -11.9 | -8.7 | -9.0 | -11.0 | -9.8 | -11.8 | -12.0 |
| **5** | -8.4 | -7.9 | -7.8 | -9.0 | -9.1 | -8.6 | -12.3 | -10.2 | -11.8 | -8.7 | -8.7 | -10.7 | -9.7 | -11.7 | -11.7 |
| **6** | -8.3 | -7.8 | -7.8 | -8.9 | -9.1 | -8.5 | -12.2 | -10.1 | -11.5 | -8.6 | -8.6 | -10.6 | -9.7 | -11.4 | -11.4 |
| **7** | -8.2 | -7.7 | -7.7 | -8.9 | -8.9 | -8.4 | -12.1 | -10.1 | -11.5 | -8.6 | -8.6 | -10.6 | -9.6 | -11.3 | -11.1 |
| **8** | -8.2 | -7.6 | -7.5 | -8.8 | -8.9 | -8.4 | -11.7 | -9.9 | -11.3 | -8.6 | -8.3 | -10.4 | -9.4 | -11.2 | -11.1 |
| **9** | -8.2 | -7.6 | -7.4 | -8.8 | -8.9 | -8.4 | -11.7 | -9.9 | -11.2 | -8.5 | -8.3 | -10.4 | -9.3 | -11.1 | -11.1 |
| **AVG** | **-8.4** | **-7.9** | **-8.0** | **-9.1** | **-9.4** | **-8.7** | **-12.3** | **-10.1** | **-11.7** | **-8.8** | **-8.9** | **-10.9** | **-9.7** | **-11.6** | **-11.6** |

**Table S10.** Binding affinity (kcal/mol) for computed for the docking poses of compounds **1-15** shown in Figure S10.

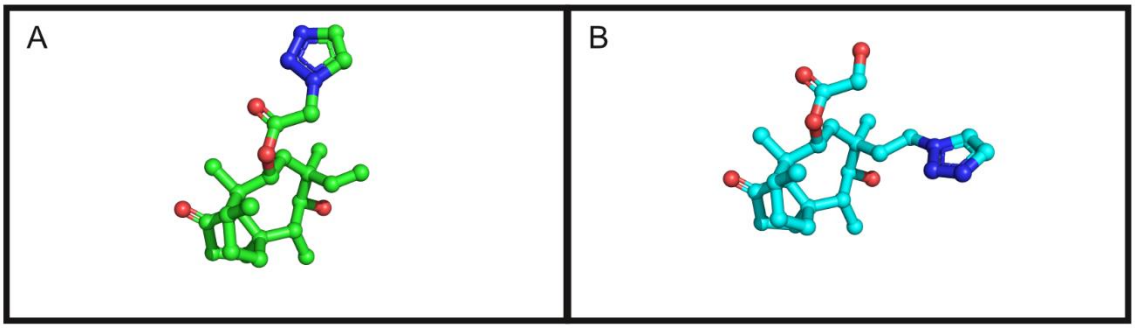


**Figure S11. Base structures for triazole-pleuromutilin C22 and C20 derivatives.** (A) base structure for the C22 triazole derivatives. (B) base structure for the C20 derivatives.

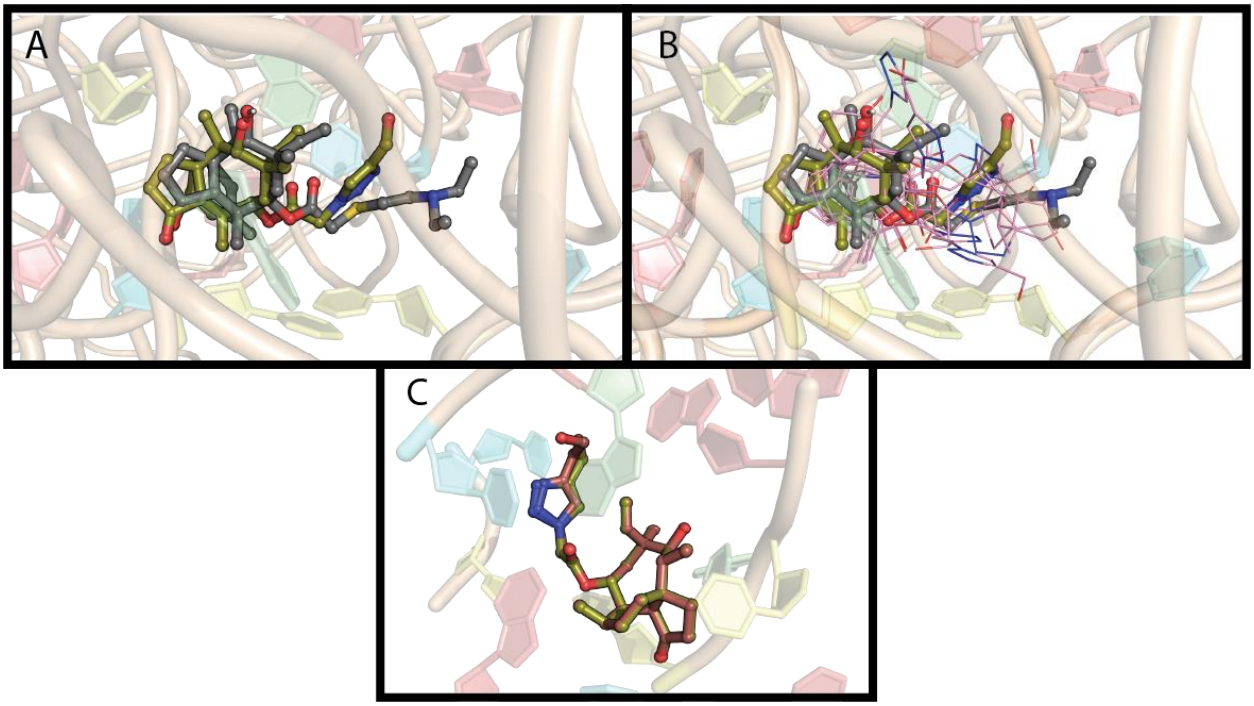


**Figure S12. Docking results of C22 derivative 18.** (A) Co-crystalized tiamulin (shown in grey sticks, colored by element) in the *D. radiodurans* 50S ribosome subunit (PDB ID: 1XBP). The

lowest energy docked pose of derivative 18 is shown in olive sticks, colored by element. (B) All poses of docked derivative 18 (lines) overlaid with the lowest redocked pose of derivative 18 (olive, colored by element) and tiamulin crystal structure (grey, colored by element) in PDB ID: 1XBP. (C) Lowest energy pose of derivative 18 (olive, sticks) overlayed with the best performing C22 derivative (derivative 19, brown, sticks) in the tiamulin binding pocket of *D. radiodurans* (PDB ID: 1XBP).

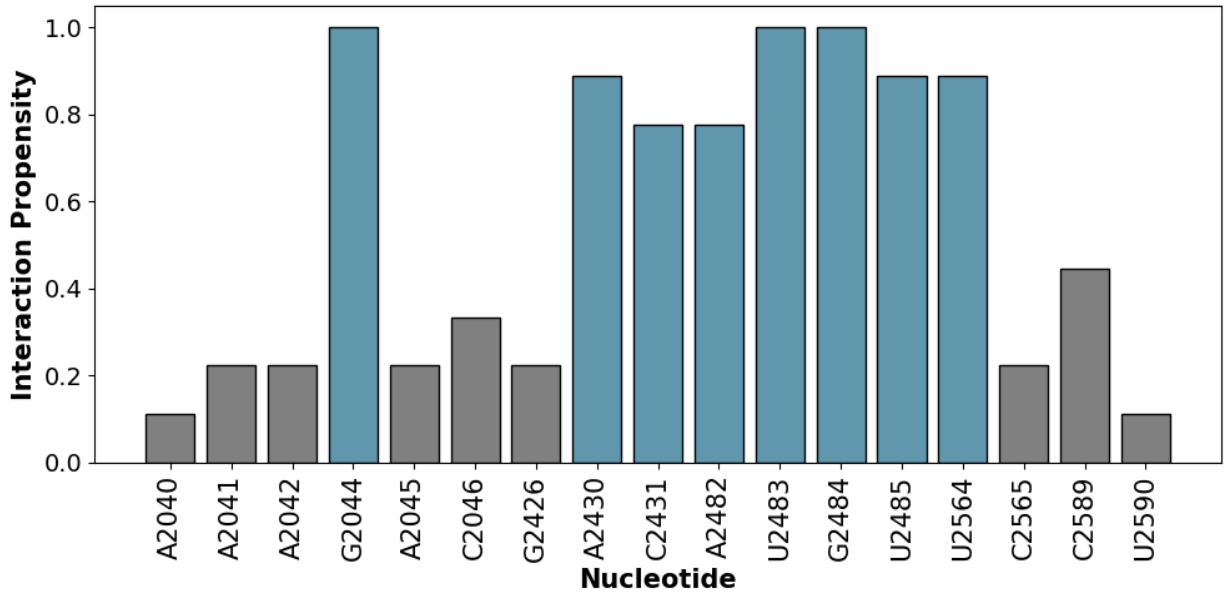


**Figure S13. Derivative 18 nucleotide interaction propensities within PDB ID: 1XBP.** Nucleotides that interacted with this derivative are shown on the x-axis. Propensity is shown in the y-axis. Bars are colored teal when the interaction threshold was over 70% for all poses. Bars are colored grey when the interaction threshold is under 70% and at least one interaction with one pose was observed.

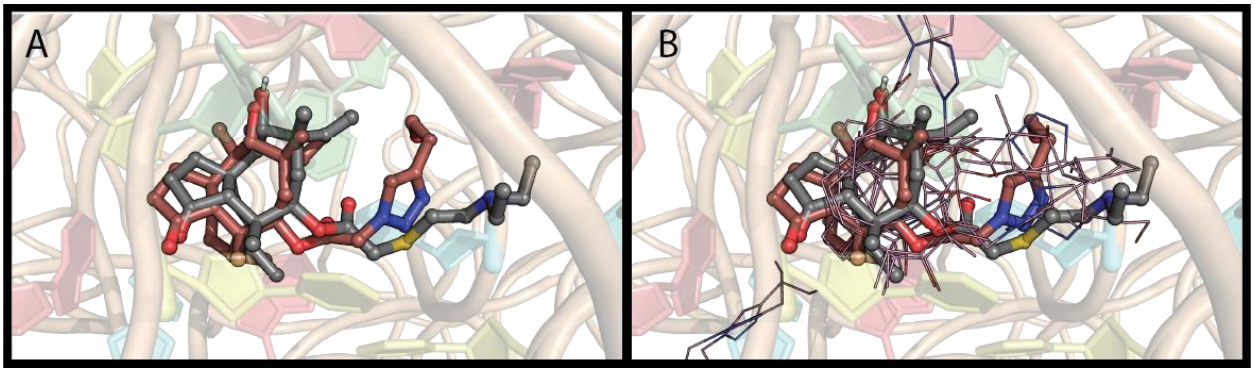


**Figure S14. Docking results of C22 derivative 19.** (A) Co-crystalized tiamulin (shown in grey sticks, colored by element) in the *D. radiodurans* 50S ribosome subunit (PDB ID: 1XBP). The olowest energy docked pose of derivative 19 is shown in olive sticks, colored by element. (B) All poses of docked derivative 19 (lines) overlaid with the lowest redocked pose of derivative 18 (olive, colored by element) and tiamulin crystal structure (grey, colored by element) in PDB ID: 1XBP. As this is the lowest energy structure, no comparative panel C is shown.

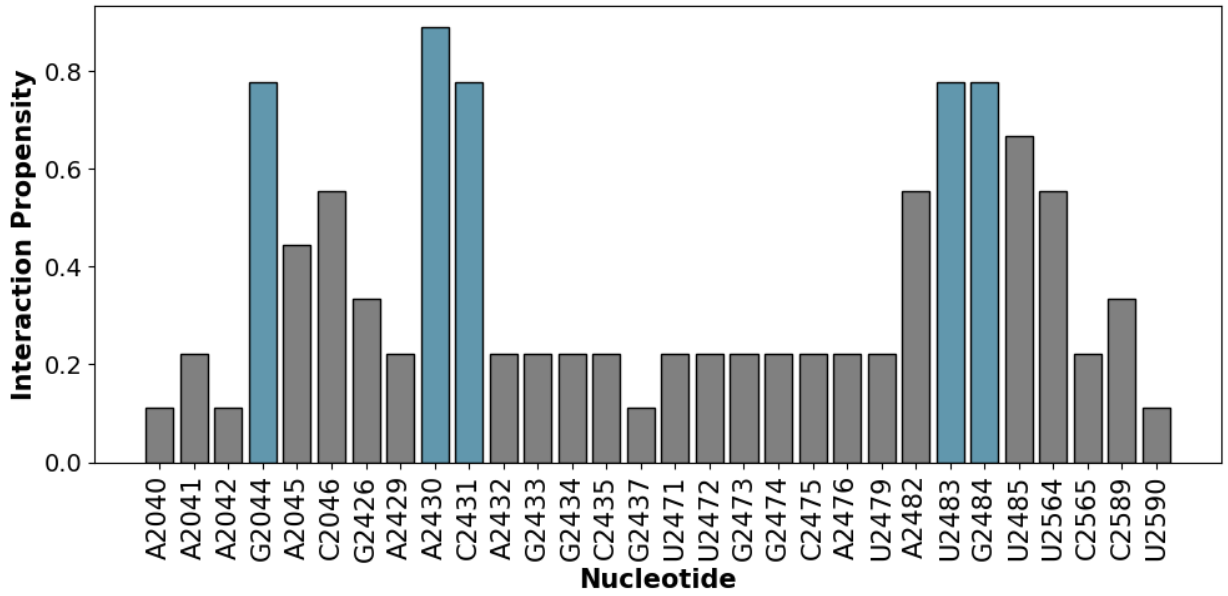


**Figure S15. Derivative 19 nucleotide interaction propensities within PDB ID: 1XBP.** Nucleotides that interacted with this derivative are shown on the x-axis. Propensity is shown in the y-axis. Bars are colored teal when the interaction threshold was over 70% for all poses. Bars are colored grey when the interaction threshold is under 70% and at least one interaction with one pose was observed.

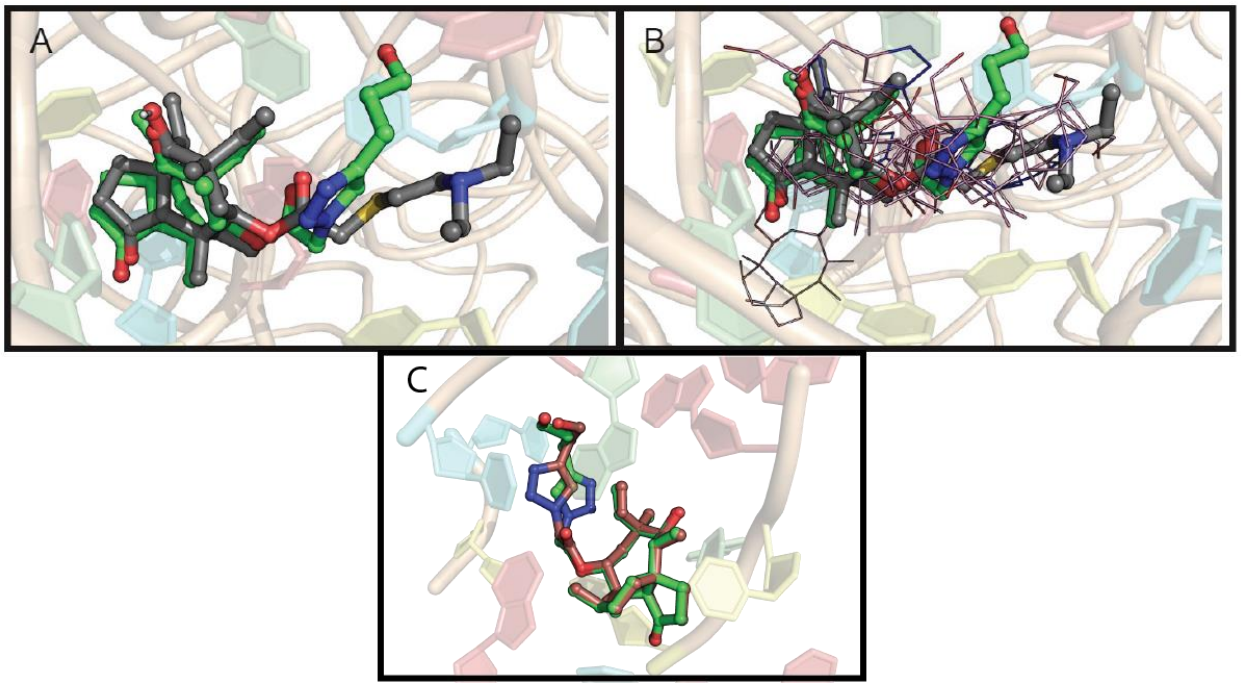


**Figure S16. Docking results of C22 derivative 20.** (A) Co-crystalized tiamulin (shown in grey sticks, colored by element) in the *D. radiodurans* 50S ribosome subunit (PDB ID: 1XBP). The lowest energy docked pose of derivative 20 is shown in light green sticks, colored by element. (B) All poses of docked derivative 20 (lines) overlaid with the lowest redocked pose of derivative 20 (light green, colored by element) and tiamulin crystal structure (grey, colored by element) in PDB ID: 1XBP. (C) Lowest energy pose of derivative 20 (light green, sticks) overlayed with the best performing C22 derivative (derivative 19, brown, sticks) in the tiamulin binding pocket of *D. radiodurans* (PDB ID: 1XBP).

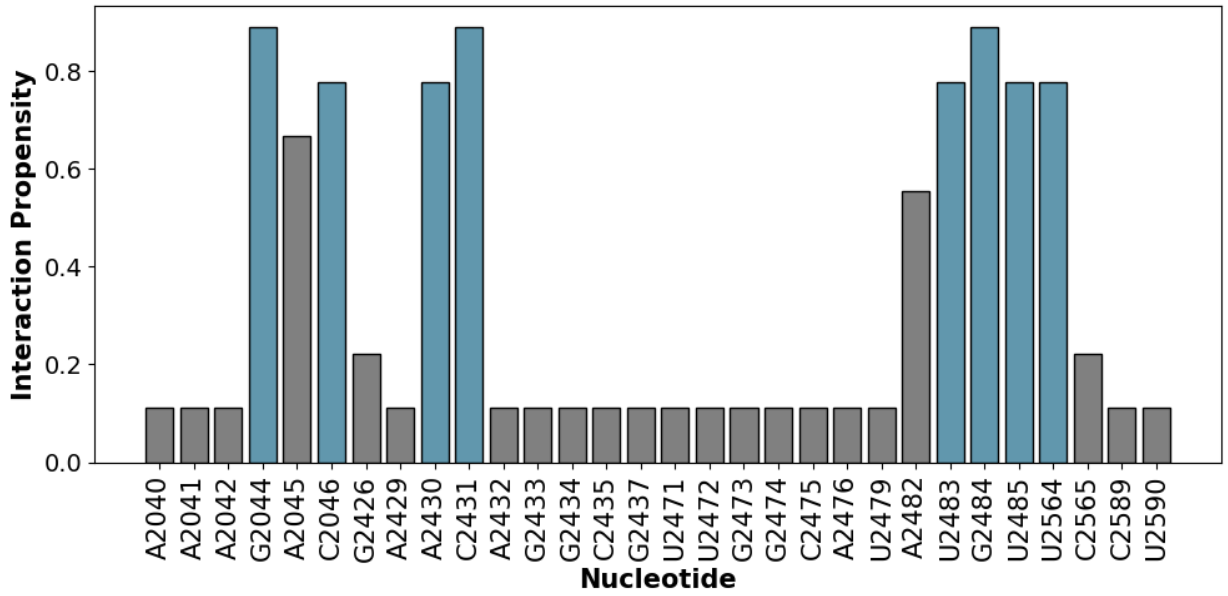


**Figure S17. Derivative 20 nucleotide interaction propensities within PDB ID: 1XBP.** Nucleotides that interacted with this derivative are shown on the x-axis. Propensity is shown in the y-axis. Bars are colored teal when the interaction threshold was over 70% for all poses. Bars are colored grey when the interaction threshold is under 70% and at least one interaction with one pose was observed.

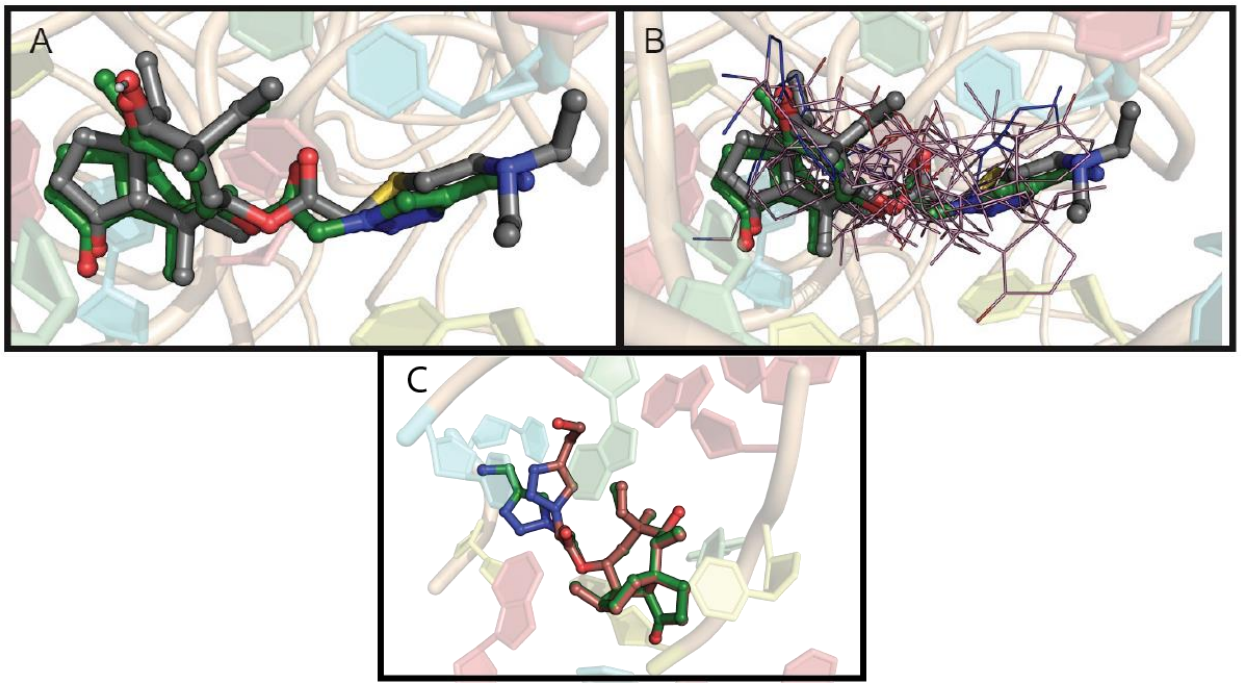


**Figure S18. Docking results of C22 derivative 21.** (A) Co-crystalized tiamulin (shown in grey sticks, colored by element) in the *D. radiodurans* 50S ribosome subunit (PDB ID: 1XBP). The lowest energy docked pose of derivative 21 is shown in green sticks, colored by element. (B) All poses of docked derivative 21 (lines) overlaid with the lowest redocked pose of derivative 21 (green, colored by element) and tiamulin crystal structure (grey, colored by element) in PDB ID: 1XBP. (C) Lowest energy pose of derivative 21 (green, sticks) overlayed with the best performing C22 derivative (derivative 19, brown, sticks) in the tiamulin binding pocket of *D. radiodurans* (PDB ID: 1XBP).

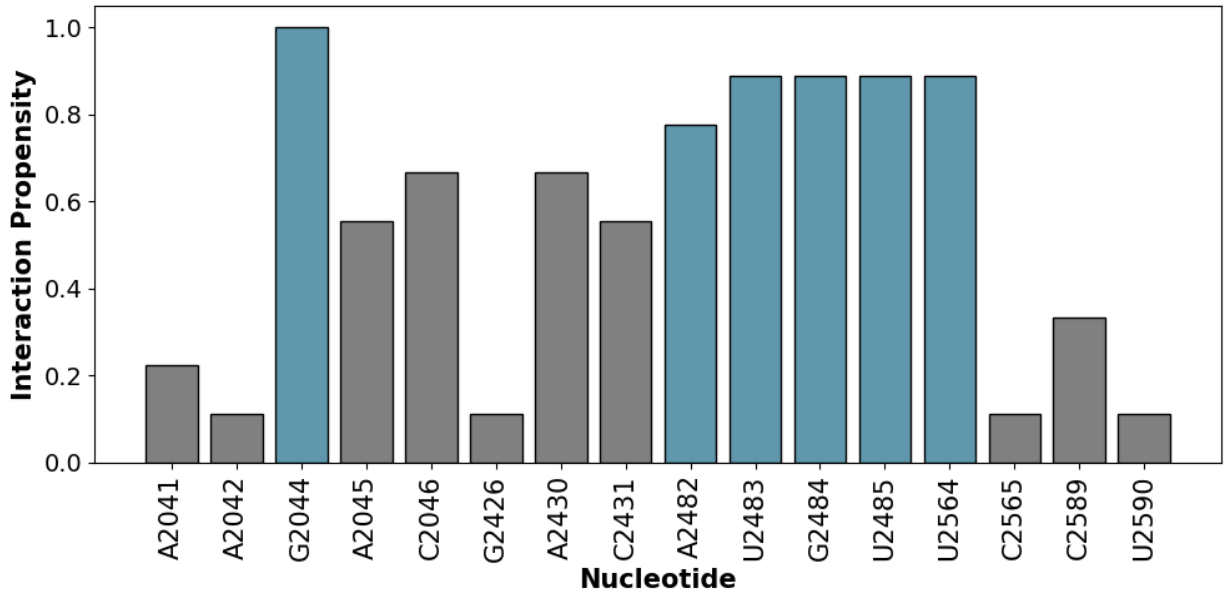


**Figure S19. Derivative 21 nucleotide interaction propensities within PDB ID: 1XBP.** Nucleotides that interacted with this derivative are shown on the x-axis. Propensity is shown in the y-axis. Bars are colored teal when the interaction threshold was over 70% for all poses. Bars are colored grey when the interaction threshold is under 70% and at least one interaction with one pose was observed.

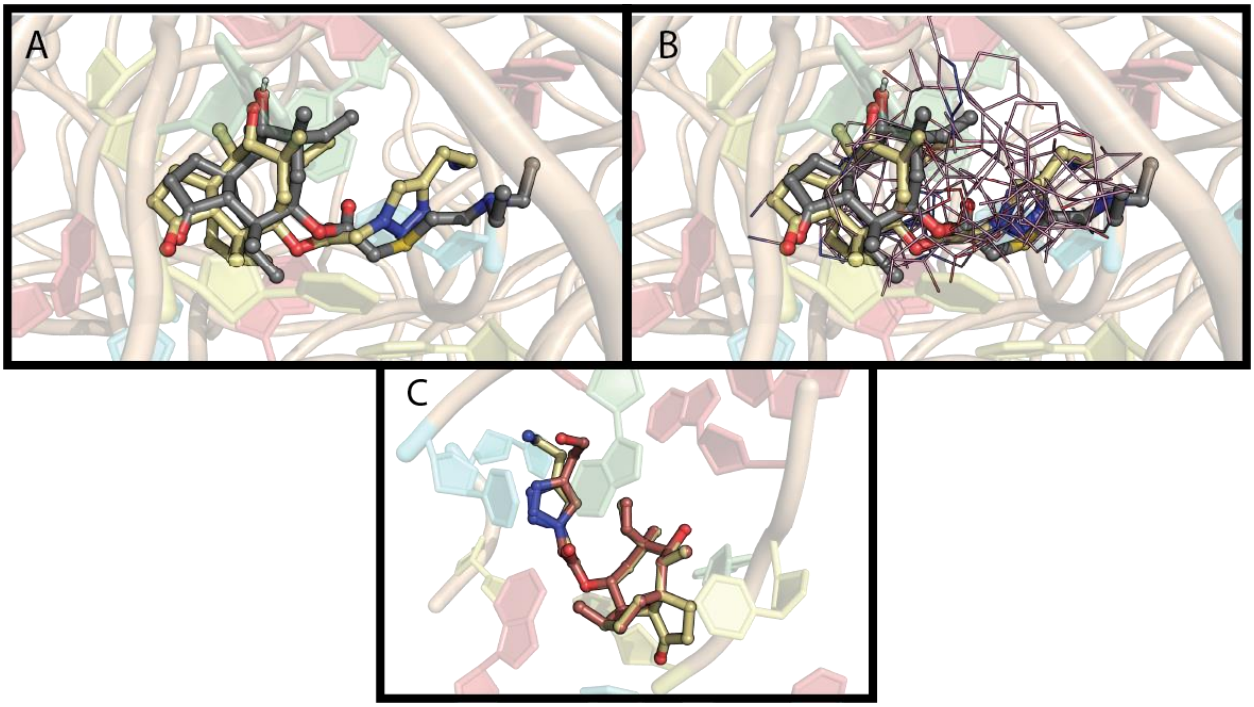


**Figure S20. Docking results of C22 derivative 22.** (A) Co-crystalized tiamulin (shown in grey sticks, colored by element) in the *D. radiodurans* 50S ribosome subunit (PDB ID: 1XBP). The lowest energy docked pose of derivative 22 is shown in yellow sticks, colored by element. (B) All poses of docked derivative 22 (lines) overlaid with the lowest redocked pose of derivative 22 (yellow, colored by element) and tiamulin crystal structure (grey, colored by element) in PDB ID: 1XBP. (C) Lowest energy pose of derivative 22 (yellow, sticks) overlayed with the best performing C22 derivative (derivative 19, brown, sticks) in the tiamulin binding pocket of *D. radiodurans* (PDB ID: 1XBP).

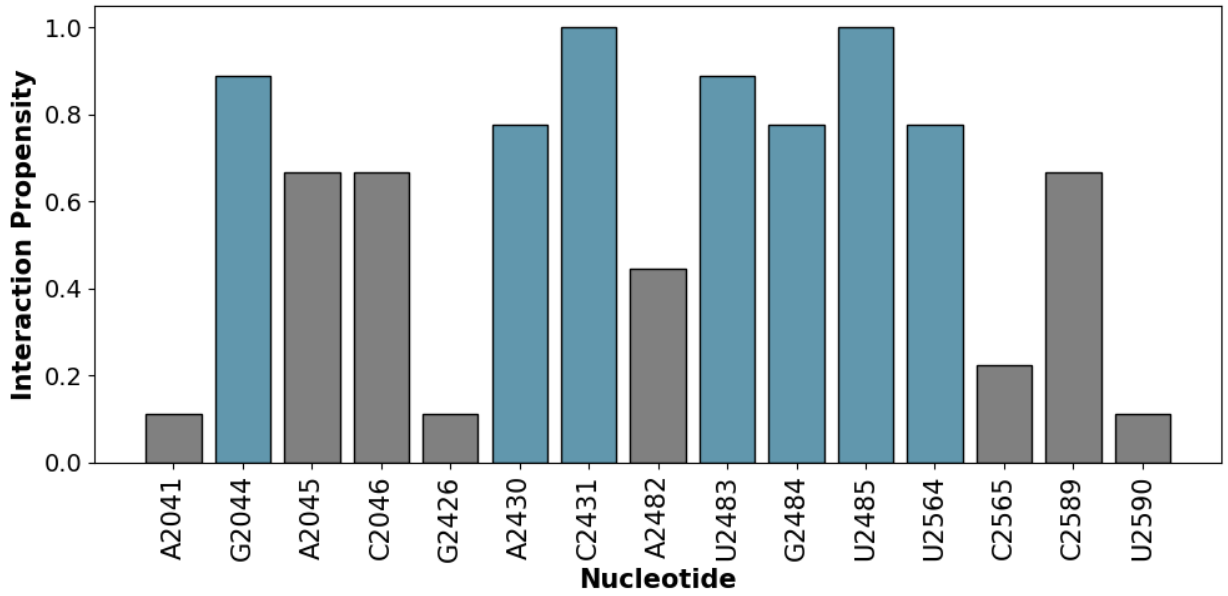


**Figure S21. Derivative 22 nucleotide interaction propensities within PDB ID: 1XBP.** Nucleotides that interacted with this derivative are shown on the x-axis. Propensity is shown in the y-axis. Bars are colored teal when the interaction threshold was over 70% for all poses. Bars are colored grey when the interaction threshold is under 70% and at least one interaction with one pose was observed.

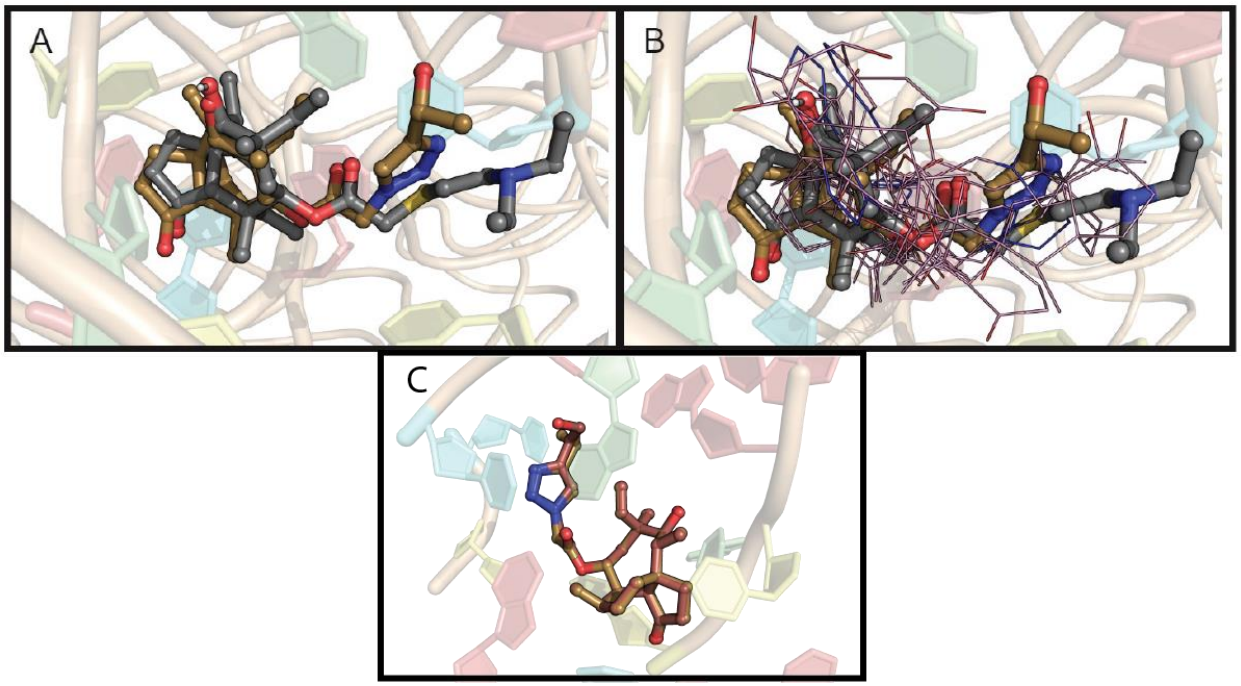


**Figure S22. Docking results of C22 derivative 23-R.** (A) Co-crystalized tiamulin (shown in grey sticks, colored by element) in the *D. radiodurans* 50S ribosome subunit (PDB ID: 1XBP). The lowest energy docked pose of derivative 23-R is shown in gold sticks, colored by element. (B) All poses of docked derivative 23-R (lines) overlaid with the lowest redocked pose of derivative 23-R (gold, colored by element) and tiamulin crystal structure (grey, colored by element) in PDB ID: 1XBP. (C) Lowest energy pose of derivative 23-R (gold, sticks) overlayed with the best performing C22 derivative (derivative 19, brown, sticks) in the tiamulin binding pocket of *D. radiodurans* (PDB ID: 1XBP).

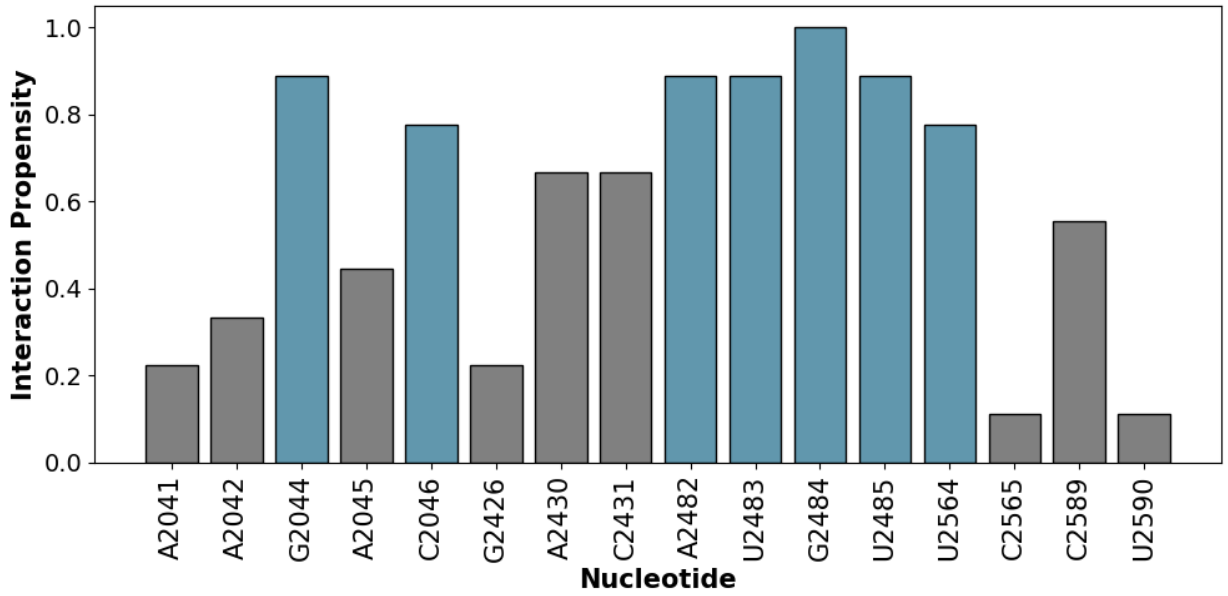


**Figure S23. Derivative 23-R nucleotide interaction propensities within PDB ID: 1XBP.** Nucleotides that interacted with this derivative are shown on the x-axis. Propensity is shown in the y-axis. Bars are colored teal when the interaction threshold was over 70% for all poses. Bars are colored grey when the interaction threshold is under 70% and at least one interaction with one pose was observed.

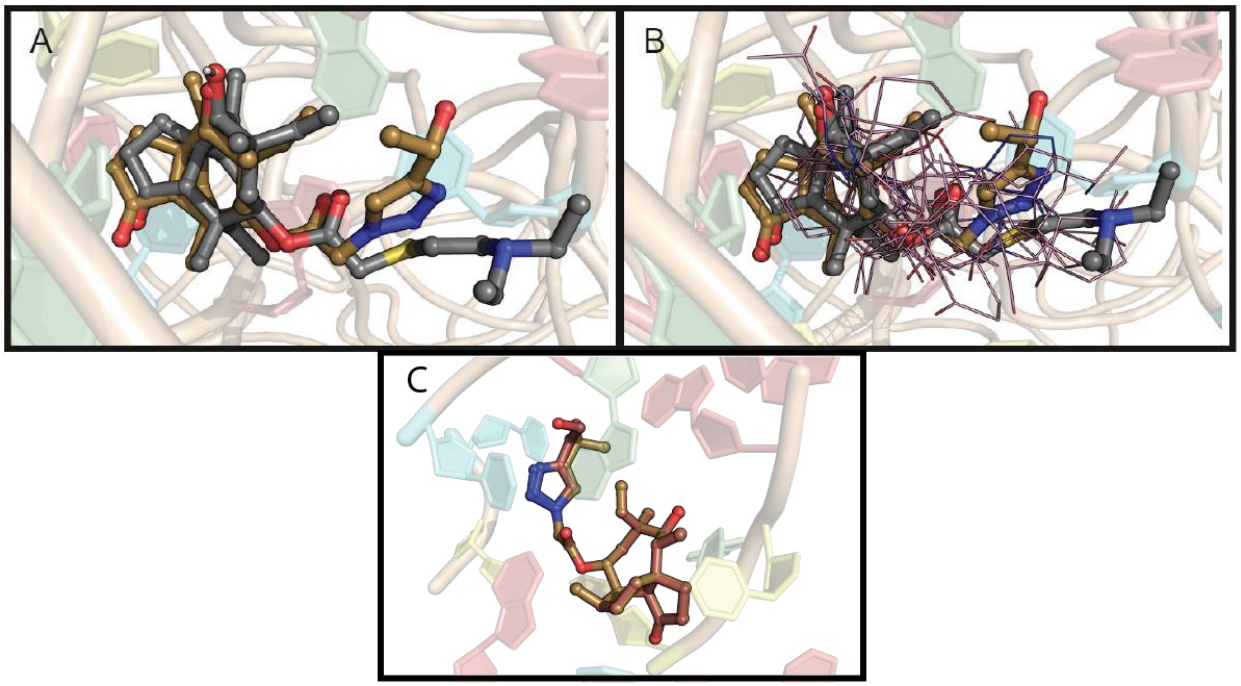


**Figure S24. Docking results of C22 derivative 23-S.** (A) Co-crystalized tiamulin (shown in grey sticks, colored by element) in the *D. radiodurans* 50S ribosome subunit (PDB ID: 1XBP). The lowest energy docked pose of derivative 23-S is shown in gold sticks, colored by element. (B) All poses of docked derivative 23-S (lines) overlaid with the lowest redocked pose of derivative 23-S (gold, colored by element) and tiamulin crystal structure (grey, colored by element) in PDB ID: 1XBP. (C) Lowest energy pose of derivative 23-S (gold, sticks) overlayed with the best performing C22 derivative (derivative 19, brown, sticks) in the tiamulin binding pocket of *D. radiodurans* (PDB ID: 1XBP).

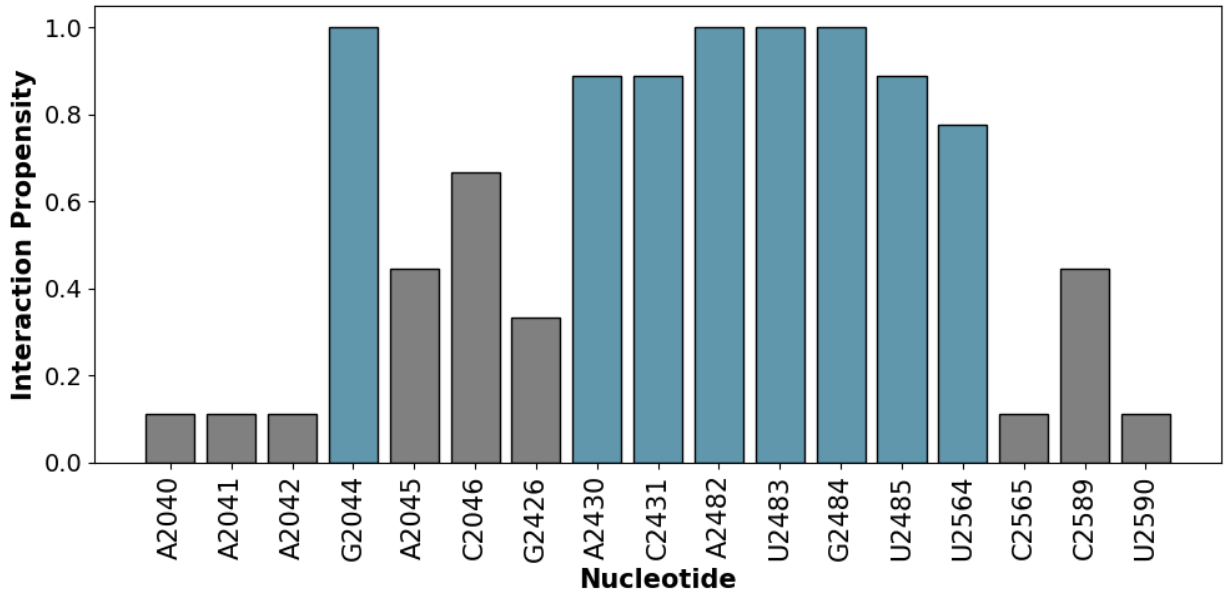


**Figure S25. Derivative 23-S nucleotide interaction propensities within PDB ID: 1XBP.** Nucleotides that interacted with this derivative are shown on the x-axis. Propensity is shown in the y-axis. Bars are colored teal when the interaction threshold was over 70% for all poses. Bars are colored grey when the interaction threshold is under 70% and at least one interaction with one pose was observed.

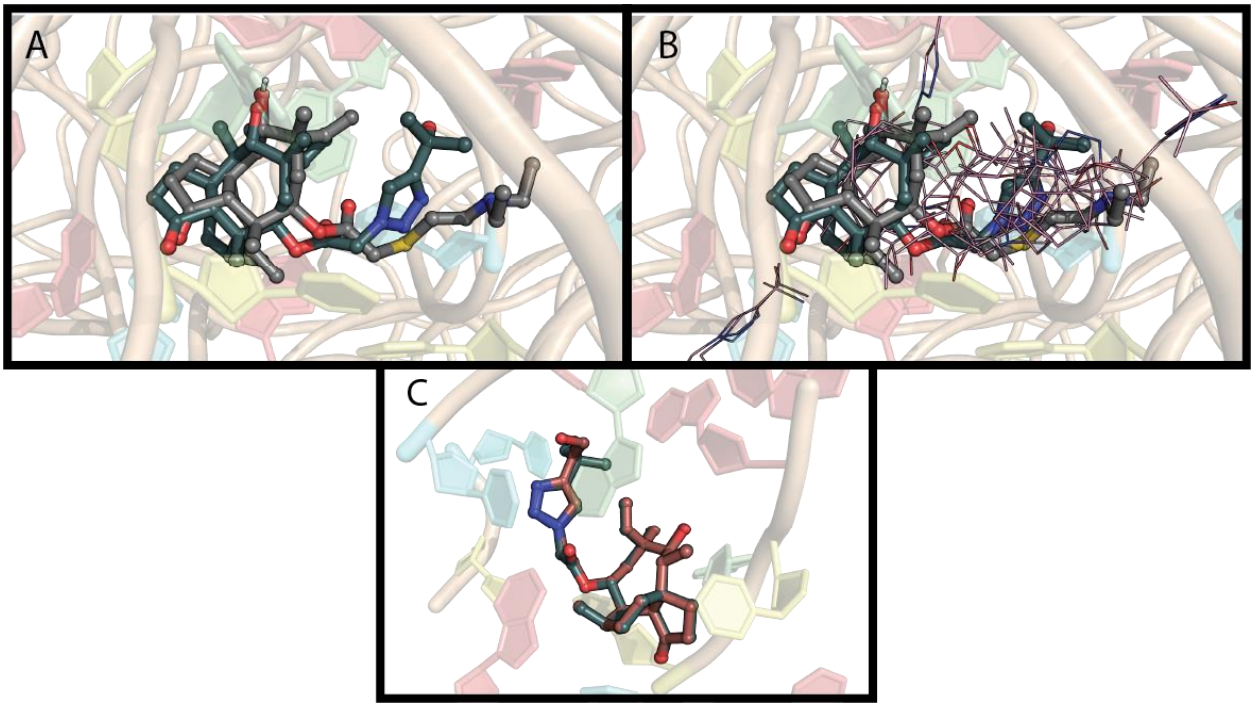


**Figure S26. Docking results of C22 derivative 24.** (A) Co-crystalized tiamulin (shown in grey sticks, colored by element) in the *D. radiodurans* 50S ribosome subunit (PDB ID: 1XBP). The lowest energy docked pose of derivative 24 is shown in teal sticks, colored by element. (B) All poses of docked derivative 24 (lines) overlaid with the lowest redocked pose of derivative 24 (teal, colored by element) and tiamulin crystal structure (grey, colored by element) in PDB ID: 1XBP. (C) Lowest energy pose of derivative 24 (teal, sticks) overlayed with the best performing C22 derivative (derivative 19, brown, sticks) in the tiamulin binding pocket of *D. radiodurans* (PDB ID: 1XBP).

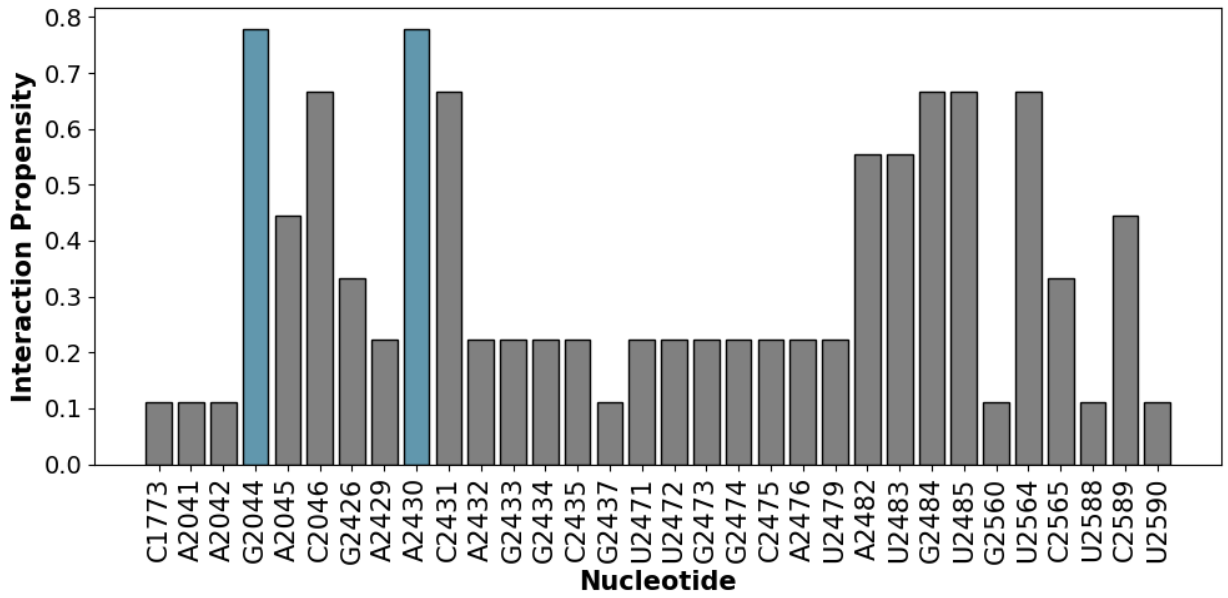


**Figure S27. Derivative 24 nucleotide interaction propensities within PDB ID: 1XBP.** Nucleotides that interacted with this derivative are shown on the x-axis. Propensity is shown in the y-axis. Bars are colored teal when the interaction threshold was over 70% for all poses. Bars are colored grey when the interaction threshold is under 70% and at least one interaction with one pose was observed.

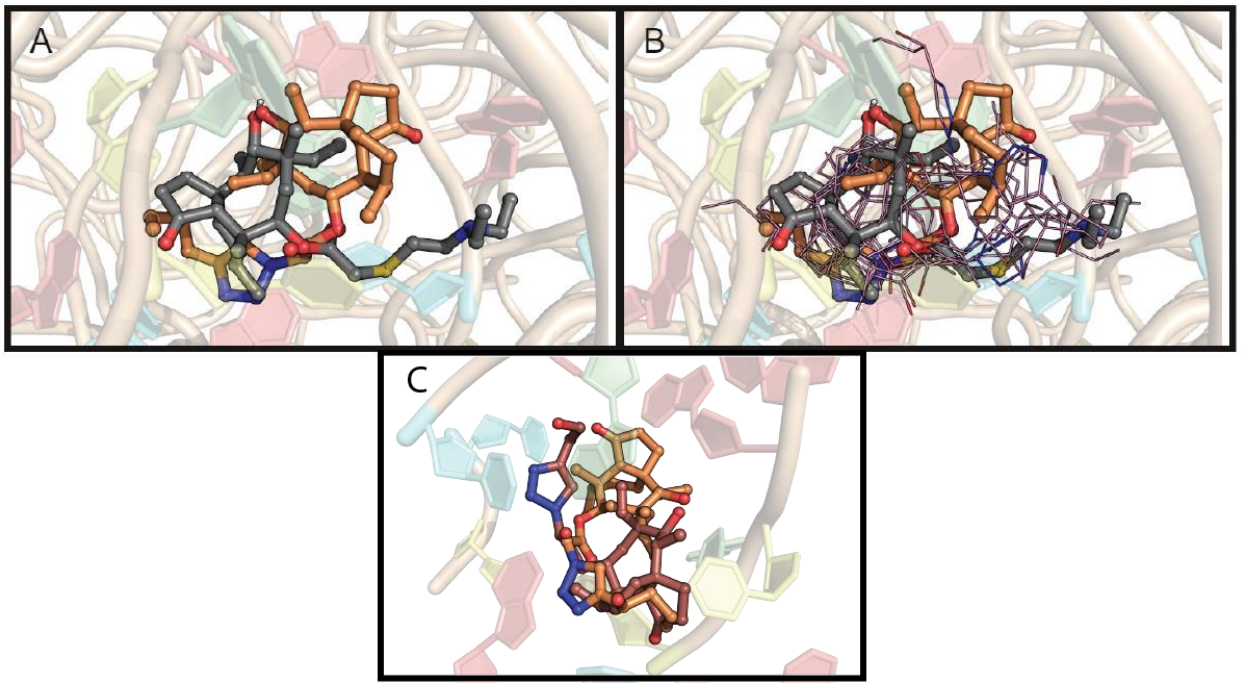


**Figure S28. Docking results of C22 derivative 25-R.** (A) Co-crystalized tiamulin (shown in grey sticks, colored by element) in the *D. radiodurans* 50S ribosome subunit (PDB ID: 1XBP). The lowest energy docked pose of derivative 25-R is shown in orange sticks, colored by element. (B) All poses of docked derivative 25-R (lines) overlaid with the lowest redocked pose of derivative 25-R (orange, colored by element) and tiamulin crystal structure (grey, colored by element) in PDB ID: 1XBP. (C) Lowest energy pose of derivative 25-R (orange, sticks) overlayed with the best performing C22 derivative (derivative 19, brown, sticks) in the tiamulin binding pocket of *D. radiodurans* (PDB ID: 1XBP).

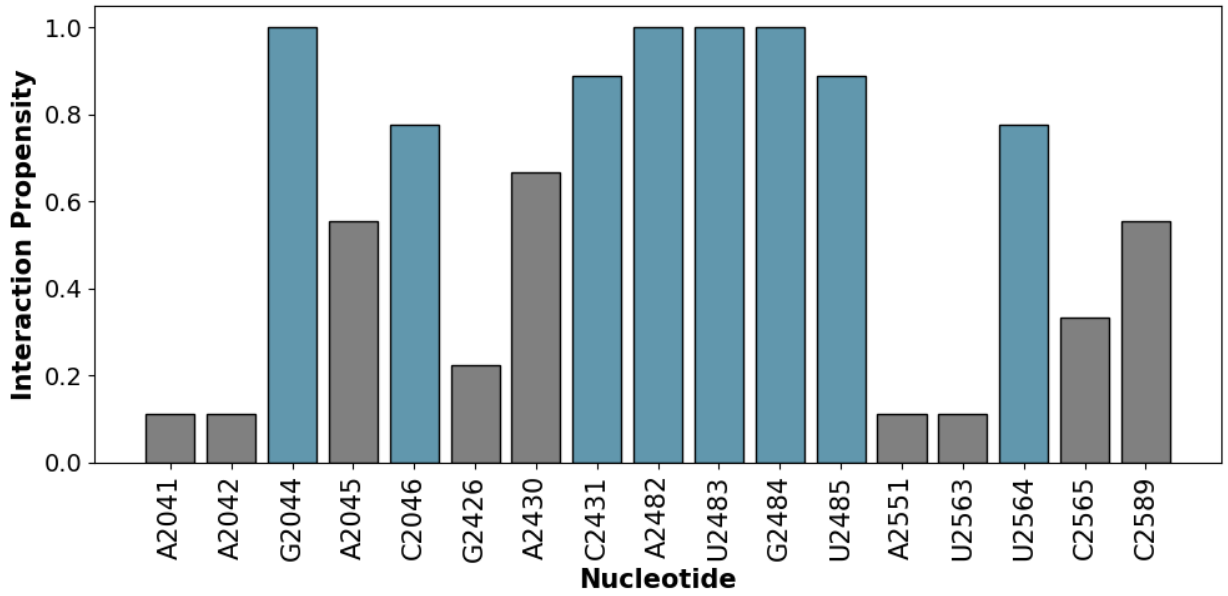


**Figure S29. Derivative 25-R nucleotide interaction propensities within PDB ID: 1XBP.** Nucleotides that interacted with this derivative are shown on the x-axis. Propensity is shown in the y-axis. Bars are colored teal when the interaction threshold was over 70% for all poses. Bars are colored grey when the interaction threshold is under 70% and at least one interaction with one pose was observed.

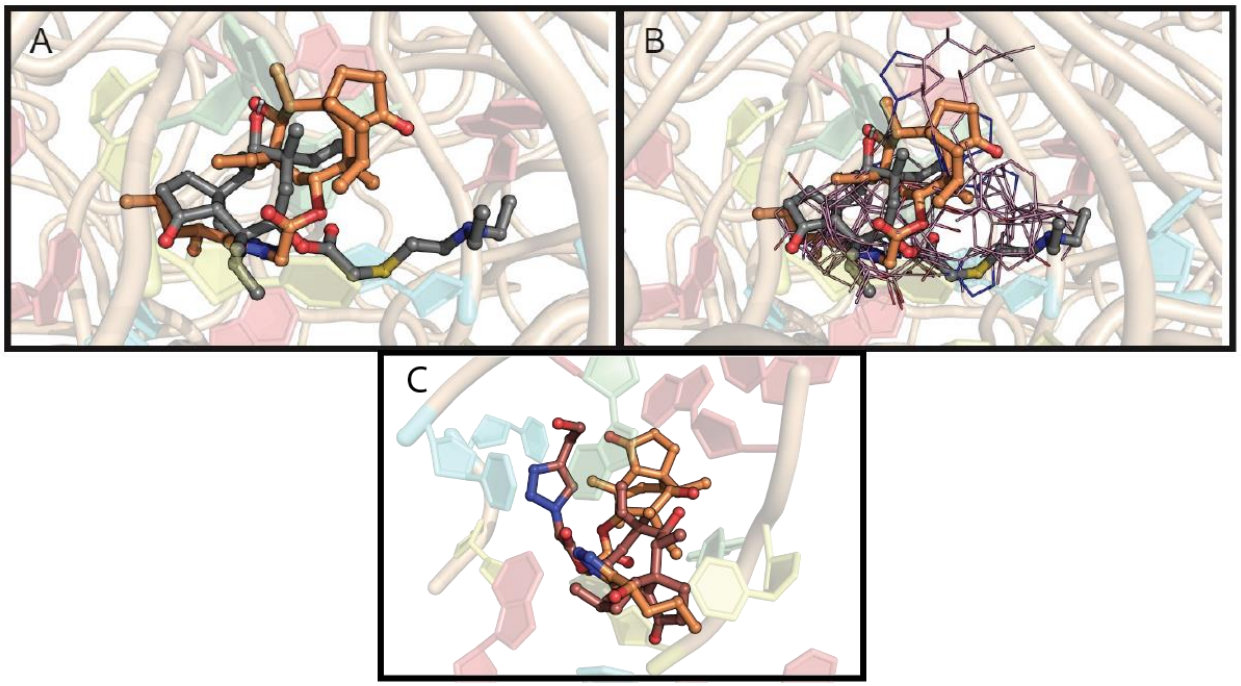


**Figure S30. Docking results of C22 derivative 25-S.** (A) Co-crystalized tiamulin (shown in grey sticks, colored by element) in the *D. radiodurans* 50S ribosome subunit (PDB ID: 1XBP). The lowest energy docked pose of derivative 25-S is shown in orange sticks, colored by element. (B) All poses of docked derivative 25-S (lines) overlaid with the lowest redocked pose of derivative 25-S (orange, colored by element) and tiamulin crystal structure (grey, colored by element) in PDB ID: 1XBP. (C) Lowest energy pose of derivative 25-S (orange, sticks) overlayed with the best performing C22 derivative (derivative 19, brown, sticks) in the tiamulin binding pocket of *D. radiodurans* (PDB ID: 1XBP).

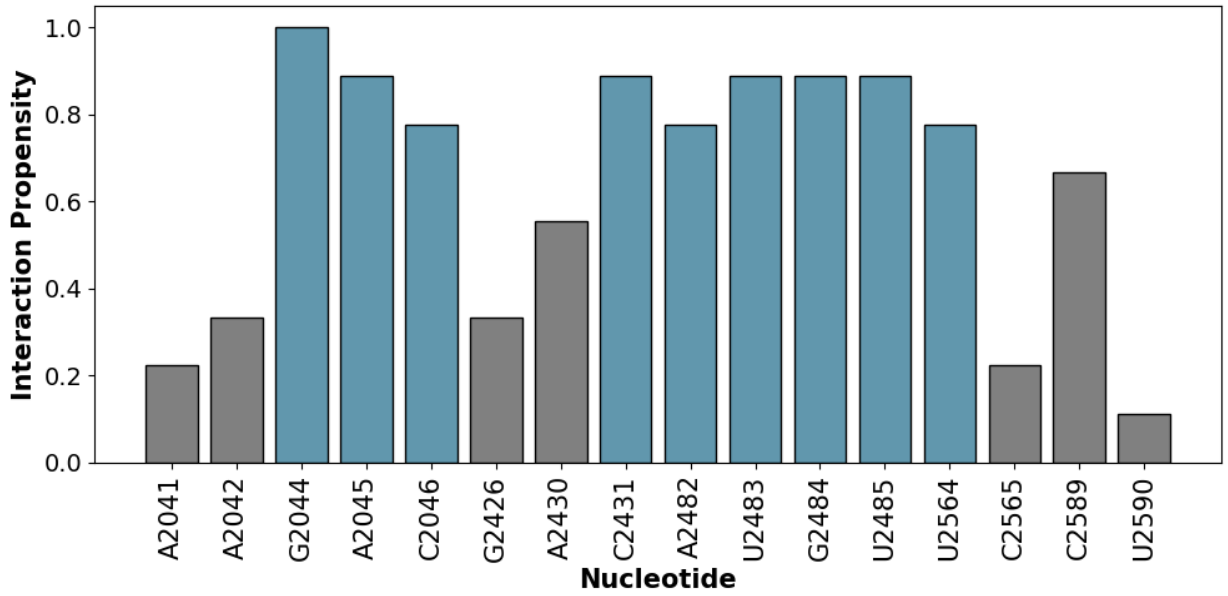


**Figure S31. Derivative 30 nucleotide interaction propensities within PDB ID: 1XBP.** Nucleotides that interacted with this derivative are shown on the x-axis. Propensity is shown in the y-axis. Bars are colored teal when the interaction threshold was over 70% for all poses. Bars are colored grey when the interaction threshold is under 70% and at least one interaction with one pose was observed.

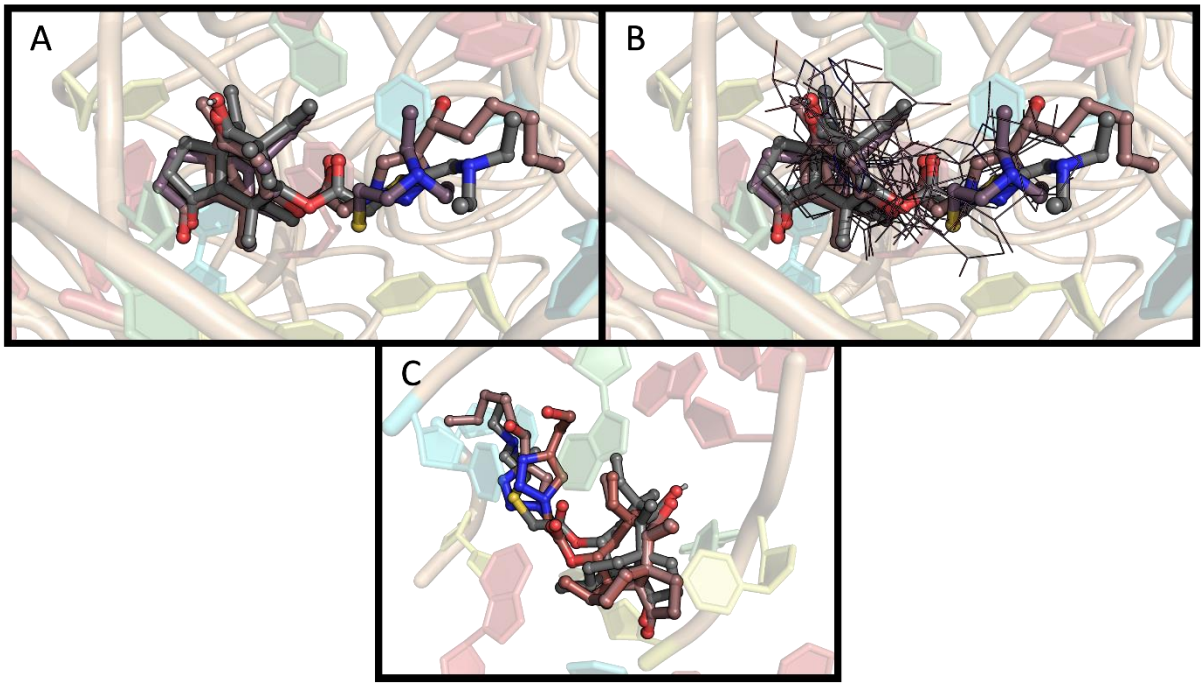


**Figure S32. Docking results of C22 derivative 26-R.** (A) Co-crystalized tiamulin (shown in grey sticks, colored by element) in the *D. radiodurans* 50S ribosome subunit (PDB ID: 1XBP). The lowest energy docked pose of derivative 26-R is shown in olive sticks, colored by element. (B) All poses of docked derivative 26-R (lines) overlaid with the lowest redocked pose of derivative 26-R (purple, colored by element) and tiamulin crystal structure (grey, colored by element) in PDB ID: 1XBP. (C) Lowest energy pose of derivative 26-R (purple, sticks) overlayed with the best performing C22 derivative (derivative 19, brown, sticks) in the tiamulin binding pocket of *D. radiodurans* (PDB ID: 1XBP).

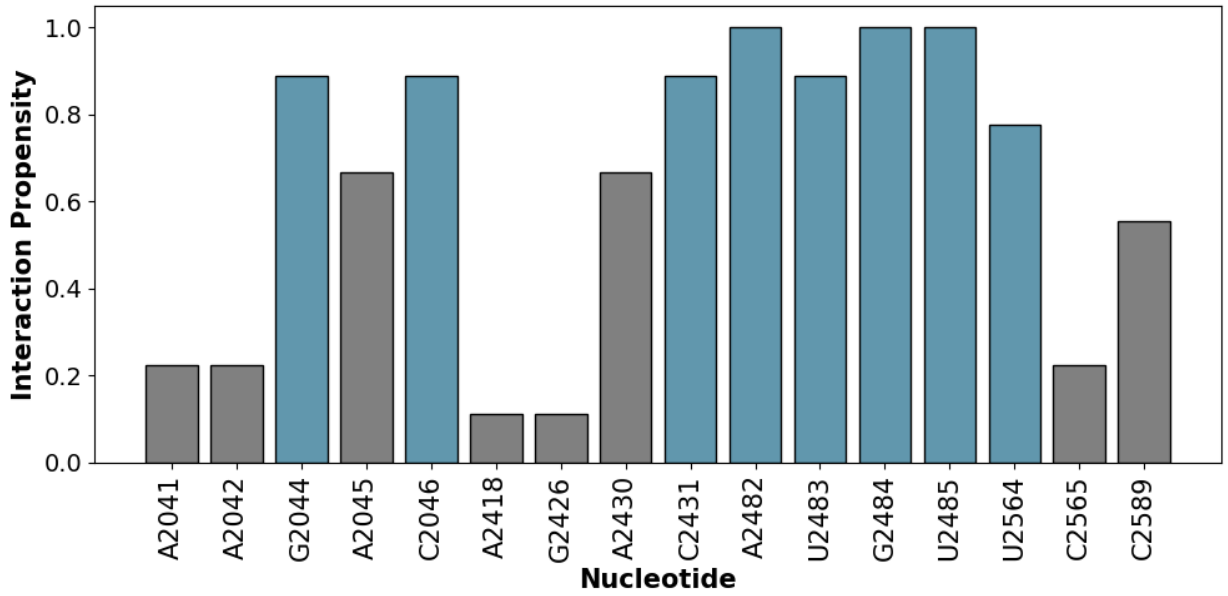


**Figure S33. Derivative 26-R nucleotide interaction propensities within PDB ID: 1XBP.** Nucleotides that interacted with this derivative are shown on the x-axis. Propensity is shown in the y-axis. Bars are colored teal when the interaction threshold was over 70% for all poses. Bars are colored grey when the interaction threshold is under 70% and at least one interaction with one pose was observed.

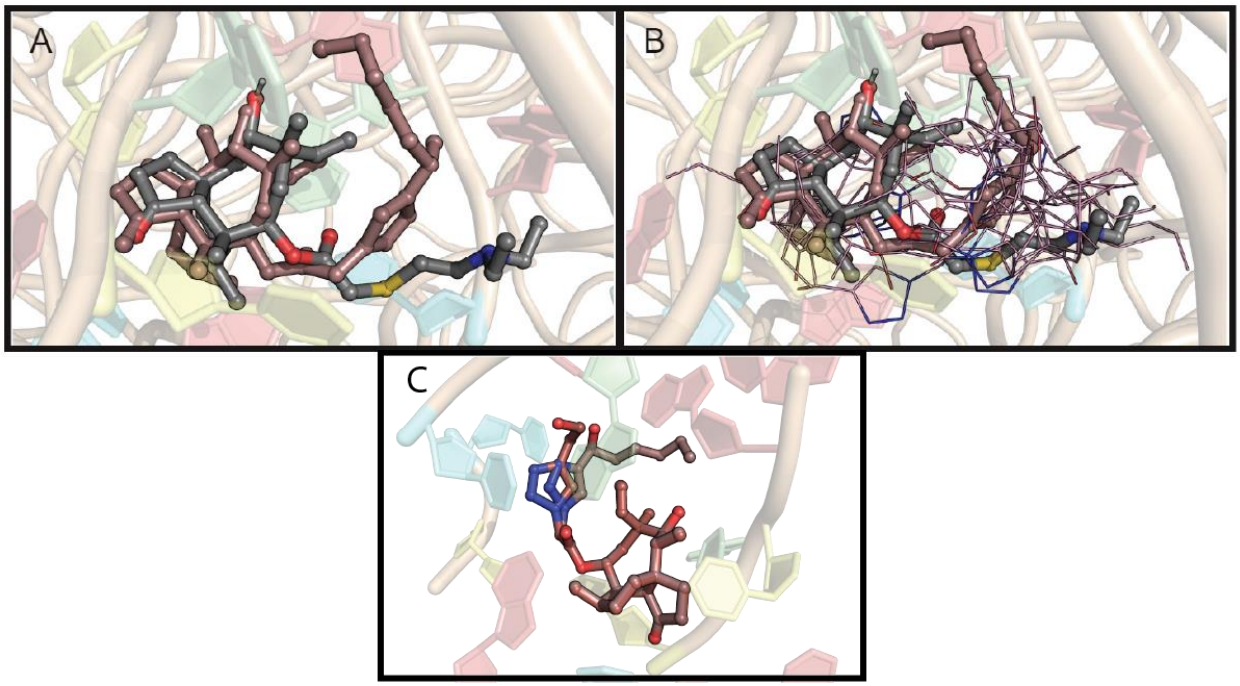


**Figure S34. Docking results of C22 derivative 26-S.** (A) Co-crystalized tiamulin (shown in grey sticks, colored by element) in the *D. radiodurans* 50S ribosome subunit (PDB ID: 1XBP). The lowest energy docked pose of derivative 26-S is shown in copper sticks, colored by element. (B) All poses of docked derivative 26-S (lines) overlaid with the lowest redocked pose of derivative 26-S (copper, colored by element) and tiamulin crystal structure (grey, colored by element) in PDB ID: 1XBP. (C) Lowest energy pose of derivative 26-S (copper, sticks) overlayed with the best performing C22 derivative (derivative 19, brown, sticks) in the tiamulin binding pocket of *D. radiodurans* (PDB ID: 1XBP).

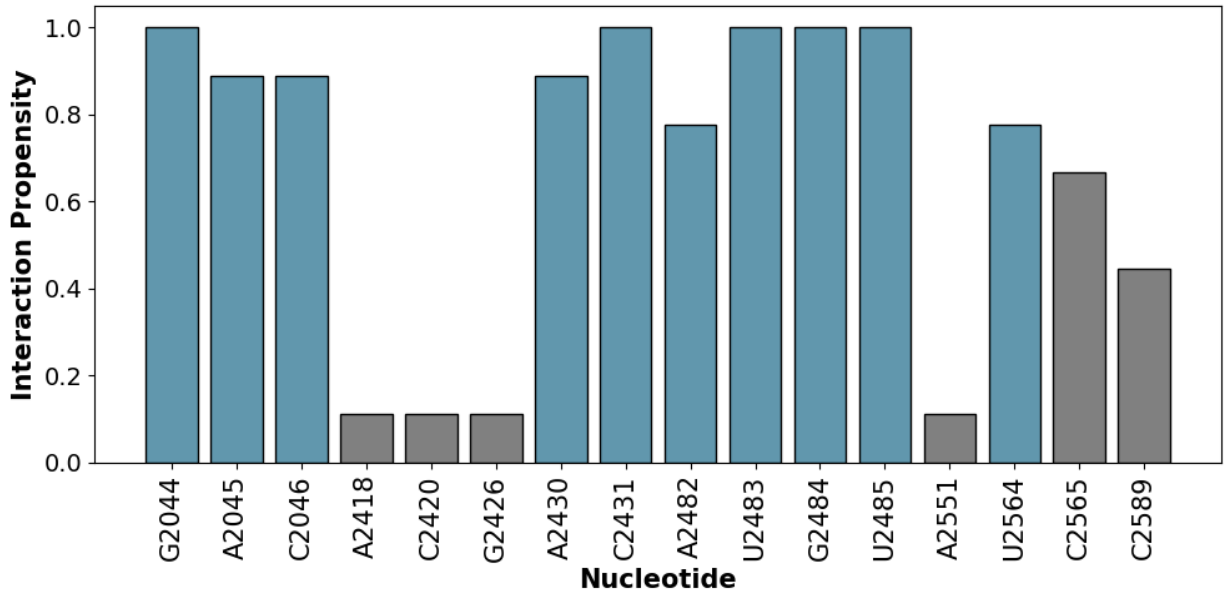


**Figure S35. Derivative 26-S nucleotide interaction propensities within PDB ID: 1XBP.** Nucleotides that interacted with this derivative are shown on the x-axis. Propensity is shown in the y-axis. Bars are colored teal when the interaction threshold was over 70% for all poses. Bars are colored grey when the interaction threshold is under 70% and at least one interaction with one pose was observed.

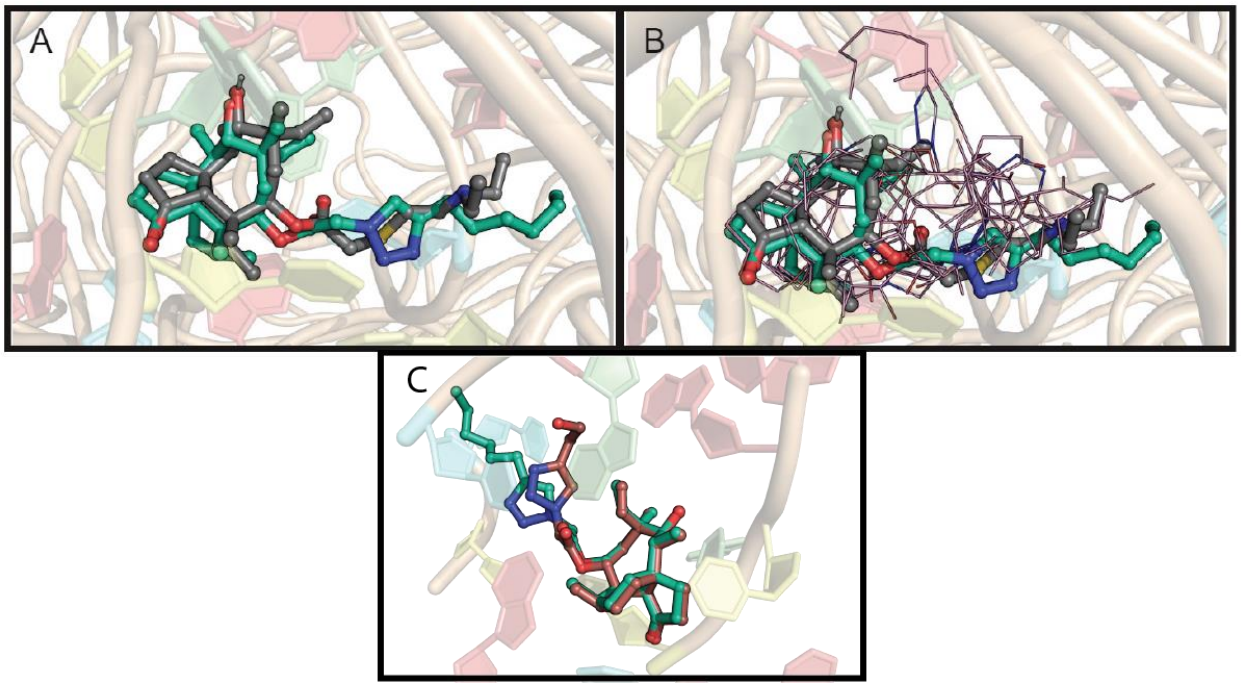


**Figure S36. Docking results of C22 derivative 27.** (A) Co-crystalized tiamulin (shown in grey sticks, colored by element) in the *D. radiodurans* 50S ribosome subunit (PDB ID: 1XBP). The lowest energy docked pose of derivative 27 is shown in cyan sticks, colored by element. (B) All poses of docked derivative 27 (lines) overlaid with the lowest redocked pose of derivative 27 (cyan, colored by element) and tiamulin crystal structure (grey, colored by element) in PDB ID: 1XBP. (C) Lowest energy pose of derivative 27 (cyan, sticks) overlayed with the best performing C22 derivative (derivative 19, brown, sticks) in the tiamulin binding pocket of *D. radiodurans* (PDB ID: 1XBP).

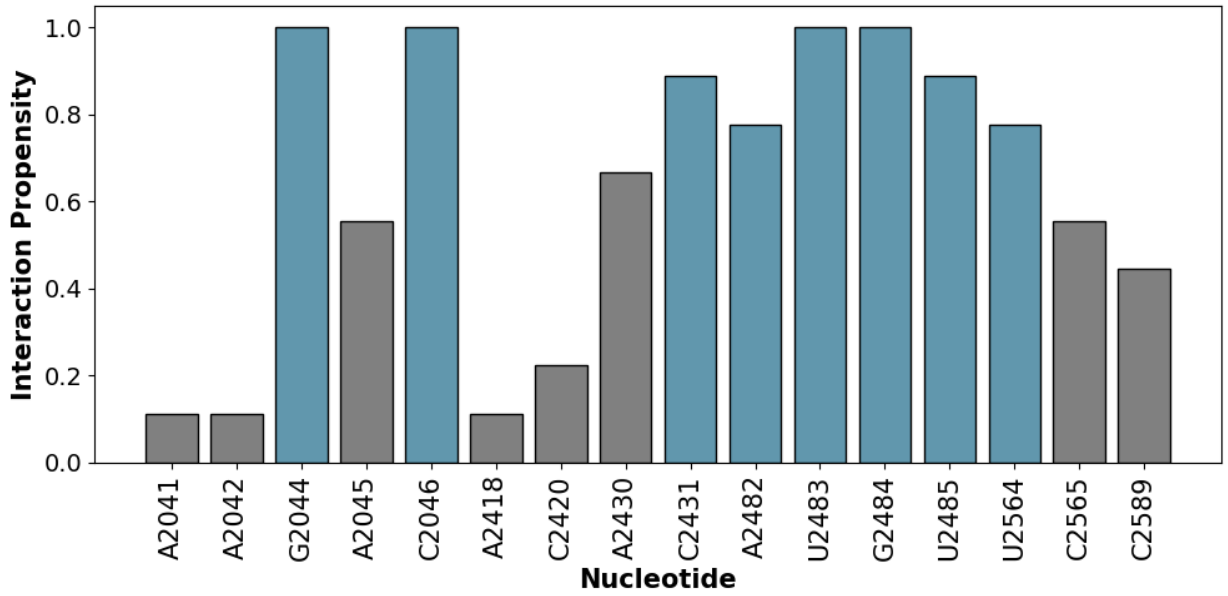


**Figure S37. Derivative 27 nucleotide interaction propensities within PDB ID: 1XBP.** Nucleotides that interacted with this derivative are shown on the x-axis. Propensity is shown in the y-axis. Bars are colored teal when the interaction threshold was over 70% for all poses. Bars are colored grey when the interaction threshold is under 70% and at least one interaction with one pose was observed.

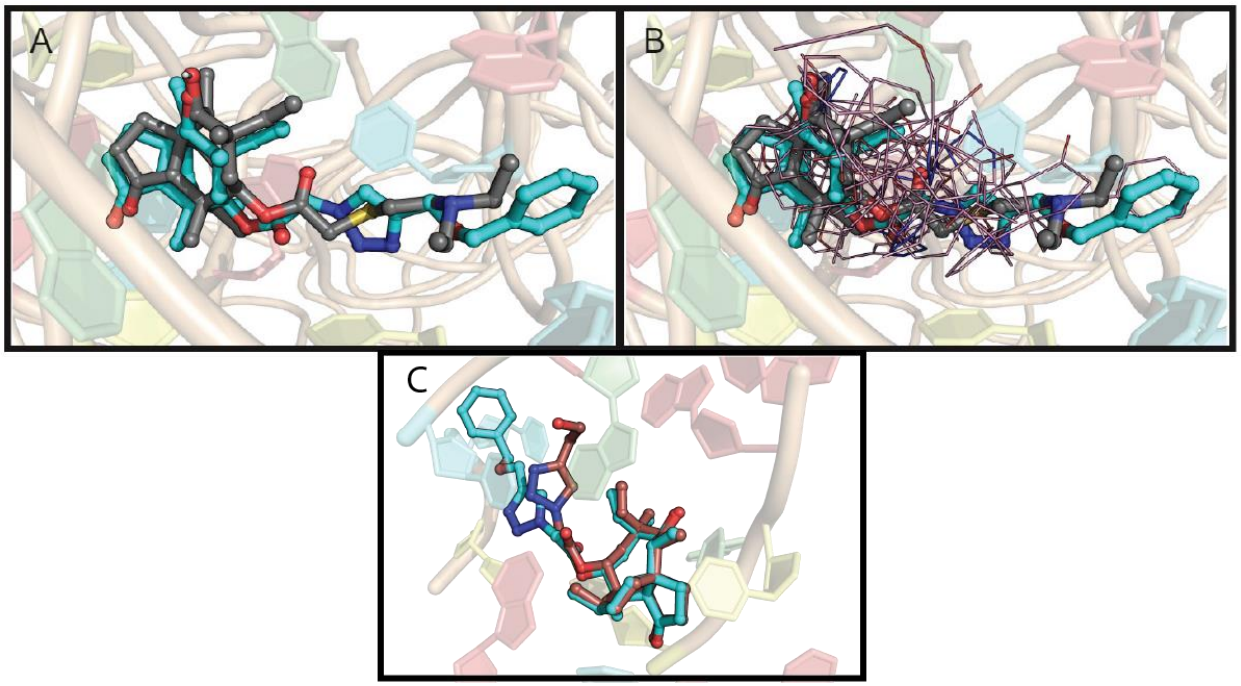


**Figure S38. Docking results of C22 derivative 28.** (A) Co-crystalized tiamulin (shown in grey sticks, colored by element) in the *D. radiodurans* 50S ribosome subunit (PDB ID: 1XBP). The lowest energy docked pose of derivative 28 is shown in light blue sticks, colored by element. (B) All poses of docked derivative 28 (lines) overlaid with the lowest redocked pose of derivative 28 (light blue, colored by element) and tiamulin crystal structure (grey, colored by element) in PDB ID: 1XBP. (C) Lowest energy pose of derivative 28 (light blue, sticks) overlayed with the best performing C22 derivative (derivative 19, brown, sticks) in the tiamulin binding pocket of *D. radiodurans* (PDB ID: 1XBP).

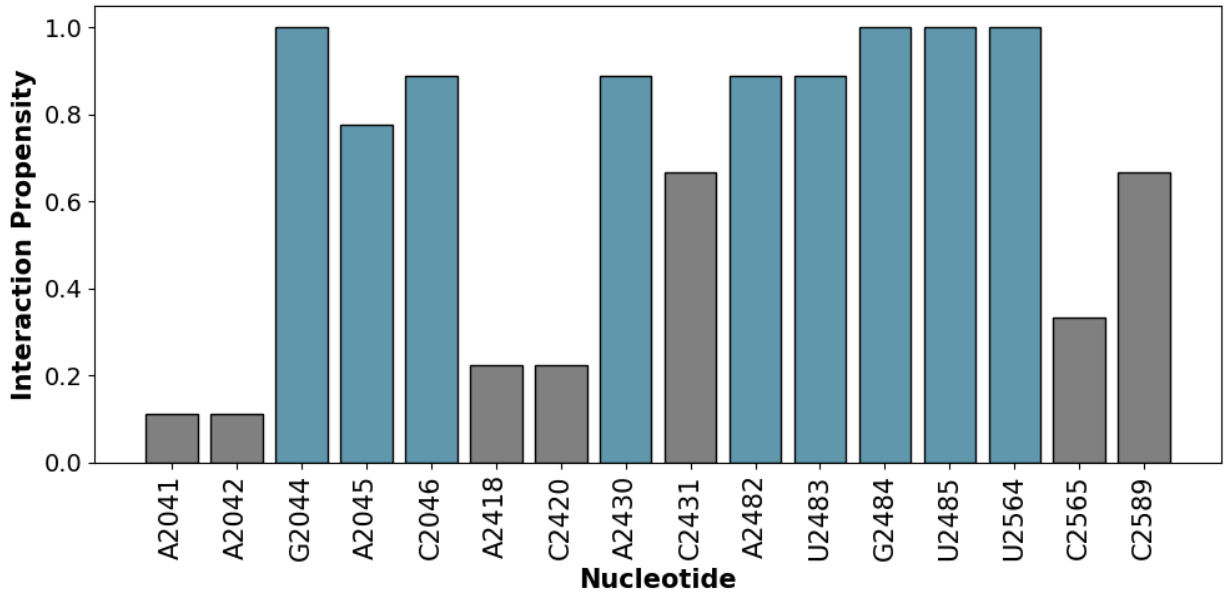


**Figure S39. Derivative 28 nucleotide interaction propensities within PDB ID: 1XBP.** Nucleotides that interacted with this derivative are shown on the x-axis. Propensity is shown in the y-axis. Bars are colored teal when the interaction threshold was over 70% for all poses. Bars are colored grey when the interaction threshold is under 70% and at least one interaction with one pose was observed.

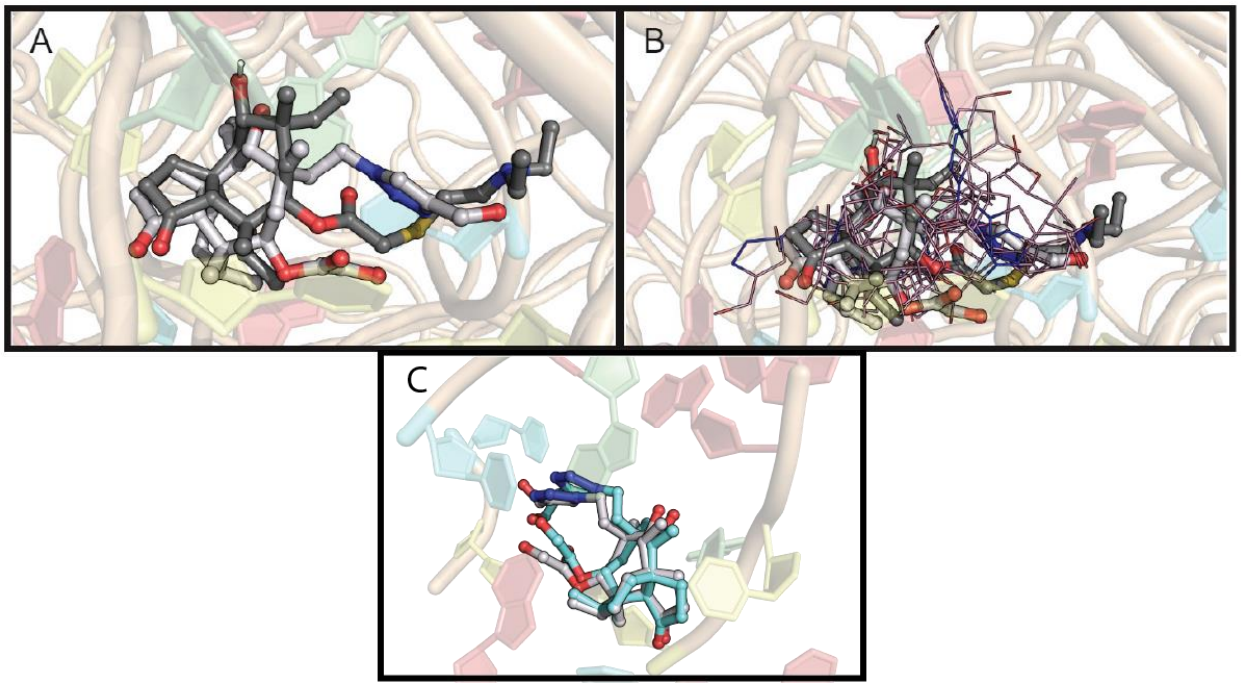


**Figure S40. Docking results of C20 derivative 31.** (A) Co-crystalized tiamulin (shown in grey sticks, colored by element) in the *D. radiodurans* 50S ribosome subunit (PDB ID: 1XBP). The lowest energy docked pose of derivative 31 is shown in white sticks, colored by element. (B) All poses of docked derivative 31 (lines) overlaid with the lowest redocked pose of derivative 31 (white, colored by element) and tiamulin crystal structure (grey, colored by element) in PDB ID: 1XBP. (C) Lowest energy pose of derivative 31 (white, sticks) overlayed with the best performing C22 derivative (derivative 19, brown, sticks) in the tiamulin binding pocket of *D. radiodurans* (PDB ID: 1XBP).

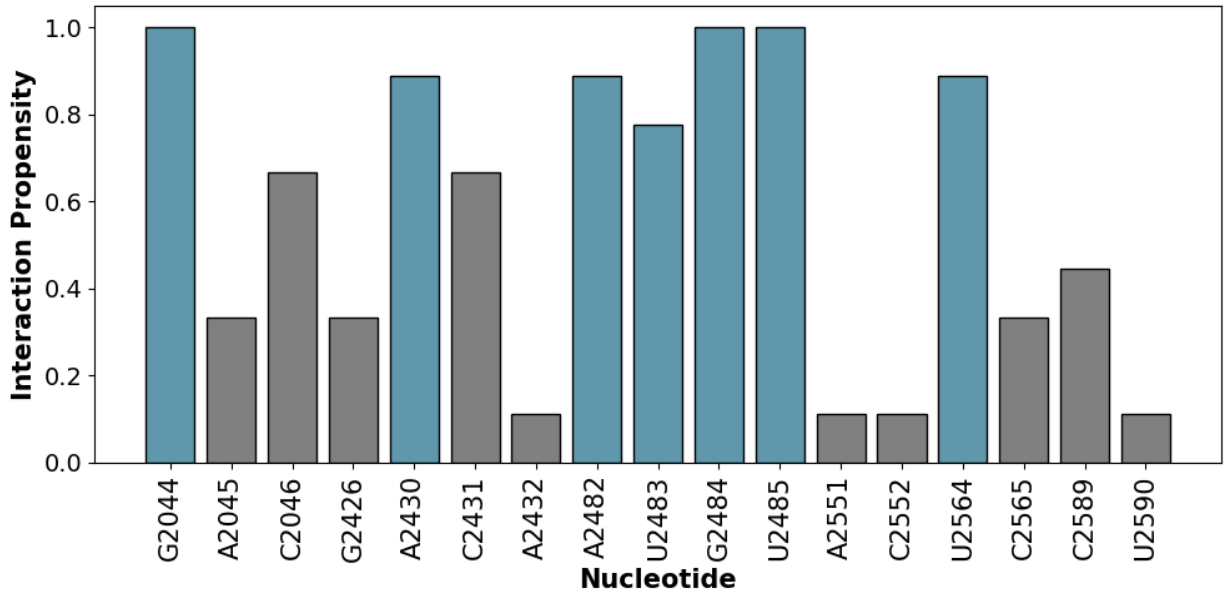


**Figure S41. Derivative 31 nucleotide interaction propensities within PDB ID: 1XBP.** Nucleotides that interacted with this derivative are shown on the x-axis. Propensity is shown in the y-axis. Bars are colored teal when the interaction threshold was over 70% for all poses. Bars are colored grey when the interaction threshold is under 70% and at least one interaction with one pose was observed.

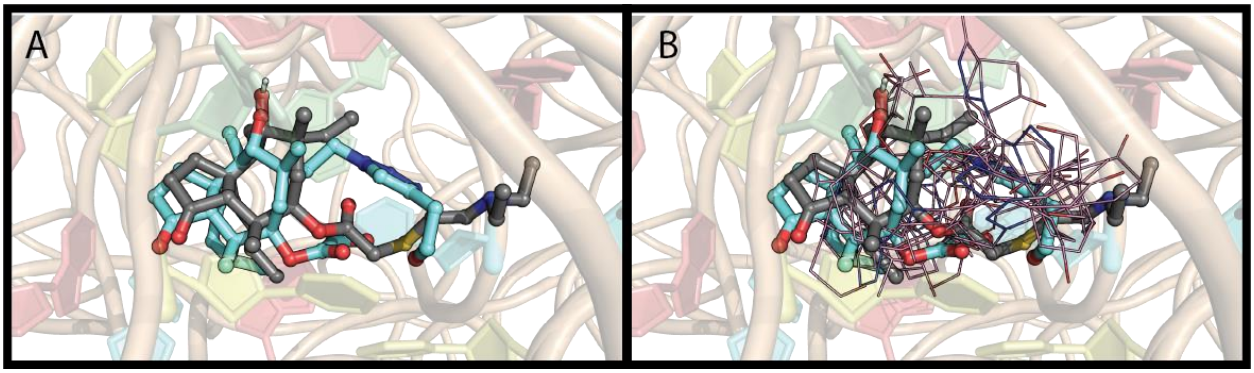


**Figure S42. Docking results of C20 derivative 32.** (A) Co-crystalized tiamulin (shown in grey sticks, colored by element) in the *D. radiodurans* 50S ribosome subunit (PDB ID: 1XBP). The lowest energy docked pose of derivative 32 is shown in olive sticks, colored by element. (B) All poses of docked derivative 32 (lines) overlaid with the lowest redocked pose of derivative 32 (olive, colored by element) and tiamulin crystal structure (grey, colored by element) in PDB ID: 1XBP. (C) Lowest energy pose of derivative 32 (olive, sticks) overlayed with the best performing C22 derivative (derivative 19, brown, sticks) in the tiamulin binding pocket of *D. radiodurans* (PDB ID: 1XBP).

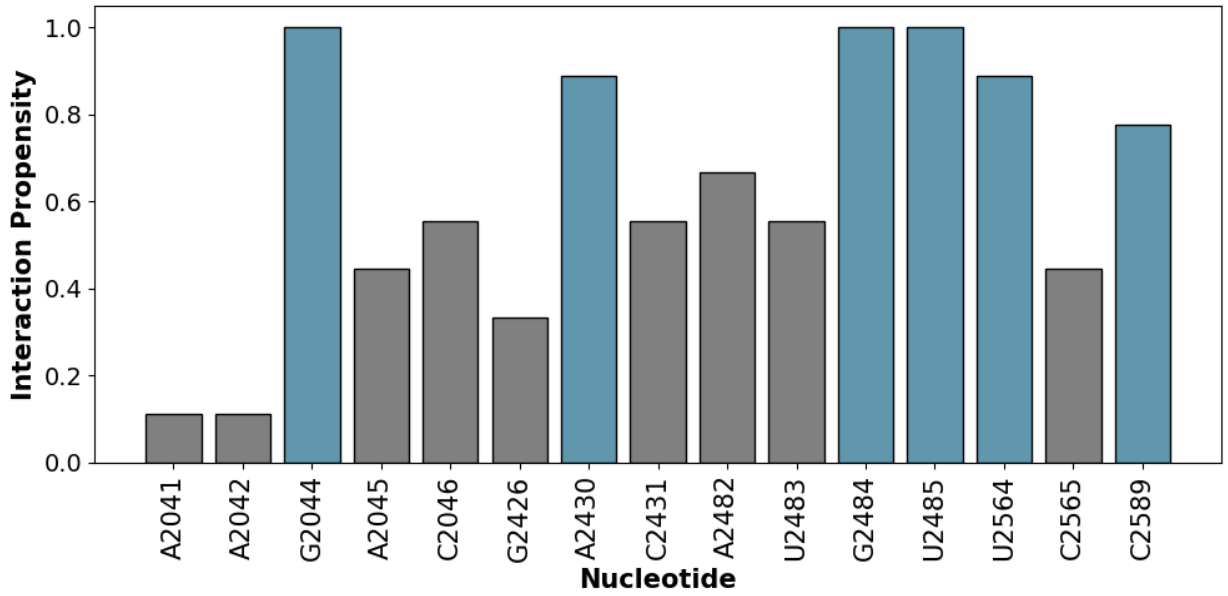


**Figure S43. Derivative 32 nucleotide interaction propensities within PDB ID: 1XBP.** Nucleotides that interacted with this derivative are shown on the x-axis. Propensity is shown in the y-axis. Bars are colored teal when the interaction threshold was over 70% for all poses. Bars are colored grey when the interaction threshold is under 70% and at least one interaction with one pose was observed.

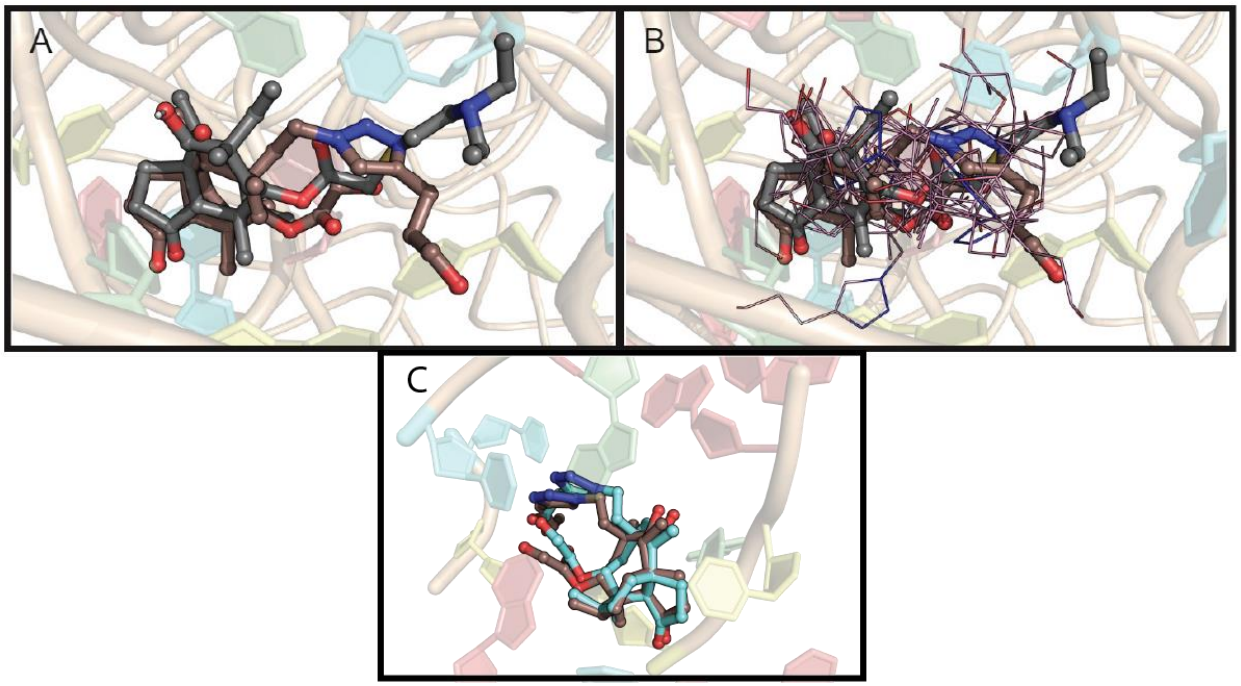


**Figure S44. Docking results of C22 derivative 33.** (A) Co-crystalized tiamulin (shown in grey sticks, colored by element) in the *D. radiodurans* 50S ribosome subunit (PDB ID: 1XBP). The lowest energy docked pose of derivative 33 is shown in olive sticks, colored by element. (B) All poses of docked derivative 33 (lines) overlaid with the lowest redocked pose of derivative 33 (olive, colored by element) and tiamulin crystal structure (grey, colored by element) in PDB ID: 1XBP. (C) Lowest energy pose of derivative 33 (olive, sticks) overlayed with the best performing C22 derivative (derivative 32, aquamarine, sticks) in the tiamulin binding pocket of *D. radiodurans* (PDB ID: 1XBP).

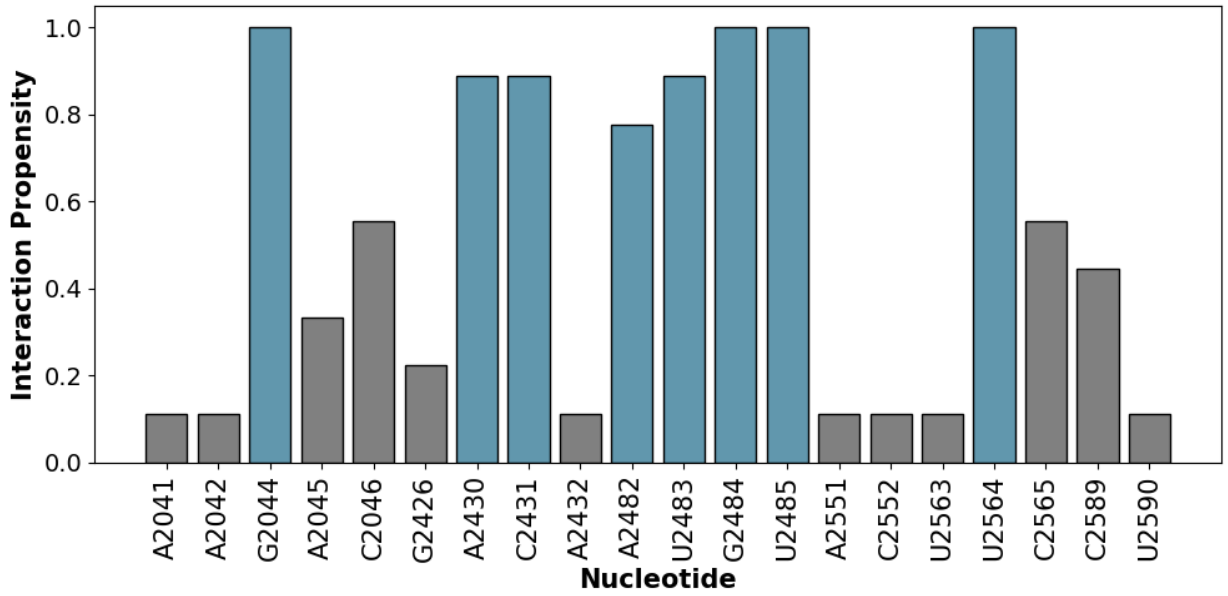


**Figure S45. Derivative 33 nucleotide interaction propensities within PDB ID: 1XBP.** Nucleotides that interacted with this derivative are shown on the x-axis. Propensity is shown in the y-axis. Bars are colored teal when the interaction threshold was over 70% for all poses. Bars are colored grey when the interaction threshold is under 70% and at least one interaction with one pose was observed.

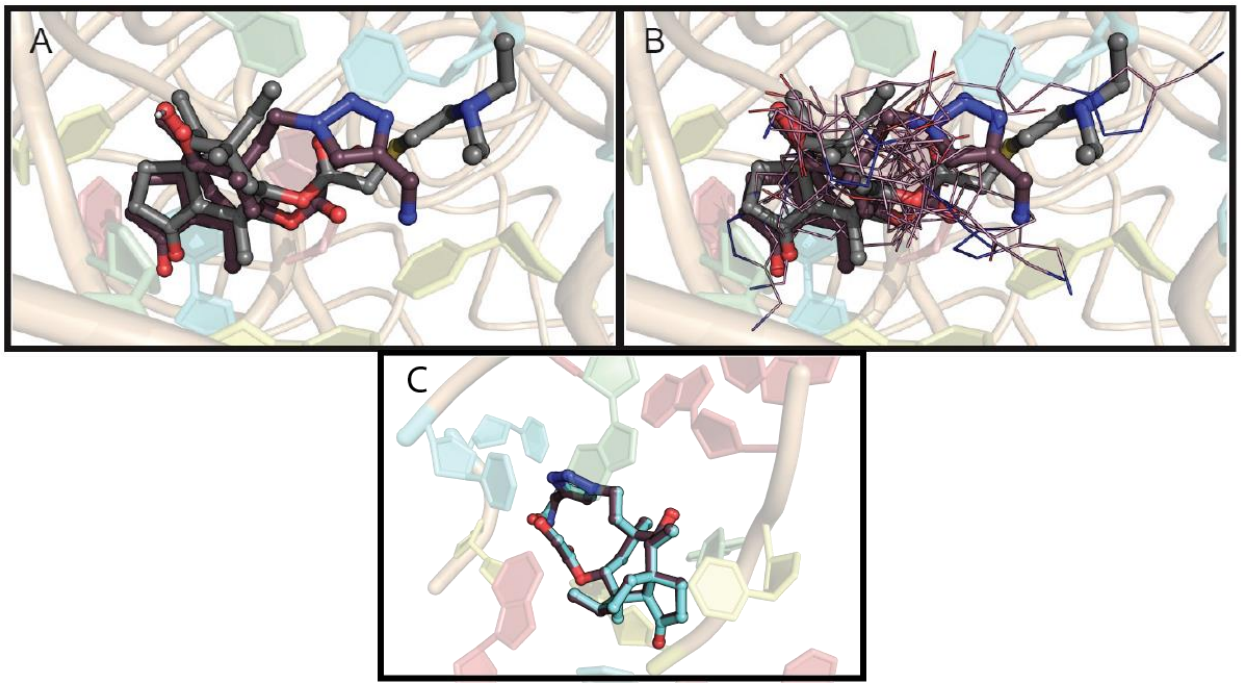


**Figure S46. Docking results of C22 derivative 34.** (A) Co-crystalized tiamulin (shown in grey sticks, colored by element) in the *D. radiodurans* 50S ribosome subunit (PDB ID: 1XBP). The lowest energy docked pose of derivative 34 is shown in olive sticks, colored by element. (B) All poses of docked derivative 34 (lines) overlaid with the lowest redocked pose of derivative 34 (olive, colored by element) and tiamulin crystal structure (grey, colored by element) in PDB ID: 1XBP. (C) Lowest energy pose of derivative 34 (olive, sticks) overlayed with the best performing C22 derivative (derivative 32, aquamarine, sticks) in the tiamulin binding pocket of *D. radiodurans* (PDB ID: 1XBP).

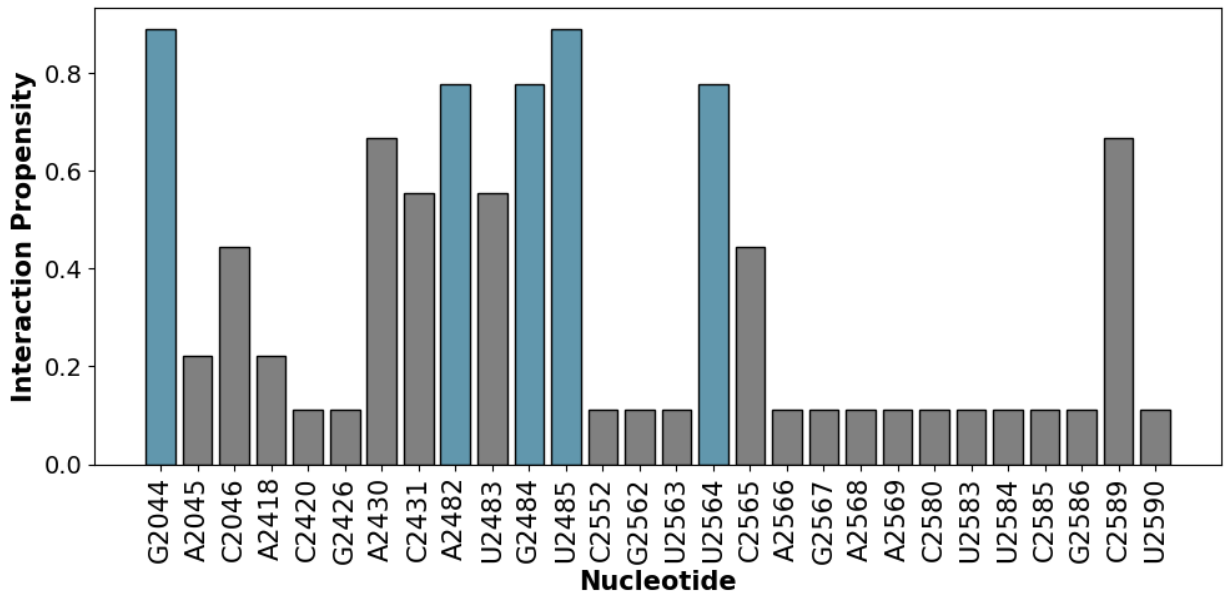


**Figure S47. Derivative 34 nucleotide interaction propensities within PDB ID: 1XBP.** Nucleotides that interacted with this derivative are shown on the x-axis. Propensity is shown in the y-axis. Bars are colored teal when the interaction threshold was over 70% for all poses. Bars are colored grey when the interaction threshold is under 70% and at least one interaction with one pose was observed.

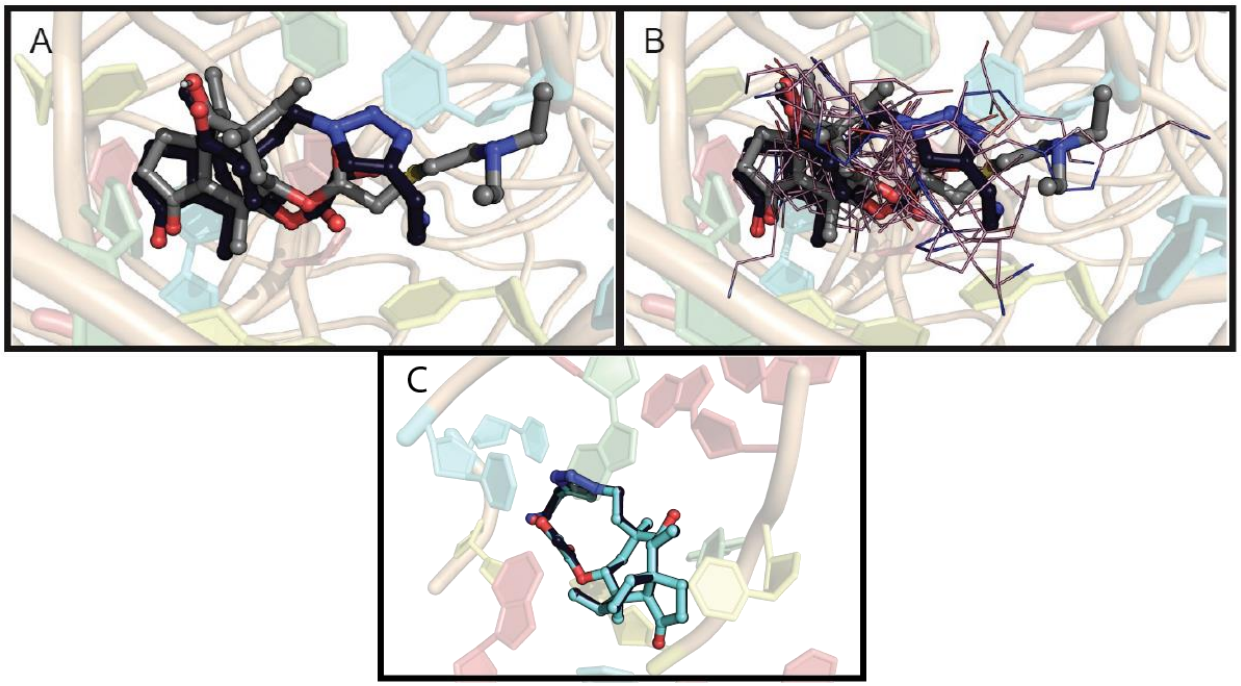


**Figure S48. Docking results of C22 derivative 35.** (A) Co-crystalized tiamulin (shown in grey sticks, colored by element) in the *D. radiodurans* 50S ribosome subunit (PDB ID: 1XBP). The lowest energy docked pose of derivative 35 is shown in black sticks, colored by element. (B) All poses of docked derivative 35 (lines) overlaid with the lowest redocked pose of derivative 35 (black, colored by element) and tiamulin crystal structure (grey, colored by element) in PDB ID: 1XBP. (C) Lowest energy pose of derivative 35 (black, sticks) overlayed with the best performing C22 derivative (derivative 32, aquamarine, sticks) in the tiamulin binding pocket of *D. radiodurans* (PDB ID: 1XBP).

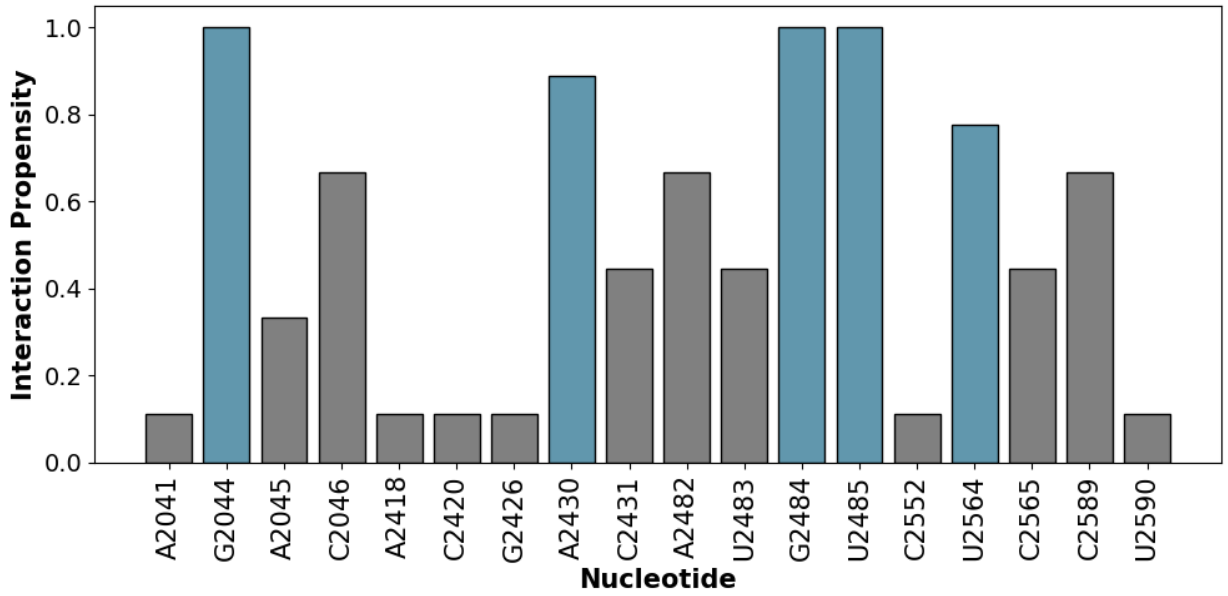


**Figure S49. Derivative 35 nucleotide interaction propensities within PDB ID: 1XBP.** Nucleotides that interacted with this derivative are shown on the x-axis. Propensity is shown in the y-axis. Bars are colored teal when the interaction threshold was over 70% for all poses. Bars are colored grey when the interaction threshold is under 70% and at least one interaction with one pose was observed.

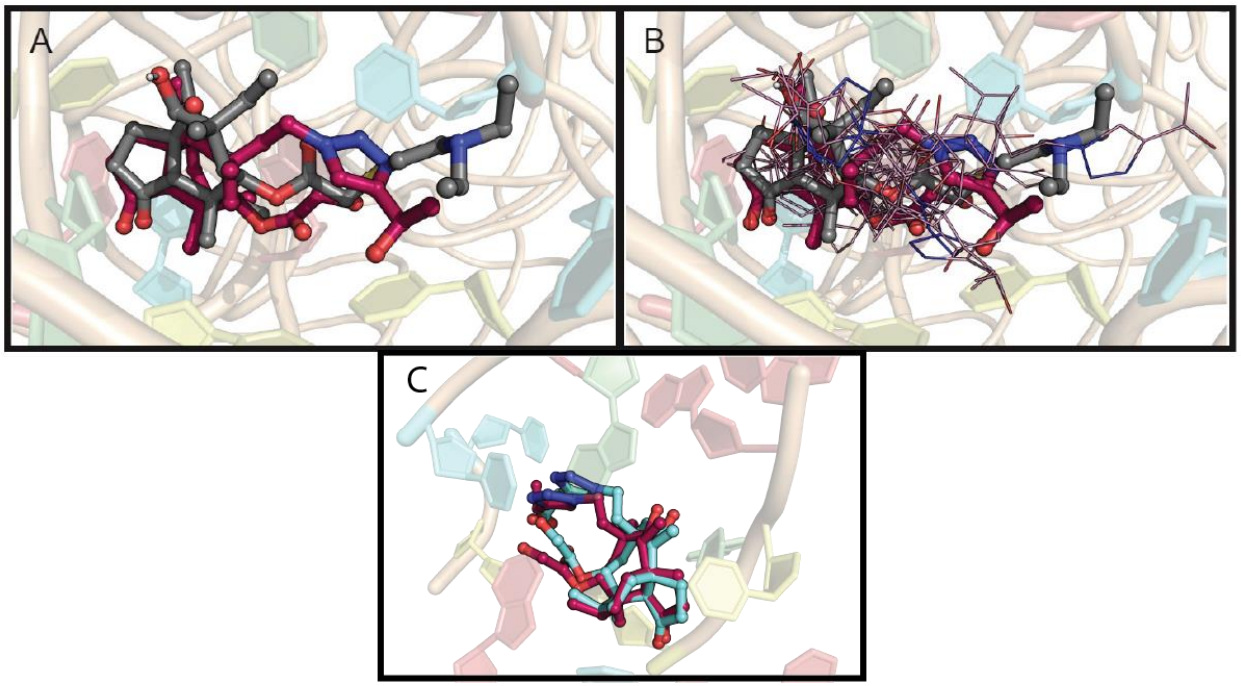


**Figure S50. Docking results of C22 derivative 36-R.** (A) Co-crystalized tiamulin (shown in grey sticks, colored by element) in the *D. radiodurans* 50S ribosome subunit (PDB ID: 1XBP). The lowest energy docked pose of derivative 36-R is shown in red sticks, colored by element. (B) All poses of docked derivative 36-R (lines) overlaid with the lowest redocked pose of derivative 36-R (red, colored by element) and tiamulin crystal structure (grey, colored by element) in PDB ID: 1XBP. (C) Lowest energy pose of derivative 36-R (red, sticks) overlayed with the best performing C22 derivative (derivative 32, aquamarine, sticks) in the tiamulin binding pocket of *D. radiodurans* (PDB ID: 1XBP).

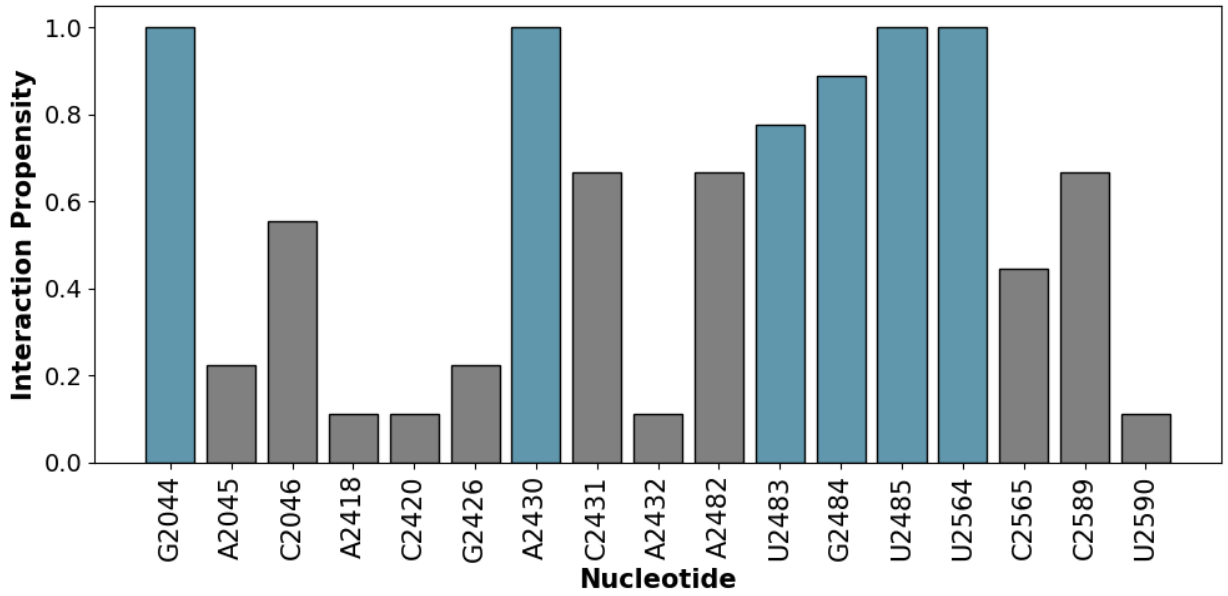


**Figure S51. Derivative 36-R nucleotide interaction propensities within PDB ID: 1XBP.** Nucleotides that interacted with this derivative are shown on the x-axis. Propensity is shown in the y-axis. Bars are colored teal when the interaction threshold was over 70% for all poses. Bars are colored grey when the interaction threshold is under 70% and at least one interaction with one pose was observed.

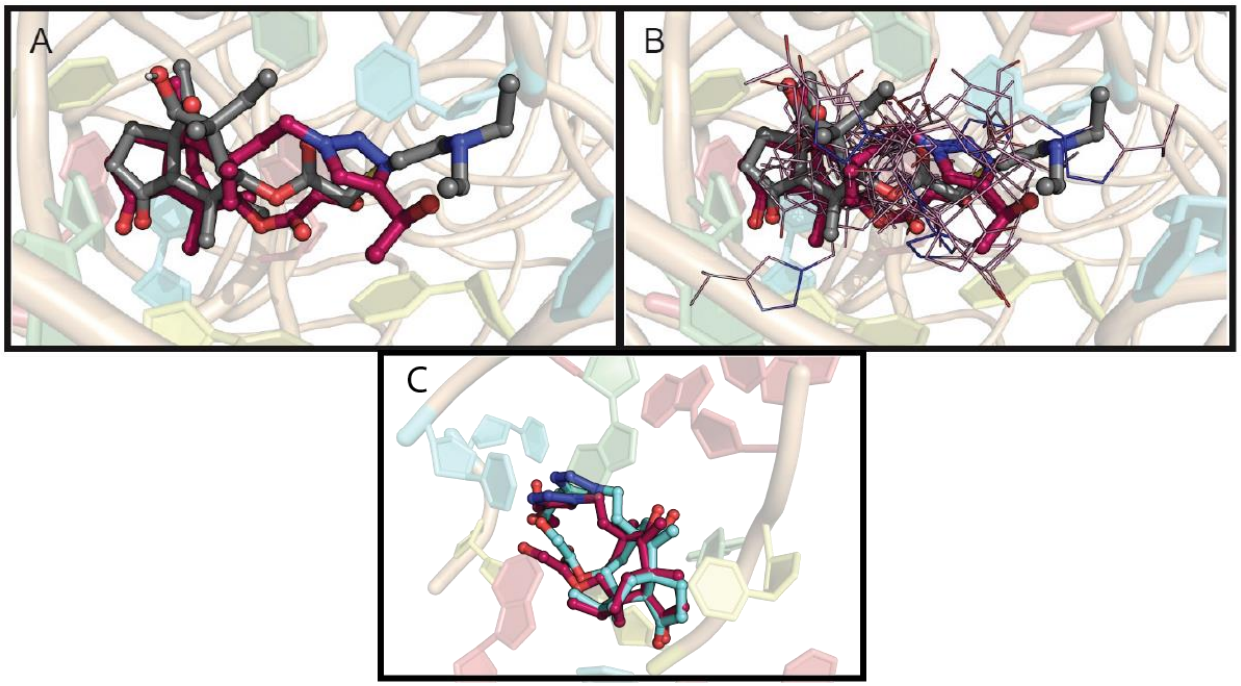


**Figure S52. Docking results of C22 derivative 36-S.** (A) Co-crystalized tiamulin (shown in grey sticks, colored by element) in the *D. radiodurans* 50S ribosome subunit (PDB ID: 1XBP). The lowest energy docked pose of derivative 36-S is shown in red sticks, colored by element. (B) All poses of docked derivative 36-S (lines) overlaid with the lowest redocked pose of derivative 36-S (red, colored by element) and tiamulin crystal structure (grey, colored by element) in PDB ID: 1XBP. (C) Lowest energy pose of derivative 36-S (red, sticks) overlayed with the best performing C22 derivative (derivative 32, aquamarine, sticks) in the tiamulin binding pocket of *D. radiodurans* (PDB ID: 1XBP).

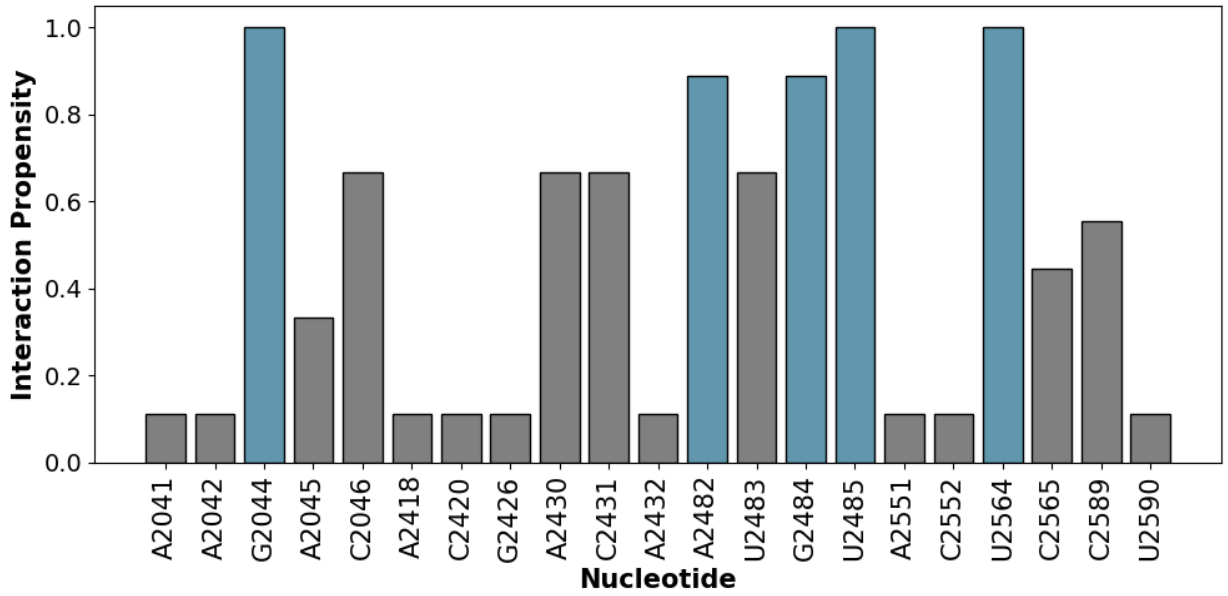


**Figure S53. Derivative 36-S nucleotide interaction propensities within PDB ID: 1XBP.** Nucleotides that interacted with this derivative are shown on the x-axis. Propensity is shown in the y-axis. Bars are colored teal when the interaction threshold was over 70% for all poses. Bars are colored grey when the interaction threshold is under 70% and at least one interaction with one pose was observed.

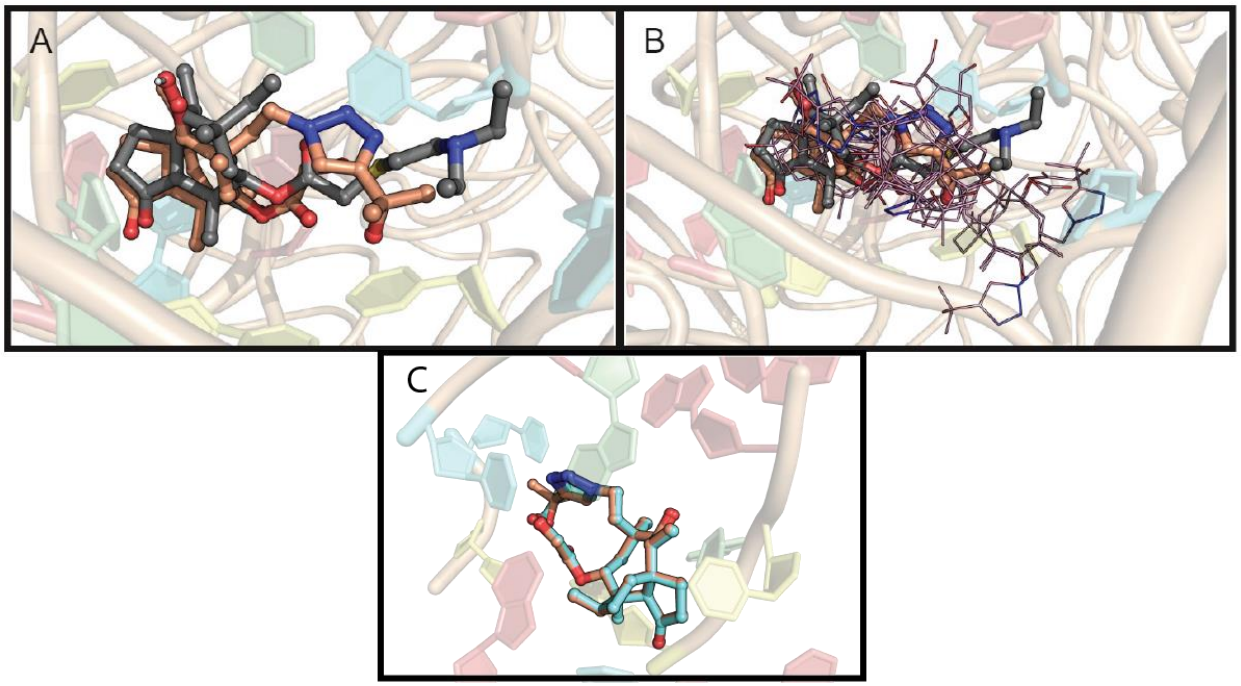


**Figure S54. Docking results of C22 derivative 37.** (A) Co-crystalized tiamulin (shown in grey sticks, colored by element) in the *D. radiodurans* 50S ribosome subunit (PDB ID: 1XBP). The lowest energy docked pose of derivative 37 is shown in light orange sticks, colored by element. (B) All poses of docked derivative 37 (lines) overlaid with the lowest redocked pose of derivative 37 (light orange, colored by element) and tiamulin crystal structure (grey, colored by element) in PDB ID: 1XBP. (C) Lowest energy pose of derivative 37 (light orange, sticks) overlayed with the best performing C22 derivative (derivative 32, aquamarine, sticks) in the tiamulin binding pocket of *D. radiodurans* (PDB ID: 1XBP).

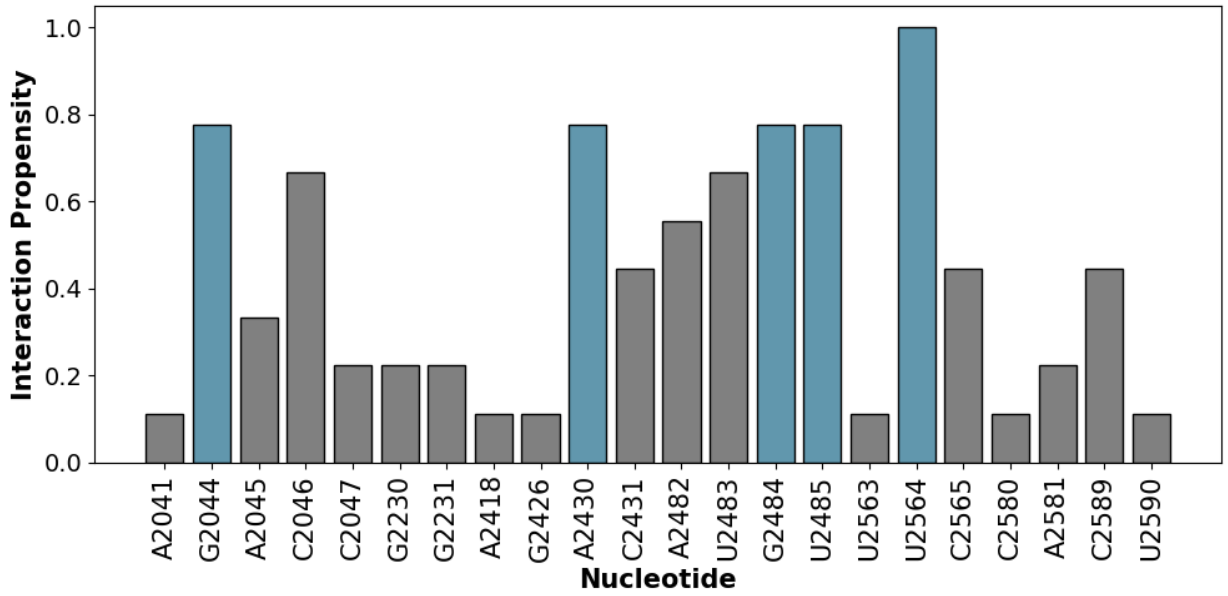


**Figure S55. Derivative 37 nucleotide interaction propensities within PDB ID: 1XBP.** Nucleotides that interacted with this derivative are shown on the x-axis. Propensity is shown in the y-axis. Bars are colored teal when the interaction threshold was over 70% for all poses. Bars are colored grey when the interaction threshold is under 70% and at least one interaction with one pose was observed.

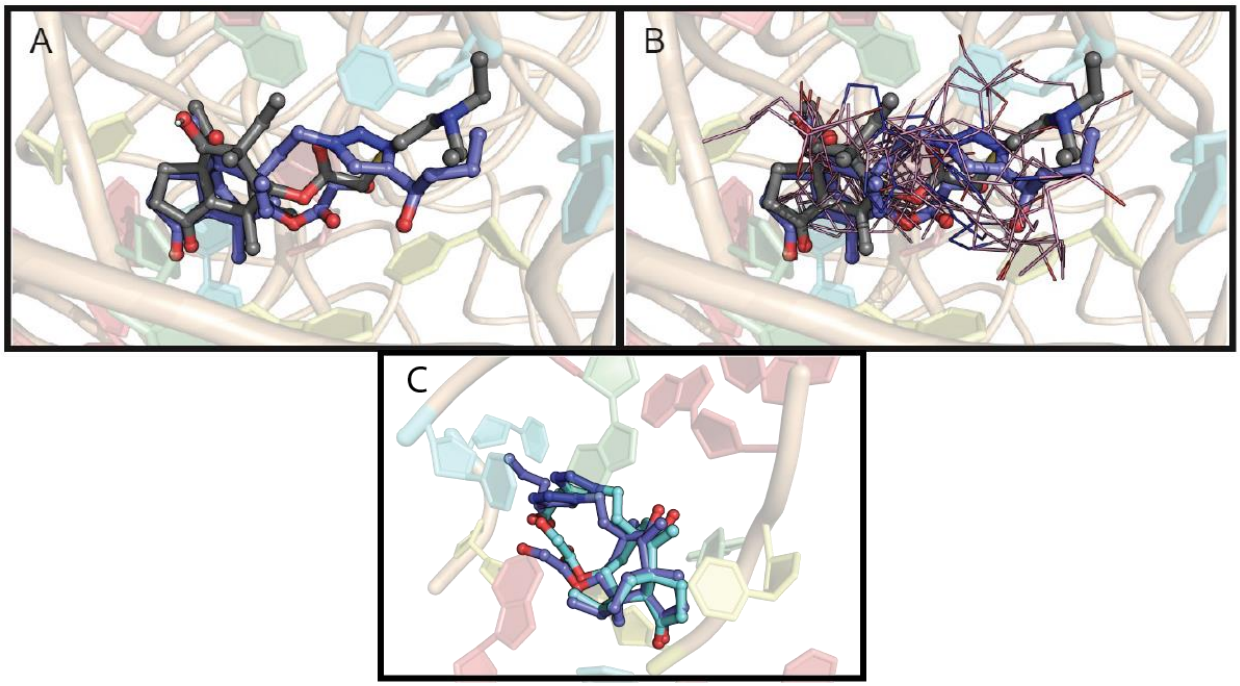


**Figure S56. Docking results of C22 derivative 39-R.** (A) Co-crystalized tiamulin (shown in grey sticks, colored by element) in the *D. radiodurans* 50S ribosome subunit (PDB ID: 1XBP). The lowest energy docked pose of derivative 39-R is shown in dark blue sticks, colored by element. (B) All poses of docked derivative 39-R (lines) overlaid with the lowest redocked pose of derivative 39-R (dark blue, colored by element) and tiamulin crystal structure (grey, colored by element) in PDB ID: 1XBP. (C) Lowest energy pose of derivative 39-R (dark blue, sticks) overlayed with the best performing C22 derivative (derivative 32, aquamarine, sticks) in the tiamulin binding pocket of *D. radiodurans* (PDB ID: 1XBP).

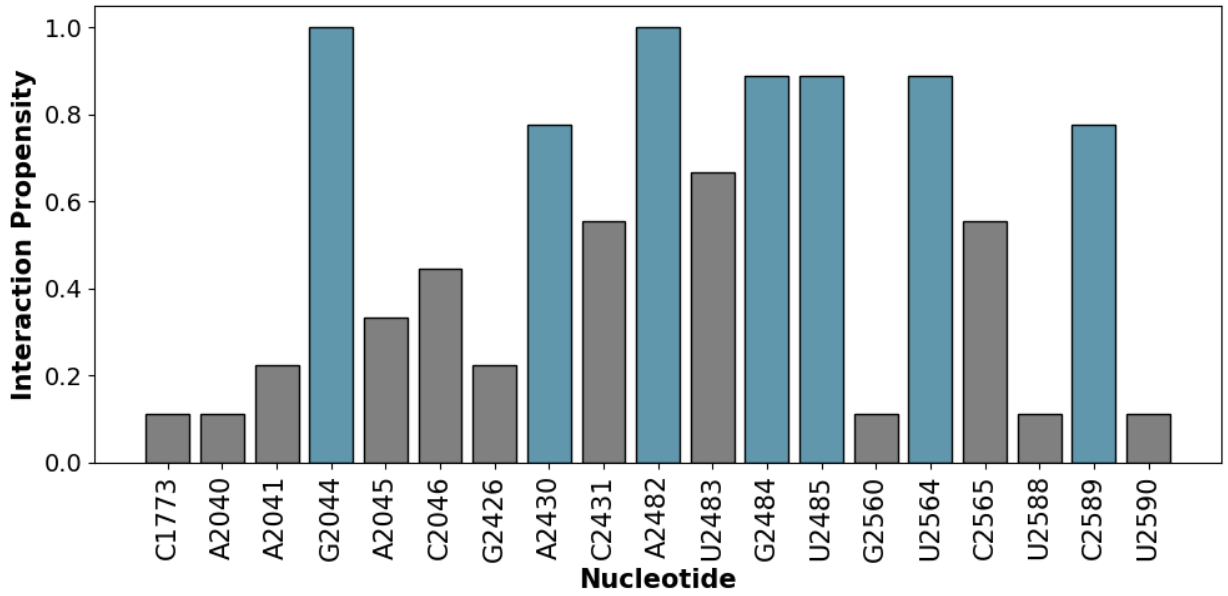


**Figure S57. Derivative 39-R nucleotide interaction propensities within PDB ID: 1XBP.** Nucleotides that interacted with this derivative are shown on the x-axis. Propensity is shown in the y-axis. Bars are colored teal when the interaction threshold was over 70% for all poses. Bars are colored grey when the interaction threshold is under 70% and at least one interaction with one pose was observed.

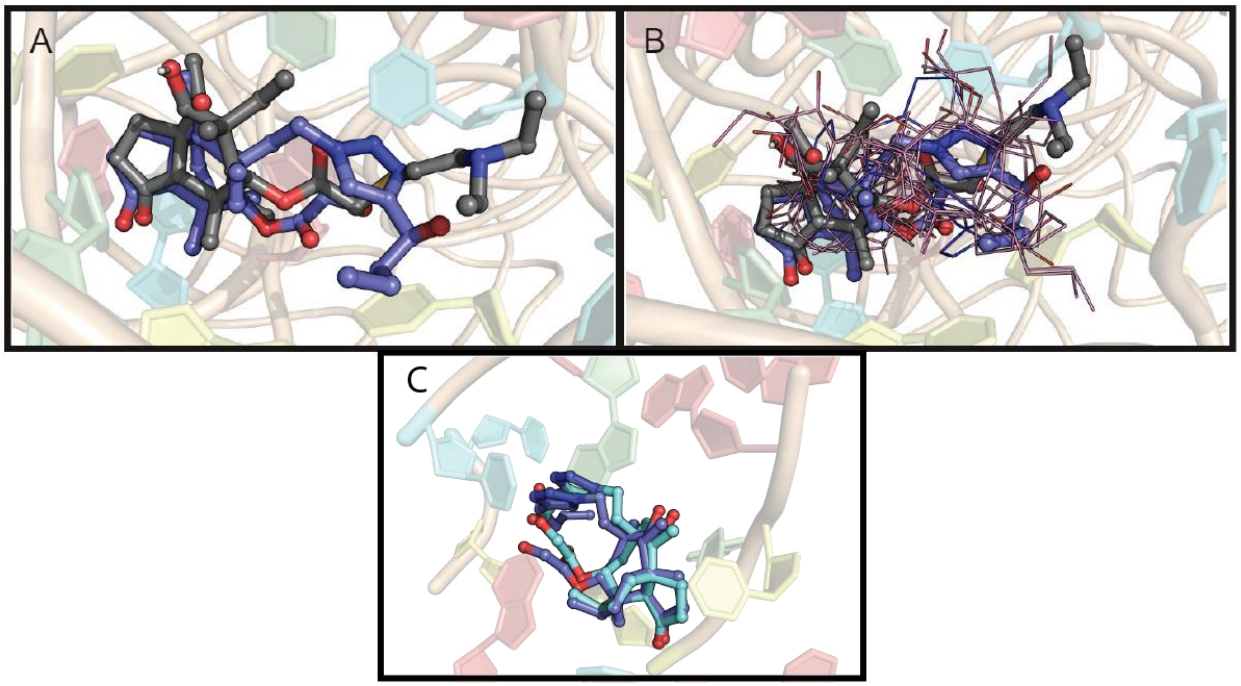


**Figure S58. Docking results of C22 derivative 39-S.** (A) Co-crystalized tiamulin (shown in grey sticks, colored by element) in the *D. radiodurans* 50S ribosome subunit (PDB ID: 1XBP). The lowest energy docked pose of derivative 39-S is shown in dark blue sticks, colored by element. (B) All poses of docked derivative 39-S (lines) overlaid with the lowest redocked pose of derivative 39-S (dark blue, colored by element) and tiamulin crystal structure (grey, colored by element) in PDB ID: 1XBP. (C) Lowest energy pose of derivative 39-S (dark blue, sticks) overlayed with the best performing C22 derivative (derivative 32, aquamarine, sticks) in the tiamulin binding pocket of *D. radiodurans* (PDB ID: 1XBP).

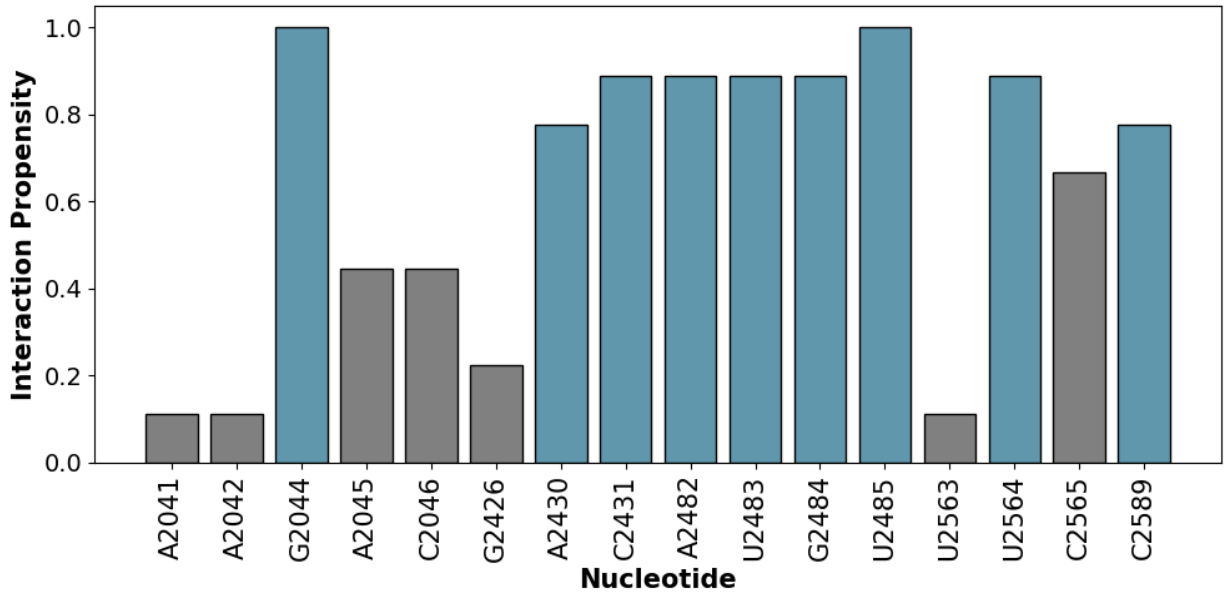


**Figure S59. Derivative 39-S nucleotide interaction propensities within PDB ID: 1XBP.** Nucleotides that interacted with this derivative are shown on the x-axis. Propensity is shown in the y-axis. Bars are colored teal when the interaction threshold was over 70% for all poses. Bars are colored grey when the interaction threshold is under 70% and at least one interaction with one pose was observed.

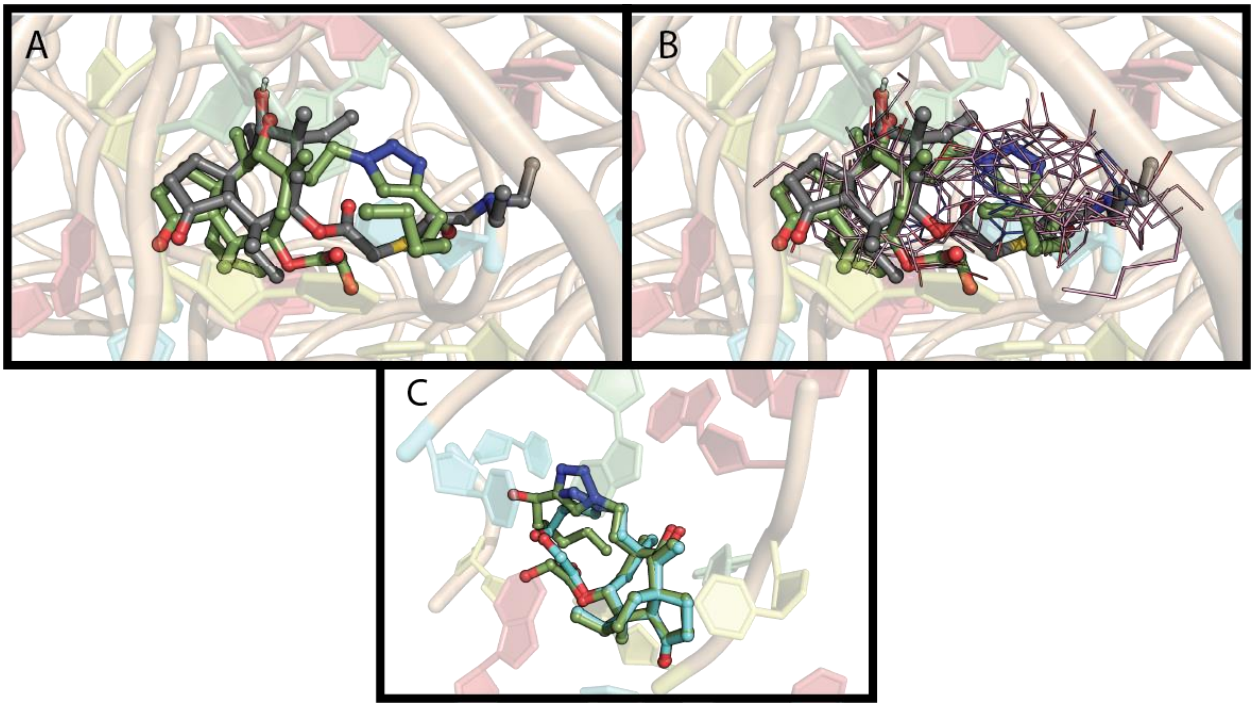


**Figure S60. Docking results of C22 derivative 40-R.** (A) Co-crystalized tiamulin (shown in grey sticks, colored by element) in the *D. radiodurans* 50S ribosome subunit (PDB ID: 1XBP). The lowest energy docked pose of derivative 40-R is shown in light green sticks, colored by element. (B) All poses of docked derivative 40-R (lines) overlaid with the lowest redocked pose of derivative 40-R (light green, colored by element) and tiamulin crystal structure (grey, colored by element) in PDB ID: 1XBP. (C) Lowest energy pose of derivative 40-R (light green, sticks) overlayed with the best performing C22 derivative (derivative 32, aquamarine, sticks) in the tiamulin binding pocket of *D. radiodurans* (PDB ID: 1XBP).

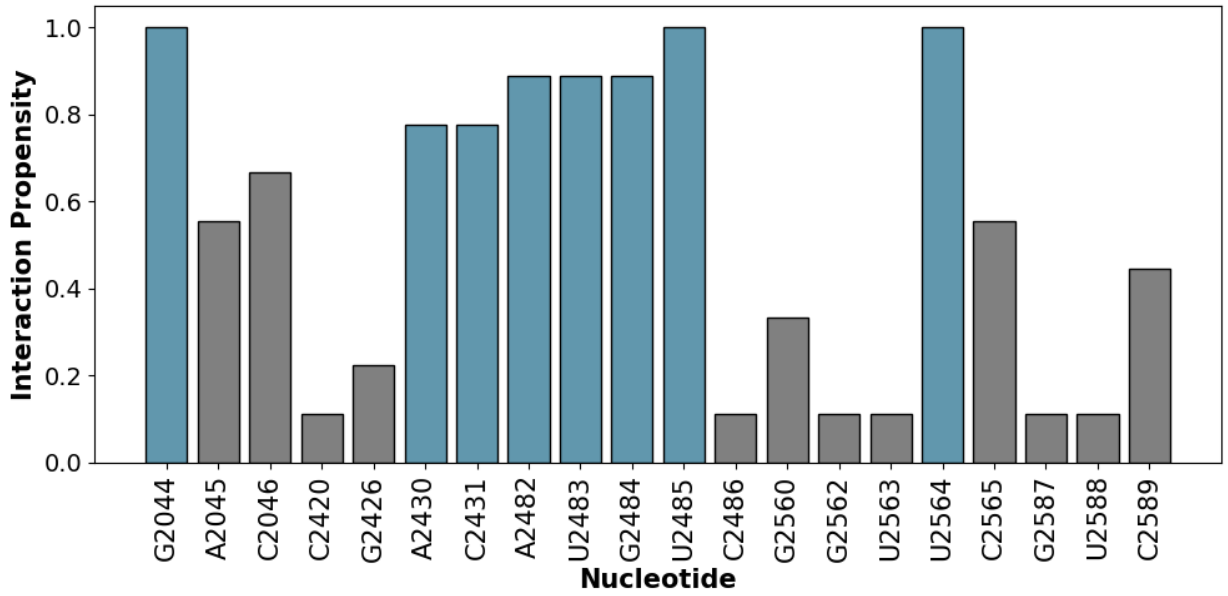


**Figure S61. Derivative 40-R nucleotide interaction propensities within PDB ID: 1XBP.** Nucleotides that interacted with this derivative are shown on the x-axis. Propensity is shown in the y-axis. Bars are colored teal when the interaction threshold was over 70% for all poses. Bars are colored grey when the interaction threshold is under 70% and at least one interaction with one pose was observed.

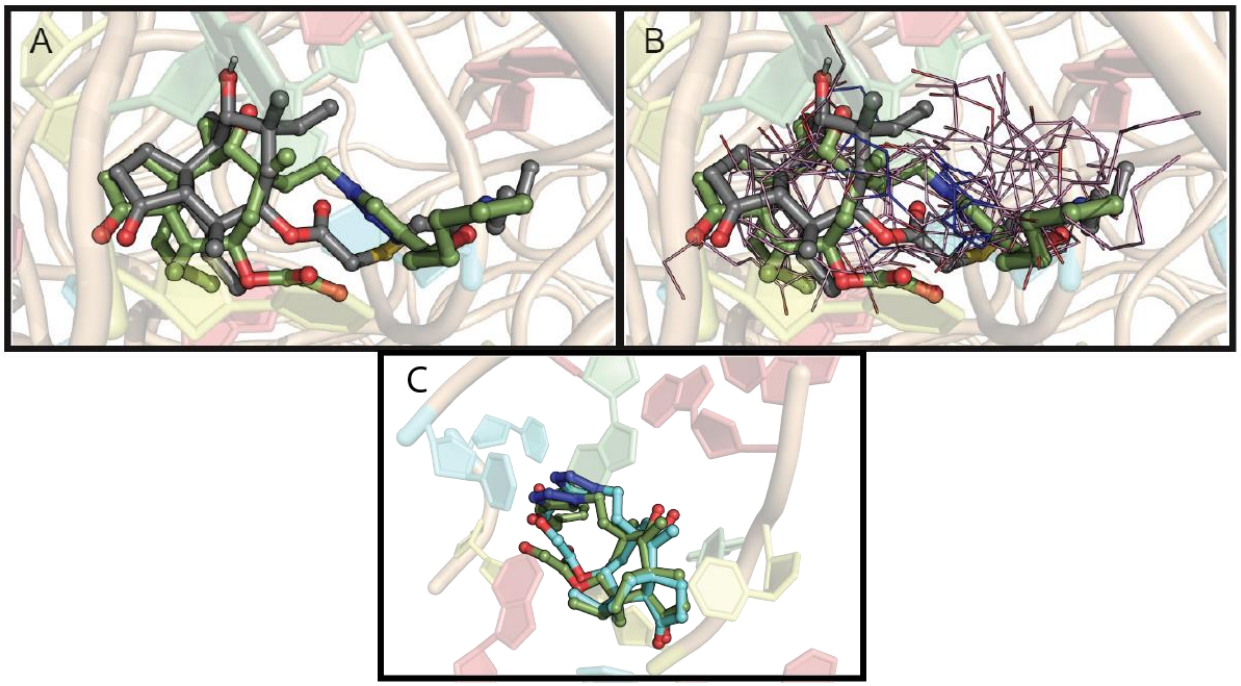


**Figure S62. Docking results of C22 derivative 40-S.** (A) Co-crystalized tiamulin (shown in grey sticks, colored by element) in the *D. radiodurans* 50S ribosome subunit (PDB ID: 1XBP). The lowest energy docked pose of derivative 40-S is shown in light green sticks, colored by element. (B) All poses of docked derivative 40-S (lines) overlaid with the lowest redocked pose of derivative 40-S (light green, colored by element) and tiamulin crystal structure (grey, colored by element) in PDB ID: 1XBP. (C) Lowest energy pose of derivative 40-S (light green, sticks) overlayed with the best performing C22 derivative (derivative 32, aquamarine, sticks) in the tiamulin binding pocket of *D. radiodurans* (PDB ID: 1XBP).

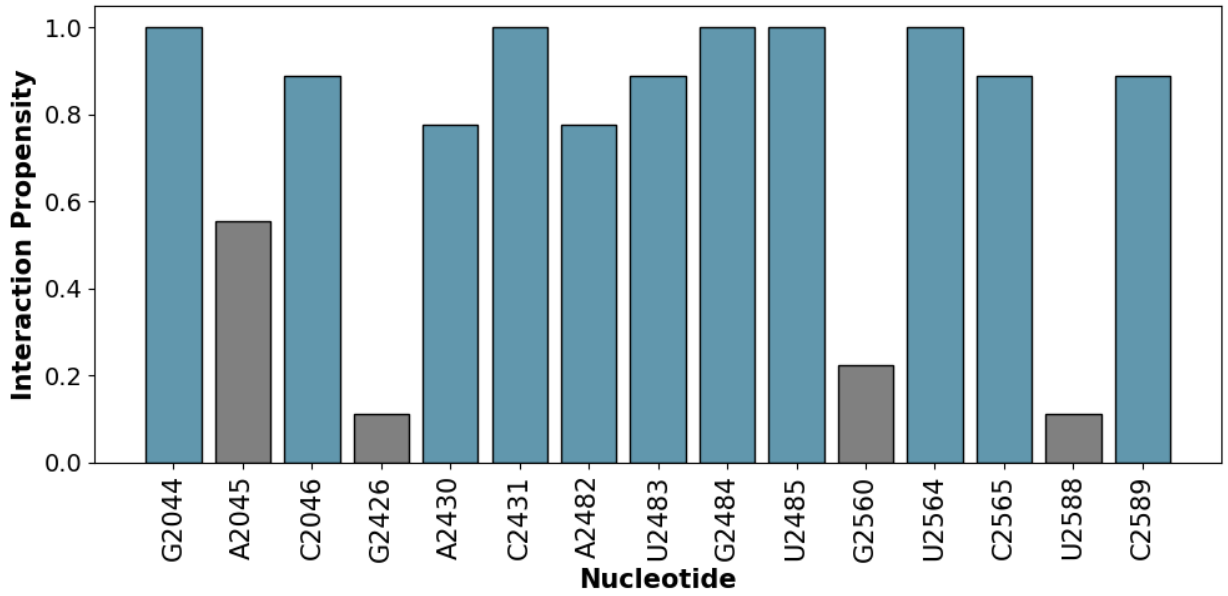


**Figure S63. Derivative 40-S nucleotide interaction propensities within PDB ID: 1XBP.** Nucleotides that interacted with this derivative are shown on the x-axis. Propensity is shown in the y-axis. Bars are colored teal when the interaction threshold was over 70% for all poses. Bars are colored grey when the interaction threshold is under 70% and at least one interaction with one pose was observed.

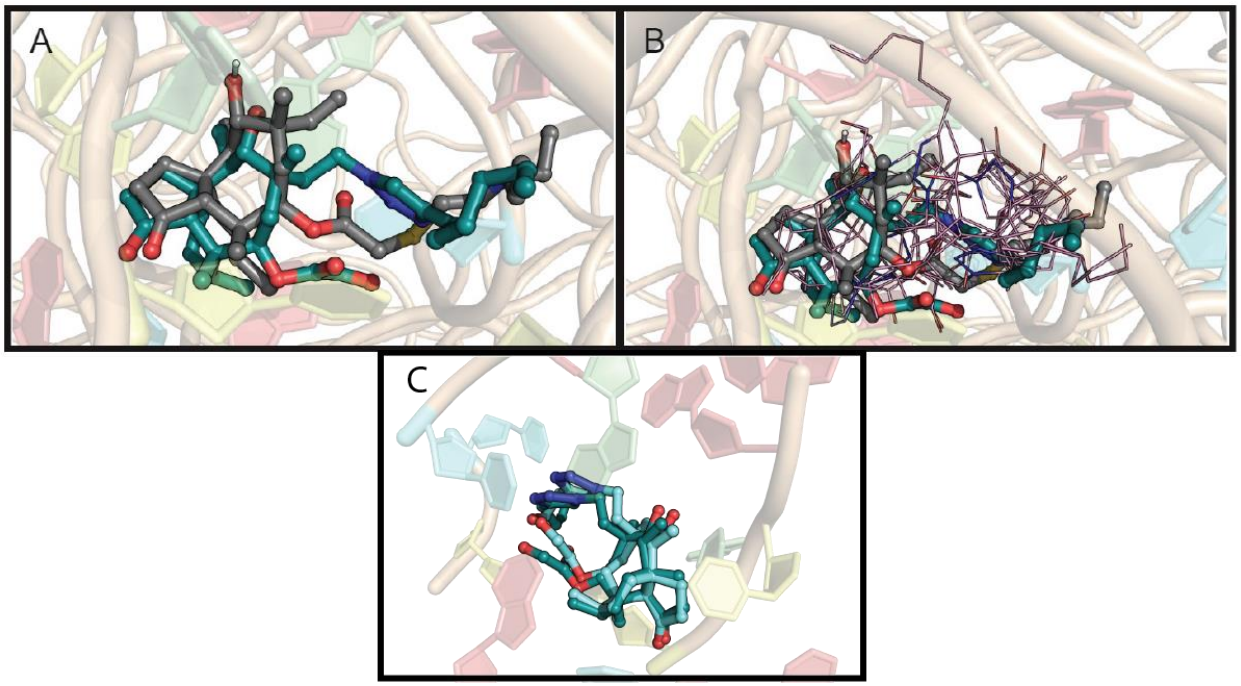


**Figure S64. Docking results of C22 derivative 41.** (A) Co-crystalized tiamulin (shown in grey sticks, colored by element) in the *D. radiodurans* 50S ribosome subunit (PDB ID: 1XBP). The lowest energy docked pose of derivative 41 is shown in teal sticks, colored by element. (B) All poses of docked derivative 41 (lines) overlaid with the lowest redocked pose of derivative 41 (teal, colored by element) and tiamulin crystal structure (grey, colored by element) in PDB ID: 1XBP. (C) Lowest energy pose of derivative 41 (teal, sticks) overlayed with the best performing C22 derivative (derivative 32, aquamarine, sticks) in the tiamulin binding pocket of *D. radiodurans* (PDB ID: 1XBP).

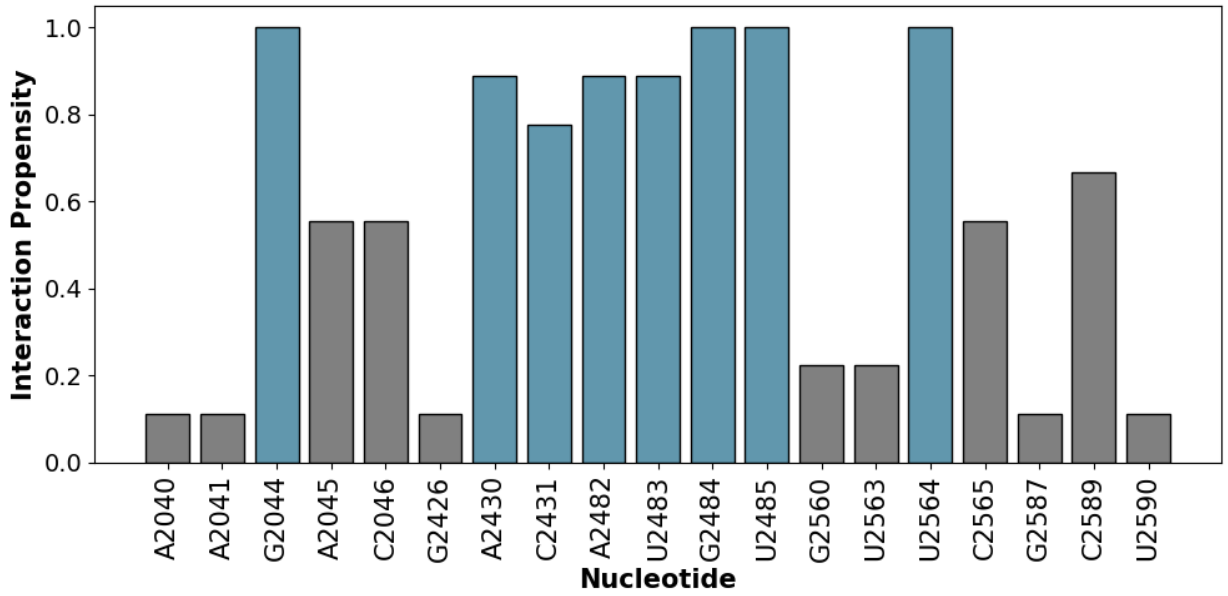


**Figure S65. Derivative 41 nucleotide interaction propensities within PDB ID: 1XBP.** Nucleotides that interacted with this derivative are shown on the x-axis. Propensity is shown in the y-axis. Bars are colored teal when the interaction threshold was over 70% for all poses. Bars are colored grey when the interaction threshold is under 70% and at least one interaction with one pose was observed.

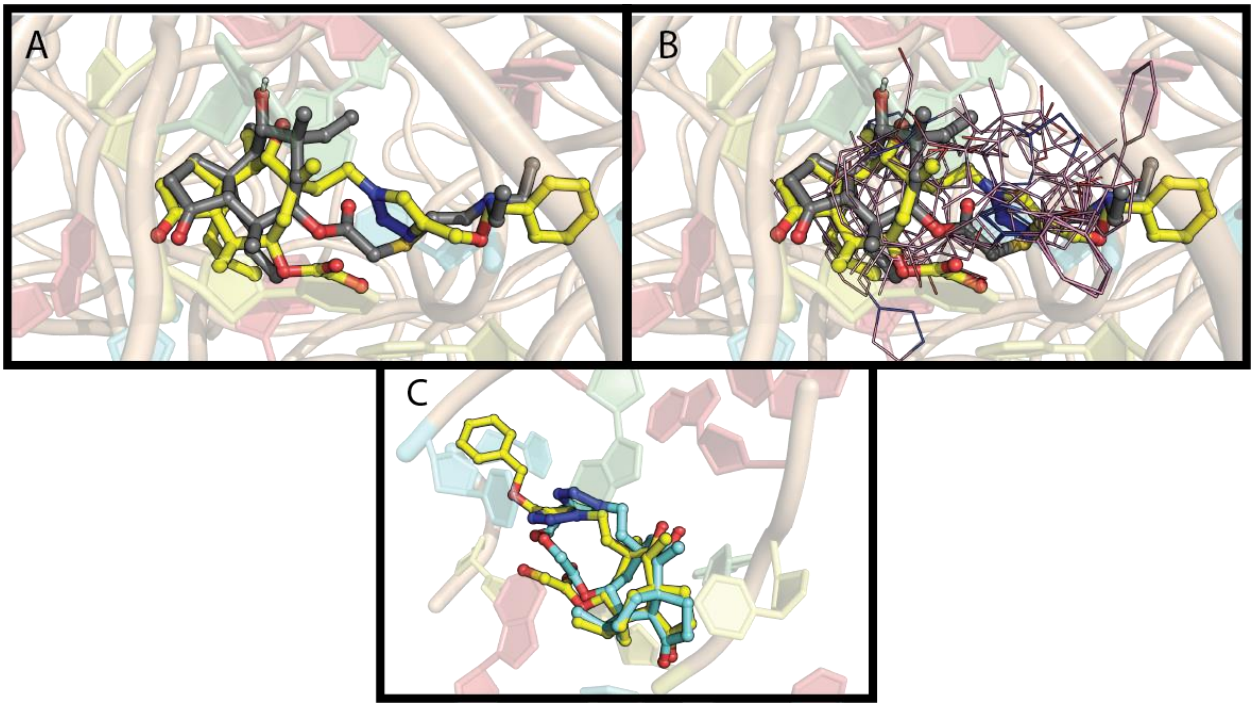


**Figure S66. Docking results of C22 derivative 38.** (A) Co-crystalized tiamulin (shown in grey sticks, colored by element) in the *D. radiodurans* 50S ribosome subunit (PDB ID: 1XBP). The lowest energy docked pose of derivative 38 is shown in yellow sticks, colored by element. (B) All poses of docked derivative 38 (lines) overlaid with the lowest redocked pose of derivative 38 (yellow, colored by element) and tiamulin crystal structure (grey, colored by element) in PDB ID: 1XBP. (C) Lowest energy pose of derivative 38 (yellow, sticks) overlayed with the best performing C22 derivative (derivative 32, aquamarine, sticks) in the tiamulin binding pocket of *D. radiodurans* (PDB ID: 1XBP).

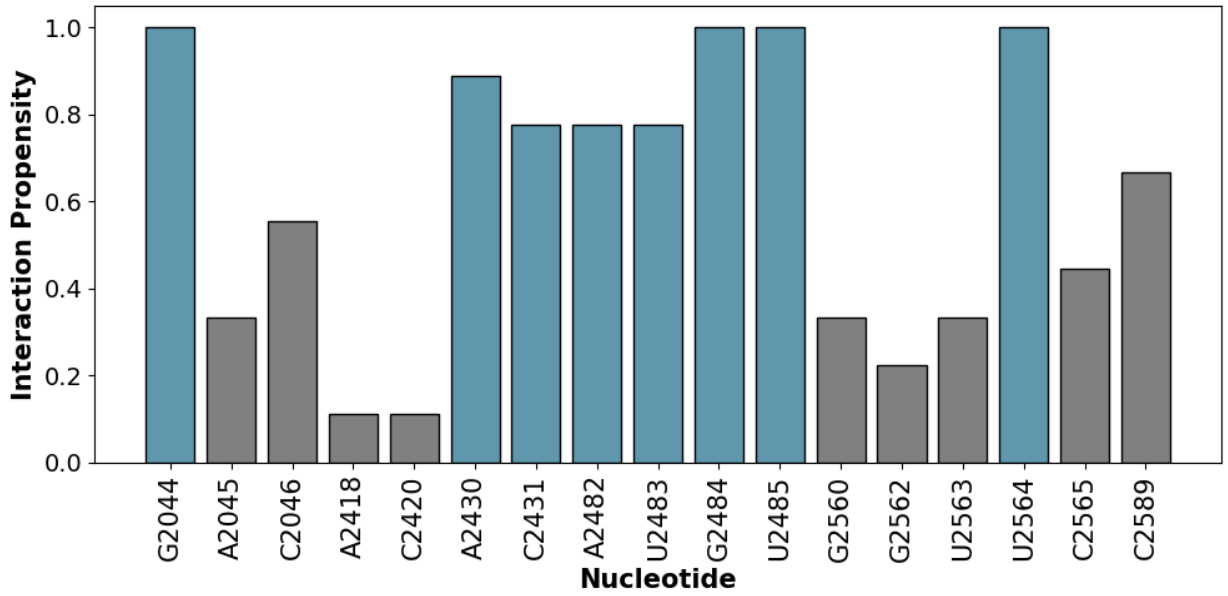


**Figure S67. Derivative 38 nucleotide interaction propensities within PDB ID: 1XBP.** Nucleotides that interacted with this derivative are shown on the x-axis. Propensity is shown in the y-axis. Bars are colored teal when the interaction threshold was over 70% for all poses. Bars are colored grey when the interaction threshold is under 70% and at least one interaction with one pose was observed.

**Table S11. C22 Chemical property data predicted by Qikprop**

| Derivative ID | 18 | 19 | 20 | 23 | 24 | 21-R | 21-S |
|---|---|---|---|---|---|---|---|
| Reactive Functional Group | hetero-hetero single bond/hetero-hetero single bond/acetal or analog | hetero-hetero single bond/hetero-hetero single bond/acetal or analog | hetero-hetero single bond/hetero-hetero single bond/acetal or analog | hetero-hetero single bond/hetero-hetero single bond/acetal or analog | hetero-hetero single bond/hetero-hetero single bond/acetal or analog | hetero-hetero single bond/hetero-hetero single bond/acetal or analog | hetero-hetero single bond/hetero-hetero single bond/acetal or analog |
| No. of Primary Metabolites | 4 | 4 | 4 | 5 | 5 | 4 | 4 |
| Vina Lowest Free Energy (kcal/mol) | -9.8 | -10.6 | -9.4 | -9.6 | -9.8 | -10.0 | -10.0 |
| Average All Poses Vina Free Energy (kcal/mol) | -9.1 | -9.7 | -8.8 | -8.9 | -9.1 | -9.6 | -9.4 |
| Heavy Atom Count | 33 | 34 | 35 | 33 | 34 | 34 | 34 |
| Ligand Effeciency [lowest energy pose] | -0.297 | -0.312 | -0.269 | -0.291 | -0.288 | -0.294 | -0.294 |
| Ligand Effeciency [all poses] | -0.28 | -0.29 | -0.25 | -0.27 | -0.27 | -0.28 | -0.28 |
| Molecular Wt. (g/mol) | 469.7 | 483.7 | 497.7 | 468.7 | 482.7 | 483.7 | 483.7 |
| Molecular Volume ($Å^3$) | 1369.3 | 1407.0 | 1468.7 | 1376.1 | 1435.5 | 1414.7 | 1418.5 |
| Total SASA ($Å^2$) | 695.9 | 713.7 | 746.7 | 695.2 | 732.8 | 715.6 | 727.1 |
| logP (M) [octanol/water] | -0.019 | 0.133 | 0.465 | -0.446 | -0.233 | 0.38 | 0.334 |
| % Human Oral Absorption in GI (±20%) | 37 | 37 | 39 | 23 | 22 | 43 | 42 |

| Derivative ID | 22 | 25-R | 25-S | 26-R | 26-S | 27 | 28 |
|---|---|---|---|---|---|---|---|
| Reactive Functional Group | hetero-hetero single bond/hetero-hetero single bond/acetal or analog | hetero-hetero single bond/hetero-hetero single bond/acetal or analog | hetero-hetero single bond/hetero-hetero single bond/acetal or analog | hetero-hetero single bond/hetero-hetero single bond/acetal or analog | hetero-hetero single bond/hetero-hetero single bond/acetal or analog | hetero-hetero single bond/hetero-hetero single bond/acetal or analog | hetero-hetero single bond/hetero-hetero single bond/acetal or analog |
| No. of Primary Metabolites | 4 | 4 | 4 | 3 | 4 | 3 | 4 |
| Vina Lowest Free Energy (kcal/mol) | -10.2 | -9.5 | -9.6 | -9.5 | -9.1 | -9.4 | -10.7 |
| Average All Poses Vina Free Energy (kcal/mol) | -9.4 | -9.1 | -9.0 | -9.3 | -8.7 | -9.1 | -10.0 |
| Heavy Atom Count | 35 | 36 | 36 | 38 | 38 | 37 | 40 |
| Ligand Effeciency [lowest energy pose] | -0.291 | -0.264 | -0.267 | -0.250 | -0.239 | -0.254 | -0.268 |
| Ligand Effeciency [all poses] | -0.27 | -0.25 | -0.25 | -0.24 | -0.23 | -0.25 | -0.25 |
| Molecular Wt. (g/mol) | 497.7 | 511.7 | 511.7 | 539.8 | 539.8 | 523.8 | 565.8 |
| Molecular Volume ($Å^3$) | 1479.8 | 1497.6 | 1526.4 | 1603.7 | 1636.5 | 1637.4 | 1701.5 |
| Total SASA ($Å^2$) | 754.9 | 724.7 | 765.5 | 802.8 | 816.4 | 839.0 | 863.5 |
| logP (M) [octanol/water] | 1.043 | 0.908 | 0.982 | 1.442 | 1.586 | 2.494 | 2.235 |
| % Human Oral Absorption in GI (±20%) | 47 | 34 | 34 | 38 | 37 | 60 | 58 |

**Table S12. C20 Chemical property data predicted by Qikprop**

| Derivative ID | 31 | 32 | 33 | 36 | 37 | 34-R | 34-S |
|---|---|---|---|---|---|---|---|
| Reactive Functional Group | hetero-hetero single bond/hetero-hetero single bond/acetal or analog | hetero-hetero single bond/hetero-hetero single bond/acetal or analog | hetero-hetero single bond/hetero-hetero single bond/acetal or analog | hetero-hetero single bond/hetero-hetero single bond/acetal or analog | hetero-hetero single bond/hetero-hetero single bond/acetal or analog | hetero-hetero single bond/hetero-hetero single bond/acetal or analog | hetero-hetero single bond/hetero-hetero single bond/acetal or analog |
| No. of Primary Metabolites | 5 | 5 | 5 | 5 | 6 | 5 | 4 |
| Vina Lowest Free Energy (kcal/mol) | -9.3 | -9.1 | -9.4 | -9.2 | -9.1 | -9.5 | -9.5 |
| Average All Poses Vina Free Energy (kcal/mol) | -8.7 | -8.2 | -8.6 | -8.7 | -8.0 | -8.9 | -8.8 |
| Heavy Atom Count | 34 | 35 | 36 | 34 | 35 | 35 | 35 |
| Ligand Effeciency [lowest energy pose] | -0.274 | -0.260 | -0.261 | -0.271 | -0.260 | -0.271 | -0.271 |
| Ligand Effeciency [all poses] | -0.26 | -0.23 | -0.24 | -0.25 | -0.23 | -0.25 | -0.25 |
| Molecular Wt. (g/mol) | 485.7 | 499.7 | 513.7 | 484.7 | 498.7 | 499.7 | 499.7 |
| Molecular Volume ($Å^3$) | 1446.5 | 1499.8 | 1565.8 | 1391.3 | 1522.8 | 1446.2 | 1516.7 |
| Total SASA ($Å^2$) | 765.3 | 793.9 | 831.5 | 706.4 | 810.3 | 751.3 | 804.5 |
| logP (M) [octanol/water] | -0.805 | -0.64 | -0.28 | -1.449 | -1.018 | -0.515 | -0.372 |
| % Human Oral Absorption in GI (±20%) | 23 | 21 | 11 | 8 | 7 | 31 | 28 |

| Derivative ID | 35 | 39-R | 39-S | 40-R | 40-S | 41 | 38 |
|---|---|---|---|---|---|---|---|
| Reactive Functional Group | hetero-hetero single bond/hetero-hetero single bond/acetal or analog | hetero-hetero single bond/hetero-hetero single bond/acetal or analog | hetero-hetero single bond/hetero-hetero single bond/acetal or analog | hetero-hetero single bond/hetero-hetero single bond/acetal or analog | hetero-hetero single bond/hetero-hetero single bond/acetal or analog | hetero-hetero single bond/hetero-hetero single bond/acetal or analog | hetero-hetero single bond/hetero-hetero single bond/acetal or analog |
| No. of Primary Metabolites | 5 | 4 | 4 | 5 | 4 | 4 | 4 |
| Vina Lowest Free Energy (kcal/mol) | -9.6 | -9.4 | -9.3 | -9.4 | -9.1 | -9.1 | -10.6 |
| Average All Poses Vina Free Energy (kcal/mol) | -8.9 | -8.7 | -8.7 | -8.7 | -8.4 | -8.4 | -9.8 |
| Heavy Atom Count | 36 | 37 | 37 | 39 | 39 | 38 | 41 |
| Ligand Effeciency [lowest energy pose] | -0.267 | -0.254 | -0.251 | -0.241 | -0.233 | -0.239 | -0.259 |
| Ligand Effeciency [all poses] | -0.25 | -0.24 | -0.24 | -0.22 | -0.21 | -0.22 | -0.24 |
| Molecular Wt. (g/mol) | 513.7 | 527.7 | 527.7 | 555.8 | 555.8 | 539.8 | 581.8 |
| Molecular Volume ($Å^3$) | 1556.5 | 1566.2 | 1622.8 | 1583.9 | 1646.5 | 1719.6 | 1793.3 |
| Total SASA ($Å^2$) | 823.0 | 817.9 | 859.7 | 790.2 | 836.2 | 912.4 | 942.3 |
| logP (M) [octanol/water] | 0.256 | 0.104 | 0.234 | 0.433 | 0.57 | 1.718 | 1.514 |
| % Human Oral Absorption in GI (±20%) | 20 | 22 | 19 | 27 | 24 | 33 | 31 |

**Table S13. Different ranking systems.**

| Derivative ID | 18 | 19 | 20 | 23 | 24 | 21-R | 21-S | 22 | 25 | 25 | 26-R | 26-S | 27 | 28 | 31 | 32 | 33 | 36 | 37 | 34-R | 34-S | 35 | 39-R | 39-S | 40-R | 40-S | 41 | 38 |
|---|---|---|---|---|---|---|---|---|---|---|---|---|---|---|---|---|---|---|---|---|---|---|---|---|---|---|---|---|
| MIC Rank | 3 | 1 | 5 | 6 | 2 | 4 | 4 | 8 | 10 | 10 | 7 | 7 | 9 | 3 | 13 | 13 | 13 | 12 | 13 | 13 | 13 | 13 | 13 | 13 | 11 | 11 | 13 | 13 |
| LE Rank (lowest energy pose) [3 sig figs] | 2 | 1 | 8 | 4 | 5 | 3 | 3 | 4 | 11 | 10 | 17 | 19 | 15 | 9 | 6 | 13 | 12 | 7 | 13 | 7 | 7 | 10 | 15 | 16 | 18 | 20 | 19 | 14 |
| LE Rank (lowest energy pose) [2 sig figs] | 2 | 1 | 4 | 3 | 3 | 3 | 3 | 3 | 5 | 4 | 6 | 7 | 6 | 4 | 4 | 5 | 5 | 4 | 5 | 4 | 4 | 4 | 6 | 6 | 7 | 8 | 7 | 5 |
| LE Rank (average energy) [3 sig figs] | 4 | 1 | 10 | 5 | 6 | 2 | 3 | 5 | 10 | 11 | 13 | 19 | 12 | 11 | 7 | 18 | 15 | 8 | 19 | 9 | 10 | 12 | 16 | 17 | 20 | 22 | 21 | 14 |
| LE Rank (average energy) [2 sig figs] | 2 | 1 | 5 | 3 | 3 | 2 | 2 | 3 | 5 | 5 | 6 | 7 | 5 | 5 | 4 | 7 | 6 | 5 | 7 | 5 | 5 | 5 | 6 | 6 | 8 | 9 | 8 | 6 |

Ligand efficiency based on lowest energy pose up to three significant figures showed the greatest agreement with the MIC ranks.

**Table S14. Ranking by the C22 subgroup.**

| Derivative ID | 18 | 19 | 20 | 23 | 24 | 21-R | 21-S | 22 | 25-R | 25-S | 26-R | 26-S | 27 | 28 |
|---|---|---|---|---|---|---|---|---|---|---|---|---|---|---|
| MIC Rank | 3 | 1 | 5 | 6 | 2 | 4 | 4 | 8 | 10 | 10 | 7 | 7 | 9 | 3 |
| LE Rank (lowest energy pose) [3 sig figs] | 2 | 1 | 6 | 4 | 5 | 3 | 3 | 4 | 9 | 8 | 11 | 12 | 10 | 7 |

**Table S15. Ranking be the C20 subgroup.**

| Derivative ID | 31 | 32 | 33 | 36 | 37 | 34-R | 34-S | 35 | 39-R | 39-S | 40-R | 40-S | 41 | 38 |
|---|---|---|---|---|---|---|---|---|---|---|---|---|---|---|
| MIC Rank | 3 | 3 | 3 | 2 | 3 | 3 | 3 | 3 | 3 | 3 | 1 | 1 | 3 | 3 |
| LE Rank (lowest energy pose) [3 sig figs] | 1 | 5 | 4 | 2 | 5 | 2 | 2 | 3 | 7 | 8 | 9 | 11 | 10 | 6 |

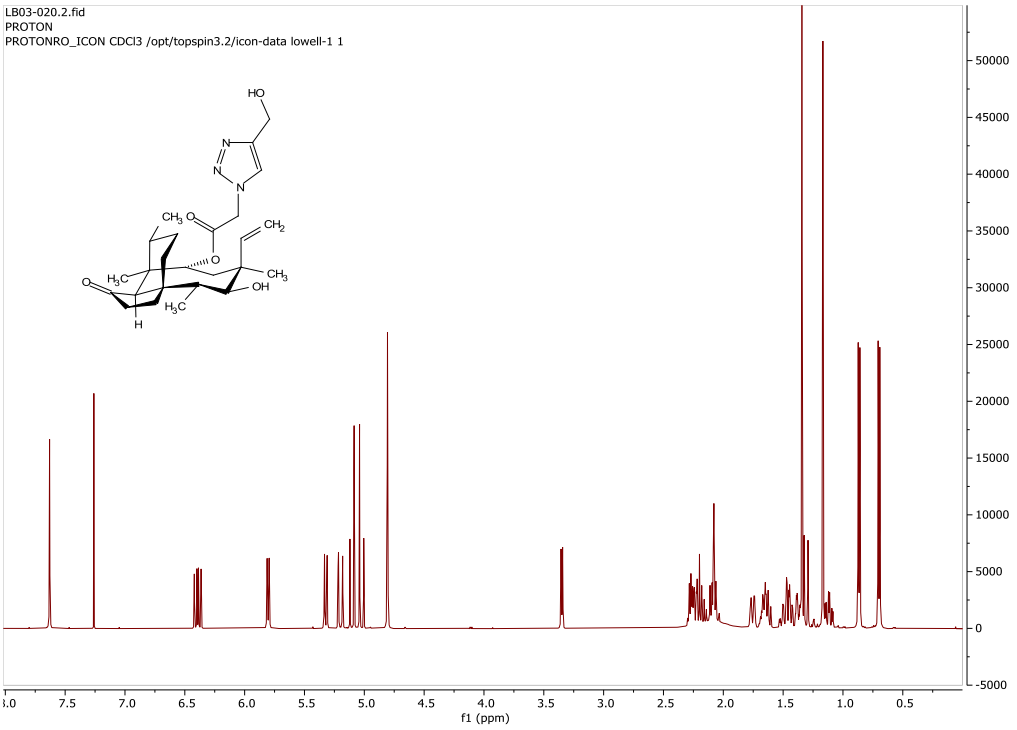


**Figure S68.** $^{1}$H-NMR (500 MHz, $CDCl_3$) of **18**.

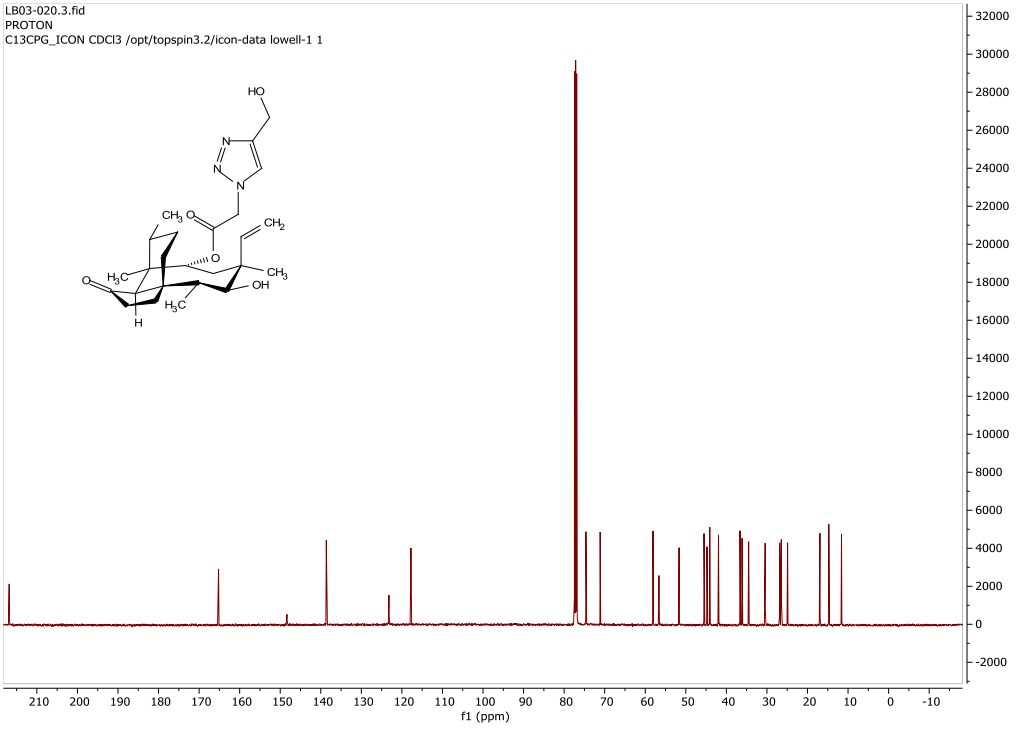


**Figure S69.** $^{13}$C-NMR (125 MHz, $CDCl_3$) of **18**.

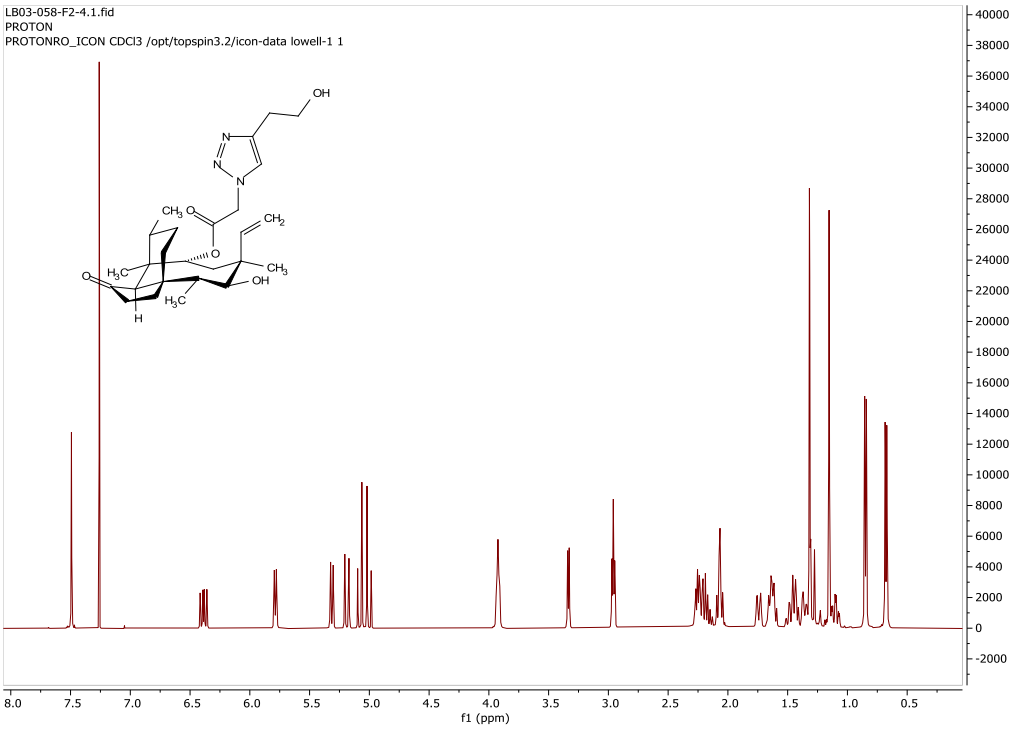


**Figure S70.** $^{1}$H NMR ($CDCl_3$, 500 MHz) of **19**.

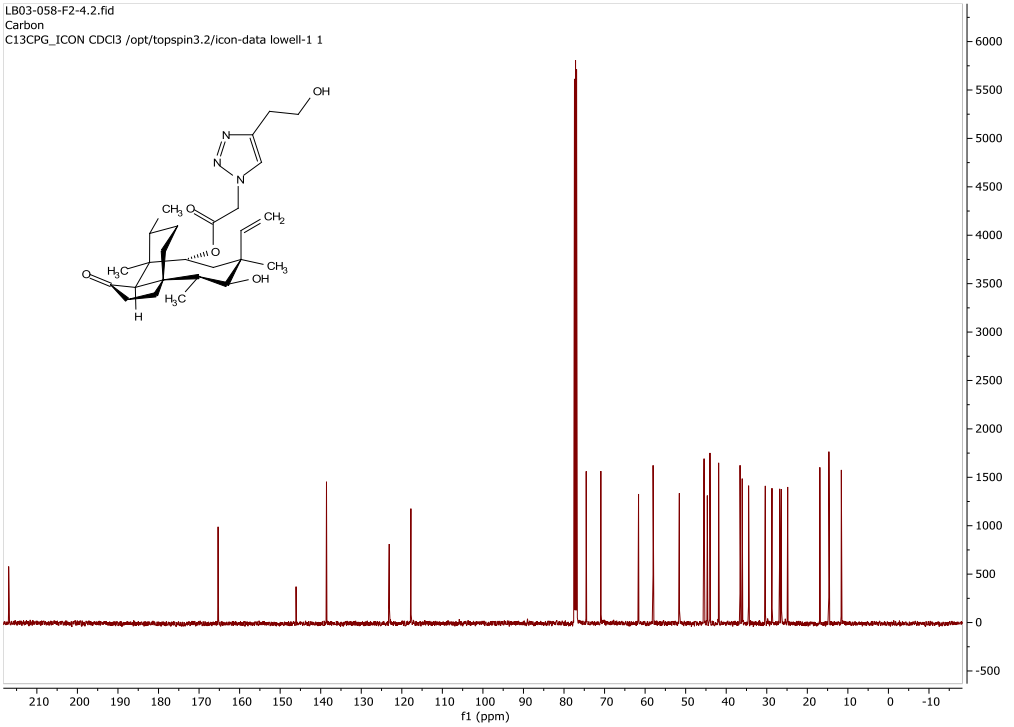


**Figure S71.** $^{13}$C NMR ($CDCl_3$, 125 MHz) of **19**.

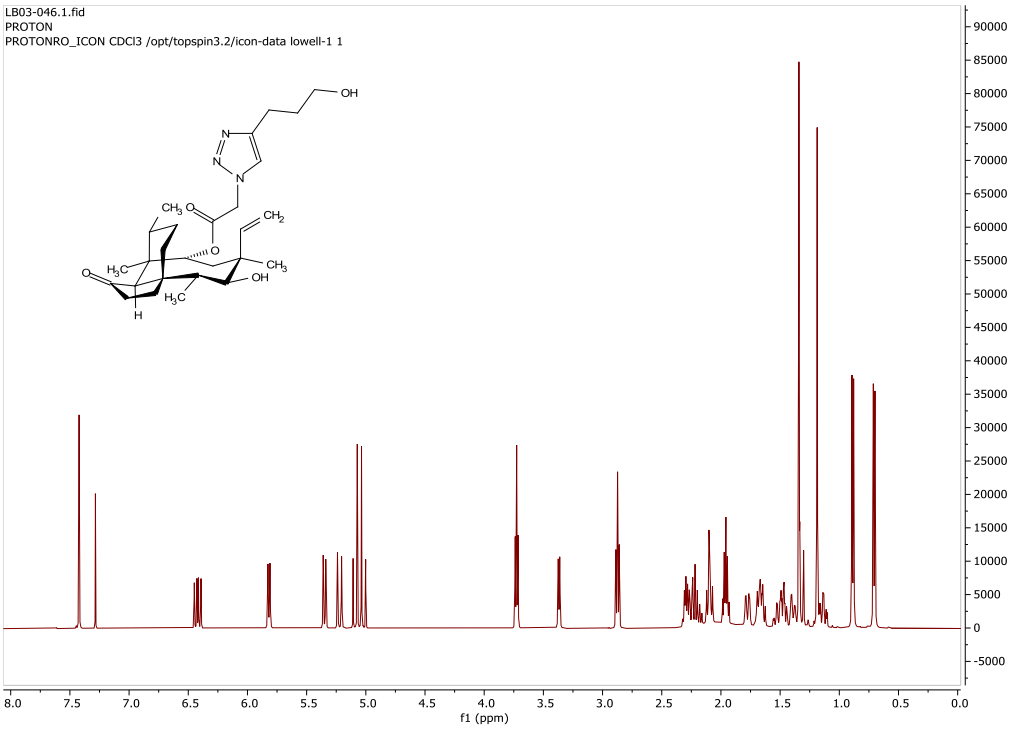


**Figure S72.** $^{1}$H NMR ($CDCl_3$, 500 MHz) of **20**.

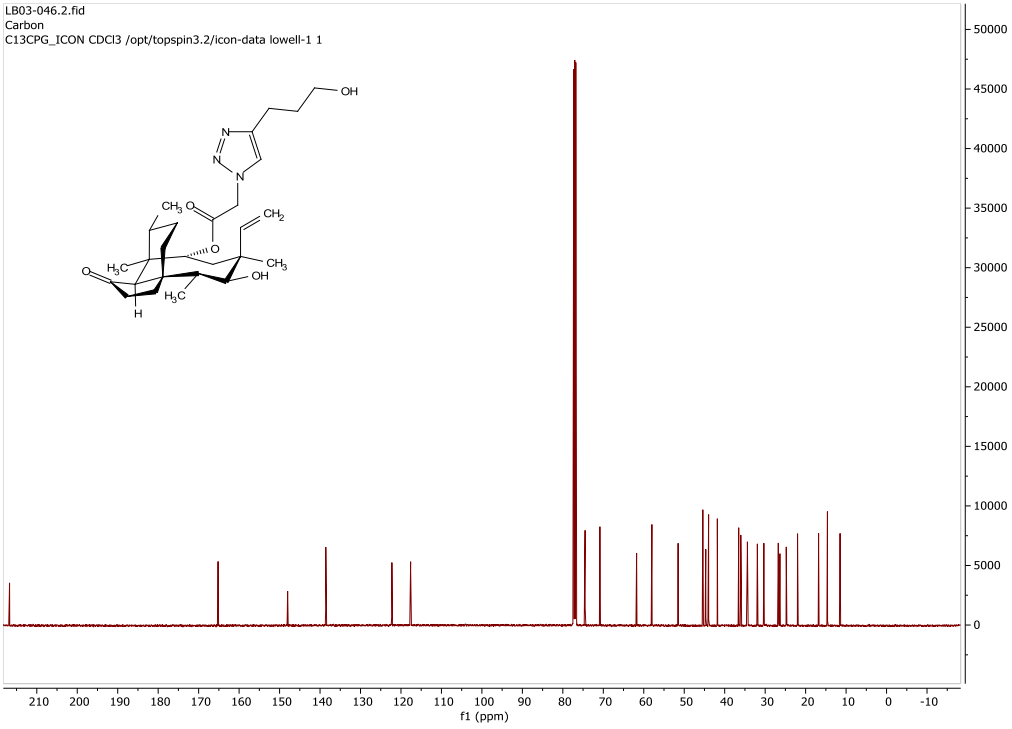


**Figure S73.** $^{13}$C NMR ($CDCl_3$, 125 MHz) of **20**.

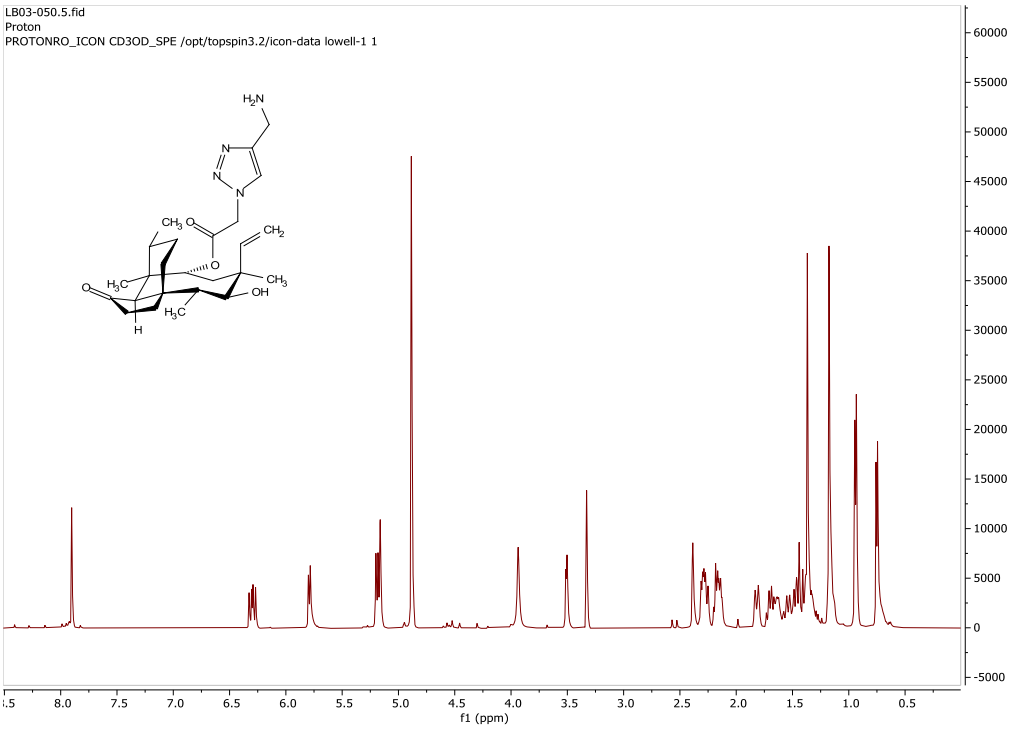


**Figure S74.** $^{1}$H NMR ($CD_3OD$, 500 MHz) of **21**.

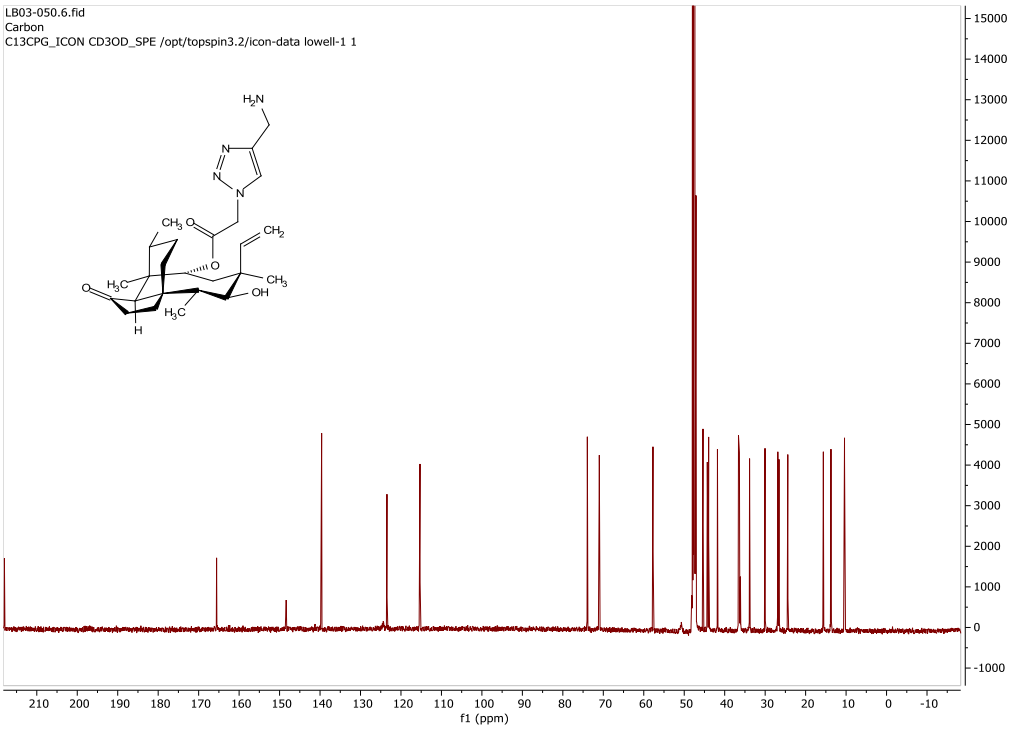


**Figure S75.** $^{13}$C NMR ($CD_3OD$, 125 MHz) of **21**.

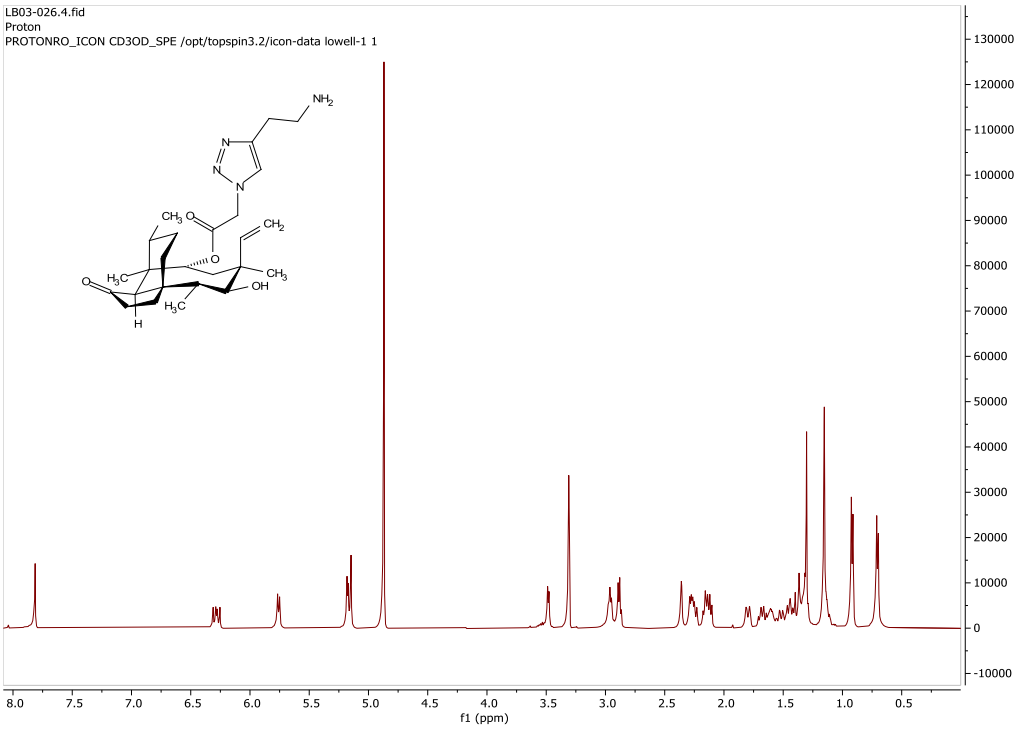


**Figure S76.** $^{1}$H NMR ($CD_3OD$, 500 MHz) of **22**.

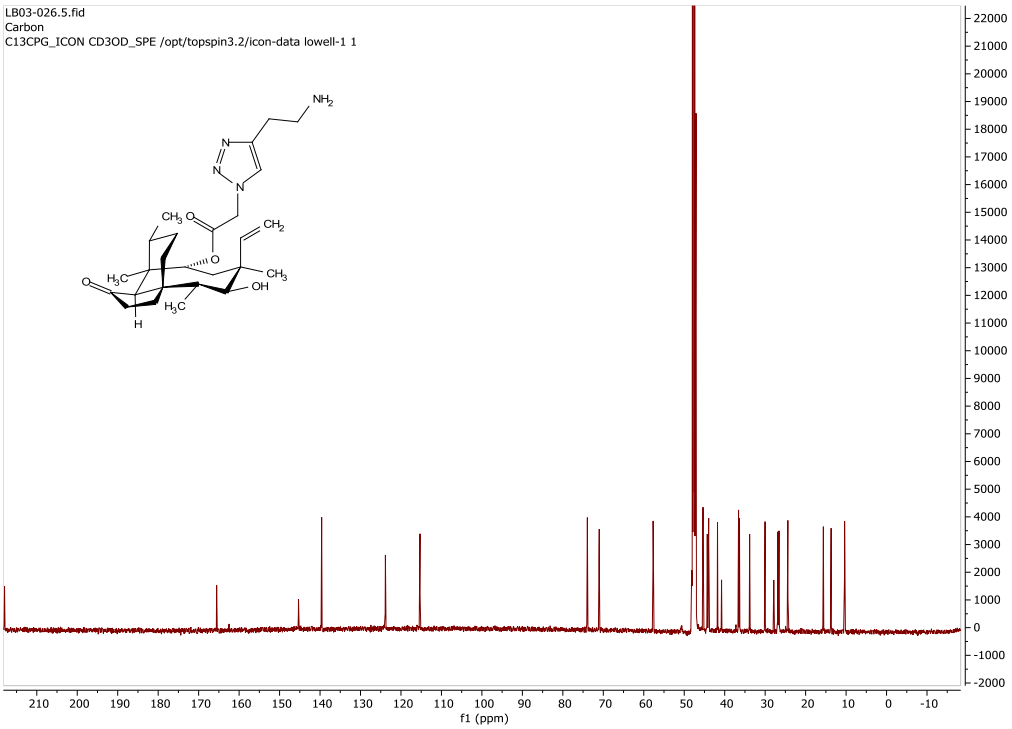


**Figure S77.** $^{13}$C NMR ($CD_3OD$, 125 MHz) of **22**.

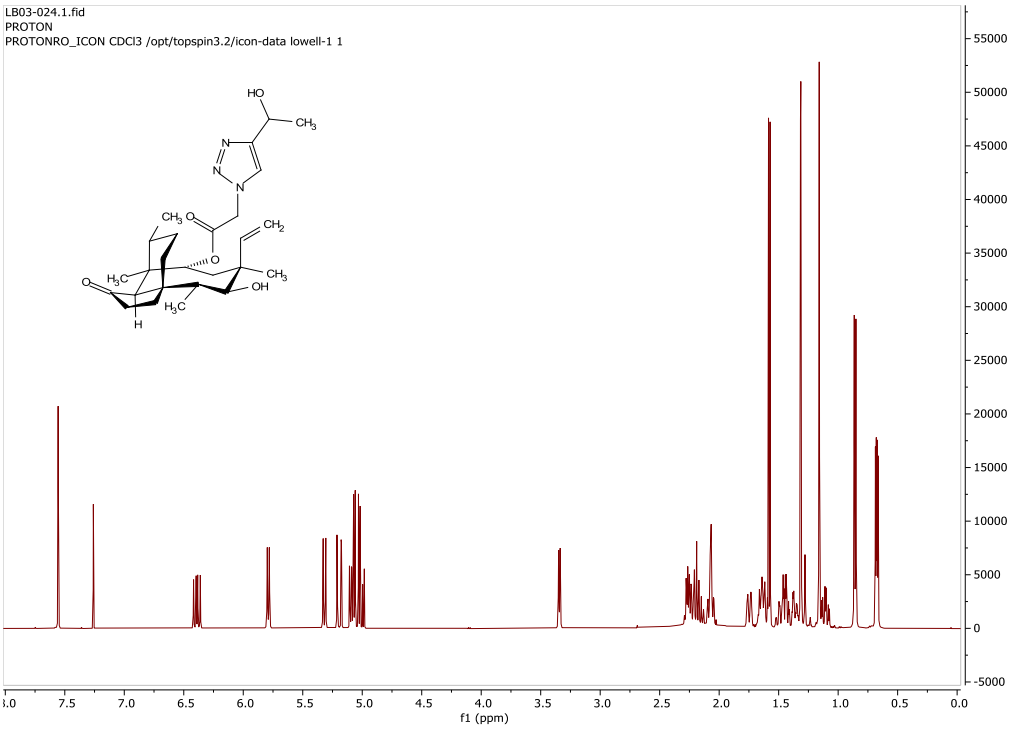


**Figure S78.** $^{1}$H NMR ($CDCl_3$, 500 MHz) of **23**.

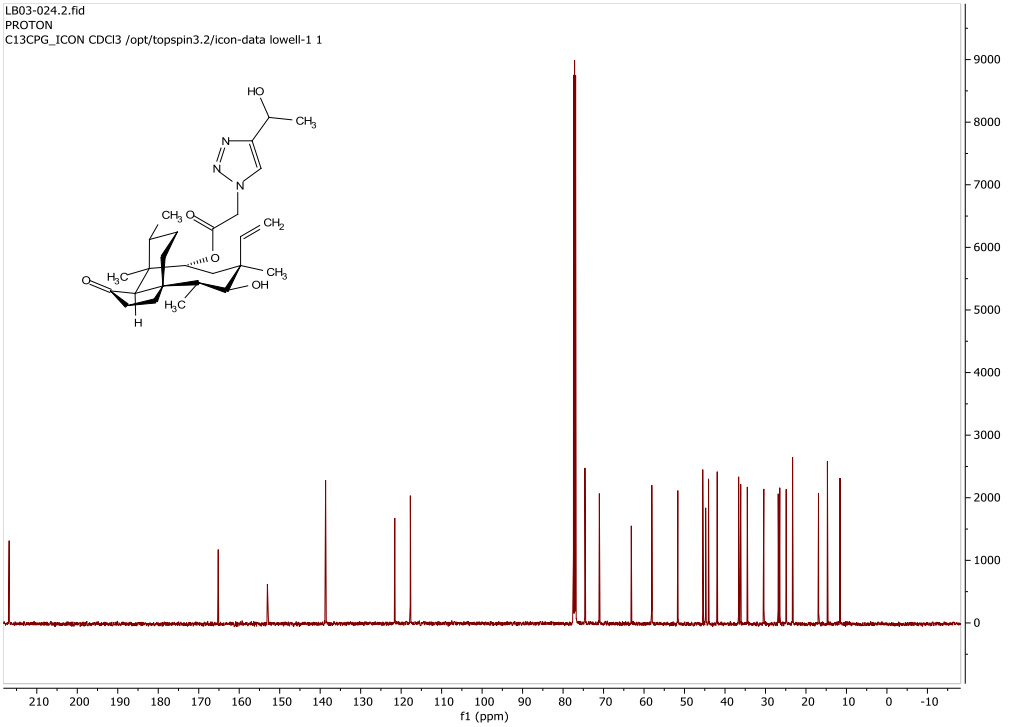


**Figure S79.** $^{13}$C NMR ($CDCl_3$, 125 MHz) of **23**.

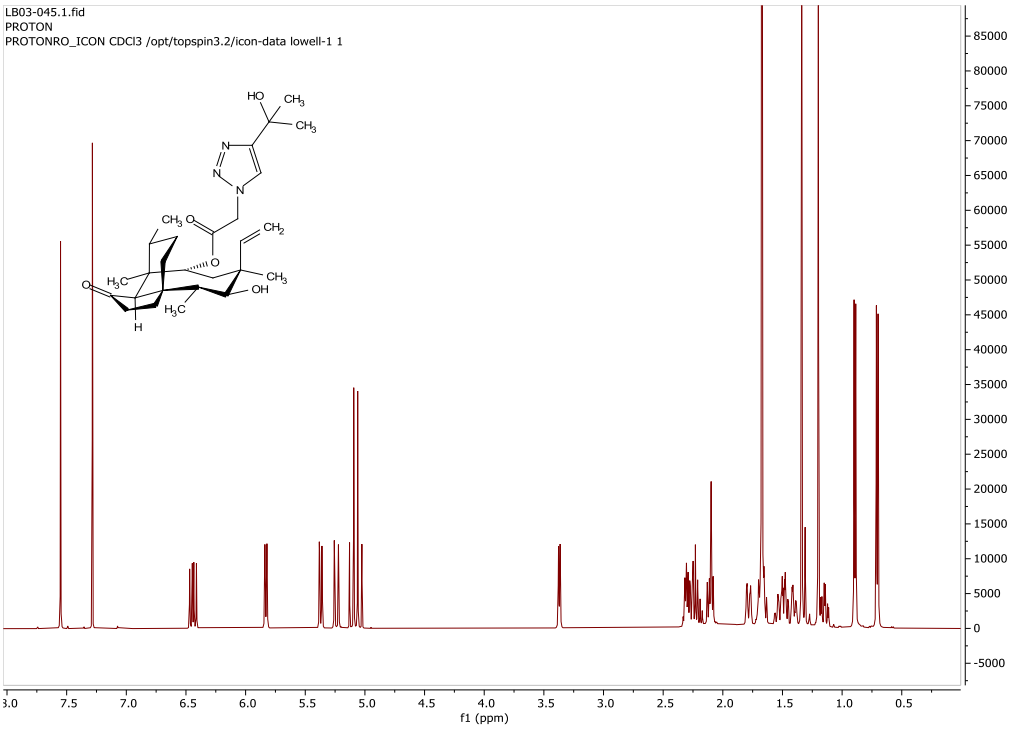


**Figure S80.** $^{1}$H NMR ($CDCl_3$, 500 MHz) of **24**.

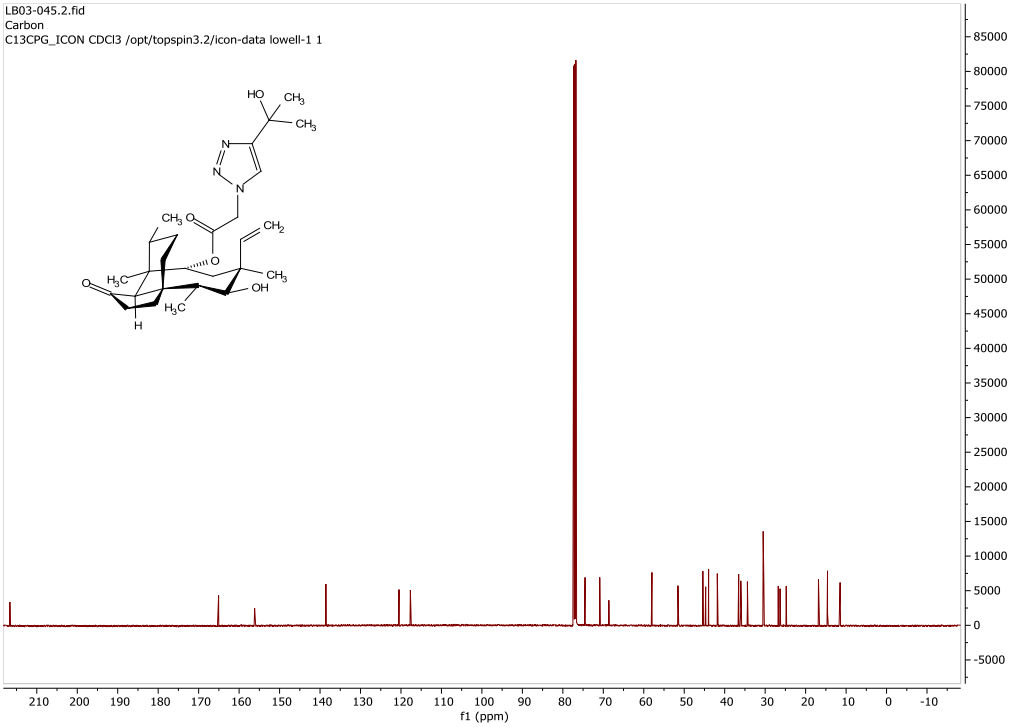


**Figure S81.** $^{13}$C NMR ($CDCl_3$, 125 MHz) of **24**.

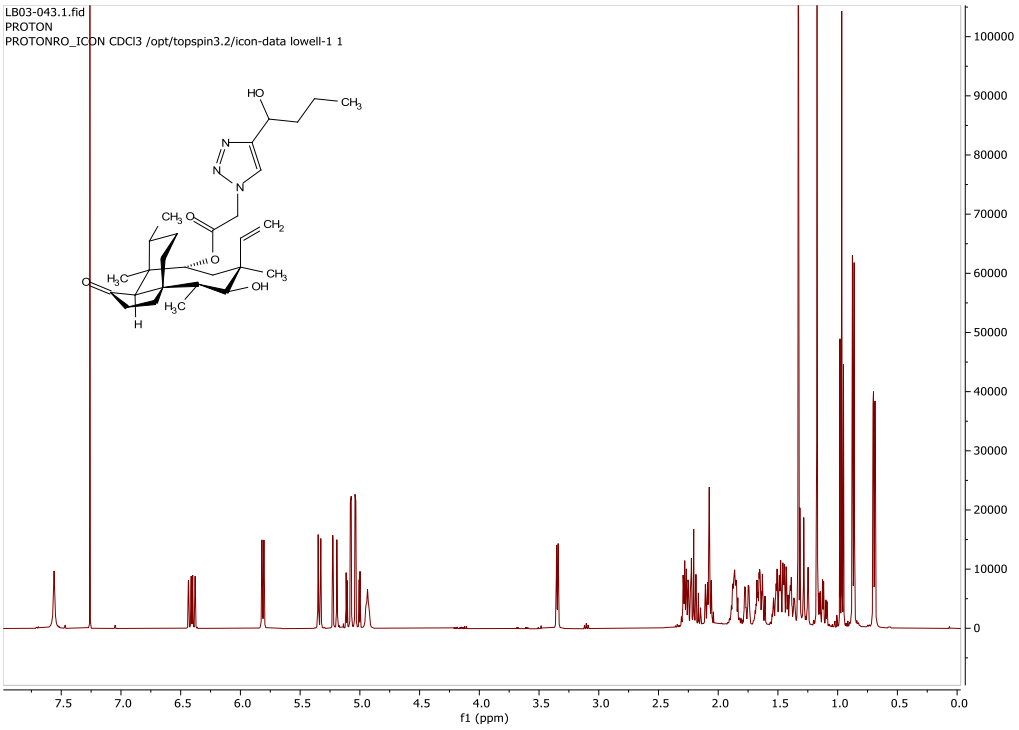


**Figure S82.** $^{1}$H NMR ($CDCl_3$, 500 MHz) of **25**.

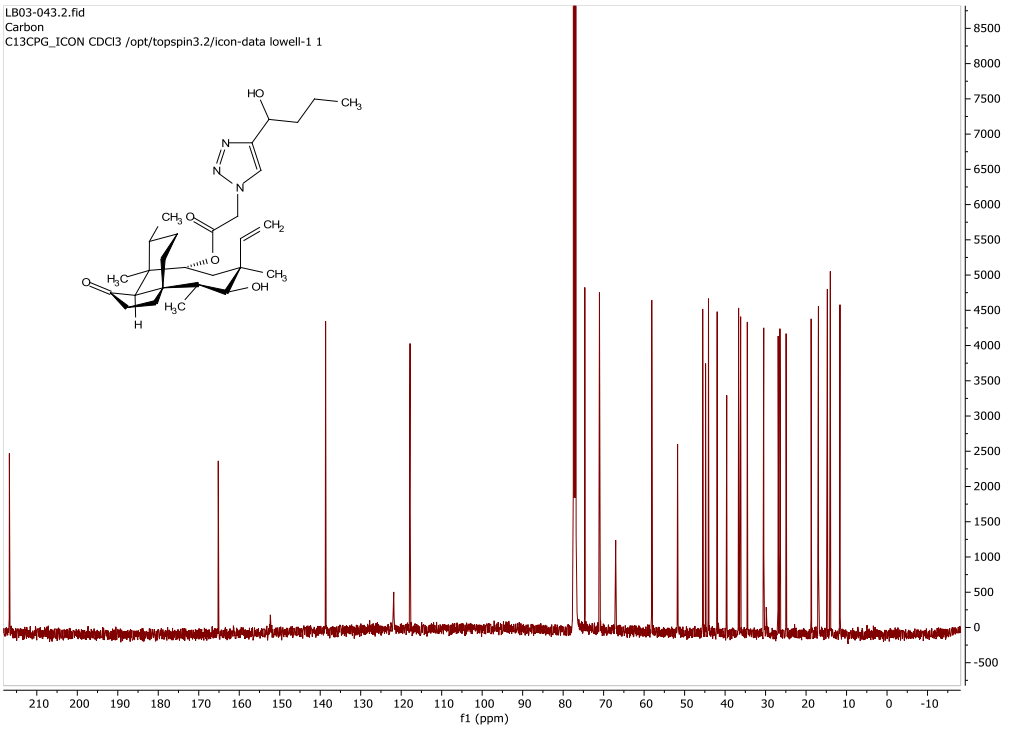


**Figure S83.** $^{13}$C NMR ($CDCl_3$, 125 MHz) of **25**.

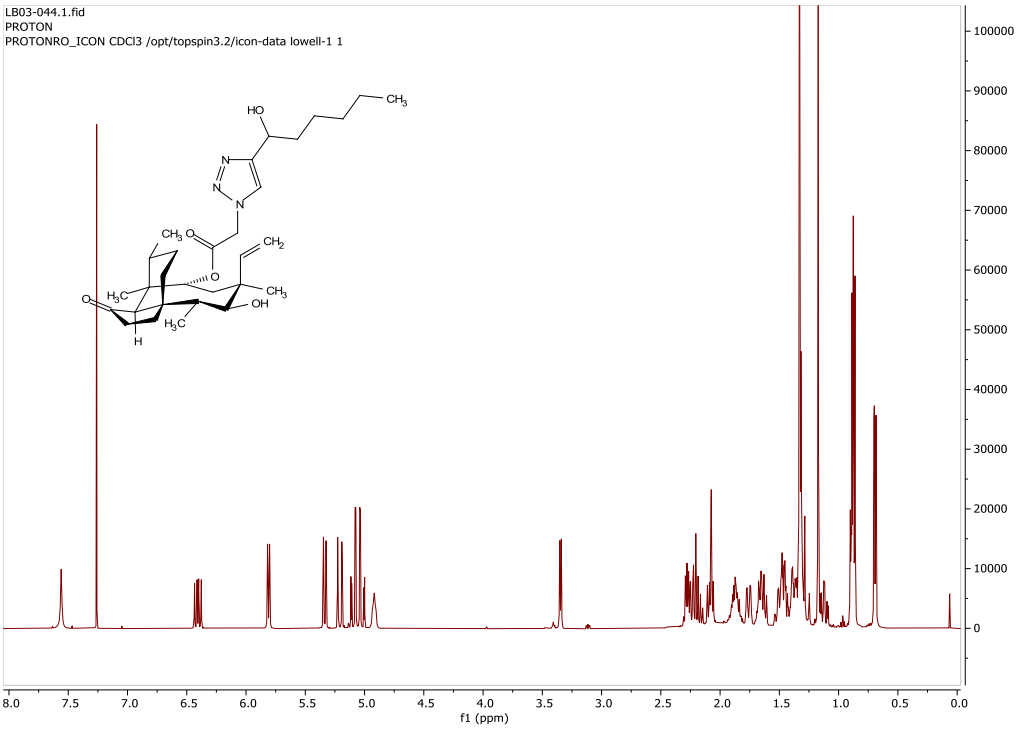


**Figure S84.** $^{1}$H NMR ($CDCl_3$, 500 MHz) of **26**.

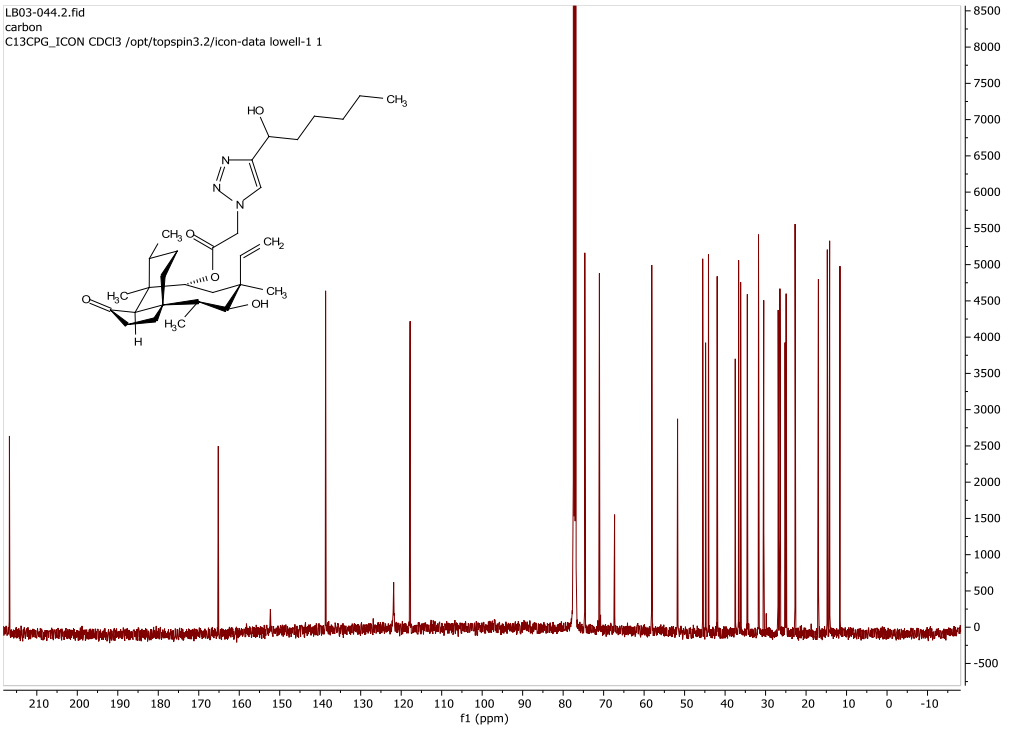


**Figure S85.** $^{13}$C NMR ($CDCl_3$, 125 MHz) of **26**.

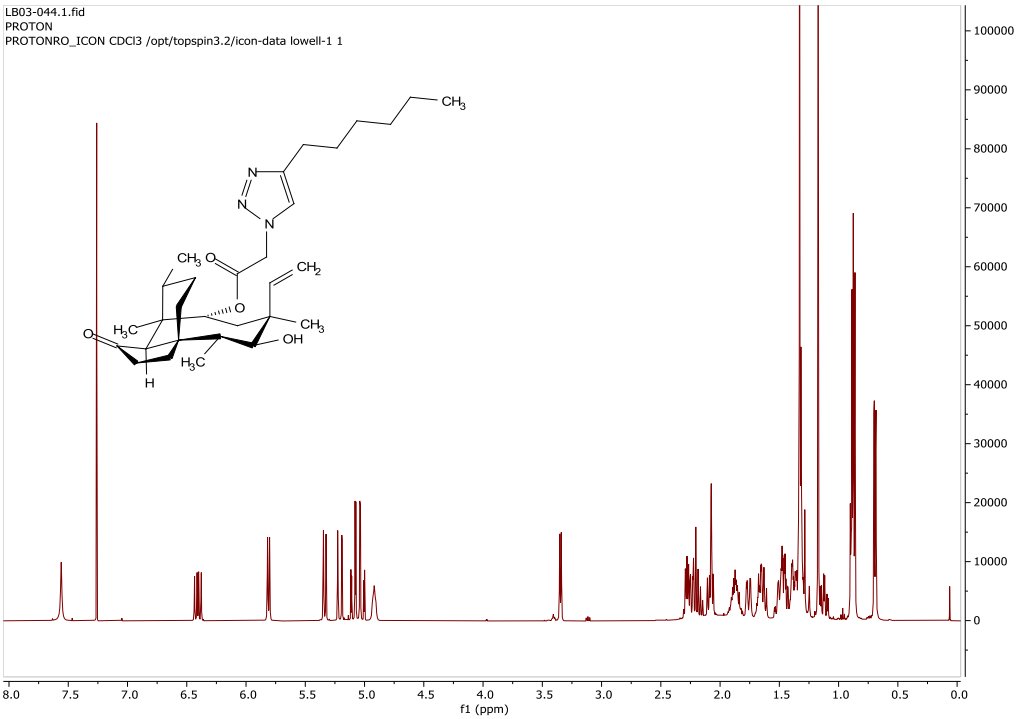


**Figure S86.** $^{1}$H NMR ($CDCl_3$, 500 MHz) of **27**.

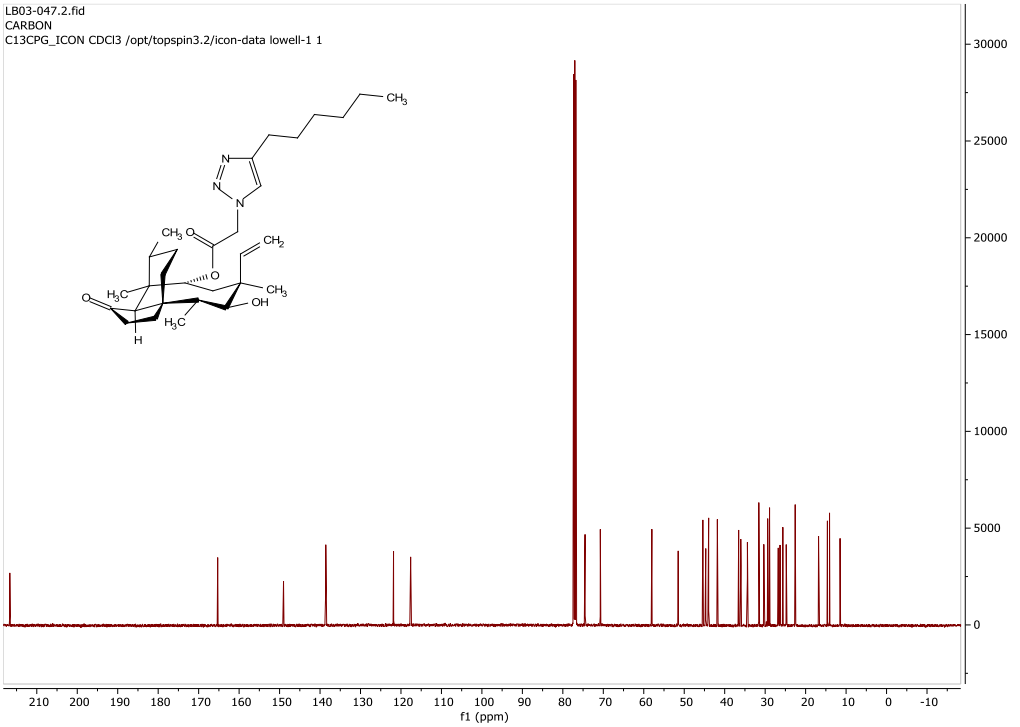


**Figure S87.** $^{13}$C NMR ($CDCl_3$, 125 MHz) of **27**.

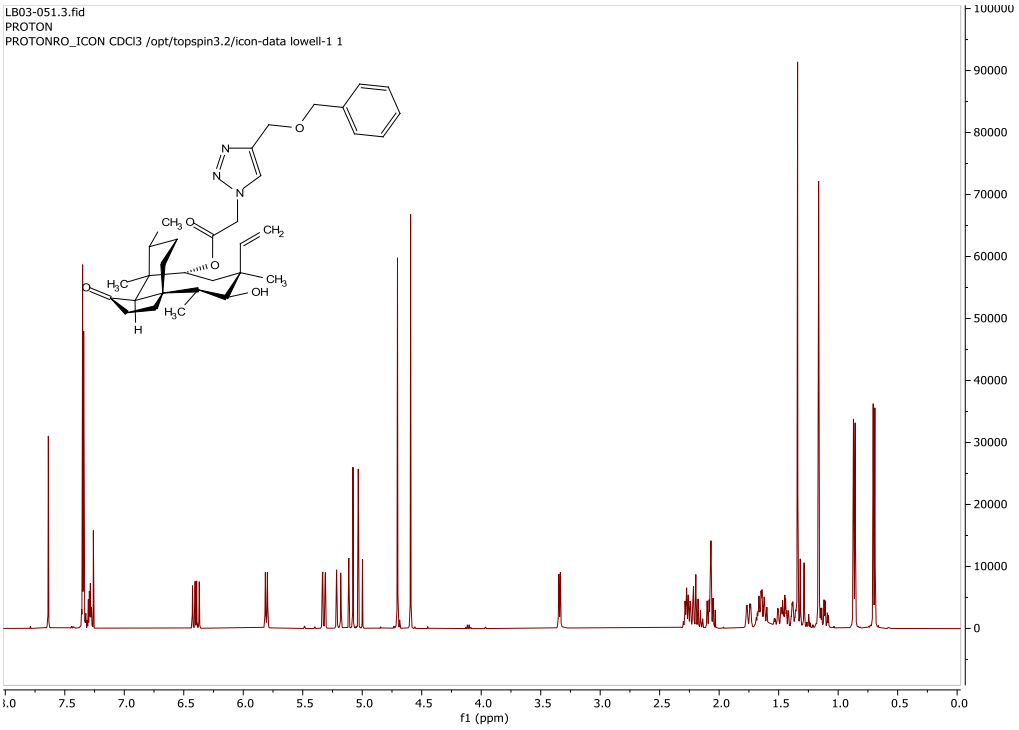


**Figure S88.** $^{1}$H NMR ($CDCl_3$, 500 MHz) of **28**.

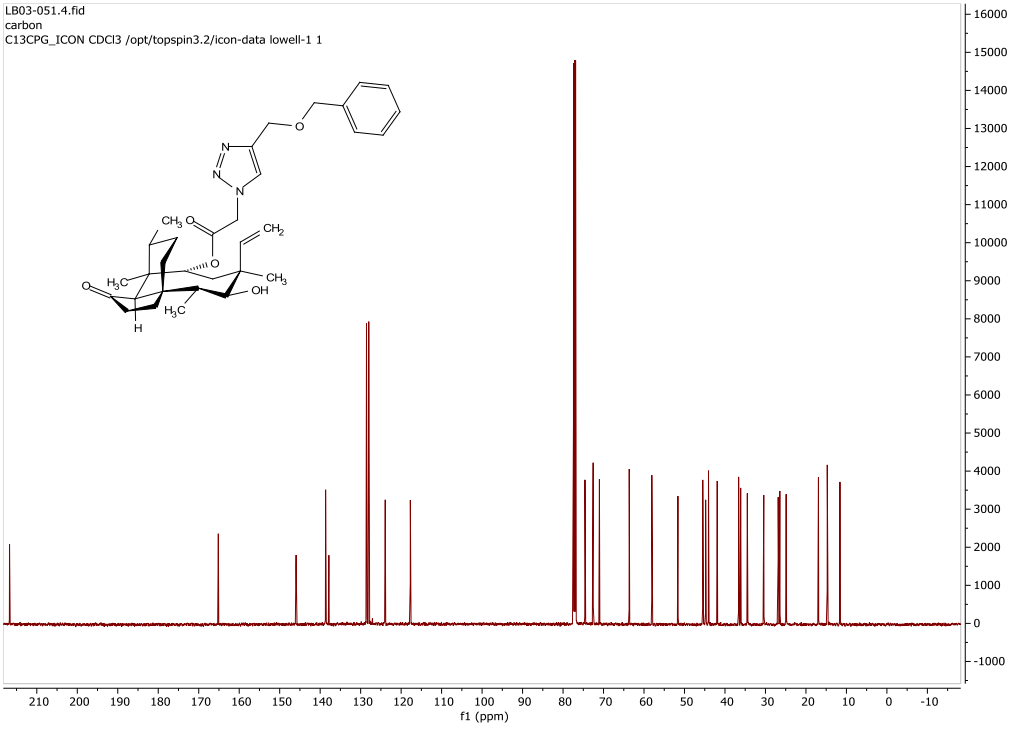


**Figure S89.** $^{13}$C NMR ($CDCl_3$, 125 MHz) of **28**.

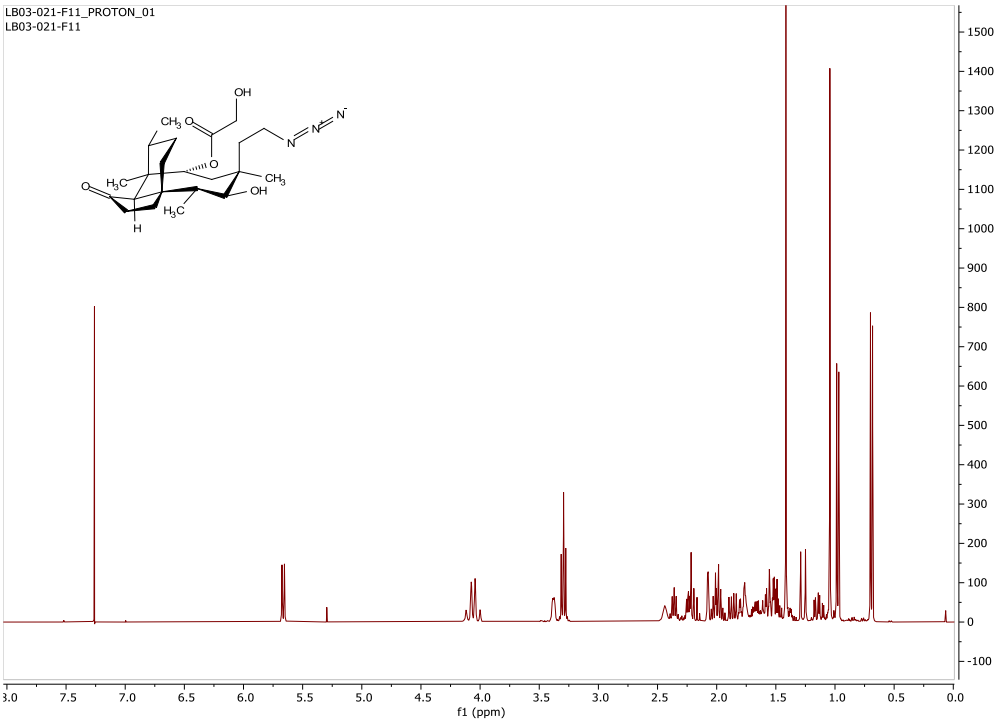


**Figure S90.** $^{1}$H NMR ($CDCl_3$, 500 MHz) of **30**.

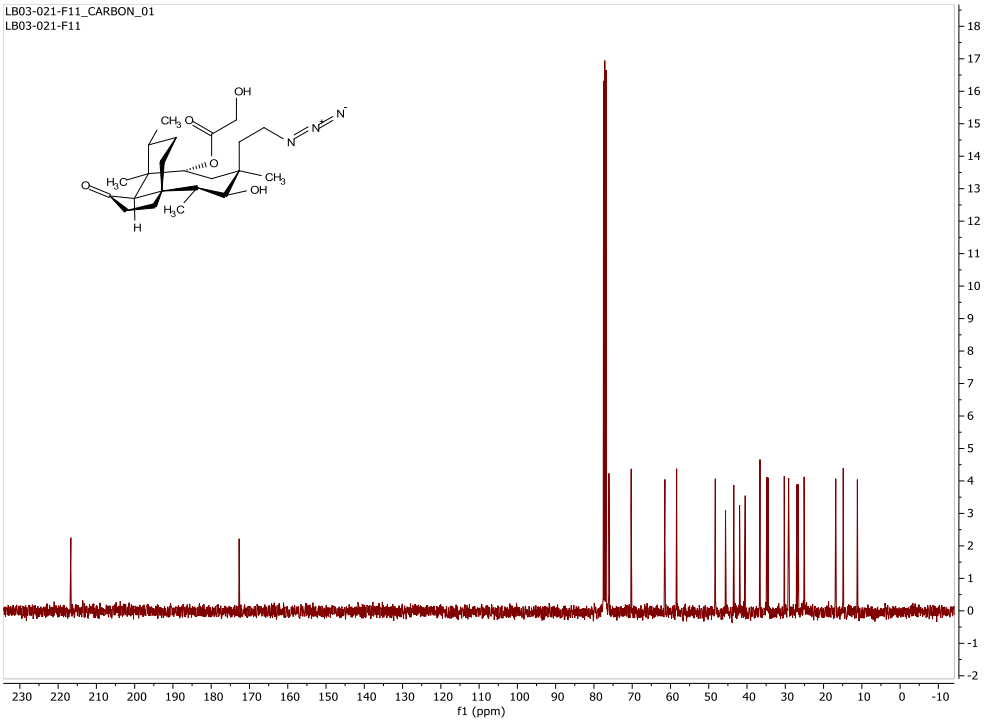


**Figure S91.** $^{13}$C NMR ($CDCl_3$, 125 MHz) of **30**.

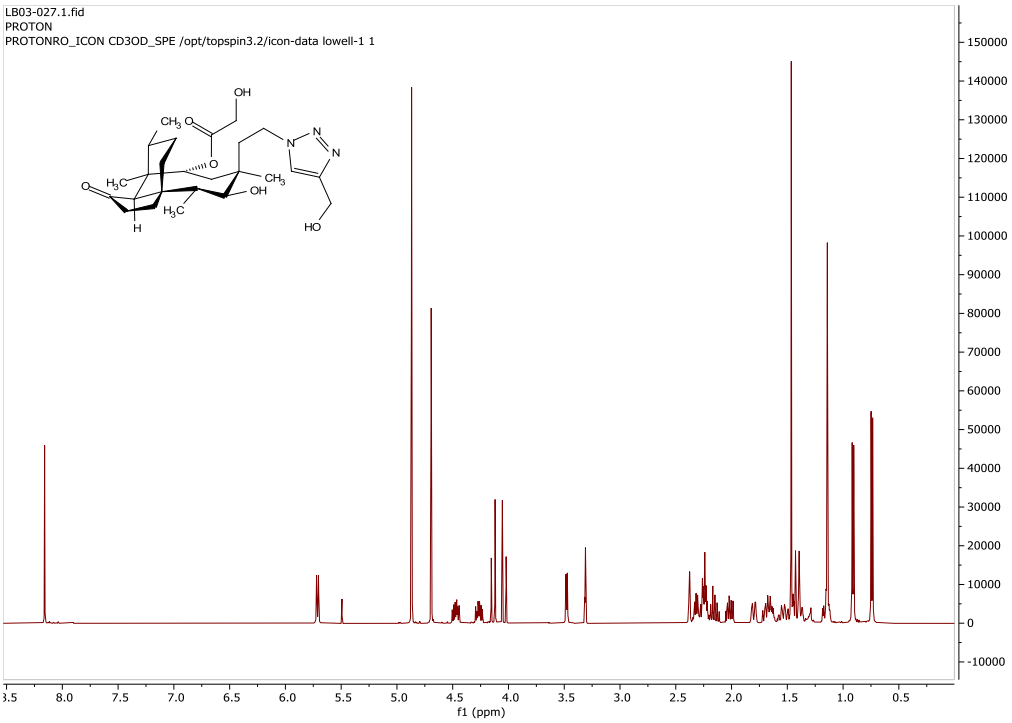


**Figure S92.** $^{1}$H NMR ($CD_3OD$, 500 MHz) of **31**.

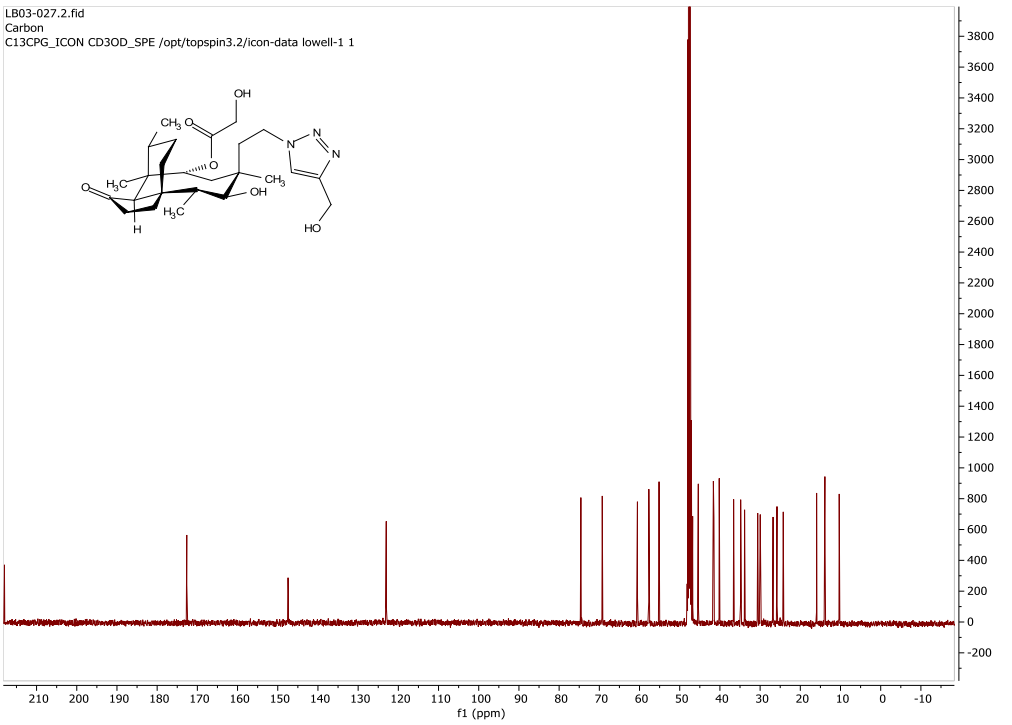


**Figure S93.** $^{13}$C NMR ($CD_3OD$, 125 MHz) of **31**.

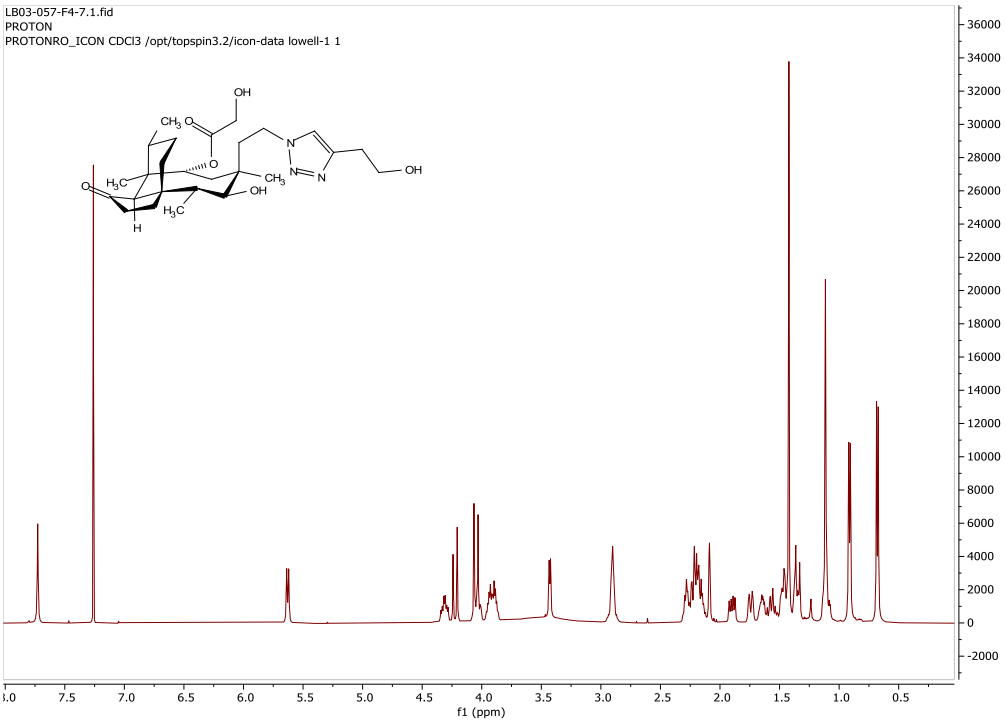


**Figure S94.** $^{1}$H NMR ($CDCl_3$, 500 MHz) of **32**.

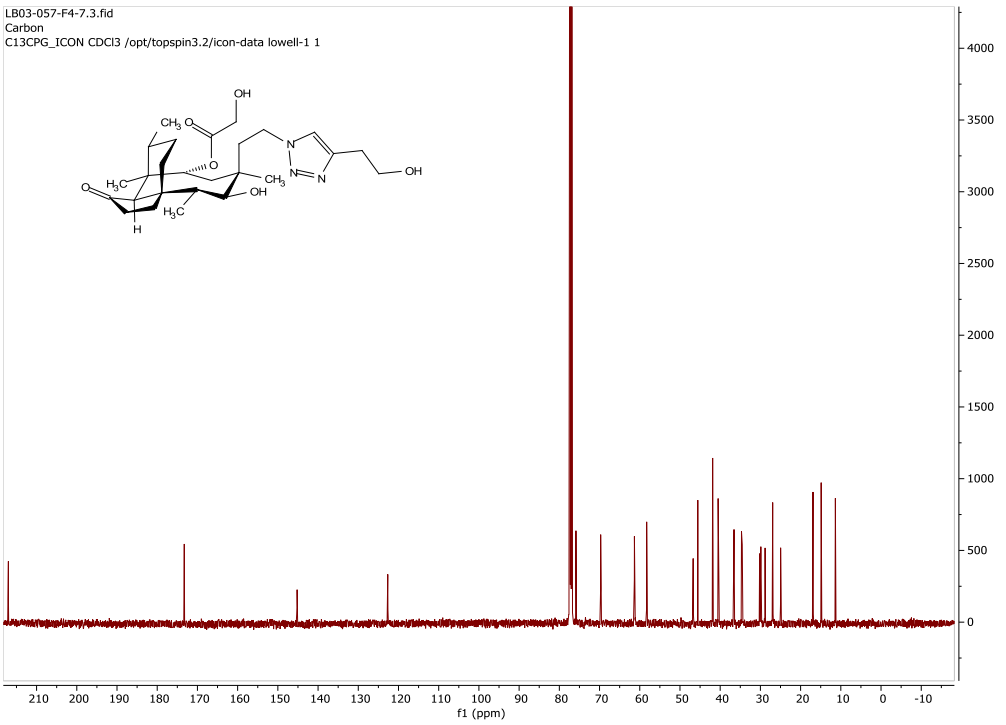


**Figure S95.** $^{13}$C NMR ($CDCl_3$, 125 MHz) of **32**.

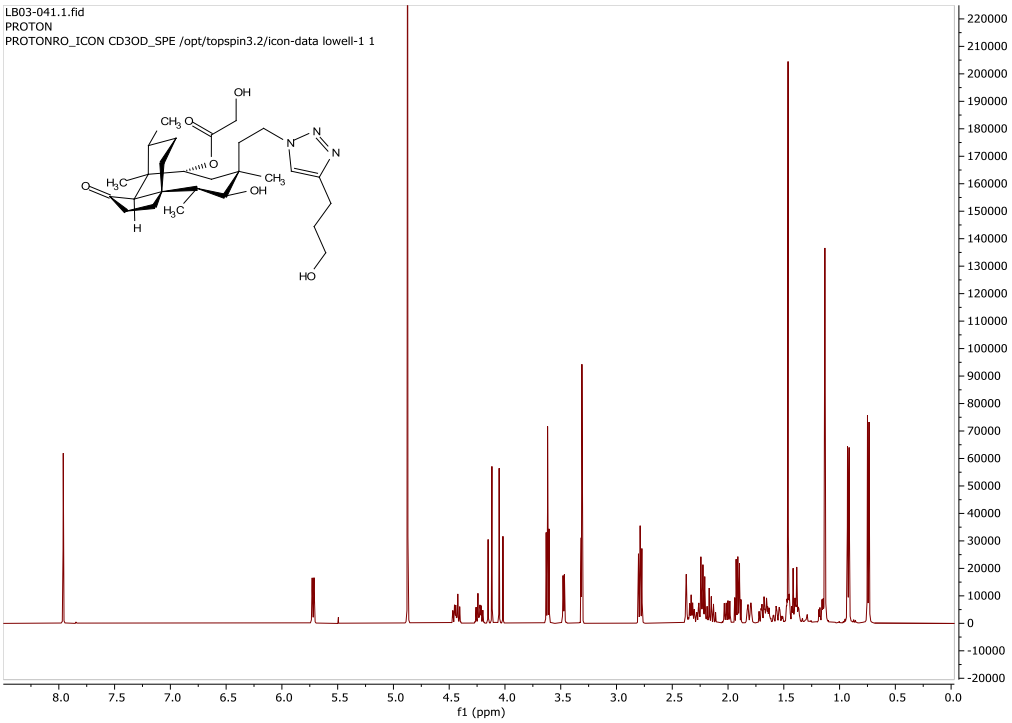


**Figure S96.** $^{1}$H NMR ($CD_3OD$, 500 MHz) of **33**.

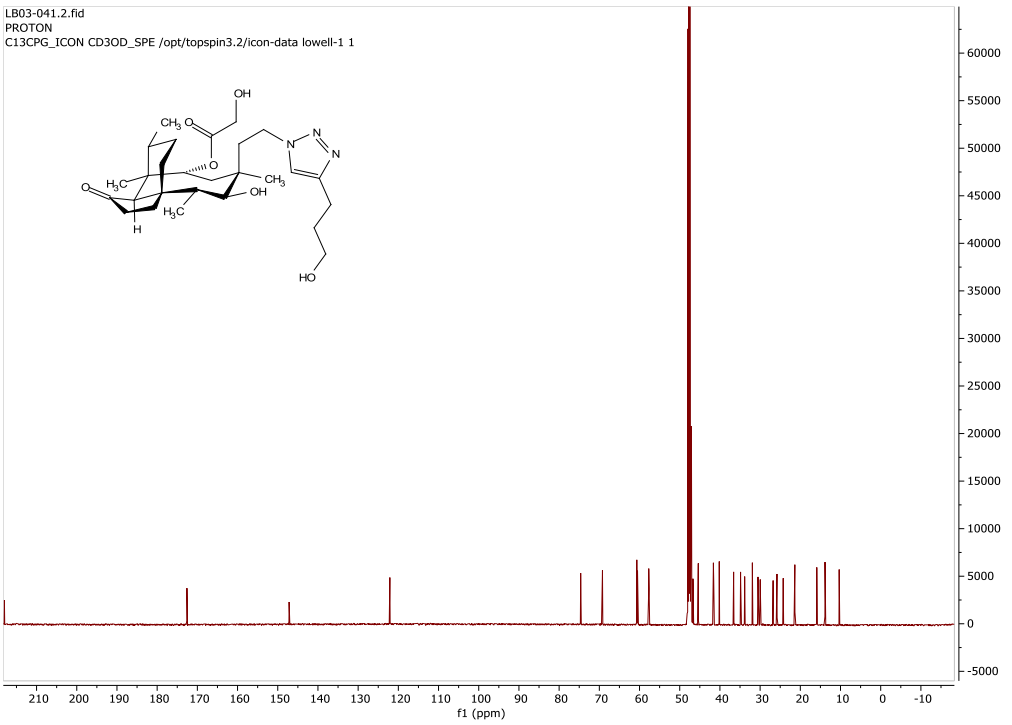


**Figure S97.** $^{13}$C NMR ($CD_3OD$, 125 MHz) of **33**.

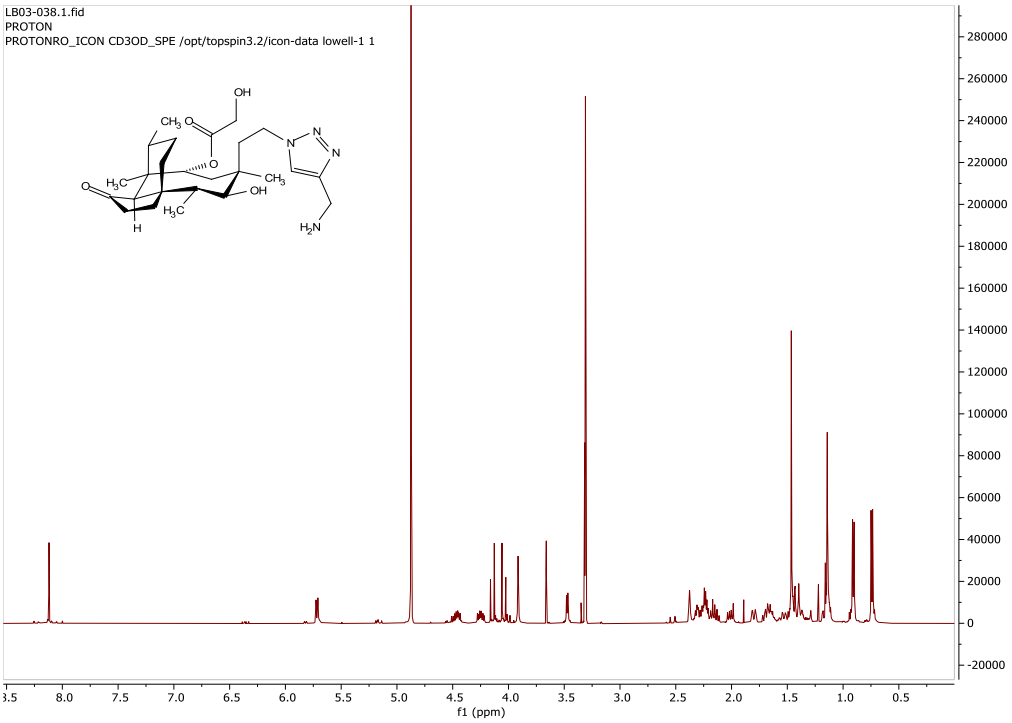


**Figure S98.** $^{1}$H NMR ($CD_3OD$, 500 MHz) of **34**.

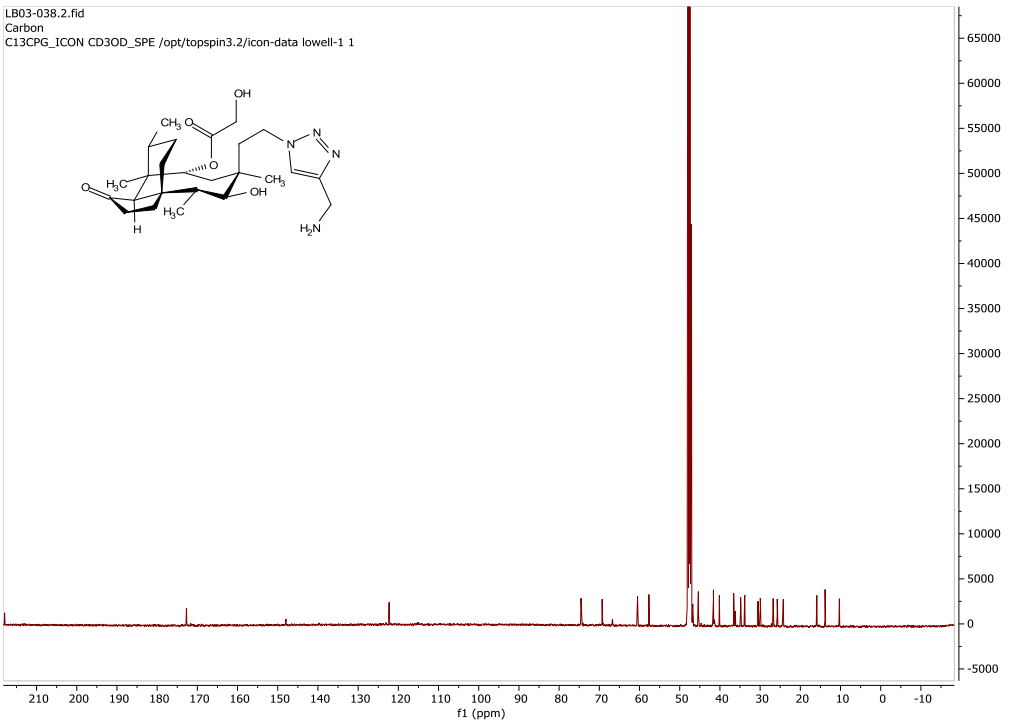


**Figure S99.** $^{13}$C NMR ($CD_3OD$, 125 MHz) of **34**.

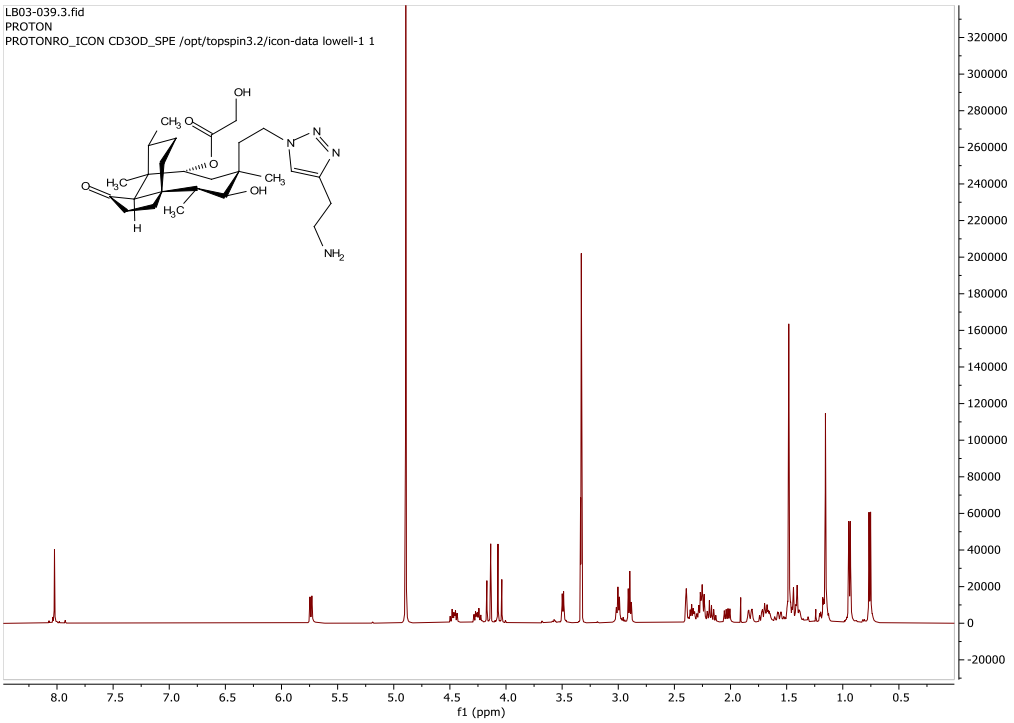


**Figure S100.** $^{1}$H NMR ($CD_3OD$, 500 MHz) of **35**.

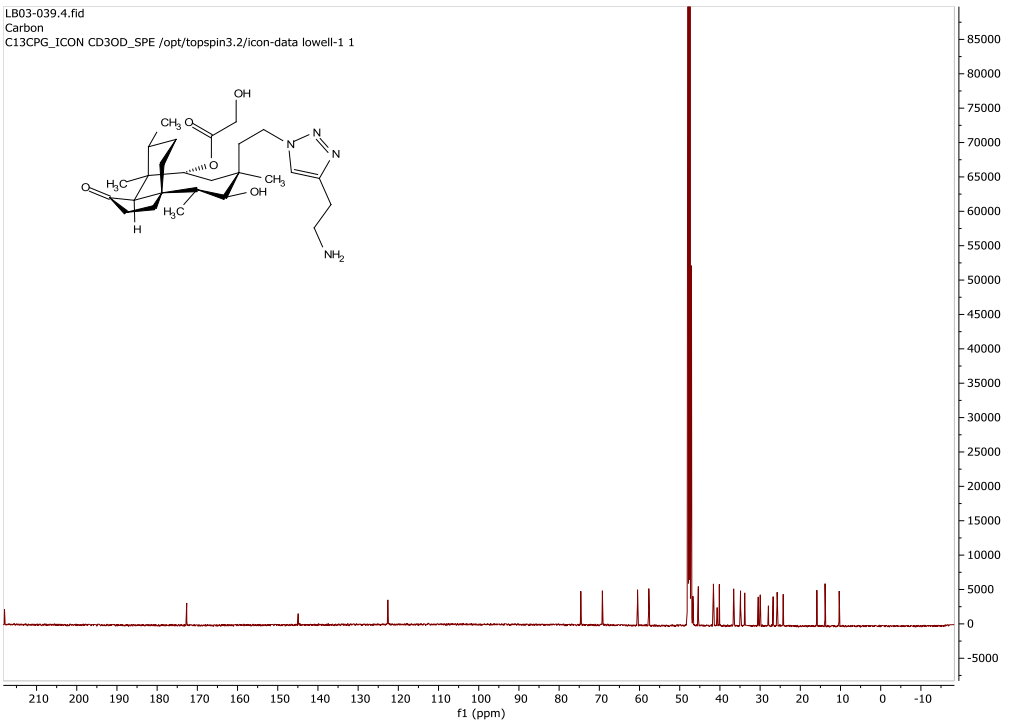


**Figure S101.** $^{13}$C NMR ($CD_3OD$, 125 MHz) of **35**.

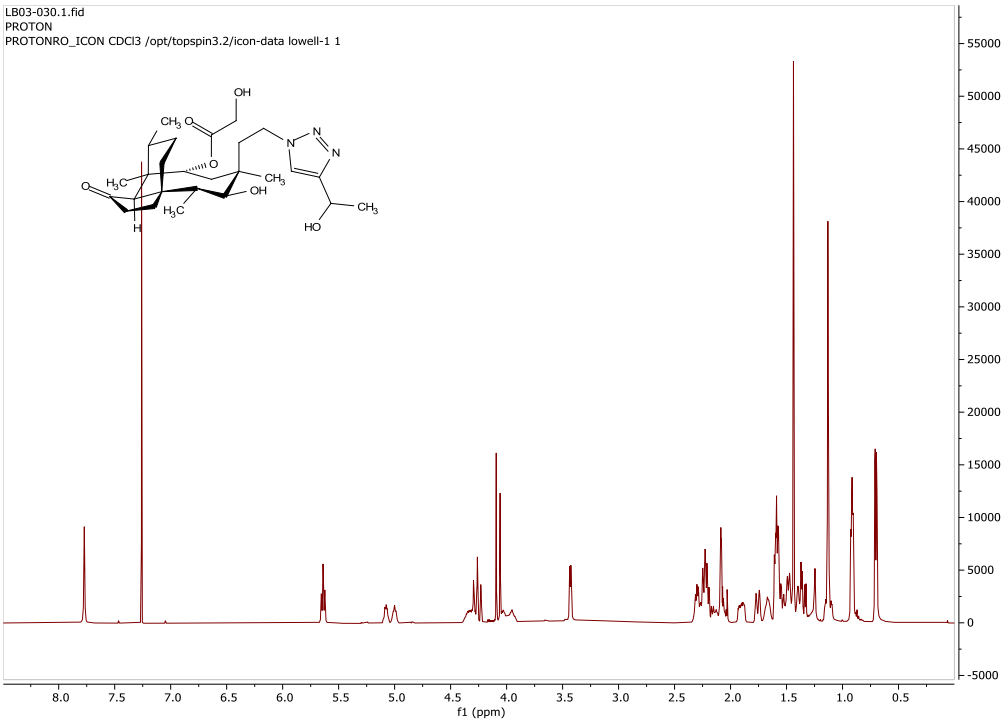


**Figure S102.** $^{1}$H NMR ($CDCl_3$, 500 MHz) of **36**.

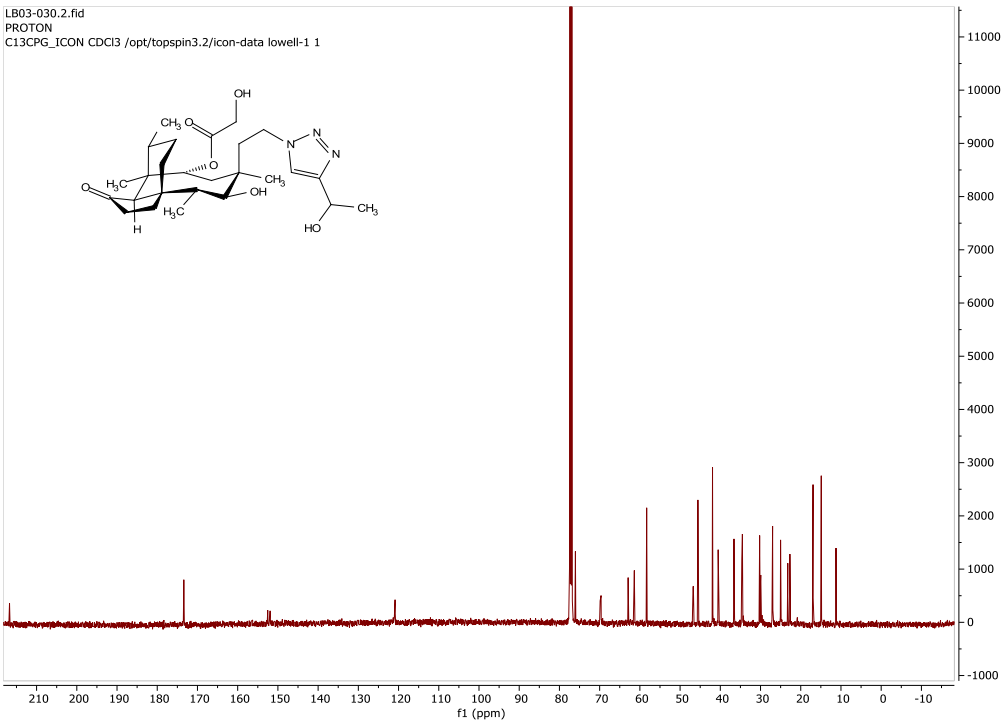


**Figure S103.** $^{13}$C NMR ($CDCl_3$, 125 MHz) of **36**.

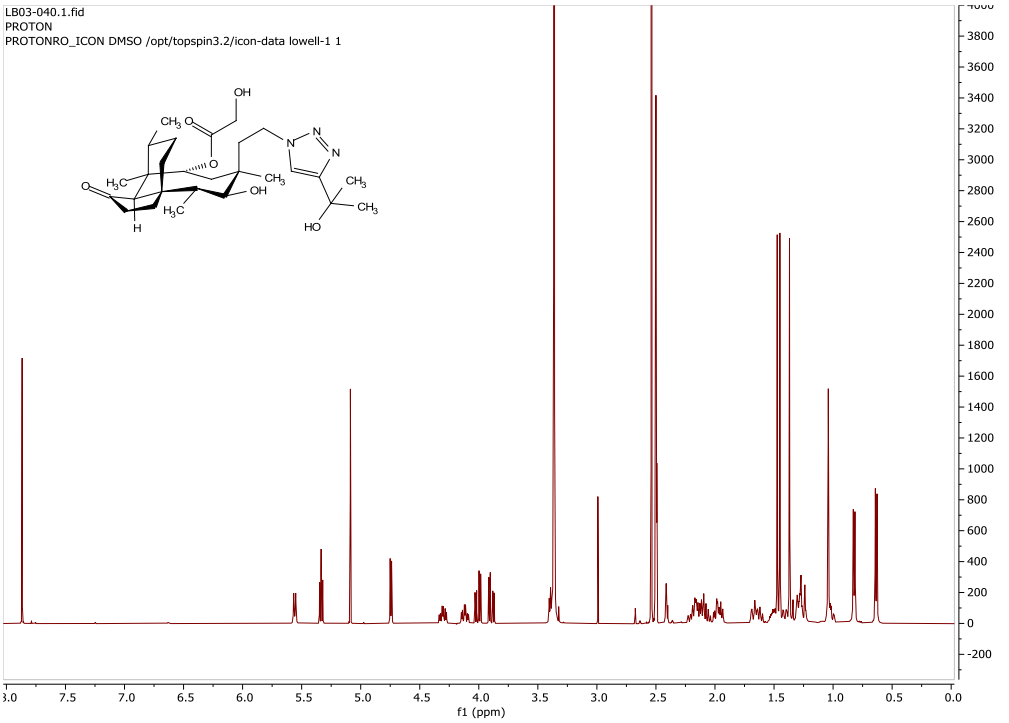


**Figure S104.** $^{1}$H NMR ($(CD_3)_2SO$, 500 MHz) of **37**.

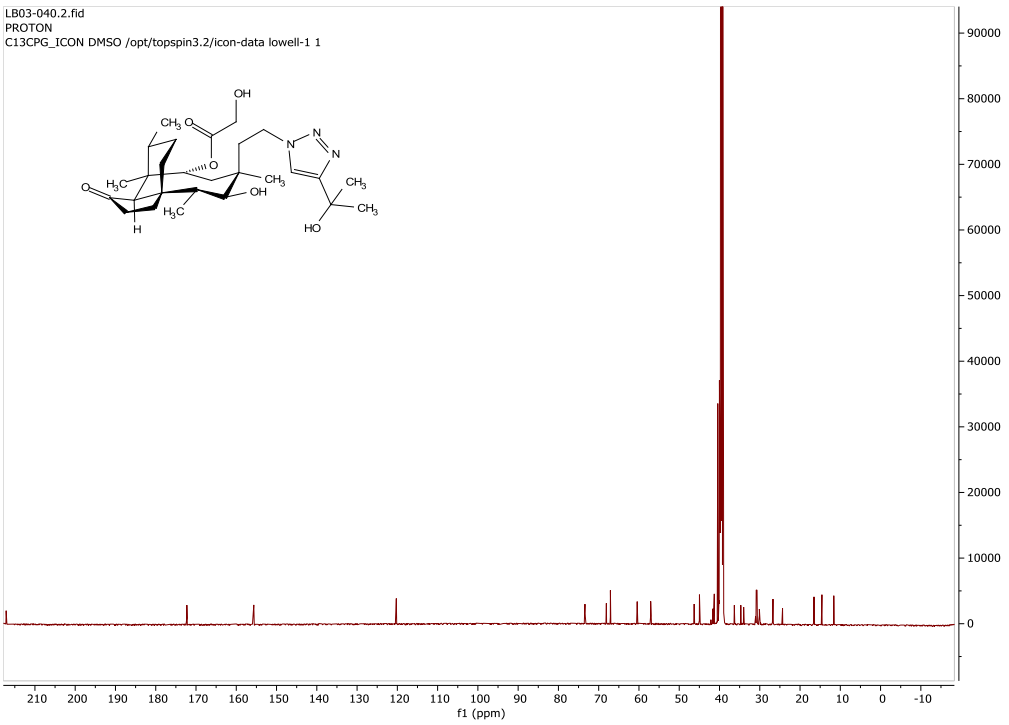


**Figure S105.** $^{13}$C NMR ($(CD_3)_2SO$, 125 MHz) of **37**.

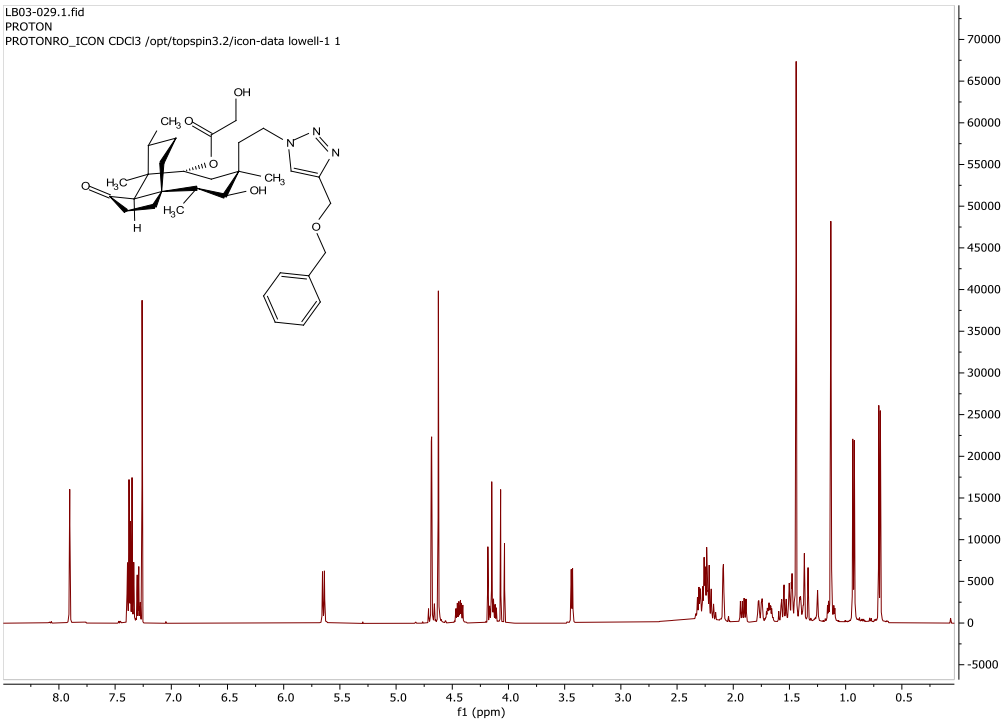


**Figure S106.** $^{1}$H NMR ($CDCl_3$, 500 MHz) of **38**.

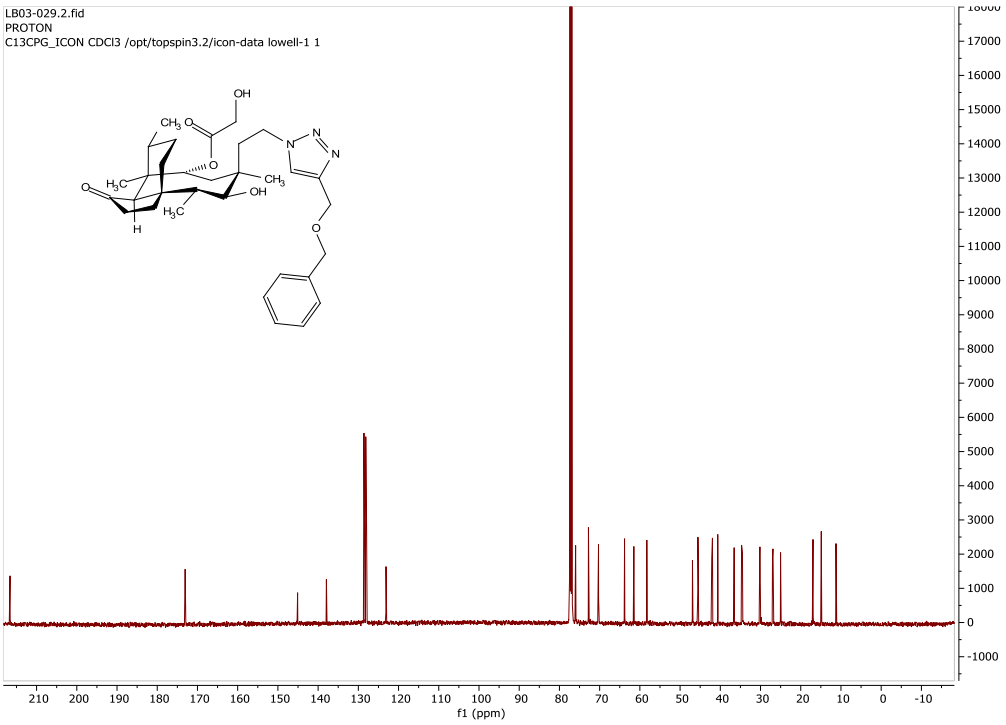


**Figure S107.** $^{13}$C NMR ($CDCl_3$, 125 MHz) of **38**.

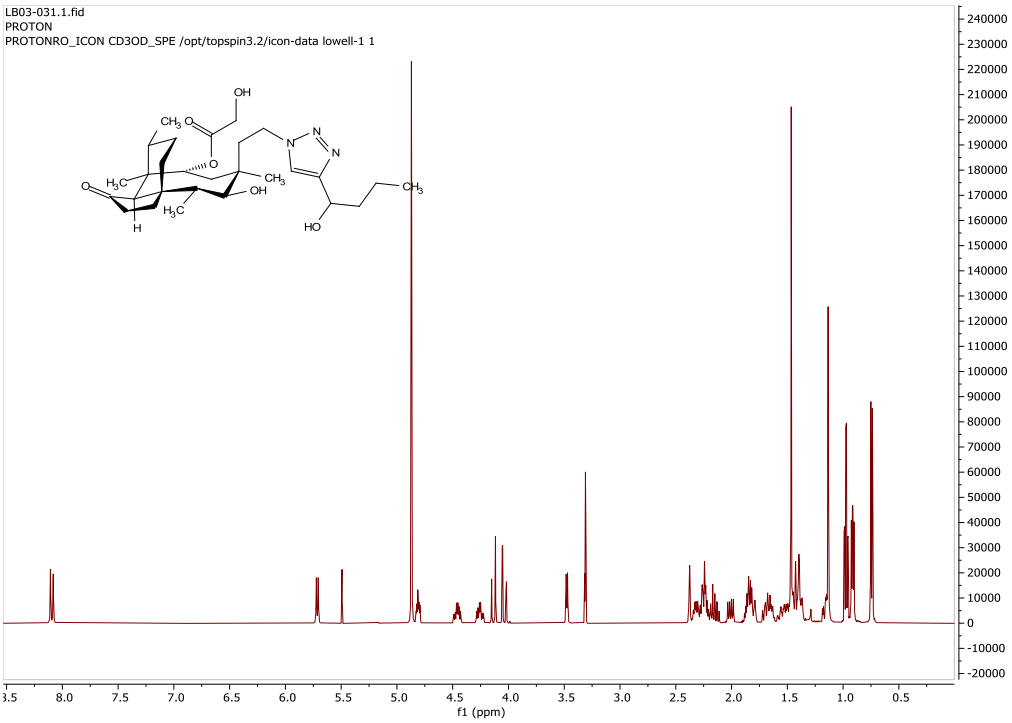


**Figure S108.** $^{1}$H NMR ($CD_3OD$, 500 MHz) of **39**.

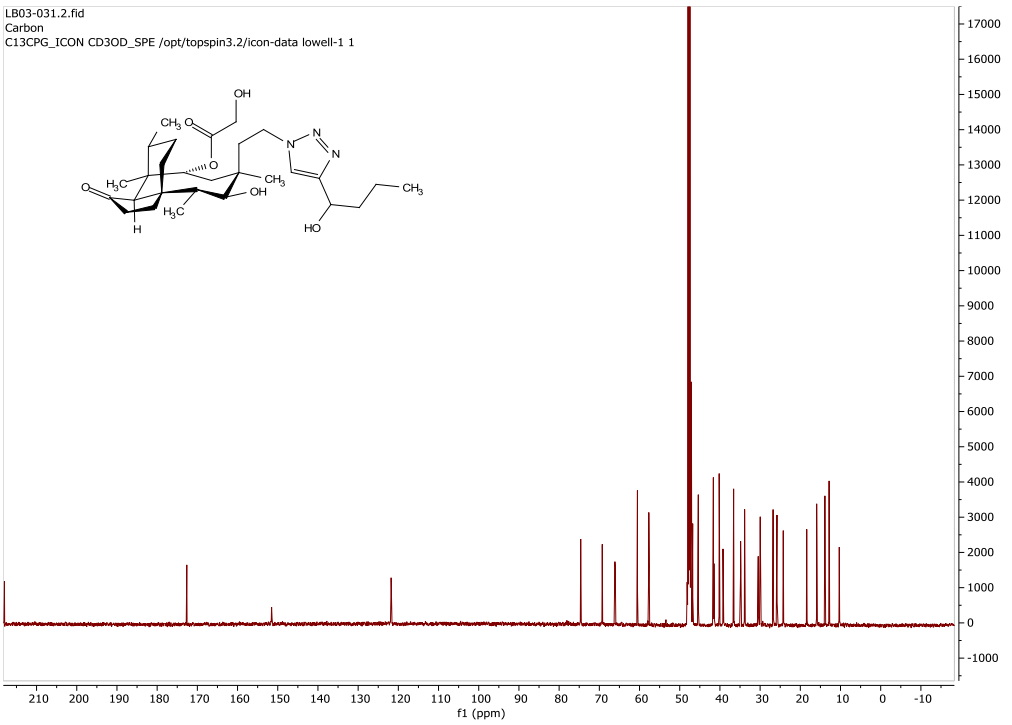


**Figure S109.** $^{13}$C NMR ($CD_3OD$, 125 MHz) of **39**.

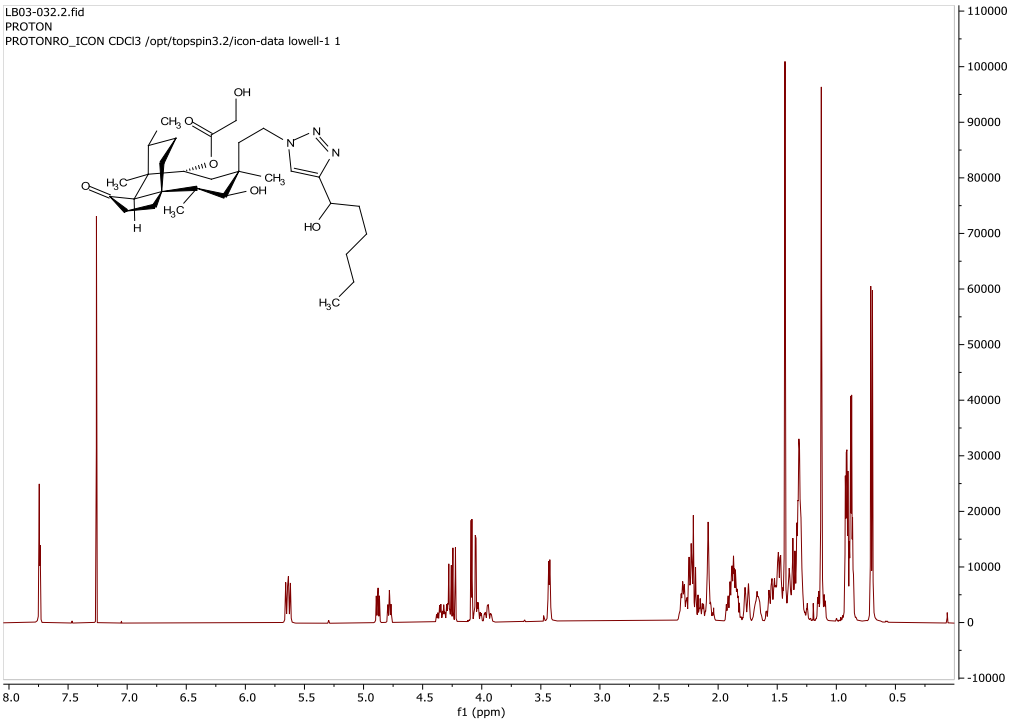


**Figure S110.** $^{1}$H NMR ($CDCl_3$, 500 MHz) of **40**.

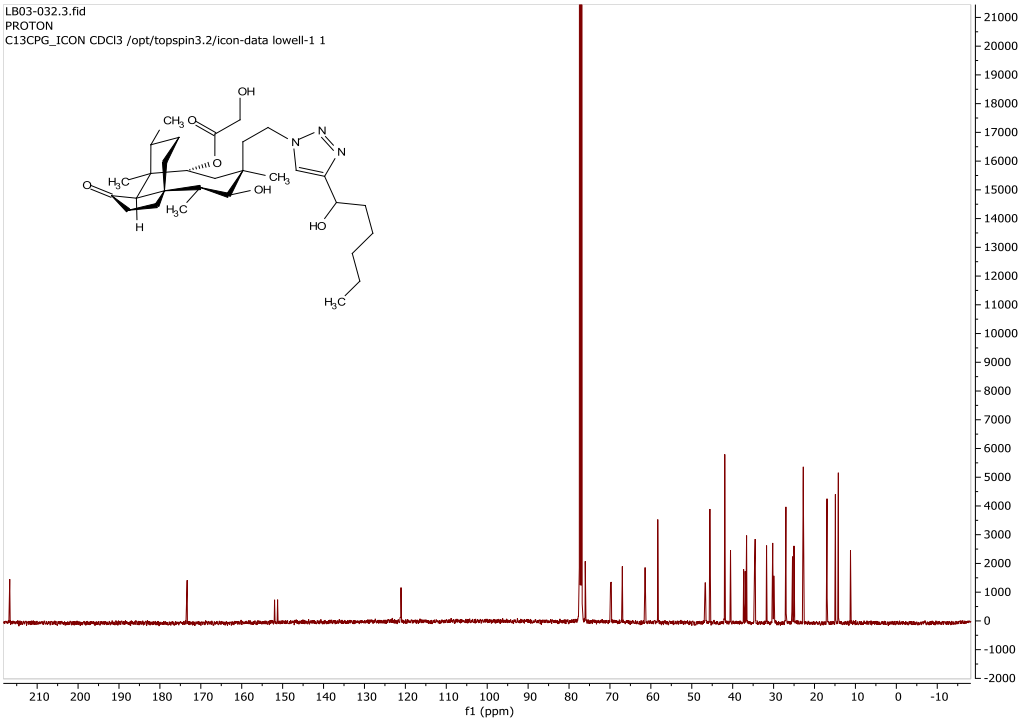


**Figure S111.** $^{13}$C NMR ($CDCl_3$, 125 MHz) of **40**.

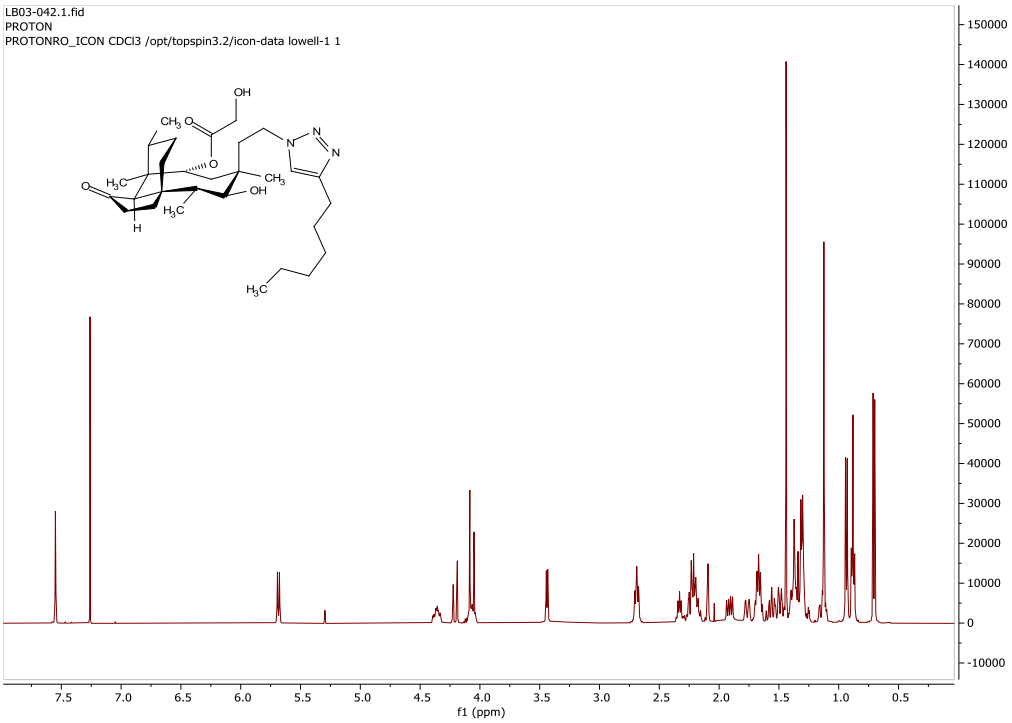


**Figure S112.** $^{1}$H NMR ($CDCl_3$, 500 MHz) of **41**.

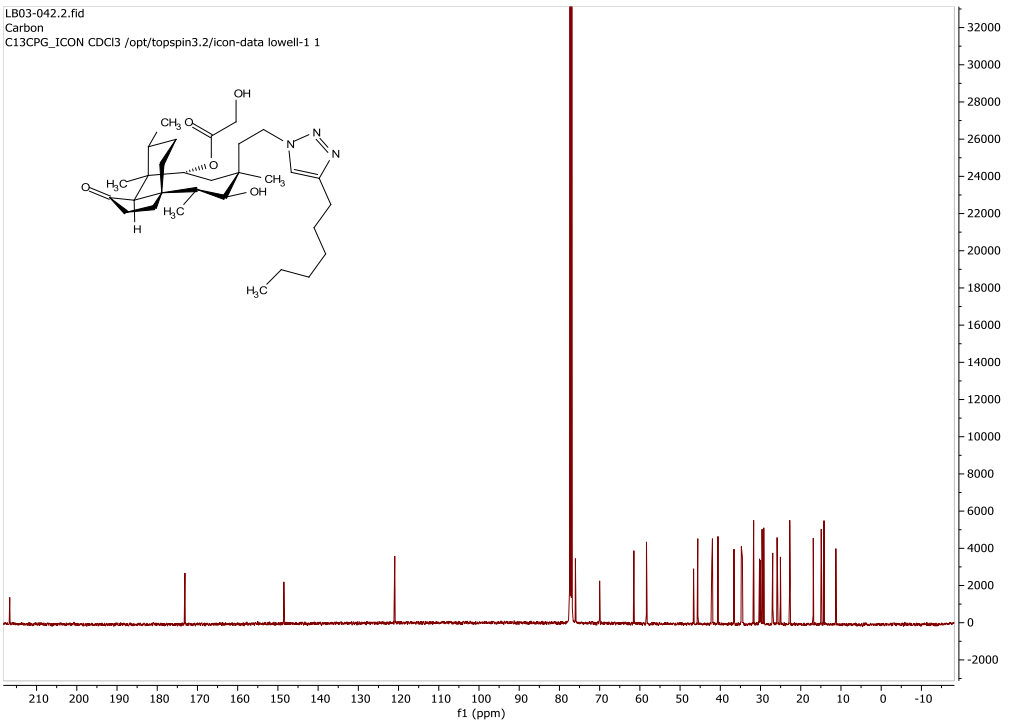


**Figure S113.** $^{13}$C NMR ($CDCl_3$, 125 MHz) of **41**.

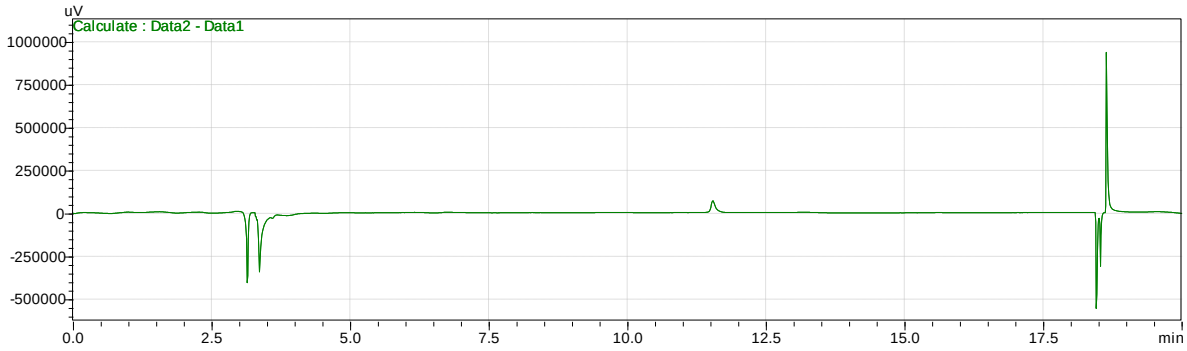


**Figure S114.** HPLC trace of (3a*R*,4*R*,5*S*,7*S*,8*S*,9*R*,9a*S*,12*R*)-8-hydroxy-4,7,9,12-tetramethyl-3-oxo-7-vinyldecahydro-4,9a-propanocyclopenta[8]annulen-5-yl 2-azidoacetate (**17**)

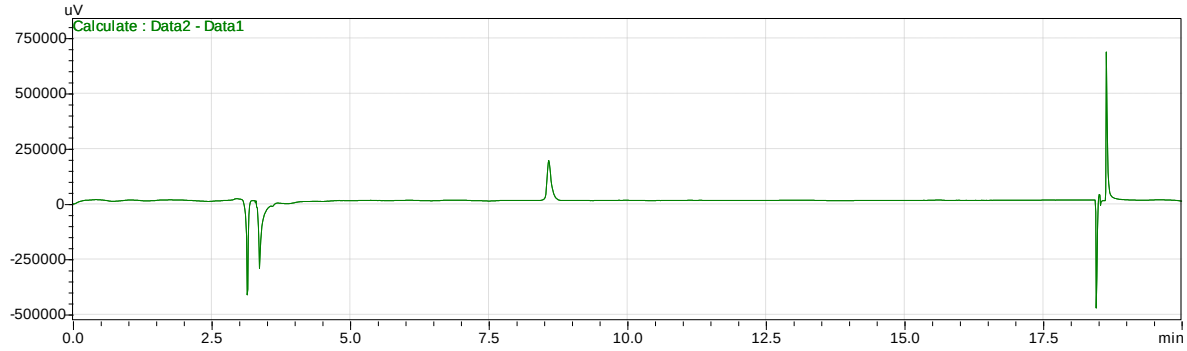


**Figure S115.** HPLC trace of (3a*R*,4*R*,5*S*,7*S*,8*S*,9*R*,9a*S*,12*R*)-8-Hydroxy-4,7,9,12-tetramethyl-3-oxo-7-vinyldecahydro-4,9a-propanocyclopenta[8]annulen-5-yl 2-(4-(hydroxymethyl)-1*H*-1,2,3-triazol-1-yl)acetate (**18**).

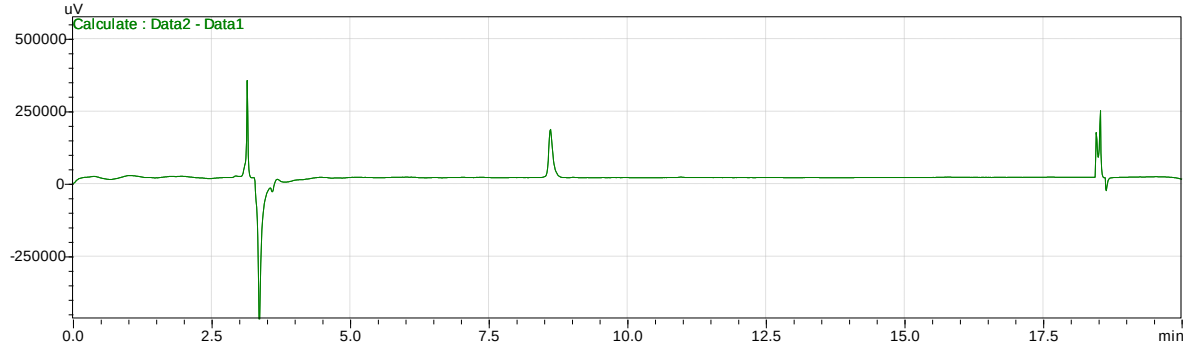

**Figure S116.** HPLC trace of (3a*R*,4*R*,5*S*,7*S*,8*S*,9*R*,9a*S*,12*R*)-8-Hydroxy-4,7,9,12-tetramethyl-3-oxo-7-vinyldecahydro-4,9a-propanocyclopenta[8]annulen-5-yl 2-(4-(2-hydroxyethyl)-1*H*-1,2,3-triazol-1-yl)acetate (**19**).

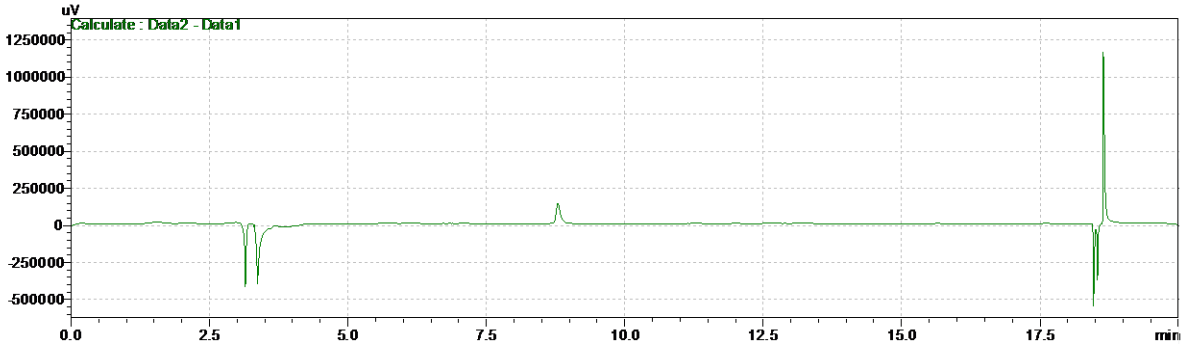


**Figure S117.** HPLC trace of (3a*R*,4*R*,5*S*,7*S*,8*S*,9*R*,9a*S*,12*R*)-8-Hydroxy-4,7,9,12-tetramethyl-3-oxo-7-vinyldecahydro-4,9a-propanocyclopenta[8]annulen-5-yl 2-(4-(3-hydroxypropyl)-1*H*-1,2,3-triazol-1-yl)acetate (**20**).

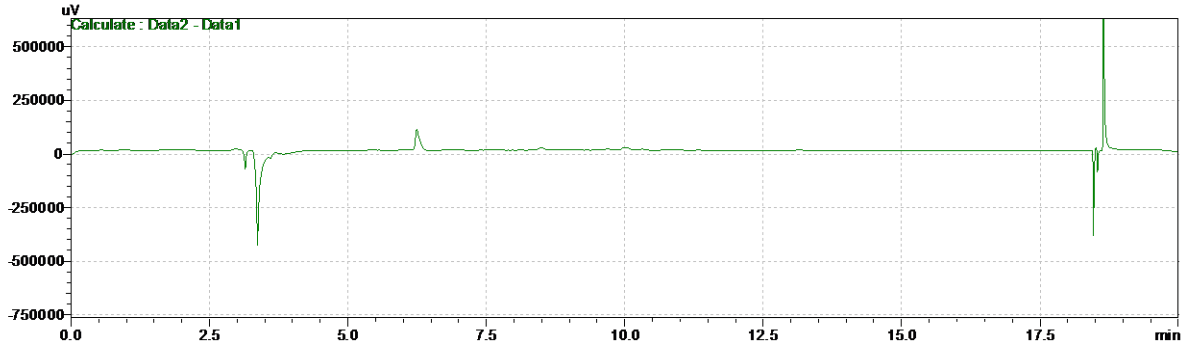


**Figure S118.** HPLC trace of (3a*R*,4*R*,5*S*,7*S*,8*S*,9*R*,9a*S*,12*R*)-8-Hydroxy-4,7,9,12-tetramethyl-3-oxo-7-vinyldecahydro-4,9a-propanocyclopenta[8]annulen-5-yl 2-(4-(aminomethyl)-1*H*-1,2,3-triazol-1-yl)acetate (**21**).

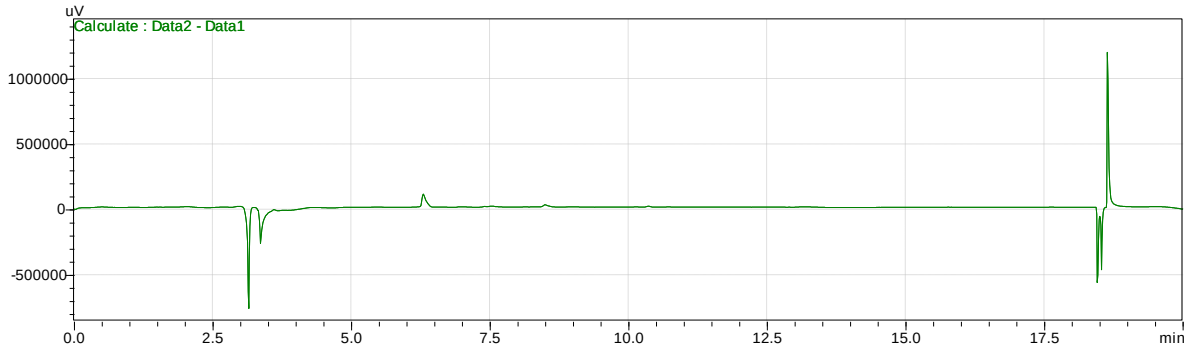


**Figure S119.** HPLC trace of (3a*R*,4*R*,5*S*,7*S*,8*S*,9*R*,9a*S*,12*R*)-8-Hydroxy-4,7,9,12-tetramethyl-3-oxo-7-vinyldecahydro-4,9a-propanocyclopenta[8]annulen-5-yl 2-(4-(2-aminoethyl)-1*H*-1,2,3-triazol-1-yl)acetate (**22**).

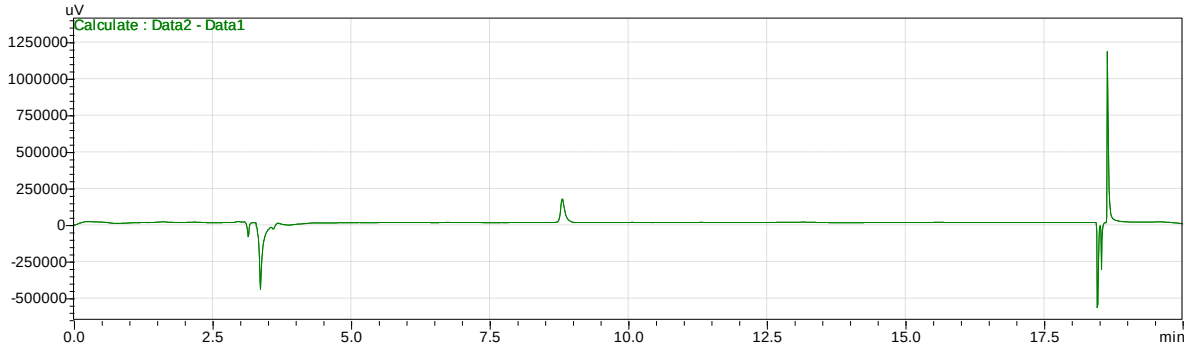


**Figure S120.** HPLC trace of (3a*R*,4*R*,5*S*,7*S*,8*S*,9*R*,9a*S*,12*R*)-8-Hydroxy-4,7,9,12-tetramethyl-3-oxo-7-vinyldecahydro-4,9a-propanocyclopenta[8]annulen-5-yl 2-(4-(1-hydroxyethyl)-1*H*-1,2,3-triazol-1-yl)acetate (**23**).

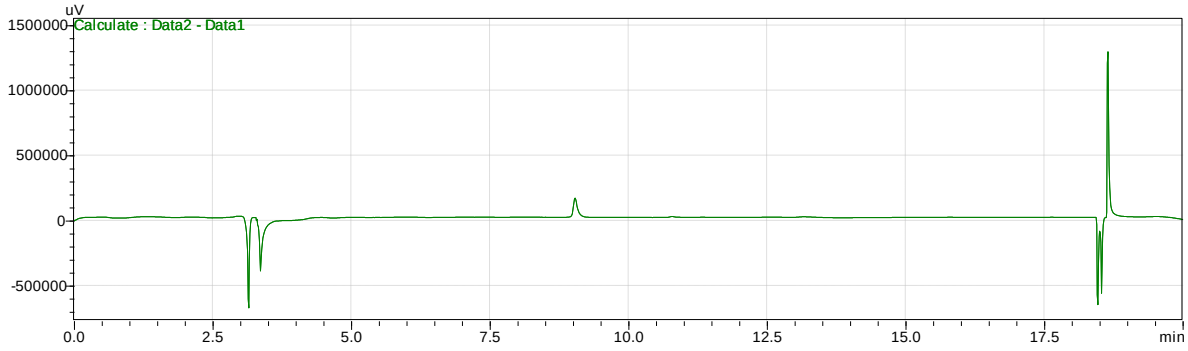

**Figure S121.** HPLC trace of (3a*R*,4*R*,5*S*,7*S*,8*S*,9*R*,9a*S*,12*R*)-8-Hydroxy-4,7,9,12-tetramethyl-3-oxo-7-vinyldecahydro-4,9a-propanocyclopenta[8]annulen-5-yl 2-(4-(2-hydroxypropan-2-yl)-1*H*-1,2,3-triazol-1-yl)acetate (**24**).

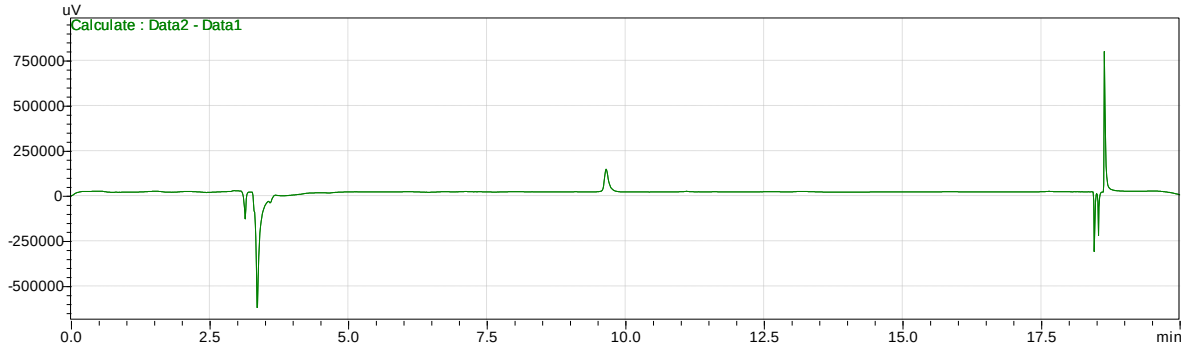


**Figure S122.** HPLC trace of (3a*R*,4*R*,5*S*,7*S*,8*S*,9*R*,9a*S*,12*R*)-8-Hydroxy-4,7,9,12-tetramethyl-3-oxo-7-vinyldecahydro-4,9a-propanocyclopenta[8]annulen-5-yl 2-(4-(1-hydroxybutyl)-1*H*-1,2,3-triazol-1-yl)acetate (**25**).

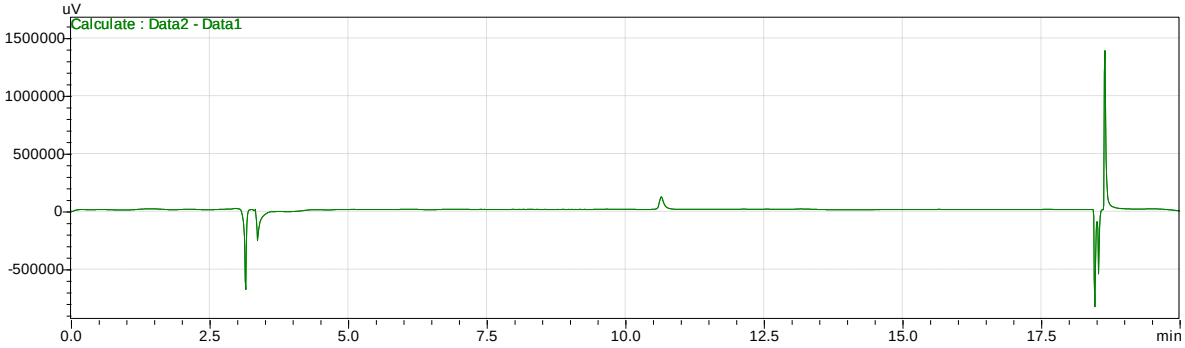


**Figure S123.** HPLC trace of (3a*R*,4*R*,5*S*,7*S*,8*S*,9*R*,9a*S*,12*R*)-8-Hydroxy-4,7,9,12-tetramethyl-3-oxo-7-vinyldecahydro-4,9a-propanocyclopenta[8]annulen-5-yl 2-(4-(1-hydroxyhexyl)-1*H*-1,2,3-triazol-1-yl)acetate (**26**).

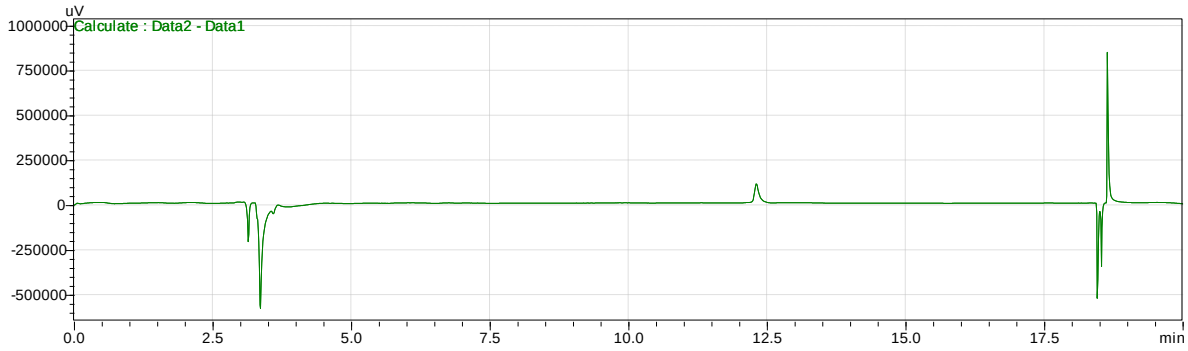


**Figure S124.** HPLC trace of (3a*R*,4*R*,5*S*,7*S*,8*S*,9*R*,9a*S*,12*R*)-8-Hydroxy-4,7,9,12-tetramethyl-3-oxo-7-vinyldecahydro-4,9a-propanocyclopenta[8]annulen-5-yl 2-(4-hexyl-1*H*-1,2,3-triazol-1-yl)acetate **(27**).

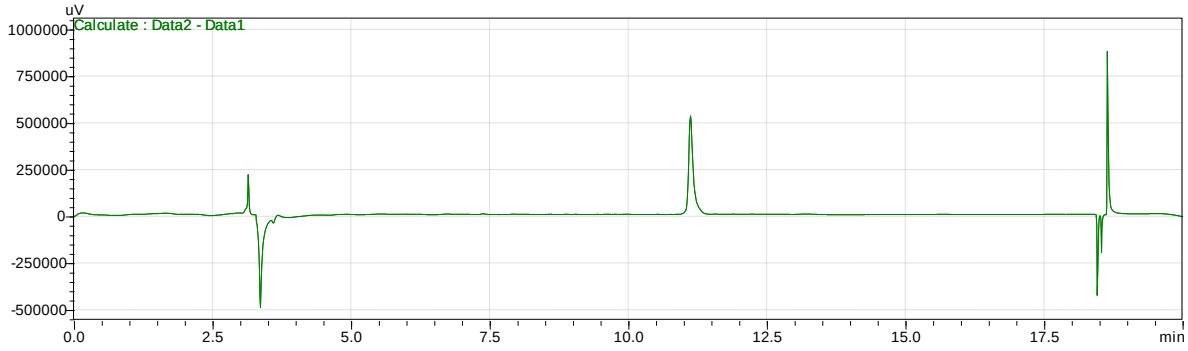


**Figure S125.** HPLC trace of (3a*R*,4*R*,5*S*,7*S*,8*S*,9*R*,9a*S*,12*R*)-8-Hydroxy-4,7,9,12-tetramethyl-3-oxo-7-vinyldecahydro-4,9a-propanocyclopenta[8]annulen-5-yl 2-(4-((benzyloxy)methyl)-1*H*-1,2,3-triazol-1-yl)acetate (**28**).

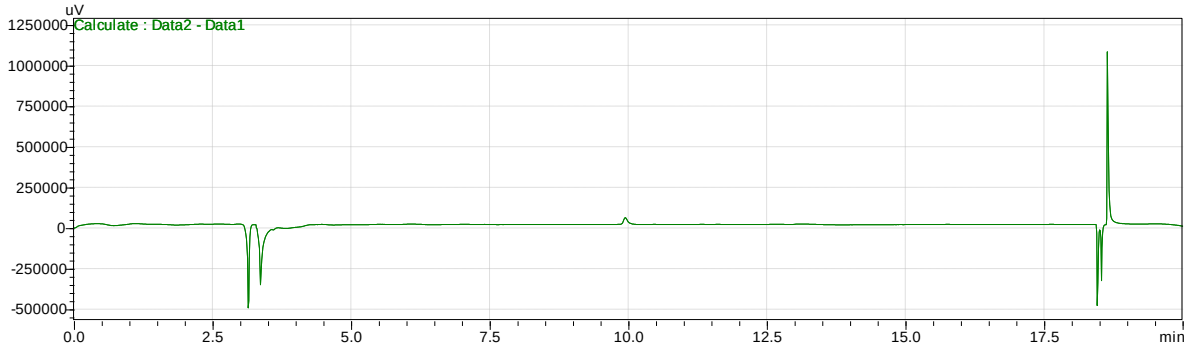

**Figure S126.** HPLC trace of (3a*R*,4*R*,5*S*,7*R*,8*S*,9*R*,9a*S*,12*R*)-7-(2-azidoethyl)-8-hydroxy-4,7,9,12-tetramethyl-3-oxodecahydro-4,9a-propanocyclopenta[8]annulen-5-yl 2-hydroxyacetate (**30**).

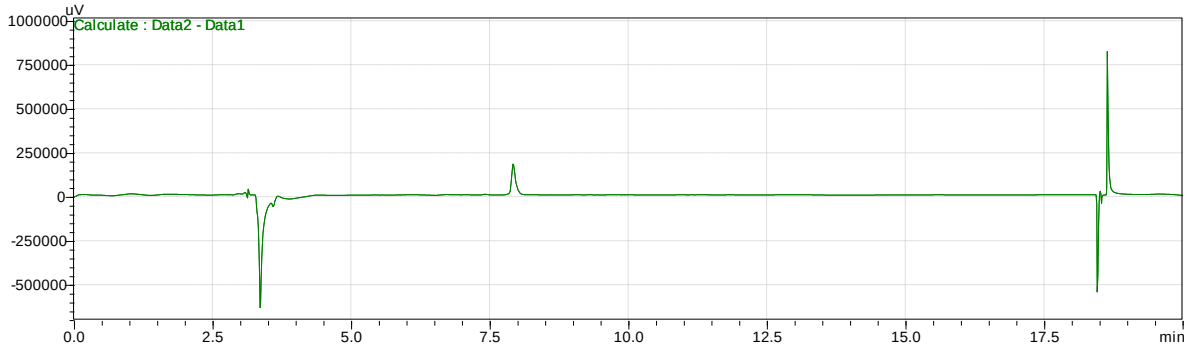


**Figure S127.** HPLC trace of (3a*R*,4*R*,5*S*,7*R*,8*S*,9*R*,9a*S*,12*R*)-8-Hydroxy-7-(2-(4-(hydroxymethyl)-1*H*-1,2,3-triazol-1-yl)ethyl)-4,7,9,12-tetramethyl-3-oxodecahydro-4,9a-propanocyclopenta[8]annulen-5-yl 2-hydroxyacetate (**31**).

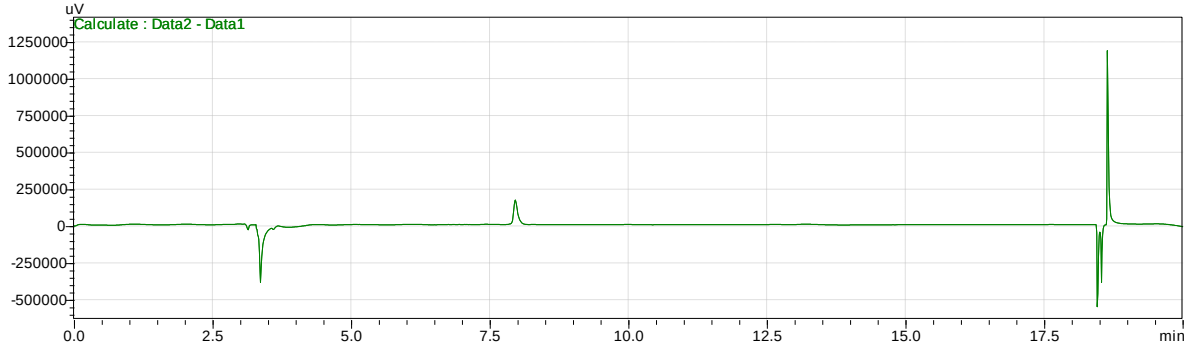


**Figure S128.** HPLC trace of (3a*R*,4*R*,5*S*,7*R*,8*S*,9*R*,9a*S*,12*R*)-8-Hydroxy-7-(2-(4-(2-hydroxyethyl)-1*H*-1,2,3-triazol-1-yl)ethyl)-4,7,9,12-tetramethyl-3-oxodecahydro-4,9a-propanocyclopenta[8]annulen-5-yl 2-hydroxyacetate (**32**).

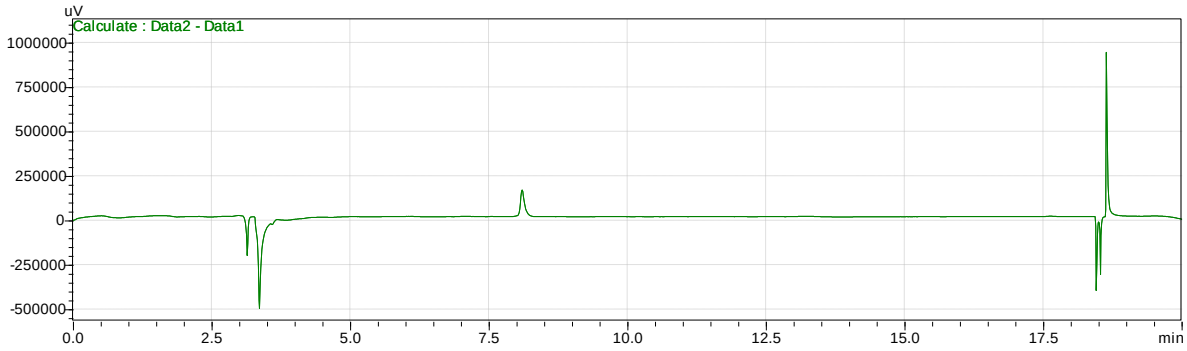


**Figure S129.** HPLC trace of (3a*R*,4*R*,5*S*,7*R*,8*S*,9*R*,9a*S*,12*R*)-8-Hydroxy-7-(2-(4-(3-hydroxypropyl)-1*H*-1,2,3-triazol-1-yl)ethyl)-4,7,9,12-tetramethyl-3-oxodecahydro-4,9a-propanocyclopenta[8]annulen-5-yl 2-hydroxyacetate (**33**).

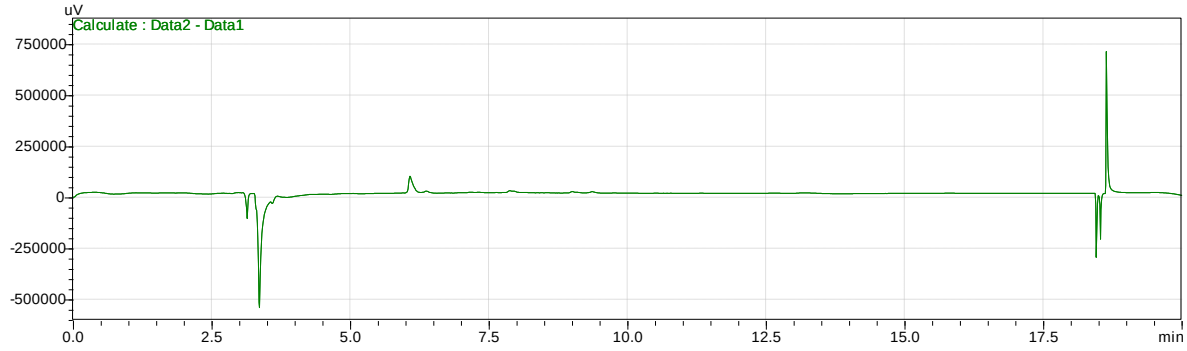


**Figure S130.** HPLC trace of (3a*R*,4*R*,5*S*,7*R*,8*S*,9*R*,9a*S*,12*R*)-7-(2-(4-(Aminomethyl)-1*H*-1,2,3-triazol-1-yl)ethyl)-8-hydroxy-4,7,9,12-tetramethyl-3-oxodecahydro-4,9a-propanocyclopenta[8]annulen-5-yl 2-hydroxyacetate (**34**).

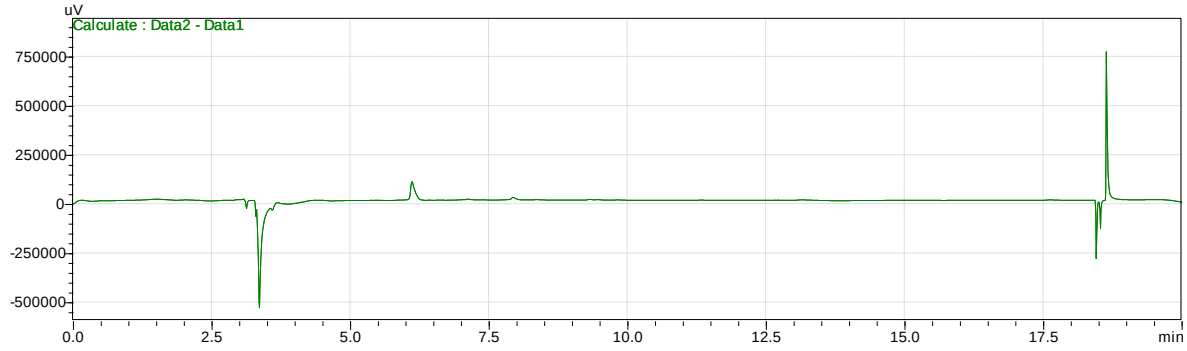

**Figure S131.** HPLC trace of (3a*R*,4*R*,5*S*,7*R*,8*S*,9*R*,9a*S*,12*R*)-7-(2-(4-(2-Aminoethyl)-1*H*-1,2,3-triazol-1-yl)ethyl)-8-hydroxy-4,7,9,12-tetramethyl-3-oxodecahydro-4,9a-propanocyclopenta[8]annulen-5-yl 2-hydroxyacetate (**35**).

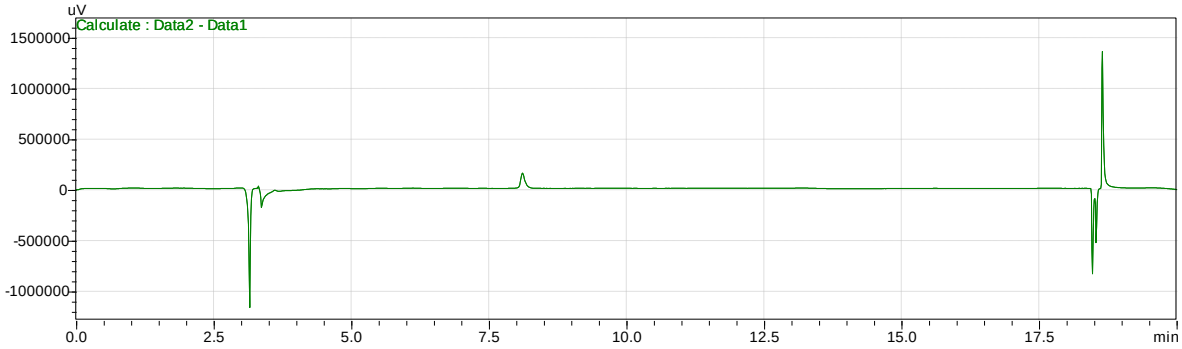


**Figure S132.** HPLC trace of (3a*R*,4*R*,5*S*,7*R*,8*S*,9*R*,9a*S*,12*R*)-8-Hydroxy-7-(2-(4-(1-hydroxyethyl)-1*H*-1,2,3-triazol-1-yl)ethyl)-4,7,9,12-tetramethyl-3-oxodecahydro-4,9a-propanocyclopenta[8]annulen-5-yl 2-hydroxyacetate (**36**).

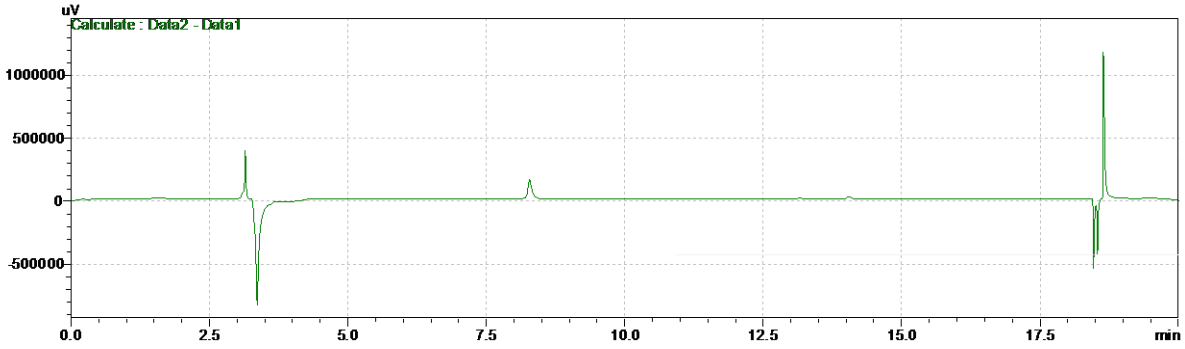


**Figure S133.** HPLC trace of (3a*R*,4*R*,5*S*,7*R*,8*S*,9*R*,9a*S*,12*R*)-8-Hydroxy-7-(2-(4-(2-hydroxypropan-2-yl)-1*H*-1,2,3-triazol-1-yl)ethyl)-4,7,9,12-tetramethyl-3-oxodecahydro-4,9a-propanocyclopenta[8]annulen-5-yl 2-hydroxyacetate (**37**).

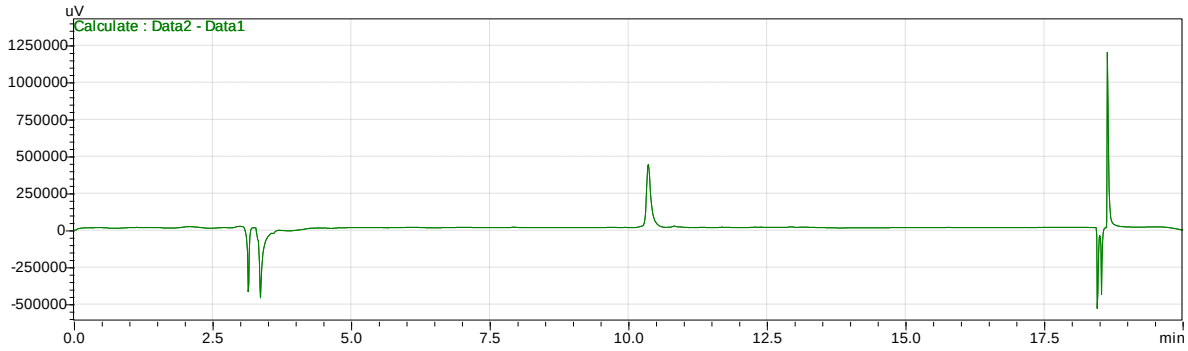


**Figure S134.** HPLC trace of (3a*R*,4*R*,5*S*,7*R*,8*S*,9*R*,9a*S*,12*R*)-7-(2-(4-((Benzyloxy)methyl)-1*H*-1,2,3-triazol-1-yl)ethyl)-8-hydroxy-4,7,9,12-tetramethyl-3-oxodecahydro-4,9a-propanocyclopenta[8]annulen-5-yl 2-hydroxyacetate (**38**).

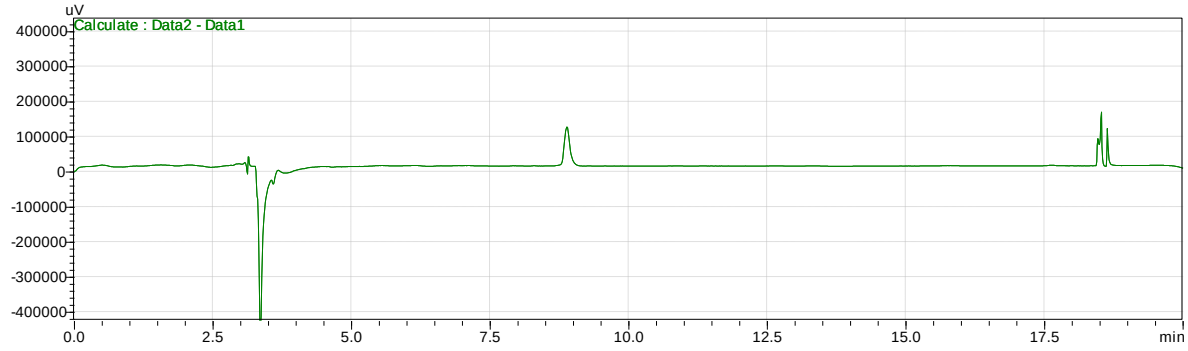


**Figure S135.** HPLC trace of (3a*R*,4*R*,5*S*,7*R*,8*S*,9*R*,9a*S*,12*R*)-8-Hydroxy-7-(2-(4-(1-hydroxybutyl)-1*H*-1,2,3-triazol-1-yl)ethyl)-4,7,9,12-tetramethyl-3-oxodecahydro-4,9a-propanocyclopenta[8]annulen-5-yl 2-hydroxyacetate (**39**).

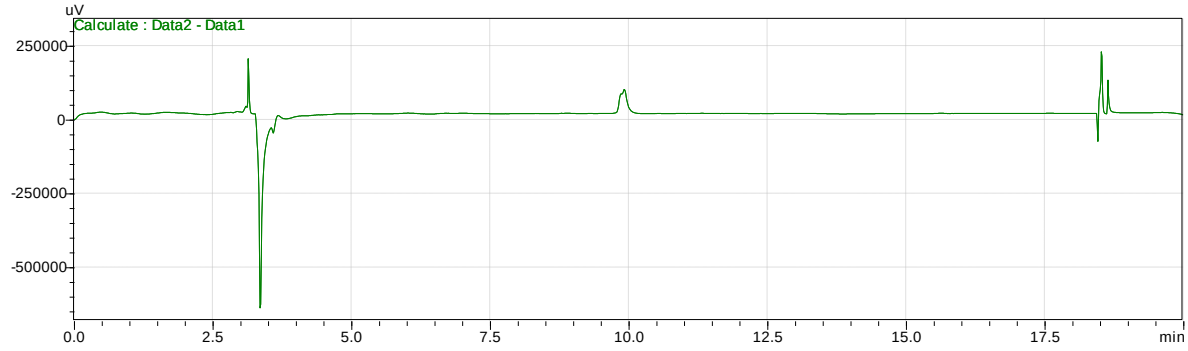

**Figure S136.** HPLC trace of **(**3a*R*,4*R*,5*S*,7*R*,8*S*,9*R*,9a*S*,12*R*)-8-Hydroxy-7-(2-(4-(1-hydroxyhexyl)-1*H*-1,2,3-triazol-1-yl)ethyl)-4,7,9,12-tetramethyl-3-oxodecahydro-4,9a-propanocyclopenta[8]annulen-5-yl 2-hydroxyacetate (**40**).

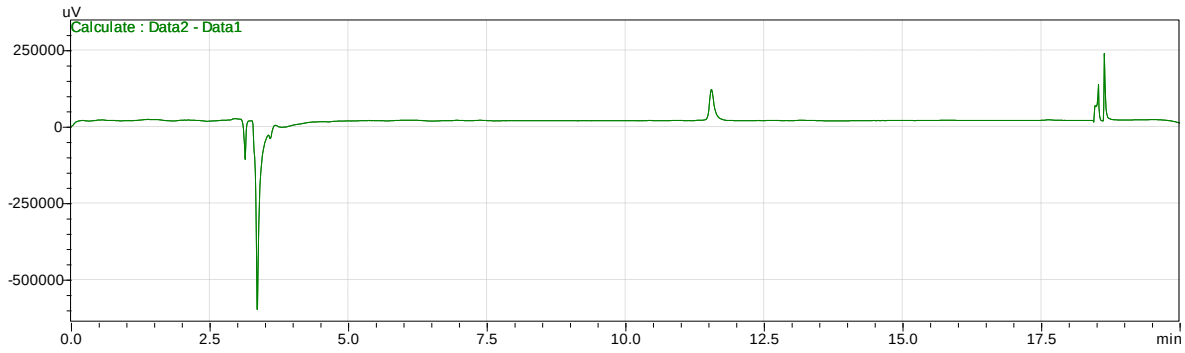


**Figure S137.** HPLC trace of (3a*R*,4*R*,5*S*,7*R*,8*S*,9*R*,9a*S*,12*R*)-7-(2-(4-Hexyl-1*H*-1,2,3-triazol-1-yl)ethyl)-8-hydroxy-4,7,9,12-tetramethyl-3-oxodecahydro-4,9a-propanocyclopenta[8]annulen-5-yl 2-hydroxyacetate (**41**).

**Table S16 Crystal data and structure refinement for cs2691 (29).**

| | |
|---|---|
| Identification code | cs2691 (Compound 29) |
| Empirical formula | $C_{22}H_{33}ClO_4$ |
| Formula weight | 396.93 |

| | |
|---|---|
| Temperature/K | 100.01(12) |
| Crystal system | monoclinic |
| Space group | $P2_1$ |
| a/Å | 9.11080(10) |
| b/Å | 10.79720(10) |
| c/Å | 10.52760(10) |
| α/° | 90 |
| β/° | 98.1430(10) |
| γ/° | 90 |
| Volume/Å$^3$ | 1025.171(18) |
| Z | 2 |
| $\rho_{calc}$g/cm$^3$ | 1.286 |
| μ/mm$^{-1}$ | 1.845 |
| F(000) | 428.0 |
| Crystal size/mm$^3$ | 0.28 × 0.24 × 0.12 |
| Radiation | Cu Kα (λ = 1.54184) |
| 2Θ range for data collection/° | 8.484 to 154.956 |

| | |
|---|---|
| Index ranges | $-11 \leq h \leq 11$, $-13 \leq k \leq 13$, $-11 \leq l \leq 13$ |
| Reflections collected | 26076 |
| Independent reflections | 4328 [$R_{int}$ = 0.0500, $R_{sigma}$ = 0.0310] |
| Data/restraints/parameters | 4328/1/252 |
| Goodness-of-fit on $F^2$ | 1.088 |
| Final R indexes [I>=2σ (I)] | $R_1$ = 0.0336, $wR_2$ = 0.0897 |
| Final R indexes [all data] | $R_1$ = 0.0339, $wR_2$ = 0.0900 |
| Largest diff. peak/hole / e $Å^{-3}$ | 0.20/-0.22 |
| Flack parameter | -0.023(7) |

**Table S17 Bond Lengths for cs2691 (29).**

| Atom | Atom | Length/Å | Atom | Atom | Length/Å |
|---|---|---|---|---|---|
| Cl1 | C10 | 1.765(2) | C4 | C18 | 1.553(3) |
| O1 | C1 | 1.472(2) | C5 | C6 | 1.568(3) |
| O1 | C9 | 1.338(3) | C5 | C19 | 1.542(3) |
| O2 | C9 | 1.195(3) | C6 | C7 | 1.553(3) |
| O3 | C16 | 1.218(3) | C7 | C8 | 1.550(3) |
| O4 | C6 | 1.431(3) | C7 | C20 | 1.516(3) |
| C1 | C2 | 1.560(3) | C7 | C22 | 1.545(3) |
| C1 | C8 | 1.539(3) | C9 | C10 | 1.521(3) |
| C2 | C3 | 1.559(3) | C12 | C13 | 1.536(3) |
| C2 | C11 | 1.541(3) | C12 | C14 | 1.532(3) |
| C2 | C12 | 1.555(3) | C14 | C15 | 1.526(3) |
| C3 | C4 | 1.555(3) | C16 | C17 | 1.512(3) |
| C3 | C16 | 1.538(3) | C17 | C18 | 1.524(3) |
| C4 | C5 | 1.557(3) | C20 | C21 | 1.318(3) |
| C4 | C15 | 1.548(3) | | | |

**Table S18 Bond Angles for cs2691 (29).**

| Atom | Atom | Atom | Angle/° | Atom | Atom | Atom | Angle/° |
|---|---|---|---|---|---|---|---|
| C9 | O1 | C1 | 118.59(16) | C7 | C6 | C5 | 113.16(17) |
| O1 | C1 | C2 | 106.63(16) | C8 | C7 | C6 | 112.95(17) |
| O1 | C1 | C8 | 105.64(16) | C20 | C7 | C6 | 108.82(18) |
| C8 | C1 | C2 | 116.18(17) | C20 | C7 | C8 | 112.46(18) |
| C3 | C2 | C1 | 108.57(16) | C20 | C7 | C22 | 108.52(18) |
| C11 | C2 | C1 | 109.03(17) | C22 | C7 | C6 | 108.27(17) |
| C11 | C2 | C3 | 109.97(17) | C22 | C7 | C8 | 105.61(17) |
| C11 | C2 | C12 | 111.17(17) | C1 | C8 | C7 | 119.18(18) |
| C12 | C2 | C1 | 111.57(16) | O1 | C9 | C10 | 107.21(18) |
| C12 | C2 | C3 | 106.47(16) | O2 | C9 | O1 | 126.8(2) |
| C4 | C3 | C2 | 117.72(17) | O2 | C9 | C10 | 126.0(2) |
| C16 | C3 | C2 | 117.78(17) | C9 | C10 | Cl1 | 111.39(17) |
| C16 | C3 | C4 | 102.97(17) | C13 | C12 | C2 | 116.34(18) |
| C3 | C4 | C5 | 115.78(17) | C14 | C12 | C2 | 111.60(17) |
| C15 | C4 | C3 | 107.55(17) | C14 | C12 | C13 | 109.79(18) |

**Table S18 Bond Angles for cs2691 (29).**

| Atom | Atom | Atom | Angle/° | Atom | Atom | Atom | Angle/° |
|---|---|---|---|---|---|---|---|
| C15 | C4 | C5 | 111.08(17) | C15 | C14 | C12 | 112.26(18) |
| C15 | C4 | C18 | 108.91(17) | C14 | C15 | C4 | 114.67(17) |
| C18 | C4 | C3 | 102.32(16) | O3 | C16 | C3 | 127.0(2) |
| C18 | C4 | C5 | 110.71(17) | O3 | C16 | C17 | 123.40(19) |
| C4 | C5 | C6 | 113.54(17) | C17 | C16 | C3 | 109.41(19) |
| C19 | C5 | C4 | 110.37(17) | C16 | C17 | C18 | 105.01(17) |
| C19 | C5 | C6 | 111.19(17) | C17 | C18 | C4 | 104.99(18) |
| O4 | C6 | C5 | 112.04(17) | C21 | C20 | C7 | 126.5(2) |
| O4 | C6 | C7 | 106.36(16) | | | | |

**Table S19 Hydrogen Bonds for cs2691 (29).**

| D | H | A | d(D-H)/Å | d(H-A)/Å | d(D-A)/Å | D-H-A/° |
|---|---|---|---|---|---|---|
| O4 | H4 | O3[1] | 0.76(4) | 2.07(4) | 2.825(2) | 171(4) |

[1]1-X,-1/2+Y,2-Z

**Table S20 Torsion Angles for cs2691 (29).**

| A | B | C | D | Angle/° | A | B | C | D | Angle/° |
|---|---|---|---|---|---|---|---|---|---|
| O1 | C1 | C2 | C3 | 166.49(15) | C5 | C4 | C18 | C17 | -163.05(17) |
| O1 | C1 | C2 | C11 | 46.7(2) | C5 | C6 | C7 | C8 | -68.2(2) |
| O1 | C1 | C2 | C12 | -76.5(2) | C5 | C6 | C7 | C20 | 57.4(2) |
| O1 | C1 | C8 | C7 | 134.09(18) | C5 | C6 | C7 | C22 | 175.19(18) |
| O1 | C9 | C10 | Cl1 | -175.85(14) | C6 | C7 | C8 | C1 | 66.0(2) |
| O2 | C9 | C10 | Cl1 | 4.9(3) | C6 | C7 | C20 | C21 | -162.9(2) |
| O3 | C16 | C17 | C18 | 170.5(2) | C8 | C1 | C2 | C3 | 49.1(2) |
| O4 | C6 | C7 | C8 | 168.34(17) | C8 | C1 | C2 | C11 | -70.7(2) |
| O4 | C6 | C7 | C20 | -66.0(2) | C8 | C1 | C2 | C12 | 166.11(17) |
| O4 | C6 | C7 | C22 | 51.8(2) | C8 | C7 | C20 | C21 | -36.9(3) |
| C1 | O1 | C9 | O2 | -5.5(3) | C9 | O1 | C1 | C2 | 126.73(18) |
| C1 | O1 | C9 | C10 | 175.25(16) | C9 | O1 | C1 | C8 | -109.09(19) |
| C1 | C2 | C3 | C4 | 64.4(2) | C11 | C2 | C3 | C4 | -176.44(17) |
| C1 | C2 | C3 | C16 | -171.35(17) | C11 | C2 | C3 | C16 | -52.1(2) |
| C1 | C2 | C12 | C13 | 64.7(2) | C11 | C2 | C12 | C13 | -57.3(2) |

**Table S20 Torsion Angles for cs2691 (29).**

| A | B | C | D | Angle/° | A | B | C | D | Angle/° |
|---|---|---|---|---|---|---|---|---|---|
| C1 | C2 | C12 | C14 | -62.4(2) | C11 | C2 | C12 | C14 | 175.71(17) |
| C2 | C1 | C8 | C7 | -108.0(2) | C12 | C2 | C3 | C4 | -55.9(2) |
| C2 | C3 | C4 | C5 | -73.2(2) | C12 | C2 | C3 | C16 | 68.4(2) |
| C2 | C3 | C4 | C15 | 51.7(2) | C12 | C14 | C15 | C4 | 54.2(2) |
| C2 | C3 | C4 | C18 | 166.32(16) | C13 | C12 | C14 | C15 | 171.70(17) |
| C2 | C3 | C16 | O3 | 34.3(3) | C15 | C4 | C5 | C6 | -164.49(17) |
| C2 | C3 | C16 | C17 | -150.48(17) | C15 | C4 | C5 | C19 | 69.9(2) |
| C2 | C12 | C14 | C15 | -57.8(2) | C15 | C4 | C18 | C17 | 74.5(2) |
| C3 | C2 | C12 | C13 | -177.02(18) | C16 | C3 | C4 | C5 | 155.40(17) |
| C3 | C2 | C12 | C14 | 55.9(2) | C16 | C3 | C4 | C15 | -79.73(19) |
| C3 | C4 | C5 | C6 | -41.5(2) | C16 | C3 | C4 | C18 | 34.9(2) |
| C3 | C4 | C5 | C19 | -167.09(18) | C16 | C17 | C18 | C4 | 27.4(2) |
| C3 | C4 | C15 | C14 | -48.4(2) | C18 | C4 | C5 | C6 | 74.4(2) |
| C3 | C4 | C18 | C17 | -39.1(2) | C18 | C4 | C5 | C19 | -51.3(2) |
| C3 | C16 | C17 | C18 | -5.0(2) | C18 | C4 | C15 | C14 | -158.61(18) |

**Table S20 Torsion Angles for cs2691 (29).**

| A | B | C | D | Angle/° | A | B | C | D | Angle/° |
|---|---|---|---|---|---|---|---|---|---|
| C4 | C3 | C16 | O3 | 165.7(2) | C19 | C5 | C6 | O4 | -9.5(2) |
| C4 | C3 | C16 | C17 | -19.1(2) | C19 | C5 | C6 | C7 | -129.73(19) |
| C4 | C5 | C6 | O4 | -134.66(18) | C20 | C7 | C8 | C1 | -57.7(2) |
| C4 | C5 | C6 | C7 | 105.1(2) | C22 | C7 | C8 | C1 | -175.89(18) |
| C5 | C4 | C15 | C14 | 79.2(2) | C22 | C7 | C20 | C21 | 79.5(3) |

**Crystal Data for cs2691 (Compound 29)**. $C_{22}H_{33}ClO_4$ ($M$ =396.93 g/mol): monoclinic, space group $P2_1$ (no. 4), $a$ = 9.11080(10) Å, $b$ = 10.79720(10) Å, $c$ = 10.52760(10) Å, $\beta$ = 98.1430(10)°, $V$ = 1025.171(18) Å$^3$, $Z$ = 2, $T$ = 100.01(12) K, μ(Cu Kα) = 1.845 mm$^{-1}$, *Dcalc* = 1.286 g/cm$^3$, 26076 reflections measured (8.484° ≤ 2Θ ≤ 154.956°), 4328 unique ($R_{int}$ = 0.0500, $R_{sigma}$ = 0.0310) which were used in all calculations. The final $R_1$ was 0.0336 (I > 2σ(I)) and $wR_2$ was 0.0900 (all data).

## 2.7 References

1. Murray, C. J.; Ikuta, K. S.; Sharara, F.; Swetschinski, L.; Robles Aguilar, G.; Gray, A.; Han, C.; Bisignano, C.; Rao, P.; Wool, E.; Johnson, S. C.; Browne, A. J.; Chipeta, M. G.; Fell, F.; Hackett, S.; Haines-Woodhouse, G.; Kashef Hamadani, B. H.; Kumaran, E. A. P.; McManigal, B.; Agarwal, R.; Akech, S.; Albertson, S.; Amuasi, J.; Andrews, J.; Aravkin, A.; Ashley, E.; Bailey, F.; Baker, S.; Basnyat, B.; Bekker, A.; Bender, R.; Bethou, A.; Bielicki, J.; Boonkasidecha, S.; Bukosia, J.; Carvalheiro, C.; Castañeda-Orjuela, C.; Chansamouth, V.; Chaurasia, S.; Chiurchiù, S.; Chowdhury, F.; Cook, A. J.; Cooper, B.; Cressey, T. R.; Criollo-Mora, E.; Cunningham, M.; Darboe, S.; Day, N. P. J.; De Luca, M.; Dokova, K.; Dramowski, A.; Dunachie, S. J.; Eckmanns, T.; Eibach, D.; Emami, A.; Feasey, N.; Fisher-

Pearson, N.; Forrest, K.; Garrett, D.; Gastmeier, P.; Giref, A. Z.; Greer, R. C.; Gupta, V.; Haller, S.; Haselbeck, A.; Hay, S. I.; Holm, M.; Hopkins, S.; Iregbu, K. C.; Jacobs, J.; Jarovsky, D.; Javanmardi, F.; Khorana, M.; Kissoon, N.; Kobeissi, E.; Kostyanev, T.; Krapp, F.; Krumkamp, R.; Kumar, A.; Kyu, H. H.; Lim, C.; Limmathurotsakul, D.; Loftus, M. J.; Lunn, M.; Ma, J.; Mturi, N.; Munera-Huertas, T.; Musicha, P.; Mussi-Pinhata, M. M.; Nakamura, T.; Nanavati, R.; Nangia, S.; Newton, P.; Ngoun, C.; Novotney, A.; Nwakanma, D.; Obiero, C. W.; Olivas-Martinez, A.; Olliaro, P.; Ooko, E.; Ortiz-Brizuela, E.; Peleg, A. Y.; Perrone, C.; Plakkal, N.; Ponce-De-Leon, A.; Raad, M.; Ramdin, T.; Riddell, A.; Roberts, T.; Robotham, J. V.; Roca, A.; Rudd, K. E.; Russell, N.; Schnall, J.; Scott, J. A. G.; Shivamallappa, M.; Sifuentes-Osornio, J.; Steenkeste, N.; Stewardson, A. J.; Stoeva, T.; Tasak, N.; Thaiprakong, A.; Thwaites, G.; Turner, C.; Turner, P.; Van Doorn, H. R.; Velaphi, S.; Vongpradith, A.; Vu, H.; Walsh, T.; Waner, S.; Wangrangsimakul, T.; Wozniak, T.; Zheng, P.; Sartorius, B.; Lopez, A. D.; Stergachis, A.; Moore, C.; Dolecek, C.; Naghavi, M., Global burden of bacterial antimicrobial resistance in 2019: a systematic analysis. *The Lancet* **2022,** *399* (10325), 629-655.

2. *No time to wait: Securing the future from drug-resistant infections*; Interagency Coordination Group on Antimicrobial Resistance: 2019.

3. Ventola, C. L., The antibiotic resistance crisis: Part 1: Causes and threats. *P T* **2015,** *40* (4), 277-283.

4. Newman, D. J.; Cragg, G. M., Natural products as sources of new drugs over the nearly four decades from 01/1981 to 09/2019. *J. Nat. Prod.* **2020,** *83* (3), 770-803.

5. Kavanagh, F.; Hervey, A.; Robbins, W. J., Antibiotic substances from Basidiomycetes: VIII. *Pleurotus multilus* (Fr.) Sacc. and *Pleurotus passeckerianus* Pilat. *Proc. Natl. Acad. Sci. U. S. A.* **1951,** *37* (9), 570.

6. Egger, H.; Reinshagen, H., New pleuromutilin derivatives with enhanced antimicrobial activity. II. Structure-activity correlations. *J. Antibiot.* **1976,** *29* (9), 915-922.

7. Schlünzen, F.; Pyetan, E.; Fucini, P.; Yonath, A.; Harms, J. M., Inhibition of peptide bond formation by pleuromutilins: the structure of the 50S ribosomal subunit from *Deinococcus radiodurans* in complex with tiamulin. *Mol. Microbiol.* **2004,** *54* (5), 1287-1294.

8. Davidovich, C.; Bashan, A.; Auerbach-Nevo, T.; Yaggie, R. D.; Gontarek, R. R.; Yonath, A., Induced-fit tightens pleuromutilins binding to ribosomes and remote interactions enable their selectivity. *Proc. Natl. Acad. Sci. U. S. A.* **2007,** *104* (11), 4291-4296.

9. Goethe, O.; Heuer, A.; Ma, X.; Wang, Z.; Herzon, S. B., Antibacterial properties and clinical potential of pleuromutilins. *Nat. Prod. Rep.* **2019,** *36* (1), 220-247.

10. Fazakerley, N. J.; Procter, D. J., Synthesis and synthetic chemistry of pleuromutilin. *Tetrahedron* **2014,** *70* (39), 6911-6930.

11. Prince, W.; Obermayr, F.; Ivezic-Schoenfeld, Z.; Lell, C.; Wicha, W.; Strickmann, D.; Tack, K.; Novak, R. In *A phase 2 study comparing the safety and efficacy of two doses of BC-3781 versus vancomycin in acute bacterial skin and skin structure infections (ABSSSI), abstr. L-966. Abstr. 51st Intersci*, Program and Abstracts of the 51st Interscience Conference on Antimicrobial Agents and Chemotherapy (Chicago). Washington, DC: American Society for Microbiology, 2011.

12. Rittenhouse, S.; Biswas, S.; Broskey, J.; McCloskey, L.; Moore, T.; Vasey, S.; West, J.; Zalacain, M.; Zonis, R.; Payne, D., Selection of retapamulin, a novel pleuromutilin for topical use. *Antimicrob. Agents Chemother.* **2006,** *50* (11), 3882-3885.

13. Czok, R.; Meingassner, J. G.; Mieth, H.; Schutze, E. Antibiotic compositions for treating coccidiosis. US patent 4,148,890, 1979.

14. Burch, D. G. S.; Ripley, P. H.; Zeisl, E. Veterinary use of a pleuromutilin derivative. US Patent 6,130,250, 2000.

15. Jacobs, M. R., Retapamulin: a semisynthetic pleuromutilin compound for topical treatment of skin infections in adults and children. *Future Microbiol.* **2007,** *2* (6), 591-600.

16. Hunt, A., FDA approves new antibiotic to treat community-acquired bacterial pneumonia. www.fda.gov/news-events/press-announcements, 2019.
17. Paukner, S.; Riedl, R., Pleuromutilins: Potent drugs for resistant bugs—Mode of action and resistance. *Cold Spring Harb. Perspect. Med.* **2017,** *7* (1), a027110.
18. Yan, K.; Madden, L.; Choudhry, A. E.; Voigt, C. S.; Copeland, R. A.; Gontarek, R. R., Biochemical characterization of the interactions of the novel pleuromutilin derivative retapamulin with bacterial ribosomes. *Antimicrob. Agents Chemother.* **2006,** *50* (11), 3875-3881.
19. Gentry, D. R.; Rittenhouse, S. F.; McCloskey, L.; Holmes, D. J., Stepwise exposure of *Staphylococcus aureus* to pleuromutilins Is associated with stepwise acquisition of mutations in rplC and minimally affects susceptibility to retapamulin. *Antimicrob. Agents Chemother.* **2007,** *51* (6), 2048-2052.
20. Bozorov, K.; Zhao, J.; Aisa, H. A., 1,2,3-Triazole-containing hybrids as leads in medicinal chemistry: A recent overview. *Biorg. Med. Chem.* **2019,** *27* (16), 3511-3531.
21. Jain, A.; Piplani, P., Exploring the chemistry and therapeutic potential of triazoles: A comprehensive literature review. *Mini-Rev. Med. Chem.* **2019,** *19* (16), 1298-1368.
22. Marzi, M.; Farjam, M.; Kazeminejad, Z.; Shiroudi, A.; Kouhpayeh, A.; Zarenezhad, E., A recent overview of 1,2,3-triazole-containing hybrids as novel antifungal agents: Focusing on synthesis, mechanism of action, and structure-activity relationship (SAR). *Journal of Chemistry* **2022,** *2022*, 1-50.
23. Lolk, L.; Pøhlsgaard, J.; Jepsen, A. S.; Hansen, L. H.; Nielsen, H.; Steffansen, S. I.; Sparving, L.; Nielsen, A. B.; Vester, B.; Nielsen, P., A click chemistry approach to pleuromutilin conjugates with nucleosides or acyclic nucleoside derivatives and their binding to the bacterial ribosome. *J. Med. Chem.* **2008,** *51* (16), 4957-4967.
24. Dreier, I.; Kumar, S.; Søndergaard, H.; Rasmussen, M. L.; Hansen, L. H.; List, N. H.; Kongsted, J.; Vester, B.; Nielsen, P., A click chemistry approach to pleuromutilin derivatives, part 2: Conjugates with acyclic nucleosides and their ribosomal binding and antibacterial activity. *J. Med. Chem.* **2012,** *55* (5), 2067-2077.
25. Dreier, I.; Hansen, L. H.; Nielsen, P.; Vester, B., A click chemistry approach to pleuromutilin derivatives. Part 3: Extended footprinting analysis and excellent MRSA inhibition for a derivative with an adenine phenyl side chain. *Bioorg. Med. Chem. Lett.* **2014,** *24* (4), 1043-1046.
26. Heidtmann, C. V.; Voukia, F.; Hansen, L. N.; Soerensen, S. H.; Urlund, B.; Nielsen, S.; Pedersen, M.; Kelawi, N.; Andersen, B. N.; Pedersen, M.; Reinholdt, P.; Kongsted, J.; Nielsen, C. U.; Klitgaard, J. K.; Nielsen, P., Discovery of a potent adenine-benzyltriazolo-pleuromutilin conjugate with pronounced antibacterial activity against MRSA. *J. Med. Chem.* **2020,** *63* (24), 15693-15708.
27. Zhang, Z.; Li, K.; Zhang, G.-Y.; Tang, Y.-Z.; Jin, Z., Design, synthesis and biological activities of novel pleuromutilin derivatives with a substituted triazole moiety as potent antibacterial agents. *Eur. J. Med. Chem.* **2020,** *204*, 112604.
28. Zhang, G.-Y.; Zhang, Z.; Li, K.; Liu, J.; Li, B.; Jin, Z.; Liu, Y.-H.; Tang, Y.-Z., Design, synthesis and biological evaluation of novel pleuromutilin derivatives containing piperazine and 1,2,3-triazole linker. *Bioorg. Chem.* **2020,** *105*, 104398.
29. Stresser, D. M.; Broudy, M. I.; Ho, T.; Cargill, C. E.; Blanchard, A. P.; Sharma, R.; Dandeneau, A. A.; Goodwin, J. J.; Turner, S. D.; Erve, J. C. L.; Patten, C. J.; Dehal, S. S.; Crespi, C. L., Highly selective inhibition of human CYP3A *in vitro* by azamulin and evidence that inhibition is irreversible. *Drug Metab. Disposition* **2004,** *32* (1), 105-112.
30. Thirring, K.; Heilmayer, W.; Riedl, R.; Kollmann, H.; Ivezic-Schoenfeld, Z.; Wicha, W.; Paukner, S.; Strickmann, D. Preparation of 12-epi-pleuromutilin derivatives as antimicrobial agents. WO2015110481A1, 2015.
31. Xianfeng, L.; Lunde, C. S.; Jacobs, R. T.; Yasheen, Z. Boron-containing small molecules. WO 2017/151492 A1, 2017.

32. Himo, F.; Lovell, T.; Hilgraf, R.; Rostovtsev, V. V.; Noodleman, L.; Sharpless, K. B.; Fokin, V. V., Copper (I)-catalyzed synthesis of azoles. DFT study predicts unprecedented reactivity and intermediates. *J. Am. Chem. Soc.* **2005,** *127* (1), 210-216.
33. Riedl, K., Studies on pleuromutilin and some of its derivatives. *J. Antibiot.* **1976,** *29* (2), 132-139.
34. Chappe, B.; Musikas, H.; Marie, D.; Ourisson, G., Synthesis of three acyclic all-*trans*-tetraterpene diols, putative precursors of bacterial lipids. *Bull. Chem. Soc. Jpn.* **1988,** *61* (1), 141-148.
35. Ding, R.; He, Y.; Wang, X.; Xu, J.; Chen, Y.; Feng, M.; Qi, C., Treatment of alcohols with tosyl chloride does not always lead to the formation of tosylates. *Molecules* **2011,** *16* (7), 5665-5673.
36. Osorio, L. S.; Ionta, M.; Demuner, A. J.; Sousa, B. L. d.; Ferraz, G. O.; Varejão, E. V.; Ferreira-Silva, G. A.; Pilau, E. J.; Silva, E.; Santos, M. H. d., Synthesis of 1, 2, 3-triazole derivatives of hydnocarpic acid isolated from *Carpotroche brasiliensis* seed oil and evaluation of antiproliferative activity. *J. Braz. Chem. Soc.* **2020,** *31*, 2500-2510.
37. Li, X.; Chen, P.; Liu, G., Iodine(III) reagent (ABX—N3)-induced intermolecular anti-Markovnikov hydroazidation of unactivated alkenes. *Sci China Chem.* **2019,** *62* (11), 1537-1541.
38. Li, H.; Shen, S.-J.; Zhu, C.-L.; Xu, H., Direct intermolecular anti-Markovnikov hydroazidation of unactivated olefins. *J. Am. Chem. Soc.* **2019,** *141* (23), 9415-9421.
39. Lengerli, D.; Ibis, K.; Nural, Y.; Banoglu, E., The 1,2,3-triazole "all-in-one" ring system in drug discovery: a good bioisostere, a good pharmacophore, a good linker, and a versatile synthetic tool. *Expert Opin. Drug Discov.* **2022**, null-null.
40. Treitler, D. S.; Leung, S., How Dangerous Is Too Dangerous? A Perspective on Azide Chemistry. *J. Org. Chem.* **2022,** *87* (17), 11293-11295.
41. Hassner, A.; Stern, M.; Gottlieb, H. E.; Frolow, F., Synthetic methods. 33. Utility of a polymeric azide reagent in the formation of di- and triazidomethane. Their NMR spectra and the x-ray structure of derived triazoles. *The Journal of Organic Chemistry* **1990,** *55* (8), 2304-2306.
42. Patel, D.; Kosmidis, C.; Seo Susan, M.; Kaatz Glenn, W., Ethidium Bromide MIC Screening for Enhanced Efflux Pump Gene Expression or Efflux Activity in Staphylococcus aureus. *Antimicrob. Agents Chemother.* **2010,** *54* (12), 5070-5073.
43. Zgurskaya, H. I.; Krishnamoorthy, G.; Ntreh, A.; Lu, S., Mechanism and Function of the Outer Membrane Channel TolC in Multidrug Resistance and Physiology of Enterobacteria. *Front Microbiol* **2011,** *2*, 189.
44. Gordon, N. C.; Wareham, D. W., Multidrug-resistant Acinetobacter baumannii: mechanisms of virulence and resistance. *Int. J. Antimicrob. Agents* **2010,** *35* (3), 219-226.
45. König, G.; Sokkar, P.; Pryk, N.; Heinrich, S.; Möller, D.; Cimicata, G.; Matzov, D.; Dietze, P.; Thiel, W.; Bashan, A.; Bandow Julia, E.; Zuegg, J.; Yonath, A.; Schulz, F.; Sanchez-Garcia, E., Rational prioritization strategy allows the design of macrolide derivatives that overcome antibiotic resistance. *Proc. Natl. Acad. Sci. U. S. A.* **2021,** *118* (46), e2113632118.
46. Tessaro, F.; Scapozza, L., How 'Protein-Docking' Translates into the New Emerging Field of Docking Small Molecules to Nucleic Acids? *Molecules* **2020,** *25* (12).
47. Trott, O.; Olson, A. J., AutoDock Vina: improving the speed and accuracy of docking with a new scoring function, efficient optimization, and multithreading. *J. Comput. Chem.* **2010,** *31* (2), 455-461.
48. Friesner, R. A.; Murphy, R. B.; Repasky, M. P.; Frye, L. L.; Greenwood, J. R.; Halgren, T. A.; Sanschagrin, P. C.; Mainz, D. T., Extra precision Glide: Docking and scoring incorporating a model of hydrophobic enclosure for protein−ligand complexes. *J. Med. Chem.* **2006,** *49* (21), 6177-6196.
49. Ruiz-Carmona, S.; Alvarez-Garcia, D.; Foloppe, N.; Garmendia-Doval, A. B.; Juhos, S.; Schmidtke, P.; Barril, X.; Hubbard, R. E.; Morley, S. D., rDock: A Fast, Versatile and Open Source Program for Docking Ligands to Proteins and Nucleic Acids. *PLoS Comp. Biol.* **2014,** *10* (4), e1003571.
50. Kufareva, I.; Abagyan, R., Methods of protein structure comparison. *Methods Mol Biol* **2012,** *857*, 231-257.

51. Carter, A. P.; Clemons, W. M.; Brodersen, D. E.; Morgan-Warren, R. J.; Wimberly, B. T.; Ramakrishnan, V., Functional insights from the structure of the 30S ribosomal subunit and its interactions with antibiotics. *Nature* **2000,** *407* (6802), 340-348.
52. Borovinskaya, M. A.; Shoji, S.; Holton, J. M.; Fredrick, K.; Cate, J. H. D., A steric block in translation caused by the antibiotic spectinomycin. *ACS Chem. Bio.* **2007,** *2* (8), 545-552.
53. Eyal, Z.; Matzov, D.; Krupkin, M.; Paukner, S.; Riedl, R.; Rozenberg, H.; Zimmerman, E.; Bashan, A.; Yonath, A., A novel pleuromutilin antibacterial compound, its binding mode and selectivity mechanism. *Sci. Re.* **2016,** *6* (1), 39004.
54. Svidritskiy, E.; Ling, C.; Ermolenko, D. N.; Korostelev, A. A., Blasticidin S inhibits translation by trapping deformed tRNA on the ribosome. *Proc. Natl. Acad. Sci. U. S. A.* **2013,** *110* (30), 12283-12288.
55. Serrano, C. M.; Kanna Reddy, H. R.; Eiler, D.; Koch, M.; Tresco, B. I. C.; Barrows, L. R.; VanderLinden, R. T.; Testa, C. A.; Sebahar, P. R.; Looper, R. E., Unifying the aminohexopyranose- and peptidyl-nucleoside antibiotics: Implications for antibiotic design. *Angew. Chem. Int. Ed.* **2020,** *59* (28), 11330-11333.
56. Garreau De Loubresse, N.; Prokhorova, I.; Holtkamp, W.; Rodnina, M. V.; Yusupova, G.; Yusupov, M., Structural basis for the inhibition of the eukaryotic ribosome. *Nature* **2014,** *513* (7519), 517-522.
57. Svidritskiy, E.; Korostelev, A. A., Mechanism of inhibition of translation termination by blasticidin S. *J. Mol. Biol.* **2018,** *430* (5), 591-593.
58. Hansen, J. L.; Moore, P. B.; Steitz, T. A., Structures of five antibiotics bound at the peptidyl transferase center of the large ribosomal subunit. *J. Mol. Biol.* **2003,** *330* (5), 1061-1075.
59. Schrodinger, L. *Maestro* New York, NY 2021.
60. Schrodinger, L. *The PyMOL Molecular Graphics System, Version 8*, 2021.
61. RSCB Protein Data Bank. RSCB PDB: 2021.
62. Morris, G. M.; Huey, R.; Lindstrom, W.; Sanner, M. F.; Belew, R. K.; Goodsell, D. S.; Olson, A. J., AutoDock4 and AutoDockTools4: Automated docking with selective receptor flexibility. *J. Comput. Chem.* **2009,** *30* (16), 2785-2791.
63. *CrysAlisPro Software System*, v1.171.41.105a; Rigaku Oxford Diffraction: Rigaku Corporation, Oxford, UK, 2021.
64. Sheldrick, G. M., SHELXT–Integrated space-group and crystal-structure determination. *Acta Crystallogr. A: Found. Adv.* **2015,** *71* (1), 3-8.
65. Sheldrick, G. M., Crystal structure refinement with SHELXL. *Acta Crystallogr. C Struct. Chem.* **2015,** *71* (1), 3-8.
66. Dolomanov, O. V.; Bourhis, L. J.; Gildea, R. J.; Howard, J. A.; Puschmann, H., OLEX2: a complete structure solution, refinement and analysis program. *J. Appl. Crystallogr.* **2009,** *42* (2), 339-341.
67. Parsons, S.; Flack, H. D.; Wagner, T., Use of intensity quotients and differences in absolute structure refinement. *Acta Crystallogr. B: Struct. Sci. Cryst. Eng. Mater.* **2013,** *69* (3), 249-259.
68. Hergenrother, P. J.; Llabani, E. Compounds that induce ferroptic cell death. WO2020/210158, 2020.
69. Bąchor, R.; Setner, B.; Kluczyk, A.; Stefanowicz, P.; Szewczuk, Z., The unusual hydrogen-deuterium exchange ofα-carbon protons in N-substituted glycine-containing peptides. *J. Mass Spectrom.* **2014,** *49* (1), 43-49.

# Chapter 3. Engineering pleuromutilin epimers to engage an unexploited ribosomal binding pocket

Logan M. Breiner,[1,2,†] Micah Hoernig,[3,†] Benjamin Y. Killam,[4,†] Marion LoPresti,[3] Abdallah S. Abdelsattar,[2,5] Ahmed A. Abouelkhair,[2,5] Anthony J. Briganti,[3] Roman P. Slowinksi,[1,3] Nancy J. Vogelaar,[3,6] Iza Kopec,[4] Mohamed N. Seleem,[2,5,7*] Yury S. Polikanov,[4,8,9,*] Anne M. Brown,[2,3,10,*] Andrew N. Lowell[1,2,11,*]

[1] Department of Chemistry, Virginia Polytechnic Institute and State University (Virginia Tech), Blacksburg, Virginia 24061, USA

[2] Center for Emerging, Zoonotic, and Arthropod-borne Pathogens, Virginia Polytechnic Institute and State University (Virginia Tech), Blacksburg, Virginia 24061, USA

[3] Department of Biochemistry, Virginia Tech, Blacksburg, Virginia 24061, USA

[4] Department of Biological Sciences, University of Illinois at Chicago, Chicago, IL 60607, USA

[5] Center for One Health Research, Virginia Tech, Blacksburg, VA, 24061, USA

[6] Virginia Tech Center for Drug Discovery Screening Laboratory, Virginia Tech, Blacksburg, VA 24061, USA

[7] Department of Biomedical Sciences and Pathobiology, Virginia-Maryland College of Veterinary Medicine, Virginia Tech, Blacksburg, Virginia 24061, USA

[8] Center for Biomolecular Sciences, University of Illinois at Chicago, Chicago, IL 60607, USA

[9] Department of Pharmaceutical Sciences, University of Illinois at Chicago, Chicago, IL 60607, USA

[10] Research and Informatics, Virginia Tech, Blacksburg, Virginia 24061, USA

[11] Faculty of Health Sciences, Virginia Tech, Blacksburg, VA, USA

† These authors contributed equally to this work.

This study has been submitted for publication.

## 3.1 Abstract

Optimizing the bioactivity of natural product–derived antibiotics is an inherently challenging process, particularly when targeting complex macromolecular assemblies like the bacterial ribosome. Yet such efforts are essential for the rational design and development of next-generation antibiotics. Pleuromutilin derivatives are of particular value given their recent approval for systemic human use and low frequency of resistance development. While most efforts have focused on C22-substituted thioglycolates, identifying new functionalization sites is critical for advancing this antibiotic class. Leveraging structural insights from computational modeling, we identified C12 as a novel derivatization site amenable to divergent semisynthetic modification. To access this site, we epimerized C12 and applied an optimized anti-Markovnikov hydroazidation strategy to activate C20 for rapid diversification into a triazole library using CuAAC click chemistry. Biological evaluation confirmed that aromatic triazole substituents exhibited the best activity. Docking analysis guided structure-based refinements, resulting in derivatives with sub-mg/mL antimicrobial potency. X-ray crystallography revealed that the novel triazole arm binds in a previously unexploited region of the ribosomal A-site, with mechanism-of-action and toxicity studies confirming selectivity. Notably, C22 functionality did not impact activity. Collectively, these findings define a new ribosomal binding region for pleuromutilin and provide a framework for further structurally and computationally guided semisynthetic derivatization.

## 3.2 Introduction

Antimicrobial resistance (AMR) is a global health crisis, responsible for 1.3 million deaths annually[1] and expected to worsen without new therapeutic interventions.[2] One key approach to expanding treatment options is semisynthesis, the iterative improvement of established antibiotics to enhance efficacy. Over the past four decades, semisynthesis has yielded more than 60% of newly

approved small-molecule antimicrobials[3] and created most frontline antibiotics prescribed in the US, including amoxicillin, azithromycin, and doxycycline.[4] Continued innovation in this area is essential for efficiently leveraging evolutionarily optimized chemical space to counteract resistance.

At a foundational level, semisynthesis is the derivatization of complex natural products, which typically have a high degree of three-dimensionality—including rings, a high $sp^3$ to $sp^2$ ratio, and multiple stereocenters—that confers their specificity and potency as antibiotics. By modifying the complete scaffold, semisynthesis further enhances these inherent properties, offering a distinct advantage over traditional medicinal chemistry. In contrast, fully synthetic approaches often prioritize simpler, lower-dimensional scaffolds to address challenges such as route length, scalability, and starting material availability. However, this simplification can limit binding and reduce specificity.[5] Despite these challenges, fully synthetic campaigns have produced key antibiotics, such as linezolid,[6] and the recently developed lincosamide-inspired antibiotics iboxamycin[7, 8] and cresomycin as resistance breakers.[9]

Despite its widespread use, semisynthesis remains challenging to implement efficiently. Because the scaffold itself typically constitutes the essential pharmacophore, it must remain largely intact to preserve activity. Thus, the key to effective semisynthesis is the selective modification of functional groups, a process hindered by two primary obstacles: (i) in the absence of structural or mechanistic data, modifications are often guided by ease of functionalization rather than biological relevance, potentially abolishing activity, and (ii) highly desirable sites may be unreactive or lack regioselectivity, necessitating lengthier procedures and protecting groups. Consequently, approaches that facilitate site identification and enable highly selective functionalization are crucial for advancing semisynthetic antibiotic development.

Pleuromutilins are particularly well-suited for continued semisynthetic development because of their low propensity for resistance emergence[10] and the challenges associated with their several impressive total syntheses.[11-14] Substitution at the C22 position of pleuromutilin (**1**, **Figure 1**) via a straightforward sequence of activation and nucleophilic displacement of the primary alcohol—especially with thiols—has been extensively explored, yielding several medically[15, 16] and veterinary relevant drugs,[17] such as **2** and **3**. However, further derivatization at this site has provided diminishing returns. Structural assessments have shown that other functional groups, including the C3 ketone, C11 alcohol, and carbonyl of the C21 ester, are critical for ribosomal binding,[18] and recent total synthesis efforts confirm that preserving the tricyclic mutilin core is essential for activity.[19]

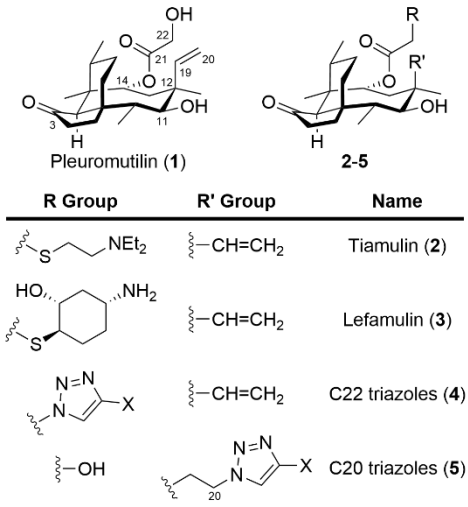


**Figure 1**. Representative pleuromutilin class antibiotics and derivatization sites.

Building on these findings, we previously implemented a computationally supported strategy to synthesize libraries of triazole pleuromutilin derivatives, targeting both the traditional C22 position (**4**) or the sole remaining reactive site, the C19-C20 vinyl group at C12 (**5**).[20] Triazoles were chosen for their ease of assembly, their formation tolerating a wide range of

functional groups, and their increasing recognition as medically relevant pharmacophores.[21] Their potential to engage in π-stacking and hydrogen bonding with ribosomal nucleotides further supported their selection. Our previous work[20] showed that the required C22 azide was accessible through established methods, but generating the C20 azide in a single step required a novel approach—an essential consideration for efficient semisynthesis. The C22 derivatives generally retained activity comparable to pleuromutilin, but the C20 derivatives were inactive. Computational docking revealed that while both series positioned the mutilin core within the pleuromutilin binding pocket, the C20-triazolyl-functionalized series adopted a suboptimal conformation. To better engage the pocket normally occupied by the C14 thioglycolate arm of tiamulin (**2**), this series shifted, twisting their hydrophobic core out of the proper orientation and disrupting key hydrogen bonding interactions of the C3 ketone, C11 alcohol, and C21 ester carbonyl.

While these results demonstrated that C20 functionalization with triazoles on *native* pleuromutilin did not enhance activity, further investigation through molecular docking and pharmacophore analysis suggested that the C12 methyl group, rather than the C12 vinyl group, was better positioned for derivatization. Supporting this approach, Nabriva Therapeutics previously showed that C12 epimerization, followed by oxidative scission of the C19/C20 bond and reductive amination, could give rise to active derivatives[22] as had recent synthetic approaches.[23] These epimerized compounds not only retained activity against Gram-positive pathogens but also exhibited improved potency against select Gram-negative bacteria.

Building on computationally guided design, we sought to exploit this newly identified ribosomal binding region with C12-epimerized, C20-triazole derivatives displaying both pleuromutilin and tiamulin functionality at C22. Further refinement revealed that aromatic

triazoles conferred the highest antimicrobial activity, independent of C22 substitution. Structural data illustrated that the reoriented C20 triazole arm engages a distinct ribosomal binding pocket, with *in vitro* assays confirming selectivity for the bacterial ribosome. This seamless integration of computational modeling, synthetic chemistry, biological evaluation, and structural analysis highlights the power of semisynthesis in antibiotic discovery and its potential for expanding ribosome-targeting therapeutics.

## 3.3 Results and discussion

### 3.3.1 Synthetic approach to 12-epi-pleuromutilin and tiamulin triazole derivatives

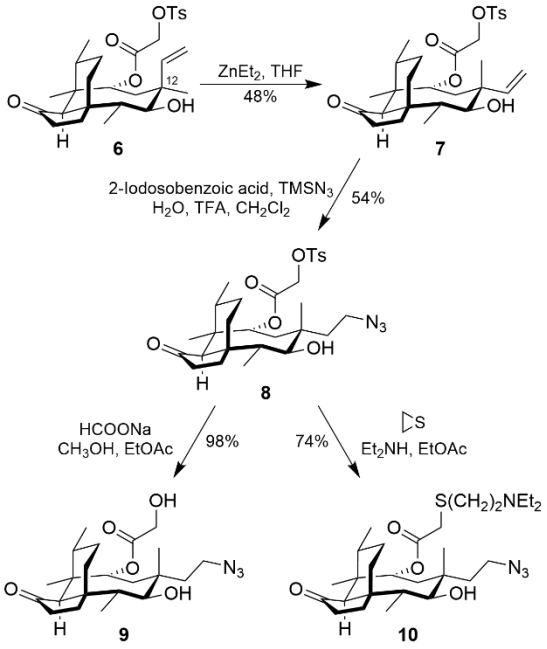


**Scheme 1**. Synthetic pathway to epimerized, hydroazidated intermediates

22-*O*-Tosylpleuromutilin (**6**, **Scheme 1**) was synthesized from pleuromutilin (**1**) in 92% yield following established literature procedures,[24] while minimizing formation of the C22-chloro byproduct.[20] To generate the epimerized derivatives, we adapted an improved version[22] of Berner's earlier finding[25] that alkyl zinc reagents can invert the C12 position of **6**. The alkyl zinc reagent

reacts with the secondary alcohol of **6**, coordinating the vinyl group and facilitating a retro-Ene–type reaction that opens the eight-membered ring between C11 and C12. Upon reclosure, thermodynamic epimerization at C12 yielded a 47:53 mixture of **6** and its C12 epimer (**7**) by NMR, consistent with literature values,[22] while avoiding generation of cyclopropanoid byproducts observed using other methods.[25] Multiple rounds of chromatography enabled over 90% recovery of **7**, a 48% yield. Although we found that tiamulin (**2**) underwent C12 epimerization with even higher conversion (2:3 tiamulin:*epi*-tiamulin as assessed by NMR), chromatographic separation of this mixture was extremely inefficient. Thus, we adopted a late-stage divergent strategy to generate either pleuromutilin-type (C22 = OH) or tiamulin-type (C22 = $S(CH_2)_2NEt_2$) triazole derivatives from **8** as a common intermediate.

With **7** in hand, radical anti-Markovnikov hydroazidation using 2-iodosobenzoic acid (IBA) as a catalyst[26] generated C20-azido intermediate **8**. The tosylate was not only tolerated—a surprising result given the nucleophilic environment from excess azide—but also appeared to enhance product formation, improving the yield of **8** to 54% compared to 32% for native pleuromutilin under the same conditions.[20] We believe the tosylate serves as a protecting group for the primary alcohol of pleuromutilin, preventing side reactions with $TMSN_3$. Without this protection, transient silylation, followed by hydrolysis, would catalytically consume the azidation reagent, decreasing the yield.[20] These findings suggest that radical azidation conditions can be broadly applied to natural products, even those with reactive functionality, expanding opportunities to introduce diversity via click chemistry in medicinal chemistry and natural products derivatization.

After installation of the azide handle (**8**), the synthesis diverged to generate *epi*-pleuromutilin or *epi*-tiamulin triazoles. The *epi*-pleuromutilin series, to be derived from **9**, was

prepared by deprotecting the tosylate of **8** to reveal the C22 alcohol (**9**). Deprotection was achieved under mild conditions by first displacing the tosylate with formate, followed by solvolysis of the resulting formate ester. This transformation gave a quantitative yield and required no purification, although recrystallization from benzene proved facile, even on scales as small as 100 mg. For the *epi*-tiamulin series based on hydroazide **10**, common intermediate **8** was treated with a freshly generated solution of *N*,*N*-diethyl-(2-amino)ethanethiol, furnishing **10** in good yield (74%). This yield surpassed prior reports for tiamulin synthesis (~54%),[27] an improvement we attribute to increased amounts of reactants and longer reaction times. Both processes proceeded in high yield under mild conditions, preserving the integrity of the azide for subsequent cycloaddition.

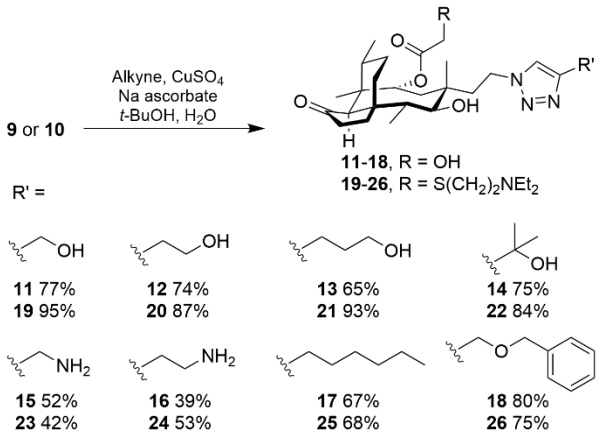


**Scheme 2**. Structure and yields of 12-*epi*-20-triazolyl pleuromutilins and tiamulins

To obtain the triazole derivatives, advanced intermediates **9** and **10** (**Scheme 2**) were subjected to copper-catalyzed azide/alkyne cycloaddition (CuAAC) conditions using the Sharpless protocol.[28] Some reagents exhibited poor solubility in the highly polar water:*tert*-butanol solvent system, but heating the mixture to 70 °C enabled production of both series in good to excellent yields. As observed with previous cycloadditions,[20] alkynes bearing free amines gave lower yields (**15-16**, **23-24**), likely due to amine coordination with copper, which slows $Cu^{2+}$ reduction to the

active $Cu^{1+}$ species,[29] or due to $Cu^{2+}$ catalyzing amine oxidation because the presence of residual $O_2$.[30] Despite these challenges, all compounds were obtained in sufficient quantities for biological evaluation. Notably, CuAAC efficiency was comparable between the C22 hydroxide (**9**) and the diethylaminoethane thiol (**10**), highlighting the robustness of this approach.

### 3.3.2 Aromatic derivatization of epimeric triazoles increases antimicrobial activity

The *epi*-C12 C20-triazole pleuromutilin (**11**-**18**) and tiamulin (**19**-**26**) derivatives were evaluated in broth microdilution assays to determine their minimum inhibitory concentrations (MIC) against a panel of bacterial strains. Testing included five *Staphylococcus aureus* strains (one susceptible and four methicillin-resistant), two *Escherichia coli* variants (wild-type and a TolC efflux pump knockout), two vancomycin-resistant *Enterococcus faecium*, and *Enterococcus faecalis* (**Table 1**). Additional screening was conducted against *Shigella flexneri*, *Salmonella enterica*, *Acinetobacter baumannii*, *Klebsiella pneumoniae*, and *Pseudomonas aeruginosa* (**SI Table S1**).

Within the *epi*-pleuromutilin series (**Table 1**), homologated alcohols (**11**–**13**) and amines (**15** and **16**) lost activity against *S. aureus*, with MIC values at least 8-fold less potent than the parent compound **1**. This effect was less pronounced in the *E. coli* efflux pump TolC knockout strain (*E. coli* Δ*tolC*), where these derivatives were comparable to or slightly less active than **1**; however, all were inactive against wild-type *E. coli*. Against VRE strains, the linear alcohols and amines showed activity comparable to **1**. The branched-chain alcohol **14** generally matched the activity of the other alcohols but was more variable. In contrast, longer aliphatic and aromatic chains were more potent. Hexyl derivative **17** generally retained activity in the *S. aureus* and VRE strains, and matched **1** against *E. coli*. Of the *epi*-pleuromutilin triazole derivatives, the most potent was benzyl ether derivative **18**, exhibiting a 2-fold to 4-fold increase in activity against *S. aureus*

strains, including MRSA subtypes. While **18** remained inactive against wild-type *E. coli*, its potency against *E. coli* Δ*tolC* was comparable to **1**. It also demonstrated promising activity against *E. faecium*, showing comparable or improved MIC values relative to **1**.

For the *epi*-tiamulin series, the alcohol (**19**–**22**) and amine (**23** and **24**) triazole derivatives also exhibited reduced activity against the tested strains, though the loss was less pronounced than in the *epi*-pleuromutilin series. The hexyl derivative (**25**) lost activity against the MRSA and *E. coli* but retained activity against susceptible *S. aureus* and was variable against the *E. faecium*, suggesting attenuation by efflux or other resistance mechanisms. Consistent with the *epi*-pleuromutilin series, the benzyl ether derivative **26** had the highest potency, with MIC values comparable or slightly improved over the tiamulin parent compound. Overall, the tiamulin analogs were generally more potent than their pleuromutilin counterparts, possibly due to subtle ribosomal differences between the different organisms,[31] variations in cellular uptake, or unrecognized context-specific effects[32] related to protein production.[33, 34]

While most compounds were inactive against the variety of tested Gram-negative strains (**SI Table S1**), tiamulin amine triazole derivatives **23** and **24** stood out as the most potent. Both exhibited detectable activity against *E. coli* (**Table 1**) and inhibited *S. flexneri* at 32 μg/mL (**SI Table S1**). The enhanced activity of **23** and **24** is likely due to improved uptake as the additional amine group increases positive charge at physiological pH, facilitating interactions with the negatively charged outer membrane of Gram-negative bacteria, such as *S. flexneri* and *E. coli*.[35] These findings, consistent with literature precedent,[36] suggest that further structural modifications could expand the potential of pleuromutilin derivatives against Gram-negative pathogens.

The epimeric synthetic intermediates (**7**, **8**, **9**, and **10**, **Table 1**) also generally retained high activity against *S. aureus* strains, with **7** showing the greatest potency. Against *E. coli* Δ*tolC*, all

four derivatives exhibited submicromolar activity, but they were completely inactive against wild-

| Compound | *S. aureus* ATCC 6538P | MRSA ATCC 43300 | MRSA NRS 123 (USA400) | MRSA NRS 384 (USA300) | VRSA VRS 10 (USA100) | *E. coli* BW 25113 (wt) | *E. coli* JW 51103 ΔtolC | VRE | *E. faecium* HM-965 |
|---|---|---|---|---|---|---|---|---|---|
| **11** | 16 | >32 | 8 | 16 | 32 | >64 | 1 | 4 | 1 |
| **12** | 16 | 16 | 4 | 8 | 8 | >64 | 1 | 4 | 0.5 |
| **13** | 16 | 32 | 4 | 8 | 16 | >64 | 2 | 4 | 1 |
| **14** | 16 | 32 | 8 | 8 | 1 | >64 | 2 | 16 | 2 |
| **15** | 32 | >32 | 16 | 32 | 32 | >64 | 0.5 | 4 | 1 |
| **16** | 16 | >32 | 16 | 32 | 32 | >64 | 1 | 16 | 1 |
| **17** | 1 | 2 | 0.5 | 1 | 8 | >64 | 1 | 2 | 1 |
| **18** | 0.5 | 1 | 0.25 | 0.25 | 0.25 | >64 | 0.25 | 1 | 0.5 |
| **1** | 2 | 2 | 0.5 | 1 | 0.5 | >64 | 0.5 | 8 | 0.5 |
| | | | | | | | | | |
| **19** | 4 | 32 | 2 | 4 | 4 | >64 | 0.5 | 2 | 0.5 |
| **20** | 4 | 8 | 1 | 2 | 2 | >64 | 0.5 | 2 | 0.5 |
| **21** | 4 | 16 | 1 | 2 | 2 | >64 | 0.5 | 2 | 0.5 |
| **22** | 4 | 16 | 2 | 4 | 4 | >64 | 1 | 4 | 1 |
| **23** | 8 | 32 | 8 | 16 | 16 | 64 | 0.25 | 4 | 4 |
| **24** | 4 | 32 | 4 | 8 | 16 | 64 | 0.125 | 4 | 2 |
| **25** | 1 | 4 | 8 | 8 | 1 | >64 | 2 | 1 | 1 |
| **26** | 0.5 | 2 | 0.25 | 0.5 | 0.5 | >64 | 0.25 | 0.5 | 0.25 |
| **2** | 1 | 2 | 0.5 | 0.5 | 0.5 | >64 | 0.125 | 2 | 0.25 |
| | | | | | | | | | |
| **7** | 0.5 | 0.5 | 1 | 1 | 0.5 | >64 | 2 | 2 | 1 |
| **8** | 0.5 | 1 | 2 | 4 | 1 | >64 | 1 | >32 | 2 |
| **9** | 2 | 2 | 1 | 2 | 1 | >64 | 0.25 | 8 | 1 |
| **10** | 2 | 4 | 2 | 4 | 1 | >64 | 0.25 | 2 | 1 |

**Table 1**. Minimum inhibitory concentrations (MIC) of the initial series of compounds in select organisms. All MIC values are in μg/mL. Compounds were inactive against two strains of *Enterococcus faecalis*, *Salmonella enterica*, *Acinetobacter baumannii*, *Klebsiella pneumoniae*, and *Pseudomonas aeruginosa* (**Table S1**). Compounds **23** and **24**

type *E. coli*. In VRE strains, their activity was comparable to pleuromutilin, except for **8**, which showed reduced potency.

The most potent derivatives from each series were the benzyloxymethylene-terminated triazoles (**18** and **26**) followed by the aromatic toluenesulfonate intermediate **7**. We hypothesize that the aromatic functionality of these compounds favorably interacts with the nucleotide-rich bacterial 70S ribosome, enhancing their on-target activity. Among these compounds, **18** was

generally the most potent, exhibiting MIC values as low as 0.25 ug/mL, particularly against a subset of MRSA strains. Compound **26** was nearly as effective and showed a slight advantage against VRE strains. These results contrast sharply with the non-C12 epimerized analog of **18**, which was previously[20] found to be inactive (MIC ≥64 ug/mL) across all tested organisms, as were other non-epimerized C20 triazoles. The high activity of **18** and **26** conclusively demonstrates that the C12 vinyl group is a suitable site for derivatization, provided that the pendant triazole adopts a suitable orientation—an insight not immediately apparent from the ribosome-bound tiamulin crystal structure.[37]

### 3.3.3 Computationally investigating epimeric pleuromutilin and tiamulin triazole derivatives in the PTC

Pleuromutilin antibiotics bind to the peptidyl transferase center (PTC) in the large ribosomal subunit with the tricyclic mutilin core binding in a hydrophobic pocket of the A site and the C14 substituents extending toward the P site. This nearly complete occlusion of both A and P sites prevents proper accommodation of the CCA ends of both A- and P-site tRNA substrates, even during the first elongation cycle.[10, 37] To refine atomistic insights into how the various triazole arms influence binding and to guide further derivatization, we applied our ribosome docking methodology[20, 38, 39] to the *epi*-C12 C20-triazole derivatives using the *Deinococcus radiodurans* 50S ribosome structure containing tiamulin (PDB ID: 1XBP)[37], the best available structure when this work commenced. Despite recent advances in nucleotide docking technology from our group [20, 39] and others,[40, 41] ribosomal RNA remains a particularly complex drug target. Our GNINA-based[42] docking approach leverages a genetic algorithm to sample a broad conformational space, which is essential for modeling RNA-ligand interactions as traditional scoring functions often fall short. By incorporating a CNN-based deep-learning scoring method, this approach enhances pose

ranking and improves identification of new relevant molecular interactions within the ribosome (**Figure S61**).

The pleuromutilin series (**11–18**) exhibited greater variability in docking orientations within the ribosomal binding cavity compared to the tiamulin series (**19–26**). This difference is attributed to the increased conformational consistency observed when both the triazole and thioglycolate arms are present, as seen in the tiamulin series (**Figures S64–S65**). Specifically, the mutilin core of the pleuromutilin derivatives docked closer to C2565 and A2045 than crystallized tiamulin but was positioned further from A2430 and C2431. In contrast, the tiamulin derivatives maintained stable interactions of the mutilin core with A2430 and C2431, likely due to the presence of the thioglycolate arm, which helps anchor the core within the pocket.

Interaction fingerprint heatmap analysis (**Figure S61**) identified novel interactions in many C20 triazole derivatives that were absent in docked poses of tiamulin and pleuromutilin. These new interactions were more frequent in tiamulin derivatives, likely due to the consistency imparted by the longer thioglycolate arm. One of the most notable new interactions involved C1773, which predominately interacts with longer C20 triazole arms (**17**–**18**, **25**–**26**). Additional interactions with A2041, A2042, and U2588 were also more frequent in tiamulin derivatives, again attributed to the thioglycolate arm. In contrast, pleuromutilin derivatives showed less consistent interactions with these nucleotides, likely due to the smaller C14 glycolate arm allowing greater variability in mutilin core positioning within the binding pocket.

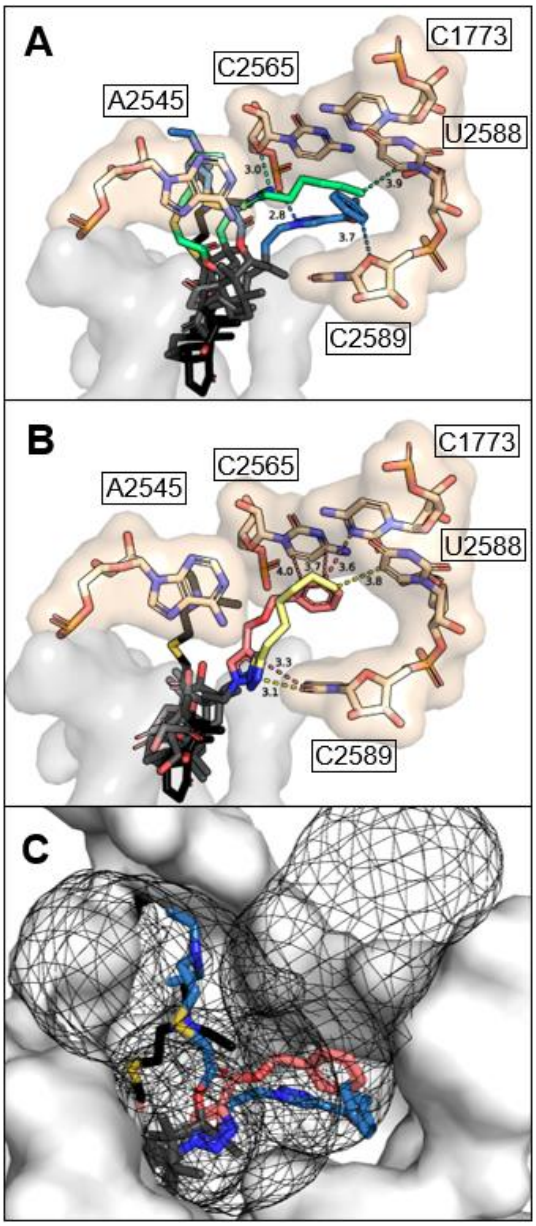


**Figure 2**. Predicted poses of pleuromutilin and tiamulin compounds in the *D. radiodurans* ribosome (PDB ID: 1XBP). **A)** Key interactions of pleuromutilin derivatives **17** (yellow) and **18** (salmon) with select nucleotides. **B)** Key interactions of tiamulin derivatives **25** (green) and **26** (blue). Co-crystallized tiamulin is shown in black; interactions of all derivatives and poses shown in **Figures S62** and **S63**. **C)** Volumetric capacity of the binding cavity as defined using CAVER 3.0.3.

Additional interactions between the C20 triazole or mutilin core with G2560, G2562, and G2563 were frequently observed, particularly in tiamulin derivatives. Within the tiamulin series (**Figure S63**), the steric constraints imposed by the thioglycolate and triazole arms promoted greater conformational consistency within the binding pocket, leading to more stable and favorable docking poses. In contrast, pleuromutilin derivatives (**Figure S62**) exhibited a broader positional distribution within the cavity due to their smaller glycolic acid arm, which increased variability in core positioning. Notably, derivatives with greater docking consistency and core stability generally correlated with better MIC values (**Table 1**).

Analysis of specific poses (**Figures 2A** and **2B**) revealed that the long C20 triazole arm in **17**, **18**, **25**, and **26** extend deeper into the A site than their parent molecules, tiamulin or pleuromutilin. These derivatives engage a previously unaccessed ribosomal region, bounded by C1773, C2565, U2588, and C2589, leading to new nucleotides interactions. Among these interactions, the triazoles frequently positioned near A2045 and C2589, in some poses forming pi-stacking contacts. The terminal aromatic portion of the benzyloxymethyl triazoles (**18** and **26**) also showed enhanced interactions with C2565, C2589, and U2588, among others (**Figure S61**), aligning with their hither MIC potency (**Table 1**). Beyond these direct interactions, CAVER[43] analysis identified a spacious binding pocket in this region (**Figure 2C**), suggesting that aromatic substituents could further optimize engagement with underlying nucleotides. These docking insights were instrumental in guiding synthetic derivation and provided key insights for rationalizing the design of subsequent derivative sets.

### 3.3.4 Design, synthesis, and testing of epimeric aryl triazole series

#### 3.3.4.1 Synthesis

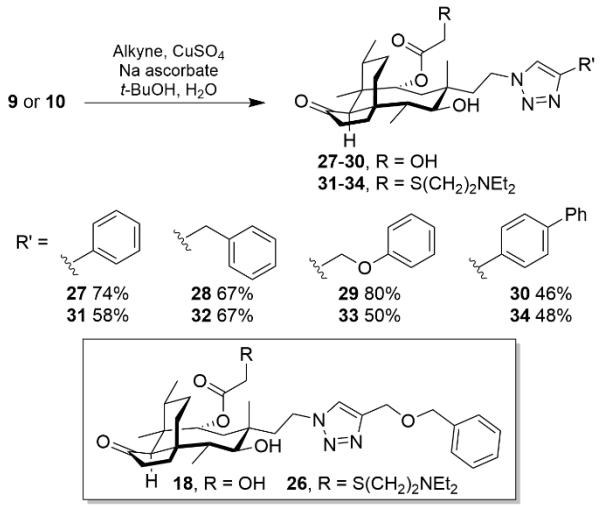


**Scheme 3**. Structure and yields of aromatic *epi*-C12 C20-triazole pleuromutilins and tiamulins. *Inset:* The highly active benzyloxymethylene triazoles that provided the basis of this SAR.

Based on these results, a combination of oxa-functionality and aromaticity off the C20 triazole appeared to be critical for activity. To probe this hypothesis, we synthesized (**Scheme 3**) a series of aromatic triazoles for both pleuromutilin (**27**–**30**) and tiamulin (**31**–**34**) designed to explore the available binding space of this new ribosomal region. Hydroazidation of **7** (**Scheme 1**) furnished **8**, which then diverged via hydrolysis or aminothiolation to generate **9** and **10**, the key intermediates for CuAAC cycloaddition. This reaction produced the pleuromutilin (**27**-**30**) and tiamulin (**31**-**34**) triazole series in yields ranging from 46% to 80% (**Scheme 3**). Together with top-performing derivatives **18** and **26** (*inset*), these compounds enabled structure-activity relationship (SAR) studies, assessing length and oxa-functionality in *epi*-C12 C20-triazole mutilins bearing aromatic substituents.

### 3.3.4.2 Antimicrobial testing

These series of aromatic *epi*-C12 pleuromutilin and tiamulin triazole derivatives were tested against a variety of pathogens (**Table 2**, **Table S1**). Compared to pleuromutilin and tiamulin,

the aromatic derivatives were equipotent against Gram-negative pathogens but showed significant activity gains against Gram-positive strains. Unlike the initial triazole series (**Table 1**), where tiamulin derivatives generally outperformed their pleuromutilin counterparts, the aromatic pleuromutilin triazoles were more effective against *S. aureus* strains, including MRSA. Notably, **27** and **30** showed ng/mL MIC values, suggesting that a more rigid orientation of aromatic functionality enhances activity against *S. aureus* activity and that larger groups, such as biphenyl **30**, are well accommodated. In contrast, the tiamulin analogues outperformed pleuromutilin derivatives against VRE, with the original benzyloxymethyl derivative **26** and phenyl derivative **31** exhibiting up to 4-fold higher activity relative to tiamulin. For more flexible chains, the presence of oxygen functionality off the triazole may be important as the benzyl triazoles **28** and **32** showed reduced potency compared to **18**, **29**, **26**, and **33**.

| **Compound** | ***S. aureus* ATCC 6538P** | **MRSA ATCC 43300** | **MRSA NRS 123 (USA400)** | **MRSA NRS 384 (USA300)** | **VRSA VRS 10 (USA100)** | ***E. coli* BW 25113 (wt)** | ***E. coli* JW 51103 (ΔtolC)** | **VRE** | ***E. faecium* HM-965** |
|---|---|---|---|---|---|---|---|---|---|
| **27** | 0.25 | 0.5 | 0.25 | 0.25 | 0.25 | >64 | 0.5 | 2 | 0.5 |
| **28** | 2 | 4 | 0.5 | 1 | 1 | >64 | 0.5 | 8 | 1 |
| **29** | 0.5 | 1 | 0.25 | 0.25 | 0.25 | >64 | 0.25 | 2 | 0.25 |
| **30** | 0.25 | 0.5 | 0.25 | 0.25 | 0.5 | >64 | 4 | 1 | 0.25 |
| **18** | 0.5 | 1 | 0.25 | 0.25 | 0.25 | >64 | 0.25 | 1 | 0.5 |
| **1** | 2 | 2 | 0.5 | 1 | 0.5 | >64 | 0.5 | 8 | 0.5 |
| | | | | | | | | | |
| **31** | 0.5 | 2 | 0.25 | 0.5 | 0.25 | >64 | 0.25 | 0.5 | 0.25 |
| **32** | 1 | 4 | 1 | 2 | 1 | >64 | 0.5 | 1 | 0.5 |
| **33** | 0.5 | 2 | 0.25 | 0.25 | 0.25 | >64 | 0.25 | 1 | 0.5 |
| **34** | 1 | 4 | 1 | 2 | 2 | >64 | 4 | 1 | 0.5 |
| **26** | 0.5 | 2 | 0.25 | 0.5 | 0.5 | >64 | 0.25 | 0.5 | 0.25 |
| **2** | 1 | 2 | 0.5 | 0.5 | 0.5 | >64 | 0.125 | 2 | 0.25 |

**Table 2**. Minimum inhibitory concentrations (MIC) of the aromatic compound series. All MIC values are in μg/mL.

Compounds were inactive against *Enterococcus faecalis*, *Shigella flexneri*, *Salmonella enterica*, *Acinetobacter*

### 3.3.4.3 Triazole derivatives target protein synthesis in vivo and in vitro

Because the new triazole derivatives are semisynthetic analogs of the PTC-targeting antibiotics pleuromutilin (**1**, PLE) and tiamulin (**2**, TIA), we expected them to bind to the bacterial ribosome inhibiting protein synthesis. However, epimerization and bulky C20 substituents could potentially alter their intracellular target. To confirm that protein synthesis remained the primary mode of action, we tested top-performing derivatives **18**, **27**, **30**, **26**, and **31** using an *in vivo* reporter system designed to distinguish between DNA replication and protein synthesis inhibitors.[44] In this assay, sub-inhibitory concentrations of antibacterial compounds that stall translation (e.g., erythromycin, ERY) induce expression of the far-red fluorescent protein reporter Katushka2S (**Figure 3A**, ERY, red pseudocolor ring). Compounds that trigger SOS response, such as inhibitors of DNA gyrase (e.g., ciprofloxacin, CIP), induce the expression of Red Fluorescent Protein (RFP) reporter (**Figure 3A**, CIP, green pseudocolor ring). When *E. coli ΔtolC* cells carrying the dual reporter plasmid were exposed to triazole derivatives **18**, **27**, **30**, **26**, and **31** or the parent antibiotics, a strong induction of Katushka2S expression was universally observed (**Figure 3A**, red pseudocolor rings). This result is consistent with protein synthesis remaining the primary target of the PLE and TIA derivatives.

To evaluate the intrinsic translation-inhibitory potential of new PLE and TIA derivatives, independent of their cellular uptake and efflux, we assessed their ability to suppress *in vitro* protein synthesis. The addition of these compounds to a cell-free transcription-translation system based on *E. coli* S30 extract resulted in dose-dependent inhibition of green fluorescent protein (GFP) synthesis in both series. GFP fluorescence was monitored over two hours, reaching a plateau at the endpoint. At the lowest concentration of 1 μM, neither the parent nor derivative compounds significantly inhibited translation relative to the no-antibiotic control. However, at 30 μM—a

ribosome saturating concentration—all compounds except **27** and **26** exhibited inhibition levels comparable to the no-template control. For comparative analysis, all drugs were tested at 8 μM (**Figure 3B, C**).

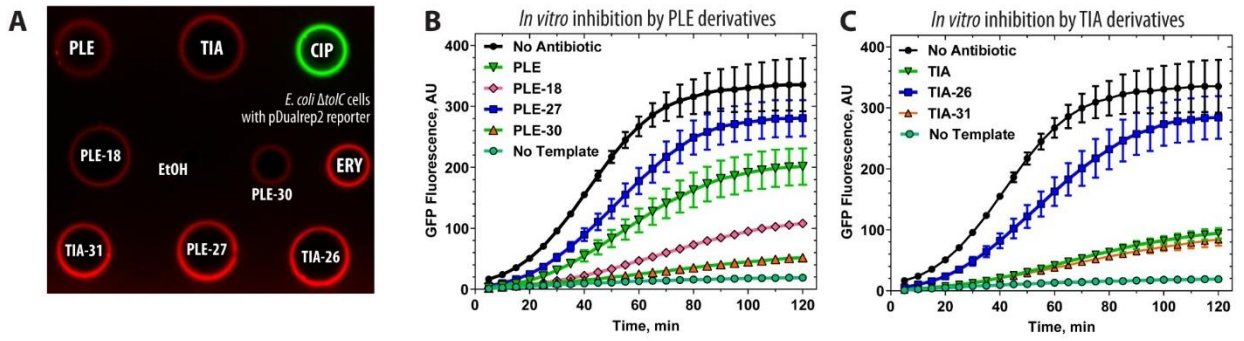


**Figure 3. New PLE and TIA derivatives inhibit protein synthesis both *in vivo* and *in vitro*.** (**A**) *In vivo* testing of antibiotic activity using *E. coli* BW25113 Δ*tolC* strain carrying pDualrep2 plasmid. The induction of the red fluorescent protein (RFP) expression (green halo around the inhibition zone) is triggered by DNA-damage, while the induction of Katushka2S protein (red halo) occurs in response to ribosome stalling. Ciprofloxacin (CIP) and erythromycin (ERY) are used as positive controls. Ethanol (EtOH) is a negative control. The image is an overlay of the two images from the independent detections of RFP (Cy3 mode) or Katushka2S (Cy5 mode) by ChemiDoc MP (Bio-Rad) with RFP fluorescence shown in green pseudocolor and Katushka2S fluorescence shown in red pseudocolor. (**B**, **C**) Inhibition of protein synthesis by pleuromutilin (B), tiamulin (C), and their new derivatives in the *in vitro* cell-free transcription-translation coupled system. The relative fluorescence of *in vitro* synthesized GFP is shown. Error bars represent standard deviations of the mean of three independent measurements.

Among the pleuromutilin-derived compounds (**Figure 3B**), **18** and **30** exhibited significantly stronger inhibition of protein synthesis than the parent compound PLE (**1**), whereas **27** was the weakest translation inhibitor. For the tiamulin-derived compounds (**Figure 3C**), **31** showed inhibition comparable to parent TIA (**2**), while **26** was markedly less effective. Although some variation was expected due to the use of *E. coli* ribosomes in the *in vitro* translation system, these results largely align with MIC data from the *E. coli* Δ*tolC* knockout strain. However, **30**, despite being the least effective compound in *E. coli* Δ*tolC* MIC assays, exhibited the strongest inhibition of translation among all derivatives and parents. This enhanced translation inhibition correlates with structural data—albeit from a different ribosome—suggesting that the additional π-stacking interaction with C2610 (*vida infra*) may have strengthened its ribosomal binding, thereby increasing its efficacy *in vitro*. However, the same triazole extension that enhances binding may also hinder ribosomal access *in vivo*, potentially explaining the discrepancies between *in vivo* and *in vitro* results.

#### 3.3.4.4 Cytotoxicity testing of top aromatic derivatives

Cytotoxicity data were collected for the initial benzyloxymethylene triazoles (**18** and **26**) and the highly active phenyl triazoles (**27** and **31**) to assess their viability as lead compounds. In monkey kidney fibroblast cells (**Figure 4A**), **18** and **27** exhibited no cytotoxicity at the highest tested concentration (64 µg/mL). However, the corresponding *epi*-tiamulin derivatives (**26** and **31**) showed toxicity at 16-32 ug/mL. Neither pleuromutilin (**1**) nor tiamulin (**2**) exhibited cytotoxic at any tested concentration. In the human endocervical epithelial cell line ME-180 (**Figure 4B**), the same overall trends were observed, though all compounds except **18**—including pleuromutilin (**1**) and tiamulin (**2**)—began to exhibit cytotoxicity at higher concentrations. Compared to **1** and **2**, which exhibited toxicity at 32 µg/mL and 16 ug/mL, respectively, compound **18** remained non-

toxic up to 64 µg/mL. Compound **27** was slightly more toxic than pleuromutilin and tiamulin at 64 µg/mL, but remained nontoxic at concentrations of 32 µg/mL or lower. In contrast, **26** and **31** began showing toxicity at 16 µg/mL.

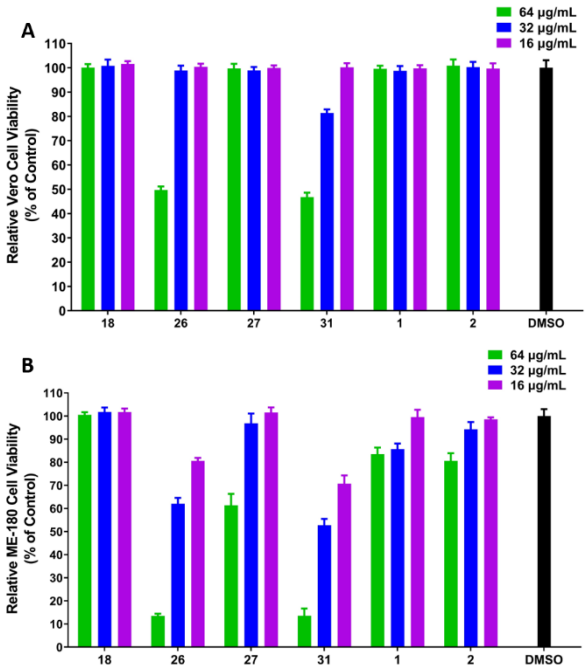


**Figure 4.** *In vitro* cytotoxicity evaluation of key compounds against A) monkey kidney fibroblast cells Vero cells. B) A) human endocervical epithelial cells (ME-180). Error bars represent the standard deviations

The high potency of **18** and **27** (0.25–2 µg/mL) against drug resistant Gram-positive pathogens alongside their low cytotoxicity suggests a selectivity index suitable for human use. The lower toxicity of **18**, **27**, and tiamulin compared to disubstituted derivatives **26** and **31** suggests that simultaneous substitution of both the C22 and C20 positions—with a thioether and triazole-aromatic pendant group, respectively—may contribute to increased toxicity, at least with tiamulin-type thioethers. Moreover, the strong efficacy of **18** and **27**, which matches that of their tiamulin

counterparts **26** and **31**, suggests that refining the C22 position *after* optimizing the triazole constituent could enhance activity even further.

### 3.3.4.5 Aromatic moieties of new triazole derivatives establish unique interactions with the ribosome

To further investigate functional role of aromatic additions, we determined the high-resolution X-ray crystal structures of the 70S ribosomes from the Gram-negative bacterium *Thermus thermophilus* (*Tth*) complexed with the five best-performing derivatives—**18**, **27**, **30**, **26**, and **31**—at 2.70-2.90 Å resolution (**Table S2**). The obtained Fourier maps (**Figure 5**) revealed strong positive electron density with characteristics closely resembling the structural features of each individual compound, allowing us to unambiguously position all chemical groups within the pleuromutilin scaffold. For direct comparison, we also determined the structures of ribosome-bound parent compounds pleuromutilin (**1**) and tiamulin (**2**).

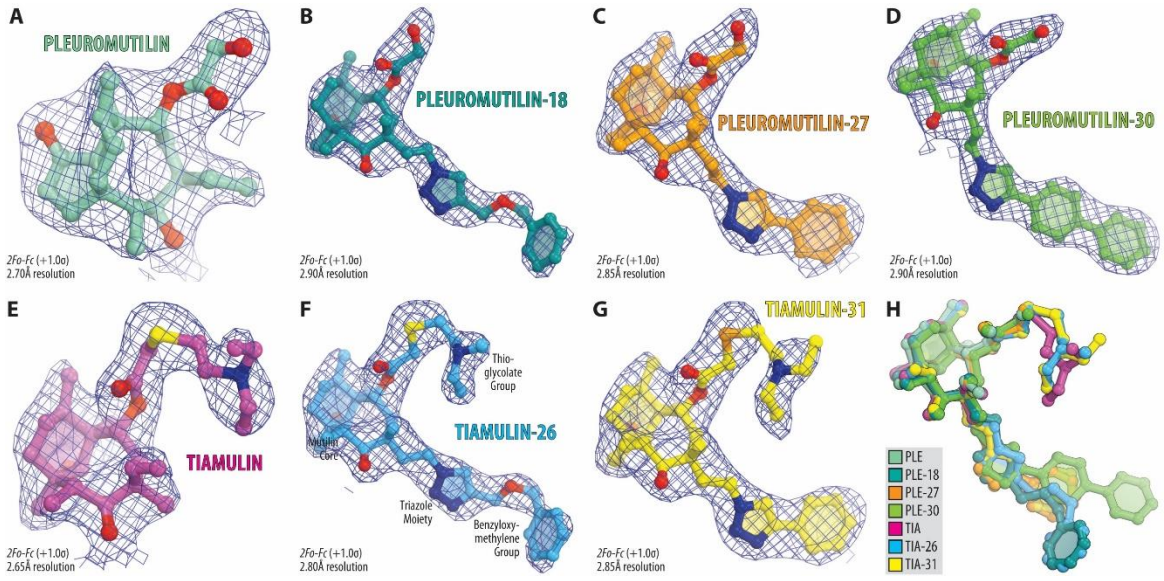


**Figure 5. Electron density maps of ribosome-bound pleuromutilin (A-D) and tiamulin (E-G) derivatives.** 2*Fo-Fc* Fourier electron density maps of pleuromutilin (**1**, A, light teal), **18** (B,

teal), **27** (C, orange), **30** (D, green), tiamulin (**2**, E, magenta), **26** (F, light blue), and **31** (G, yellow) in complex with the *T. thermophilus* 70S ribosome (blue mesh). The refined model of each molecule is displayed in its respective electron density after the refinement contoured at 1.0σ. Carbon atoms are colored specific to each compound; nitrogen atoms are blue, oxygen atoms are red. (**H**) Superposition of the new structures of the derivatives with each other. All structures were aligned based on domain V of the 23S rRNA.

Our structural data reveal that all compounds engage the bacterial ribosome in similar ways. Importantly, the positions of the tricyclic mutilin cores remain conserved in the A site, stabilized through a combination of hydrophobic interactions and H-bonding (**Figure 6**). More specifically, all studied derivatives establish the same H-bond between the C21 carbonyl oxygen and the N2 atom of nucleotide G2061 (*E. coli* numbering) of the 23S rRNA, mirroring the parent compounds. Additionally, the C3 carbonyl group forms an H-bond with the ribose 2'-hydroxyl of the G2505 in **30**, **26**, and **31**, with a weaker interaction in **18** and **27**, based on relative distance. Notably, while the C11 alcohol **26** and **31** forms H-bonds with the G2505 phosphate group, this interaction is absent in **18**, **27** and **30**.

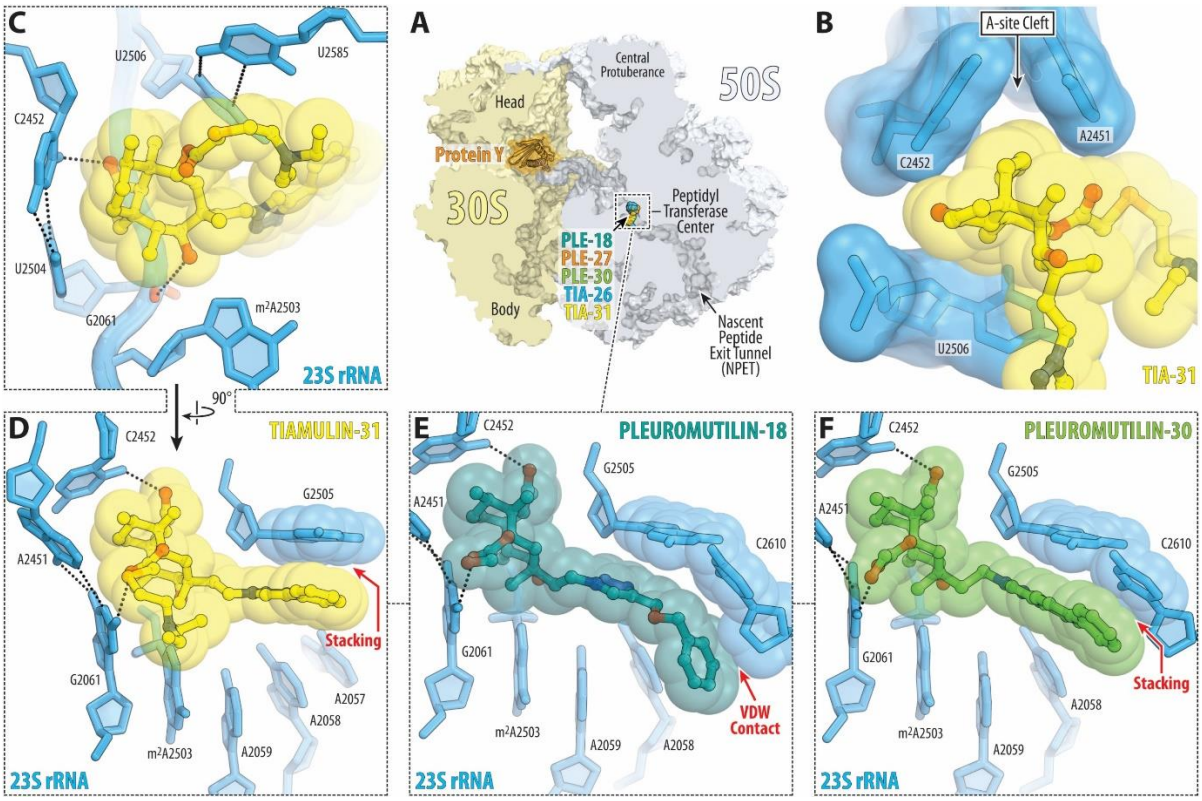


**Figure 6. Structures of PLE and TIA derivatives in complex with the bacterial ribosome.** (**A)** Overview of the binding site for PLE-**18** (teal), PLE-**27** (orange), PLE-**30** (green), TIA-**26** (light blue), and TIA-**31** (yellow) in the PTC of the *T. thermophilus* 70S ribosome showing the 30S subunit (light yellow), the 50S subunit (light blue), and the ribosome-bound protein Y (orange). (**B**) Detailed view of TIA-**31** bound in the PTC, highlighting the characteristic intercalation of the mutilin core of the molecule into the A-site cleft formed by nucleotides A2451 and C2452 of the 23S rRNA (*E. coli* numbering of the rRNA nucleotides is used throughout). (**C-F**) Close-up views of TIA-**31** (C, D), PLE-**18** (E), and PLE-**30** (F) in the PTC of the 70S ribosome, highlighting its stacking/VDW contacts (red labels) and H-bond interactions (dashed lines) with the nucleotides of the 23S rRNA. Note that the triazole ring of all the compounds engages in pi-pi stacking interactions with the nucleobase G2505. The additional phenyl group in compounds PLE-**27** and TIA-**31** extends this stacking interaction, whereas the second phenyl group of PLE-30

extends further, also engaging the nucleobase of C2610. The phenyl group of the longer benzyloxymethyl arms of PLE-**18** and TIA-**26** has VDW contacts with the ribose of C2610.

Our structures reveal that adding the C20-triazole group off the *epi*-C12 position of the mutilin core facilitates π-π stacking interactions with the G2505 nucleobase. This new hydrophobic contact enhances engagement between the derivatives and their binding site, in agreement with the improved MIC values of these derivatives relative to their parent compounds (**Table 2**). Further benzene ring extensions off the triazole, as in **27** and **31**, increased contact with G2505. Additional π-stacking interactions were only observed in **30**, where a biphenyl system extends the terminal ring further than in other compounds. This elongation enables **30** to encroach π-stack with the C2610 nucleobase. Peculiarly, benzyloxymethylene extensions (as in compounds **18** and **26**) did not introduce any additional π-stacking interactions. However, the phenyl group of the benzyloxymethyl arms maintained van der Waals (VDW) contacts with the nearby C2610 ribose. The flexibility of these benzyloxymethylene groups of **18** and **26**, as judged by the relatively weak electron density (**Figure 5**), suggests that they may form multiple contacts not captured in the static structure. Collectively, these findings demonstrate that the C20-triazoles on C12-epimeric mutilins engage the ribosome through new π-stacking interactions and highlight further opportunities to refine pendant aryl functionality for enhanced target engagement.

Finally, the thioglycolate arm at C22, present in tiamulin (**2**) and its derivatives **26** and **31**, extends further into the P site. However, the distal diethylamino group is not well resolved in the structures and does not form additional interactions within the PTC of the ribosome, suggesting that it is not coordinated. Instead, it may interfere with the canonical placement of the formyl-methionyl moiety of the initiator tRNA during the initiation of protein synthesis. The high flexibility and lack of additional contacts from the thioglycolate arm cannot explain the increase

in potency of tiamulin (**2**) compared to pleuromutilin (**1**). One possible explanation is that C22-thioglycolate substitution enhances bacterial uptake rather than contributing to target engagement. However, the absence of a parallel increase in activity between C22-OH triazole derivatives (**18** and **27**) with their C22-thioglycolated counterparts (**26** and **31**) suggests that this effect is not universal and that additional factors influence potency.

The mutilin cores of all studied derivatives bind consistently to the A and P sites of the PTC, likely inhibiting protein synthesis initiation by preventing accommodation of both tRNAs into the PTC. This orientation suggests that the observed antimicrobial activity is primarily driven by target engagement (affinity). Indeed, incorporation of the triazoles and their extensions introduces additional ribosome interactions, which likely increases binding affinity. It should be noted, however, that the additional π-stacking interaction observed with **30** does not improve MIC values (**Table 2**) in Gram-positive strains compared to **27**, which is one benzene ring shorter. Thus, our structural data indicates that the most beneficial modification is the addition of the C20 aromatic triazole off the epimeric C12 position of the mutilin core. The relative lack of contacts of the aromatic substituents off the triazole ring—with the exception of **30**—suggests multiple avenues for further derivatization to enhance affinity. Meanwhile, the thioglycolate arm at C22 in **26** and **31** does not establish additional ribosomal contacts, nor does it improve activity relative to C22-hydroxy counterparts **18** and **27**. This suggests that C22 modifications affect factors beyond binding, making it a viable site for further derivatization in turn.

#### 3.3.4.6 Activity correlations and outcomes

The antimicrobial activity and cytotoxicity profile of these *epi*-C12 pleuromutilin aromatic triazole derivatives reveal a large therapeutic window, with target engagement supported by multiple lines of evidence. Structural data confirms binding within the pleuromutilin core pocket,

with triazole modifications extending into the A site, introducing new π-stacking interactions between the ribosome and the triazole ring. While these structural snapshots provide direct evidence of engagement, they do not capture the full dynamic binding landscape. Molecular docking suggests that certain derivatives may adopt conformations beyond those observed in static structures, explaining activity trends not solely attributable to resolved binding interactions. Medicinal chemistry data further reinforces this perspective—for instance, the drastic MIC shift between **11** and **18** suggests aromatic functional groups off the triazole are critical for activity, even in cases where direct binding contacts were not captured crystallographically.

Beyond direct target engagement, calculated drug properties may help explain discrepancies in efficacy trends. Comparative assessment of activity versus ADME properties (**Table S3**) revealed that cLogP values above 3.58 and total polar surface areas below 124 Å$^2$ for the pleuromutilin derivatives (134 Å$^2$ for tiamulin derivatives) correlates with higher activity, suggesting that both permeability and lipophilicity influence potency. This property analysis provides a framework for reconciling cases where enhanced in vitro activity (**Figure 3B**) does not translate to improved MIC values (**Table 2**), as seen with **30**. Finally, computational docking of newly obtained crystal structures (**Figures S66** and **S67**) provides additional insight into potential drug-ribosome interactions. Threse results reinforce the need to integrate structural validation, computational modeling, and pharmacokinetic considerations alongside synthesis to fully optimize antibiotic efficacy.

### 3.4 Conclusions

In summary, C12 epimerization and C20-triazole functionalization via anti-Markovnikov hydroazidation yielded active pleuromutilin (C22 hydroxy) and tiamulin (C22 thioglycolate) derivatives with 4- to 8-fold increases in antimicrobial activity relative to parent compounds. The

top-performing derivatives exhibited strong activity against drug-resistant *S. aureus* strains without increased cytotoxicity. Structural data indicate that activity enhancements stem from new π-stacking interactions between the triazole and G2505 nucleobase. Computational modeling further suggests this binding region can accommodate large aromatic functional groups, offering additional avenues for potency optimization. Notably, the C22-thioglycolate tiamulin derivatives (**26** and **31**) were only equivalent in activity to their C22-hydroxy counterparts (**18** and **27**), indicating that C22 modifications influence factors beyond direct ribosomal binding. Accordingly, stepwise refinement of the C22 position after C12 epimeric C20 triazole optimization may yield derivatives with even greater activity. Future work will continue to leveraging computational and structural insight to develop these compounds into lead candidates for *in vivo* testing and next-generation pleuromutilin antibiotics.

## ACKNOWLEDGMENTS

This research was supported by grant funding from Virginia's Commonwealth Health Research Board. Funding was also provided by the Lay Nam Chang Dean's Discovery Fund, the CeZAP Interdisciplinary Team-building Pilot Grant, CeZAP ID-IGEP graduate student mini-grant (L.M.B.), and Virginia Tech startup funds (A.N.L). We thank the Virginia Tech Center for Drug Discovery for assistance with plate preparation for antimicrobial assays.

We thank the staff at NE-CAT beamlines 24ID-C and 24ID-E for help with X-ray diffraction data collection, especially Drs. Malcolm Capel, Frank Murphy, Surajit Banerjee, Igor Kourinov, David Neau, Jonathan Schuermann, Narayanasami Sukumar, Anthony Lynch, James Withrow, Kay Perry, Ali Kaya, and Cyndi Salbego.

This work is based upon research conducted at the Northeastern Collaborative Access Team beamlines (24ID-C and 24ID-E), which are funded by the National Institute of General Medical Sciences from the National Institutes of Health [grant P30-GM124165 to NE-CAT]. The Eiger 16M detector on 24ID-E beamline is funded by an NIH-ORIP HEI grant [S10-OD021527 to NE-CAT]. This research used resources of the Advanced Photon Source, a US Department of Energy (DOE) Office of Science User Facility operated for the DOE Office of Science by Argonne National Laboratory under Contract No. DE-AC02-06CH11357. This work is also based upon research conducted at the Center for BioMolecular Structure beamlines (17ID-1 and 17ID-2), which are primarily supported by the National Institute of General Medical Sciences from the National Institutes of Health [P30-GM133893] and by the DOE Office of Biological and Environmental Research [KP1605010]. NSLS2 is a U.S. DOE Office of Science User Facility operated under Contract No. DE-SC0012704. This publication resulted from the data collected using the beamtime obtained through NE-CAT BAG proposal #311950.

This work was supported by the National Institute of General Medical Sciences of the National Institutes of Health [grants R01-GM132302 and R35-GM151957 to Y.S.P.], Illinois State startup funds [to Y.S.P.]. The funders had no role in study design, data collection and analysis, decision to publish, or manuscript preparation.

**AUTHOR CONTRIBUTIONS STATEMENT**

L.M.B., R.P.S., and A.N.L. designed and performed the chemical synthesis, purification, and characterization of pleuromutilin compounds; M.H., M.L., A.J.B., and A.M.B. designed and performed computational docking experiments. B.Y.K., I.K., and Y.S.P. designed and performed X-ray crystallography experiments and determined the structures of ribosome-bound synthetic pleuromutilin compounds; L.M.B., B.Y.K., A.S.A., A.A.A., and N.J.V. performed antimicrobial

and other biochemical assays. A.N.L., A.M.B., Y.S.P., and M.N.S. designed and supervised the experiments. All authors interpreted the results. All authors contributed to the writing and editing of the manuscript.

**COMPETING INTERESTS STATEMENT**

The authors declare no competing interests.

### 3.5 General methods

#### 3.5.1 Synthetic methods

Unless otherwise noted, chemical reagents and solvents were purchased from EMD Millipore, Oakwood Chemical, Sigma-Aldrich, and Thermo Fisher Scientific. Unless otherwise specified, all reactions were carried out under an atmosphere of dry nitrogen in dried glassware. Commercially available starting materials and reagents were used as received or purified prior to use if necessary. Triethylamine was distilled from calcium hydride, and pyridine was distilled from potassium hydroxide. Pleuromutilin was purchased as a commercial compound from TRC Canada. Analytical thin layer chromatography was performed Supelco 0.25 mm silica gel 60 $F_{254}$ plates. Visualization was accomplished by irradiation with a 254 nm UV lamp or by staining with an aqueous solution of ceric ammonium molybdate, an acidified ethanolic solution of *p*-anisaldehyde, or a basified solution of potassium permanganate. Chromatography was performed using a forced flow of the indicated solvent system on SiliCycle SiliaFlash P60 silica gel (40-63 μm) or via automated flash chromatography using a Biotage Selekt system with SiliCycle SiliaSep or Teledyne RediSepRf gold chromatography columns. Deionized water was obtained from the house deionized water system.

$^{1}$H NMR spectra were recorded on a Bruker Avance II 500 MHz spectrometer. Chemical shifts are reported in parts per million from tetramethylsilane (0 ppm) using the solvent resonance as an internal standard ($CDCl_3$ 7.26 ppm, $CD_3OD$ 3.31 ppm, DMSO-$d_6$ 2.50 ppm). Data are reported as follows: chemical shift, multiplicity (s=singlet, d=doublet, t=triplet, q=quartet, m=multiplet, br=broad), number of protons, and coupling constants. Proton decoupled $^{13}$C NMR were recorded on a Bruker Avance II 500 MHz (125 MHz) spectrometer. Chemical shifts are reported in ppm from tetramethylsilane (0 ppm) using the solvent resonance as an internal standard ($CDCl_3$ 7.26 ppm, $CD_3OD$ 3.31 ppm, DMSO-$d_6$ 2.50 ppm). High resolution mass spectra were obtained on an Agilent Technologies 6220 TOF LC/MS or a Waters Synapt Q-TOF G2 in the Department of Chemistry and the VT-Mass Spectrometry Incubator at the Virginia Polytechnic Institute and State University. Specific rotations were obtained on a Jasco P-2000 polarimeter.

### 3.5.2 Broth microdilution assays

Media and solutions were autoclaved or sterile filtered prior to use and manipulations were carried out in a laminar flow hood. Antibacterial testing was performed in polypropylene 96-well flat bottom plates in triplicate. The minimal inhibitory concentration (MIC) of derivatives **5**-**32** was assessed against *Staphylococcus aureus* ATCC 6538P, methicillin-resistant *S. aureus* (MRSA) ATCC 43300, *Enterococcus faecalis* ATCC 29212, vancomycin-resistant *Enterococcus* (VRE), *Escherichia coli* ΔTolC, *E. coli* MC1061, *Klebsiella pneumoniae* ATCC 29665, *Pseudomonas aeruginosa*, *Acinetobacter baumannii* ATCC 17978, *Shigella flexneri* (BS103), *Salmonella enterica* (ATCC 14028) using serial dilutions. Pleuromutilin (TRC Canada) and tiamulin (Elanco US) were used as positive controls and the vehicle as a negative control. Stock solutions of each compound were prepared at 1.28 mg/mL in DMSO and serially diluted in DMSO to create master plates. From the master plates, 5 μL of each dilution was applied to test plates using a Bravo

automated liquid transfer system (Agilent). Bacteria previously grown overnight (37 °C, 120 – 200 RPM), in LB broth were diluted to an OD600 of 0.05 in cation-adjusted Mueller-Hinton broth, grown to an OD600 of ~0.5, and diluted to an OD600 of 0.004 in cation-adjusted Mueller-Hinton broth. These diluted cultures were applied to the test plates (195 μL per test well) resulting in final concentrations of the test compounds of 32-0.25 μg/mL. The plates were incubated at 37 °C for 16–18 h, except for VRE and *E. faecalis*, which were incubated at 37 °C for 24 h. Inhibition was determined by measuring the optical density at 600 nm (OD600) with a Cytation 3 plate reader (BioTek). The optical density measurements were normalized to the positive and negative controls. The MIC was the lowest concentration that inhibited >90% of growth. After the first round of testing, an expanded range of *Enterococci* (*E. faecalis* NR31971, *E. faecalis* NR31972, and *E. faecium* HM-965) and *Staphylococcus aureus* (VRSA VRS10 (USA100), MRSA NRS123 (USA400), and MRSA NRS384 (USA300)) strains were tested via the following methods: The minimum inhibitory concentrations (MICs) of the compounds and control drugs were determined using the broth microdilution method, according to guidelines outlined by the Clinical and Laboratory Standards Institute (CLSI).[45] Bacteria were grown aerobically overnight at 37°C on tryptone soy agar plates. Afterwards, a bacterial solution equivalent to 0.5 McFarland standard was prepared and diluted in cationic adjusted muller hinton broth (CA-MHB) to achieve a bacterial concentration of about $5 \times 10^5$ CFU/mL, and seeded in 96-well well plates. Compounds and control drugs were added in the first row of the 96-well plates and serially diluted along the plates. Plates were then incubated aerobically at 37°C for 20-24 hours. MICs reported are the minimum concentrations of the compounds/control drugs that could completely inhibit the visual growth of the bacteria.

### 3.5.3 Synthesis

**(3a*R*,4*R*,5*R*,7*R*,8*S*,9*R*,9a*S*,12*R*)-8-hydroxy-4,7,9,12-tetramethyl-3-oxo-7-vinyldecahydro-4,9a-propanocyclopenta[8]annulen-5-yl 2-(tosyloxy)acetate (7)**: To a stirring, degassed solution of **6** (4.00 g, 7.51 mmol) in refluxing dry tetrahydrofuran (20 mL), was added 1.0 M diethyl zinc in hexanes (4.1 mL, 4.1 mmol) slowly over 5 minutes. The transparent, slightly yellow solution was stirred for 7 h at reflux. After cooling, the solution was quenched by the addition of water (0.45 mL) while stirring. The resulting suspension was filtered through Celite, washed with THF, and the filtrate was concentrated to afford a white foam. This residue was purified via automated flash chromatography (80 g Silicycle SiliaSep silica column, 7% acetone/toluene, impure fractions resubjected to chromatography using identical conditions) to give **7** (1.93 g, 48%) as a white foam. Spectral data were in accord with those previously reported.[22]

**(3a*R*,4*R*,5*R*,7*S*,8*S*,9*R*,9a*S*,12*R*)-7-(2-azidoethyl)-8-hydroxy-4,7,9,12-tetramethyl-3-oxodecahydro-4,9a-propanocyclopenta[8]annulen-5-yl 2-(tosyloxy)acetate (8)**: A stirring suspension of **7** (1.122 g, 2.105 mmol) and benziodoxole (500 mg, 1.89 mmol) in $CH_2Cl_2$ (2.50 mL) was purged and refilled with $N_2$ three times and then kept under a positive pressure of nitrogen, after which $H_2O$ (106 µL, 5.89 mmol) was added with stirring. The white suspension was cooled to 0 °C (ice bath). $TMSN_3$ (2.10 mL, 16.0 mmol) was added and after 5 min, TFA (32.0 µL, 0.418 mmol) was added. The reaction was warmed to rt and stirred for 16 h resulting in a slightly yellow suspension. The mixture was diluted with EtOAc (15 mL), washed with saturated aqueous $NaHCO_3$ (20 mL), washed with brine (10 mL), dried over $Na_2SO_4$, and concentrated to afford a yellow foam. The residue was purified by automated flash chromatography (40 g Silicycle SiliaSep $SiO_2$ column, 9% EtOAc/$CH_2Cl_2$) to give **8** (706 mg, 58%) as a white foam: $^1$H NMR (500 MHz, $CDCl_3$) δ 7.84 (d, *J* = 8.1 Hz, 2H), 7.38 (d, *J* = 8.1 Hz, 2H), 5.62 (d, *J* = 8.4 Hz, 1H), 4.49 (s, 2H), 3.52 – 3.48 (m, 1H), 3.48 – 3.38 (m, 2H), 2.48 (s, 3H), 2.34 – 2.18 (m, 3H), 2.12 (dd,

*J* = 15.7, 8.4 Hz, 1H), 2.01 (d, *J* = 2.7 Hz, 1H), 1.84 (dt, *J* = 14.8, 7.5 Hz, 1H), 1.80 – 1.75 (m, 1H), 1.72 – 1.62 (m, 2H), 1.62 – 1.55 (m, 2H), 1.53 – 1.46 (m, 2H), 1.43 (d, *J* = 1.1 Hz, 3H), 1.41 – 1.35 (m, 1H), 1.13 (td, *J* = 14.0, 4.5 Hz, 1H), 1.07 (s, 3H), 1.01 (d, *J* = 15.8 Hz, 1H), 0.96 (d, *J* = 7.1 Hz, 3H), 0.64 (d, *J* = 7.0 Hz, 3H); $^{13}$C NMR (126 MHz, $CDCl_3$) δ 216.7, 165.1, 145.5, 132.7, 130.1, 128.2, 72.0, 70.8, 65.1, 58.2, 47.6, 45.5, 42.5, 41.9, 41.0, 40.6, 36.6, 34.9, 34.6, 30.3, 26.9, 25.1, 21.8, 18.0, 16.7, 15.0, 11.1; HRMS (ESI) calcd for $C_{29}H_{41}N_3O_7SNa$ $[M+Na]^+$ 598.2557, found 598.2553; $[\alpha]_D^{25}$ = -12 (c = 1.1, $CH_3OH$).

**(3a*R*,4*R*,5*R*,7*S*,8*S*,9*R*,9a*S*,12*R*)-7-(2-azidoethyl)-8-hydroxy-4,7,9,12-tetramethyl-3-oxodecahydro-4,9a-propanocyclopenta[8]annulen-5-yl 2-hydroxyacetate (9)**: To a stirring solution of **8** (299 mg, 0.519 mmol) in EtOAc (5 mL) and $CH_3OH$ (15 mL) was added sodium formate (349 mg, 5.13 mmol). The suspension was heated to 70 °C (oil bath) and stirred for 28 h. After cooling, the mixture was concentrated and the residue was partitioned between EtOAc (15 mL) and water (4 mL). The organic layer was washed with brine (10 mL), dried over $Na_2SO_4$, and concentrated to afford **9** (214 mg, 98%) as an amorphous white solid. A small sample was precipitated from benzene for characterization purposes. $^1$H NMR (500 MHz, $CDCl_3$) δ 5.68 (d, *J* = 8.5 Hz, 1H), 4.11 (d, *J* = 17.1 Hz, 1H), 4.04 (d, *J* = 17.1 Hz, 1H), 3.53 (d, *J* = 6.2 Hz, 1H), 3.50 – 3.39 (m, 2H), 2.36 (p, *J* = 7.1 Hz, 1H), 2.32 – 2.22 (m, 2H), 2.21 – 2.13 (m, 1H), 2.03 (d, *J* = 2.8 Hz, 1H), 1.87 (dt, *J* = 14.8, 7.5 Hz, 1H), 1.80 (dq, *J* = 14.6, 3.1 Hz, 1H), 1.71 – 1.47 (m, 6H), 1.45 (s, 3H), 1.44 – 1.37 (m, 1H), 1.19 – 1.10 (m, 4H), 1.04 (d, *J* = 15.8 Hz, 1H), 0.98 (d, *J* = 7.1 Hz, 3H), 0.71 (d, *J* = 7.1 Hz, 3H); $^{13}$C NMR (126 MHz, $CDCl_3$) δ 216.7, 172.2, 71.9, 70.2, 61.3, 58.1, 47.5, 45.4, 42.6, 41.9, 40.9, 40.5, 36.6, 34.8, 34.5, 30.2, 26.8, 25.0, 18.0, 16.7, 14.9, 11.0; HRMS (ESI) calcd for $C_{22}H_{35}N_3O_5Na$ $[M+Na]^+$ 444.2469, found 444.2471; $[\alpha]_D^{25}$ = -12 (c = 1.1, $CH_3OH$).

**(3a*R*,4*R*,5*R*,7*S*,8*S*,9*R*,9a*S*,12*R*)-7-(2-azidoethyl)-8-hydroxy-4,7,9,12-tetramethyl-3-oxodecahydro-4,9a-propanocyclopenta[8]annulen-5-yl 2-((2-(diethylamino)ethyl)thio)acetate (10)**: To a stirring solution of $Et_2NH$ (92.0 µL, 0.889 mmol) in EtOAc (0.5 mL), thiirane (53.0 µL, 0.891 mmol) was added slowly via syringe. Azido-*epi*-tosylpleuromutilin **8** (329 mg, 0.571 mmol) dissolved in EtOAc (0.7 mL) was added. The solution was heated to 45 °C (oil bath) and stirred for 4 h. Additional thiirane (53.0 µL, 0.891 mmol) and $Et_2NH$ (92.0 µL, 0.889 mmol) were added. After stirring for 16 h, the mixture was cooled and concentrated, resulting in a yellow oil. This residue was purified by flash chromatography ($SiO_2$, 4% (10:1 $CH_3OH$:$NH_4OH$)/$CH_2Cl_2$) to give **10** (227 mg, 74%) as a faintly yellow oil: $^1$H NMR (500 MHz, $CDCl_3$) δ 5.57 (d, *J* = 8.4 Hz, 1H), 3.50 (t, *J* = 6.2 Hz, 1H), 3.47 – 3.36 (m, 2H), 3.18 (s, 2H), 2.73 (br s, 4H), 2.58 (q, *J* = 7.2 Hz, 4H), 2.34 (p, *J* = 6.9 Hz, 1H), 2.31 – 2.16 (m, 2H), 2.12 (dd, *J* = 15.8, 8.5 Hz, 1H), 2.00 (d, *J* = 2.8 Hz, 1H), 1.87 – 1.73 (m, 3H), 1.68 – 1.61 (m, 1H), 1.61 – 1.51 (m, 3H), 1.51 – 1.46 (m, 1H), 1.45 (s, 3H), 1.40 – 1.33 (m, 1H), 1.12 (td, *J* = 14.2, 4.6 Hz, 1H), 1.08 (s, 3H), 1.07 – 1.01 (m, 7H), 0.94 (d, *J* = 7.1 Hz, 3H), 0.73 (d, *J* = 6.9 Hz, 3H); $^{13}$C NMR (126 MHz, $CDCl_3$) δ 217.0, 169.1, 72.1, 69.7, 58.4, 52.4, 47.6, 47.1, 45.6, 42.8, 41.9, 41.0, 40.5, 36.9, 34.8, 34.7, 34.6, 30.4, 30.1, 27.0, 25.2, 18.2, 17.0, 15.1, 11.7, 11.1; HR-MS (ESI) calcd for $C_{28}H_{49}N_4O_4S$ $[M+H]^+$ 537.3469, found 537.3467; $[\alpha]_D^{25}$ = -4.7 (c = 0.78, $CH_3OH$).

**General Method for Triazole Formation**: Following the conditions of Sharpless,[28] 20-azido-12-*epi*-pleuromutilin (**9**) or 20-azido-12-*epi*-tiamulin (**10**) (0.05–0.1 mmol, 1 equiv.), sodium ascorbate (0.25 equiv.), alkyne (1.1 equiv.), 10.8 mM $CuSO_4$ (5 mol %), and *t*-BuOH (0.20-0.40 mL) were combined and heated to 70 °C (oil bath) for 3-18 h. After cooling, the mixture was diluted with EtOAc (10 mL), $H_2O$ (2 mL), and brine (1 mL). The layers were separated, and the aqueous was extracted with EtOAc (10 mL). The combined organic layers were washed with brine

(5 mL), dried over $Na_2SO_4$, and concentrated. The residue was purified using column chromatography ($SiO_2$) with the indicated mobile phase.

**(3a*R*,4*R*,5*R*,7*S*,8*S*,9*R*,9a*S*,12*R*)-8-hydroxy-7-(2-(4-(hydroxymethyl)-1*H*-1,2,3-triazol-1-yl)ethyl)-4,7,9,12-tetramethyl-3-oxodecahydro-4,9a-propanocyclopenta[8]annulen-5-yl 2-hydroxyacetate (11)**: Prepared from **9** according to the general method for triazole formation and purified using flash chromatography ($SiO_2$, 12% $CH_3OH/CH_2Cl_2$) to give **11** (25.9 mg, 77%) as a white glass: $^1$H NMR (500 MHz, $CD_3OD$) δ 7.92 (s, 1H), 5.69 (d, *J* = 8.3 Hz, 1H), 4.66 (s, 2H), 4.59 (ddd, *J* = 13.6, 10.1, 6.2 Hz, 1H), 4.50 (ddd, *J* = 13.6, 10.1, 5.6 Hz, 1H), 4.05 (d, *J* = 17.1 Hz, 1H), 3.98 (d, *J* = 17.1 Hz, 1H), 3.61 (d, *J* = 6.2 Hz, 1H), 2.39 – 2.25 (m, 3H), 2.21 – 2.02 (m, 3H), 1.92 – 1.78 (m, 2H), 1.73 (ddd, *J* = 13.2, 11.3, 8.8 Hz, 1H), 1.66 – 1.51 (m, 2H), 1.46 (ddd, *J* = 12.6, 9.7, 2.1 Hz, 1H), 1.41 (s, 3H), 1.40 – 1.34 (m, 1H), 1.16 (dd, *J* = 14.2, 4.6 Hz, 1H), 1.12 (s, 3H), 1.07 (d, *J* = 15.7 Hz, 1H), 0.96 (d, *J* = 7.1 Hz, 3H), 0.72 (d, *J* = 6.7 Hz, 3H); $^{13}$C NMR (126 MHz, $CD_3OD$) δ 219.4, 173.2, 149.0, 124.1, 72.4, 70.4, 61.8, 58.9, 56.5, 47.8, 46.7, 44.0, 43.6, 43.0, 41.5, 38.0, 36.6, 35.3, 31.6, 28.1, 25.9, 18.6, 17.1, 15.3, 11.6; HR-MS (ESI) calcd for $C_{25}H_{40}N_3O_6$ $[M+H]^+$ 478.2912, found 478.2906; $[\alpha]_D^{23}$ = -14 (c = 1.2, $CH_3OH$).

**(3a*R*,4*R*,5*R*,7*S*,8*S*,9*R*,9a*S*,12*R*)-8-hydroxy-7-(2-(4-(2-hydroxyethyl)-1*H*-1,2,3-triazol-1-yl)ethyl)-4,7,9,12-tetramethyl-3-oxodecahydro-4,9a-propanocyclopenta[8]annulen-5-yl 2-hydroxyacetate (12)**: Prepared from **9** according to the general method for triazole formation and purified using flash chromatography ($SiO_2$, 11% $CH_3OH/CH_2Cl_2$) to give **12** (25.2 mg, 74%) as a white glass: $^1$H NMR (500 MHz, $CD_3OD$) δ 7.79 (s, 1H), 5.68 (d, *J* = 8.3 Hz, 1H), 4.57 (ddd, *J* = 13.7, 9.8, 6.4 Hz, 1H), 4.47 (ddd, *J* = 13.7, 9.7, 5.6 Hz, 1H), 4.05 (d, *J* = 17.1 Hz, 1H), 3.98 (d, *J* = 17.1 Hz, 1H), 3.79 (t, *J* = 6.7 Hz, 2H), 3.59 (d, *J* = 6.2 Hz, 1H), 2.89 (t, *J* = 6.7 Hz, 2H), 2.38 – 2.25 (m, 3H), 2.20 – 2.10 (m, 2H), 2.03 (dd, *J* = 15.7, 8.4 Hz, 1H), 1.89 – 1.78 (m, 2H), 1.72 (ddd,

*J* = 13.2, 11.2, 8.8 Hz, 1H), 1.66 – 1.50 (m, 2H), 1.46 (ddd, *J* = 12.9, 9.8, 2.3 Hz, 1H), 1.40 (s, 3H), 1.39 – 1.34 (m, 1H), 1.16 (dd, *J* = 14.1, 4.6 Hz, 1H), 1.12 (s, 3H), 1.05 (d, *J* = 15.7 Hz, 1H), 0.96 (d, *J* = 7.1 Hz, 3H), 0.72 (d, *J* = 6.8 Hz, 3H); $^{13}$C NMR (126 MHz, $CD_3OD$) δ 219.4, 173.2, 146.5, 123.9, 72.3, 70.4, 62.1, 61.8, 58.9, 47.7, 46.7, 43.9, 43.6, 43.0, 41.5, 38.0, 36.6, 35.3, 31.6, 29.9, 28.1, 25.9, 18.6, 17.1, 15.3, 11.6; HR-MS (ESI) calcd for $C_{26}H_{42}N_3O_6$ $[M+H]^+$ 492.3068, found 492.3075; $[\alpha]_D^{23}$ = -15 (c = 1.2, $CH_3OH$).

**(3a*R*,4*R*,5*R*,7*S*,8*S*,9*R*,9a*S*,12*R*)-8-hydroxy-7-(2-(4-(3-hydroxypropyl)-1*H*-1,2,3-triazol-1-yl)ethyl)-4,7,9,12-tetramethyl-3-oxodecahydro-4,9a-propanocyclopenta[8]annulen-5-yl 2-hydroxyacetate (13)**: Prepared from **9** according to the general method for triazole formation and purified using flash chromatography ($SiO_2$, 10% $CH_3OH/CH_2Cl_2$) to give **13** (22.4 mg, 65%) as a white glass: $^1$H NMR (500 MHz, $CD_3OD$) δ 7.75 (s, 1H), 5.68 (d, *J* = 8.3 Hz, 1H), 4.58 (ddd, *J* = 13.9, 9.6, 6.6 Hz, 1H), 4.45 (ddd, *J* = 14.1, 9.7, 5.3 Hz, 1H), 4.05 (d, *J* = 17.1 Hz, 1H), 3.97 (d, *J* = 17.1 Hz, 1H), 3.66 (d, *J* = 6.2 Hz, 1H), 3.58 (t, *J* = 6.4 Hz, 2H), 2.79 – 2.72 (m, 2H), 2.39 – 2.25 (m, 3H), 2.21 – 2.07 (m, 2H), 1.97 (dd, *J* = 15.8, 8.3 Hz, 1H), 1.91 – 1.79 (m, 4H), 1.74 (ddd, *J* = 13.4, 11.2, 8.8 Hz, 1H), 1.66 – 1.43 (m, 3H), 1.38 (s, 3H), 1.37 – 1.32 (m, 1H), 1.19 – 1.12 (m, 1H), 1.11 (s, 3H), 1.03 (d, *J* = 15.7 Hz, 1H), 0.96 (d, *J* = 7.1 Hz, 3H), 0.71 (d, *J* = 6.8 Hz, 3H); $^{13}$C NMR (126 MHz, $CD_3OD$) δ 219.4, 173.2, 149.0, 123.2, 72.4, 70.4, 62.0, 61.8, 58.9, 47.7, 46.7, 44.0, 43.6, 43.0, 41.6, 38.0, 36.6, 35.3, 33.3, 31.6, 28.1, 25.9, 22.7, 18.6, 17.1, 15.3, 11.6; HR-MS (ESI) calcd for $C_{27}H_{44}N_3O_6$ $[M+H]^+$ 506.3230, found 506.3225; $[\alpha]_D^{24}$ = -12 (c = 1.1, $CH_3OH$).

**(3a*R*,4*R*,5*R*,7*S*,8*S*,9*R*,9a*S*,12*R*)-8-hydroxy-7-(2-(4-(2-hydroxypropan-2-yl)-1*H*-1,2,3-triazol-1-yl)ethyl)-4,7,9,12-tetramethyl-3-oxodecahydro-4,9a-propanocyclopenta[8]annulen-5-yl 2-hydroxyacetate (14)**: Prepared from **9** according to the general method for triazole formation and purified using flash chromatography ($SiO_2$, 7% $CH_3OH/CH_2Cl_2$) to give **14** (26.2 mg, 75%) as a

white glass: $^{1}$H NMR (500 MHz, $CDCl_3$) δ 7.49 (s, 1H), 5.64 (d, *J* = 8.3 Hz, 1H), 4.50 – 4.39 (m, 2H), 4.09 (d, *J* = 17.1 Hz, 1H), 4.02 (d, *J* = 17.1 Hz, 1H), 3.58 (d, *J* = 6.1 Hz, 1H), 2.77 (br s, 4H), 2.34 (p, *J* = 7.2 Hz, 1H), 2.29 – 2.23 (m, 1H), 2.18 (q, *J* = 9.6 Hz, 1H), 2.14 – 2.07 (m, 1H), 2.06 (s, 1H), 2.00 (dd, *J* = 15.6, 8.4 Hz, 1H), 1.84 (ddd, *J* = 13.8, 9.6, 6.6 Hz, 1H), 1.76 (dq, *J* = 14.6, 3.1 Hz, 1H), 1.67 – 1.62 (m, 1H), 1.60 (s, 3H), 1.59 (s, 3H), 1.53 – 1.42 (m, 2H), 1.40 – 1.34 (m, 1H), 1.38 (s, 3H), 1.16 – 1.08 (m, 1H), 1.14 (s, 3H), 1.03 (d, *J* = 15.6 Hz, 1H), 0.96 (d, *J* = 7.0 Hz, 3H), 0.67 (d, *J* = 7.0 Hz, 3H); $^{13}$C NMR (126 MHz, $CDCl_3$) δ 217.1, 172.3, 155.9, 119.6, 71.9, 70.1, 68.5, 61.4, 58.0, 53.6, 46.8, 45.5, 42.9, 42.8, 41.9, 40.7, 36.7, 35.1, 34.6, 30.5, 27.0, 25.1, 18.0, 16.8, 15.0, 11.3; HR-MS (ESI) calcd for $C_{27}H_{44}N_3O_6$ $[M+H]^+$ 506.3230 found 506.3225; $[\alpha]_D^{25}$ = -10 (c = 1.3, $CH_3OH$).

**(3a*R*,4*R*,5*R*,7*S*,8*S*,9*R*,9a*S*,12*R*)-7-(2-(4-(aminomethyl)-1*H*-1,2,3-triazol-1-yl)ethyl)-8-hydroxy-4,7,9,12-tetramethyl-3-oxodecahydro-4,9a-propanocyclopenta[8]annulen-5-yl 2-hydroxyacetate (15)**: Prepared from **9** according to the general method for triazole formation and purified using flash chromatography ($SiO_2$, 16% (10:1 MeOH:$NH_4OH$)/$CH_2Cl_2$) to give **15** (21.1 mg, 52%) as a faintly yellow glass: $^{1}$H NMR (500 MHz, $CD_3OD$) δ 7.86 (s, 1H), 5.69 (d, *J* = 8.3 Hz, 1H), 4.58 (ddd, *J* = 13.6, 10.0, 6.2 Hz, 1H), 4.50 (ddd, *J* = 13.7, 10.0, 5.7 Hz, 1H), 4.05 (d, *J* = 17.1 Hz, 1H), 3.98 (d, *J* = 17.1 Hz, 1H), 3.89 (s, 2H), 3.60 (d, *J* = 6.2 Hz, 1H), 2.39 – 2.26 (m, 3H), 2.20 – 2.11 (m, 2H), 2.08 (dd, *J* = 15.7, 8.4 Hz, 1H), 1.89 – 1.79 (m, 2H), 1.72 (ddd, *J* = 13.1, 11.2, 8.9 Hz, 1H), 1.67 – 1.51 (m, 2H), 1.47 (ddd, *J* = 13.2, 9.7, 2.2 Hz, 1H), 1.41 (s, 3H), 1.40 – 1.34 (m, 1H), 1.19 – 1.14 (m, 1H), 1.12 (s, 3H), 1.06 (d, *J* = 15.6 Hz, 1H), 0.96 (d, *J* = 7.1 Hz, 3H), 0.72 (d, *J* = 6.9 Hz, 3H); $^{13}$C NMR (126 MHz, $CD_3OD$) δ 219.4, 173.2, 149.5, 123.3, 72.4, 70.4, 61.8, 58.9, 47.8, 46.7, 44.0, 43.6, 43.0, 41.6, 38.1, 37.4, 36.6, 35.3, 31.6, 28.1, 25.9, 18.6,

17.1, 15.3, 11.6; HR-MS (ESI) calcd for $C_{25}H_{41}N_4O_5$ $[M+H]^+$ 477.3071, found 477.3072; $[\alpha]_D^{24}$ = -16 (c = 0.97, $CH_3OH$).

**(3a*R*,4*R*,5*R*,7*S*,8*S*,9*R*,9a*S*,12*R*)-7-(2-(4-(2-aminoethyl)-1*H*-1,2,3-triazol-1-yl)ethyl)-8-hydroxy-4,7,9,12-tetramethyl-3-oxodecahydro-4,9a-propanocyclopenta[8]annulen-5-yl 2-hydroxyacetate (16)**: Prepared from **9** according to the general method for triazole formation and purified using flash chromatography ($SiO_2$, 18% (10:1 MeOH:$NH_4OH$)/$CH_2Cl_2$) to give **16** (13.6 mg, 39%) as a faintly yellow, glass: $^1$H NMR (500 MHz, $CD_3OD$) δ 7.81 (s, 1H), 5.68 (d, *J* = 8.3 Hz, 1H), 4.59 (ddd, *J* = 13.7, 9.6, 6.6 Hz, 1H), 4.47 (ddd, *J* = 13.7, 9.7, 5.5 Hz, 1H), 4.04 (d, *J* = 17.0 Hz, 1H), 3.98 (d, *J* = 17.1 Hz, 1H), 3.63 (d, *J* = 6.2 Hz, 1H), 2.98 (t, *J* = 7.1 Hz, 2H), 2.87 (t, *J* = 7.1 Hz, 2H), 2.38 – 2.24 (m, 3H), 2.20 – 2.10 (m, 2H), 1.99 (dd, *J* = 15.7, 8.4 Hz, 1H), 1.84 (dddd, *J* = 23.5, 14.2, 6.7, 2.0 Hz, 2H), 1.73 (ddd, *J* = 13.1, 11.1, 8.8 Hz, 1H), 1.66 – 1.51 (m, 2H), 1.47 (ddd, *J* = 12.7, 9.5, 2.3 Hz, 1H), 1.39 (s, 3H), 1.38-1.34 (m, 1H), 1.19-1.12 (m, 1H), 1.12 (s, 3H), 1.03 (d, *J* = 15.6 Hz, 1H), 0.96 (d, *J* = 7.1 Hz, 3H), 0.72 (d, *J* = 6.8 Hz, 3H); $^{13}$C NMR (126 MHz, $CD_3OD$) δ 219.4, 173.2, 146.5, 123.7, 72.3, 70.4, 61.8, 58.9, 47.8, 46.7, 43.9, 43.6, 43.0, 41.9, 41.6, 38.0, 36.6, 35.3, 31.6, 28.7, 28.1, 25.9, 18.6, 17.1, 15.3, 11.6; HR-MS (ESI) calcd for $C_{26}H_{43}N_4O_5$ $[M+H]^+$ 491.3228, found 491.3246; $[\alpha]_D^{24}$ = -10 (c = 0.72, $CH_3OH$).

**(3a*R*,4*R*,5*R*,7*S*,8*S*,9*R*,9a*S*,12*R*)-7-(2-(4-hexyl-1*H*-1,2,3-triazol-1-yl)ethyl)-8-hydroxy-4,7,9,12-tetramethyl-3-oxodecahydro-4,9a-propanocyclopenta[8]annulen-5-yl 2-hydroxyacetate (17)**: Prepared from **9** according to the general method for triazole formation and purified using flash chromatography ($SiO_2$, 70% EtOAC/$CH_2Cl_2$) to give **17** (24.7 mg, 67%) as a white glass: $^1$H NMR (500 MHz, $CDCl_3$) δ 7.27 (s, 1H), 5.65 (d, *J* = 8.4 Hz, 1H), 4.51 – 4.39 (m, 2H), 4.08 (d, *J* = 17.1 Hz, 1H), 4.01 (d, *J* = 17.0 Hz, 1H), 3.61 (d, *J* = 6.2 Hz, 1H), 2.66 (t, *J* = 7.7 Hz, 2H), 2.34 (p, *J* = 6.9 Hz, 1H), 2.30 – 2.08 (m, 4H), 2.05 (d, *J* = 2.6 Hz, 1H), 2.00 (dd, *J* = 15.7,

8.5 Hz, 1H), 1.84 (ddd, *J* = 13.8, 9.6, 6.5 Hz, 1H), 1.76 (dq, *J* = 14.5, 3.1 Hz, 1H), 1.68 – 1.57 (m, 4H), 1.56 – 1.41 (m, 2H), 1.38 (s, 3H), 1.36 – 1.23 (m, 7H), 1.14 (s, 3H), 1.10 (dd, *J* = 14.0, 4.2 Hz, 1H), 1.02 (d, *J* = 15.6 Hz, 1H), 0.97 (d, *J* = 7.0 Hz, 3H), 0.87 (t, *J* = 6.8 Hz, 3H), 0.67 (d, *J* = 7.0 Hz, 3H); $^{13}$C NMR (126 MHz, $CDCl_3$) δ 216.9, 172.3, 148.7, 120.7, 71.7, 70.2, 61.4, 58.0, 46.6, 45.5, 42.9, 42.8, 41.9, 40.8, 36.7, 35.1, 34.6, 31.7, 30.5, 29.5, 29.0, 27.0, 25.7, 25.1, 22.7, 18.0, 16.8, 14.9, 14.2, 11.3; HR-MS (ESI) calcd for $C_{30}H_{50}N_3O_5$ $[M+H]^+$ 532.3744, found 532.3748; $[\alpha]_D^{25}$ = -8.5 (c = 1.3, $CH_3OH$).

**(3a*R*,4*R*,5*R*,7*S*,8*S*,9*R*,9a*S*,12*R*)-7-(2-(4-((benzyloxy)methyl)-1*H*-1,2,3-triazol-1-yl)ethyl)-8-hydroxy-4,7,9,12-tetramethyl-3-oxodecahydro-4,9a-propanocyclopenta[8]annulen-5-yl 2-hydroxyacetate (18)**: Prepared from **9** according to the general method for triazole formation and purified using flash chromatography ($SiO_2$, 70% EtOAC/$CH_2Cl_2$) to give **18** (31.1 mg, 80%) as a white glass: $^1$H NMR (500 MHz, $CDCl_3$) δ 7.55 (s, 1H), 7.36 – 7.32 (m, 4H), 7.32 – 7.27 (m, 1H), 5.65 (d, *J* = 8.4 Hz, 1H), 4.65 (d, *J* = 1.7 Hz, 2H), 4.58 (d, *J* = 1.3 Hz, 2H), 4.54 – 4.36 (m, 2H), 4.08 (d, *J* = 17.1 Hz, 1H), 4.01 (d, *J* = 17.1 Hz, 1H), 3.55 – 3.51 (m, 1H), 2.38 – 2.24 (m, 2H), 2.22 – 2.10 (m, 3H), 2.07 – 2.01 (m, 3H), 1.90 – 1.79 (m, 1H), 1.76 (dq, *J* = 14.6, 3.1 Hz, 1H), 1.70 – 1.62 (m, 1H), 1.62 – 1.43 (m, 2H), 1.42 – 1.35 (m, 1H), 1.40 (s, 3H), 1.15 (s, 3H), 1.11 (dd, *J* = 14.3, 4.4 Hz, 1H), 1.05 (d, *J* = 15.7 Hz, 1H), 0.95 (d, *J* = 7.0 Hz, 3H), 0.68 (d, *J* = 7.0 Hz, 3H); $^{13}$C NMR (126 MHz, $CDCl_3$) δ 216.6, 172.2, 145.3, 137.7, 128.5, 127.93, 127.88, 122.6, 72.7, 71.9, 70.0, 63.6, 61.3, 57.9, 46.7, 45.3, 42.8, 42.7, 41.8, 40.6, 36.5, 34.9, 34.4, 30.3, 26.9, 25.0, 17.8, 16.7, 14.8, 11.0; HR-MS (ESI) calcd for $C_{32}H_{46}N_3O_6$ $[M+H]^+$ 568.3381, found 568.3392; $[\alpha]_D^{25}$ = -13.0 (c = 0.82, $CH_3OH$).

**(3a*R*,4*R*,5*R*,7*S*,8*S*,9*R*,9a*S*,12*R*)-8-hydroxy-7-(2-(4-(hydroxymethyl)-1*H*-1,2,3-triazol-1-yl)ethyl)-4,7,9,12-tetramethyl-3-oxodecahydro-4,9a-propanocyclopenta[8]annulen-5-yl 2-((2-(diethylamino)ethyl)thio)acetate (19)**: Prepared from **10** according to the general method for triazole formation and purified using flash chromatography ($SiO_2$, 9.5% (10:1 MeOH:$NH_4OH$)/$CH_2Cl_2$) to give **19** (23.8 mg, 95%) as a clear, colorless oil: $^1$H NMR (500 MHz, $CDCl_3$) δ 7.60 (s, 1H), 5.56 (d, *J* = 8.3 Hz, 1H), 4.70 (s, 2H), 4.52 – 4.38 (m, 2H), 3.59 (t, *J* = 6.3 Hz, 1H), 3.17 (s, 2H), 2.96 (dd, *J* = 6.5, 3.0 Hz, 1H), 2.73 (s, 4H), 2.59 (q, *J* = 7.1 Hz, 4H), 2.36 – 2.06 (m, 6H), 2.02 – 1.95 (m, 1H), 1.88 – 1.80 (m, 1H), 1.75 (dq, *J* = 14.5, 3.0 Hz, 1H), 1.68 – 1.58 (m, 2H), 1.53 (qd, *J* = 13.5, 3.3 Hz, 1H), 1.45 – 1.33 (m, 2H), 1.40 (s, 3H), 1.15 – 1.12 (m, 1H), 1.11 (s, 3H), 1.05 (t, *J* = 7.2 Hz, 6H), 0.95 (d, *J* = 7.0 Hz, 3H), 0.71 (d, *J* = 7.0 Hz, 3H); $^{13}$C NMR (126 MHz, $CDCl_3$) δ 217.3, 169.1, 148.2, 122.1, 71.9, 69.8, 58.1, 56.3, 52.3, 47.0, 46.8, 45.5, 42.9, 42.7, 41.9, 40.6, 36.9, 35.1, 34.6 (2C), 30.5, 29.9, 27.0, 25.1, 18.0, 17.0, 15.1, 11.5 (2C), 11.3; HR-MS (ESI) calcd for $C_{31}H_{53}N_4O_5S$ $[M+H]^+$ 593.3731, found 593.3741; $[\alpha]_D^{25}$ = -8.6 (c = 1.2, $CH_3OH$).

**(3a*R*,4*R*,5*R*,7*S*,8*S*,9*R*,9a*S*,12*R*)-8-hydroxy-7-(2-(4-(2-hydroxyethyl)-1*H*-1,2,3-triazol-1-yl)ethyl)-4,7,9,12-tetramethyl-3-oxodecahydro-4,9a-propanocyclopenta[8]annulen-5-yl 2-((2-(diethylamino)ethyl)thio)acetate (20)**: Prepared from **10** according to the general method for triazole formation and purified using flash chromatography ($SiO_2$, 9.5% (10:1 MeOH:$NH_4OH$)/$CH_2Cl_2$) to give **20** (23.9 mg, 87%) as a clear, colorless oil: $^1$H NMR (500 MHz, $CDCl_3$) δ 7.45 (s, 1H), 5.55 (d, *J* = 8.3 Hz, 1H), 4.53 – 4.41 (m, 2H), 3.89 (t, *J* = 5.9 Hz, 2H), 3.38 (t, *J* = 6.3 Hz, 1H), 3.17 (s, 2H), 3.06 (s, 1H), 2.92 (td, *J* = 5.7, 2.2 Hz, 2H), 2.74 – 2.68 (m, 4H), 2.57 (q, *J* = 7.2 Hz, 4H), 2.39 (d, *J* = 6.5 Hz, 1H), 2.36 – 2.26 (m, 2H), 2.22 – 2.13 (m, 2H), 2.08 – 2.00 (m, 2H), 1.83 – 1.77 (m, 1H), 1.74 (dd, *J* = 14.5, 3.1 Hz, 1H), 1.68 – 1.61 (m, 1H), 1.58 –

1.48 (m, 2H), 1.45 – 1.38 (m, 1H), 1.42 (s, 3H), 1.38 – 1.32 (m, 1H), 1.14 – 1.09 (m, 1H), 1.11 (s, 3H), 1.06 – 1.01 (m, 1H), 1.03 (t, *J* = 7.2 Hz, 6H), 0.92 (d, *J* = 7.1 Hz, 3H), 0.71 (d, *J* = 7.0 Hz, 3H); $^{13}$C NMR (126 MHz, $CDCl_3$) δ 216.8, 169.0, 145.7, 121.9, 71.5, 69.6, 61.5, 57.9, 52.3, 46.9, 46.5, 45.3, 42.5, 42.4, 41.7, 40.4, 36.7, 34.9, 34.5, 34.4, 30.4, 30.1, 28.8, 26.9, 25.0, 18.3, 16.9, 14.9, 11.6, 11.1; HR-MS (ESI) calcd for $C_{32}H_{55}N_4O_5S$ $[M+H]^+$ 607.3888, found 607.3883; $[\alpha]_D^{25}$ = -5.2 (c = 0.84, $CH_3OH$).

**(3a*R*,4*R*,5*R*,7*S*,8*S*,9*R*,9a*S*,12*R*)-8-hydroxy-7-(2-(4-(3-hydroxypropyl)-1*H*-1,2,3-triazol-1-yl)ethyl)-4,7,9,12-tetramethyl-3-oxodecahydro-4,9a-propanocyclopenta[8]annulen-5-yl 2-((2-(diethylamino)ethyl)thio)acetate (21)**: Prepared from **10** according to the general method for triazole formation and purified using flash chromatography ($SiO_2$, 9.5% (10:1 MeOH:$NH_4OH$)/$CH_2Cl_2$) to give **21** (26.2 mg, 93%) as a clear, colorless oil: $^1$H NMR (500 MHz, $CDCl_3$) δ 7.37 (s, 1H), 5.59 (d, *J* = 8.3 Hz, 1H), 4.51 – 4.42 (m, 2H), 3.68 (s, 1H), 3.62 (t, *J* = 6.3 Hz, 1H), 3.20 (s, 2H), 2.82 (t, *J* = 7.2 Hz, 2H), 2.74 (s, 4H), 2.61 – 2.56 (m, 4H), 2.38 (t, *J* = 6.8 Hz, 1H), 2.29 (d, *J* = 10.6 Hz, 1H), 2.22 (t, *J* = 9.4 Hz, 1H), 2.19 – 2.11 (m, 1H), 2.08 (s, 1H), 2.01 (dd, *J* = 15.8, 8.5 Hz, 1H), 1.95 – 1.85 (m, 3H), 1.78 (dq, *J* = 14.4, 3.1 Hz, 1H), 1.70 – 1.61 (m, 2H), 1.55 (dd, *J* = 13.5, 3.3 Hz, 1H), 1.51 – 1.35 (m, 3H), 1.43 (s, 3H), 1.18 – 1.13 (m, 1H), 1.15 (s, 3H), 1.10 – 1.03 (m, 8H), 0.98 (d, *J* = 7.0 Hz, 3H), 0.74 (d, *J* = 7.0 Hz, 3H); $^{13}$C NMR (126 MHz, $CDCl_3$) δ 216.9, 169.0, 147.7, 121.0, 71.8, 69.6, 61.7, 58.0, 52.3, 46.9, 46.5, 45.4, 42.8, 42.6, 41.7, 40.5, 36.7, 34.9, 34.5, 34.5, 31.9, 30.4, 30.1, 26.9, 25.0, 22.1, 18.0, 16.9, 14.9, 11.6, 11.1; HR-MS (ESI) calcd for $C_{33}H_{57}N_4O_5S$ $[M+H]^+$ 621.4044, found 621.4038; $[\alpha]_D^{25}$ = -11 (c = 1.0, $CH_3OH$).

**(3a*R*,4*R*,5*R*,7*S*,8*S*,9*R*,9a*S*,12*R*)-8-hydroxy-7-(2-(4-(2-hydroxypropan-2-yl)-1*H*-1,2,3-triazol-1-yl)ethyl)-4,7,9,12-tetramethyl-3-oxodecahydro-4,9a-propanocyclopenta[8]annulen-5-yl 2-**

**((2-(diethylamino)ethyl)thio)acetate (22)**: Prepared from **10** according to the general method for triazole formation and purified using flash chromatography ($SiO_2$, 7.5% (10:1 MeOH:$NH_4OH$)/$CH_2Cl_2$) to give **22** (23.7 mg, 84%) as a clear, colorless oil: $^1$H NMR (500 MHz, $CDCl_3$) δ 7.49 (s, 1H), 5.59 (d, *J* = 8.3 Hz, 1H), 4.47 (dq, *J* = 9.3, 6.9 Hz, 2H), 3.60 (t, *J* = 6.0 Hz, 1H), 3.20 (s, 2H), 2.78 – 2.68 (m, 4H), 2.62 (s, 1H), 2.58 (q, *J* = 7.2 Hz, 4H), 2.38 (p, *J* = 7.2 Hz, 1H), 2.34 – 2.26 (m, 1H), 2.23 – 2.11 (m, 2H), 2.07 (s, 1H), 2.06 – 1.99 (m, 1H), 1.87 (ddd, *J* = 13.8, 9.6, 6.6 Hz, 1H), 1.78 (dq, *J* = 15.1, 3.4 Hz, 1H), 1.69 – 1.58 (m, 3H), 1.63 (s, 3H), 1.62 (s, 3H), 1.58 – 1.53 (m, 1H), 1.52 – 1.46 (m, 1H), 1.44 (s, 3H), 1.42 – 1.35 (m, 1H), 1.17 – 1.13 (m, 1H), 1.15 (s, 3H), 1.08 (d, *J* = 16.0 Hz, 1H), 1.05 (t, *J* = 7.2 Hz, 6H), 0.97 (d, *J* = 7.0 Hz, 3H), 0.74 (d, *J* = 6.9 Hz, 3H); $^{13}$C NMR (126 MHz, $CDCl_3$) δ 216.9, 169.0, 155.9, 119.2, 71.8, 69.5, 68.4, 58.0, 52.3, 46.9, 46.5, 45.4, 42.8, 42.6, 41.7, 40.5, 36.7, 34.9, 34.54, 34.48, 30.5, 30.4, 30.1, 26.9, 25.0, 18.0, 16.9, 15.0, 11.7, 11.1; HR-MS (ESI) calcd for $C_{33}H_{57}N_4O_5S$ $[M+H]^+$ 621.4044, found 621.4048; $[\alpha]_D^{25}$ = -10 (c = 1.3, $CH_3OH$).

**(3a*R*,4*R*,5*R*,7*S*,8*S*,9*R*,9a*S*,12*R*)-7-(2-(4-(aminomethyl)-1*H*-1,2,3-triazol-1-yl)ethyl)-8-hydroxy-4,7,9,12-tetramethyl-3-oxodecahydro-4,9a-propanocyclopenta[8]annulen-5-yl 2-((2-(diethylamino)ethyl)thio)acetate (23)**: Prepared from **10** according to the general method for triazole formation and purified using flash chromatography ($SiO_2$, 10% (10:1 MeOH:$NH_4OH$)/$CH_2Cl_2$) to give **23** (11.1 mg, 42%) as a clear, yellowish glass: $^1$H NMR (500 MHz, $CDCl_3$) δ 7.51 (s, 1H), 5.57 (d, *J* = 8.3 Hz, 1H), 4.46 (t, *J* = 8.6 Hz, 2H), 3.97 (s, 1H), 3.54 (d, *J* = 6.1 Hz, 1H), 3.18 (s, 2H), 2.75 – 2.69 (m, 4H), 2.56 (q, *J* = 7.2 Hz, 4H), 2.36 – 2.11 (m, 9H), 2.07 – 2.00 (m, 2H), 1.88 – 1.82 (m, 1H), 1.79 – 1.73 (m, 1H), 1.66 – 1.60 (m, 1H), 1.56 (q, *J* = 13.0 Hz, 2H), 1.42 (s, 3H), 1.39 – 1.33 (m, 1H), 1.14 – 1.08 (m, 1H), 1.12 (s, 3H), 1.03 (t, *J* = 7.1 Hz, 6H), 0.94 (d, *J* = 7.0 Hz, 3H), 0.72 (d, *J* = 7.0 Hz, 3H); $^{13}$C NMR (126 MHz, $CDCl_3$) δ

216.9, 169.2, 149.1, 121.1, 72.0, 69.6, 58.2, 52.4, 47.1 (2C), 46.7, 45.5, 42.9, 42.8, 41.9, 40.6, 36.8, 35.0, 34.7, 34.6, 30.5, 30.3, 27.0, 25.2, 18.1, 17.0, 15.1, 11.8, 11.2; HR-MS (ESI) calcd for $C_{31}H_{54}N_5O_4S$ $[M+H]^+$ 592.3891, found 592.3892, $[\alpha]_D^{25}$ = -13.8 (c = 0.555, $CH_3OH$).

**(3a*R*,4*R*,5*R*,7*S*,8*S*,9*R*,9a*S*,12*R*)-7-(2-(4-(2-aminoethyl)-1*H*-1,2,3-triazol-1-yl)ethyl)-8-hydroxy-4,7,9,12-tetramethyl-3-oxodecahydro-4,9a-propanocyclopenta[8]annulen-5-yl 2-((2-(diethylamino)ethyl)thio)acetate (24)**: Prepared from **10** according to the general method for triazole formation and purified using flash chromatography ($SiO_2$, 12% (10:1 MeOH:$NH_4OH$)/$CH_2Cl_2$) to give **24** (14.4 mg, 53%) as a clear, yellowish oil: $^1$H NMR (500 MHz, $CDCl_3$) δ 7.49 (s, 1H), 5.59 (d, *J* = 8.3 Hz, 1H), 4.62 (dt, *J* = 15.2, 7.9 Hz, 1H), 4.46 – 4.38 (m, 1H), 3.20 (s, 2H), 3.06 (br s, 1H), 3.03 (d, *J* = 6.2 Hz, 1H), 2.94 – 2.88 (m, 1H), 2.86 – 2.80 (m, 1H), 2.76 – 2.69 (m, 4H), 2.57 (q, *J* = 7.2 Hz, 4H), 2.40 – 2.22 (m, 7H), 2.20 – 2.11 (m, 2H), 2.09 (s, 1H), 1.77 – 1.64 (m, 3H), 1.59 – 1.50 (m, 1H), 1.48 – 1.43 (m, 1H), 1.47 (s, 3H), 1.40 – 1.32 (m, 2H), 1.15 – 1.09 (1, 4H) 1.12 (s, 3H), 1.08 – 1.01 (m, 1H), 1.04 (t, *J* = 7.11 Hz, 6H), 0.87 (d, *J* = 7.0 Hz, 3H), 0.74 (d, *J* = 7.1 Hz, 3H); $^{13}$C NMR (126 MHz, $CDCl_3$) δ 216.8, 169.1, 145.7, 122.2, 70.5, 69.6, 57.8, 52.3, 47.0, 46.4, 45.3, 42.2, 42.0, 41.7, 41.3, 40.4, 36.6, 35.0, 34.5, 34.3, 30.5, 30.2, 28.4, 26.9, 24.8, 18.8, 16.9, 15.0, 11.8, 11.2; HR-MS (ESI) calcd for $C_{32}H_{56}N_5O_4S$ $[M+H]^+$ 606.4048, found 606.4042; $[\alpha]_D^{25}$ = -12.6 (c = 0.715, $CH_3OH$).

**(3a*R*,4*R*,5*R*,7*S*,8*S*,9*R*,9a*S*,12*R*)-7-(2-(4-hexyl-1*H*-1,2,3-triazol-1-yl)ethyl)-8-hydroxy-4,7,9,12-tetramethyl-3-oxodecahydro-4,9a-propanocyclopenta[8]annulen-5-yl 2-((2-(diethylamino)ethyl)thio)acetate (25)**: Prepared from **10** according to the general method for triazole formation and purified using flash chromatography ($SiO_2$, 5% (10:1 MeOH:$NH_4OH$)/$CH_2Cl_2$) to give **25** (19.9 mg, 68%) as a clear, colorless oil: $^1$H NMR (500 MHz, $CDCl_3$) δ 7.27 (s, 1H), 5.57 (d, *J* = 8.2 Hz, 1H), 4.44 (ddd, *J* = 9.5, 6.5, 2.9 Hz, 2H), 3.57 (t, *J* =

6.3 Hz, 1H), 3.17 (s, 2H), 2.74 – 2.68 (m, 4H), 2.66 (t, *J* = 7.0 Hz, 2H), 2.55 (q, *J* = 7.2 Hz, 4H), 2.36 (p, *J* = 7.1 Hz, 1H), 2.31 (dd, *J* = 6.4, 1.6 Hz, 1H), 2.29 – 2.23 (m, 1H), 2.22 – 2.10 (m, 2H), 2.06 – 2.00 (m, 2H), 1.85 (ddd, *J* = 13.8, 9.2, 6.9 Hz, 1H), 1.76 (dq, *J* = 14.5, 3.1 Hz, 1H), 1.67 – 1.57 (m, 4H), 1.56 – 1.49 (m, 1H), 1.48 – 1.42 (m, 1H), 1.41 (s, 3H), 1.39 – 1.25 (m, 7H), 1.16 – 1.10 (m, 1H), 1.13 (s, 3H), 1.07 (d, *J* = 15.5 Hz, 1H), 1.03 (t, *J* = 7.1 Hz, 6H), 0.95 (d, *J* = 7.1 Hz, 3H), 0.89 – 0.84 (m, 3H), 0.72 (d, *J* = 7.0 Hz, 3H); $^{13}$C NMR (126 MHz, $CDCl_3$) δ 216.9, 169.2, 148.8, 120.6, 71.9, 69.6, 58.2, 52.4, 47.1, 46.5, 45.5, 42.9, 42.8, 41.8, 40.6, 36.8, 35.0, 34.7, 34.6, 31.7, 30.5, 30.3, 29.6, 29.1, 27.0, 25.8, 25.1, 22.7, 18.1, 17.0, 15.1, 14.2, 11.8, 11.2; HR-MS (ESI) calcd for $C_{36}H_{63}N_4O_4S$ $[M+H]^+$ 647.4564, found 647.4556; $[\alpha]_D^{25}$ = -14.5 (c = 0.965, $CH_3OH$).

**(3a*R*,4*R*,5*R*,7*S*,8*S*,9*R*,9a*S*,12*R*)-7-(2-(4-((benzyloxy)methyl)-1*H*-1,2,3-triazol-1-yl)ethyl)-8-hydroxy-4,7,9,12-tetramethyl-3-oxodecahydro-4,9a-propanocyclopenta[8]annulen-5-yl 2-((2-(diethylamino)ethyl)thio)acetate (26)**: Prepared from **10** according to the general method for triazole formation and purified using flash chromatography ($SiO_2$, 5% (10:1 MeOH:$NH_4OH$)/$CH_2Cl_2$) to give **26** (22.4 mg, 75%) as a clear, colorless oil: $^1$H NMR (500 MHz, $CDCl_3$) δ 7.48 (s, 1H), 7.27 – 7.26 (m, 4H), 7.24 – 7.19 (m, 1H), 5.50 (d, *J* = 8.3 Hz, 1H), 4.58 (s, 2H), 4.51 (s, 2H), 4.44 – 4.37 (m, 2H), 3.44 (t, *J* = 6.2 Hz, 1H), 3.10 (s, 2H), 2.68 – 2.60 (m, 4H), 2.48 (q, *J* = 7.1 Hz, 4H), 2.28 (p, *J* = 6.9 Hz, 1H), 2.25 – 2.16 (m, 1H), 2.12 (t, *J* = 9.5 Hz, 1H), 2.09 – 1.94 (m, 4H), 1.82 – 1.75 (m, 1H), 1.68 (dq, *J* = 14.5, 3.1 Hz, 1H), 1.60 – 1.55 (m, 1H), 1.53 – 1.40 (m, 2H), 1.39 – 1.34 (m, 1H), 1.35 (s, 3H), 1.32 – 1.26 (m, 1H), 1.08 – 0.99 (m, 2H), 1.06 (s, 3H), 0.95 (t, *J* = 7.2 Hz, 6H), 0.86 (d, *J* = 7.1 Hz, 3H), 0.65 (d, *J* = 7.0 Hz, 3H); $^{13}$C NMR (126 MHz, $CDCl_3$) δ 216.8, 169.2, 145.5, 137.9, 128.6, 128.0, 127.9, 122.6, 72.7, 72.2, 69.6, 63.8, 58.1, 52.4, 47.1, 46.7, 45.5, 42.95, 42.86, 41.8, 40.6, 36.8, 35.0, 34.6, 34.5, 30.5, 30.3, 27.0, 25.2,

18.0, 17.0, 15.1, 11.8, 11.1; HR-MS (ESI) calcd for $C_{38}H_{59}N_4O_5S$ $[M+H]^+$ 683.4201, found 683.4217; $[\alpha]_D^{25}$ = -14.2 (c = 1.10, $CH_3OH$).

**(3a*R*,4*R*,5*R*,7*S*,8*S*,9*R*,9a*S*,12*R*)-8-hydroxy-4,7,9,12-tetramethyl-3-oxo-7-(2-(4-phenyl-1*H*-1,2,3-triazol-1-yl)ethyl)decahydro-4,9a-propanocyclopenta[8]annulen-5-yl 2-hydroxyacetate (27)**: Prepared from **9** according to the general method for triazole formation and purified using automated flash chromatography (Teledyne RediSepRf gold 4g $SiO_2$ column, 25 then 47% EtOAC/$CH_2Cl_2$) to give **27** (17.3 mg, 74%) as a colorless glass: $^1$H NMR (500 MHz, $CDCl_3$) δ 7.79 – 7.76 (m, 2H), 7.75 (s, 1H), 7.44 – 7.37 (m, 2H), 7.35 – 7.30 (m, 1H), 5.66 (d, *J* = 8.4 Hz, 1H), 4.63 – 4.42 (m, 2H), 4.09 (d, *J* = 17.1 Hz, 1H), 4.02 (d, *J* = 17.1 Hz, 1H), 3.59 (d, *J* = 6.2 Hz, 1H), 2.53 (s, 1H), 2.36 (p, *J* = 6.9 Hz, 1H), 2.30 – 2.16 (m, 3H), 2.09 – 2.03 (m, 2H), 1.90 (ddd, *J* = 13.9, 9.7, 6.2 Hz, 1H), 1.76 (dq, *J* = 14.6, 3.2 Hz, 1H), 1.69 – 1.62 (m, 1H), 1.62 – 1.55 (m, 1H), 1.54 – 1.49 (m, 1H), 1.48 – 1.44 (m, 1H), 1.43 – 1.35 (m, 1H), 1.40 (s, 3H), 1.18 (s, 3H), 1.16 – 1.09 (m, 1H), 1.06 (d, *J* = 15.6 Hz, 1H), 0.97 (d, *J* = 7.1 Hz, 3H), 0.68 (d, *J* = 7.2 Hz, 3H); $^{13}$C NMR (126 MHz, $CDCl_3$) δ 216.7, 172.3, 148.1, 130.5, 129.0, 128.4, 125.8, 119.7, 71.9, 70.2, 61.5, 58.0, 46.9, 45.5, 42.9, 42.8, 42.0, 40.8, 36.6, 35.1, 34.5, 30.5, 27.0, 25.1, 18.0, 16.8, 14.9, 11.2; HR-MS (ESI) calcd for $C_{30}H_{42}N_3O_5$ $[M+H]^+$ 524.3118, found 524.3121; $[\alpha]_D^{24}$ = -16.8 (c = 0.870, $CH_3OH$).

**(3a*R*,4*R*,5*R*,7*S*,8*S*,9*R*,9a*S*,12*R*)-7-(2-(4-benzyl-1*H*-1,2,3-triazol-1-yl)ethyl)-8-hydroxy-4,7,9,12-tetramethyl-3-oxodecahydro-4,9a-propanocyclopenta[8]annulen-5-yl 2-hydroxyacetate (28)**: Prepared from **9** according to the general method for triazole formation and purified using automated flash chromatography (Teledyne RediSepRf gold 4g $SiO_2$ column, 38 then 54% EtOAC/$CH_2Cl_2$) to give **28** (16.4 mg, 67%) as a colorless glass: $^1$H NMR (500 MHz, $CDCl_3$) δ 7.31 – 7.26 (m, 2H), 7.24 – 7.20 (m, 3H), 7.16 (s, 1H), 5.63 (d, *J* = 8.4 Hz, 1H), 4.46 –

4.36 (m, 2H), 4.07 (d, *J* = 17.1 Hz, 1H), 4.04 (s, 2H), 4.01 (d, *J* = 17.1 Hz, 1H), 3.50 (d, *J* = 6.2 Hz, 1H), 2.35 – 2.30 (m, 1H), 2.29 – 2.22 (m, 1H), 2.21 – 2.16 (m, 1H), 2.15 – 2.07 (m, 2H), 2.05 – 1.98 (m, 2H), 1.85 – 1.78 (m, 1H), 1.75 (dq, *J* = 14.5, 3.2 Hz, 1H), 1.69 – 1.60 (m, 1H), 1.57 – 1.46 (m, 2H), 1.46 – 1.33 (m, 2H), 1.38 (s, 3H), 1.14 – 1.08 (m, 1H), 1.12 (s, 3H), 1.01 (d, *J* = 15.7 Hz, 1H), 0.93 (d, *J* = 7.1 Hz, 3H), 0.67 (d, *J* = 7.1 Hz, 3H); $^{13}$C NMR (126 MHz, $CDCl_3$) δ 216.7, 172.3, 148.0, 139.1, 128.8 (2C), 126.7, 121.5, 77.4, 71.9, 70.2, 61.4, 58.0, 46.6, 45.4, 42.7, 41.9, 40.7, 36.6, 35.0, 34.5, 32.4, 30.5, 27.0, 25.1, 18.0, 16.8, 14.9, 11.2; HR-MS (ESI) calcd for $C_{31}H_{44}N_3O_5$ $[M+H]^+$ 538.3275, found 538.3281; $[\alpha]_D^{23}$ = -3.65 (c = 0.855, $CH_3OH$).

**(3a*R*,4*R*,5*R*,7*S*,8*S*,9*R*,9a*S*,12*R*)-8-hydroxy-4,7,9,12-tetramethyl-3-oxo-7-(2-(4-(phenoxymethyl)-1*H*-1,2,3-triazol-1-yl)ethyl)decahydro-4,9a-propanocyclopenta[8]annulen-5-yl 2-hydroxyacetate (29)**: Prepared from **9** according to the general method for triazole formation and purified using automated flash chromatography (Teledyne RediSepRf gold 4g $SiO_2$ column, 38 then 58% EtOAC/$CH_2Cl_2$) to give **29** (20.3 mg, 80%) as a colorless glass: $^1$H NMR (500 MHz, $CDCl_3$) δ 7.64 (s, 1H), 7.35 – 7.29 (m, 2H), 7.02 – 6.96 (m, 3H), 5.67 (d, *J* = 8.4 Hz, 1H), 5.20 (s, 2H), 4.60 – 4.46 (m, 2H), 4.11 (d, *J* = 17.1 Hz, 1H), 4.05 (d, *J* = 17.1 Hz, 1H), 3.54 (d, *J* = 6.2 Hz, 1H), 2.40 – 2.33 (m, 1H), 2.33 – 2.27 (m, 1H), 2.24 – 2.04 (m, 5H), 1.93 – 1.85 (m, 1H), 1.78 (dq, *J* = 14.5, 3.1 Hz, 1H), 1.72 – 1.65 (m, 1H), 1.63 – 1.38 (m, 5H), 1.43 (s, 3H), 1.18 (s, 3H), 1.17 – 1.10 (m, 1H), 1.08 (d, *J* = 15.6 Hz, 1H), 0.97 (d, *J* = 7.0 Hz, 3H), 0.71 (d, *J* = 7.0 Hz, 3H); $^{13}$C NMR (126 MHz, $CDCl_3$) δ 216.5, 172.2, 158.1, 144.5, 129.6, 122.7, 121.3, 114.7, 77.2, 71.9, 70.0, 61.9, 61.3, 57.9, 46.7, 45.3, 42.7, 41.8, 40.6, 36.5, 34.9, 34.4, 30.3, 26.9, 25.0, 17.8, 16.7, 14.8, 11.0; HR-MS (ESI) calcd for $C_{31}H_{44}N_3O_6$ $[M+H]^+$ 554.3224, found 554.3228; $[\alpha]_D^{23}$ = -8.28 (c = 1.07, $CH_3OH$).

**(3a*R*,4*R*,5*R*,7*S*,8*S*,9*R*,9a*S*,12*R*)-7-(2-(4-([1,1'-biphenyl]-4-yl)-1*H*-1,2,3-triazol-1-yl)ethyl)-8-hydroxy-4,7,9,12-tetramethyl-3-oxodecahydro-4,9a-propanocyclopenta[8]annulen-5-yl 2-hydroxyacetate (30)**: Prepared from **9** according to the general method for triazole formation and purified using flash chromatography ($SiO_2$, 70% EtOAC/hexane) to give **30** (13.1 mg, 46%) as an amorphous, white solid: $^1$H NMR (500 MHz, $CDCl_3$) δ 7.86 (dt, *J* = 8.2, 2.2 Hz, 2H), 7.80 (s, 1H), 7.65 (dt, *J* = 8.2, 2.2 Hz, 2H), 7.63 – 7.60 (m, 2H), 7.45 (dt, *J* = 7.5, 1.3 Hz, 2H), 7.36 (dt, *J* = 7.5, 1.3 Hz, 1H), 5.67 (d, *J* = 8.4 Hz, 1H), 4.64 – 4.48 (m, 2H), 4.10 (d, *J* = 17.2 Hz, 1H), 4.03 (d, *J* = 17.1 Hz, 1H), 3.60 (d, *J* = 6.2 Hz, 1H), 2.38 (t, *J* = 6.9 Hz, 1H), 2.34 – 2.14 (m, 4H), 2.10 – 2.04 (m, 2H), 1.97 – 1.88 (m, 1H), 1.77 (dq, *J* = 14.5, 3.0 Hz, 1H), 1.70 – 1.36 (m, 6H), 1.41 (s, 3H), 1.19 (s, 3H), 1.14 (td, *J* = 14.1, 4.6 Hz, 1H), 1.08 (d, *J* = 15.6 Hz, 1H), 0.98 (d, *J* = 7.1 Hz, 3H), 0.69 (d, *J* = 7.2 Hz, 3H); $^{13}$C NMR (126 MHz, $CDCl_3$) δ 216.5, 172.2, 147.7, 141.0, 140.5, 129.3, 128.9, 127.6, 127.5 , 127.0, 126.1, 119.6, 71.9, 70.1, 61.3, 57.9, 46.8, 45.4, 42.8, 42.7, 41.8, 40.7, 36.5, 35.0, 34.4, 30.3, 26.9, 25.1, 17.9, 16.7, 14.8, 11.1; HR-MS (ESI) calcd for $C_{36}H_{46}N_3O_5$ $[M+H]^+$, 600.3431, found 600.3436; $[\alpha]_D^{24}$ = -24.7 (c = 0.720, $CH_3OH$).

**(3a*R*,4*R*,5*R*,7*S*,8*S*,9*R*,9a*S*,12*R*)-8-hydroxy-4,7,9,12-tetramethyl-3-oxo-7-(2-(4-phenyl-1*H*-1,2,3-triazol-1-yl)ethyl)decahydro-4,9a-propanocyclopenta[8]annulen-5-yl 2-((2-(diethylamino)ethyl)thio)acetate (31)**: Prepared from **10** according to the general method for triazole formation and purified using flash chromatography ($SiO_2$, 5% (10:1 MeOH:$NH_4OH$)/$CH_2Cl_2$) to give **31** (17.9 mg, 58%) as a clear, colorless oil: $^1$H NMR (500 MHz, $CDCl_3$) δ 7.81 – 7.78 (m, 3H), 7.44 – 7.39 (m, 2H), 7.35 – 7.31 (m, 1H), 5.58 (d, *J* = 8.3 Hz, 1H), 4.61 – 4.49 (m, 2H), 3.55 (t, *J* = 6.1 Hz, 1H), 3.19 (s, 2H), 2.74 (br s, 4H), 2.59 (br s, 4H), 2.38 (p, *J* = 7.1 Hz, 1H), 2.32 – 2.13 (m, 3H), 2.12 – 2.03 (m, 2H), 1.97 – 1.90 (m, 2H), 1.79 – 1.72 (m, 1H), 1.70 – 1.63 (m, 1H), 1.60 – 1.52 (m, 2H), 1.50 – 1.44 (m, 1H), 1.43 (s, 3H), 1.40 – 1.35 (m,

1H), 1.16 (s, 3H), 1.15 – 1.09 (m, 2H), 1.05 (t, *J* = 7.1 Hz, 6H), 0.96 (d, *J* = 7.0 Hz, 3H), 0.73 (d, *J* = 7.0 Hz, 3H); $^{13}$C NMR (126 MHz, $CDCl_3$) δ 216.7, 169.2, 148.1, 130.7, 129.0, 128.3, 125.8, 119.7, 72.2, 69.6, 58.2, 52.4, 47.1, 46.8, 45.5, 42.8 (2C), 41.9, 40.7, 36.8, 35.0, 34.7, 34.5, 30.5, 30.2, 27.0, 25.2, 18.1, 17.0, 15.1, 11.7, 11.1; HR-MS (ESI) calcd for $C_{36}H_{55}N_4O_4S$ $[M+H]^+$ 639.3938, found 639.3938; $[\alpha]_D^{24}$ = -18 (c = 0.40, $CH_3OH$).

**(3a*R*,4*R*,5*R*,7*S*,8*S*,9*R*,9a*S*,12*R*)-7-(2-(4-benzyl-1*H*-1,2,3-triazol-1-yl)ethyl)-8-hydroxy-4,7,9,12-tetramethyl-3-oxodecahydro-4,9a-propanocyclopenta[8]annulen-5-yl 2-((2-(diethylamino)ethyl)thio)acetate (32)**: Prepared from **10** according to the general method for triazole formation and purified using flash chromatography ($SiO_2$, 6% (10:1 MeOH:$NH_4OH$)/$CH_2Cl_2$) to give **32** (21.9 mg, 67%) as a clear, colorless oil: $^1$H NMR (500 MHz, $CDCl_3$) δ 7.31 – 7.27 (m, 2H), 7.25 – 7.20 (m, 3H), 7.16 (d, *J* = 0.8 Hz, 1H), 5.56 (d, *J* = 8.3 Hz, 1H), 4.42 (t, *J* = 8.0 Hz, 2H), 4.05 (s, 2H), 3.48 – 3.44 (m, 1H), 3.17 (s, 2H), 2.73 – 2.66 (m, 4H), 2.54 (q, *J* = 7.1 Hz, 4H), 2.34 (p, *J* = 7.0 Hz, 1H), 2.30 – 2.23 (m, 1H), 2.21 – 2.14 (m, 1H), 2.14 – 2.09 (m, 1H), 2.05 (dd, *J* = 16.5, 8.1 Hz, 1H), 2.01 (d, *J* = 3.2 Hz, 1H), 1.91 (d, *J* = 6.0 Hz, 1H), 1.82 (dt, *J* = 13.9, 7.8 Hz, 1H), 1.74 (dq, *J* = 14.5, 3.1 Hz, 1H), 1.67 – 1.62 (m, 1H), 1.57 – 1.47 (m, 2H), 1.44 – 1.40 (m, 1H), 1.41 (s, 3H), 1.40 – 1.33 (m, 1H), 1.14 – 1.08 (m, 1H), 1.10 (s, 3H), 1.06 (d, *J* = 15.8 Hz, 1H), 1.01 (t, *J* = 7.1 Hz, 6H), 0.91 (d, *J* = 7.1 Hz, 3H), 0.72 (d, *J* = 7.0 Hz, 3H); $^{13}$C NMR (126 MHz, $CDCl_3$) δ 216.6, 169.1, 147.9, 139.1, 128.70, 128.67, 126.5, 121.3, 72.0, 69.4, 58.0, 52.3, 47.0, 46.4, 45.3, 42.65, 42.62, 41.7, 40.4, 36.7, 34.8, 34.5, 34.4, 32.3, 30.4, 30.3, 26.9, 25.0, 18.0, 16.9, 14.9, 11.8, 11.0; HR-MS (ESI) calcd for $C_{37}H_{57}N_4O_4S$ $[M+H]^+$ 653.4095, found 653.4115; $[\alpha]_D^{24}$ = -6.50 (c = 0.600, $CH_3OH$).

**(3a*R*,4*R*,5*R*,7*S*,8*S*,9*R*,9a*S*,12*R*)-8-hydroxy-4,7,9,12-tetramethyl-3-oxo-7-(2-(4-(phenoxymethyl)-1*H*-1,2,3-triazol-1-yl)ethyl)decahydro-4,9a-propanocyclopenta[8]annulen-5-yl 2-((2-(diethylamino)ethyl)thio)acetate (33)**: Prepared from **10** according to the general method for triazole formation and purified using automated flash chromatography (Teledyne RediSepRf gold 4 g $SiO_2$ column, 7% (10:1 MeOH:$NH_4OH$)/$CH_2Cl_2$) to give **33** (15.2 mg, 50%) as a clear, colorless oil: $^1$H NMR (500 MHz, $CDCl_3$) δ 7.64 (s, 1H), 7.31 – 7.27 (m, 2H), 6.99 – 6.95 (m, 3H), 5.57 (d, *J* = 8.3 Hz, 1H), 5.19 (d, *J* = 0.7 Hz, 2H), 4.51 (t, *J* = 7.1 Hz, 2H), 3.48 (t, *J* = 6.1 Hz, 1H), 3.19 (s, 2H), 2.81 – 2.69 (m, 4H), 2.64 – 2.55 (m, 4H), 2.38 – 2.26 (m, 2H), 2.23 – 2.13 (m, 2H), 2.08 (dd, *J* = 15.8, 8.4 Hz, 1H), 2.02 (d, *J* = 2.7 Hz, 1H), 1.93 – 1.86 (m, 1H), 1.75 (dd, *J* = 14.5, 3.0 Hz, 1H), 1.71 (d, *J* = 6.0 Hz, 1H), 1.69 – 1.62 (m, 1H), 1.59 – 1.48 (m, 2H), 1.48 – 1.41 (m, 1H), 1.43 (s, 3H), , 1.41 – 1.34 (m, 1H), 1.16 – 1.13 (m, 1H) 1.13 (s, 3H), 1.12 – 1.09 (m, 1H), 1.05 (br s, 6H), 0.93 (d, *J* = 7.1 Hz, 3H), 0.73 (d, *J* = 7.1 Hz, 3H); $^{13}$C NMR (126 MHz, $CDCl_3$) δ 216.6, 169.2, 158.3, 144.6, 129.7, 122.8, 121.4, 114.8, 72.3, 69.6, 62.1, 58.1, 52.4, 47.1, 46.8, 45.4, 42.84, 42.81, 41.8, 40.6, 36.8, 35.0, 34.7, 34.6, 34.5, 30.5, 27.0, 25.2, 18.0, 17.0, 15.1, 11.7, 11.1; HR-MS (ESI) calcd for $C_{37}H_{57}N_4O_5S$ $[M+H]^+$ 669.4044, found 669.4045; $[\alpha]_D^{24}$ = -5.7 (c = 0.40, $CH_3OH$).

**(3a*R*,4*R*,5*R*,7*S*,8*S*,9*R*,9a*S*,12*R*)-7-(2-(4-([1,1'-biphenyl]-4-yl)-1*H*-1,2,3-triazol-1-yl)ethyl)-8-hydroxy-4,7,9,12-tetramethyl-3-oxodecahydro-4,9a-propanocyclopenta[8]annulen-5-yl 2-((2-(diethylamino)ethyl)thio)acetate (34)**: Prepared from **10** according to the general method for triazole formation and purified using flash chromatography ($SiO_2$, 6% (10:1 MeOH:$NH_4OH$)/$CH_2Cl_2$) to give **34** (27.0 mg, 48%) as a colorless glass: $^1$H NMR (500 MHz, $CDCl_3$) δ 7.87 – 7.84 (m, 2H), 7.81 (s, 1H), 7.66 – 7.63 (m, 2H), 7.63 – 7.60 (m, 2H), 7.47 – 7.42 (m, 2H), 7.37 – 7.33 (m, 1H), 5.60 (d, *J* = 8.3 Hz, 1H), 4.61 – 4.48 (m, 2H), 3.62 – 3.55 (m, 1H),

3.19 (s, 2H), 2.77 – 2.66 (m, *J* = 4.4 Hz, 4H), 2.56 (q, *J* = 7.2 Hz, 4H), 2.39 (p, *J* = 6.9 Hz, 1H), 2.32 – 2.24 (m, 2H), 2.24 – 2.14 (m, 2H), 2.12 – 2.06 (m, 2H), 1.94 (ddd, *J* = 13.8, 9.7, 6.3 Hz, 1H), 1.80 – 1.72 (m, 1H), 1.68 – 1.34 (m, 6 H), 1.41 (s, 3H), 1.17 (s, 3H), 1.14 – 1.08 (m, 2H), 1.03 (t, *J* = 7.1 Hz, 6H), 0.97 (d, *J* = 7.0 Hz, 3H), 0.73 (d, *J* = 7.0 Hz, 3H); $^{13}$C NMR (126 MHz, $CDCl_3$) δ 216.9, 169.2, 147.8, 141.0, 140.6, 129.6, 129.0, 127.7, 127.6, 127.1, 126.2, 119.8, 72.1, 69.6, 58.2, 52.4, 47.1, 46.9, 45.5, 42.94, 42.87, 41.9, 40.7, 36.8, 35.1, 34.7, 34.6, 30.5, 30.2, 27.0, 25.2, 18.1, 17.0, 15.1, 11.8, 11.2; HR-MS (ESI) calcd for $C_{42}H_{59}N_4O_4S$ $[M+H]^+$ 715.4252, found 715.4260; $[\alpha]_D^{24}$ = -18.4 (c = 1.41, $CH_3OH$).

**Figure S1.** $^{1}H$ NMR of **8** (500 MHz, $CDCl_3$)

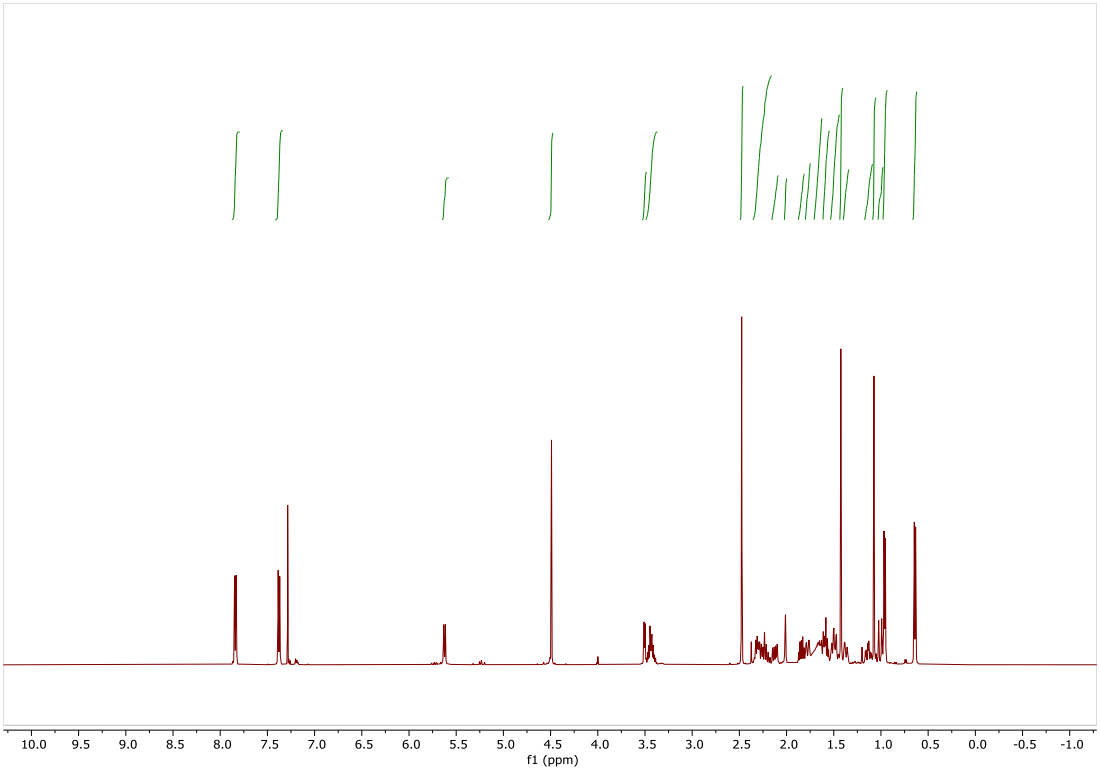


**Figure S2.** $^{13}C$ NMR of **8** (500 MHz, $CDCl_3$)

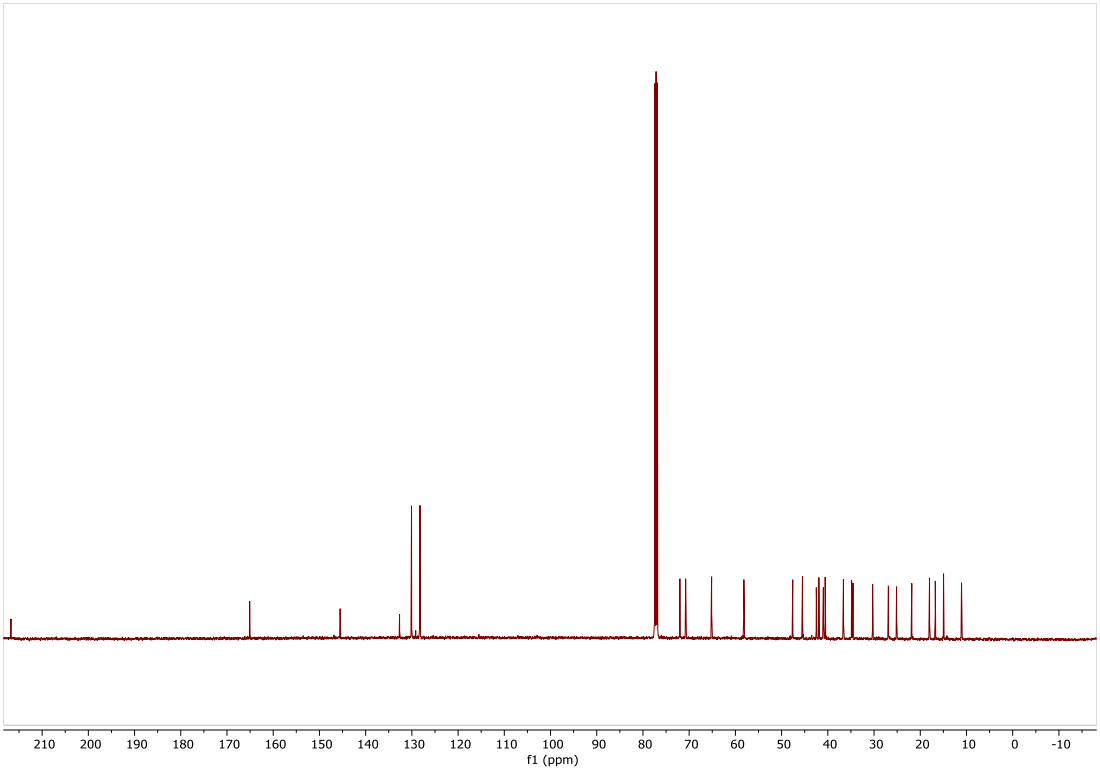

**Figure S3.** $^{1}$H NMR of **9** plus trace PhH (500 MHz, $CDCl_3$)

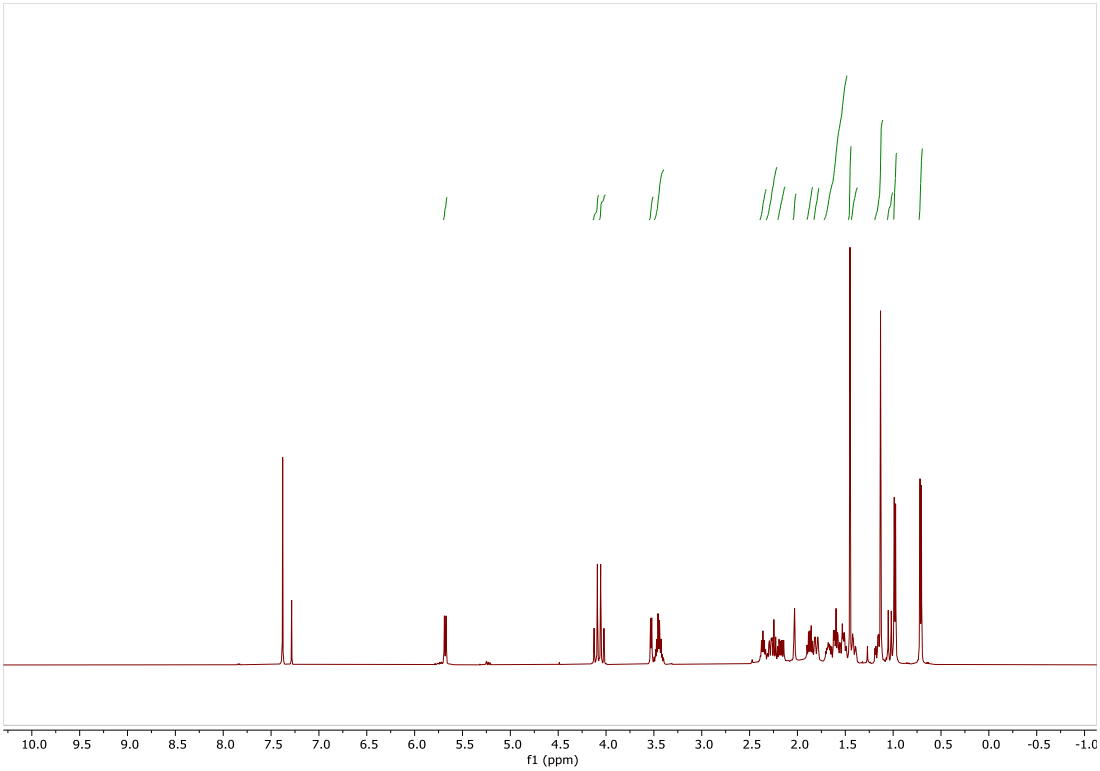


**Figure S4.** $^{13}$C NMR of **9** plus trace PhH (500 MHz, $CDCl_3$)

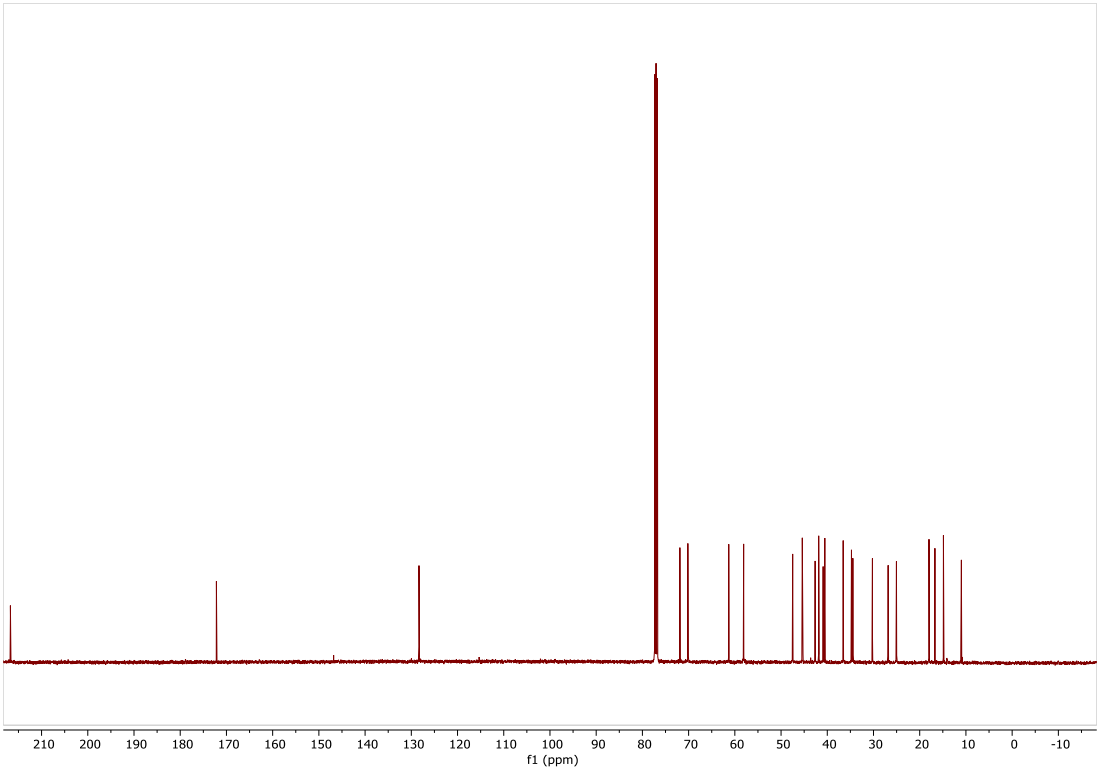

**Figure S5.** $^{1}H$ NMR of **10** (500 MHz, $CDCl_3$)

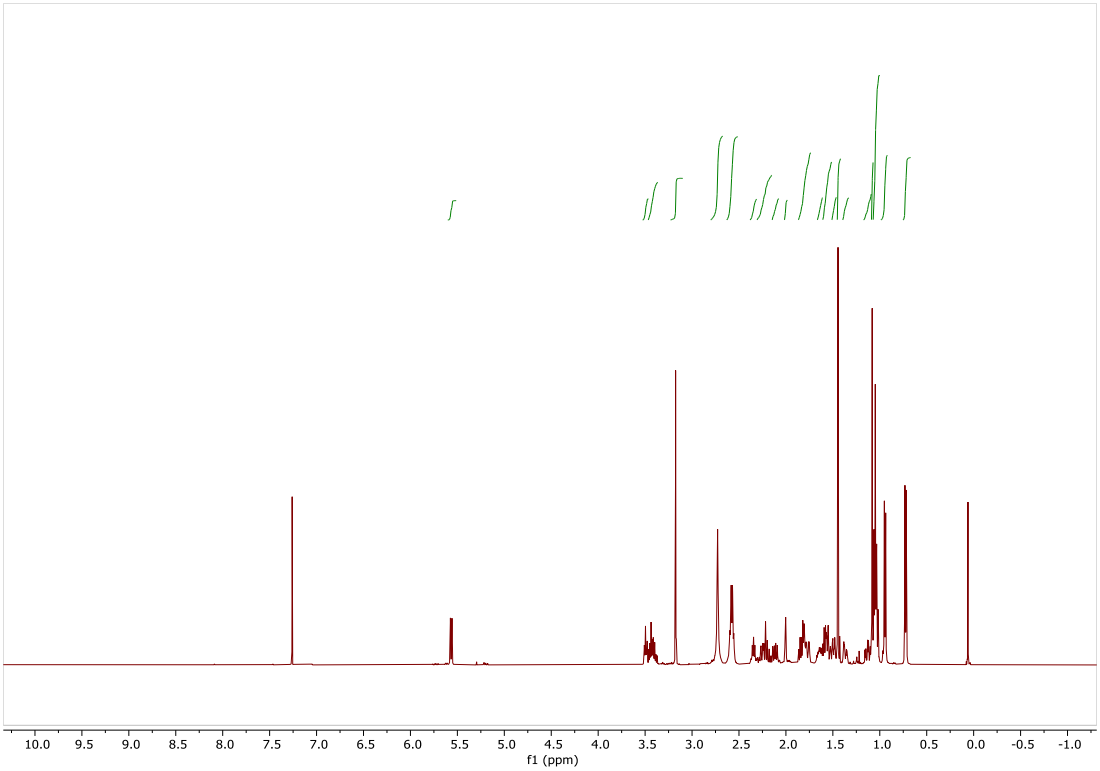


**Figure S6.** $^{13}C$ NMR of **10** (500 MHz, $CDCl_3$)

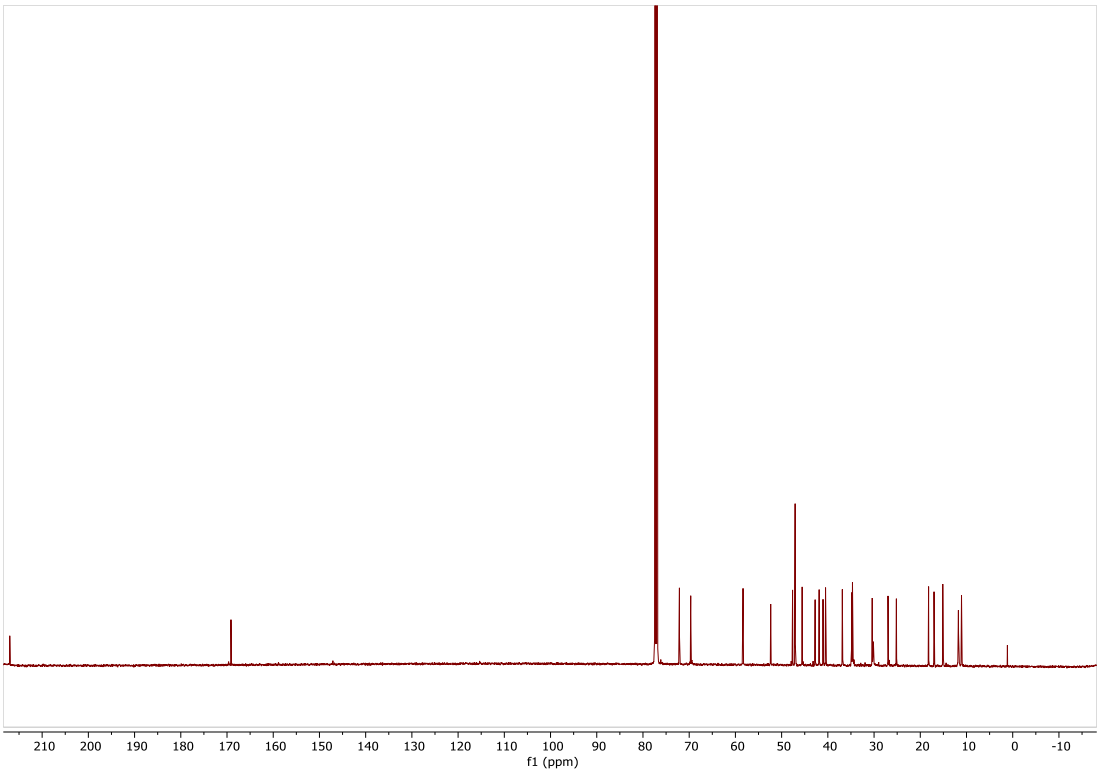

**Figure S7.** $^{1}$H NMR of **11** (500 MHz, $CD_3OD$)

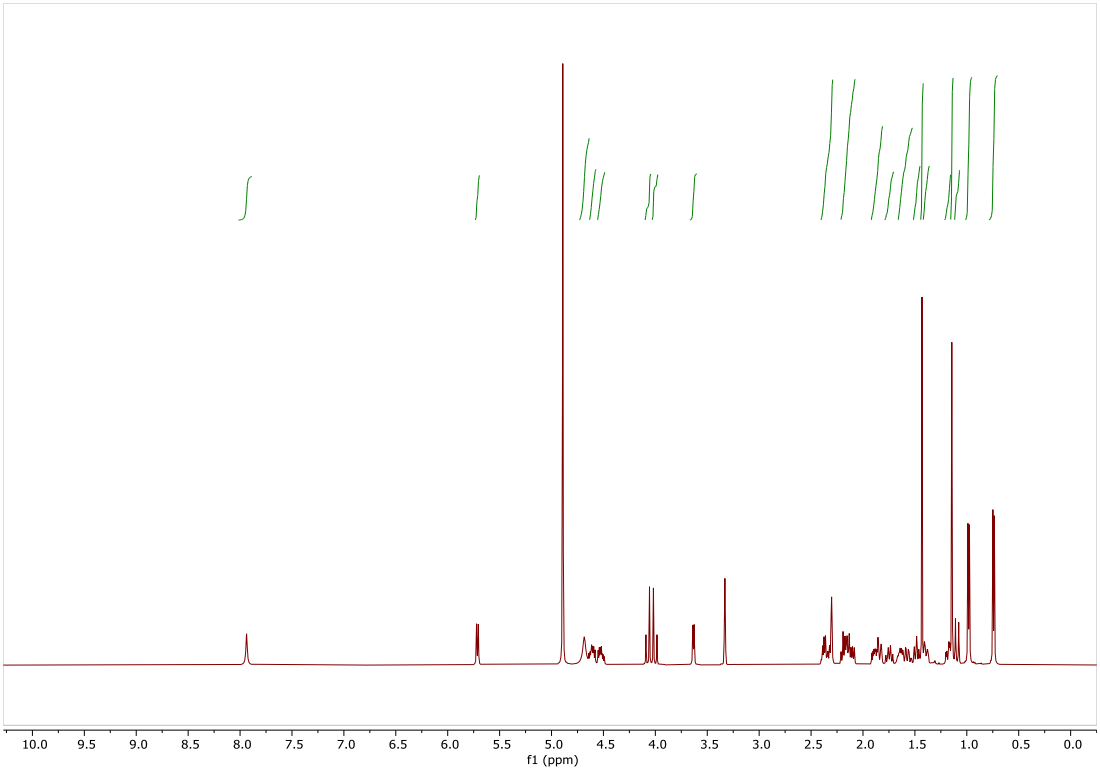


**Figure S8.** $^{13}$C NMR of **11** (500 MHz, $CD_3OD$)

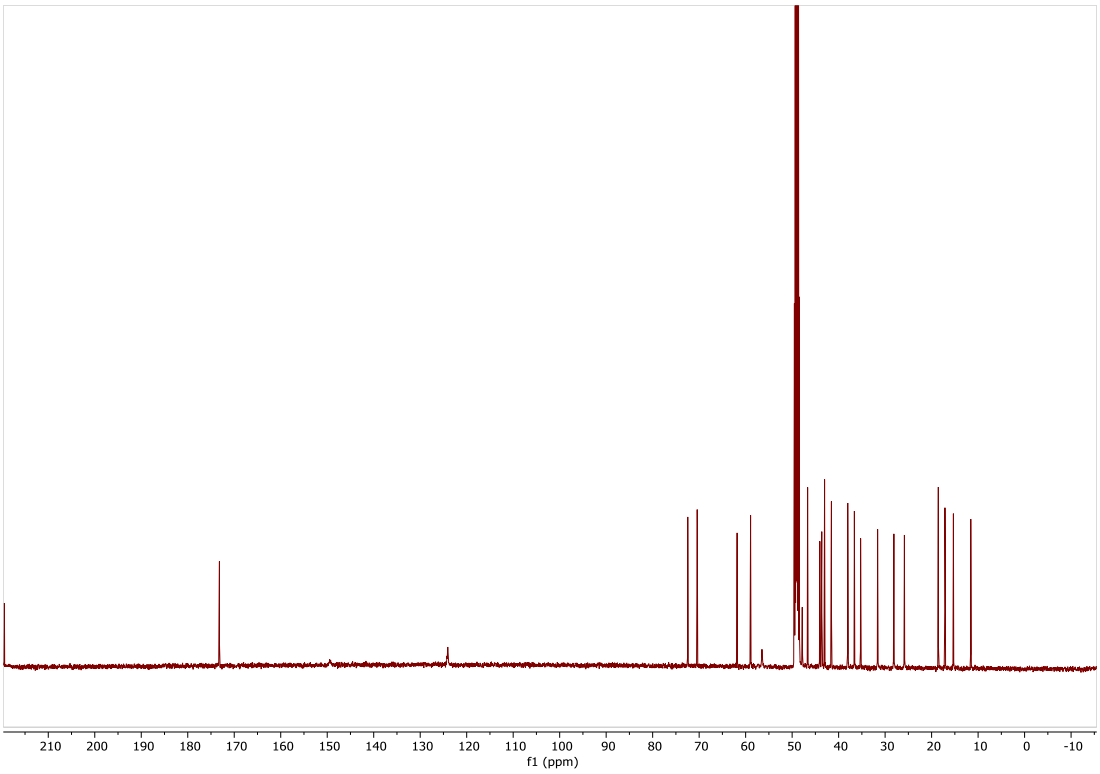

**Figure S9.** $^{1}$H NMR of **12** (500 MHz, $CD_3OD$)

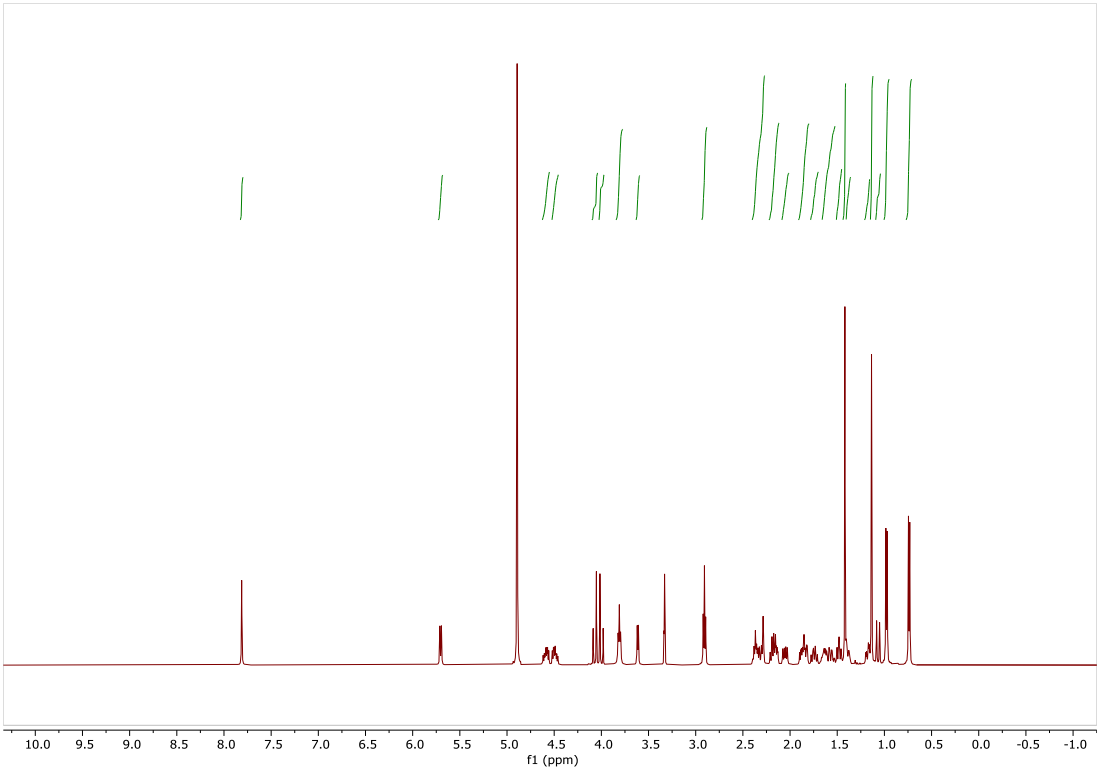


**Figure S10.** $^{13}$C NMR of **12** (500 MHz, $CD_3OD$)

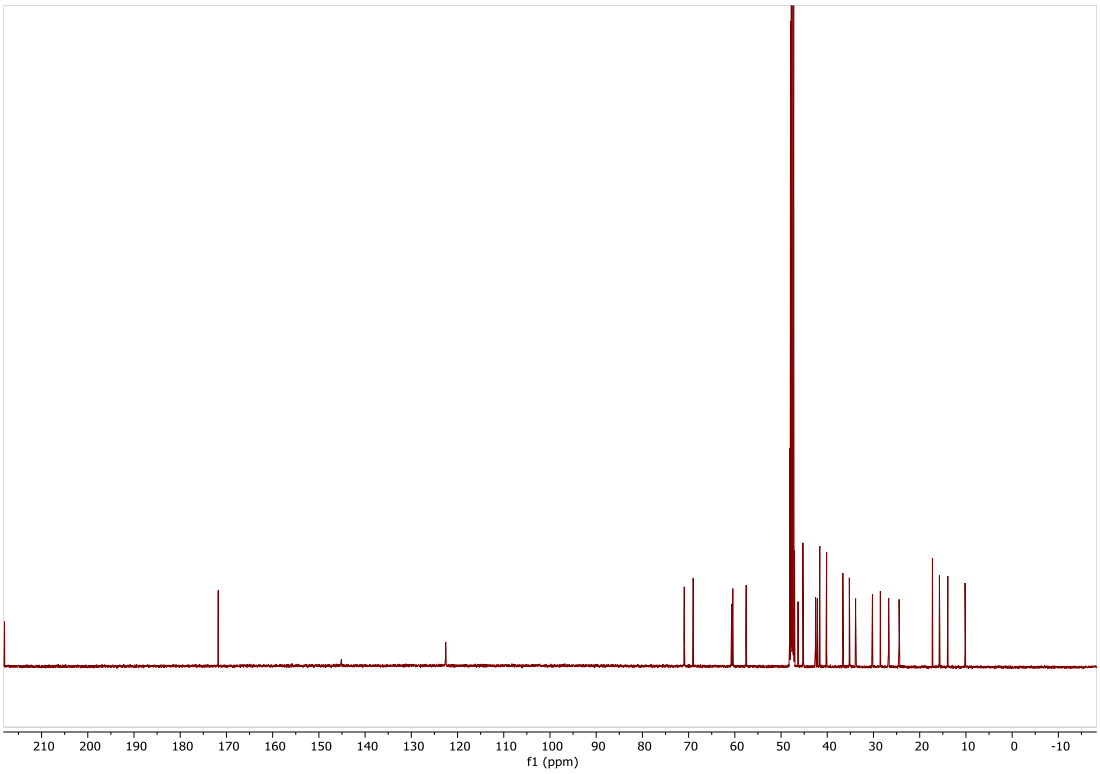

**Figure S11.** $^{1}$H NMR of **13** (500 MHz, $CD_3OD$)

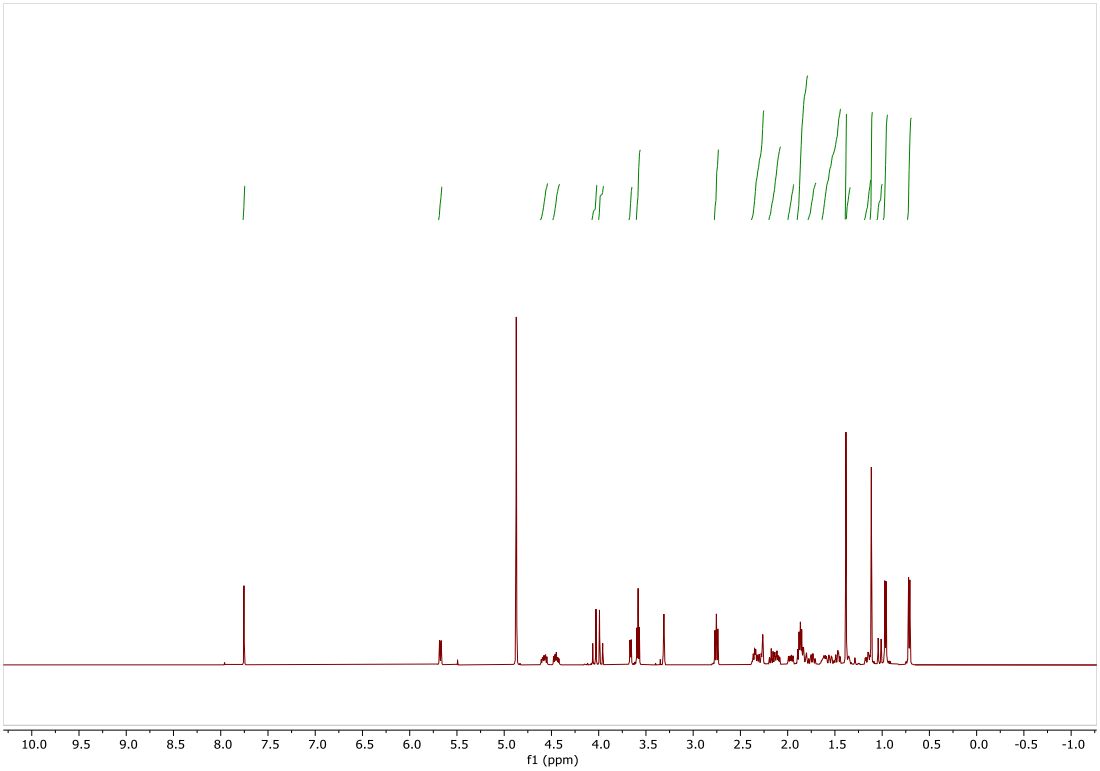


**Figure S12.** $^{13}$C NMR of **13** (500 MHz, $CD_3OD$)

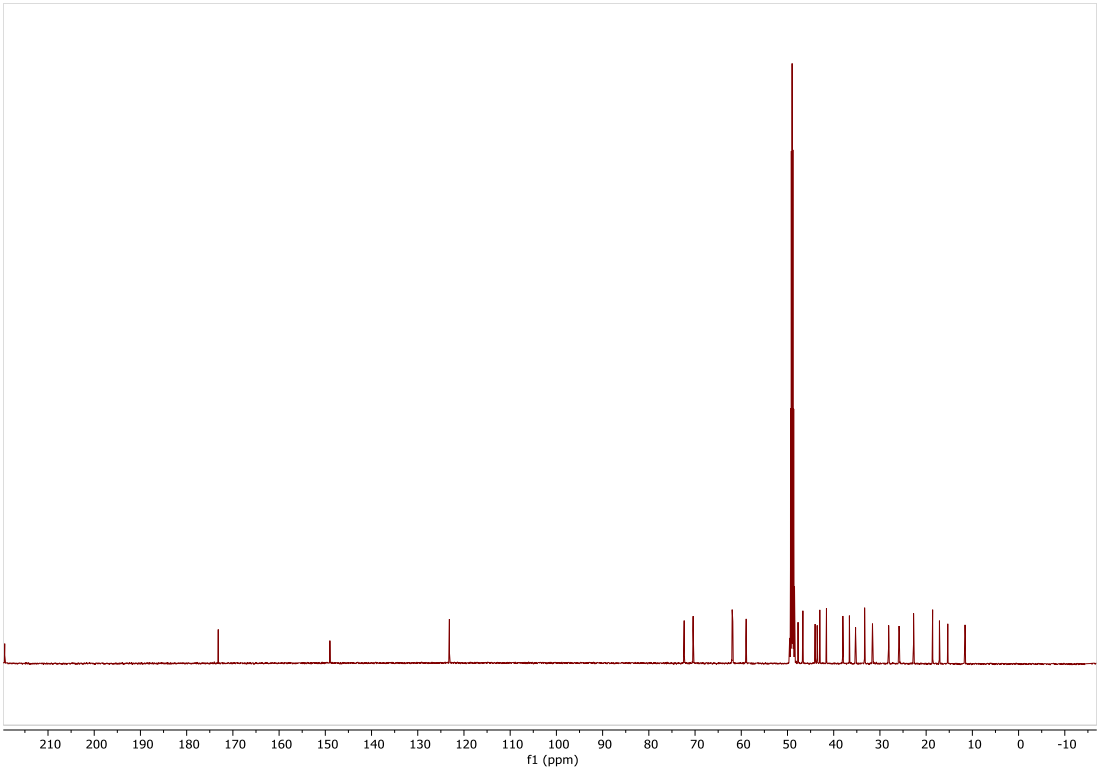

**Figure S13.** $^{1}$H NMR of **14** (500 MHz, $CDCl_3$)

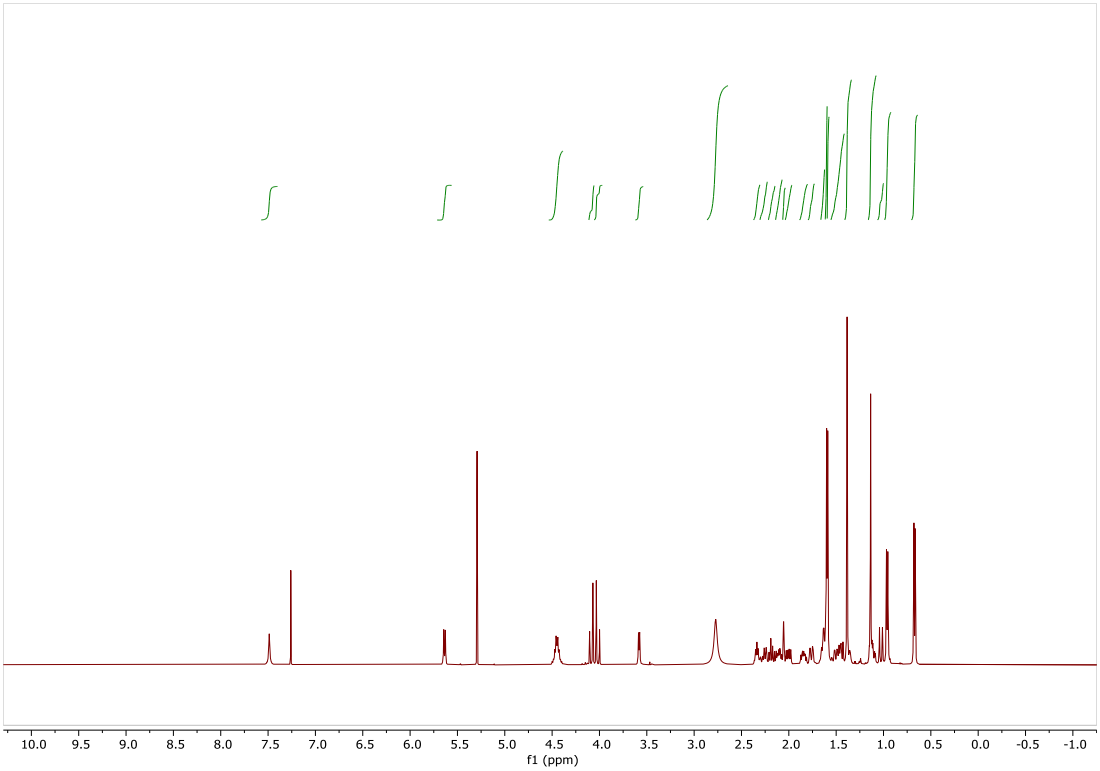


**Figure S14.** $^{13}$C NMR of **14** (500 MHz, $CDCl_3$)

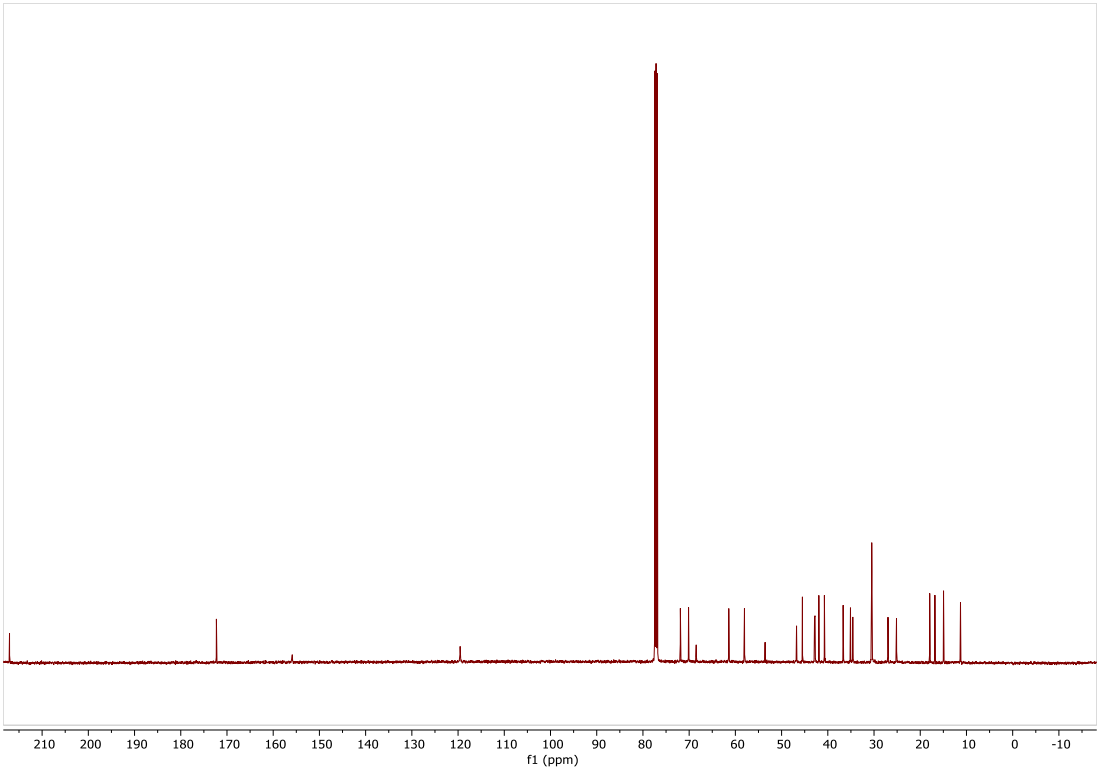

**Figure S15.** $^{1}$H NMR of **15** (500 MHz, $CD_3OD$)

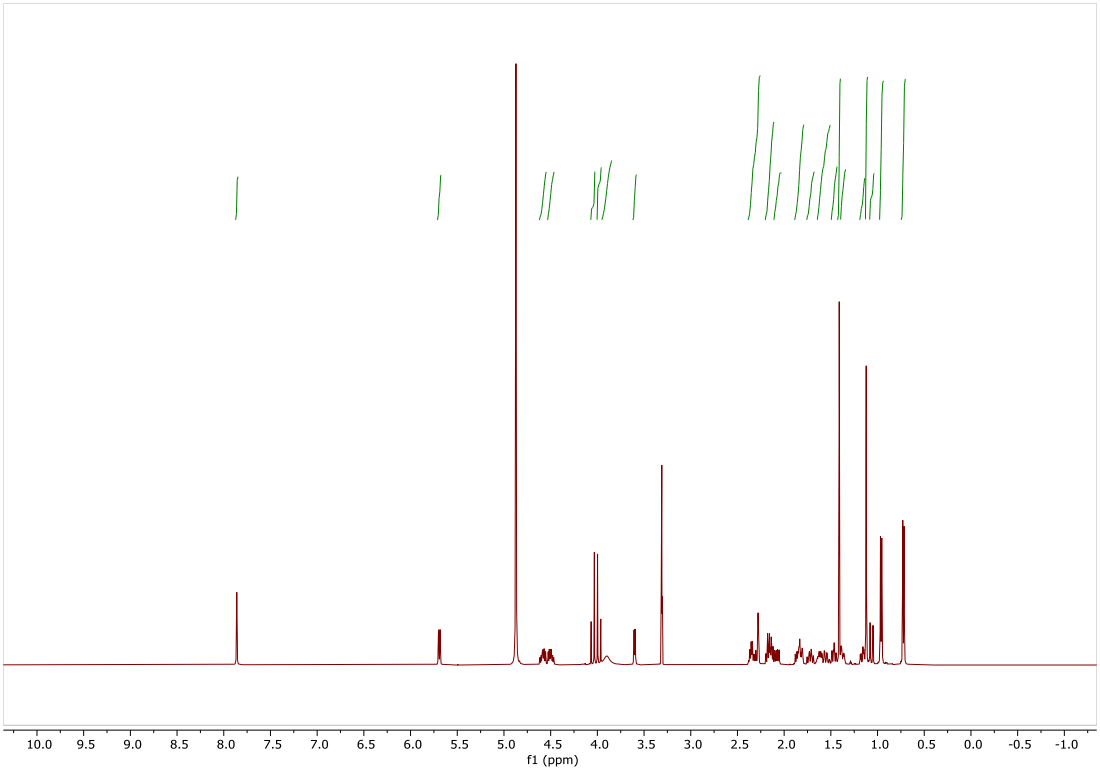


**Figure S16.** $^{13}$C NMR of **15** (500 MHz, $CD_3OD$)

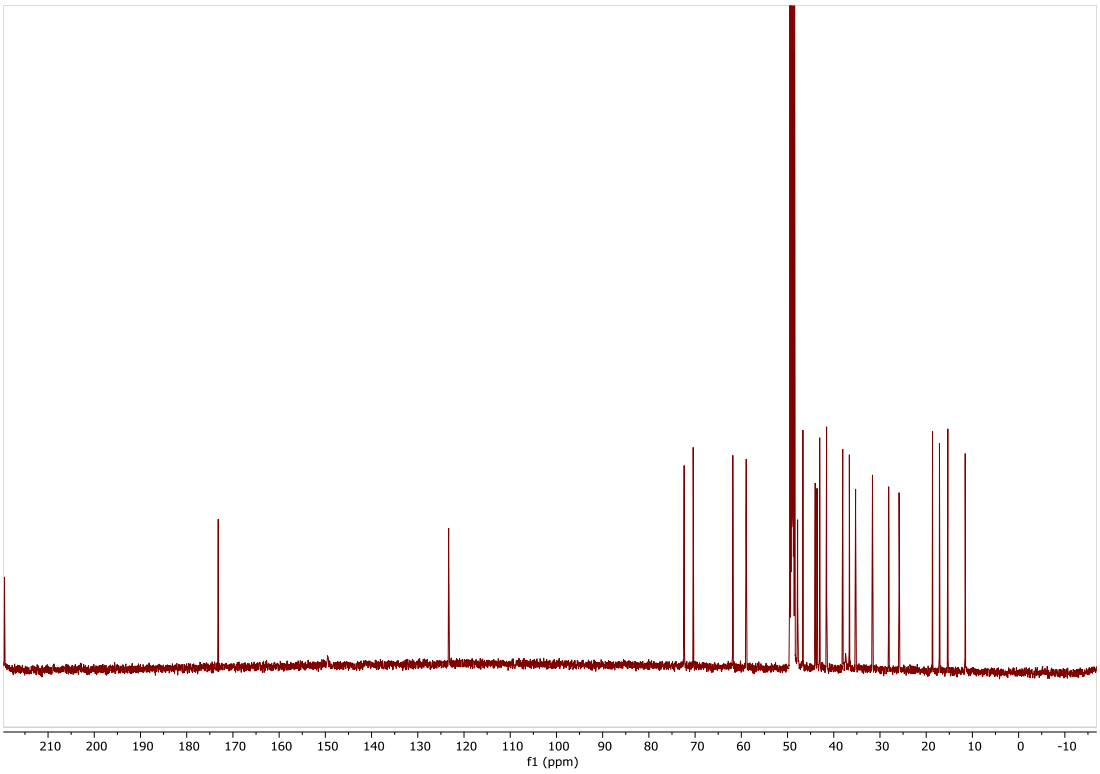

**Figure S17.** $^{1}$H NMR of **16** (500 MHz, $CD_3OD$)

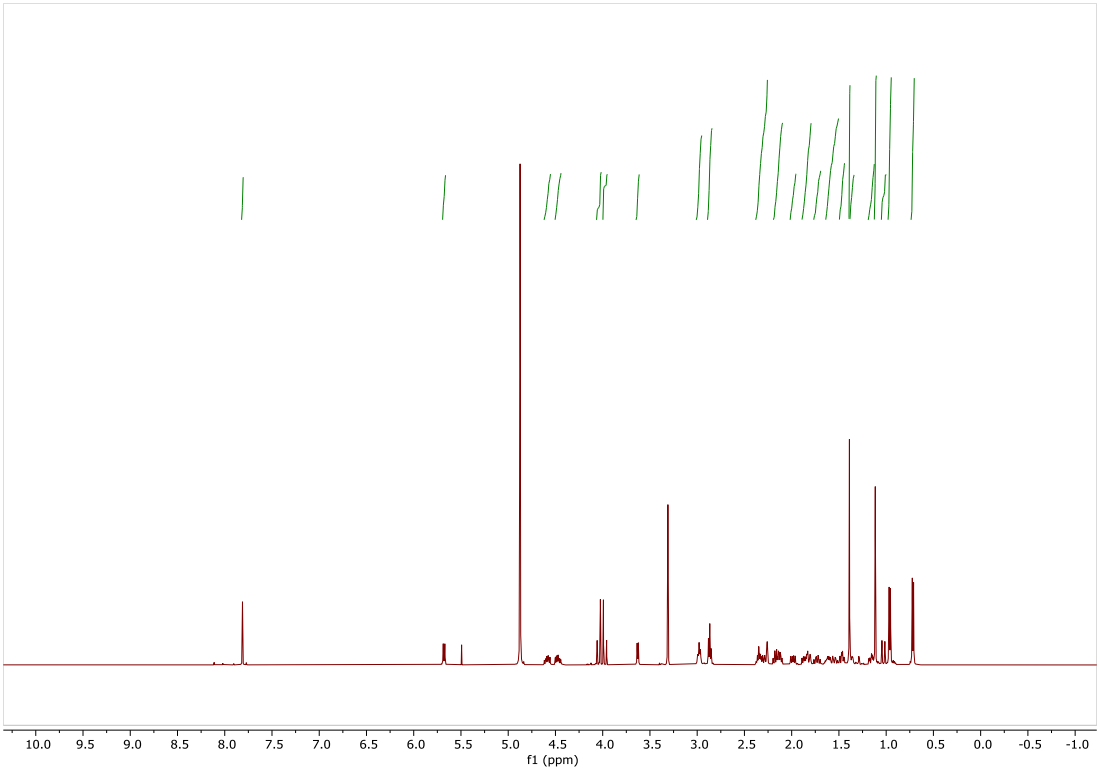


**Figure S18.** $^{13}$C NMR of **16** (500 MHz, $CD_3OD$)

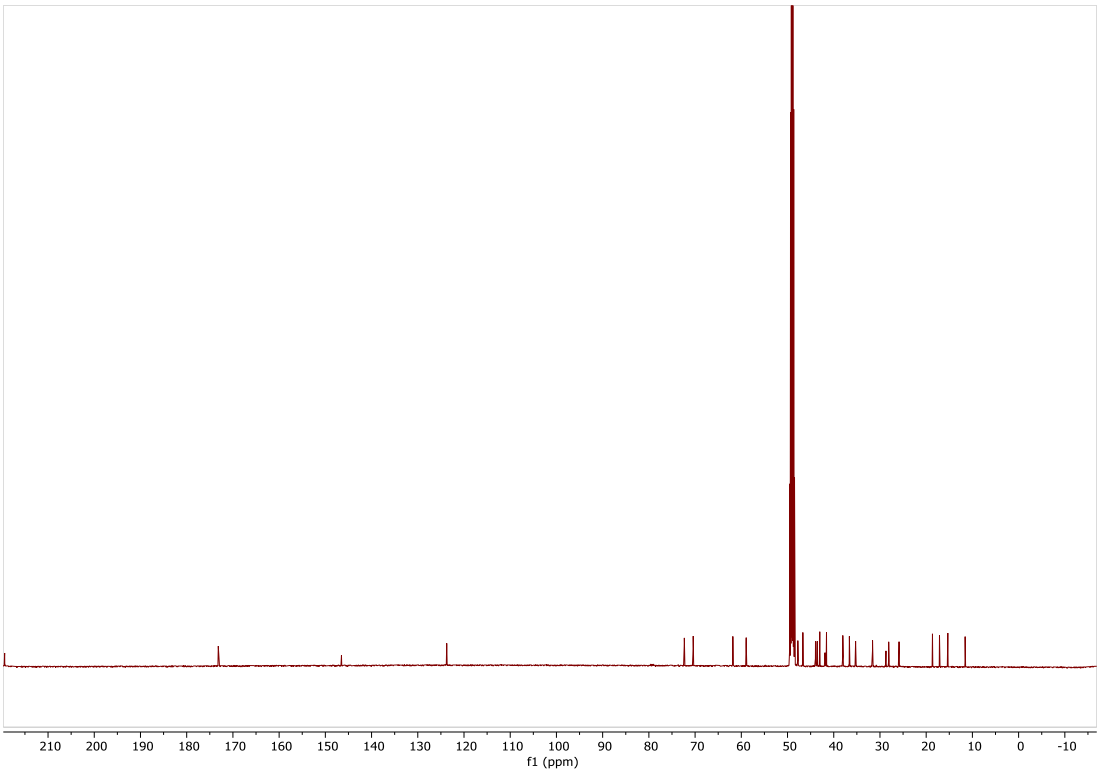

**Figure S19.** $^{1}$H NMR of **17** (500 MHz, $CDCl_3$)

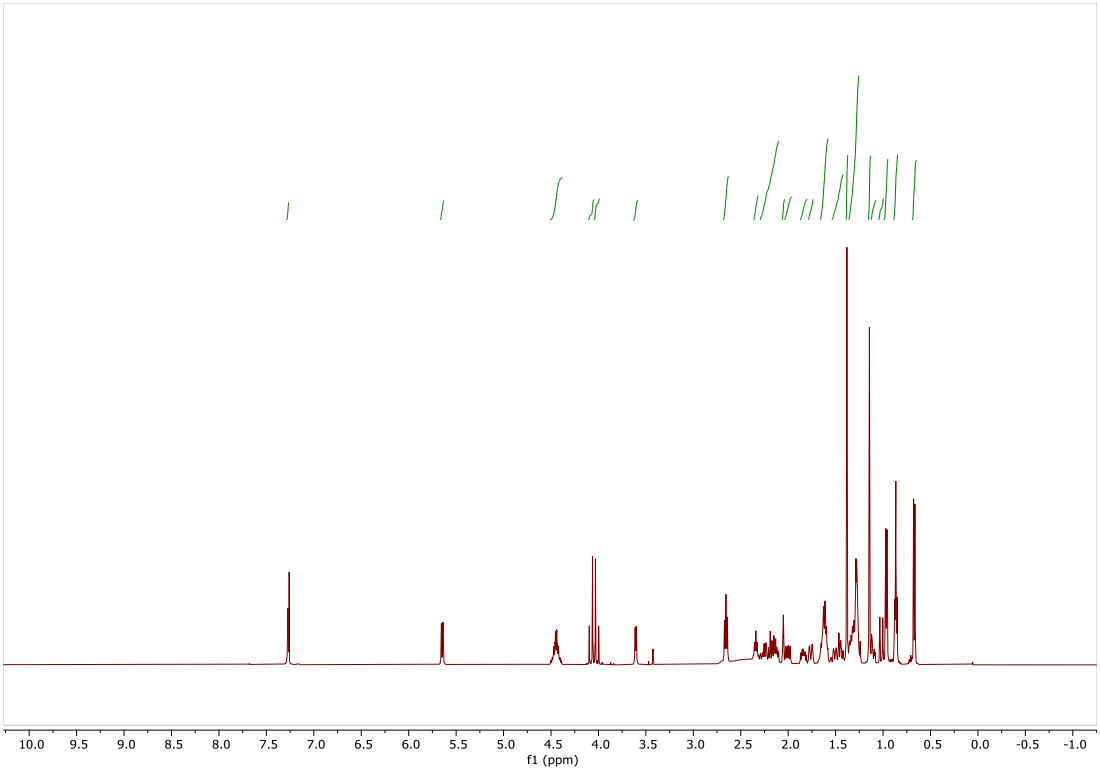


**Figure S20.** $^{13}$C NMR of **17** (500 MHz, $CDCl_3$)

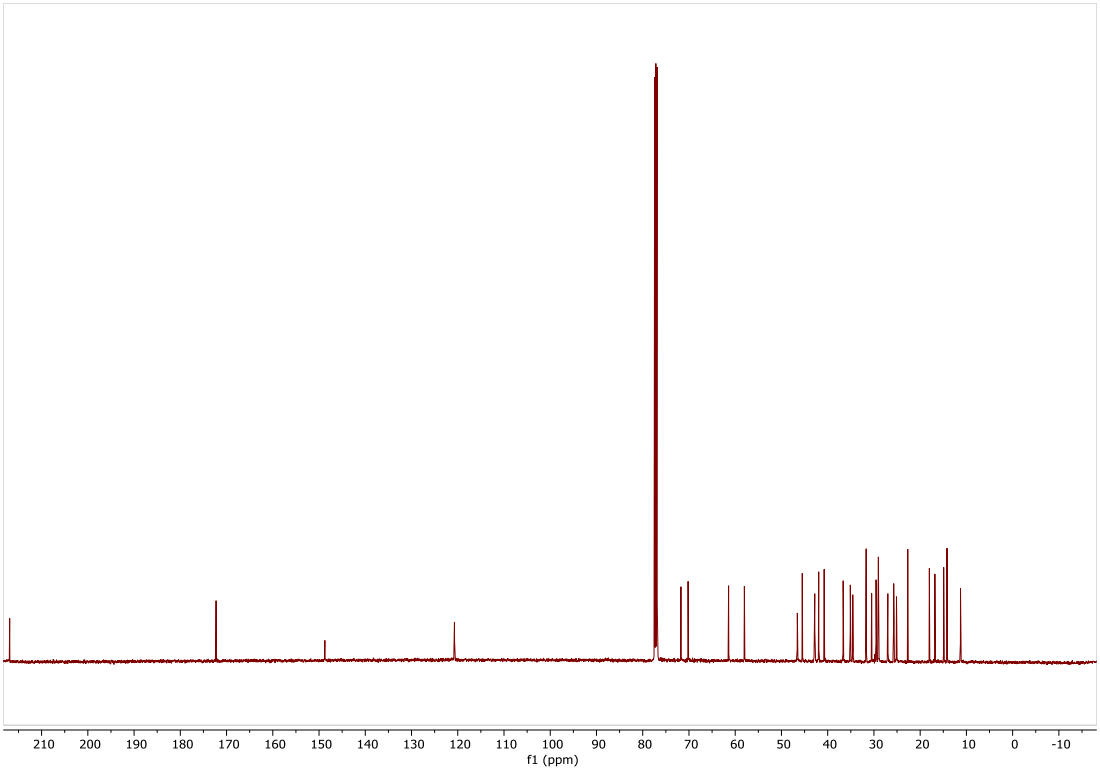

**Figure S21.** $^{1}H$ NMR of **18** plus $CH_2Cl_2$ (500 MHz, $CDCl_3$)

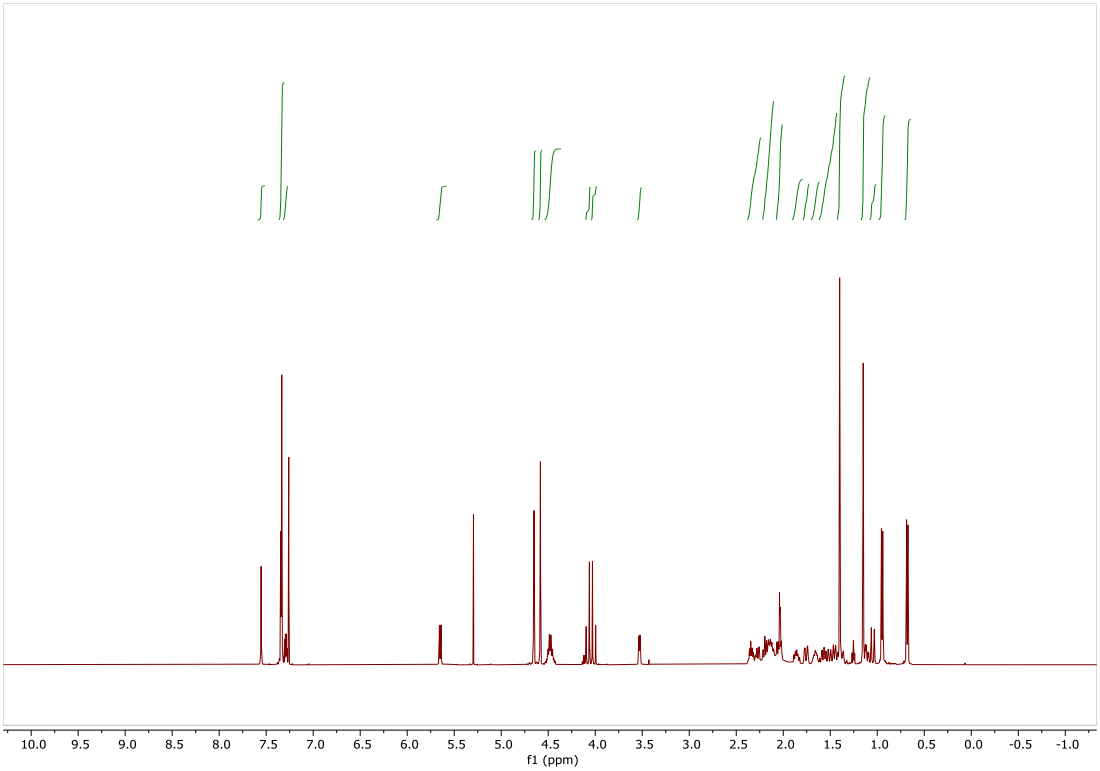


**Figure S22.** $^{13}C$ NMR of **18** plus $CH_2Cl_2$ (500 MHz, $CDCl_3$)

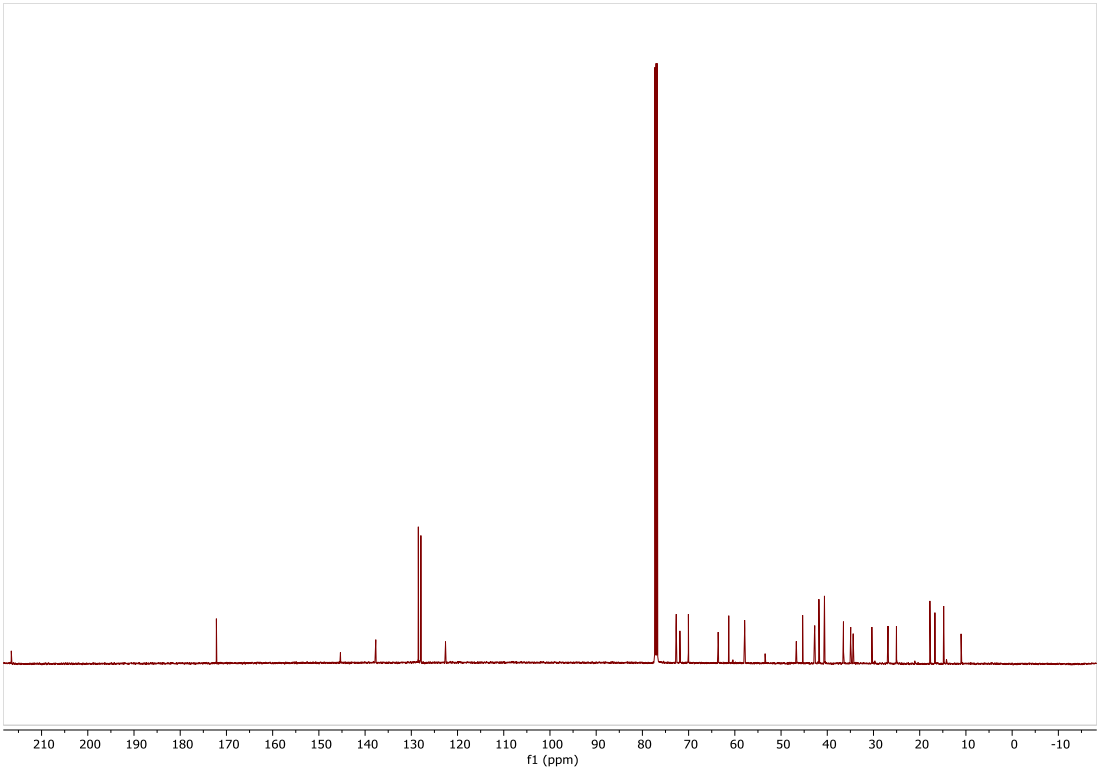

**Figure S23.** $^{1}$H NMR of **19** (500 MHz, $CDCl_3$)

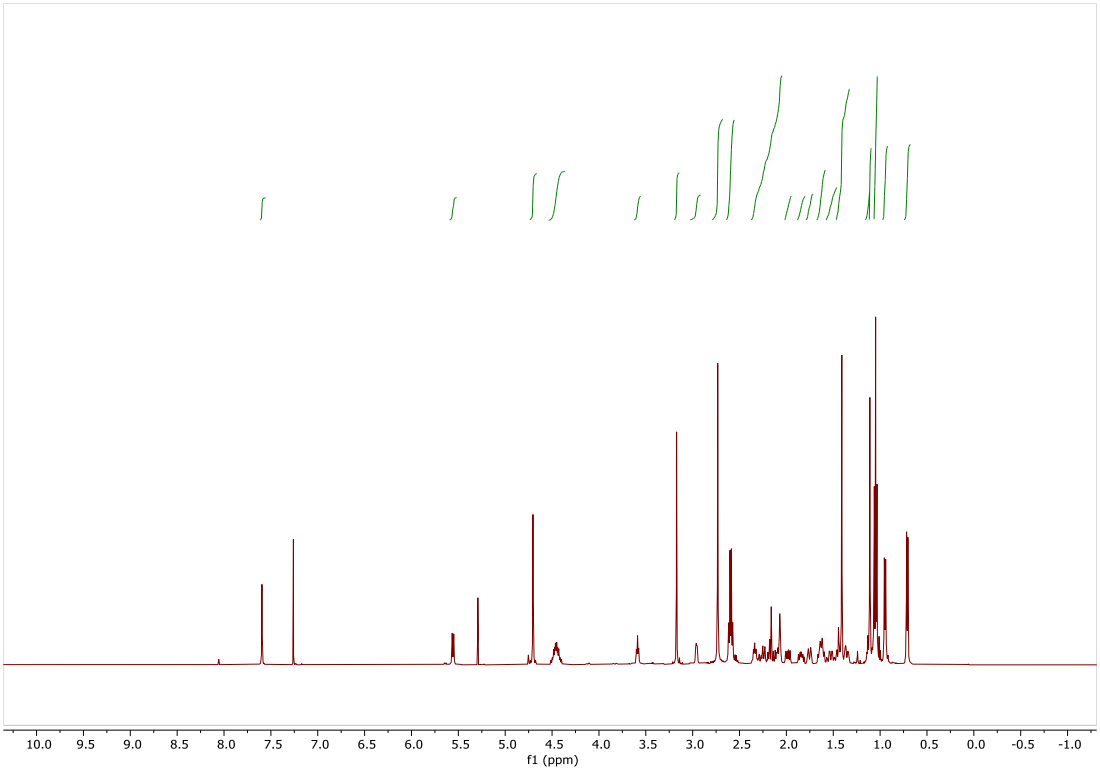


**Figure S24.** $^{13}$C NMR of **19** (500 MHz, $CDCl_3$)

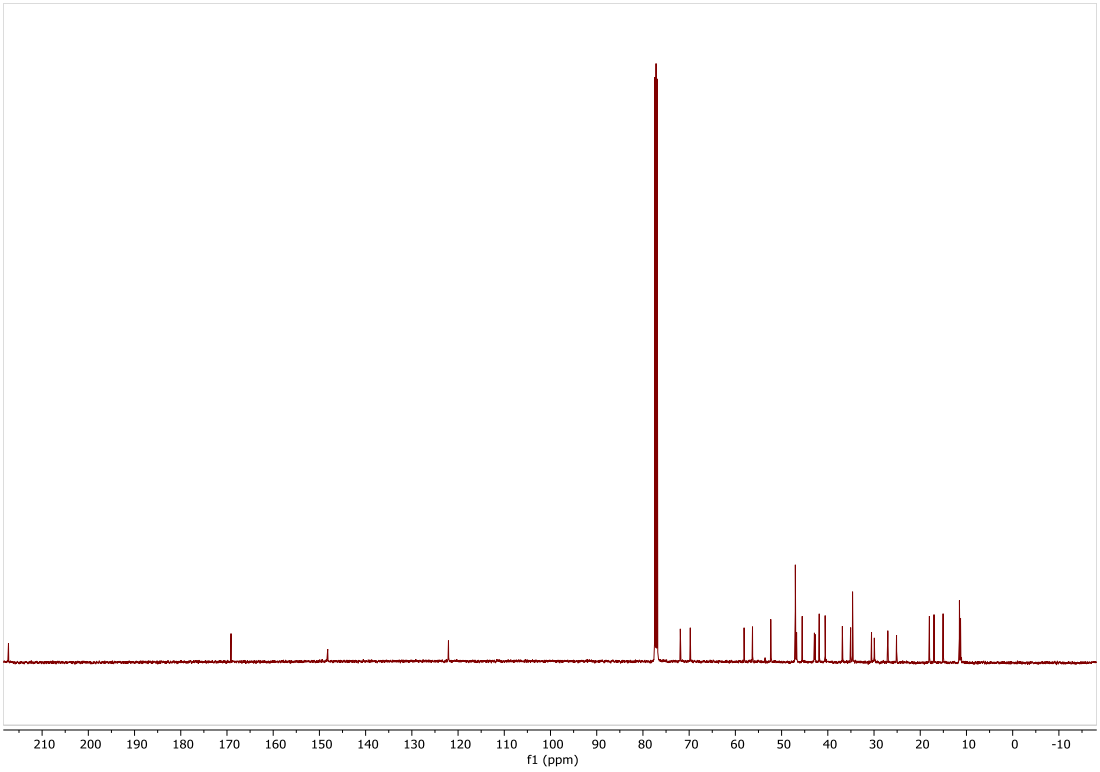

**Figure S25.** $^{1}$H NMR of **20** (500 MHz, $CDCl_3$)

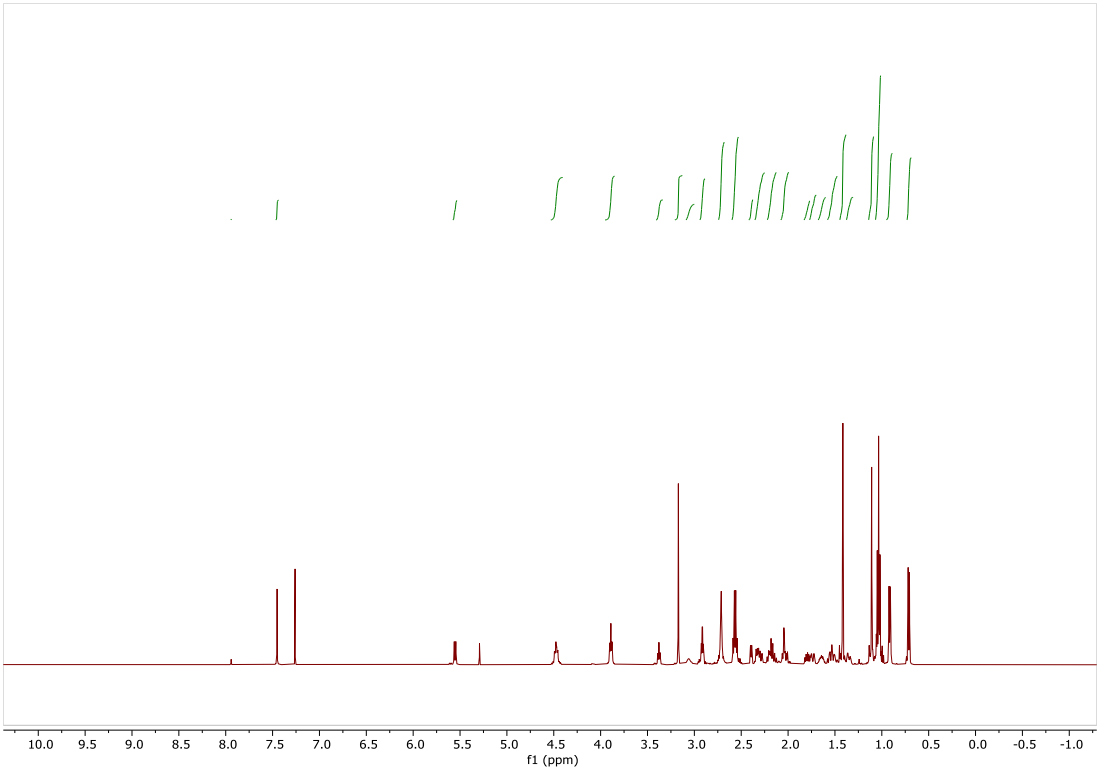


**Figure S26.** $^{13}$C NMR of **20** (500 MHz, $CDCl_3$)

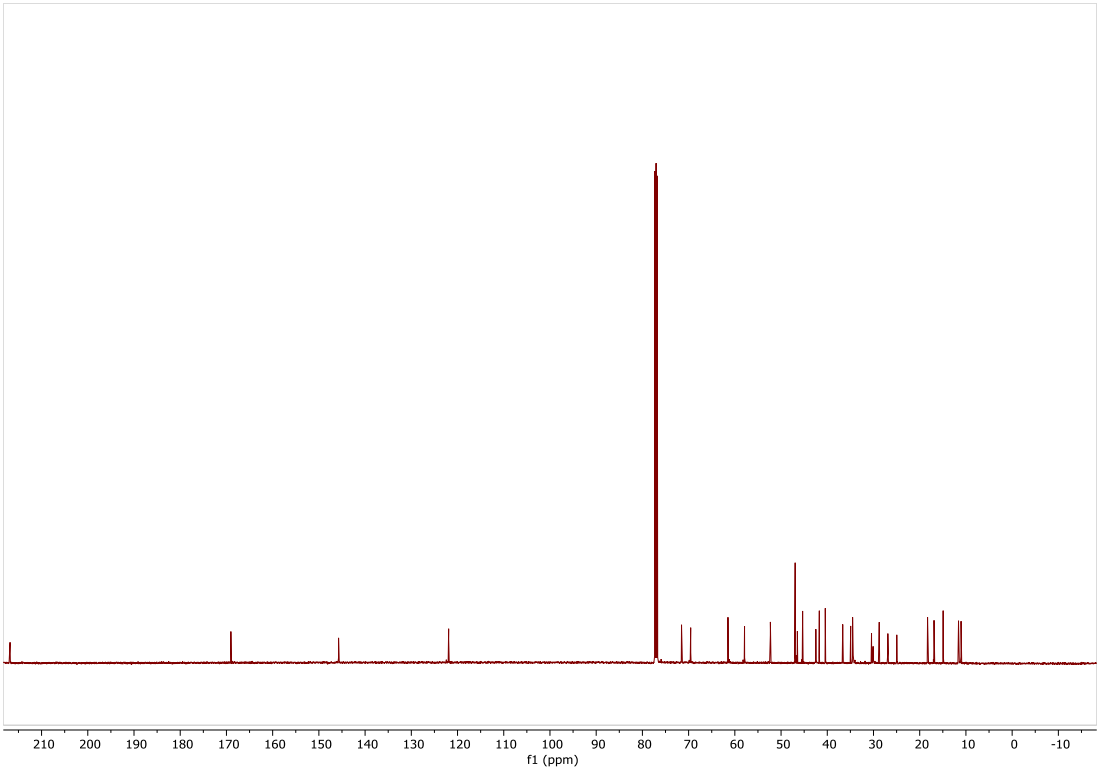

**Figure S27.** $^{1}$H NMR of **21** + trace $CH_2Cl_2$ (500 MHz, $CDCl_3$)

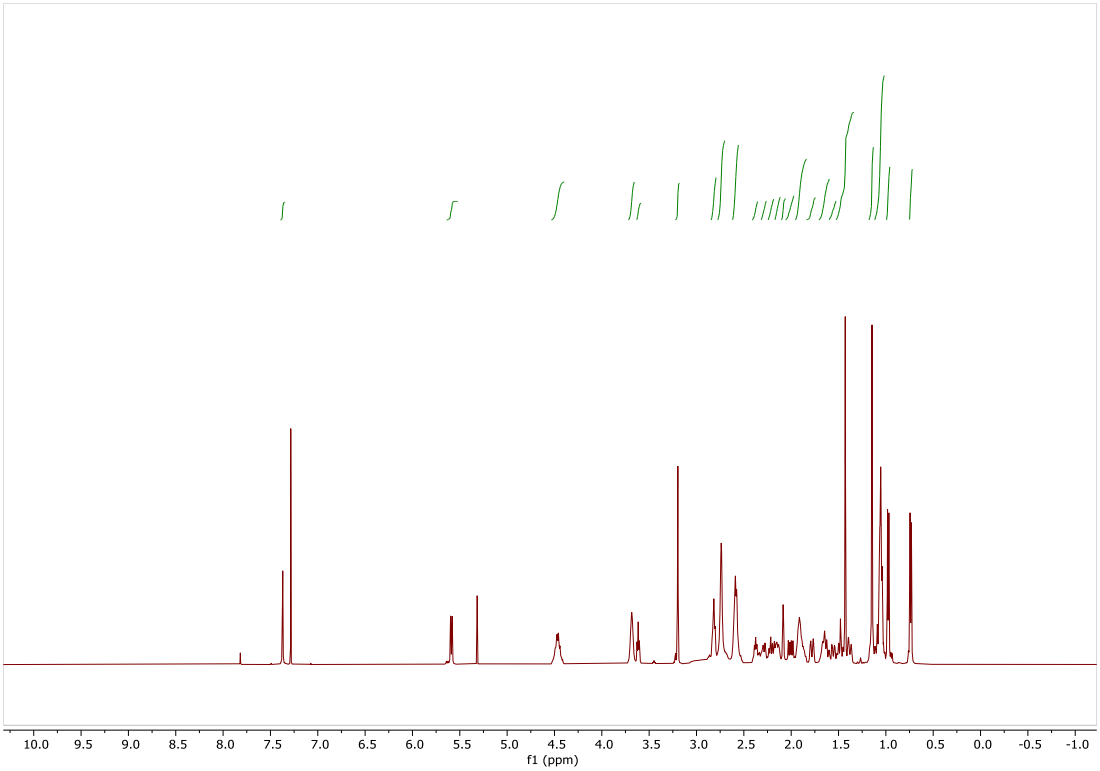


**Figure S28.** $^{13}$C NMR of **21** + trace $CH_2Cl_2$ (500 MHz, $CDCl_3$)

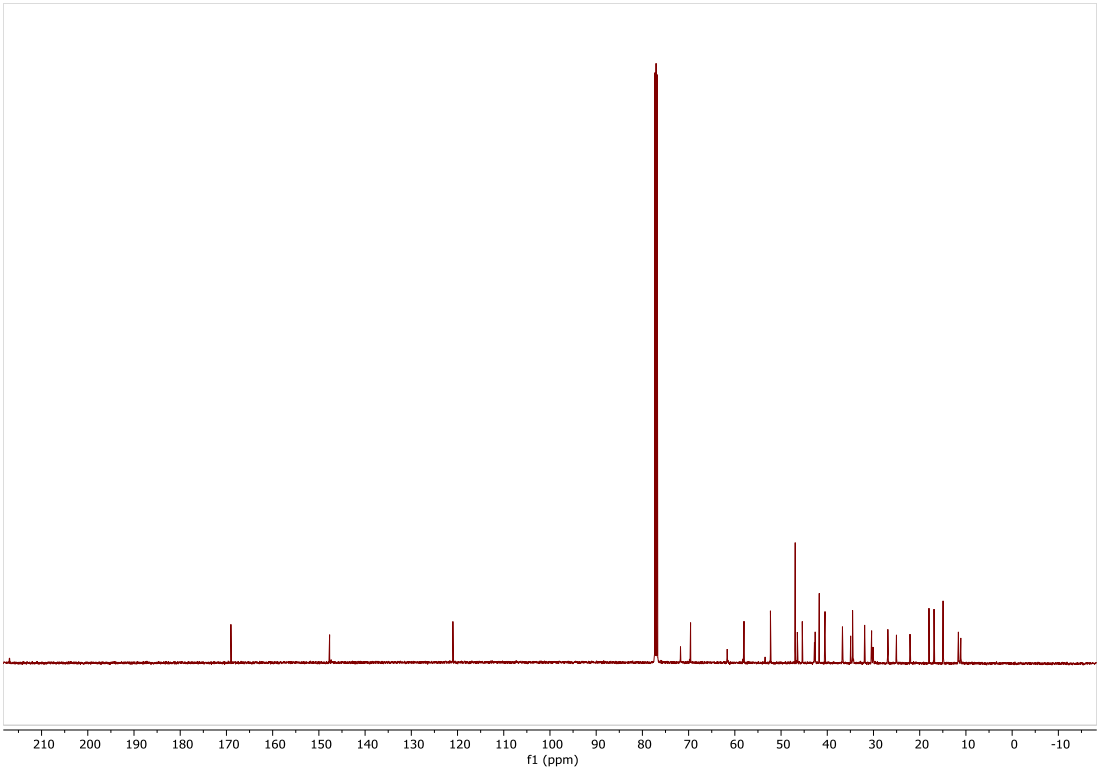

**Figure S29.** $^{1}$H NMR of **22** + trace $CH_2Cl_2$ (500 MHz, $CDCl_3$)

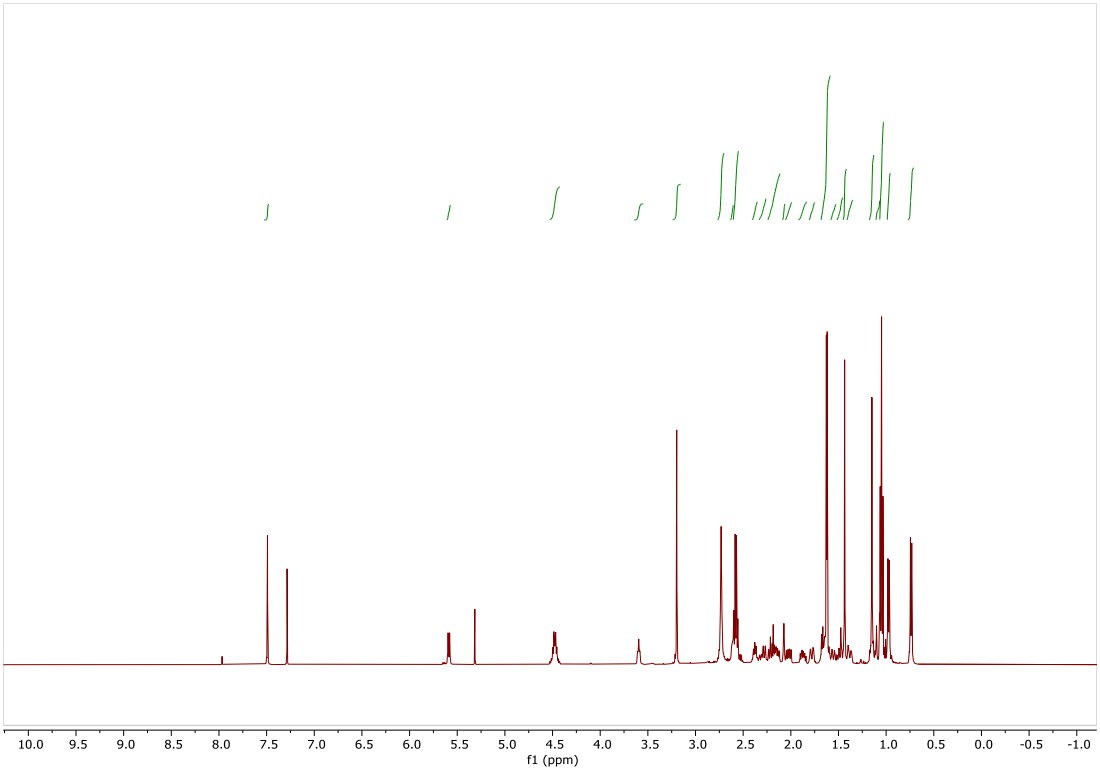


**Figure S30.** $^{13}$C NMR of **22** (500 MHz, $CDCl_3$)

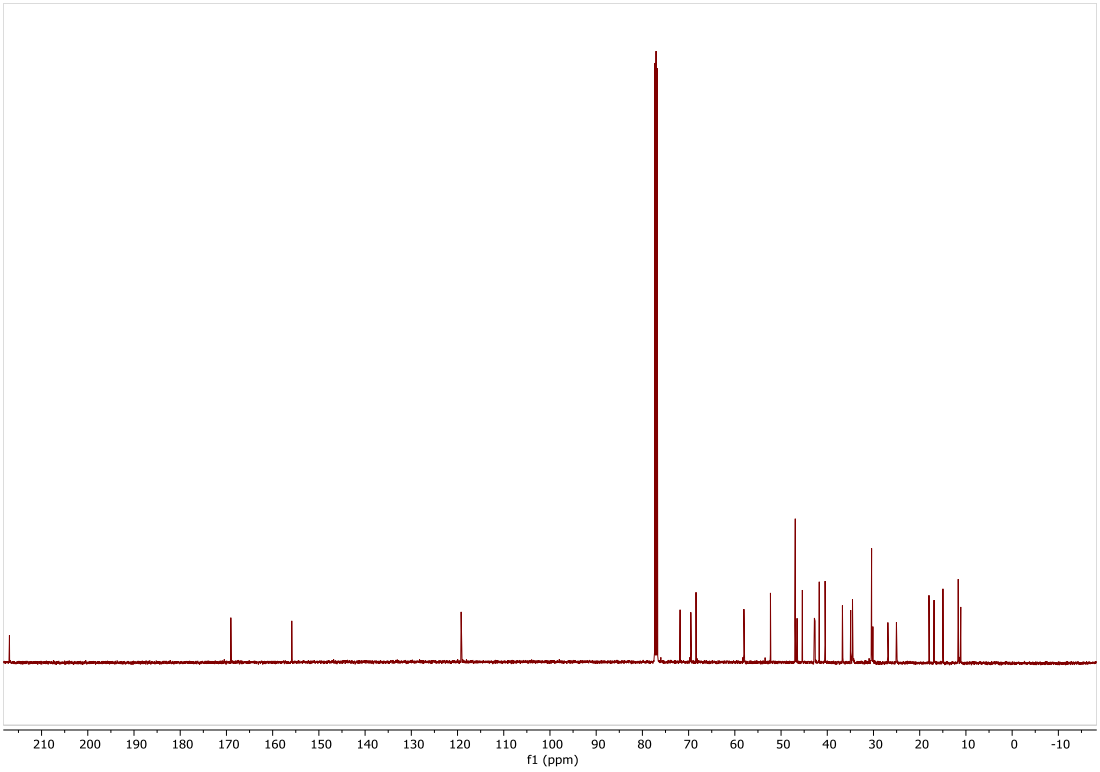

**Figure S31.** $^{1}$H NMR of **23** (500 MHz, $CDCl_3$)

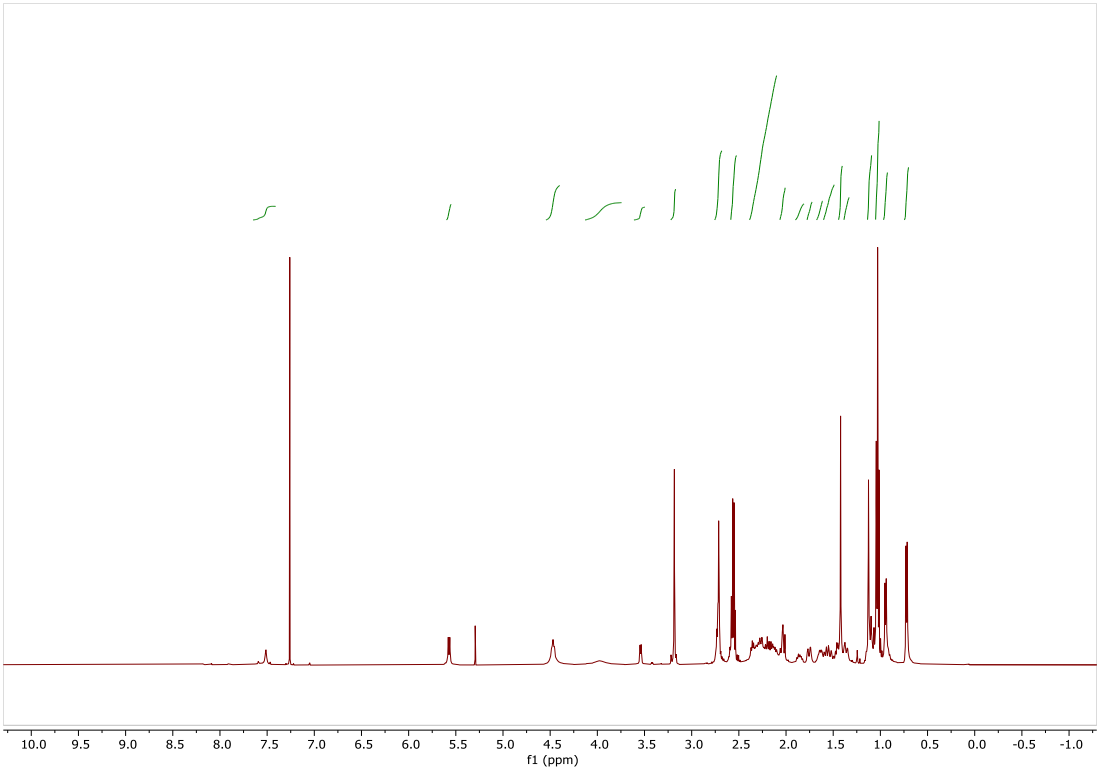


**Figure S32.** $^{13}$C NMR of **23** (500 MHz, $CDCl_3$)

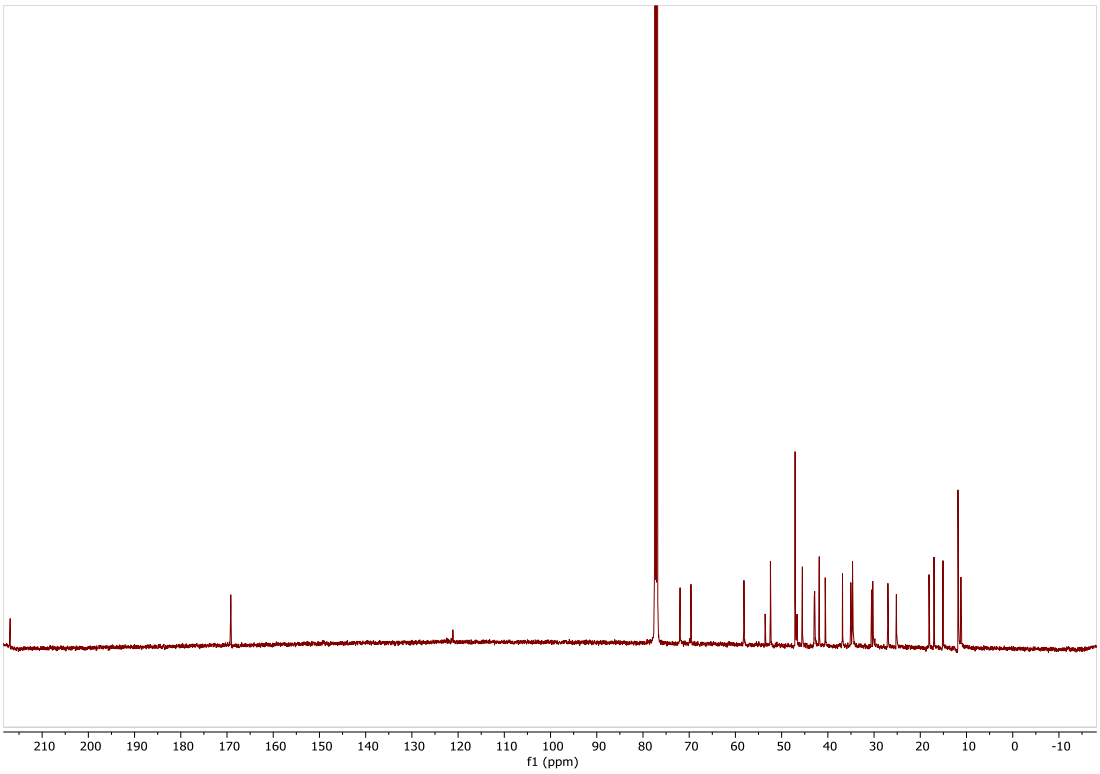

**Figure S33.** $^{1}$H NMR of **24** + trace $CH_2Cl_2$ (500 MHz, $CDCl_3$)

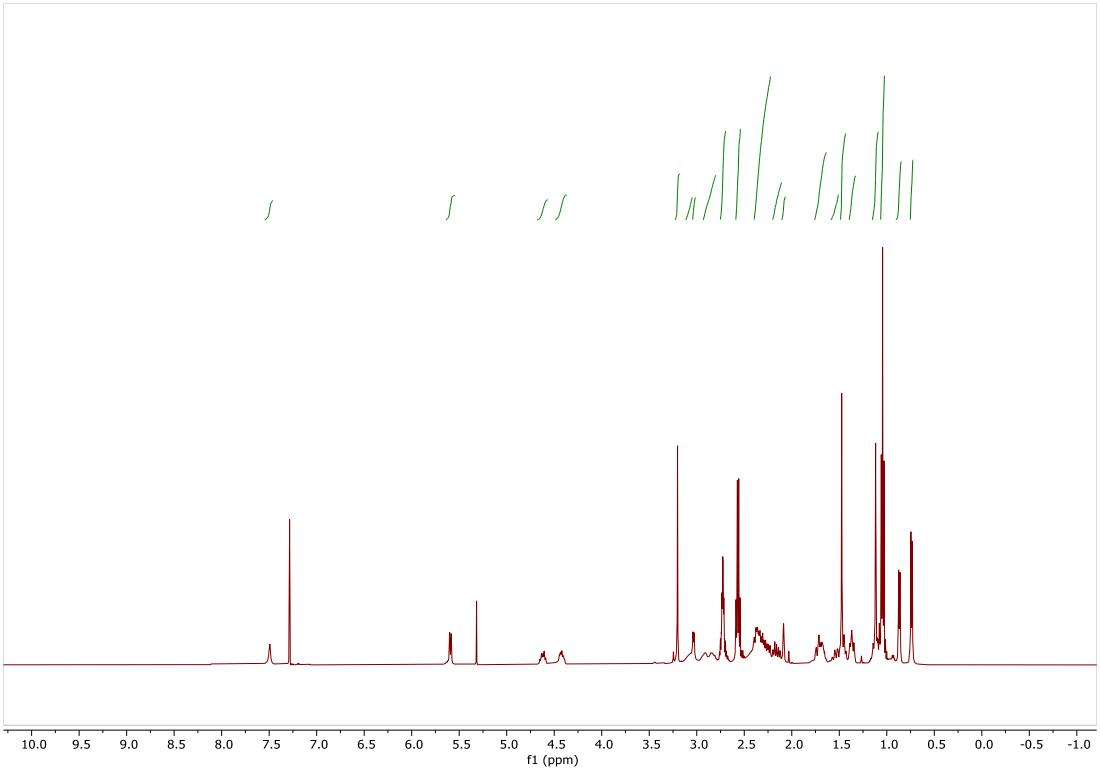


**Figure S34.** $^{13}$C NMR of **24** + trace $CH_2Cl_2$ (500 MHz, $CDCl_3$)

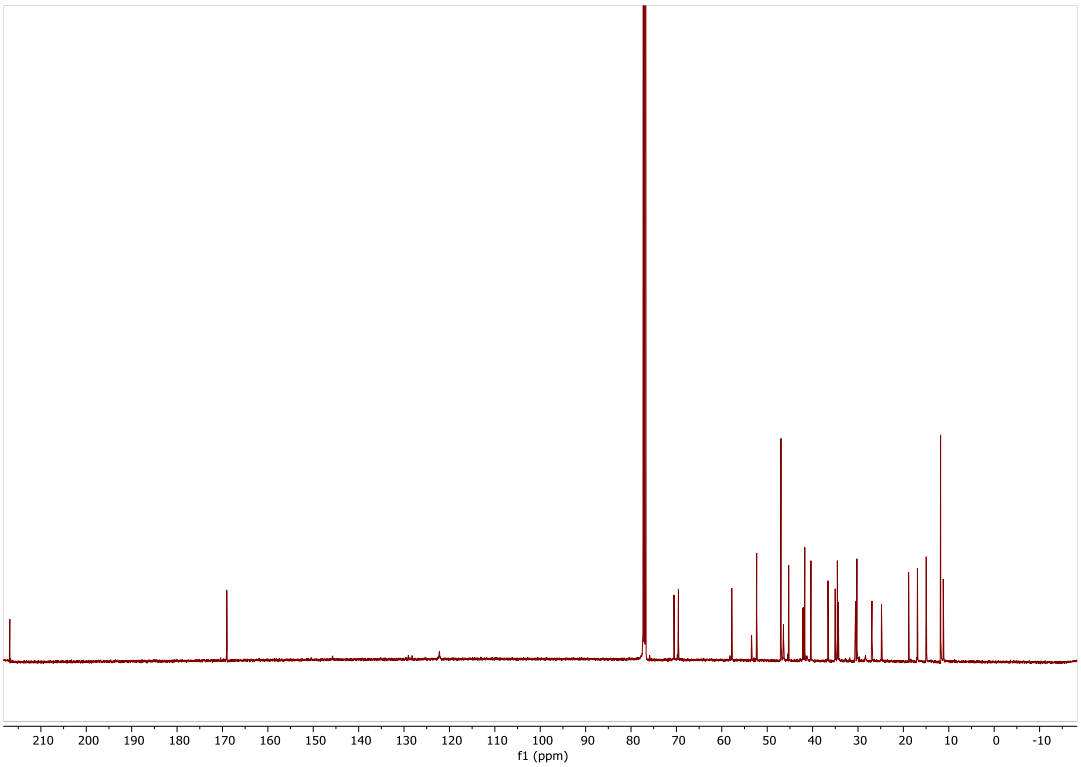

**Figure S35.** $^{1}$H NMR of **25** (500 MHz, $CDCl_3$)

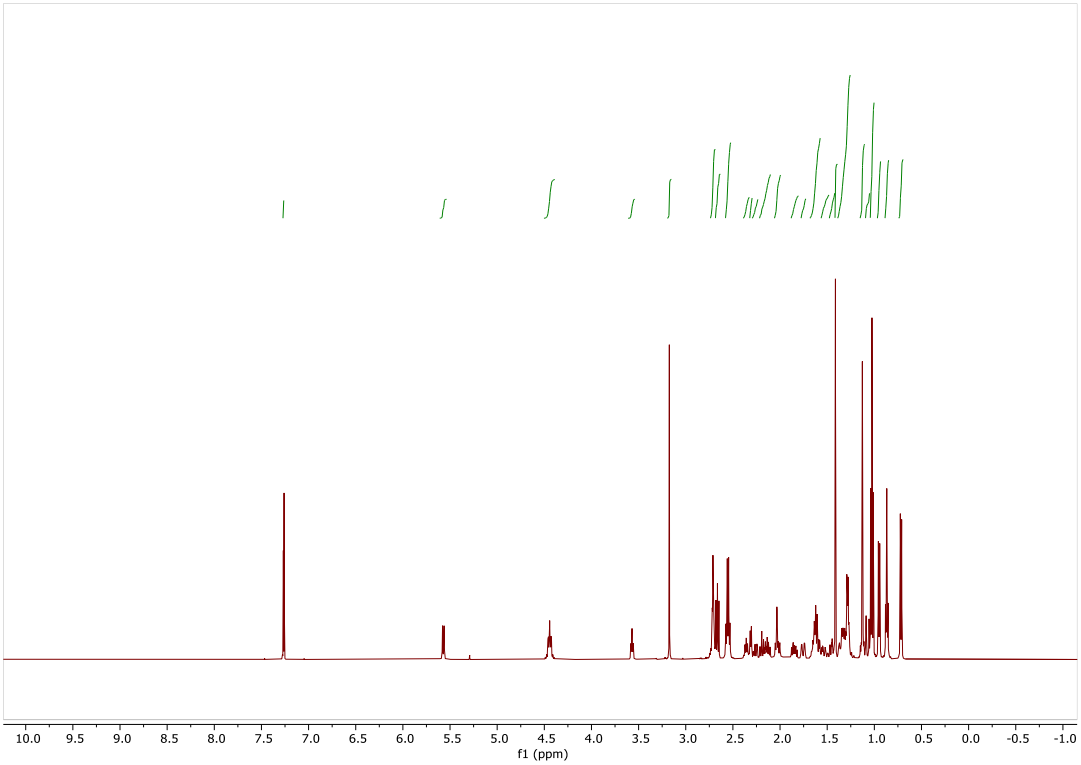


**Figure S36.** $^{13}$C NMR of **25** (500 MHz, $CDCl_3$)

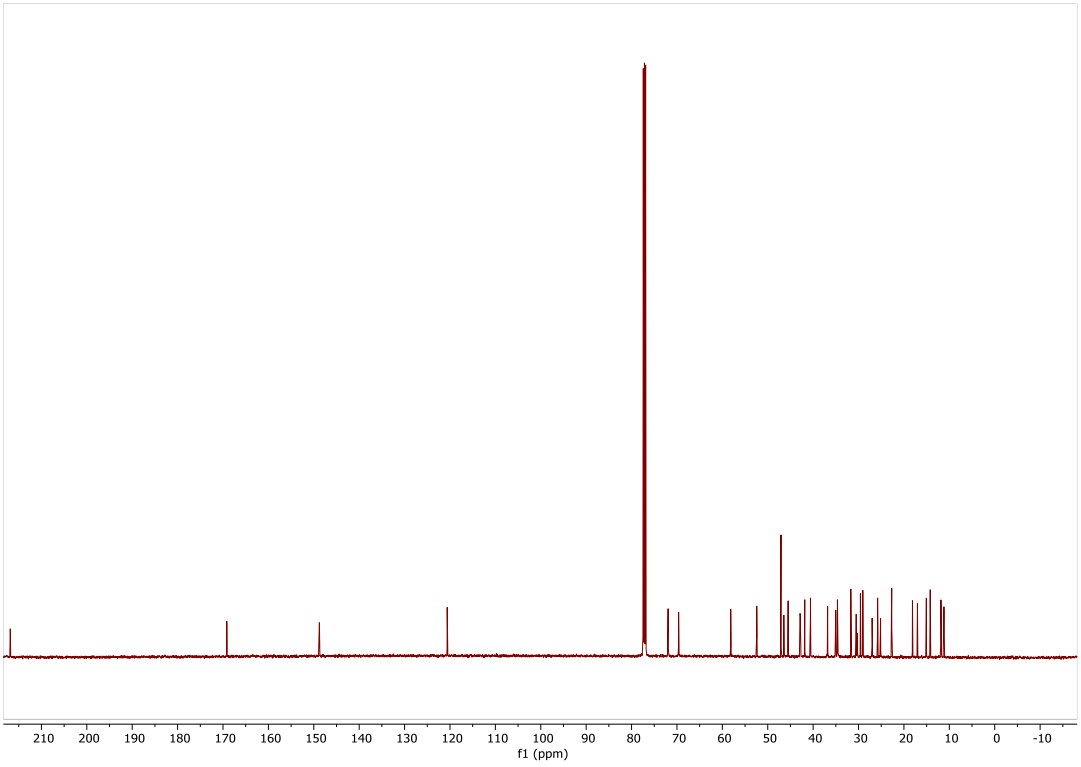

**Figure S37.** $^{1}$H NMR of **26** (500 MHz, $CDCl_3$)

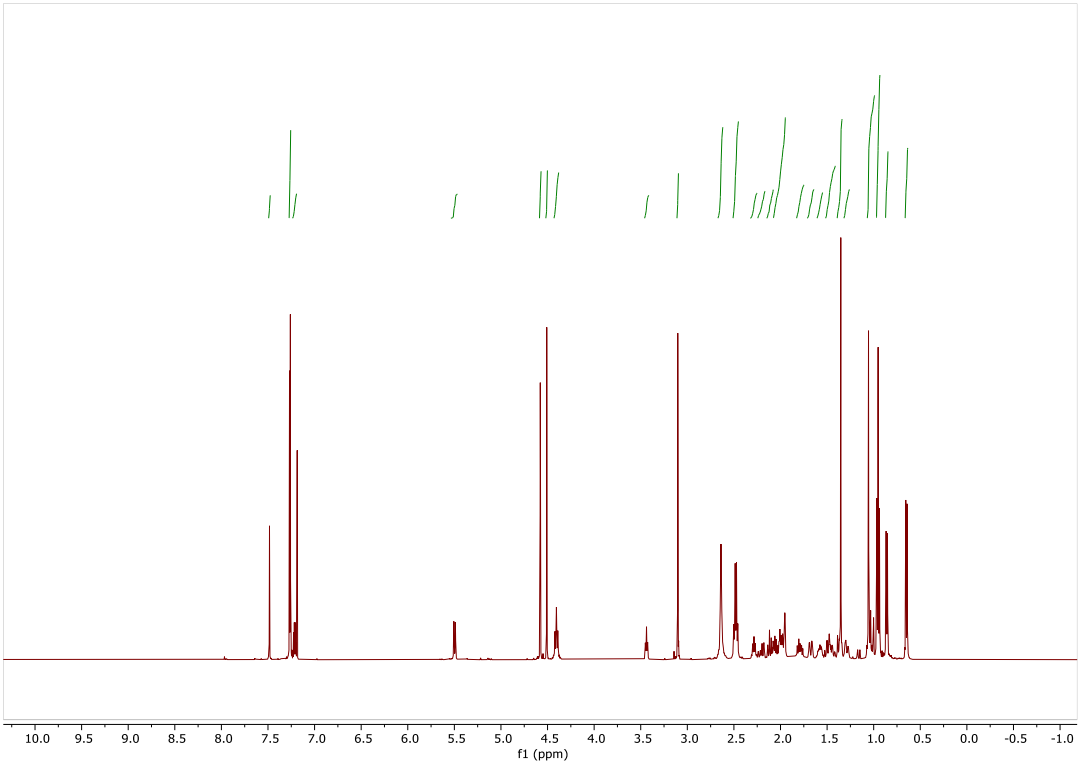


**Figure S38.** $^{13}$C NMR of **26** (500 MHz, $CDCl_3$)

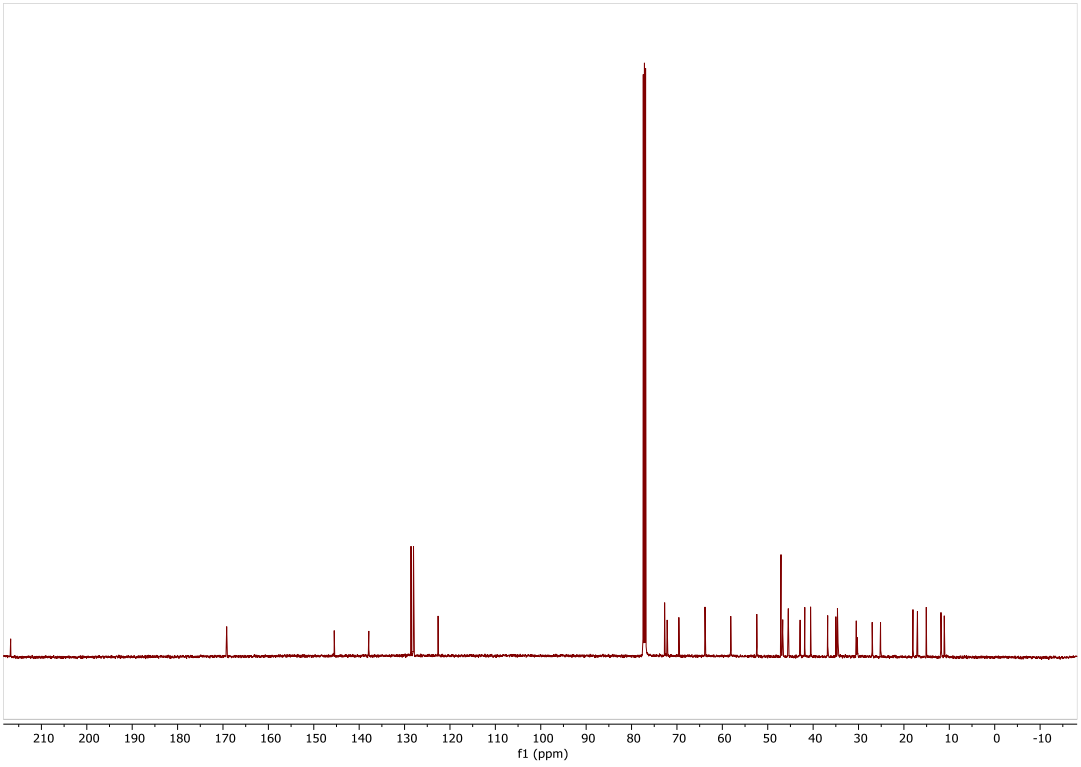

**Figure S39.** $^{1}$H NMR of **27** (500 MHz, $CDCl_3$)

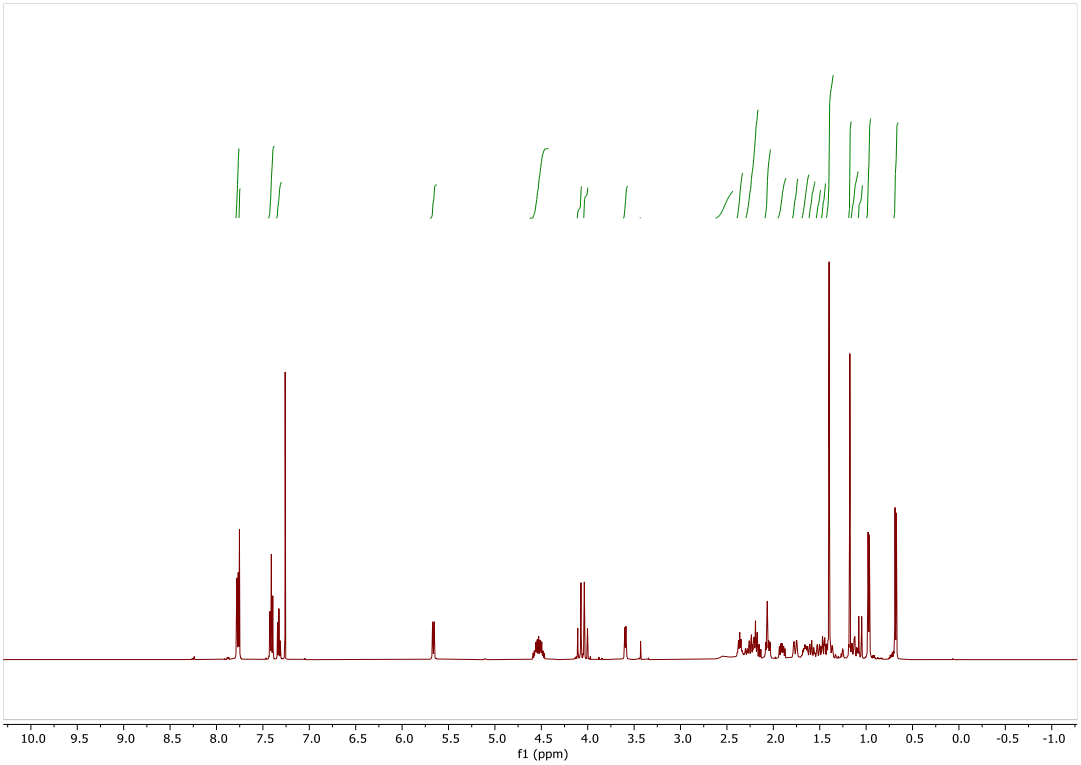


**Figure S40.** $^{13}$C NMR of **27** (500 MHz, $CDCl_3$)

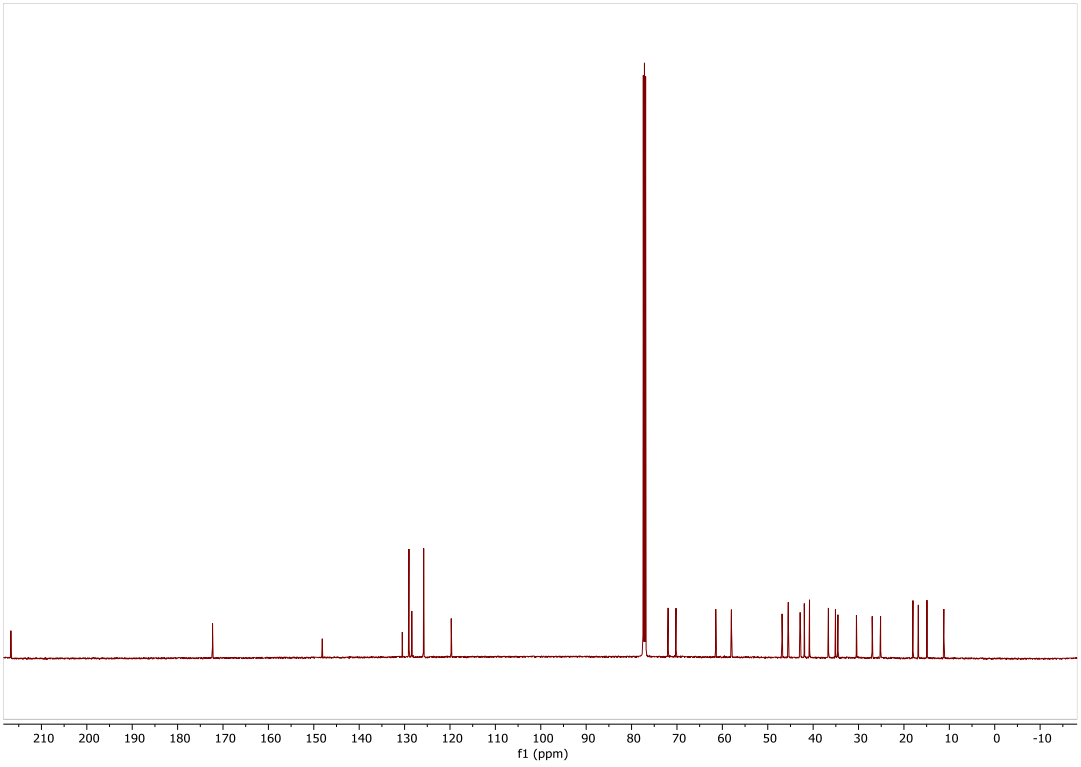

**Figure S41.** $^{1}$H NMR of **28** (500 MHz, $CDCl_3$)

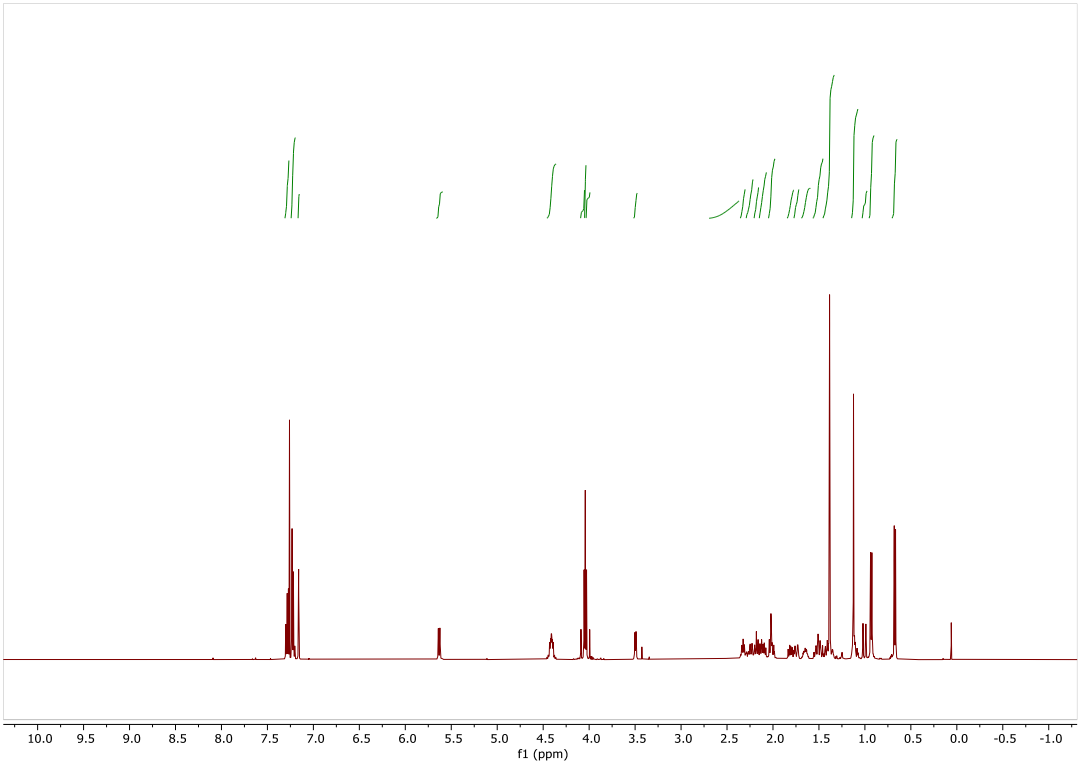


**Figure S42.** $^{13}$C NMR of **28** (500 MHz, $CDCl_3$)

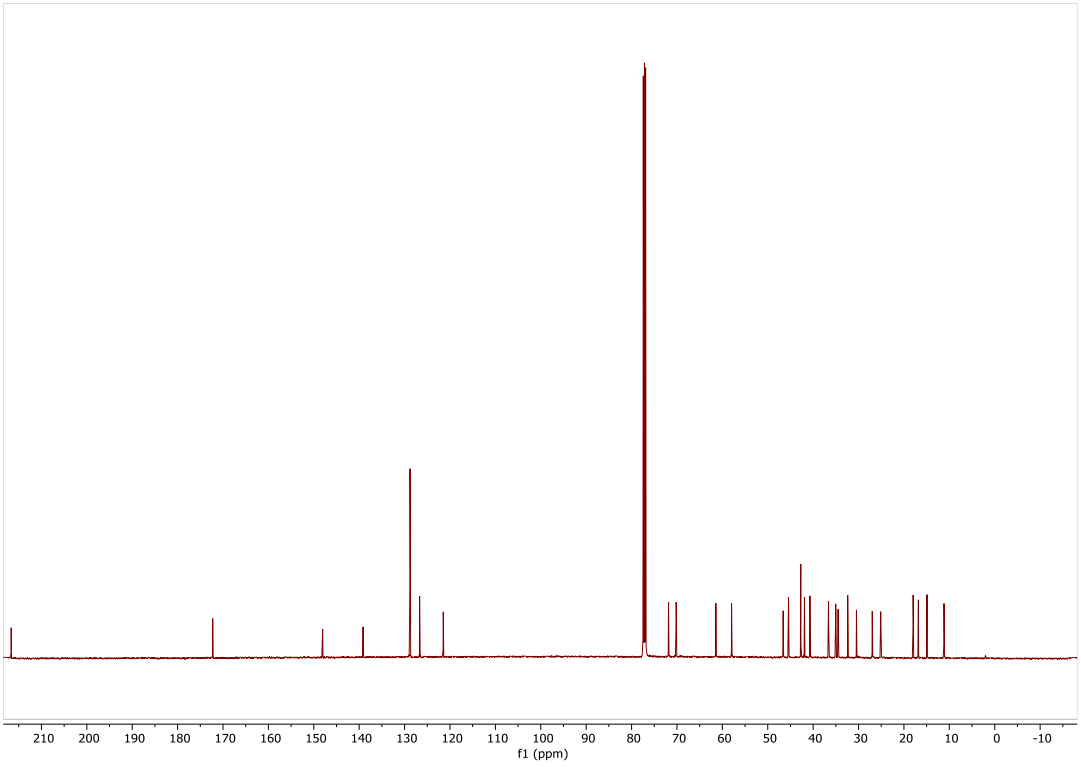

**Figure S43.** $^{1}$H NMR of **29** (500 MHz, $CDCl_3$)

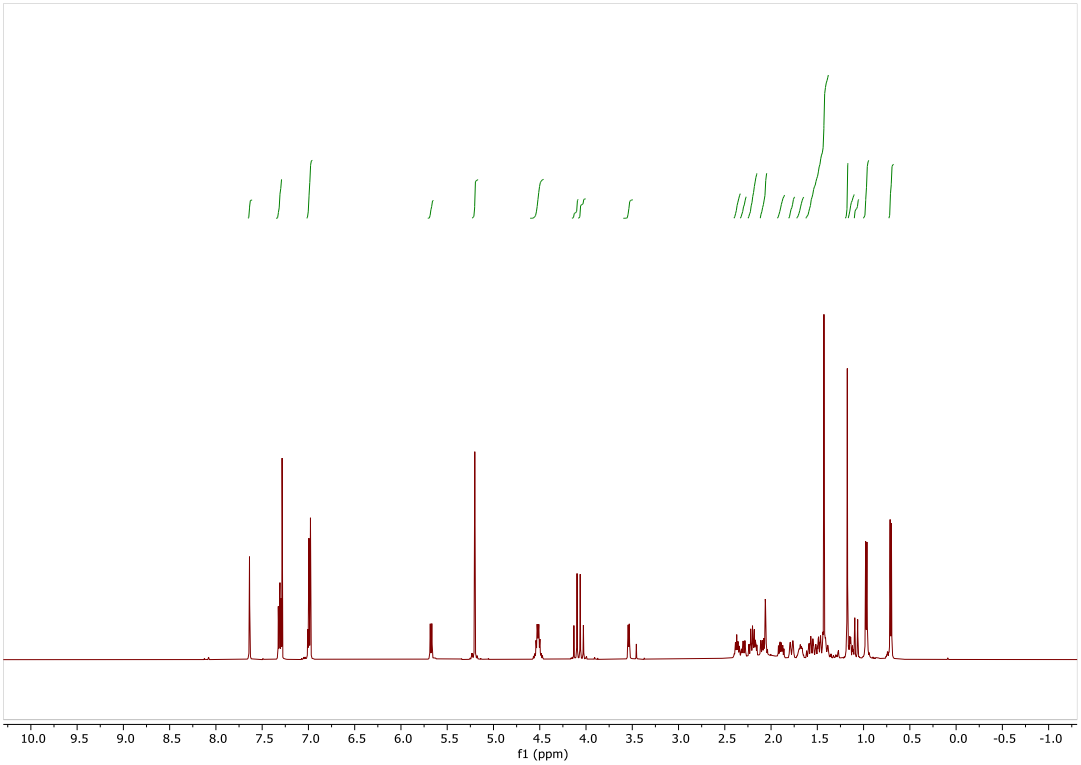


**Figure S44.** $^{13}$C NMR of **29** (500 MHz, $CDCl_3$)

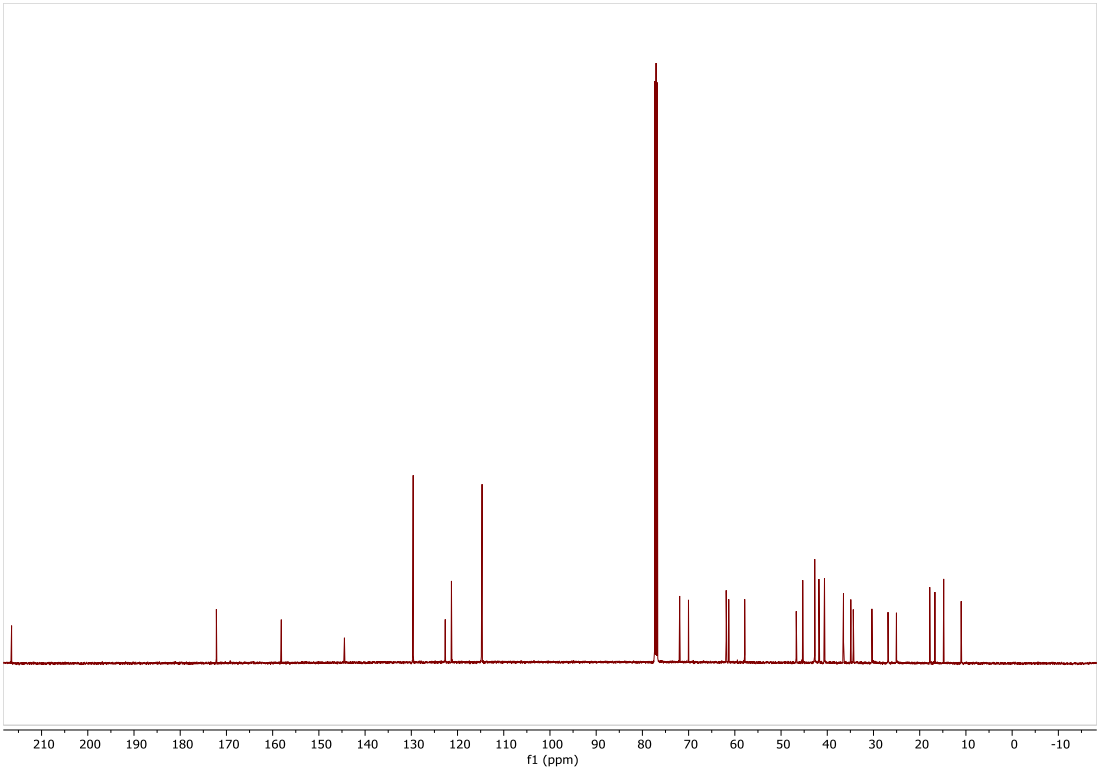

**Figure S45.** $^{1}$H NMR of **30** (500 MHz, $CDCl_3$)

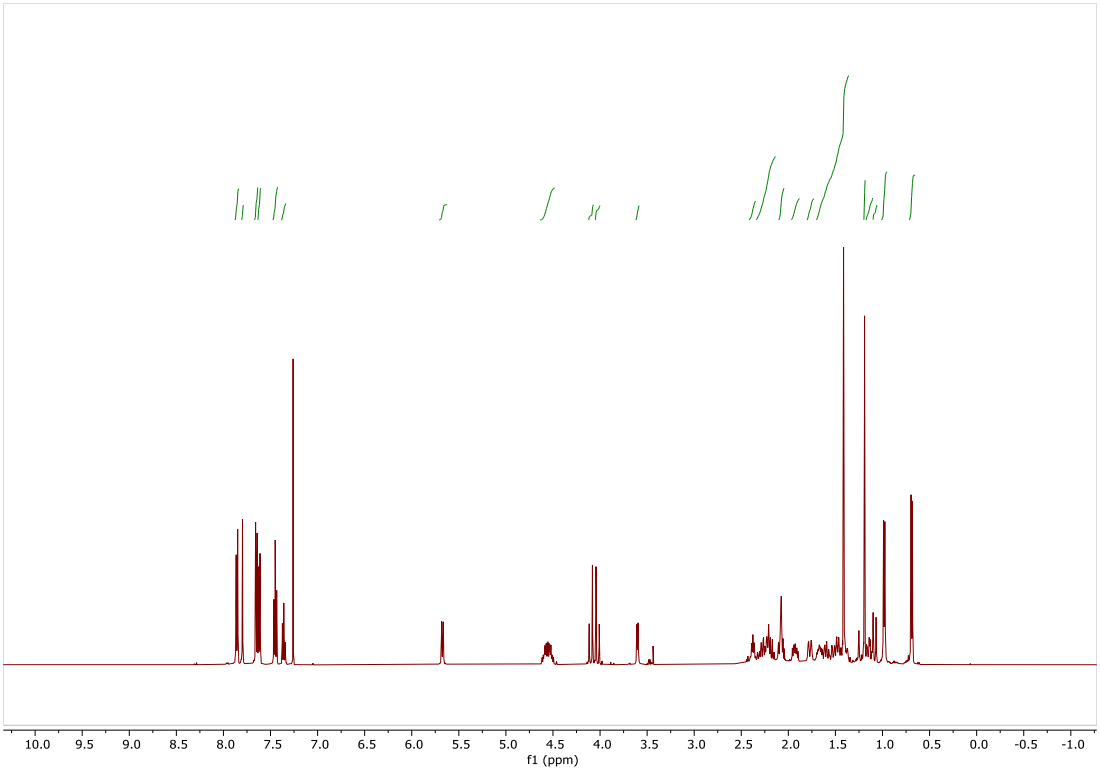


**Figure S46.** $^{13}$C NMR of **30** (500 MHz, $CDCl_3$)

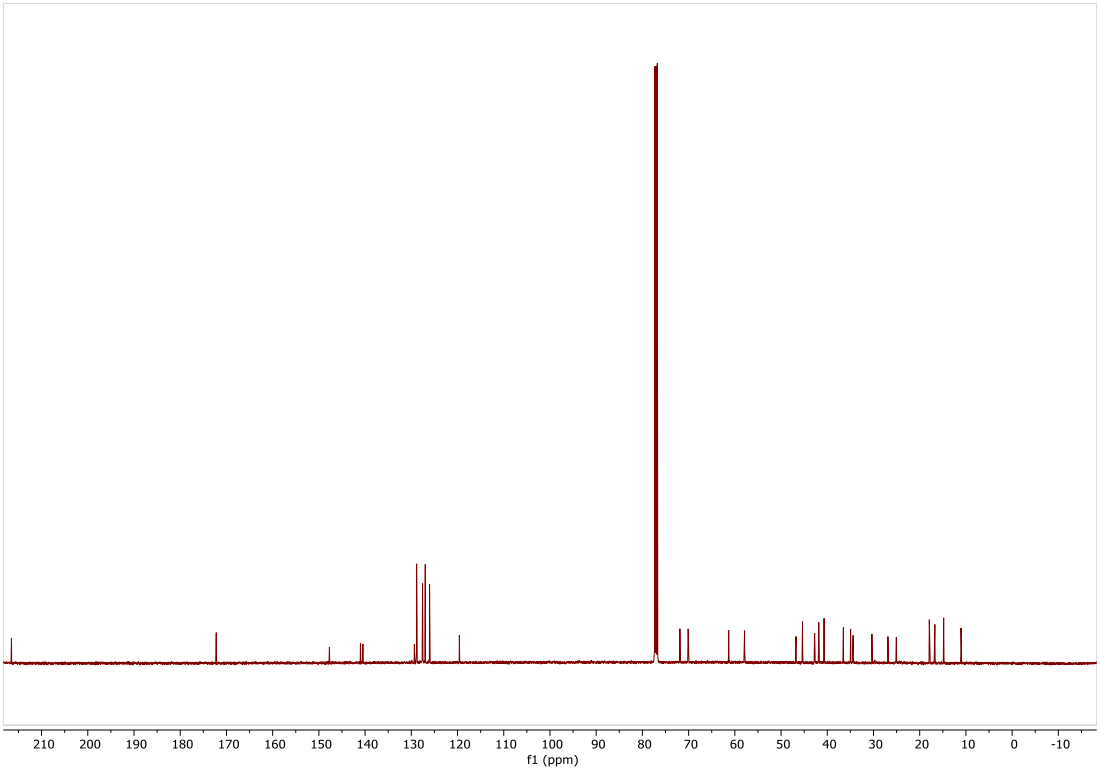

**Figure S47.** $^{1}$H NMR of **31** (500 MHz, $CDCl_3$)

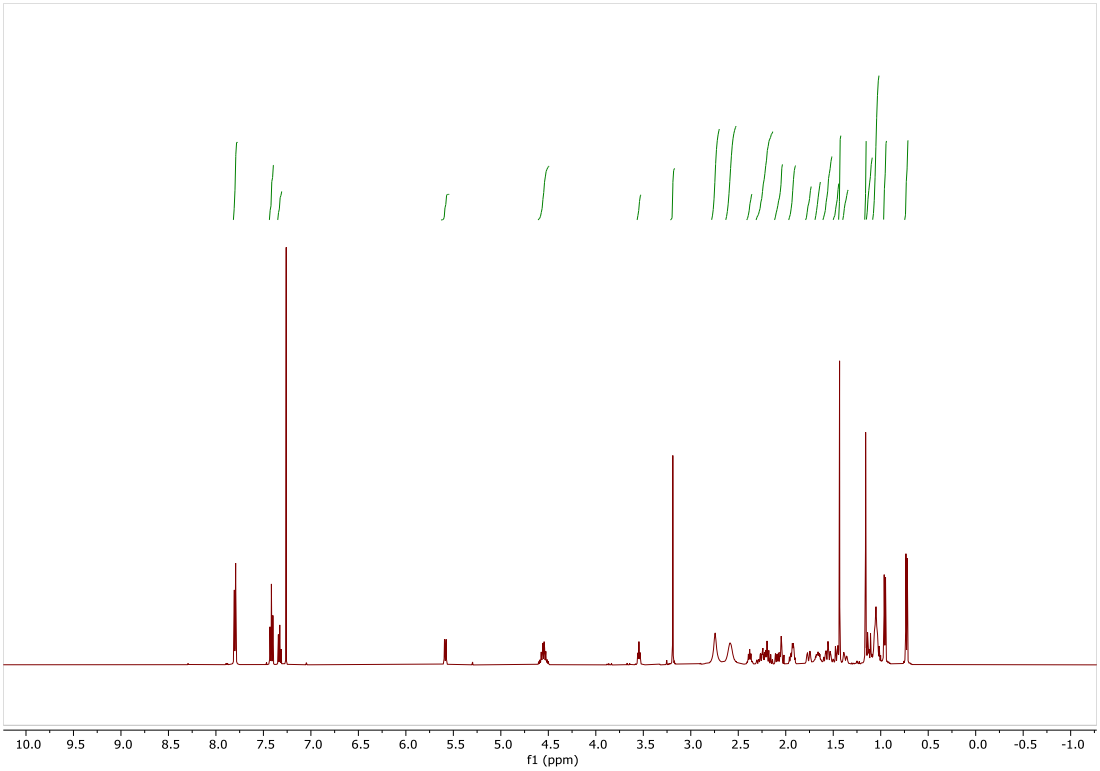


**Figure S48.** $^{13}$C NMR of **31** (500 MHz, $CDCl_3$)

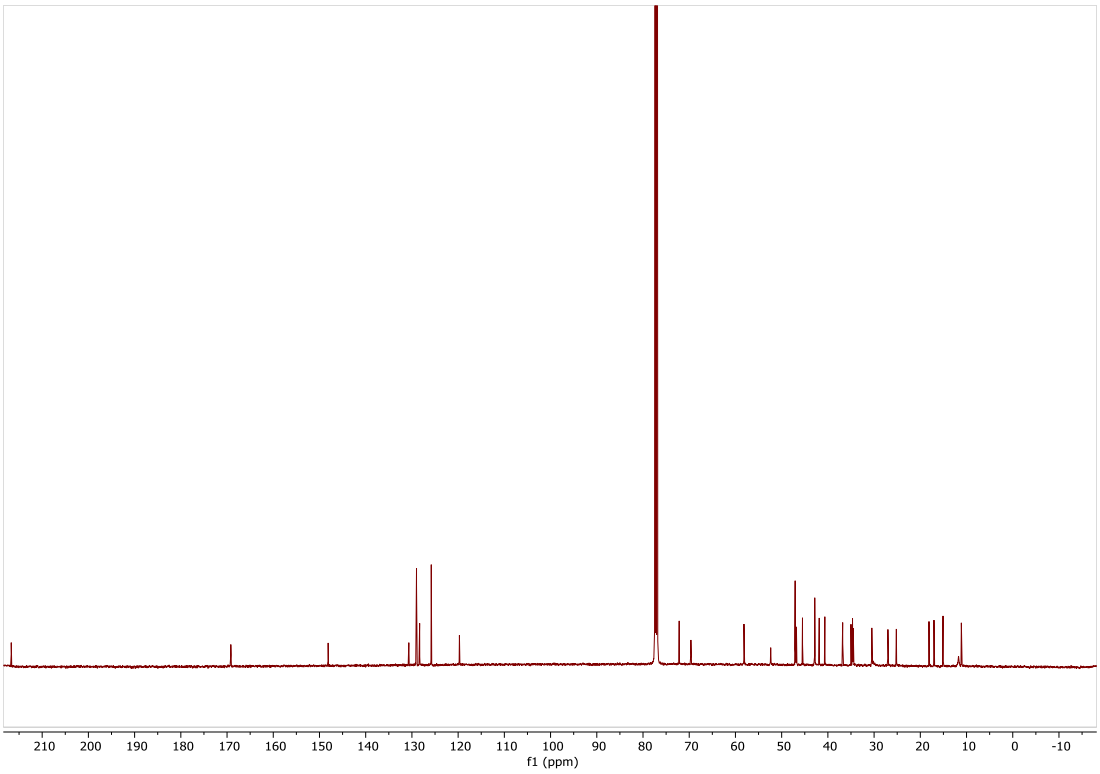

**Figure S49.** $^{1}$H NMR of **32** (500 MHz, $CDCl_3$)

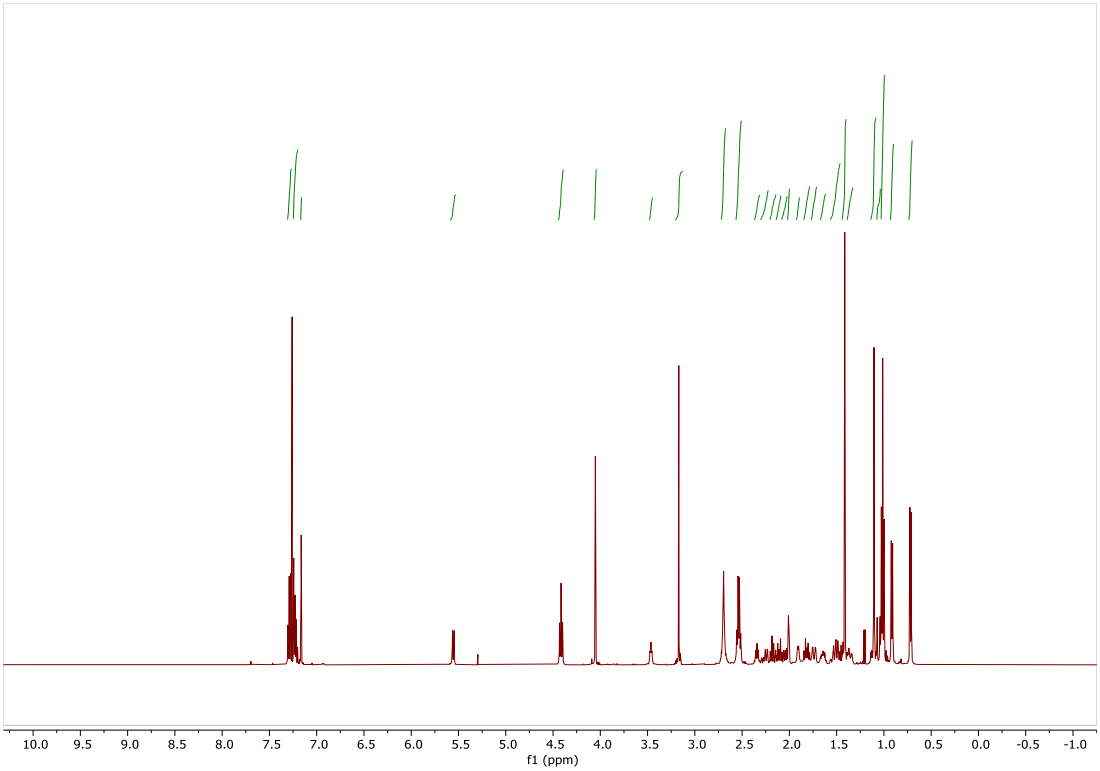


**Figure S50.** $^{13}$C NMR of **32** (500 MHz, $CDCl_3$)

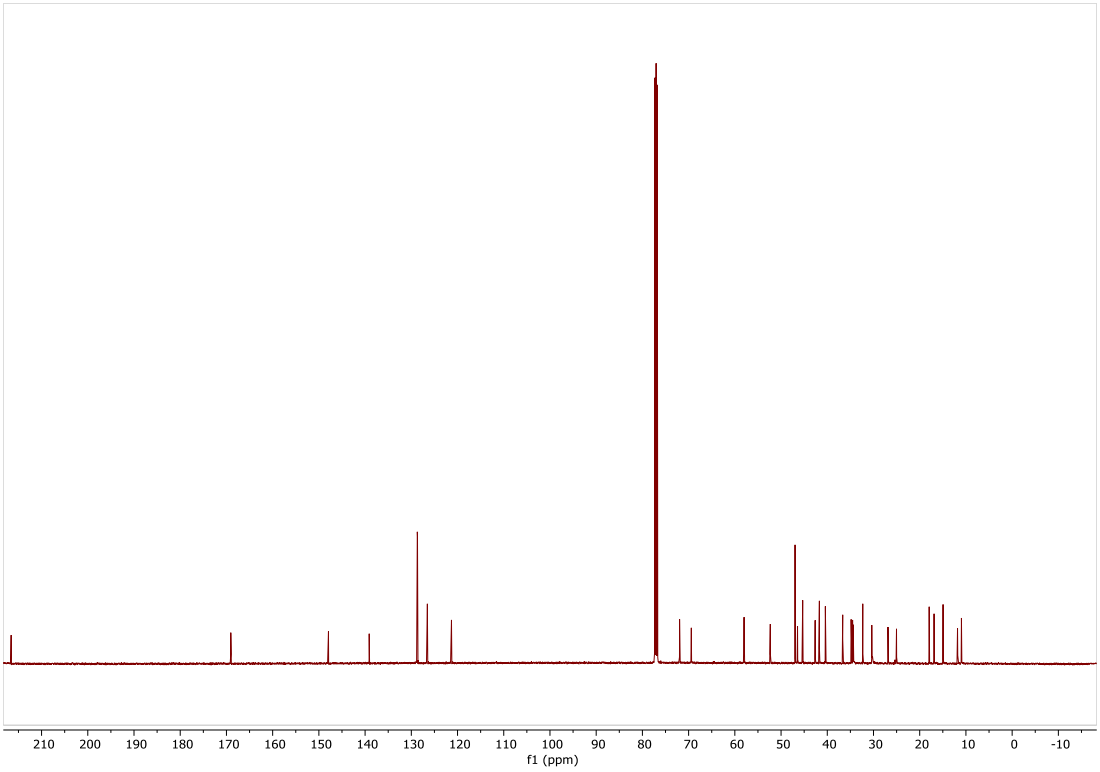

**Figure S51.** $^{1}$H NMR of **33** (500 MHz, $CDCl_3$)

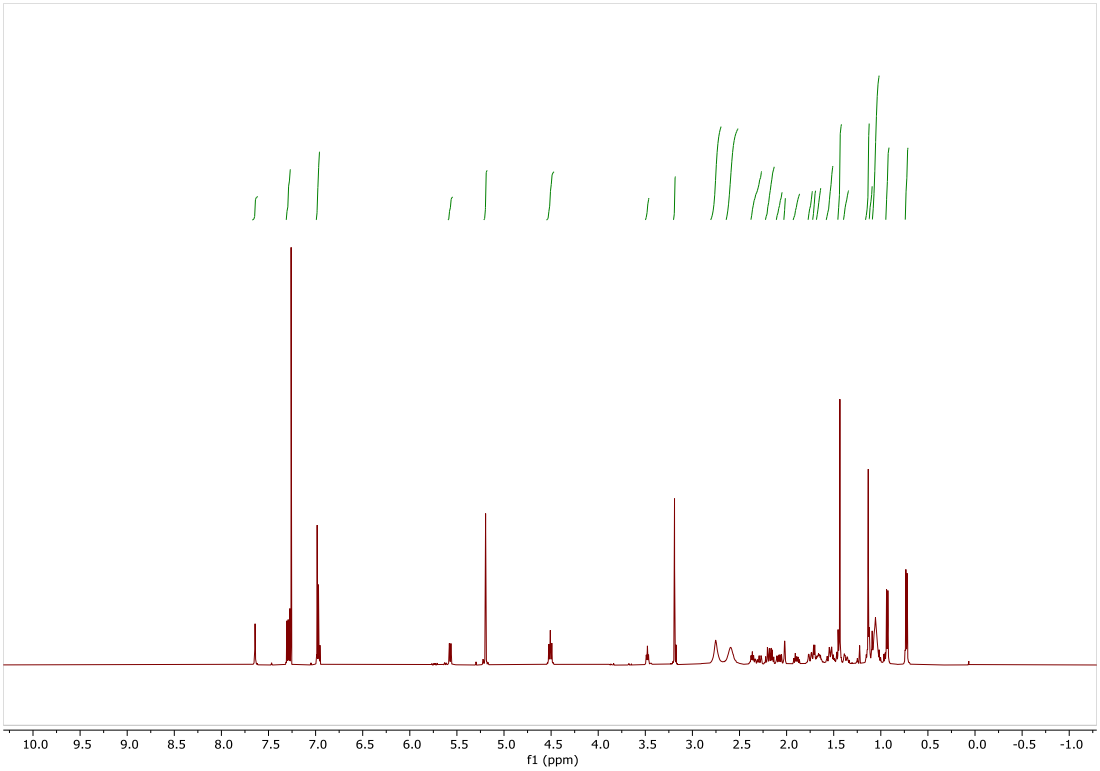


**Figure S52.** $^{13}$C NMR of **33** (500 MHz, $CDCl_3$)

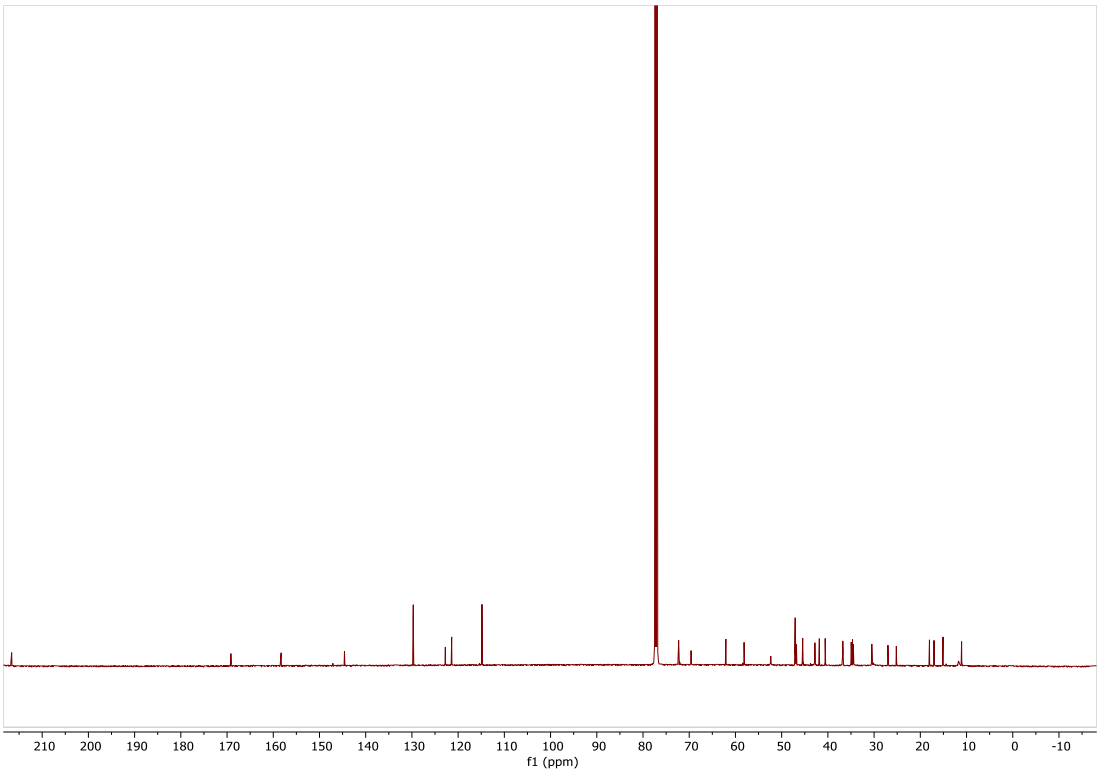

**Figure S53.** $^{1}$H NMR of **34** (500 MHz, $CDCl_3$)

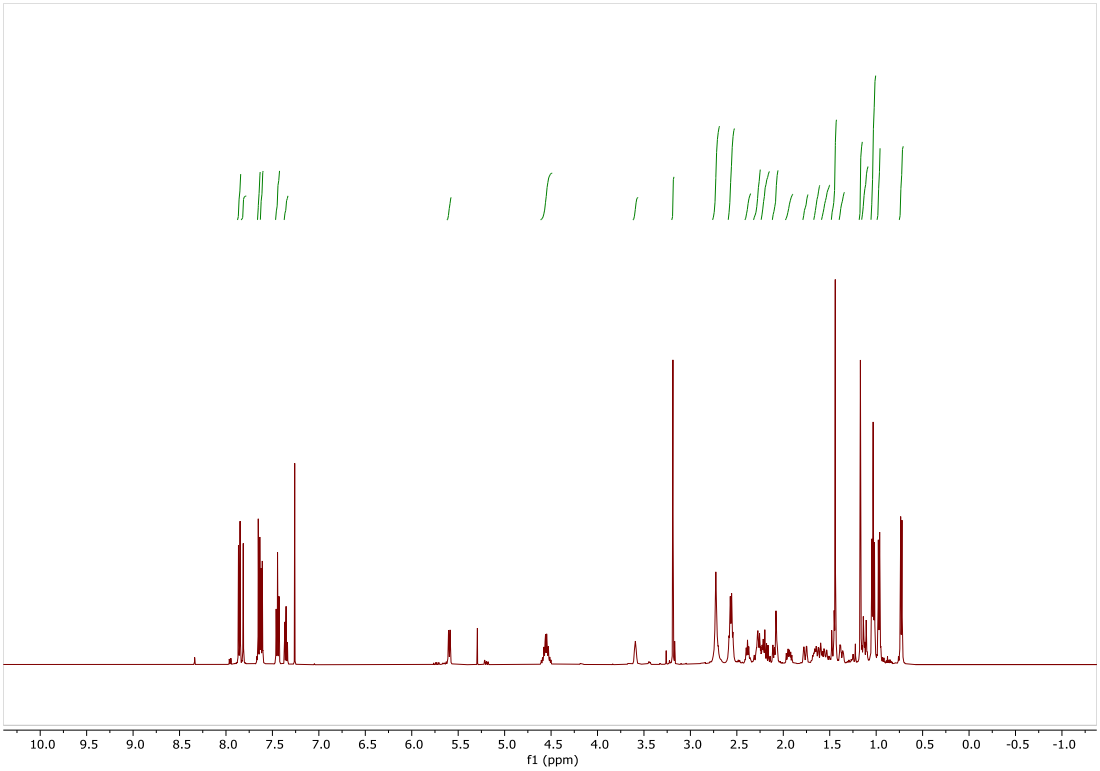


**Figure S54.** $^{13}$C NMR of **34** (500 MHz, $CDCl_3$)

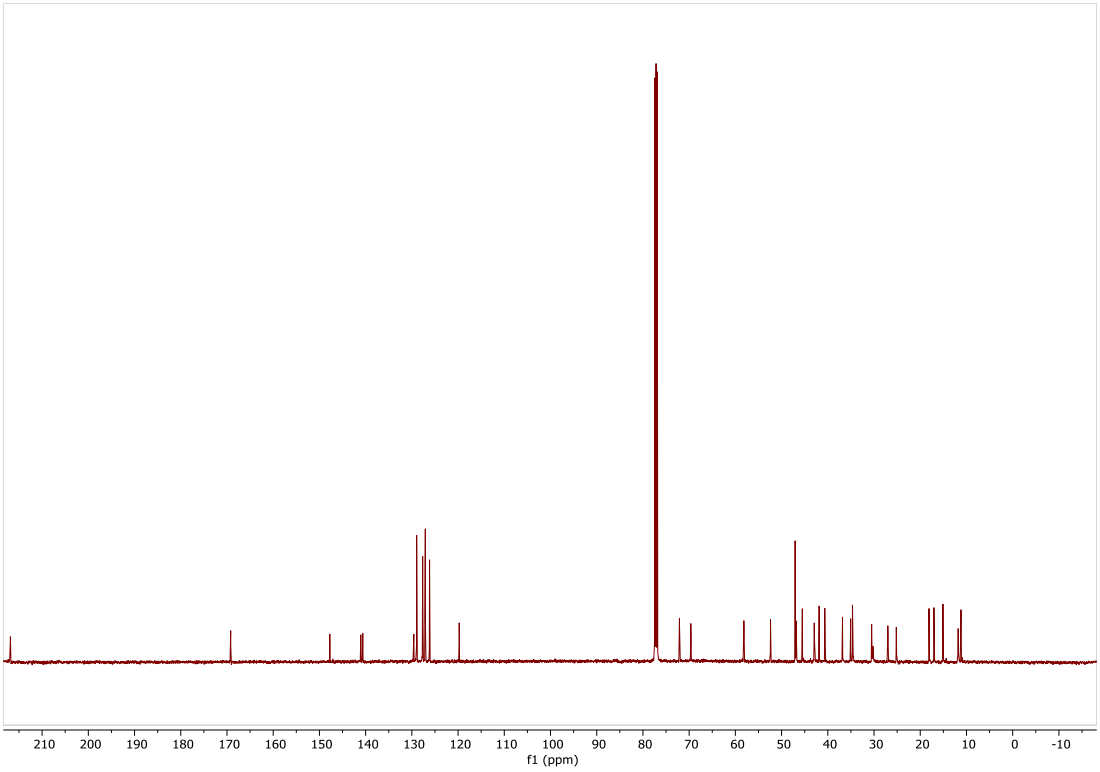

**Representative HPLC Traces for compounds 11-34**

The following chromatograms are all blank subtracted.

**Figure S55.** HPLC trace of **18**

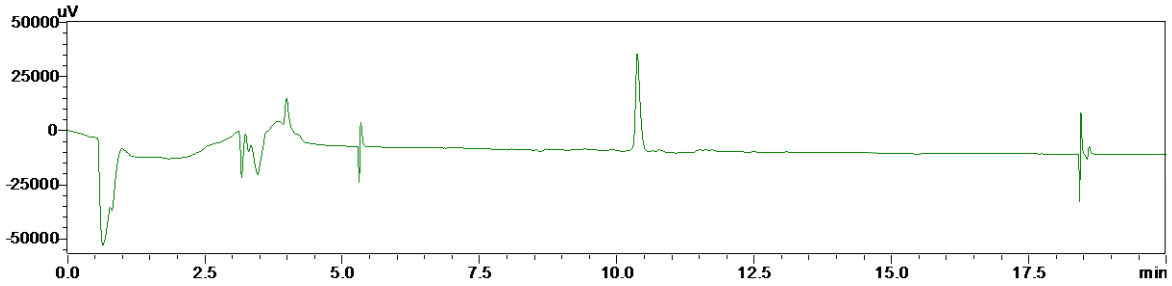


**Figure S56.** HPLC trace of **26**

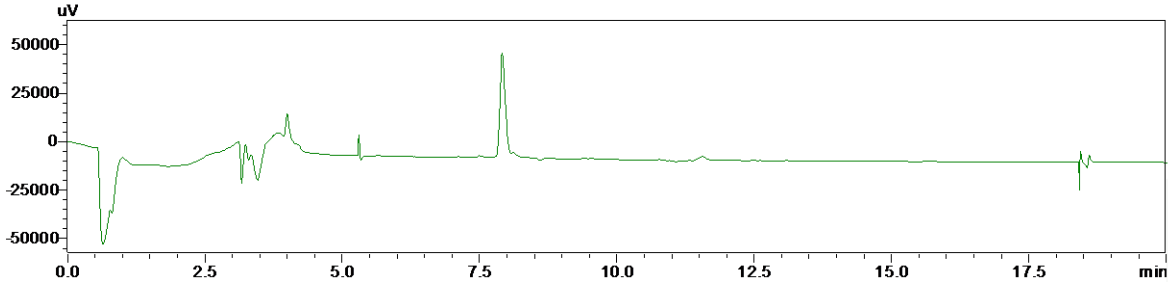


**Figure S57.** HPLC trace of **27**

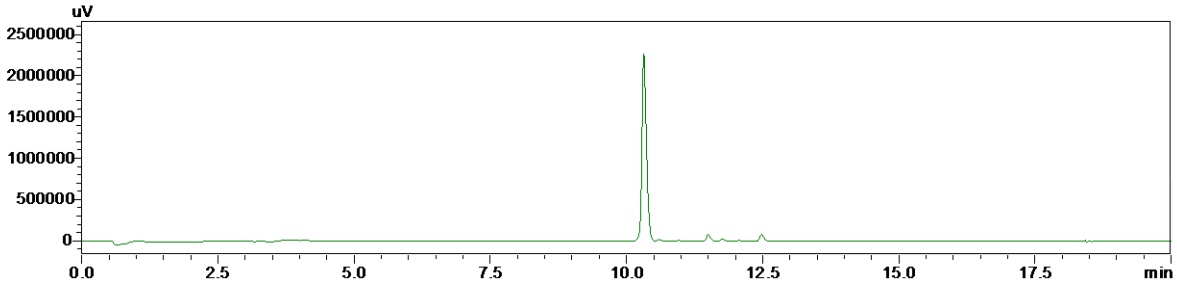


**Figure S58.** HPLC trace of **30**

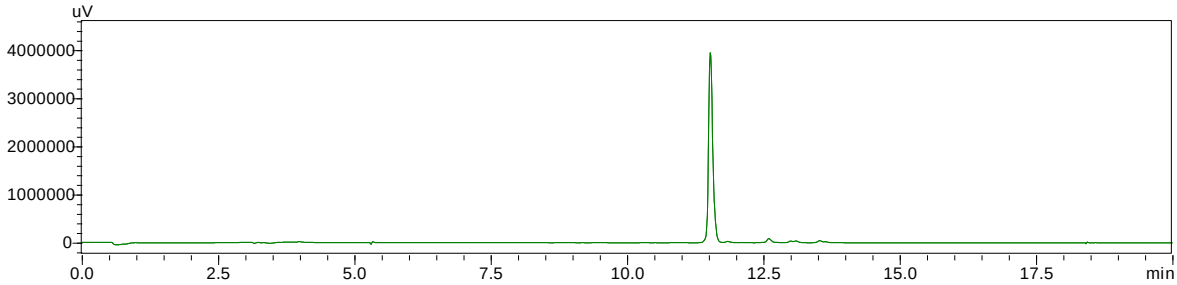


**Figure S59.** HPLC trace of **31**

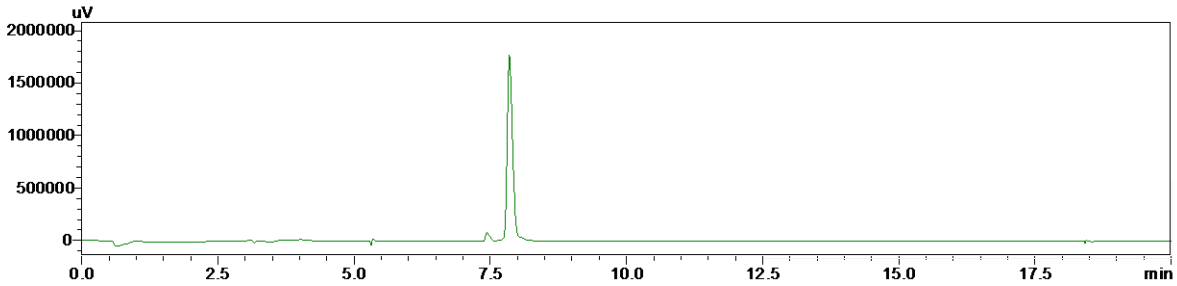


**Figure S60.** HPLC trace of **34**

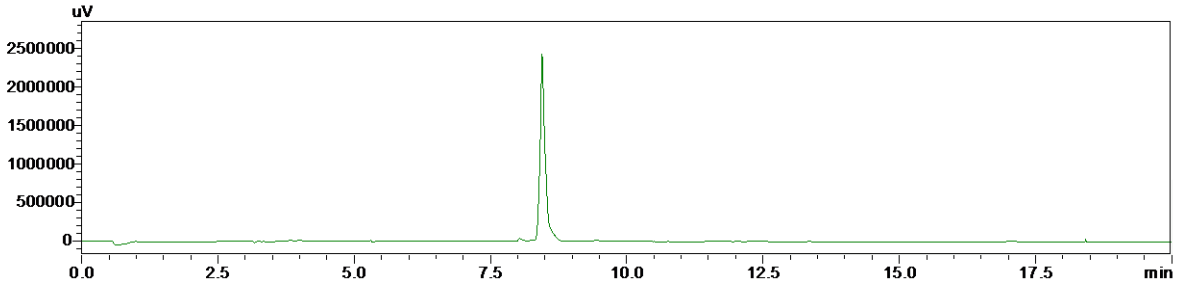

| **Test agents/** Control drugs | **E. faecalis** | **S. flexneri** | **S. enterica** | **A. baumannii** | **K. pneumoniae** | **P. aeruginosa** |
|---|---|---|---|---|---|---|
| **7** | >32 | >32 | >32 | >32 | >32 | >32 |
| **8** | >32 | >32 | >32 | >32 | >32 | >32 |
| **13** | >32 | >32 | >32 | >32 | >32 | >32 |
| **11** | >32 | >32 | >32 | >32 | >32 | >32 |
| **12** | >32 | >32 | >32 | >32 | >32 | >32 |
| **15** | >32 | >32 | >32 | >32 | >32 | >32 |
| **13** | >32 | >32 | >32 | >32 | >32 | >32 |
| **16** | >32 | >32 | >32 | >32 | >32 | >32 |
| **17** | >32 | >32 | >32 | >32 | >32 | >32 |
| **14** | >32 | >32 | >32 | >32 | >32 | >32 |
| **18** | >32 | >32 | >32 | >32 | >32 | >32 |
| **10** | >32 | >32 | >32 | >32 | >32 | >32 |
| **19** | >32 | >32 | >32 | >32 | >32 | >32 |
| **20** | >32 | >32 | >32 | >32 | >32 | >32 |
| **21** | >32 | >32 | >32 | >32 | >32 | >32 |
| **23** | >32 | 32 | >32 | >32 | >32 | >32 |
| **24** | >32 | 32 | >32 | >32 | >32 | >32 |
| **22** | >32 | >32 | >32 | >32 | >32 | >32 |
| **25** | >32 | >32 | >32 | >32 | >32 | >32 |
| **26** | >32 | >32 | >32 | >32 | >32 | >32 |
| **29** | >32 | >32 | >32 | >32 | >32 | >32 |
| **28** | >32 | >32 | >32 | >32 | >32 | >32 |
| **27** | >32 | >32 | >32 | >32 | >32 | >32 |
| **33** | >32 | >32 | >32 | >32 | >32 | >32 |
| **32** | >32 | >32 | >32 | >32 | >32 | >32 |
| **31** | >32 | >32 | >32 | >32 | >32 | >32 |
| **6** | >32 | >32 | >32 | >32 | >32 | >32 |
| **30** | >32 | >32 | >32 | >32 | >32 | >32 |
| **34** | >32 | >32 | >32 | >32 | >32 | >32 |
| Pleuromutilin | >32 | >32 | >32 | >32 | >32 | >32 |
| Tiamulin | >32 | >32 | >32 | >32 | >32 | >32 |

**Table S1. MICs (µg/mL) using serial dilution against less susceptible organisms.**

### 3.5.4 In silico methods for molecular docking and analysis

The *D. radiodurans* tiamulin-bound 50S ribosome structure (PDB ID: 1XBP)[37] was used for molecular docking. To more efficiently perform molecular docking, and in line with previous workflows,[20, 39] the 50S ribosome structure was clipped to a radius of 40 Å from the center of the tiamulin binding pocket. Redocking of tiamulin into this clipped structure was performed using GNINA[42] with a box coordinate of (182, -105, -144) and a box size of (30 by 30 by 30 Å) to confirm ability to replicate resolved tiamulin placement in the PTC binding pocket. Redocking of tiamulin into the clipped 50S ribosome structure yielded nine poses with a best pose RMSD value of 1.867, indicating reasonable alignment of tiamulin docking poses to crystallographic data. This molecular docking protocol was applied to all compounds docked in this study. For docking, compounds **1**, **2**, **11**-**34** were built using ChemDraw 23.1.1 software, saved as .pdb files using Chem3D 23.1.1 for import into GNINA, and the nonpolar hydrogens were removed. The other structures, *E. coli* (PDB IDs: 8CEU, 8CGV),[46] *S. aureus* (PDB ID: 5HL7),[47] and *T. thermophilus* (this study, EC126, EC136, EC148, EC158, and ECR14 containing derivatives **18**, **26**, **27**, **30**, and **31**) were aligned or superpositioned to the *D. radiodurans* 50S ribosome structure to utilize the same workflow. Each pose was evaluated both quantitatively and qualitatively using Schrodinger Maestro v2025-1.[48] Visualizations were performed in PyMOL v. 2.3.1 and 3.0.[49] From these poses, interaction fingerprints from Schrodinger [50, 51] were obtained and identified by contacts between heavy atoms involved in the same type of interaction (e.g., hydrogen bonds, π-π stacking, van der Waals interactions) within a distance threshold of 4.0 Å. These interactions were quantified using frequency heatmap graphs (**Figure S61**) to represent their aggregate occurrence and visualized to quantitatively identify new interactions (**Figures S62** and **S63**). As per the computational portion of the manuscript, *D. radiodurans* numbering is used in **Figures S61**–**S65**.

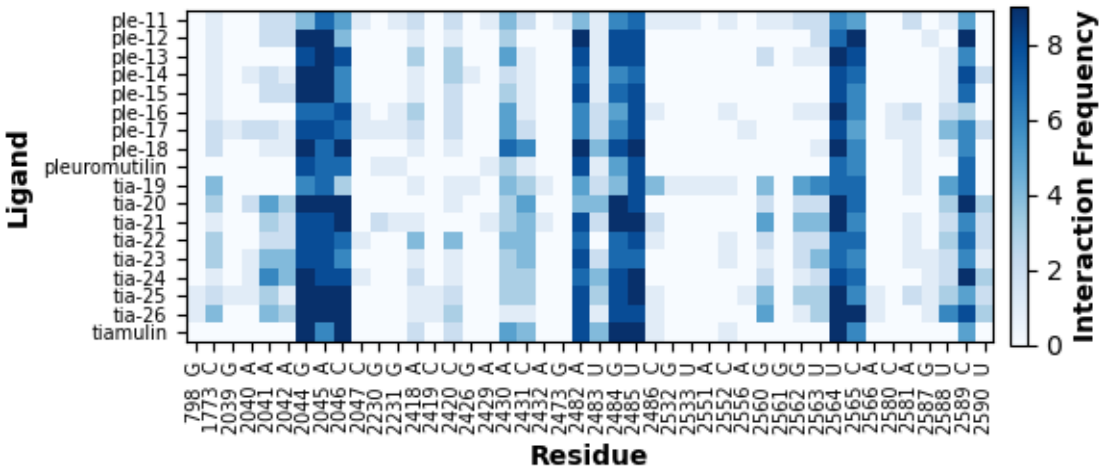


**Figure S61.** Heatmaps comparing the interaction fingerprints for docked poses of **11**–**26**, pleuromutilin (**1**), and redocked tiamulin (**2**) in 1XBP. Darker blue indicates higher interaction frequency of that interaction across poses.

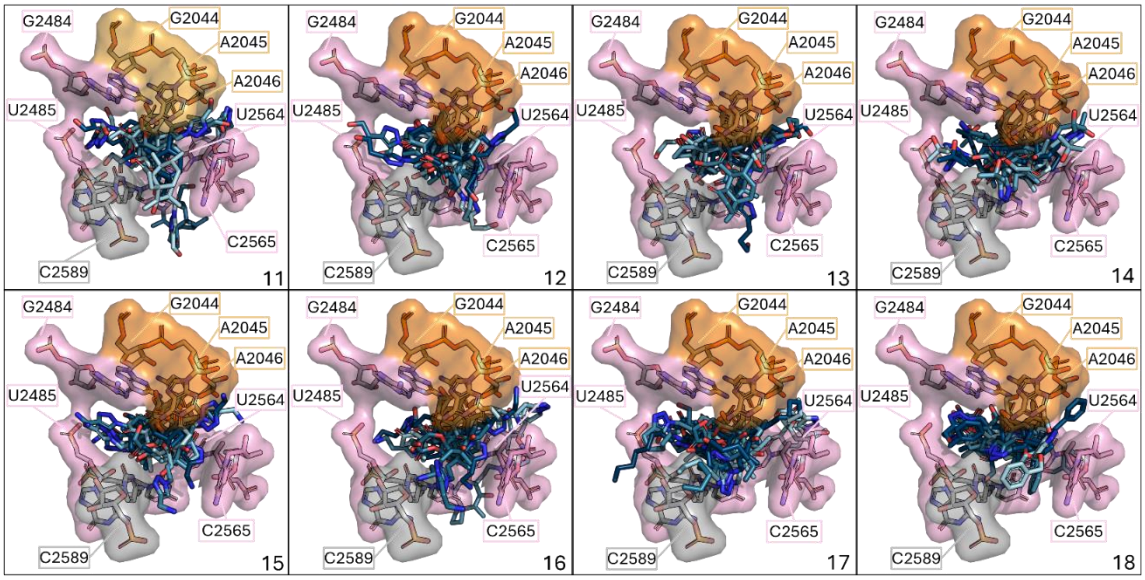


**Figure S62.** The nine poses for pleuromutilin derivatives **11**–**18** in docking into 1XBP[37] using GNINA.[42] Poses are shown as sticks and colored in a blue gradient where light blue is pose 1 and dark blue is pose 9. Nucleotides with high frequency interactions identified from the heatmap are

shown highlighted in pink for the A-site, orange for the P-site, and grey for all others as sticks and the surface.

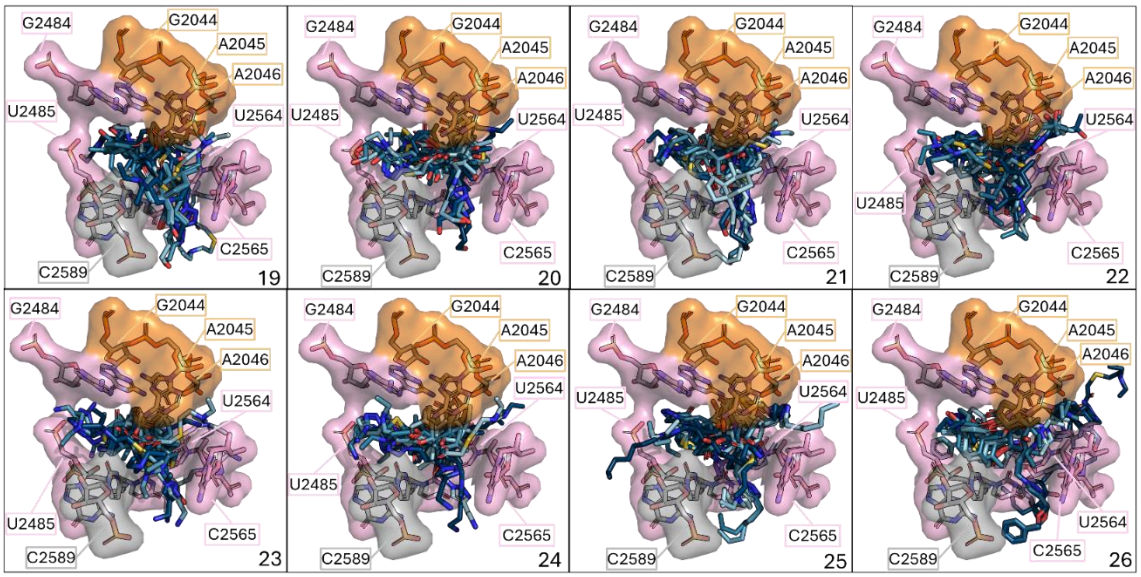


**Figure S63.** The nine docked poses for tiamulin derivatives **19**–**26** in 1XBP[37] using GNINA.[42] Poses are shown as sticks and colored in a blue gradient where light blue is pose 1 and dark blue is pose 9. Nucleotides with high frequency interactions identified from the heatmap are shown highlighted in pink for the A-site, orange for the P-site, and grey for all others as sticks and the surface.

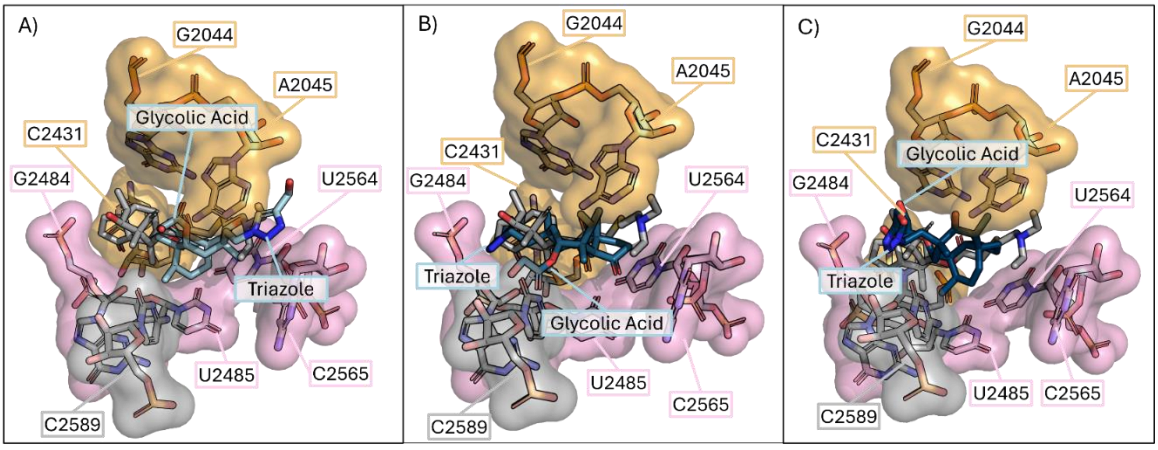

**Figure S64. Configurations of pleuromutilin derivatives docked to the 1XBP structure.** Three main configurations resulted from docking as shown by this example using **11**. The glycolic acid and triazole arms are labeled in blue. The crystal tiamulin is show as light grey sticks for reference. P-site nucleotides are shown in orange, A-site in pink, and all others in grey as sticks and surface. **A)** In pose 1, the glycolic acid arm points towards G2044 and A2045 and the triazole towards U2564 and U2565. **B)** In pose 6, the glycolic acid arm points towards C2589 and the triazole towards C2431. **C)** In pose 8, the glycolic acid points towards C2431, and the triazole towards G2484 and C2589.

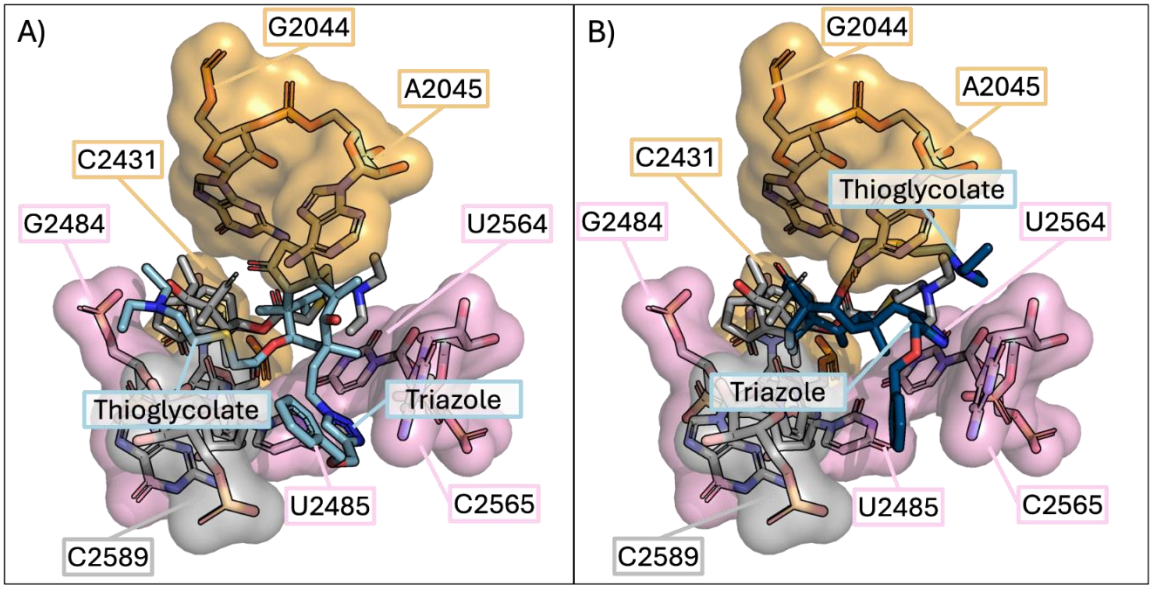


**Figure S65. Configurations of tiamulin derivatives docked to the 1XBP structure.** Two main configurations resulted from docking as shown by this example using **26**. The thioglycolate arm and triazole arm are labeled in blue. The crystal tiamulin is show as light grey sticks for reference. P-site nucleotides are shown in orange, A-site in pink, and all others in grey as sticks and surface. **A)** In pose 2, the thioglycolate points towards G2484 and the triazole points towards C2589 and C2565. **B)** In pose 7, the triazole arm still points towards C2565, but the thioglycolate arm towards G2044 and A2045.

### 3.5.5 Docking comparison of ribosome structures containing pleuromutilin derivatives

With the recent publication of additional pleuromutilin-bound ribosome crystal structures and our own co-crystallization efforts with top derivatives, we employed our docking analyses to assess structural variations and their impact on binding (**Figure S66**) and cavity size (**Figure S67**). *E. coli* numbering is used in this section for simplicity of comparison.

The binding pocket of *D. radiodurans* 50S ribosome (1XBP) is notably smaller due to the positioning of C2610 and A2062 (**Figure S67**). In this structure, the carbonyl group of C2610 is 6.3 Å from the C6-amino group of A2062, with U2585 and U2586 further constricting the cavity. Among the various structures, A2062 exhibits significant conformational diversity, adopting three distinct orientations across the ribosome structures. In *T. thermophilus* (PDB IDs: EC126, EC148, EC158, and ECR14), A2062 is parallel to the pocket, whereas in *D. radiodurans* (PDB ID: 1XBP),[37] *E. coli* (PDB IDs: 8CEU and 8CGV),[46] *S. aureus* (PDB ID: 5HL7),[47] *T. thermophilus* (PDB ID: EC136), it is perpendicular. Among the perpendicular conformations, the C6-amino group of A2062 points outward in *E. coli* (PDB IDs: 8CEU and 8CGV),[46] *S. aureus* (PDB ID: 5HL7),[47] *T. thermophilus* (PDB ID: EC136), but inward toward the pocket in *D. radiodurans* 50S ribosome (PDB ID: 1XBP).[37]

Pocket openness is further influenced by G2505 and G2061, with the distance between the phosphate backbone oxygen of G2505 and N7 of G2061 varying across structures. This distance is greatest in *D. radiodurans* 50S ribosome (PDB ID: 1XBP)[37] (7.2 Å) and smallest in *T. thermophilus* (PDB ID: EC158) (6.3 Å), correlating with A2062 conformations. Tighter G2505–G2061 interactions (6.3–6.7 Å) align with an A2062 parallel conformation, intermediate distances (6.7–7.0 Å) correspond to A2062 in a perpendicular but outward-facing orientation, and the largest

separation in *D. radiodurans* 50S ribosome (PDB ID: 1XBP)[37] coincides with A2062 flipped inward.

Another significant variation occurs at U2506, which orients downward in D. *radiodurans* 50S ribosome[37] but upward in all other structures. Despite this difference, docking suggests that interactions between the ligand and G2505/U2506 remain favorable due to steric constraints imposed by C2610, which shifts the binding pocket downward. Indeed, the orientation of C2610 (C2589 in *D. radiodurans* numbering) is in a different position and interferes with the natural extension of the triazole arms if the cocrystallized derivatives in this study. These observations underscore the dynamic flexibility of RNA binding pockets and highlight the importance of capturing conformational heterogeneity for drug discovery.

Docking of derivatives **18**, **26**, **27**, **30**, and **31** into ribosomes from *E. coli* (PDB IDs: 8CEU, 8CGV),[46] *S. aureus* (PDB ID: 5HL7),[47] and *T. thermophilus* (this study) revealed a conserved binding orientation but distinct positional variations relative to co-crystallized ligands. In *T. thermophilus* ribosome structures, consistently between docked poses the mutilin core is positioned between nucleotides A2505, U2609 and C2610 with the C20 triazole arm extending toward A2503 and A2062, inconsistent with crystallographic data. This is due to the conformational shift of C2610 downward instead of into the pocket creating extra space for the core to fit. The triazole arm either reoriented toward the mutilin core of the co-crystallized ligand or extended outward toward A2062, C2063, and A2439.

A2062 conformational changes influenced docking orientation as compared to D. *radiodurans* 50S ribosome. In *T. thermophilus* (PDB IDs: EC126, EC148, EC158, and ECR14), where A2062 adopts an open parallel conformation, the mutilin core docked closer to U2585 and C2586, enabling interactions between the triazole or terminal phenyl ring and A2062. Conversely,

in ribosomes from *E. coli* (PDB IDs: 8CEU, 8CGV),[46] *S. aureus* (PDB ID: 5HL7),[47] and *T. thermophilus* (PDB ID: EC136), A2062 assumes a closed perpendicular conformation, reducing steric accessibility and shifting the mutilin core toward the terminal phenyl group of the co-crystallized ligand. In tiamulin derivatives, a similar trend emerged: when A2062 was open, the triazole arm oriented toward U2506 and the thioglycolate arm toward A2062; when closed, the mutilin core shifted closer to the co-crystallized ligand, with the thioglycolate arm extending toward U2609 and the triazole arm toward A2503 and G2061.

While the docking results do not fully align with the observed binding conformations in the EC series structures, they still provide valuable insights into key interactions that stabilize ligand positioning. Docking initially served to guide the synthesis campaign by identifying promising structures and novel derivatization sites, ultimately leading to successful optimization and compounds with competitive MIC values based on at the time available structural information. Notably, the docking highlights the role of A2062 flexibility in dictating ligand orientation and the importance of G2505–G2061 spacing in pocket accessibility. Additionally, docking correctly predicts trends in triazole and thioglycolate arm positioning relative to A2062 and U2506, reinforcing the structural determinants of binding. These findings suggest that while static docking methods may not fully capture the range of RNA conformational changes observed in crystal structures, they remain useful for identifying key binding interactions and rationalizing ligand modifications. Critically, the interplay of the EC series introducing a novel binding pocket conformation with computational docking protocols offers new opportunities for targeting the flexible conformational landscape of the PTC pocket in antibiotic design.

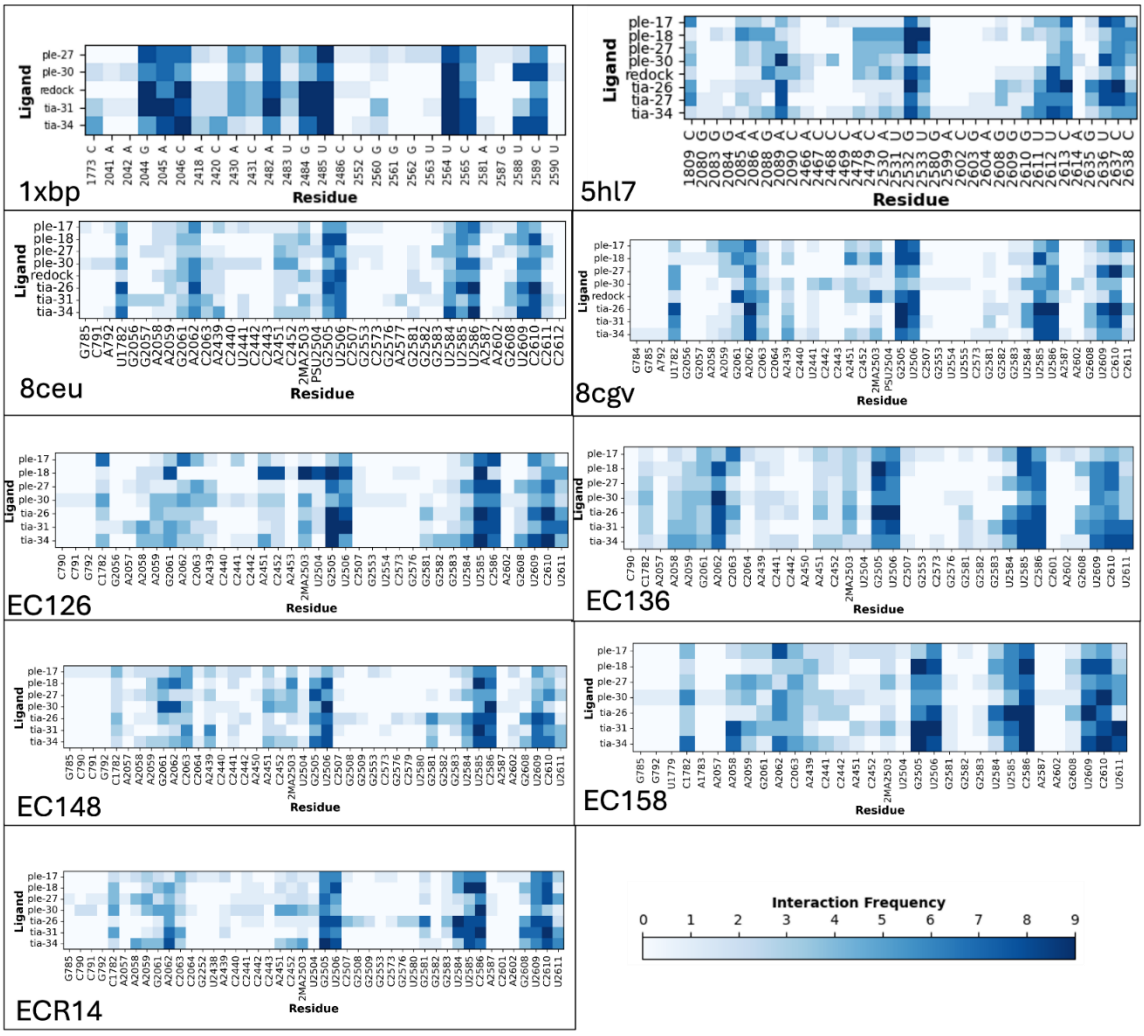


**Figure S66.** Heatmaps comparing interacting residue fingerprints of docked poses from each ligand into each relevant structure. The shade of each individual square reflects the frequency of interaction of each dock comprising 9 poses output by GNINA.[42]

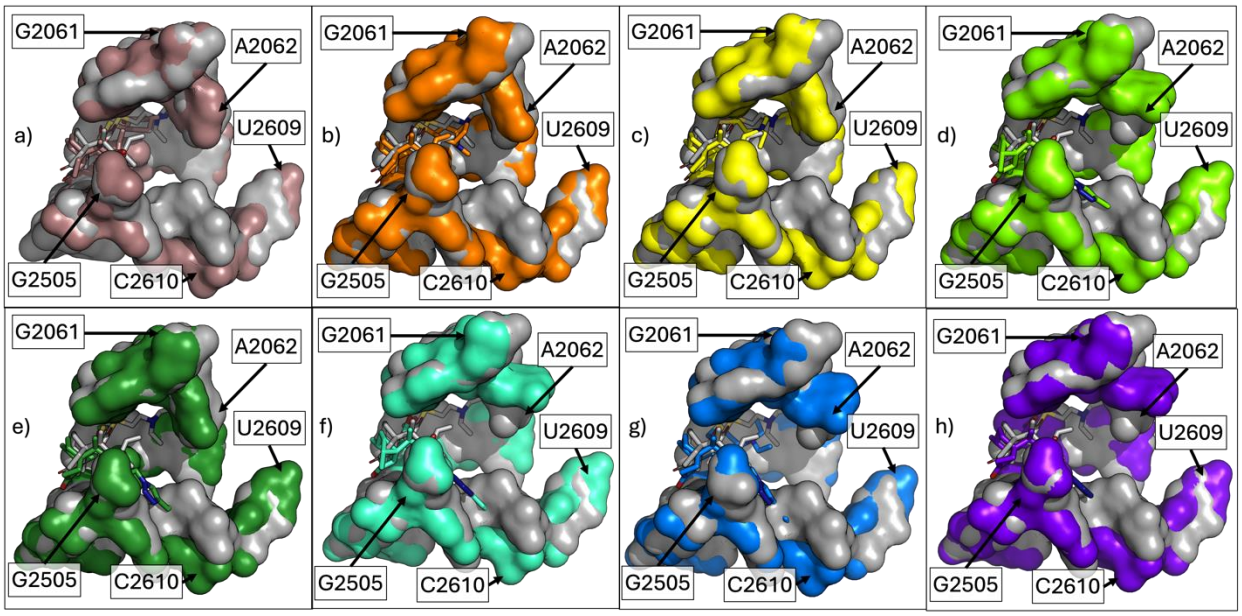


**Figure S67. Comparison of 1XBP to other crystal structures.** The surface is shown for all structures, and the crystal structure ligands are shown as sticks and colored the same as their parent structure and by element. 1XBP[37] is colored grey in all images, a) 5HL7[47] is pink, b) 8CEU is orange,[46] c) 8CGV is yellow,[46] d) EC126 is yellow green, e) EC136 is dark green, f) EC148 is green-cyan, g) EC158 is blue, and h) ECR14 is purple. *E. coli* numbering is used throughout.

### 3.5.6 In vivo detection of translation inhibitors using pDualrep2 reporter strain

For the *in vivo* bioactivity test (**Figure 3A**), we used the reporter *E. coli* BW25113 ΔtolC-pDualrep2 strain as described previously[44, 52, 53]. Briefly, cells were grown overnight at 37°C in LB medium supplemented with 100 µg/mL of ampicillin (Amp), diluted 1:100 (v/v), grown to $OD_{600}$ ~1.2 and 3 ml of the culture, containing ~$10^9$ colony forming units were poured on top of a LB/agar plate supplemented with 100 µg/mL of ampicillin. After a 5-minute of incubation, the remaining liquid was aspirated, and the plate was allowed to dry. Individual antibiotics dissolved in ethanol were applied to the agar surface: 1 µL of the solutions of pleuromutilin (2 mM) or

tiamulin (2 mM); 1.5 µL of the solutions of PLE-**18** (2 mM), PLE-**27** (2 mM), TIA-**26** (2 mM), or TIA-**31** (2 mM); 4 µL of the solution of PLE-**30** (2 mM); 2 µL of the solutions of erythromycin (2 mM) or ciprofloxacin (30 mM in $H_2O$) as well as an ethanol control. After overnight incubation at 37°C, the plate was photographed by ChemiDoc MP imager (Bio-Rad, USA) using "Cy3-blot" mode for RFP fluorescence and "Cy5-blot" mode for Katushka2S fluorescence.

### 3.5.7 In vitro translation inhibition assay

*In vitro* assessment of inhibition of synthesis of green fluorescent protein (GFP) by the tested compounds (**Figure 3B, C**) was accomplished as described previously[52, 54]. Briefly, a GFP expression plasmid was transcribed and translated using the PURExpress *in vitro* protein synthesis kit (New England Biolabs, USA). The 5 µL transcription-translation reactions, assembled according to the manufacturer protocol, were programmed with 200 ng of the plasmid template DNA. When needed, the reactions were supplemented with the tested compounds at the required concentrations. The reactions were placed into the wells of the black wall/clear bottom 384-well plates (Corning, USA), and plates were incubated at 37°C in a microplate reader (Tecan Infinite M-plex). The progression of the reaction was monitored in real-time by measuring fluorescence every 5 minutes for 4 hours ($l_{ex}$ = 488 nm, $l_{em}$ = 520 nm). The dose-dependent inhibition of translation was recorded after reactions proceeded for 60 minutes, a time point corresponding to the linear slope of the reaction. Graphing of the obtained results was carried out using GraphPad Prism software (version 9.0).

### 3.5.8 X-ray crystallographic structure determination

In this work, we used *T. thermophilus* 70S ribosomes complexed with *E. coli* protein Y merely as a tool to obtain structures of higher resolution. This approach is based on our previous finding that binding of PY to a vacant 70S ribosome stabilizes it by locking the head of the 30S subunit in an unrotated state, which leads to overall better diffraction and substantially higher structural resolution[55, 56]. Additionally, by competing with the binding of mRNAs and tRNAs to the ribosome, PY purges any residual ribosome-bound tRNAs carried over during ribosome purification, thereby increasing the homogeneity of the ribosomes and, thus, improving their crystallizability and diffraction[57]. Since the binding site of PY is located on the small ribosomal subunit, it does not interfere with the binding of any ribosomal antibiotics targeting PTC or NPET located at the heart of the large ribosomal subunit. As a result, by using ribosome-PY complexes, we obtained better resolution and overall higher quality electron density maps of the ribosome-bound pleuromutilin drugs than possible otherwise.

Wild-type 70S ribosomes from *T. thermophilus* (strain HB8) were prepared as described previously[56, 58, 59]. Ribosome complexes with *E. coli* protein Y, and pleuromutilin derivatives were formed by mixing 5 μM *Tth* 70S ribosomes with 100 μM PY, followed by the addition of each of the compounds to the final concentration of 250 μM. All *Tth* 70S ribosome complexes were formed in the buffer containing 5 mM HEPES-KOH (pH 7.6), 50 mM KCl, 10 mM $NH_4Cl$, and 10 mM $Mg(CH_3COO)_2$, and then crystallized in the buffer containing 100 mM Tris-HCl (pH 7.6), 2.9% (v/v) PEG-20K, 9-10% (v/v) MPD, 175 mM arginine, 0.5 mM β-mercaptoethanol. Crystals were grown by the vapor diffusion method in sitting drops at 19°C, stabilized and cryo-protected stepwise using a series of buffers with increasing MPD concentrations (25%, 30%, 35%) until reaching the final concentration of 40% (v/v) MPD as described previously[55-58, 60, 61]. After

stabilization, crystals were flash-frozen using a nitrogen cryo-stream at 80°K (Oxford Cryosystems, UK).

Collection and processing of the X-ray diffraction data, model building, and structure refinement were performed as described in our previous reports[54, 56, 57, 59, 60, 62, 63]. Diffraction data were collected at beamlines beamlines 17ID-1 and 17ID-2 of the National Synchrotron Light Source II (Brookhaven National Laboratory). A complete dataset was collected using 0.979Å X-ray irradiation at 100K from multiple regions of the same crystal, using 0.3-degree oscillations. Raw data were integrated and scaled using the XDS software package (version from Jan 10, 2022)[64]. Molecular replacement was performed using PHASER from the CCP4 program suite (version 7.0)[65]. The search model was generated from the previously published structures of the *T. thermophilus* 70S ribosome with bound mRNA and aminoacylated tRNAs (PDB entry 6XHW)[60]. Initial molecular replacement solutions were refined by rigid-body refinement with the ribosome split into multiple domains, followed by positional and individual B-factor refinement using the PHENIX software (version 1.17)[66]. Non-crystallographic symmetry restraints were applied to four parts of the 30S ribosomal subunit (head, body, spur, and helix 44) and four parts of the 50S subunit (body, L1-stalk, L10-stalk, and C-terminus of the L9 protein). Initial PDB model and CIF restraints for the pleuromutilin derivatives were generated using CCP4 built-in PRODRG software[65]. The final PDB model was built in Coot (version 0.8.2)[67]. The statistics of data collection and refinement are compiled in **Table S2**. All figures showing atomic models were rendered using PyMOL Molecular Graphics System software (version 1.8.6, Schrödinger, www.pymol.org).

**Table S2 | X-ray data collection and refinement statistics.**

| ***Crystals*** | **70S-PYcomplex with PLE-1 PDB entry 9XXX** | **70S-PYcomplex with PLE-18 PDB entry 9XXX** | **70S-PYcomplex with PLE-27 PDB entry 9XXX** | **70S-PYcomplex with PLE-30 PDB entry 9XXX** |
|---|---|---|---|---|
| ***Diffraction data*** | | | | |
| Space group | $P2_12_12_1$ | $P2_12_12_1$ | $P2_12_12_1$ | $P2_12_12_1$ |
| Unit cell dimensions, Å (a x b x c) | 210.50 x 449.68 x 622.97 | 210.38 x 452.11 x 624.50 | 210.42 x 450.57 x 623.1 | 209.66 x 450.37 x 619.99 |
| Wavelength, Å | 0.920208 | 1.033202 | 1.033210 | 1.033210 |
| Resolution range (outer shell), Å | 364.6-2.70 (2.77-2.70) | 366.21-2.90 (2.98-2.90) | 365.11-2.85 (2.92-2.85) | 309.99-2.90 (2.98-2.90) |
| I/σI (outer shell) | 7.38 (0.90) | 5.43 (0.95) | 5.47 (0.98) | 5.35 (0.97) |
| Resolution at which I/σI=1, Å | 2.70 | 2.90 | 2.85 | 2.90 |
| Resolution at which I/σI=2, Å | 2.93 | 3.15 | 3.05 | 3.15 |
| CC(1/2) at which I/σI=1, % | 15.9 | 16.6 | 17.2 | 14.6 |
| CC(1/2) at which I/σI=2, % | 42.3 | 45.3 | 46.85 | 41.2 |
| Completeness (outer shell), % | 99.8 (99.6) | 99.5 (99.3) | 100 (99.7) | 99.6 (99.7) |
| $R_{merge}$ (outer shell)% | 34.7 (262.1) | 32.4 (182.3) | 38.7 (210.9) | 38.3 (207.0) |
| No. of crystals used | 1 | 2 | 1 | 1 |
| No. of reflections used: Total | 5,619,291 | 8,436,445 | 6,782,712 | 6,782,712 |
| No. of reflections used: Unique | 1,291,995 | 1,359,923 | 1,275,556 | 1,275,556 |
| Redundancy (outer shell) | 7.06 (7.26) | 4.35 (4.48) | 6.20 (6.11) | 5.32 (5.50) |
| ***Refinement*** | | | | |
| Resolution range of used data, Å | 40.09-2.70 | 366.21-2.90 | 365.11-2.85 | 255.35-2.90 |
| No. of reflections used | 1,591,051 | 1,290,354 | 1,358,043 | 1,273,542 |
| $R_{work}/R_{free}$, % | 20.6/26.0 | 20.6/26.8 | 20.6/26.7 | 21.0/27.3 |
| *No. of Non-Hydrogen Atoms* | | | | |
| RNA | 193,315 | 193,315 | 193,315 | 193,315 |
| Protein | 93,036 | 93,036 | 93,036 | 93,036 |
| Ions (Mg, K, Zn, Fe) | 2,544 | 2,546 | 2,545 | 2,544 |
| Waters | 9,510 | 9,511 | 9,510 | 9,508 |
| *Ramachandran Plot* | | | | |
| Favored regions, % | 89.60 | 87.63 | 88.87 | 87.69 |
| Allowed regions, % | 8.75 | 10.20 | 9.25 | 10.03 |
| Outliers, % | 1.65 | 2.18 | 1.88 | 2.28 |
| *Deviations from ideal values (RMSD)* | | | | |
| Bond, Å | 0.009 | 0.009 | 0.009 | 0.010 |
| Angle, degrees | 1.389 | 1.445 | 1.449 | 1.472 |
| Chirality | 0.058 | 0.060 | 0.060 | 0.061 |
| Planarity | 0.007 | 0.007 | 0.007 | 0.007 |

| | | | | |
|---|---|---|---|---|
| Dihedral, degrees | 17.142 | 17.352 | 17.243 | 17.767 |
| Average B-factor (overall), Å$^2$ | 50.9 | 56.2 | 49.8 | 56.2 |

**Table S2 | X-ray data collection and refinement statistics (continued).**

| ***Crystals*** | **70S-PYcomplex with TIA-2 PDB entry 9XXX** | **70S-PYcomplex with TIA-26 PDB entry 9XXX** | **70S-PYcomplex with TIA-31 PDB entry 9XXX** |
|---|---|---|---|
| ***Diffraction data*** | | | |
| Space group | $P2_12_12_1$ | $P2_12_12_1$ | $P2_12_12_1$ |
| Unit cell dimensions, Å (a x b x c) | 210.78 x 451.71 x 625.93 | 211.16 x 452.53 x 626.77 | 210.1 x 451.17 x 625.72 |
| Wavelength, Å | 0.920208 | 1.033202 | 0.920194 |
| Resolution range (outer shell), Å | 312.96-2.65 (2.72-2.65) | 366.89-2.80 (2.87-2.80) | 312.86-2.85 (2.92-2.85) |
| I/σI (outer shell) | 8.01 (0.98) | 6.45 (0.96) | 6.89 (0.93) |
| Resolution at which I/σI=1, Å | 2.65 | 2.80 | 2.85 |
| Resolution at which I/σI=2, Å | 2.87 | 3.00 | 3.09 |
| CC(1/2) at which I/σI=1, % | 18.9 | 16.6 | 16.5 |
| CC(1/2) at which I/σI=2, % | 47.7 | 44.25 | 49.0 |
| Completeness (outer shell), % | 99.7 (99.3) | 99.7 (99.4) | 100 (100) |
| $R_{merge}$ (outer shell)% | 36.1 (292.3) | 34.2 (221.7) | 40.1 (259.5) |
| No. of crystals used | 2 | 1 | 2 |
| No. of reflections used: Total | 10,126,477 | 12,011,672 | 12,011,672 |
| No. of reflections used: Unique | 1,449,347 | 1,365,790 | 1,365,790 |
| Redundancy (outer shell) | 13.03 (13.29) | 6.99 (7.17) | 8.79 (9.02) |
| ***Refinement*** | | | |
| Resolution range of used data, Å | 257.25-2.65 | 366.89-2.80 | 45.39-2.85 |
| No. of reflections used | 1,697,315 | 1,447,536 | 1,364,816 |
| $R_{work}/R_{free}$, % | 20.7/26.1 | 21.0/27.0 | 20.2/26.1 |
| *No. of Non-Hydrogen Atoms* | | | |
| RNA | 193,315 | 193,299 | 193,315 |
| Protein | 93,036 | 93,036 | 93,024 |
| Ions (Mg, K, Zn, Fe) | 2,545 | 2,544 | 2,544 |
| Waters | 9,509 | 9,506 | 9,508 |
| *Ramachandran Plot* | | | |
| Favored regions, % | 89.46 | 87.62 | 87.93 |
| Allowed regions, % | 8.69 | 9.99 | 10.03 |

| | | | |
|---|---|---|---|
| Outliers, % | 1.85 | 2.39 | 2.04 |
| *Deviations from ideal values (RMSD)* | | | |
| Bond, Å | 0.010 | 0.010 | 0.010 |
| Angle, degrees | 1.523 | 1.525 | 1.600 |
| Chirality | 0.062 | 0.062 | 0.064 |
| Planarity | 0.008 | 0.008 | 0.008 |
| Dihedral, degrees | 17.245 | 17.480 | 17.541 |
| Average B-factor (overall), $Å^2$ | 56.1 | 53.3 | 53.6 |

**Table S3:** Derivatives and their corresponding total polar surface area (TPSA) and consensus LogP calculated using Swiss ADME.[68]

| LIGAND | TOTAL POLAR SURFACE AREA ($A^2$) | CONSENSUS LOG P |
|---|---|---|
| **11** | 134.77 | 1.97 |
| **12** | 134.77 | 2.21 |
| **13** | 134.77 | 2.46 |
| **14** | 134.77 | 2.50 |
| **15** | 140.56 | 1.84 |
| **15 (CHARGED)** | 142.18 | 0.96 |
| **16** | 140.56 | 2.12 |
| **16 (CHARGED)** | 142.18 | 1.24 |
| **17** | 114.54 | 4.32 |
| **18** | 123.77 | 3.58 |
| **27** | 114.54 | 3.67 |
| **28** | 114.54 | 3.85 |
| **29** | 123.77 | 3.59 |
| **30** | 114.54 | 4.98 |
| **19** | 143.08 | 4.05 |
| **19 (CHARGED)** | 144.28 | 2.67 |
| **20** | 143.08 | 3.91 |
| **20 (CHARGED)** | 144.28 | 2.89 |
| **21** | 143.08 | 4.05 |
| **21 (CHARGED)** | 144.28 | 3.03 |
| **23** | 148.87 | 3.53 |
| **23 (CHARGED)** | 151.69 | 1.52 |
| **24** | 148.87 | 3.79 |

| | | |
|---|---|---|
| **24 (CHARGED)** | 151.69 | 1.89 |
| **22** | 143.08 | 4.09 |
| **22 (CHARGED)** | 144.28 | 3.07 |
| **25** | 122.85 | 6.01 |
| **25 (CHARGED)** | 124.05 | 4.99 |
| **26** | 132.08 | 5.32 |
| **26 (CHARGED)** | 133.28 | 4.3 |
| **31** | 122.85 | 5.41 |
| **31 (CHARGED)** | 124.05 | 4.39 |
| **32** | 122.85 | 5.64 |
| **32 (CHARGED)** | 124.05 | 4.62 |
| **33 (CHARGED)** | 132.08 | 5.38 |
| **34** | 132.28 | 4.36 |
| **34 (CHARGED)** | 124.05 | 5.76 |
| **7** | 115.35 | 4.49 |
| **8** | 165.1 | 4.29 |
| **9** | 133.58 | 2.74 |
| **10** | 141.89 | 4.51 |
| **10 (CHARGED)** | 143.09 | 3.49 |
| **1 (PLEUROMUTILIN)** | 83.83 | 3.02 |
| **2 (TIAMULIN)** | 93.34 | 3.75 |

*****Charged species are with the physiologically relevant ammonium(s)

## 3.6 References

1. Murray, C. J.; Ikuta, K. S.; Sharara, F.; Swetschinski, L.; Robles Aguilar, G.; Gray, A.; Han, C.; Bisignano, C.; Rao, P.; Wool, E.; Johnson, S. C.; Browne, A. J.; Chipeta, M. G.; Fell, F.; Hackett, S.; Haines-Woodhouse, G.; Kashef Hamadani, B. H.; Kumaran, E. A. P.; McManigal, B.; Agarwal, R.; Akech, S.; Albertson, S.; Amuasi, J.; Andrews, J.; Aravkin, A.; Ashley, E.; Bailey, F.; Baker, S.; Basnyat, B.; Bekker, A.; Bender, R.; Bethou, A.; Bielicki, J.; Boonkasidecha, S.; Bukosia, J.; Carvalheiro, C.; Castañeda-Orjuela, C.; Chansamouth, V.; Chaurasia, S.; Chiurchiù, S.; Chowdhury, F.; Cook, A. J.; Cooper, B.; Cressey, T. R.; Criollo-Mora, E.; Cunningham, M.; Darboe, S.; Day, N. P. J.; De Luca, M.; Dokova, K.; Dramowski, A.; Dunachie, S. J.; Eckmanns, T.; Eibach, D.; Emami, A.; Feasey, N.; Fisher-Pearson, N.; Forrest, K.; Garrett, D.; Gastmeier, P.; Giref, A. Z.; Greer, R. C.; Gupta, V.; Haller, S.; Haselbeck, A.; Hay, S. I.; Holm, M.; Hopkins, S.; Iregbu, K. C.; Jacobs, J.; Jarovsky, D.; Javanmardi, F.; Khorana, M.; Kissoon, N.; Kobeissi, E.; Kostyanev, T.; Krapp, F.; Krumkamp, R.; Kumar, A.; Kyu, H. H.; Lim, C.; Limmathurotsakul, D.; Loftus, M. J.; Lunn, M.; Ma, J.; Mturi, N.; Munera-Huertas, T.; Musicha, P.; Mussi-Pinhata, M. M.; Nakamura, T.; Nanavati, R.; Nangia, S.; Newton, P.; Ngoun, C.; Novotney, A.; Nwakanma, D.; Obiero, C. W.; Olivas-Martinez, A.; Olliaro, P.; Ooko, E.; Ortiz-Brizuela, E.; Peleg, A. Y.; Perrone, C.; Plakkal, N.; Ponce-De-Leon, A.; Raad, M.; Ramdin, T.; Riddell, A.; Roberts, T.; Robotham, J. V.; Roca, A.; Rudd, K. E.; Russell, N.; Schnall, J.; Scott, J. A. G.; Shivamallappa, M.; Sifuentes-Osornio, J.; Steenkeste, N.; Stewardson, A. J.; Stoeva, T.; Tasak, N.; Thaiprakong, A.; Thwaites, G.; Turner, C.; Turner, P.; Van Doorn, H. R.; Velaphi, S.; Vongpradith, A.; Vu, H.; Walsh, T.; Waner, S.; Wangrangsimakul, T.; Wozniak, T.; Zheng, P.; Sartorius, B.; Lopez, A. D.;

Stergachis, A.; Moore, C.; Dolecek, C.; Naghavi, M., Global burden of bacterial antimicrobial resistance in 2019: a systematic analysis. *The Lancet* **2022,** *399* (10325), 629-655.
2. *No time to wait: Securing the future from drug-resistant infections*; Interagency Coordination Group on Antimicrobial Resistance: 2019.
3. Newman, D. J.; Cragg, G. M., Natural products as sources of new drugs over the nearly four decades from 01/1981 to 09/2019. *J. Nat. Prod.* **2020,** *83* (3), 770-803.
4. Kurylo-Borowska, Z., [42] Edeine synthetase. *Methods Enzymol.* **1975,** *43*, 559-567.
5. Morrison, K. C.; Hergenrother, P. J., Natural products as starting points for the synthesis of complex and diverse compounds. *Nat. Prod. Rep.* **2014,** *31* (1), 6-14.
6. Ford, W. C.; Zurenko, E. G.; Barbachyn, R. M., The Discovery of Linezolid, the First Oxazolidinone Antibacterial Agent. *Curr. Drug Targets: Infect. Disord.* **2001,** *1* (2), 181-199.
7. Mason, J. D.; Terwilliger, D. W.; Pote, A. R.; Myers, A. G., Practical gram-scale synthesis of iboxamycin, a potent antibiotic candidate. *J. Am. Chem. Soc.* **2021,** *143* (29), 11019-11025.
8. Mitcheltree, M. J.; Pisipati, A.; Syroegin, E. A.; Silvestre, K. J.; Klepacki, D.; Mason, J. D.; Terwilliger, D. W.; Testolin, G.; Pote, A. R.; Wu, K. J. Y.; Ladley, R. P.; Chatman, K.; Mankin, A. S.; Polikanov, Y. S.; Myers, A. G., A synthetic antibiotic class overcoming bacterial multidrug resistance. *Nature* **2021,** *599* (7885), 507-512.
9. Wu, K. J. Y.; Tresco, B. I. C.; Ramkissoon, A.; Aleksandrova, E. V.; Syroegin, E. A.; See, D. N. Y.; Liow, P.; Dittemore, G. A.; Yu, M.; Testolin, G.; Mitcheltree, M. J.; Liu, R. Y.; Svetlov, M. S.; Polikanov, Y. S.; Myers, A. G., An antibiotic preorganized for ribosomal binding overcomes antimicrobial resistance. *Science* **2024,** *383* (6684), 721-726.
10. Paukner, S.; Riedl, R., Pleuromutilins: Potent drugs for resistant bugs—Mode of action and resistance. *Cold Spring Harb. Perspect. Med.* **2017,** *7* (1), a027110.
11. Gibbons, E. G., Total synthesis of (+-)-pleuromutilin. *J. Am. Chem. Soc.* **1982,** *104* (6), 1767-1769.
12. Fazakerley, N. J.; Helm, M. D.; Procter, D. J., Total synthesis of (+)-pleuromutilin. *Chem. Eur. J.* **2013,** *19* (21), 6718-6723.
13. Zeng, M.; Murphy, S. K.; Herzon, S. B., Development of a Modular Synthetic Route to (+)-Pleuromutilin, (+)-12-epi-Mutilins, and Related Structures. *J. Am. Chem. Soc.* **2017,** *139* (45), 16377-16388.
14. Farney, E. P.; Feng, S. S.; Schäfers, F.; Reisman, S. E., Total synthesis of (+)-pleuromutilin. *J. Am. Chem. Soc.* **2018,** *140* (4), 1267-1270.
15. Rittenhouse, S.; Biswas, S.; Broskey, J.; McCloskey, L.; Moore, T.; Vasey, S.; West, J.; Zalacain, M.; Zonis, R.; Payne, D., Selection of retapamulin, a novel pleuromutilin for topical use. *Antimicrob. Agents Chemother.* **2006,** *50* (11), 3882-3885.
16. Hunt, A., FDA approves new antibiotic to treat community-acquired bacterial pneumonia. www.fda.gov/news-events/press-announcements, 2019.
17. Czok, R.; Meingassner, J. G.; Mieth, H.; Schutze, E. Antibiotic compositions for treating coccidiosis. US patent 4,148,890, 1979.
18. Egger, H.; Reinshagen, H., New pleuromutilin derivatives with enhanced antimicrobial activity. II. Structure-activity correlations. *J. Antibiot.* **1976,** *29* (9), 915-922.
19. Goethe, O.; DiBello, M.; Herzon, S. B., Total synthesis of structurally diverse pleuromutilin antibiotics. *Nature Chemistry* **2022,** *14* (11), 1270-1277.
20. Breiner, L. M.; Briganti, A. J.; McCord, J. P.; Heifetz, M. E.; Philbrook, S. Y.; Slebodnick, C.; Brown, A. M.; Lowell, A. N., Synthesis, testing, and computational modeling of pleuromutilin 1,2,3-triazole derivatives in the ribosome. *Tetrahedron Chem* **2022,** *4*.
21. Lengerli, D.; Ibis, K.; Nural, Y.; Banoglu, E., The 1,2,3-triazole 'all-in-one' ring system in drug discovery: a good bioisostere, a good pharmacophore, a good linker, and a versatile synthetic tool. *Expert Opin. Drug Discov.* **2022,** *17* (11), 1209-1236.

22. Thirring, K.; Heilmayer, W.; Riedl, R.; Kollmann, H.; Ivezic-Schoenfeld, Z.; Wicha, W.; Paukner, S.; Strickmann, D. 12-epi pleuromutilins. 2017.
23. Murphy, S. K.; Zeng, M.; Herzon, S. B., A modular and enantioselective synthesis of the pleuromutilin antibiotics. *Science (Washington, DC, U. S.)* **2017,** *356* (6341), 956-959.
24. Xianfeng, L.; Lunde, C. S.; Jacobs, R. T.; Yasheen, Z. Boron-containing small molecules. WO 2017/151492 A1, 2017.
25. Berner, H.; Vyplel, H.; Schulz, G.; Schneider, H., Chemie der Pleuromutiline, 11. Mitt.: Konfigurationsumkehr der Vinylgruppe am Kohlenstoff 12 durch reversible Retro-En-Spaltung. *Monatshefte fr Chemie Chemical Monthly* **1986,** *117* (8-9), 1073-1080.
26. Li, H.; Shen, S.-J.; Zhu, C.-L.; Xu, H., Direct intermolecular anti-Markovnikov hydroazidation of unactivated olefins. *J. Am. Chem. Soc.* **2019,** *141* (23), 9415-9421.
27. Li, B. L., F.; Li. J.; Sun, B.; Wang, Li.; Wang, W.; Ma, S.; One-pot method for synthesizing tiamulin. CN104447449A, 2015.
28. Himo, F.; Lovell, T.; Hilgraf, R.; Rostovtsev, V. V.; Noodleman, L.; Sharpless, K. B.; Fokin, V. V., Copper (I)-catalyzed synthesis of azoles. DFT study predicts unprecedented reactivity and intermediates. *J. Am. Chem. Soc.* **2005,** *127* (1), 210-216.
29. Zhang, C. X.; Kaderli, S.; Costas, M.; Kim, E. I.; Neuhold, Y. M.; Karlin, K. D.; Zuberbühler, A. D., Copper(I)-dioxygen reactivity of [(L)Cu(I)](+) (L = tris(2-pyridylmethyl)amine): kinetic/thermodynamic and spectroscopic studies concerning the formation of Cu-O2 and Cu2-O2 adducts as a function of solvent medium and 4-pyridyl ligand substituent variations. *Inorg. Chem.* **2003,** *42* (6), 1807-24.
30. Kim, J.; Golime, G.; Kim, H. Y.; Oh, K., Copper(II)-Catalyzed Aerobic Oxidation of Amines: Divergent Reaction Pathways by Solvent Control to Imines and Nitriles. *Asian J. Org. Chem.* **2019,** *8* (9), 1674-1679.
31. Schierholz, L.; Brown, C. R.; Helena-Bueno, K.; Uversky, V. N.; Hirt, R. P.; Barandun, J.; Melnikov, S. V., A Conserved Ribosomal Protein Has Entirely Dissimilar Structures in Different Organisms. *Mol. Biol. Evol.* **2024,** *41* (1), msad254.
32. Syroegin, E. A.; Flemmich, L.; Klepacki, D.; Vazquez-Laslop, N.; Micura, R.; Polikanov, Y. S., Structural basis for the context-specific action of the classic peptidyl transferase inhibitor chloramphenicol. *Nat. Struct. Mol. Biol.* **2022,** *29* (2), 152-161.
33. Khondker, A.; Rheinstädter, M. C., How do bacterial membranes resist polymyxin antibiotics? *Commun Biol* **2020,** *3* (1), 77.
34. Qiu, H.; Si, Z.; Luo, Y.; Feng, P.; Wu, X.; Hou, W.; Zhu, Y.; Chan-Park, M. B.; Xu, L.; Huang, D., The Mechanisms and the Applications of Antibacterial Polymers in Surface Modification on Medical Devices. *Front Bioeng Biotechnol* **2020,** *8*, 910.
35. Richter, M. F.; Drown, B. S.; Riley, A. P.; Garcia, A.; Shirai, T.; Svec, R. L.; Hergenrother, P. J., Predictive compound accumulation rules yield a broad-spectrum antibiotic. *Nature* **2017,** *545* (7654), 299-304.
36. Klaus Thirring, W. H., Rosemarie Riedl, Hermann Kollmann, Zrinka Ivezic-Schoenfeld, Wolfgang Wicha, Susanne Paukner, Dirk Strickmann 12-EPI PLEUROMUTILINS. 2016.
37. Schlünzen, F.; Pyetan, E.; Fucini, P.; Yonath, A.; Harms, J. M., Inhibition of peptide bond formation by pleuromutilins: the structure of the 50S ribosomal subunit from *Deinococcus radiodurans* in complex with tiamulin. *Mol. Microbiol.* **2004,** *54* (5), 1287-1294.
38. Breiner, L. M.; Briganti, A. J.; McCord, J. P.; Heifetz, M. E.; Philbrook, S. Y.; Slebodnick, C.; Brown, A. M.; Lowell, A. N., Synthesis, testing, and computational modeling of pleuromutilin 1,2,3-triazole derivatives in the ribosome. *Tetrahedron Chem* **2022,** *4*, 100034.
39. Gannett, C.; Tiller, K.; Briganti, A. J.; Brown, A. M.; Weger-Lucarelli, J.; Lowell, A. N., Forgotten natural products: Semisynthetic development of blasticidin S as an antibiotic lead. *ACS Medicinal Chemistry Letters* **2024,** *15* (3), 362-368.

40. Sun, L.-Z.; Jiang, Y.; Zhou, Y.; Chen, S.-J., RLDOCK: A new method for predicting RNA–ligand interactions. *J. Chem. Theory Comput.* **2020,** *16* (11), 7173-7183.
41. Ruiz-Carmona, S.; Alvarez-Garcia, D.; Foloppe, N.; Garmendia-Doval, A. B.; Juhos, S.; Schmidtke, P.; Barril, X.; Hubbard, R. E.; Morley, S. D., rDock: a fast, versatile and open source program for docking ligands to proteins and nucleic acids. *PLoS Comput. Biol.* **2014,** *10* (4), e1003571.
42. McNutt, A. T.; Francoeur, P.; Aggarwal, R.; Masuda, T.; Meli, R.; Ragoza, M.; Sunseri, J.; Koes, D. R., GNINA 1.0: molecular docking with deep learning. *J. Cheminform.* **2021,** *13* (1), 43.
43. Chovancova, E.; Pavelka, A.; Benes, P.; Strnad, O.; Brezovsky, J.; Kozlikova, B.; Gora, A.; Sustr, V.; Klvana, M.; Medek, P.; Biedermannova, L.; Sochor, J.; Damborsky, J., CAVER 3.0: a tool for the analysis of transport pathways in dynamic protein structures. *PLoS Comput Biol* **2012,** *8* (10), e1002708.
44. Osterman, I. A.; Komarova, E. S.; Shiryaev, D. I.; Korniltsev, I. A.; Khven, I. M.; Lukyanov, D. A.; Tashlitsky, V. N.; Serebryakova, M. V.; Efremenkova, O. V.; Ivanenkov, Y. A.; Bogdanov, A. A.; Sergiev, P. V.; Dontsova, O. A., Sorting out antibiotics' mechanisms of action: A double fluorescent protein reporter for high-throughput screening of ribosome and DNA biosynthesis inhibitors. *Antimicrob. Agents Chemother.* **2016,** *60* (12), 7481-7489.
45. CLSI, C. L. S. I., Methods for dilution antimicrobial susceptibility tests for bacteria that grow aerobically. 2012; pp M7-A9.
46. Paternoga, H.; Crowe-McAuliffe, C.; Bock, L. V.; Koller, T. O.; Morici, M.; Beckert, B.; Myasnikov, A. G.; Grubmüller, H.; Nováček, J.; Wilson, D. N., Structural conservation of antibiotic interaction with ribosomes. *Nat. Struct. Mol. Biol.* **2023,** *30* (9), 1380-1392.
47. Eyal, Z.; Matzov, D.; Krupkin, M.; Paukner, S.; Riedl, R.; Rozenberg, H.; Zimmerman, E.; Bashan, A.; Yonath, A., A novel pleuromutilin antibacterial compound, its binding mode and selectivity mechanism. *Scientific Reports* **2016,** *6* (1), 39004.
48. Schrödinger Release 2025-1: Maestro, S., LLC, New York, NY, 2025.
49. The PyMOL Molecular Graphics System, V. S., LLC, New York, NY, 2025.
50. Duan, J.; Dixon, S. L.; Lowrie, J. F.; Sherman, W., Analysis and comparison of 2D fingerprints: Insights into database screening performance using eight fingerprint methods. *J. Mol. Graphics Modell.* **2010,** *29* (2), 157-170.
51. Schrödinger Release 2025-1: Canvas, S., LLC, New York, NY, 2025.
52. Chen, C. W.; Pavlova, J. A.; Lukianov, D. A.; Tereshchenkov, A. G.; Makarov, G. I.; Khairullina, Z. Z.; Tashlitsky, V. N.; Paleskava, A.; Konevega, A. L.; Bogdanov, A. A.; Osterman, I. A.; Sumbatyan, N. V.; Polikanov, Y. S., Binding and action of triphenylphosphonium analog of chloramphenicol upon the bacterial ribosome. *Antibiotics (Basel)* **2021,** *10* (4).
53. Paranjpe, M. N.; Marina, V. I.; Grachev, A. A.; Maviza, T. P.; Tolicheva, O. A.; Paleskava, A.; Osterman, I. A.; Sergiev, P. V.; Konevega, A. L.; Polikanov, Y. S.; Gagnon, M. G., Insights into the molecular mechanism of translation inhibition by the ribosome-targeting antibiotic thermorubin. *Nucleic Acids Res.* **2022**.
54. Tereshchenkov, A. G.; Dobosz-Bartoszek, M.; Osterman, I. A.; Marks, J.; Sergeeva, V. A.; Kasatsky, P.; Komarova, E. S.; Stavrianidi, A. N.; Rodin, I. A.; Konevega, A. L.; Sergiev, P. V.; Sumbatyan, N. V.; Mankin, A. S.; Bogdanov, A. A.; Polikanov, Y. S., Binding and action of amino acid analogs of chloramphenicol upon the bacterial ribosome. *J. Mol. Biol.* **2018,** *430* (6), 842-852.
55. Polikanov, Y. S.; Blaha, G. M.; Steitz, T. A., How hibernation factors RMF, HPF, and YfiA turn off protein synthesis. *Science* **2012,** *336* (6083), 915-918.
56. Polikanov, Y. S.; Melnikov, S. V.; Soll, D.; Steitz, T. A., Structural insights into the role of rRNA modifications in protein synthesis and ribosome assembly. *Nat. Struct. Mol. Biol.* **2015,** *22* (4), 342-344.
57. Syroegin, E. A.; Flemmich, L.; Klepacki, D.; Vazquez-Laslop, N.; Micura, R.; Polikanov, Y. S., Structural basis for the context-specific action of the classic peptidyl transferase inhibitor chloramphenicol. *Nat. Struct. Mol. Biol.* **2022,** *29* (2), 152-161.

58. Polikanov, Y. S.; Steitz, T. A.; Innis, C. A., A proton wire to couple aminoacyl-tRNA accommodation and peptide-bond formation on the ribosome. *Nat. Struct. Mol. Biol.* **2014,** *21* (9), 787-793.
59. Syroegin, E. A.; Aleksandrova, E. V.; Polikanov, Y. S., Insights into the ribosome function from the structures of non-arrested ribosome-nascent chain complexes. *Nat. Chem.* **2022**.
60. Svetlov, M. S.; Syroegin, E. A.; Aleksandrova, E. V.; Atkinson, G. C.; Gregory, S. T.; Mankin, A. S.; Polikanov, Y. S., Structure of Erm-modified 70S ribosome reveals the mechanism of macrolide resistance. *Nat. Chem. Biol.* **2021,** *17* (4), 412-420.
61. Syroegin, E. A.; Aleksandrova, E. V.; Polikanov, Y. S., Insights into the ribosome function from the structures of non-arrested ribosome-nascent chain complexes. *Nat. Chem.* **2022,** *15* (1), 143-153.
62. Svetlov, M. S.; Plessa, E.; Chen, C. W.; Bougas, A.; Krokidis, M. G.; Dinos, G. P.; Polikanov, Y. S., High-resolution crystal structures of ribosome-bound chloramphenicol and erythromycin provide the ultimate basis for their competition. *RNA* **2019,** *25* (5), 600-606.
63. Syroegin, E. A.; Aleksandrova, E. V.; Polikanov, Y. S., Structural basis for the inability of chloramphenicol to inhibit peptide bond formation in the presence of A-site glycine. *Nucleic Acids Res.* **2022,** *50* (13), 7669-7679.
64. Kabsch, W., XDS. *Acta Cryst. Sect. D Biol. Crystallogr.* **2010,** *66* (Pt 2), 125-132.
65. McCoy, A. J.; Grosse-Kunstleve, R. W.; Adams, P. D.; Winn, M. D.; Storoni, L. C.; Read, R. J., Phaser crystallographic software. *J. Appl. Crystallogr.* **2007,** *40* (Pt 4), 658-674.
66. Adams, P. D.; Afonine, P. V.; Bunkoczi, G.; Chen, V. B.; Davis, I. W.; Echols, N.; Headd, J. J.; Hung, L. W.; Kapral, G. J.; Grosse-Kunstleve, R. W.; McCoy, A. J.; Moriarty, N. W.; Oeffner, R.; Read, R. J.; Richardson, D. C.; Richardson, J. S.; Terwilliger, T. C.; Zwart, P. H., PHENIX: a comprehensive Python-based system for macromolecular structure solution. *Acta Cryst. Sect. D Biol. Crystallogr.* **2010,** *66* (Pt 2), 213-221.
67. Emsley, P.; Cowtan, K., Coot: model-building tools for molecular graphics. *Acta Cryst. Sect. D Biol. Crystallogr.* **2004,** *60*, 2126-2132.
68. Bakchi, B.; Krishna, A. D.; Sreecharan, E.; Ganesh, V. B. J.; Niharika, M.; Maharshi, S.; Puttagunta, S. B.; Sigalapalli, D. K.; Bhandare, R. R.; Shaik, A. B., An overview on applications of SwissADME web tool in the design and development of anticancer, antitubercular and antimicrobial agents: A medicinal chemist's perspective. *J. Mol. Struct.* **2022,** *1259*, 132712.

# Chapter 4. Synthesis, antibacterial testing, and anti-malarial activity of potentially electrophilic pleuromutilin derivatives

Logan M. Breiner,[1,2] Abdallah S. Abdelsattar,[2,4] Katherine R. Fike,[2,3] Michael Klemba,[2,3,5] Mohamed N. Seleem,[2,4,6]* Andrew N. Lowell[1,2,7,]*

[1] Department of Chemistry, Virginia Polytechnic Institute and State University (Virginia Tech), Blacksburg, Virginia 24061, USA

[2] Center for Emerging, Zoonotic, and Arthropod-borne Pathogens, Virginia Polytechnic Institute and State University (Virginia Tech), Blacksburg, Virginia 24061, USA

[3] Department of Biochemistry, Virginia Tech, Blacksburg, Virginia 24061, USA

[4] Center for One Health Research, Virginia Tech, Blacksburg, VA, 24061, USA

[5] Virginia Tech Center for Drug Discovery Screening Laboratory, Virginia Tech, Blacksburg, VA 24061, USA

[6] Department of Biomedical Sciences and Pathobiology, Virginia-Maryland College of Veterinary Medicine, Virginia Tech, Blacksburg, Virginia 24061, USA

[7] Faculty of Health Sciences, Virginia Tech, Blacksburg, VA, USA

## 4.1 Abstract

As we have seen, the continued development of antibiotics is crucial in the fight against antimicrobial resistance (AMR). One approach is the generation of highly potent derivatives of already existing antibiotics, with one specific type, covalent inhibitors, showing promise because of their ability to irreversibly bind to their target. Our previous work with pleuromutilin demonstrated that synthetic intermediates containing tosylate groups were highly effective. One possible explanation for this is the electrophilic nature of these derivatives and the ready tosylate leaving group allows them to covalently bind to their ribosome target. Although covalently-binding, ribosome-targeting antibiotics are rare; we were inspired to investigate this possibility. While these compounds were shown to not be covalent inhibitors against bacteria, we identified unexpected but potent activity results against malaria which makes these compounds worthy of further investigation.

## 4.2 Introduction

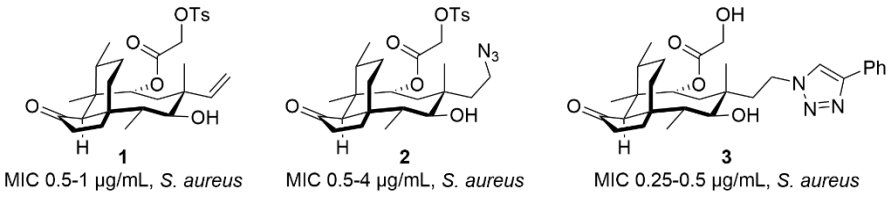


**Figure 1.** Structures of tosylated synthetic intermediates (**1**–**2**) and lead compound (**3**) with minimum inhibitory concentrations (MIC) against *S. aureus*

During our previous work with *epi*-triazolyl mutilins (Chapter 3) we observed that the synthetic intermediates, such as **1** and **2** (Figure 1), in the synthetic pathway outlined in Chapter 3, had antimicrobial activity against *Staphylococcus aureus* that surpassed that of pleuromutilin. Because of the high activity of the tosylated intermediates, we hypothesized that the tosylate may not simply be binding favorably with the underlying nucleotides of the ribosome, but might be acting as an electrophilic covalent warhead. Covalent inhibitors of the ribosome are relatively rare, with only a few being reported in the literature (tylosin[1] and puromycin[2]). Even these are not examples of true covalent binding to the underlying ribosome. Tylosin forms a labile carbinolamine with A21062[1] (*E. coli* numbering) while puromycin mimics tRNA in the A site of the ribosome and is erroneously inserted in to the growing peptide chain, causing premature termination of protein synthesis.[2] In our case, we hypothesized that a nucleotide in the ribosomal binding site of pleuromutilin might be directly displacing the tosylate leaving group, forming a true covalent bond. To test this hypothesis, we tested the previously generated tosylate (**1**) and synthesized the chloro **9**, bromo **10**, and toluyl sulfonamide **8** derivatives of the most active aryl series, **3**, as well as of 12-*epi*-pleuromutilin. The toluyl sulfonamide derivatives (**5** and **8**) were synthesized as controls to explore if it was a pharmacophore effect from the toluyl sulfonate rather

than electrophilicity and covalent attachment that provided the increase in potency. The chloro and bromo derivatives would replicate the electrophilic nature of the tosylated pleuromutilin. The electrophilic derivatives of our most potent derivative **3** would allow us to compare to **3** to see if there was an increase in potency.

### 4.3 Results and discussion

#### 4.3.1 Synthesis

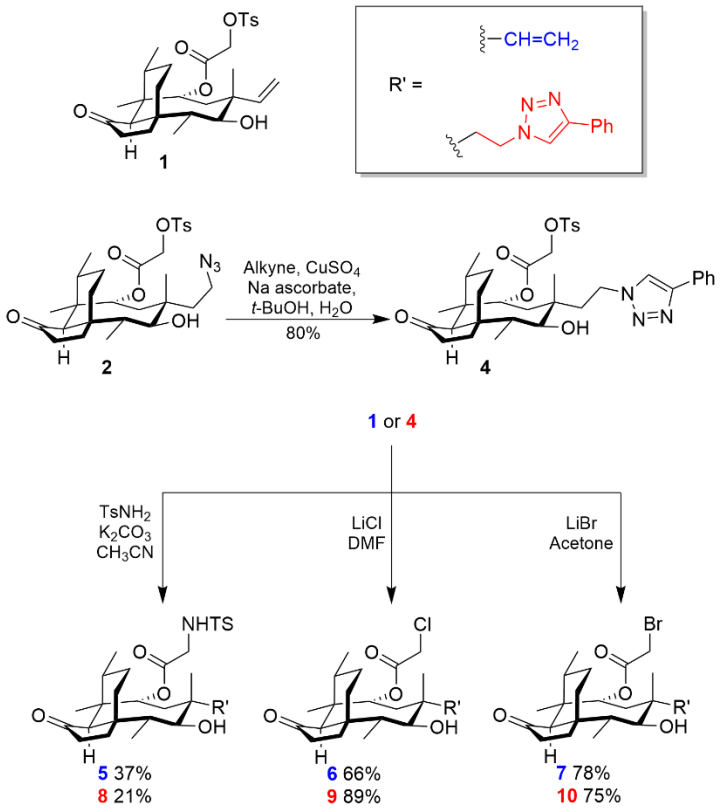


**Figure 2.** Synthesis of the electrophilic pleuromutilin series.

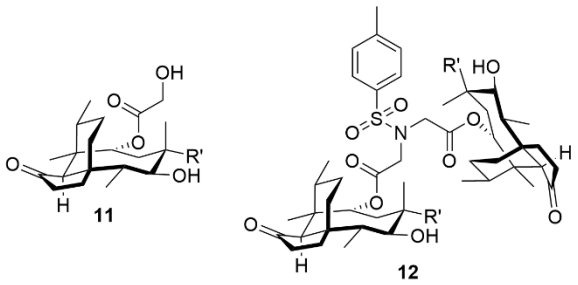


**Figure 3.** Byproducts of the nucleophilic displacement with *p*-toluenesulfonamide.

The series of derivatives were synthesized from intermediate **1** and **2** created during our earlier work (see Chapter 3). However, instead of diverging the C22 group prior to click chemistry, the tosylate was maintained through the CuAAC to give **4**. Compounds **1** and **4** were retained for testing and directly converted into the corresponding test substrates via simple nucleophilic displacement utilizing either LiCl, LiBr, or *p*-toluenesulfonamide and a base. The two derivatives containing *p*-toluenesulfonamide (**5** and **8**) suffered from low yield. This decrease in yields may be attributable to a few factors. First, the resonance of the conjugate base of the nitrogen back into the sulfonamide renders a poorer nucleophile. Second, although rigorously anhydrous conditions were used, as well as two equivalents of potassium carbonate, hydrolysis products of the tosylate were isolated (**11**, Figure 3). Additionally, despite using two equivalents of *p*-toluenesulfonamide, a double substitution product **12** was recovered, where one sulfonamide had reacted with two equivalents of **1** or **4**. This overreaction can be attributed to the presence of two acidic protons on the sulfonamide, thus allowing for an additional deprotonation and nucleophilic attack after the desired reaction has occurred. Lastly, this transformation is identical to generic reaction conditions,[3] and these yields are unoptimized as sufficient material was obtained to test the covalent binding hypothesis. In contrast to the sulfonamides, the halogenated derivatives **6**, **7**, **9**, and **10** were achieved in much better yields, even though these reactions were also taken from

generic reaction conditions with no optimization. These reactions are similar to a Finkelstein reaction where iodide displaces a smaller halogen (Cl or Br) based on the nucleophilicity of iodide and the decreased solubility of the lower halogen salts in the organic solvent driving the reaction due to Le Chatelier's principle.[4] After purification of these derivatives, special care was taken in their storage, due to the unstable nature of α-halocarbonyls.[5] Exposure to potential nucleophiles was minimized by only using halogenated solvents for characterization. Stocks were typically prepared fresh or if to be used within a week, kept as stock solutions in DMSO that were frozen at -80 °C when not in use. No odor of dimethylsulfide, which would indicate a Kornblum-type reaction where the electrophile is attacked by DMSO and dimethylsulfide eliminated to give the aldehyde, was ever detected, even upon long storage of test stock solutions.

### 4.3.2 Antimicrobial testing

| Compound | *S. aureus* 8810 | MRSA | *E. coli* MC1061 | *E. coli* ΔtolC | VRE |
|---|---|---|---|---|---|
| **1** | 0.5 | 0.5 | >32 | 0.5 | 2 |
| **4** | 1 | 0.5 | >32 | 0.25 | 16 |
| **5** | 8 | 8 | >32 | 2 | 16 |
| **6** | 0.5 | 0.5 | 4 | 0.25 | 2 |
| **7** | 2 | 2 | 4 | 1 | 4 |
| **8** | 1 | 2 | >32 | 0.25 | 4 |
| **9** | 0.25 | 0.25 | 8 | 0.25 | 0.5 |
| **10** | 1 | 1 | 16 | 0.5 | 2 |
| **TSP** | NA | NA | NA | NA | 2 |
| **3** | 0.25 | 0.5 | 1 | 0.25 | 0.5 |
| PLE | 2 | 2 | 2 | 1 | 8 |
| TIA | 1 | 2 | 2 | 0.5 | 2 |

**Table 1.** The minimum inhibitory concentrations of the suspected electrophilic derivatives (μg/mL). TSP = 22-*O*-tosylpleuromutilin (native epimer), PLE = pleuromutilin, TIA = tiamulin.

In general, the C22-chloro analogs were the most potent of their respective series. The C22-chloro 12-*epi*-pleuromutilin **6** was 4-fold more active than pleuromutilin in four of the test organisms, however in *E. coli* MC1061 it was 2-fold less active. The phenyl triazole variant with

C22-chloro substitution **9** was comparable to its 22-hydroxyl parent **3** in activity against the *S. aureus* and VRE strains and *E. coli* ΔTolC, however it was 8 times less potent in *E. coli* MC1061. The C22-bromo 12-*epi*-pleuromutilin **7** had comparable activity to pleuromutilin, as did the C22-bromo C20 phenyltriazole 12-*epi*-pleuromutilin (**10**), with the greatest change being a 16-fold decrease in potency in *E. coli* MC1061 compared to **3**. **10** also experienced a 4-fold decrease in activity compared to **3** in VRE. The tosylated derivatives **1** and **4** were comparable in all organisms, except VRE where the phenyltriazole derivative **4** had an 8-fold decrease in potency. Compound **5**, the non-electrophilic sulfonamide derivative of **1**, was 16-fold less active than **1** (parent) in the two *S. aureus* species, 4-fold less active in ΔTolC, and 8-fold less active in VRE. Compound **8**, 22-NHTs-20-phenyltriazole-12-*epi*-pleuromutilin, is an interesting case. The compound formed as an inseparable mixture with 2 equivalents of *p*-toluenesulfonamide, the desired compound making up 61% of the mass. This mixture held constant despite purification via column chromatography. Taking this into account, **8** is roughly as potent as **4** in *S. aureus* and ΔTolC and, and 4-8-fold more potent in VRE. Interestingly, all compounds containing a sulfonate or a sulfonamide at C22 were rendered inactive in *E. coli* MC1061. Both the vinyl sulfonamide **5** and its tosylate counterpart **1** may be recognized by efflux pumps, judging by the loss of activity in *E. coli* MC1061 compared to the ΔTolC strain. In the ΔTolC strain, the sulfonamide **5** was 4-fold less active than **1**, suggesting that a H-bond donor is unfavorable at this position. The retention in activity of **8** in comparison to its tosylate counterpart **4** does not match the trend of **5** and **1**. This observed activity retention may not be due directly to **8**, but due to its two associated molecules of *p*-toluenesulfonamide. Sulfonamides themselves are antibiotics which function by inhibiting dihydropteroate synthase (DHPS) which is involved in folate biosynthesis.[6] Thus, while pure **8** may be less active when

compared to **4**, there may be a synergistic effect between **8** and its residual *p*-toluenesulfonamide units.

Although the 22-chloro derivative of 12-*epi*pleuromutilin (**6**) shows promising activity, more work is necessary to determine to fully disprove it is acting as a covalently binding antibiotic. The variability in activity between the different leaving groups and inconsistency between the vinyl and phenyl triazoles suggests not only is it not covalently binding, but that a hydrogen bond as in the sulfonamide might be deleterious. The relative decrease in activity for the bromo compounds (**10** and **7**) compared to their chloro counterparts (**9** and **6**) suggests that more rapid hydrolysis back to 12-*epi*-pleuromutilin could reduce the activity of the bromo species; however, these were found to be highly active against other diseases (See section 4.3.3 below) and the phenyl triazole 12-*epi*-pleuromutilin **3** (Chapter 3) was quite active, suggesting that subtle interplays between the halogen and the underlying ribosome are responsible for activity. To better answer some of these questions, we have recently engaged in a collaboration with X-ray crystallographer Dr. Yuri S. Polikanov, at the University of Illinois at Chicago. He has previously successfully co-crystallized several of our derivatives with the ribosome, and we plan to send him our electrophilic series to establish whether they are indeed forming covalent bonds to the ribosome and determine what structural differences are responsible for the changes in activity among these compounds.

### 4.3.3 Antimalarial activity

Through the presentation of our research at the Center for Emerging Zoonotic and Arthropod-borne Pathogens (CeZAP) Infectious Disease Symposium, a multidisciplinary collaborative enterprise here at Virginia Tech, we met Dr. Michael Klemba, the director of the Virginia Tech Center for Drug Discovery Screening Lab (VTCDDSL). He had recently screened

commercial pleuromutilin derivatives and noted some activity against the malaria parasite, *P. falciparum*. We submitted our entire library of pleuromutilin derivatives to his lab for testing.

| Compound | Initial $EC_{50}$ | Retest $EC_{50}$ |
|---|---|---|
| **1** | 1810 | - |
| **TSP** | 6330 | - |
| **7** | 47 | 140 |
| **6** | 139 | 136 |

**Table 2.** Antimalarial activities (effective concentration inhibiting 50% of response, concentrations in nM) of selected compounds.

While most were unremarkable in their activity, the chloro and bromo derivatives **6** and **7** were very interesting. Tosyl pleuromutilin (**TSP**) and *epi*-tosyl pleuromutilin (**1**) had $EC_{50}$ values of 6.33 µM and 1.81 µM respectively, however the 22-chloro derivative **6** had a substantially better $EC_{50}$ value of 0.139 µM or 139 nM. The 22-bromo derivative **7** was initially more potent (47 nM) than **6** but had an anomalous curve shape. Upon further testing, **7** had an $EC_{50}$ value of 140 nM (retesting of **6** gave an $EC_{50}$ value of 136 nM). This data suggests that the C22-bromo **7** may be prone to degradation, but that the C22-chloro **6** is stable to biological conditions. Also of note is the importance of the epimerization at the C12 position, as can be seen in the differences of anti-malarial activity between native and epimerized tosyl pleuromutilin.

### 4.3.4 Cytotoxicity

The cytotoxicity of **1**, **TSP**, **6**, and **7** was determined by Abdallah (Adam) Abdelsattar of the Seleem lab. While the tosylated compounds **1** and **TSP** showed no cytotoxicity at the highest tested concentrations (128 µg/mL), **6** and **7** had $CC_{90}$ (cytotoxicity concentrations killing 90% of

cells) at 64 and 32 ug/mL respectively. The cytotoxicity of these compounds likely arises from off-target effects, due to the covalent warhead nature of the α-halo carbonyloxy moieties. α-Chloro carbonyls are selective for thiol residues, however α-bromo carbonyls are unselective, and this may explain the slight discrepancy in their cytotoxic activity.[7]

These findings are quite promising with ongoing work being performed by the Klemba lab to determine the mechanism of action of the derivatives. Toheeb Ajasa, a second-year graduate student in our lab, is taking on the mantle of a further SAR study to find even more potent pleuromutilin based anti-malarials that present a less toxic hazard.

## 4.4 Conclusion

In this chapter we have seen an interesting, albeit small, selection of work. The original hypothesis of covalently binding ribosome targeting antibiotics has not been proven, with initial results suggesting that interactions rather than covalent binding are responsible for activity. However, the anti-malarial nature of these derivatives was a serendipitous discovery. It is the intention of our lab to further elucidate the potentially electrophilic nature of these derivatives, as well as performing a full SAR study on their anti-malarial character.

## 4.5 Experimental

### 4.5.1 General synthetic

Unless otherwise noted, chemical reagents and solvents were purchased from EMD Millipore, Oakwood Chemical, Sigma-Aldrich, and Thermo Fisher Scientific. Unless otherwise specified, all reactions were carried out under an atmosphere of dry nitrogen in dried glassware. Commercially available starting materials and reagents were used as received or purified prior to use if necessary. Triethylamine was distilled from calcium hydride, and pyridine was distilled from

potassium hydroxide. Pleuromutilin was purchased as a commercial compound from TRC Canada. Analytical thin layer chromatography was performed Supelco 0.25 mm silica gel 60 $F_{254}$ plates. Visualization was accomplished by irradiation with a 254 nm UV lamp or by staining with an aqueous solution of ceric ammonium molybdate, an acidified ethanolic solution of *p*-anisaldehyde, or a basified solution of potassium permanganate. Chromatography was performed using a forced flow of the indicated solvent system on SiliCycle SiliaFlash P60 silica gel (40-63 μm) or via automated flash chromatography using a Biotage Selekt system with SiliCycle SiliaSep or Teledyne RediSepRf gold chromatography columns. Deionized water was obtained from the house deionized water system.

$^{1}$H NMR spectra were recorded on a Bruker Avance II 500 MHz spectrometer or an Agilent U4-DD2 400 MHz spectrometer. Chemical shifts are reported in parts per million from tetramethylsilane (0 ppm) using the solvent resonance as an internal standard ($CDCl_3$ 7.26 ppm). Data are reported as follows: chemical shift, multiplicity (s=singlet, d=doublet, t=triplet, q=quartet, m=multiplet, br=broad), coupling constants, and number of protons. Proton decoupled $^{13}$C NMR were recorded on a Bruker Avance II 500 MHz (126 MHz) spectrometer or an Agilent U4-DD2 400 MHz (101 MHz) spectrometer. Chemical shifts are reported in ppm from tetramethylsilane (0 ppm) using the solvent resonance as an internal standard ($CDCl_3$ 7.26 ppm). High resolution mass spectra were obtained on an Agilent Technologies 6220 TOF LC/MS or a Waters Synapt Q-TOF G2 or Thermo Exploris 120 HESI Orbitrap MS in the Department of Chemistry and the VT-Mass Spectrometry Incubator at the Virginia Polytechnic Institute and State University. Specific rotations were obtained on a Jasco P-2000 polarimeter.

### 4.5.2 Antimicrobial assay

Media components for microorganism growth were purchased from EMD Millipore, Sigma-Aldrich, Thermo Fisher Scientific, and Becton Dickinson and Company. Media and solutions were autoclaved or sterile filtered prior to use and manipulations were carried out in a laminar flow hood. Antibiotic testing was performed in polypropylene 96-well round bottom plates (Corning, Item #3365). The minimal inhibitory concentrations of the derivatives against MRSA, *S. aureus* NorA, vancomycin-resistant *Enterococcus*, *E. coli* TolC, and *A. baumanii* were tested by broth dilution using pleuromutilin as a positive control. Stock solutions were prepared at 10.0 mg/mL in DMSO (molecular biology grade). Working solutions were prepared at 2.56 mg/mL by dilution of the stock solutions with DMSO, followed by 2-fold serial dilutions in DMSO, and application of 10 µL of each dilution to 96-well plates, in duplicate. Bacteria were grown overnight in LB broth solutions from individual colonies. The overnight cultures were diluted to an $OD_{600}$ of 0.04 for outgrowth in LB. When the cultures had reached an $OD_{600}$ of 0.4-0.6 (4-6 h), the bacteria were rediluted to an $OD_{600}$ of 0.004 and applied to the plates (190 µL per well). The plates were incubated at 37 °C for 18 hours. The MIC was recorded as the lowest concentration that visibly inhibited growth of the bacteria as assessed by percent transmittance.

### 4.5.3 Synthetic procedures

**(3a*R*,4*R*,5*R*,7*S*,8*S*,9*R*,9a*S*,12*R*)-8-Hydroxy-4,7,9,12-tetramethyl-3-oxo-7-(2-(4-phenyl-1*H*-1,2,3-triazol-1-yl)ethyl)decahydro-4,9a-propanocyclopenta[8]annulen-5-yl 2-(tosyloxy)acetate (4):** Prepared from **3** according to General Method for Triazole Formation (Chapter 3) and purified via automated flash chromatography (Silicycle SiliaSep 25 g $SiO_2$ column, 40% EtOAC/$CH_2Cl_2$) to give **4** (192.5 mg, 80%) as a white foam: $^1$H NMR (500 MHz, $CDCl_3$) δ 7.81 – 7.74 (m, 5H), 7.40 (t, *J* = 7.4 Hz, 2H), 7.36 – 7.29 (m, 3H), 5.62 (d, *J* = 8.3 Hz, 1H), 4.58 – 4.40 (m, 4H), 3.58 (t, *J* = 6.1 Hz, 1H), 2.49 (d, *J* = 6.0 Hz, 1H), 2.43 (s, 3H), 2.31 (p,

*J* = 6.7 Hz, 1H), 2.27 – 2.21 (m, 1H), 2.21 – 2.11 (m, 2H), 2.08 – 1.99 (m, 2H), 1.92 (ddd, *J* = 13.9, 9.7, 6.2 Hz, 1H), 1.79 (s, 1H), 1.73 (dq, *J* = 14.4, 3.4 Hz, 1H), 1.66 – 1.55 (m, 2H), 1.52 – 1.39 (m, 2H), 1.38 – 1.31 (m, 1H), 1.37 (s, 3H), 1.14 – 1.04 (m, 2H), 1.12 (s, 3H), 0.95 (d, *J* = 7.0 Hz, 3H), 0.60 (d, *J* = 7.0 Hz, 3H); $^{13}$C NMR (126 MHz, $CDCl_3$) δ 216.7, 165.1, 148.0, 145.6, 132.6, 130.6, 130.1, 129.0, 128.3, 128.2, 125.8, 119.9, 72.0, 70.8, 65.2, 58.0, 46.8, 45.4, 42.8, 42.5, 41.9, 40.7, 36.6, 35.1, 34.5, 30.4, 26.9, 25.1, 21.8, 17.8, 16.7, 14.9, 11.2; HR-MS (ESI) calcd for $C_{37}H_{48}N_3O_7S$ $[M+H]^+$ 678.3207, found 678.3215; $[\alpha]_D^{23.7}$ = -18.4 (c = 1.40, $CHCl_3$).

**(3a*R*,4*R*,5*R*,7*R*,8*S*,9*R*,9a*S*,12*R*)-8-Hydroxy-4,7,9,12-tetramethyl-3-oxo-7-vinyldecahydro-4,9a-propanocyclopenta[8]annulen-5-yl tosylglycinate (5):** To a flame dried vial equipped with a stir bar, **1** (70.2 mg, 0.132 mmol), anhydrous $K_2CO_3$ (36.4 mg, 0.263 mmol), *p*-toluenesulfonamide (45.1 mg, 0.263 mmol), and anhydrous $CH_3CN$ (1.4 mL) were added. The vial was sealed with a Teflon-lined cap. The mixture was placed behind a blast shield, heated to 75 °C (oil bath), and stirred for 16 h, beginning as a white suspension in a clear solution, shifting to a milky white suspension at 0.5 h, and to a thick, off-white suspension containing very fine particles at 16 h. The mixture was cooled, and 0.5 mL of glacial acetic acid was added dropwise, decreasing the turbidity of the suspension, and producing more fine, off-white precipitate. The suspension was filtered through Celite (4 mm x 20 cm) using $CH_3CN$ and the filtrate concentrated. This residue was purified via automated flash chromatography (Silicycle SiliaSep 4 g $SiO_2$ column, 12-100% EtOAc/hexanes) to give an inseparable mixture of **5** (25.9 mg, 37%) and two equivalents of *p*-toluenesulfonamide as an amorphous white solid: $^1$H NMR (500 MHz, $CDCl_3$) δ 7.82 – 7.79 (m, 4H), 7.74 – 7.71 (m, 2H), 7.30 (d, *J* = 8.2 Hz, 5H), 7.28 (d, *J* = 8.3 Hz, 1H), 5.69 (dd, *J* = 17.4, 10.8 Hz, 1H), 5.52 (d, *J* = 8.4 Hz, 1H), 5.21 (dd, *J* = 10.8, 1.0 Hz, 1H), 5.19 – 5.14 (m, 2H), 4.99 (s, 4H), 3.70 (dd, *J* = 18.0, 5.5 Hz, 1H), 3.61 (dd, *J* = 18.0, 5.1 Hz, 1H), 3.39 (dd, *J* = 6.5, 2.2 Hz,

1H), 2.42 (s, 6H), 2.41 (s, 3H), 2.31 – 2.12 (m, 3H), 2.05 (d, *J* = 2.8 Hz, 1H), 2.01 – 1.94 (m, 1H), 1.76 (dq, *J* = 14.6, 3.2 Hz, 1H), 1.69 (s, 1H), 1.65 – 1.57 (m, 2H), 1.54 (d, *J* = 2.2 Hz, 1H), 1.50 – 1.38 (m, 2H), 1.36 (s, 3H), 1.34 – 1.28 (m, 1H), 1.12 – 1.04 (m, 4H), 0.96 – 0.88 (m, 4H), 0.50 (d, *J* = 7.1 Hz, 3H); $^{13}$C NMR (126 MHz, $CDCl_3$) δ 217.1, 167.9, 146.9, 143.9, 143.7, 139.2, 136.3, 129.9, 129.8, 127.4, 126.6, 115.4, 71.9, 70.6, 58.2, 45.4, 45.2, 44.8, 43.5, 41.9, 36.6, 34.5, 34.4, 30.1, 26.9, 25.0, 21.7, 21.7, 16.8, 14.9, 14.2, 10.9; HR-MS (ESI) calcd for $C_{29}H_{41}NO_6SNa$ $[M+Na]^+$ 554.2547, found 554.2554; $[\alpha]_D^{24.1}$ = 9.90 (c = 1.25, $CHCl_3$).

**(3a*R*,4*R*,5*R*,7*R*,8*S*,9*R*,9a*S*,12*R*)-8-Hydroxy-4,7,9,12-tetramethyl-3-oxo-7-vinyldecahydro-4,9a-propanocyclopenta[8]annulen-5-yl 2-chloroacetate (6):** To a flame dried vial equipped with a stir bar, **1** (67.0 mg, 0.126 mmol), anhydrous LiCl (13.5 mg, 0.318 mmol), and anhydrous DMF (0.70 mL) were added. The vial was sealed with a Teflon-lined cap, placed behind a blast shield, and heated (50 °C, oil bath) for 16 h. The mixture was cooled, diluted with EtOAc (8 mL), and washed with saturated aqueous $NH_4Cl$ solution (3x3 mL) and brine (3 mL), dried over $Na_2SO_4$, and concentrated to give a colorless glass. This residue was purified via automated flash chromatography (Silicycle SiliaSep 4 g $SiO_2$ column, 12-100% EtOAc/hexanes) to give **6** (33.0 mg, 66%) as an amorphous white solid: $^1$H NMR (500 MHz, $CDCl_3$) δ 5.76 (dd, *J* = 17.2, 11.0 Hz, 1H), 5.67 (d, *J* = 8.5 Hz, 1H), 5.26 – 5.20 (m, 2H), 4.01 (d, *J* = 15.1 Hz, 1H), 3.97 (d, *J* = 15.1 Hz, 1H), 3.46 (dd, *J* = 6.5, 2.1 Hz, 1H), 2.38 (p, *J* = 7.0 Hz, 1H), 2.32 – 2.18 (m, 2H), 2.15 – 2.07 (m, 2H), 1.83 (dq, *J* = 14.5, 3.2 Hz, 1H), 1.75 – 1.62 (m, 2H), 1.61 – 1.49 (m, 3H), 1.49 (s, 3H), 1.41 (dq, *J* = 14.7, 3.8 Hz, 1H), 1.26 (s, 3H), 1.21 – 1.11 (m, 2H), 0.99 (d, *J* = 7.0 Hz, 3H), 0.75 (d, *J* = 7.1 Hz, 3H); $^{13}$C NMR (1 26 MHz, $CDCl_3$) δ 217.0, 166.1, 146.9, 115.5, 72.0, 71.0, 58.3, 45.5, 45.4, 43.7, 42.0, 41.7, 36.8, 34.6, 34.5, 30.2, 27.0, 25.1, 17.0, 15.0, 14.3, 10.9; HR-MS (ESI) calcd for $C_{23}H_{34}ClO_6$ $(M+HCO_2^-)$ 441.2049, found 441.2057; $[\alpha]_D^{24.4}$ = 11.9 (c = 1.55, $CHCl_3$).

**(3a*R*,4*R*,5*R*,7*R*,8*S*,9*R*,9a*S*,12*R*)-8-Hydroxy-4,7,9,12-tetramethyl-3-oxo-7-vinyldecahydro-4,9a-propanocyclopenta[8]annulen-5-yl 2-bromoacetate (7):** To a flame dried vial equipped with a stir bar, **1** (82.8 mg, 0.155 mmol), anhydrous LiBr (28.3 mg, 0.326 mmol), and anhydrous acetone (0.80 mL) were added resulting in a clear, colorless solution. The vial was sealed with a Teflon-lined cap. The mixture was placed behind a blast shield, heated to 50 °C (oil bath), and stirred for 16 h resulting in a clear colorless solution over a fine white precipitate. After cooling, the reaction was diluted with EtOAc (2 mL) and filtered through Celite (4 mm x 20 cm, EtOAc). The filtrate was evaporated leaving a colorless glass. This residue was purified via automated flash chromatography (Silicycle SiliaSep 4 g $SiO_2$ column, 12-100% EtOAc/hexanes) to give **7** (53.2 mg, 78%) as an amorphous white solid: $^1$H NMR (500 MHz, $CDCl_3$) δ 5.73 (dd, *J* = 17.2, 11.1 Hz, 1H), 5.62 (d, *J* = 8.4 Hz, 1H), 5.25 – 5.16 (m, 2H), 3.76 (d, *J* = 12.3 Hz, 1H), 3.73 (d, *J* = 12.3 Hz, 1H), 3.44 (d, *J* = 6.4 Hz, 1H), 2.35 (p, *J* = 6.9 Hz, 1H), 2.30 – 2.16 (m, 2H), 2.11 (d, *J* = 2.7 Hz, 1H), 2.08 (dd, *J* = 16.1, 8.6 Hz, 1H), 1.80 (dq, *J* = 14.4, 3.2 Hz, 1H), 1.70 – 1.60 (m 2H), 1.59 – 1.47 (m, 3H), 1.46 (s, 3H), 1.38 (dq, *J* = 14.2, 3.6 Hz, 1H), 1.22 (s, 3H), 1.18 – 1.08 (m, 2H), 0.96 (d, *J* = 7.2, 3H), 0.73 (d, *J* = 7.0, 3H); $^{13}$C NMR (126 MHz, $CDCl_3$) δ 217.1, 165.9, 147.0, 115.5, 72.0, 71.0, 58.3, 45.5, 45.3, 43.6, 42.0, 36.8, 34.6, 34.5, 30.2, 27.0, 26.8, 25.1, 17.1, 15.0, 14.3, 10.9; HR-MS (ESI) calcd for $C_{23}H_{34}BrO_6$ ($M+HCO_2^-$) 485.1539, found 485.1560; $[\alpha]_D^{24.2}$ = 20.2 (c = 2.42, $CHCl_3$).

**(3a*R*,4*R*,5*R*,7*S*,8*S*,9*R*,9a*S*,12*R*)-8-Hydroxy-4,7,9,12-tetramethyl-3-oxo-7-(2-(4-phenyl-1*H*-1,2,3-triazol-1-yl)ethyl)decahydro-4,9a-propanocyclopenta[8]annulen-5-yl tosylglycinate (8):** To a flame dried vial equipped with a stir bar, **4** (79.5 mg, 0.117 mmol), anhydrous $K_2CO_3$ (74.5 mg, 0.539 mmol), *p*-toluenesulfonamide (26.0 mg, 0.152 mmol), and anhydrous $CH_3CN$ (1.0 mL) were added. The vial was sealed with a Teflon-lined cap, placed behind a blast shield, heated

to 75 °C (oil bath), and stirred for 16 h. The mixture was cooled, and glacial acetic acid (0.5 mL) was added dropwise. The suspension was filtered through Celite (4 mm x 20 cm, $CH_3CN$) and the eluant was concentrated. The residue was purified via automated flash chromatography (Silicycle SiliaSep 4 g $SiO_2$ column, 65-100% EtOAc/hexanes) to give **8** (16.7 mg, 21%) as an amorphous white solid: $^1$H NMR (500 MHz, $CDCl_3$) δ 7.79 – 7.76 (m, 2H), 7.76 (s, 1H), 7.73 (d, *J* = 7.9 Hz, 2H), 7.40 (t, *J* = 7.6 Hz, 2H), 7.32 (dd, *J* = 7.4, 1.3 Hz, 1H), 7.29 (d, *J* = 7.9 Hz, 2H), 5.51 (d, *J* = 8.4 Hz, 1H), 5.20 (q, *J* = 5.0 Hz, 1H), 4.57 – 4.44 (m, 2H), 3.70 (dd, *J* = 17.9, 5.6 Hz, 1H), 3.59 (dd, *J* = 17.9, 5.4 Hz, 1H), 3.55 (t, *J* = 5.9 Hz, 1H), 2.39 (s, 3H), 2.30 – 2.21 (m, 3H), 2.20 – 2.11 (m, 2H), 2.03 – 1.95 (m, 2H), 1.86 (ddd, *J* = 13.9, 9.7, 6.3 Hz, 1H), 1.75 – 1.72 (m, 1H), 1.64 – 1.51 (m, 2H), 1.46 – 1.35 (m, 2H), 1.34 (s, 3H), 1.33 – 1.27 (m, 1H), 1.12 – 1.02 (m, 1H), 1.04 (s, 3H), 0.96 – 0.92 (m, 4H), 0.50 (d, *J* = 7.0 Hz, 3H); $^{13}$C NMR (126 MHz, $CDCl_3$) δ 216.5, 167.9, 148.0, 143.9, 136.2, 130.4, 129.8, 128.9, 128.3, 127.3, 125.7, 119.7, 71.8, 70.6, 57.8, 46.7, 45.3, 44.8, 42.7, 42.5, 41.7, 40.6, 36.4, 34.9, 34.4, 30.3, 26.8, 25.0, 21.6, 17.7, 16.6, 14.8, 11.0; HR-MS (ESI) calcd for $C_{37}H_{49}N_4O_6S$ $[M+H]^+$ 677.3367, found 677.3378; $[\alpha]_D^{24.5}$ = -7.38 (c = 0.845, $CHCl_3$).

**(3a*R*,4*R*,5*R*,7*S*,8*S*,9*R*,9a*S*,12*R*)-8-Hydroxy-4,7,9,12-tetramethyl-3-oxo-7-(2-(4-phenyl-1*H*-1,2,3-triazol-1-yl)ethyl)decahydro-4,9a-propanocyclopenta[8]annulen-5-yl 2-chloroacetate (9):** To a flame dried vial equipped with a stir bar, **4** (48.0 mg, 0.0708 mmol), anhydrous LiCl (8.1 mg, 0.19 mmol), and anhydrous DMF (0.50 mL) were added. The vial was sealed with a Teflon-lined cap, placed behind a blast shield, heated (50 °C, oil bath), and stirred for 24 h. The mixture was cooled, diluted with EtOAc (5 mL), washed with saturated aqueous $NH_4Cl$ (3x3 mL) and brine (3 mL), dried ($Na_2SO_4$), and concentrated to give a colorless glass. This residue was purified via automated flash chromatography (Silicycle SiliaSep 4 g $SiO_2$ column, 60% EtOAc/hexanes) to

give **9** (34.0 mg, 89%) as an amorphous white solid: $^{1}$H NMR (500 MHz, $CDCl_3$) δ 7.80 – 7.76 (m, 3H), 7.42 (t, *J* = 7.0 Hz, 2H), 7.34 (dd, *J* = 7.3, 1.9 Hz, 1H), 5.63 (d, *J* = 8.4 Hz, 1H), 4.60 – 4.46 (m, 2H), 4.05 – 3.94 (m, 2H), 3.63 (t, *J* = 6.2 Hz, 1H), 2.63 (d, *J* = 6.3 Hz, 1H), 2.36 (p, *J* = 6.9 Hz, 1H), 2.32 – 2.14 (m, 3H), 2.13 – 2.07 (m, 2H), 1.93 (ddd, *J* = 13.9, 9.9, 6.2 Hz, 1H), 1.87 (s, 1H), 1.78 (dq, *J* = 14.6, 3.1 Hz, 1H), 1.72 – 1.60 (m, 2H), 1.58 – 1.49 (m, 1H), 1.49 – 1.36 (m, 2H), 1.46 (s, 3H), 1.19 (s, 3H), 1.18 – 1.12 (m, 1H), 1.11 (s, 1H), 0.99 (d, *J* = 7.1 Hz, 3H), 0.73 (d, *J* = 7.0 Hz, 3H); $^{13}$C NMR (126 MHz, $CDCl_3$) δ 216.7, 166.1, 148.0, 130.4, 128.9, 128.3, 125.7, 119.6, 71.8, 71.0, 57.9, 46.7, 45.4, 42.8, 42.7, 41.9, 41.6, 40.7, 36.6, 35.0, 34.5, 30.3, 26.9, 25.0, 17.9, 16.9, 14.8, 11.1; HR-MS (ESI) calcd for $C_{30}H_{41}ClN_3O_4$ $[M+H]^+$ 542.2786, found 542.2794; $[\alpha]_D^{23.4}$ = -21.0 (c = 1.51, $CHCl_3$).

**(3a*R*,4*R*,5*R*,7*S*,8*S*,9*R*,9a*S*,12*R*)-8-Hydroxy-4,7,9,12-tetramethyl-3-oxo-7-(2-(4-phenyl-1*H*-1,2,3-triazol-1-yl)ethyl)decahydro-4,9a-propanocyclopenta[8]annulen-5-yl 2-bromoacetate (10):** To a flame dried vial equipped with a stir bar, **4** (54.0 mg, 0.0797 mmol), anhydrous LiBr (12.8 mg, 0.15X mmol), and anhydrous acetone (0.50 mL) were added. The vial was sealed with a Teflon-lined cap, placed behind a blast shield, heated to 50 °C (oil bath) and stirred for 24 h. The initially clear solution developed a fine precipitate over the first hour of stirring. The mixture was cooled, diluted with EtOAc (2 mL), and filtered through Celite (4 mm x 20 cm, EtOAc). The filtrate was concentrated resulting in a clear glass. This residue was purified via automated flash chromatography (Silicycle SiliaSep 4 g $SiO_2$ column, 60% EtOAc/hexanes) to give **10** (35.0 mg, 75%) as an amorphous white solid: $^{1}$H NMR (500 MHz, $CDCl_3$) δ 7.81 – 7.77 (m, 2H), 7.76 (s, 1H), 7.44 – 7.39 (m, 2H), 7.36 – 7.30 (m, 1H), 5.59 (d, *J* = 8.4 Hz, 1H), 4.60 – 4.48 (m, 2H), 3.78 (d, *J* = 12.5 Hz, 1H), 3.74 (d, *J* = 12.5 Hz, 1H), 3.57 (t, *J* = 6.2 Hz, 1H), 2.35 (p, *J* = 7.0 Hz, 1H), 2.31 – 2.14 (m, 4H), 2.12 – 2.05 (m, 2H), 1.93 (ddd, *J* = 13.9, 9.6, 6.2 Hz, 1H), 1.76 (dq, *J* = 14.6,

3.2 Hz, 1H), 1.70 – 1.67 (m, 1H), 1.62 – 1.48 (m, 2H), 1.48 – 1.41 (m, 1H), 1.44 (s, 3H), 1.38 (dq, *J* = 14.6, 3.7 Hz, 1H), 1.18 – 1.06 (m, 2H), 1.16 (s, 3H), 0.96 (d, *J* = 7.0 Hz, 3H), 0.72 (d, *J* = 7.0 Hz, 3H); $^{13}$C NMR (126 MHz, $CDCl_3$) δ 216.5, 165.9, 148.0, 130.5, 128.9, 128.3, 125.7, 119.6, 71.9, 71.0, 57.9, 46.7, 45.3, 42.7, 42.5, 41.9, 40.6, 36.6, 34.9, 34.4, 30.3, 26.9, 26.7, 25.0, 17.9, 16.9, 14.8, 11.0; HR-MS (ESI) calcd for $C_{30}H_{41}BrN_3O_4$ $[M+H]^+$ 586.2280, found 586.2271; $[\alpha]_D^{23.1}$ = -15.1 (c = 1.58, $CHCl_3$).

**Figure S1.** $^{1}H$ NMR of **4** (500 MHz, $CDCl_3$)

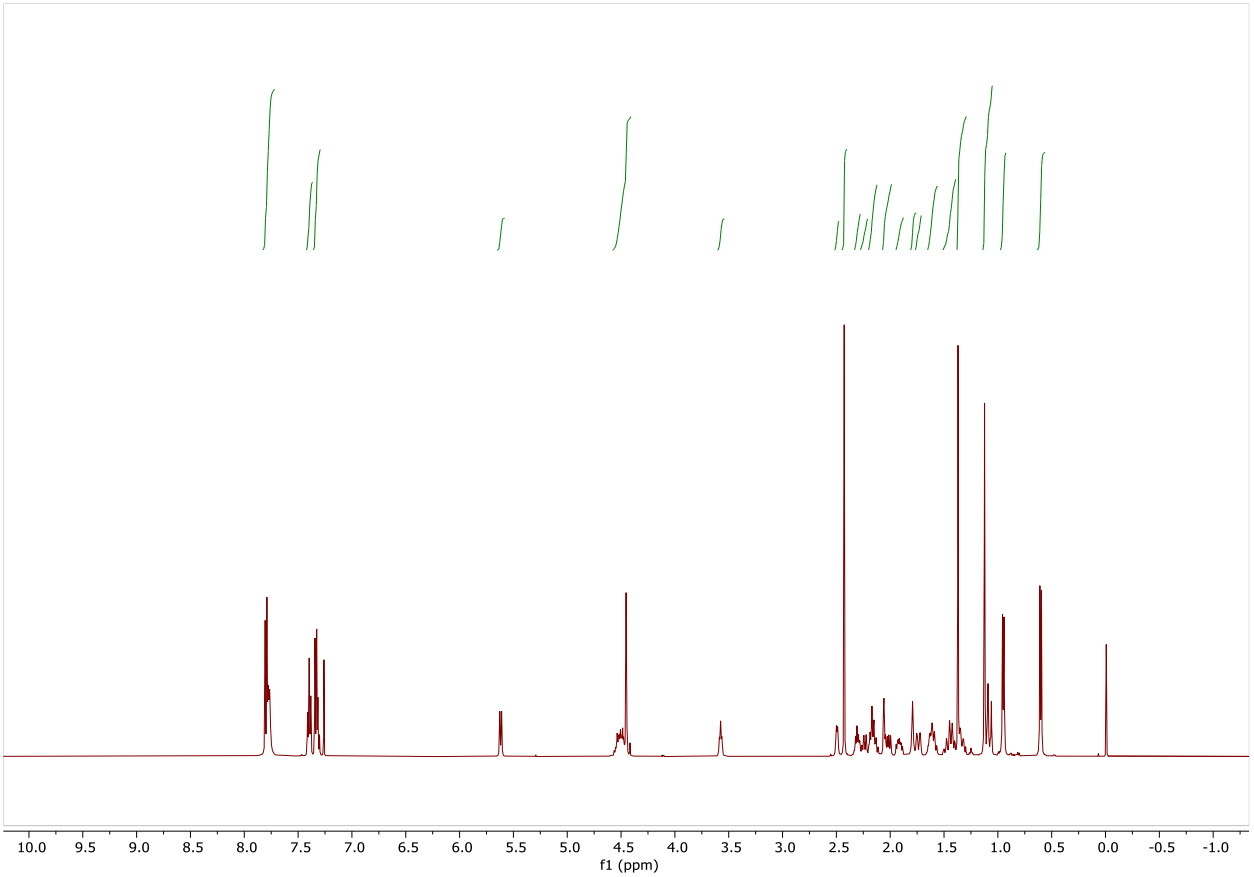


**Figure S2.** $^{13}C$ NMR of **4** (500 MHz, $CDCl_3$)

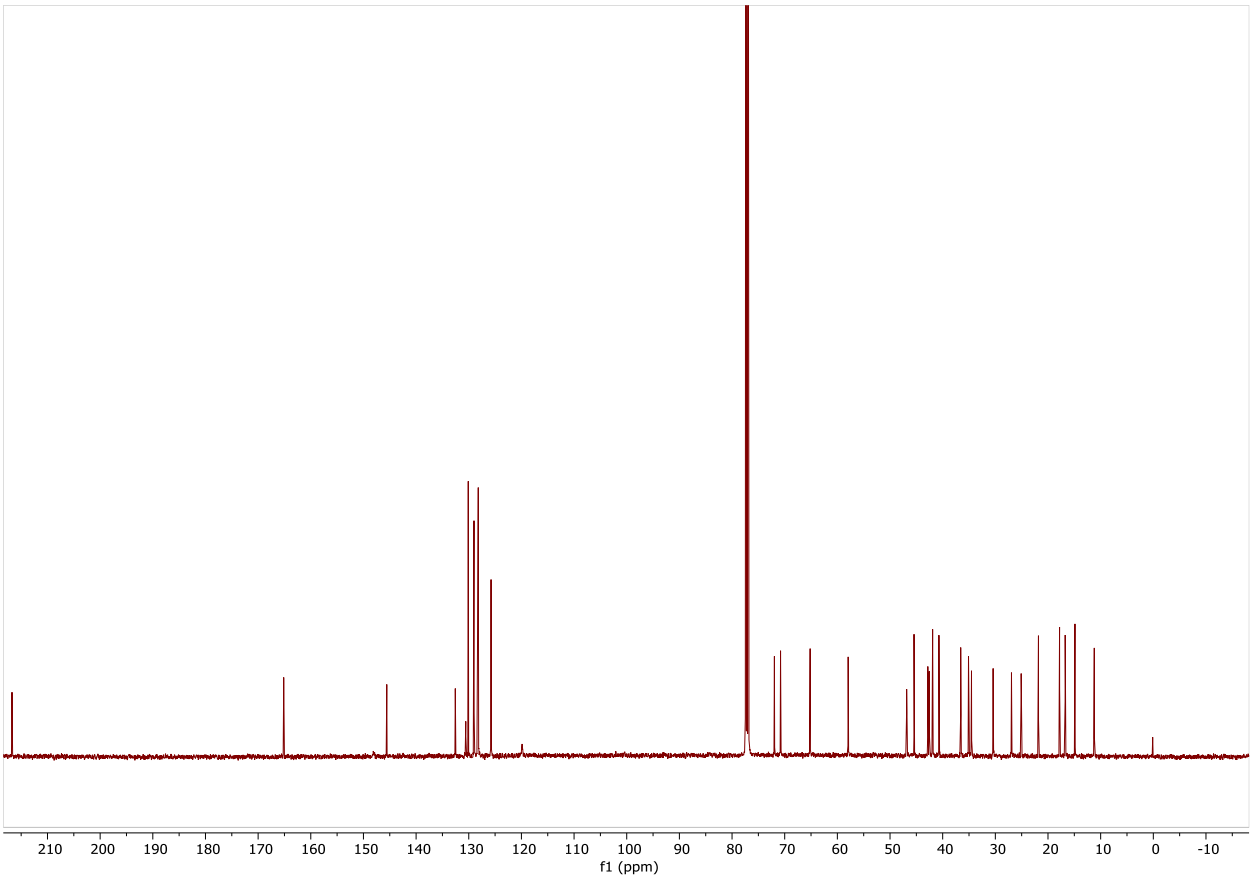


**Figure S3.** $^{1}$H NMR of **5** (500 MHz, $CDCl_3$)

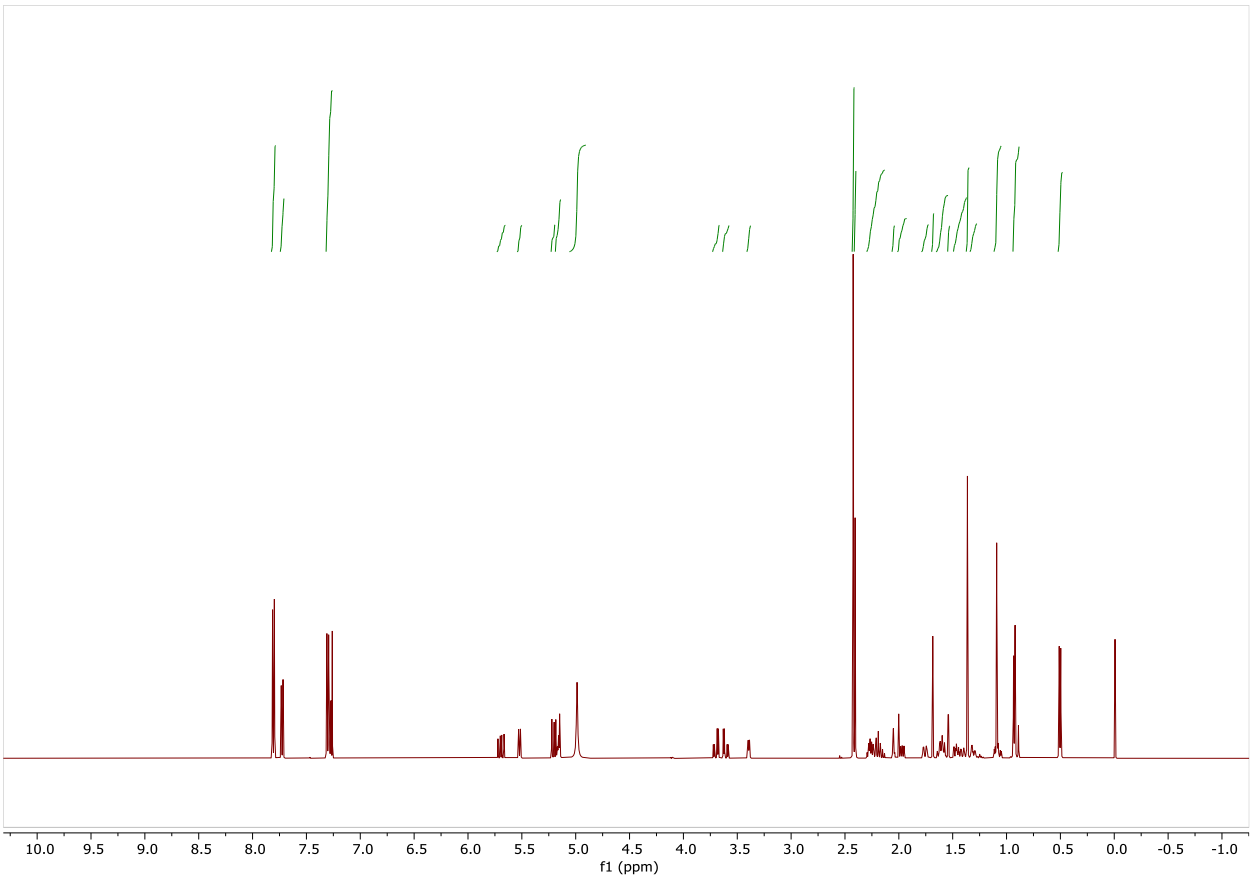


**Figure S4.** $^{13}C$ NMR of **5** (500 MHz, $CDCl_3$)

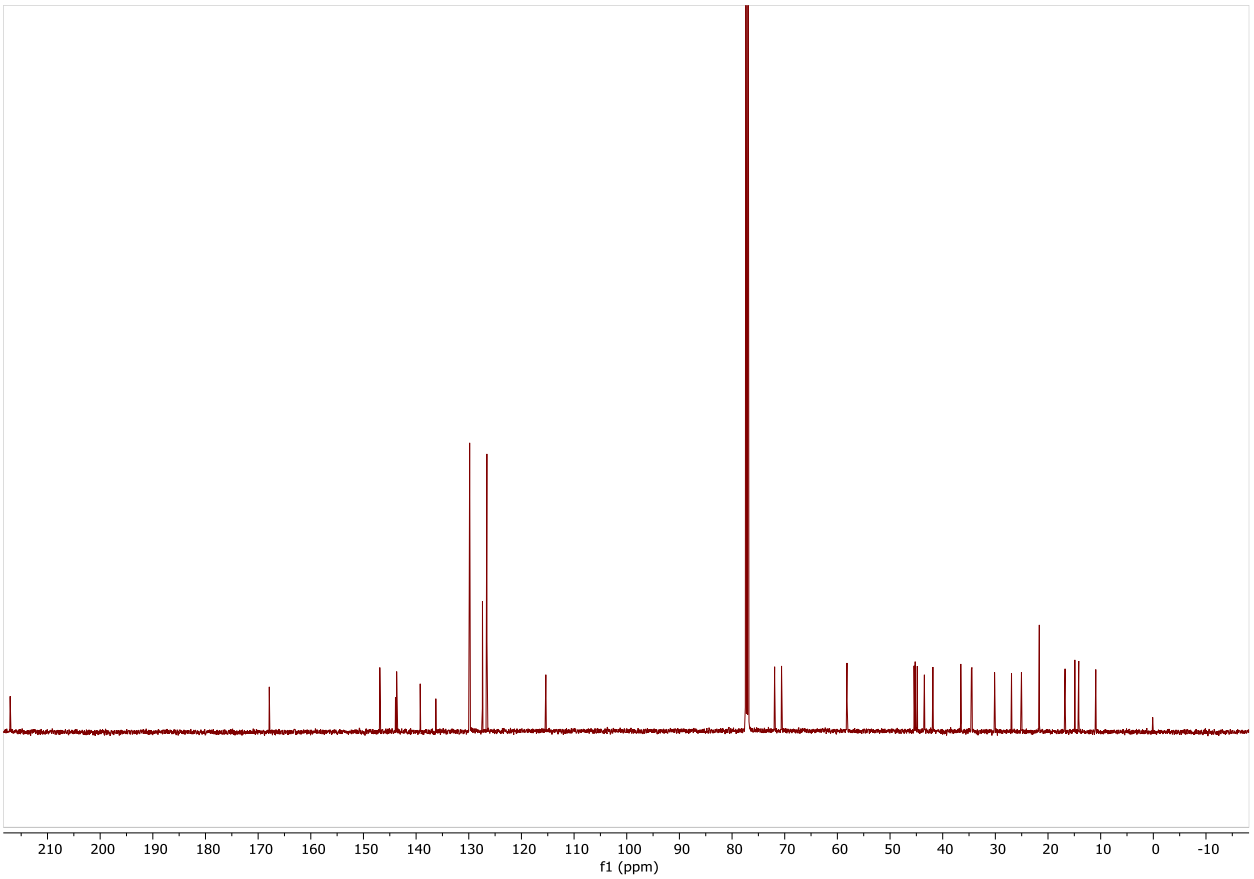


**Figure S5.** $^{1}$H NMR of **6** (500 MHz, $CDCl_3$)

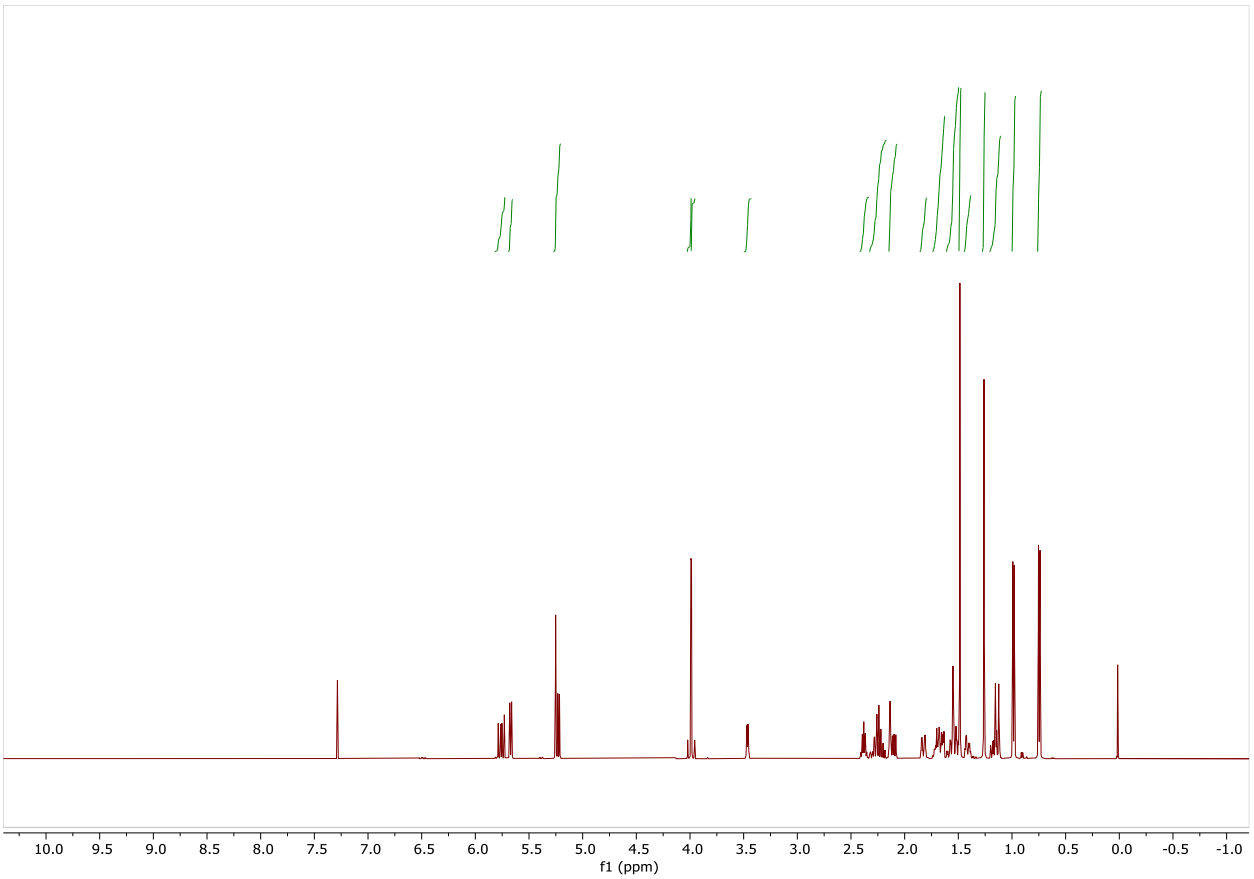


**Figure S6.** $^{13}C$ NMR of **6** (500 MHz, $CDCl_3$)

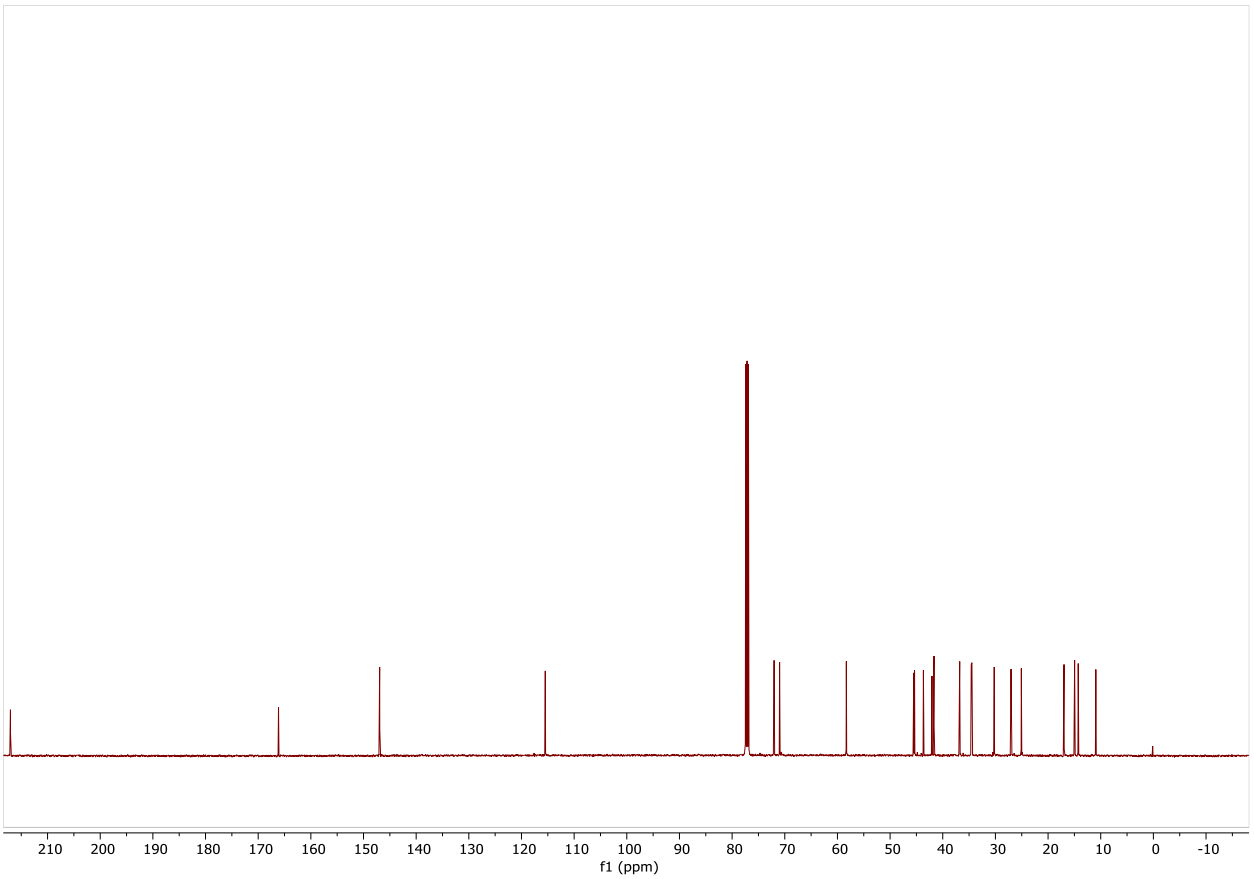


**Figure S7.** $^{1}$H NMR of **7** (500 MHz, $CDCl_3$)

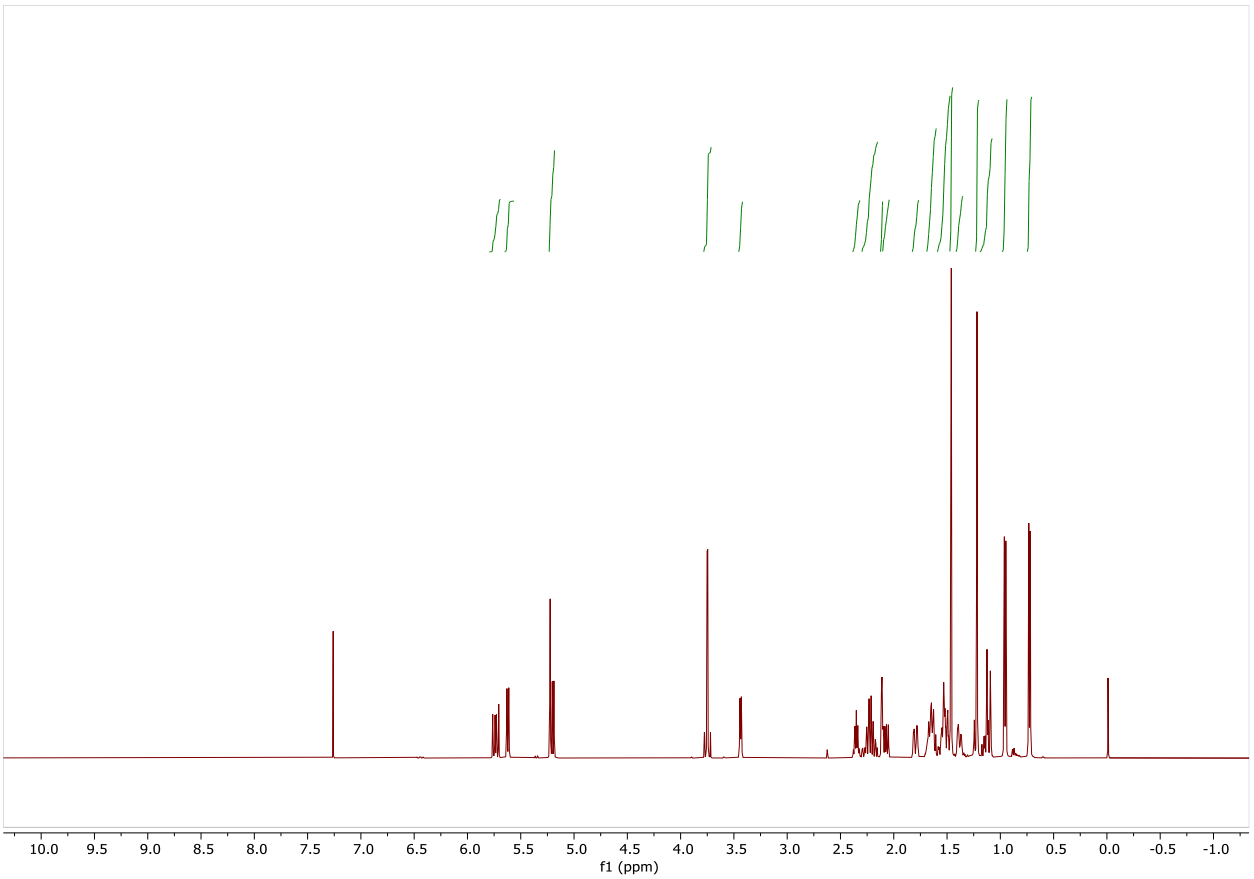


**Figure S8.** $^{13}C$ NMR of **7** (500 MHz, $CDCl_3$)

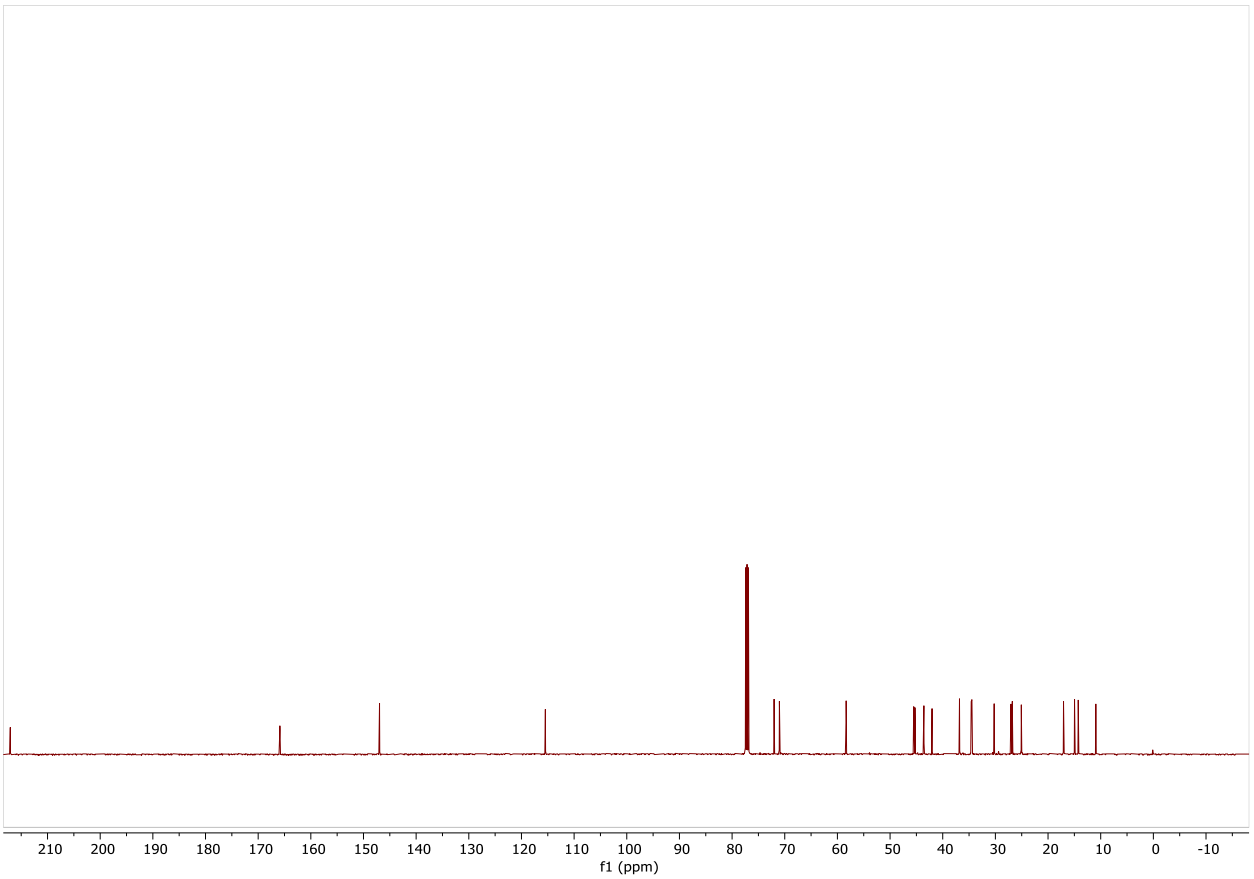


**Figure S9.** $^{1}$H NMR of **8** (500 MHz, $CDCl_3$)

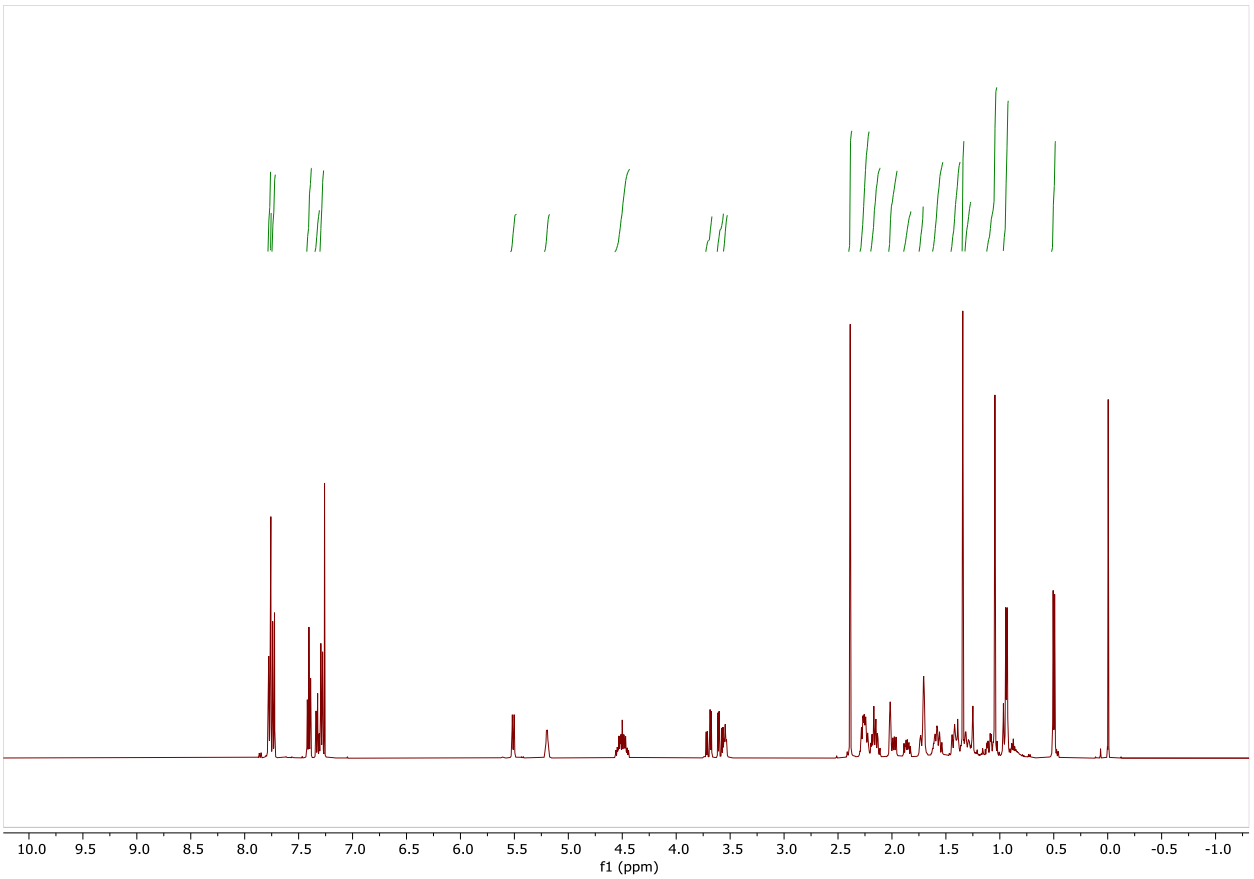


**Figure S10.** $^{13}C$ NMR of **8** (500 MHz, $CDCl_3$)

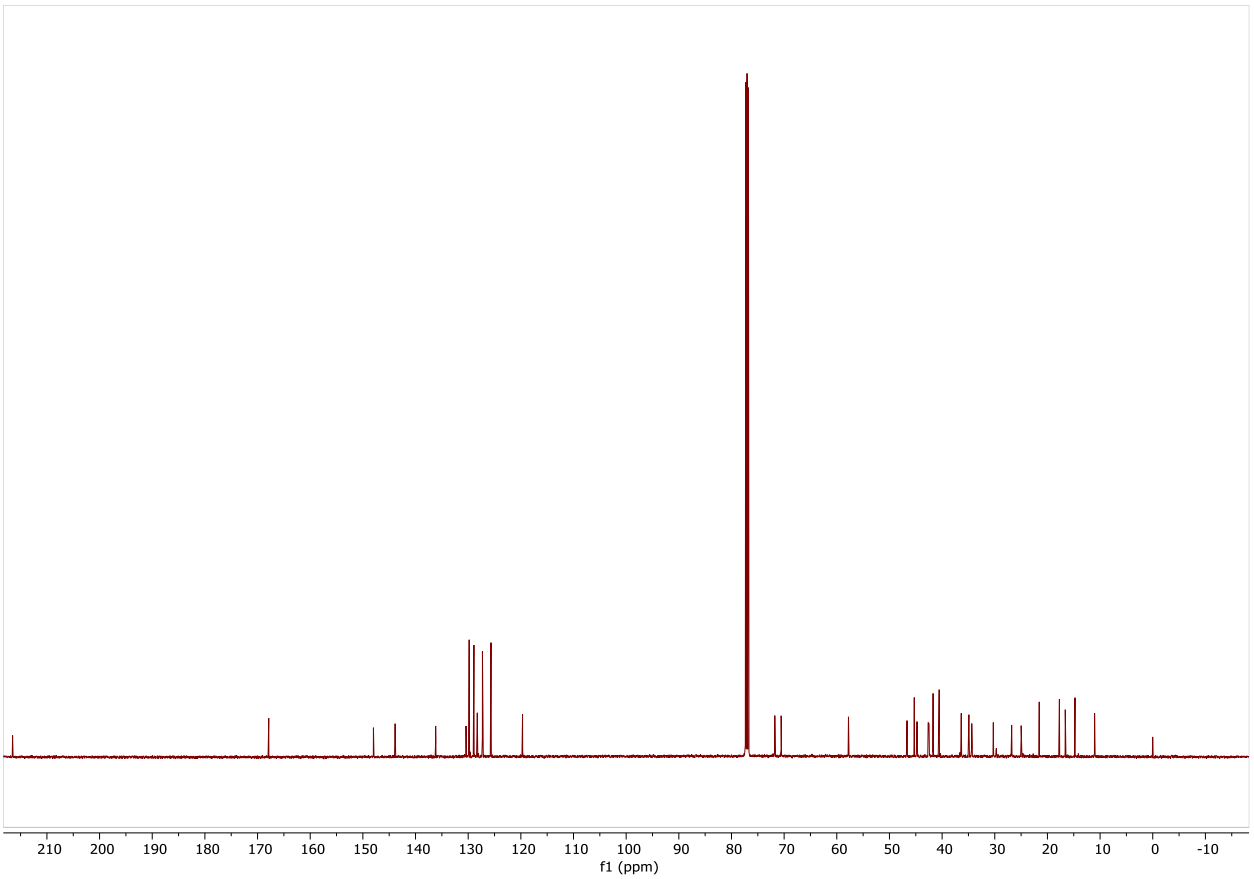


**Figure S11.** $^{1}$H NMR of **9**(500 MHz, $CDCl_3$)

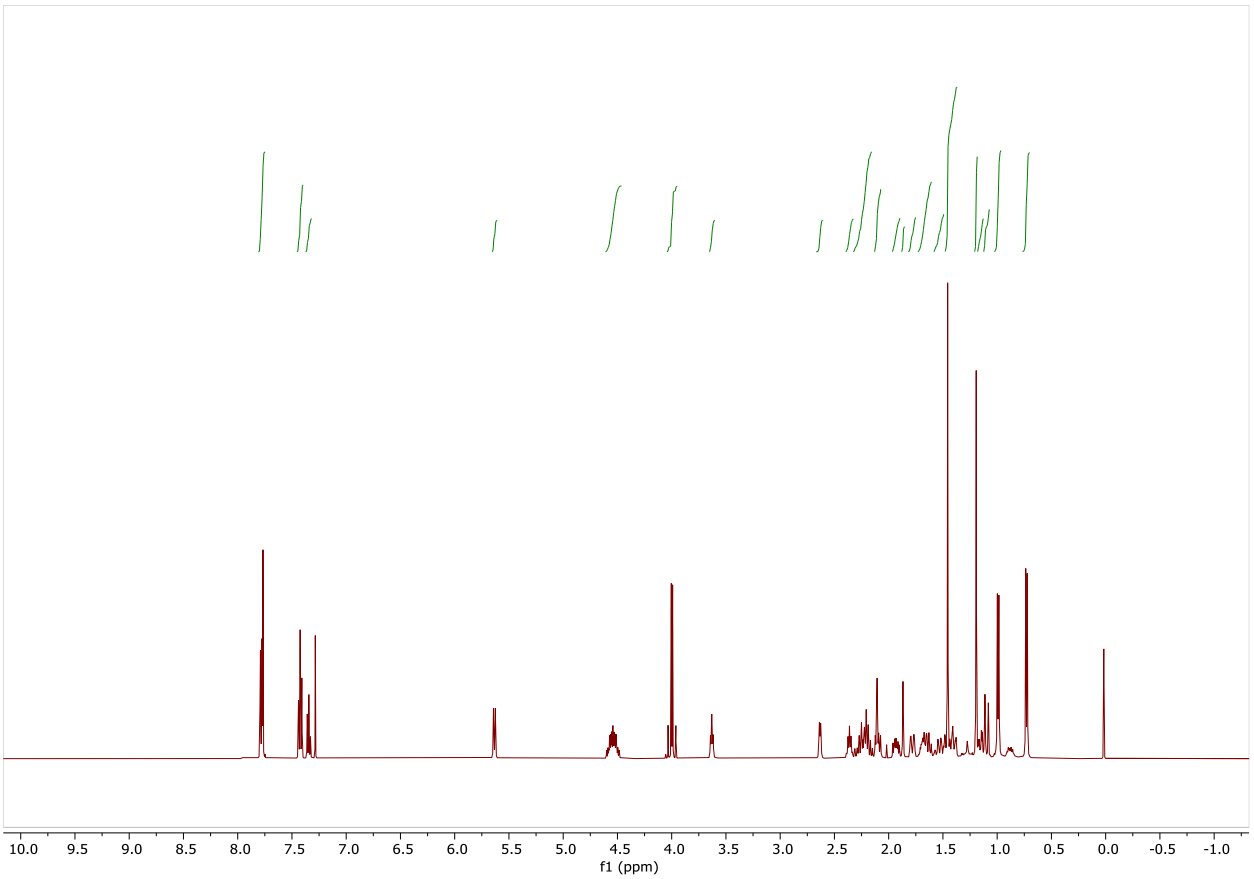


**Figure S12.** $^{13}C$ NMR of **9** (500 MHz, $CDCl_3$)

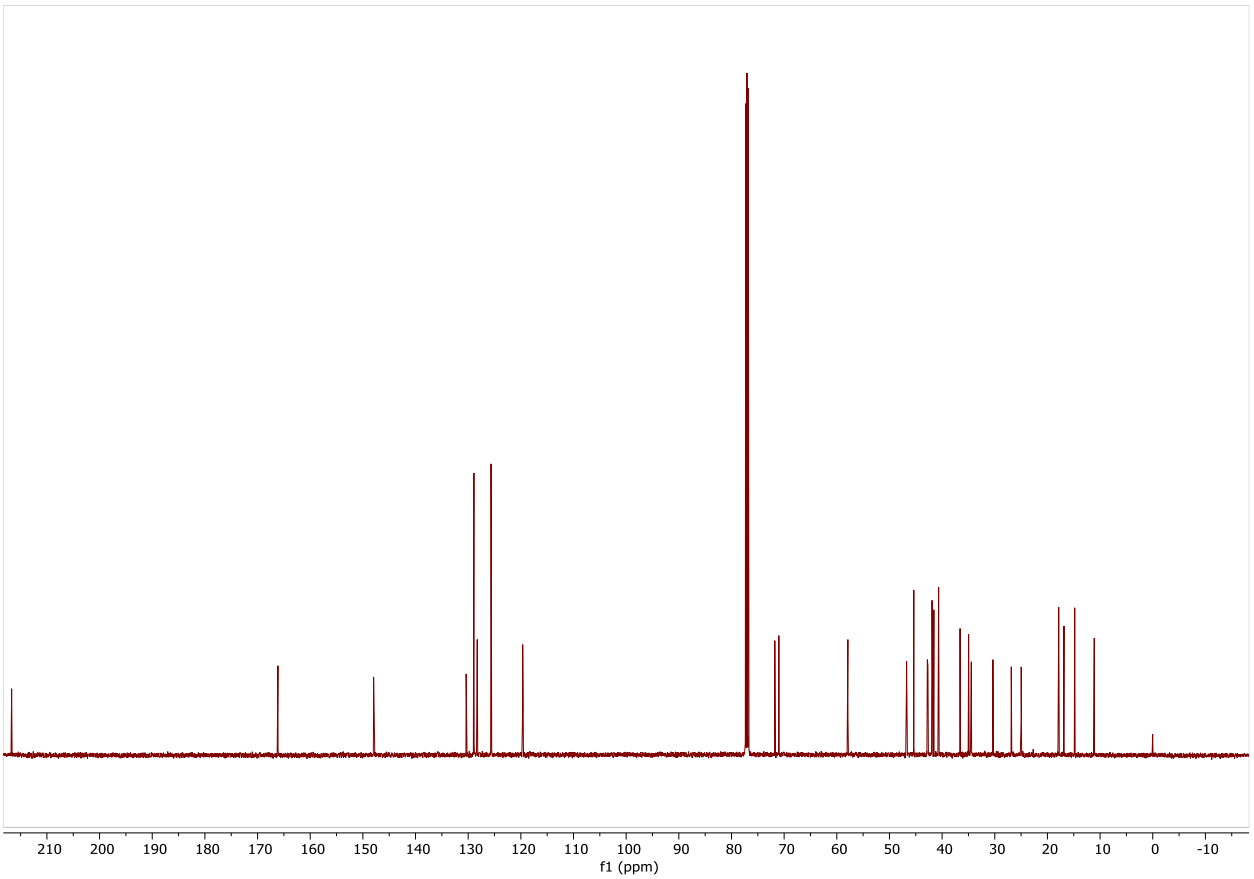


**Figure S13.** $^{1}$H NMR of **10** (500 MHz, $CDCl_3$)

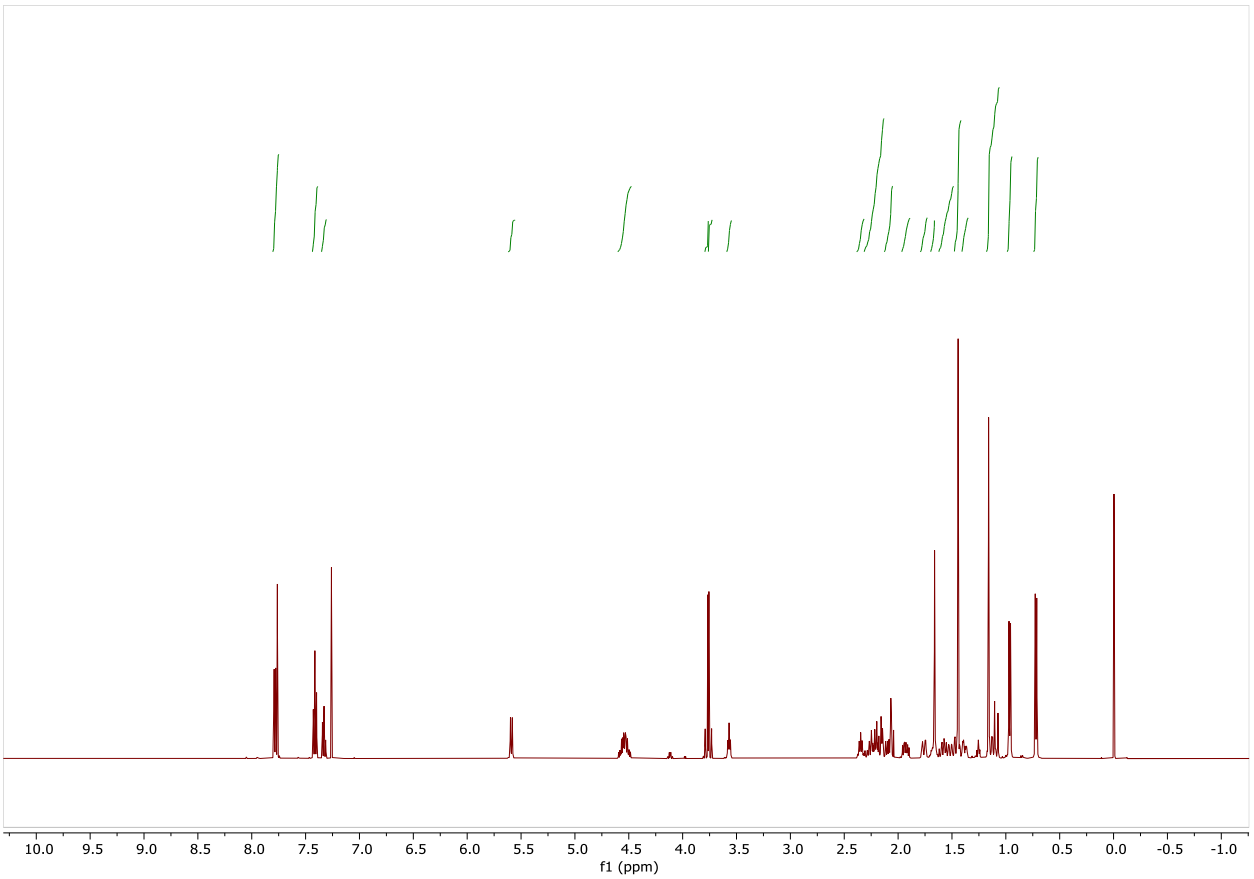


**Figure S14.** $^{13}C$ NMR of **10** (500 MHz, $CDCl_3$)

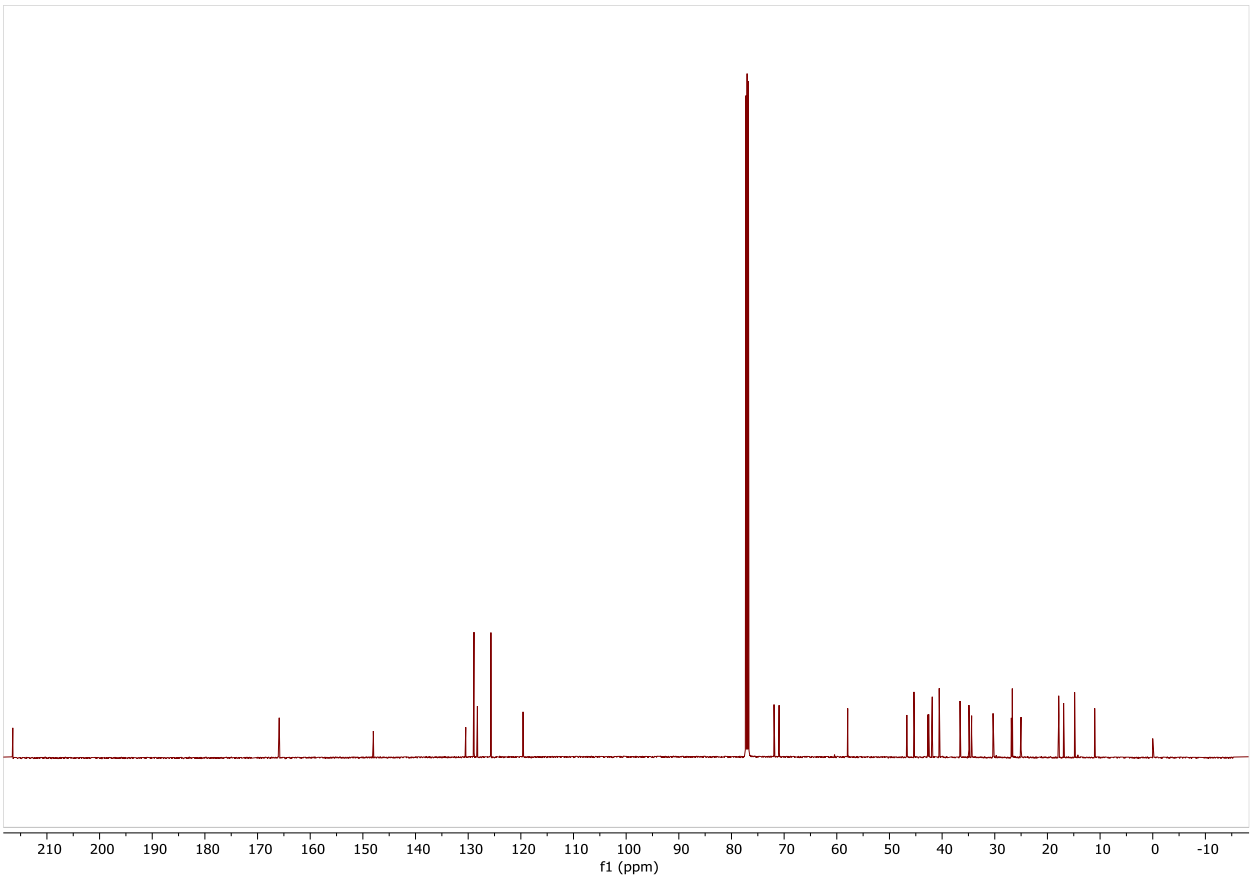


## 4.6 References

1. Hansen, J. L.; Ippolito, J. A.; Ban, N.; Nissen, P.; Moore, P. B.; Steitz, T. A., The structures of four macrolide antibiotics bound to the large ribosomal subunit. *Mol. Cell* **2002,** *10* (1), 117-128.
2. Semenkov, Y.; Shapkina, T.; Makhno, V.; Kirillov, S., Puromycin reaction for the A site-bound peptidyl-tRNA. *FEBS Lett.* **1992,** *296* (2), 207-210.
3. Wang, C.; Rago, A. J.; Dong, G., Direct β-Alkenylation of Ketones via Pd-Catalyzed Redox Cascade. *Org. Lett.* **2019,** *21* (9), 3377-3381.
4. Ervithayasuporn, V.; Pornsamutsin, N.; Prangyoo, P.; Sammawutthichai, K.; Jaroentomeechai, T.; Phurat, C.; Teerawatananond, T., One-pot synthesis of halogen exchanged silsesquioxanes: octakis(3-bromopropyl)octasilsesquioxane and octakis(3-iodopropyl)octasilsesquioxane. *Dalton Transactions* **2013,** *42* (37), 13747-13753.
5. De Kimpe, N.; Verhé, R., *The Chemistry of Alpha-Haloketones, Alpha-Haloaldehydes and Alpha-Holoimines*. Wiley: 1988; Vol. 1.
6. Lacey, R. W., Mechanism of action of trimethoprim and sulphonamides: relevance to synergy in vivo. *J. Antimicrob. Chemother.* **1979,** *5* (Supplement_B), 75-83.
7. Ábrányi-Balogh, P.; Petri, L.; Imre, T.; Szijj, P.; Scarpino, A.; Hrast, M.; Mitrović, A.; Fonovič, U. P.; Németh, K.; Barreteau, H.; Roper, D. I.; Horváti, K.; Ferenczy, G. G.; Kos, J.; Ilaš, J.; Gobec, S.; Keserű, G. M., A road map for prioritizing warheads for cysteine targeting covalent inhibitors. *European Journal of Medicinal Chemistry* **2018,** *160*, 94-107.

# Chapter 5. Highly active oligoethylene glycol pleuromutilins via systematic linker synthesis/one-pot attachment and a microscale solubility method

Logan M. Breiner,[a,b] Roman P. Slowinski,[a,c] and Andrew N. Lowell[a,b,d]*

[a]Department of Chemistry, Virginia Polytechnic Institute and State University (Virginia Tech), Blacksburg, VA 24061, USA

[b]Center for Emerging, Zoonotic, and Arthropod-borne Pathogens, Virginia Polytechnic Institute and State University (Virginia Tech), Blacksburg, VA 24061, USA

[c]Department of Biochemistry, Virginia Polytechnic Institute and State University (Virginia Tech), Blacksburg, VA 24061, USA

[d]Faculty of Health Sciences, Virginia Polytechnic Institute and State University (Virginia Tech), Blacksburg, VA 24061, USA

This study was published in the *Journal of Organic Chemistry*:

Breiner, L. M.; Slowinski, R. P.; Lowell, A. N., Highly active oligoethylene glycol pleuromutilins via systematic linker synthesis/one-pot attachment and a microscale solubility method. *The Journal of Organic Chemistry* **2025,** *90* (1), 919-924.

## 5.1 Abstract

The semisynthetic derivatization of natural products is crucial for their continued development as antibiotics. While commercial pleuromutilin derivatives depend on amines for solubility, we demonstrate high activity and solubility of oligoethylene glycol-substituted pleuromutilins achieved via a one-pot deprotection/attachment approach using thiolates protected as thioesters. The bifunctional linker synthesis is versatile and broadly applicable to other chemistries. Antibacterial assays revealed this simple glycolate modification enhanced inhibition 4-8-fold relative to pleuromutilin. A new microscale solubility method is also introduced.

## 5.2 Introduction

Antibiotics, particularly the vast majority derived from natural products, are outliers compared to typical small-molecule pharmaceuticals. In conventional medicinal chemistry, Lipinsky's Rule of Five[1] is used as a guidepost[2] and further restrictions, such as Veber's Rule (<10 rotatable bonds and <140 $Å^2$ total polar surface area), have been posited as additional indicators for drug-like molecules.[3] While synthetically developed drug-candidates seek to keep within these outlines, especially minimizing rotatable bonds to avoid conformational flexibility and thus lower potency, antibiotics routinely deviate from these rules.[4] Because natural products are fermentation-derived, semisynthetic antibiotics based on them, such as azithromycin,[5] tetracycline,[6] and Lefamulin,[7] require careful planning and the use of highly orthogonal reactions. Ideally, semisynthetic derivatives can be achieved through simple and rapid diversification of available scaffolds and quickly result in new libraries of antimicrobial compounds.

Pleuromutilin (**1**, **Figure 1**), a diterpenoid fungal secondary metabolite,[8-10] is a prime example of a successfully developed scaffold whose semisynthetic derivatives (**2**-**3**) have found use as clinical[11, 12] and veterinary[13] antibiotics. Demonstrating potent activity against Gram-positive, fastidious Gram-negative, and myco-bacteria,[14] clinically relevant pleuromutilins contain a thioether substitution at C22 linking an amine to the natural product core. These modifications enable the formation of water soluble salts, overcoming the poor water solubility of pleuromutilin itself (20 µg/mL).[15] Despite their variance from the traditional parameters of pharmaceuticals, pleuromutilin derivatives have demonstrated a propensity for resistance avoidance[14] and thus are prime targets for continued development.

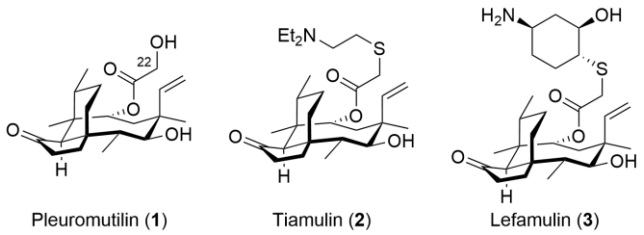


**Figure 1.** Pleuromutilin and its clinically relevant semisynthetic derivatives.

As part of ongoing efforts to synthesize conjugate antibiotics, we sought to functionalize pleuromutilin with varying length oligoethylene glycol (OEG) chains. Oligoethylene chains are attractive linker substrates because they are inexpensive, readily available, biocompatible, and water soluble.[16] By using linkers starting with a thiol and terminating with an azide, these derivatives would mimic the C22 thiol connection of all clinically approved pleuromutilin derivatives while also promoting orthogonal reaction conditions. The azide would facilitate copper-catalyzed azide alkyne cycloaddition reactions[17, 18] with other highly functionalized natural products. The excellent nucleophilicity of thiolate species would enable facile attachment to activated pleuromutilin.[19, 20] However, due to the ease with which thiols can be oxidized, this group would need to be protected prior to use.

While common,[21-26] the use of linkers to attach two or more materials tends to be system specific and is rarely discussed systematically.[27-30] We thus systemized the synthesis of azido terminated OEGs and connected them to pleuromutilin using a one-pot deprotection and attachment strategy. To our surprise, these compounds were highly active in and of themselves leading us to test them and hydroxy-terminated OEG derivatives against a series of pathogens.

## 5.3 Results and discussion

### 5.3.1 Synthesis

OEGs from di- to pentaethylene glycol (**4-7**, Scheme 1) were first monofunctionalized as the tosylate (**8-11**) by using an excess[31] of the OEGs. Treatment of **8-11** with sodium azide[32] gave azido-hydroxy OEGs **12-15**. Initial displacement with azide was chosen over the thioacetate due to their relative stabilities. The remaining hydroxy moiety of **12-15** was again activated via tosylation[31] to give **16-19**. Finally, displacement of the tosylate with thioacetate[33] was performed yielding thioesters **20-23**, masked thiols stable for storage and suitable use as nucleophiles after *in situ* deprotection.

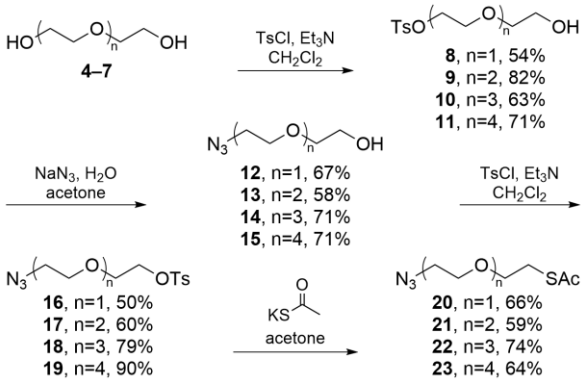


**Scheme 1.** Synthesis of azido-terminated bifunctional OEGs.

While this process was straightforward, practical challenges arose due to the linear and highly flexible nature of the linkers. Purification via recrystallization was not possible, necessitating chromatographic methods in which OEG chains behaved poorly. Due to the large number of repeating ether functional groups, products behaved very similarly to the starting materials, especially once the more polar hydroxy end groups were masked or transformed. Some OEGs also gave non-Gaussian distributions during chromatography, consistently eluting in multiple discreet peaks. Chromatographic separation only after the initial activation (to eliminate remaining OEGs and ditosylate biproducts) and after formation of the final thioacetate minimized waste while achieving purity. Complete consumption of intermediates in the intervening steps was

ensured by using an excess of the requisite nucleophile or electrophile and removal of excess reagents via extraction. Reactions were conducted under an inert atmosphere and processed rapidly because of the propensity of OEGs to form organic peroxides;[34] products and intermediates were stored cold and protected from light and oxygen.

To attach the functionalized OEGs to tosylpleuromutilin[18] (**24**, Scheme 2), we created a one-pot procedure by adapting protocols for deprotection of a thioester[33] and nucleophilic displacement using a thiolate.[19] The one-pot procedure using sodium hydroxide proved to be convenient and effective, converting **20**-**23** to **29**-**32** (n=1-4) in good yields (49-88%). The n=0 compound (**28**) was synthesized from **24** via a multistep route to avoid the generation of low-molecular weight organic azides that would violate the azide heavy atom rule and potentially be explosively unstable to friction, shock, and heat.[35] First, the tosylate of **24** was displaced using a thiolate generated from b-mercaptoethanol and sodium hydroxide to give **25**. The hydroxy-terminated **25** was then activated as tosylate **26**, which was subsequently displaced with azide to furnish **28**, completing the series of azido-terminated C22-OEG pleuromutilins where n=0-4. Contrasting with the free linkers, **28**-**32** behaved well during chromatography, likely because the pleuromutilin core added non-polar functionality that enabled better separation. The direct attachment of the azido group to C22 (**27**, not shown), was synthesized previously by direct azide displacement of **24**.[18]

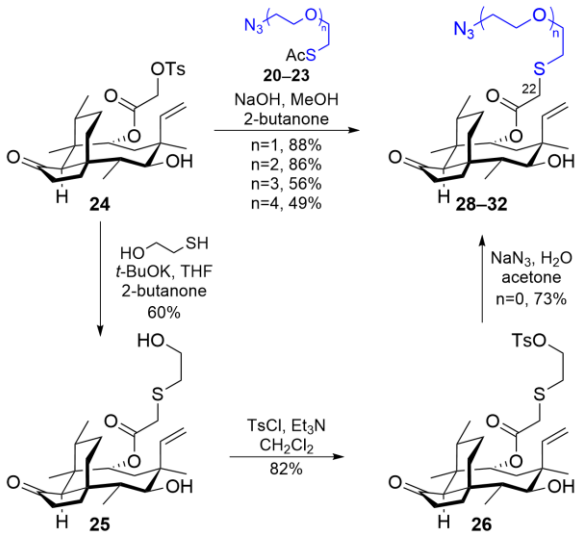


**Scheme 2.** Incorporation of azido-terminated OEGs onto the pleuromutilin scaffold.

### 5.3.2 Antibacterial testing

To determine if antimicrobial activity of PEG-derived pleuromutilins was due to the functionalized azido terminus or was an inherent property of the OEG, we synthesized hydroxy-terminated OEG chains and attached them to pleuromutilin (Scheme 3). Activation using tosyl chloride in the presence of excess OEGs proceeded as above to **8**-**11** and was expanded to include OEG6 (**35**) and OEG8 (**36**) to better assess activity as a function of increasing OEG length. Displacement using potassium thioacetate furnished hydroxy and thioester terminated OEGs **37**-**42**. Using a similar one-pot protocol, **37**-**42** were deprotected and appended onto **24** giving **43**-**48**. This work shows a straightforward way to make highly active azido- and hydroxy-terminated PEGs of various lengths with masked thiolate nucleophiles broadly suitable for use in linker chemistry and demonstrates their utility by directly attaching them via $S_N2$ reaction to activated natural products.

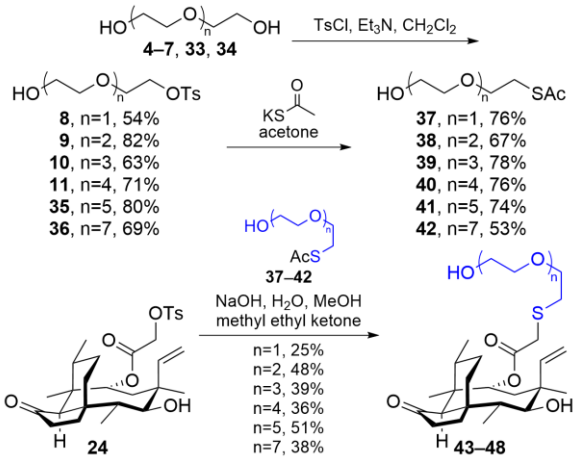


**Scheme 3.** Synthesis of hydroxy-terminated monofunctional OEGs and their incorporation onto the pleuromutilin scaffold.

Both series of OEG-pleuromutilin derivatives showed enhanced activity against Gram-positive bacteria relative to pleuromutilin (**1**, **Table 1**) with the azido-terminated compounds (**28-32**) generally showing greater activity than the hydroxy-terminated compounds (**25**, **43-48**). While the azido group directly attached to the C22 position (**27**)[18] did not significantly improve activity, shorter azido OEG chains (**28** and **29**) showed the greatest improvement in activity (8-fold improvement) with longer chain lengths (**29-32**) showing a smaller improvement in activity (4-fold improvement). While activity was good against *Staphylococcus aureus* strains and vancomycin resistant enterococcus (VRE), all compounds were inactive against *E. faecalis* (>100 mM). This general trend held true for the hydroxy OEG-pleuromutilins (**25**, **43-48**) with the addition of the longer linkers, especially OEG8 **48**, demonstrating the size limits of OEG functionalization at this site. The exception is against VRE, where all pleuromutilin-OEGs of both the $N_3$ and OH varieties showed equal activity (4x potency compared to **1**) except for **28** (8x potency), indicating the size cap had not been reached.

Pleuromutilin-OEG derivatives were inactive against the Gram-negative pathogens *Acinetobacter baumannii* and *Klebsiella pneumoniae* and were less active than **1** in *Escherichia coli* MC1061, with the same overall trend of diminishing activity with increasing chain length. However, the hydroxy series (**25**, **43**-**48**) performed better than the azide series (**28**-**32**) at equivalent lengths, a reversal of the trend seen in the Gram-positive *S. aureus*, which suggests the hydroxy-capped OEG has more favorable penetration properties than the azido-capped variants.[36] In *E. coli* with a TolC knockout (DTolC), all azide terminated pleuromutilin-OEGs were highly potent (8-fold increase over **1**) as were the shorter members of the hydroxy-terminated series. Based on these results, pleuromutilin-OEGs appear to be more easily recognized as substrates for the AcrAB-TolC efflux pump, likely because of their resemblance to non-ionic surfactants.[37]

| Compound[a] | MRSA 43300 | *S. aureus* 6538P | VRE | *E. coli* MC1061 | *E. coli* ΔTolC |
|---|---|---|---|---|---|
| **27** | 1.56 | 1.56 | 12.5 | 12.5 | 12.5 |
| **28** | 0.391 | 0.391 | 1.56 | 12.5 | 12.5 |
| **29** | 0.391 | 0.781 | 3.12 | 25 | 25 |
| **30** | 0.781 | 0.781 | 3.12 | 25 | 25 |
| **31** | 0.781 | 0.781 | 3.12 | 50 | 50 |
| **32** | 0.781 | 0.781 | 3.12 | 25 | 25 |
| **25** | 0.781 | 0.781 | 3.12 | 3.12 | 3.12 |
| **43** | 0.781 | 0.781 | 3.12 | 6.25 | 6.25 |
| **44** | 1.56 | 0.781 | 3.12 | 12.5 | 12.5 |
| **45** | 1.56 | 0.781 | 3.12 | 12.5 | 12.5 |
| **46** | 1.56 | 0.781 | 3.12 | 12.5 | 12.5 |
| **47** | 1.56 | 0.781 | 3.12 | 25 | 25 |
| **48** | 3.12 | 1.56 | 3.12 | 25 | 25 |
| **1** | 3.12 | 3.12 | 12.5 | 3.12 | 3.12 |

**Table 1.** Antibacterial activity of OEG-pleuromutilins. [a]Minimum inhibitory concentrations in mM. *E. faecalis*, *A. baumannii*, and *K. pneumoniae* were also tested but activity was >100 mM.

Efflux notwithstanding, inclusion of long, highly flexible OEG chains improved rather than worsened activity. Generally, compound optimization in medicinal chemistry seeks to reduce the number of rotatable bonds, preventing the molecule from sampling multiple conformational arrangements in the binding site—thus reducing binding efficiency—and better enabling cell membrane transit.[3] The reversal of this trend for these compounds may be because they have

enhanced uptake due to their amphiphilic nature with the hydrophobic pleuromutilin core and the hydrophilic OEG chains directly enhancing penetration through or transport across the cell membrane.[38] Another explanation may be that the binding of pleuromutilin-OEGs to their target sites is more entropically favorable compared to **1**. Highly hydrophobic molecules, such as **1**, must be contained within an ordered hydrogen bonding network, an entropically unfavorable state that is partially reduced once the molecule binds its target site, effectively shielding a portion of itself from organized solvent.[39, 40] The OEG chains may further disrupt the hydrogen-bonding network, increasing shielding and making the binding process even more entropically favorable. Another alternative, especially with regard to shorter chains having higher efficacy, is that the OEG chains may have their own discrete binding interactions within the ribosome.

### 5.3.3 Solubility assay

During the antimicrobial assays, an increase in optical density was observed at higher concentrations of pleuromutilin-OEG derivatives, specifically a visible precipitate that was morphologically distinct from the growing bacteria. Coupled with precipitation observed at a concentration range of 50-100 μM in the pleuromutilin control (a value in accord with its reported solubility),[15] this serendipitous finding suggested that we could use optical density readings to gauge solubility. Overall, we anticipated that introducing hydrophilic OEG chains onto a hydrophobic molecule, such as pleuromutilin, would enhance the water solubility of the resulting derivatives. A PEG-functionalization strategy has been used previously to create water-soluble prodrugs,[41] including an example with a pleuromutilin derivative,[42] and PEG conjugation can confer additional benefits,[43] such as increasing drug circulation in the blood and preventing its excretion, and preventing immune recognition of biologics. Our approach differs by instead using

low molecular weight OEGs, which are incorporated into the drug itself when it binds its target, and our focus on antibiotics.

Azide-terminated compounds **28**-**32** showed lower solubility at shorter chain lengths with solubility rising as the chain-length increased, showing that an increase in hydrogen bond–accepting ether groups tracks with increased solubility. The hydroxy-terminated series (**25**, **43**-**48**) all showed solubility greater than 200 µM, a minimum of a 4-fold increase relative to pleuromutilin. This result indicates that the presence of a more flexible terminal hydrogen bond-donating group is critical for increased solubility. As a common problem with pleuromutilin derivatives is their low solubility, which leads to poor bioavailability,[44] this facile method of functionalization may provide a way to create potent pleuromutilin derived antibiotics with better pharmacokinetics.[45] Furthermore, these results indicate that customary amine functionality, such as in **2**-**3**, may not be necessary for bioavailability.

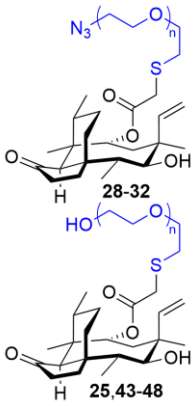


| Compound | PEG Units (n) | Solubility (µM)[a] |
|---|---|---|
| **27** | - | 50-100 |
| **28** | 0 | 25-50 |
| **29** | 1 | 25-50 |
| **30** | 2 | 50-100 |
| **31** | 3 | 100-200 |
| **32** | 4 | 100-200 |
| **25** | 0 | >200 |
| **43** | 1 | >200 |
| **44** | 2 | >200 |
| **45** | 3 | >200 |
| **46** | 4 | >200 |
| **47** | 5 | >200 |
| **48** | 7 | >200 |
| **1** | - | 50-100 |

**Table 2.** Solubility ranges of pleuromutilin OEG derivatives. [a]In 2.5% v/v DMSO/aqueous media. Concentrated solutions of the derivatives were serially diluted in 100% DMSO and then mixed with aqueous media to achieve the desired concentrations. After incubation (37 °C, 1 d), optical density was assessed using a plate reader. Listed ranges are between the soluble and insoluble wells.

While there are a variety of methods for determining solubility , they are often complicated and require substantial quantities of material.[46] By utilizing a UV-vis plate reader, the aqueous solubility of antibiotics was determined in a straightforward manner simultaneously with the minimum inhibitory concentrations. This method differs from other assay plate methods[47, 48] in that only small amounts (~50 µg) of valuable compound are needed, it is facile to conduct because it requires no evaporation stage, and it can be applied alongside other assays.

Small quantities are highly desirable when working with precious material. For example, LogP measurements are so material and labor intensive that calculated values are commonly used.[49] The efficiency of this assay could be further increased by using 384- or 1536-well plates, requiring even less material. It could also be used for non-aqueous solvent systems, provided volatility is controlled. This method could also be extended to non-druglike molecules where large quantities are undesirable, such as for highly toxic or explosive compounds.

The drawbacks of this assay are that a cosolvent was required for initial administration of the dissolved derivatives into the test wells. In this case, DMSO was used, resulting in a final concentration of 2.5% DMSO. The test concentrations are dictated by the saturation concentration of the material in the cosolvent, although reversal of the solvents could make this method applicable to non-organic soluble materials. Another drawback is that the solubility measurements are obtained as ranges and not as specific values; however, once an initial range is determined, additional assays with more precise dilutions could be used to give more accurate measurements. Lastly, supersaturation is a potential concern, but precipitation of compounds resistant to crystallization with another solvent is an established method, and the design of this assay mirrors that technique.

## 5.4 Conclusion

In summary, we have demonstrated that azido- and hydroxy-terminated OEG linkers bearing a masked thiol can be efficiently prepared and straightforwardly attached to the natural product pleuromutilin using a one-pot deprotection/attachment procedure. The resulting OEG-pleuromutilin derivatives have enhanced activity relative to the natural product as well as increased water solubility indicating that amine containing side chains may not be necessary for high activity with this class of natural product. Solubility was determined using serial dilutions in a microplate and visualized with a commonly available UV-vis plate reader, a new method which required only small amounts of compound (<100 μg). These findings and ongoing collaborations[18] enable the continued semisynthetic development of pleuromutilin for antibiotic lead discovery.

## 5.5 Experimental

### 5.5.1 General Synthetic

Unless otherwise noted, chemical reagents and solvents were purchased from EMD Millipore, Oakwood Chemical, Sigma-Aldrich, and Thermo Fisher Scientific. Unless otherwise specified, all reactions were carried out under an atmosphere of dry nitrogen in dried glassware. Commercially available starting materials and reagents were used as received or purified prior to use if necessary. Triethylamine was distilled from calcium hydride, and pyridine was distilled from potassium hydroxide. Pleuromutilin was purchased as a commercial compound from TRC Canada. Analytical thin layer chromatography was performed Supelco 0.25 mm silica gel 60 $F_{254}$ plates. Visualization was accomplished by irradiation with a 254 nm UV lamp or by staining with an aqueous solution of ceric ammonium molybdate, an acidified ethanolic solution of *p*-anisaldehyde, or a basified solution of potassium permanganate. Chromatography was performed using a forced flow of the indicated solvent system on SiliCycle SiliaFlash P60 silica gel (40-63 μm) or via automated flash chromatography using a Biotage Selekt system with SiliCycle SiliaSep or

Teledyne RediSepRf gold chromatography columns. Deionized water was obtained from the house deionized water system.

$^{1}$H NMR spectra were recorded on a Bruker Avance II 500 MHz spectrometer or an Agilent U4-DD2 400 MHz spectrometer. Chemical shifts are reported in parts per million from tetramethylsilane (0 ppm) using the solvent resonance as an internal standard ($CDCl_3$ 7.26 ppm). Data are reported as follows: chemical shift, multiplicity (s=singlet, d=doublet, t=triplet, q=quartet, m=multiplet, br=broad), coupling constants, and number of protons. Proton decoupled $^{13}$C NMR were recorded on a Bruker Avance II 500 MHz (126 MHz) spectrometer or an Agilent U4-DD2 400 MHz (101 MHz) spectrometer. Chemical shifts are reported in ppm from tetramethylsilane (0 ppm) using the solvent resonance as an internal standard ($CDCl_3$ 7.26 ppm). High resolution mass spectra were obtained on an Agilent Technologies 6220 TOF LC/MS or a Waters Synapt Q-TOF G2 or Thermo Exploris 120 HESI Orbitrap MS in the Department of Chemistry and the VT-Mass Spectrometry Incubator at the Virginia Polytechnic Institute and State University. Specific rotations were obtained on a Jasco P-2000 polarimeter.

### 5.5.2 Antimicrobial assay

Media components for microorganism growth were purchased from EMD Millipore, Sigma-Aldrich, Thermo Fisher Scientific, and Becton Dickinson and Company. Media and solutions were autoclaved or sterile filtered prior to use and manipulations were carried out in a laminar flow hood. Antibiotic testing was performed in polypropylene 96-well round bottom plates (Corning, Item #3365). The minimal inhibitory concentration of the derivatives against MRSA, *S. aureus* NorA, vancomycin-resistant *Enterococcus*, *E. coli* TolC, and *A. baumanii* was tested by broth dilution using pleuromutilin as a positive control. Stock solutions were prepared at 10.0 mg/mL in DMSO (molecular biology grade). Working solutions were prepared at 2.56 mg/mL by

dilution of the stock solutions with DMSO, followed by 2-fold serial dilutions in DMSO, and application of 10 µL of each dilution to 96-well plates, in duplicate. Bacteria were grown overnight in LB broth solutions from individual colonies. The overnight cultures were diluted to an $OD_{600}$ of 0.04 for outgrowth in LB. When the cultures had reached an $OD_{600}$ of 0.4-0.6 (4-6 h), the bacteria were rediluted to an $OD_{600}$ of 0.004 and applied to the plates (190 µL per well). The plates were incubated at 37 °C for 18 hours. The MIC was recorded as the lowest concentration that visibly inhibited growth of the bacteria as assessed by percent transmittance.

### 5.5.3 Solubility determination

Sample preparation for determination of solubility was as described in the Broth Microdilution Assay section above. The compounds were serially diluted in DMSO and the dilutions were transferred (5 µL) to 96-well plates and diluted (200 µL) with bacterial seeded cation-adjusted Mueller-Hinton broth. The concentrations of the test compounds on the plates were from 200-0.0977 µM. The plates were incubated at 37 °C for 16-24 hours depending on the test organism. OD600 measurements were taken on a Cytation 3 plate reader (BioTek). Solubility of the compounds was determined by visually assessing where precipitation for high-concentration wells ended for each compound and reporting a range based on the lowest-concentration well with precipitation and its neighboring well with no precipitation.

### 5.5.4 Synthesis

**General Method A, Preparation of Monotosylate Hydroxy OEGs:** To a round-bottomed flask equipped with a stirbar was added $CH_2Cl_2$ (0.2 M), triethylamine (2.1 equiv.) and an oligoethylene glycol (4 equiv.). With stirring, *p*-toluenesulfonyl chloride (1 equiv.) was added in one portion. The solution was allowed to stir for 12 h. The reaction was washed with aqueous solutions of 1 M $KHSO_4$ (50 mL) and saturated $NaHCO_3$ (50 mL). The organic layer was dried with $Na_2SO_4$ and concentrated. The residue was purified using column chromatography ($SiO_2$) with the indicated solvent mobile phase to afford the specific monotosylate hydroxy OEG.

**General Method B, Preparation of Azido Hydroxy OEGs: Caution!** Extended exposure of basic azides to dichloromethane can generate potentially explosive diazidomethane. All halogenated solvent should be scrupulously removed prior to creating the azido hydroxy OEGs. When using $NaN_3$, a Teflon spatula should be used to avoid sparking, acidic solutions for extraction should not be used to avoid generating toxic $HN_3$ gas, and care should be taken during weighing to avoid breathing $NaN_3$ dust. To a round-bottomed flask equipped with a stirbar and a reflux condenser was added a monotosylate hydroxy OEG prepared using Method A (1 equiv.), $NaN_3$ (2 equiv.), acetone (4 mL) and water (4 mL). With stirring, the mixture was brought to reflux and stirred for 15 h. The reaction was diluted with aqueous saturated $NaHCO_3$ (7 mL), and extracted with EtOAc (3x20 mL). The combined organics were dried with $Na_2SO_4$ and concentrated to afford the specific azido hydroxy OEG.

**General Method C, Preparation of Azido Tosylate OEGs:** To a round-bottomed flask equipped with a stirbar was added an azido hydroxy OEG prepared using Method B (1 equiv.), $CH_2Cl_2$ (20 mL), triethylamine (2 equiv.), and tosyl chloride (1.15 equiv.). The mixture was stirred at rt for 24 h. The reaction was quenched with 1 M aqueous $KHSO_4$ (20 mL), the layers were separated, and

the organic layer was washed with saturated aqueous $NaHCO_3$ (20 mL), dried with $Na_2SO_4$, and concentrated to afford the specific azido tosylate OEG.

**General Method D, Preparation of Azido Thioacetate OEGs:** To a round-bottomed flask equipped with a stirbar and was added an azido tosylate OEG prepared using Method C (1 equiv.), acetone (25 mL), and KSAc (1.4 equiv.). The mixture was stirred at rt for 9 h. The mixture was concentrated and the resulting oily salt was digested with $CH_2Cl_2$ (15 mL). The suspension was filtered through Celite ($CH_2Cl_2$), and the filtrate was concentrated to afford the specific azido thioacetate OEG.

**General Method E, Preparation of Hydroxy Thioacetate OEGs:** To a round-bottomed flask equipped with a stirbar was added a monotosyl hydroxy OEG prepared using Method A (1 equiv.), acetone (25 mL), and potassium thioacetate (1.5 equiv.). The mixture was stirred for 24 h. The mixture was concentrated and the resulting oily salt was triturated in $CH_2Cl_2$ (20 mL). The suspension was filtered through Celite ($CH_2Cl_2$), and the filtrate was concentrated to afford the specific hydroxy thioacetate OEG.

**2-(2-Hydroxyethoxy)ethyl 4-methylbenzenesulfonate (8)**: Prepared from **4** according to the general method A (2.00 g TsCl, 10.5 mmol) and purified using automated flash chromatography (SiliCycle 40g $SiO_2$ column, 0-10% $CH_3OH$ in $CH_2Cl_2$) to give **8** (1.46 g, 54%) as a colorless oil: $^1$H NMR (500 MHz, $CDCl_3$) δ 7.83 – 7.81 (m, 2H), 7.39 – 7.35 (m, 2H), 4.22 – 4.20 (m, 2H), 3.72 – 3.66 (m, 4H), 3.56 – 3.53 (m, 2H), 2.46 (s, 3H), 2.08 (s, 1H); $^{13}$C{$^1$H} NMR (126 MHz, $CDCl_3$) δ 145.0, 133.0, 129.9, 127.0, 72.5, 69.2, 68.6, 61.6, 21.7; HRMS (ESI) m/z: $[M + Na]^+$ Calcd for $C_{13}H_{20}O_6SNa$ 283.0611; Found 283.0612.

**2-(2-(2-Hydroxyethoxy)ethoxy)ethyl 4-methylbenzenesulfonate (9)**: Prepared from **5** according to the general method A (2.02 g TsCl, 10.6 mmol) and purified using automated flash chromatography (SiliCycle 40g $SiO_2$ column, 4% $CH_3OH$ in $CH_2Cl_2$) to give **9** (2.64 g, 82%) as a colorless oil: $^1H$ NMR (400 MHz, $CDCl_3$) δ 7.80 (dt, *J* = 8.6, 2.0 Hz, 2H), 7.36 – 7.32 (m, 2H), 4.18 – 4.15 (m, 2H), 3.73 – 3.68 (m, 4H), 3.61 (br s, 4H), 3.59 – 3.56 (m, 2H), 2.44 (s, 3H), 2.08 (br s, 1H); $^{13}C\{^1H\}$ NMR (101 MHz, $CDCl_3$) δ 145.0, 133.1, 130.0, 128.1, 72.6, 70.9, 70.5, 69.3, 68.8, 61.9, 21.8; HRMS (ESI) m/z: $[M + Na]^+$ Calcd for $C_{13}H_{20}O_6SNa$ 327.0872; Found 327.0869.

**2-(2-(2-(2-Hydroxyethoxy)ethoxy)ethoxy)ethyl 4-methylbenzenesulfonate (10)**: Prepared from **6** according to the general method A (2.02 g TsCl, 10.6 mmol) and purified using automated flash chromatography (SiliCycle 40g $SiO_2$ column, 4% $CH_3OH$ in $CH_2Cl_2$) to give **10** (2.29 g, 63%) as a colorless oil: $^1H$ NMR (500 MHz, $CDCl_3$) δ 7.83 – 7.79 (m, 2H), 7.35 (d, *J* = 8.1 Hz, 2H), 4.19 – 4.14 (m, 2H), 3.73 – 3.68 (m, 4H), 3.68 – 3.62 (m, 4H), 3.62 – 3.59 (m, *J* = 4.1 Hz, 6H), 2.49 (s, 1H), 2.45 (s, 3H); $^{13}C\{^1H\}$ NMR (126 MHz, $CDCl_3$) δ 144.8, 132.9, 129.8, 128.0, 72.5, 70.7, 70.6, 70.5, 70.3, 69.3, 68.7, 61.7, 21.6; HRMS (ESI) m/z: $[M + Na]^+$ Calcd for $C_{15}H_{24}O_7SNa$ 371.1134; Found 371.1144.

**14-Hydroxy-3,6,9,12-tetraoxatetradecyl 4-methylbenzenesulfonate (11)**: Prepared from **7** according to the general method A (1.00 g TsCl, 5.25 mmol) and purified using automated flash chromatography (SiliCycle 40g $SiO_2$ column, 4% $CH_3OH$ in $CH_2Cl_2$) to give **11** (1.46 g, 71%) as a colorless oil: $^1H$ NMR (500 MHz, $CDCl_3$) δ 7.82 – 7.79 (m, 2H), 7.35 (d, *J* = 8.0 Hz, 2H), 4.17 (dd, *J* = 5.5, 4.2 Hz, 2H), 3.74 – 3.60 (m, 14H), 3.60 (s, 4H), 2.71 (t, *J* = 6.2 Hz, 1H), 2.46 (s, 3H); $^{13}C\{^1H\}$ NMR (126 MHz, $CDCl_3$) δ 144.9, 133.0, 129.9, 128.1, 72.6, 70.8, 70.68, 70.66, 70.62, 70.58, 70.4, 69.4, 68.8, 61.8, 21.8; HRMS (ESI) m/z: $[M + Na]^+$ Calcd for $C_{17}H_{28}O_8SNa$ 415.1397; Found 415.1395.

**2-(2-Azidoethoxy)ethan-1-ol (12)**: Prepared from **8** (1.33 g, 5.11 mmol) according to the general method B to give **12** (0.450 g, 67%) as a colorless oil. Spectral data were in accord with those previously reported.[32]

**2-(2-(2-Azidoethoxy)ethoxy)ethan-1-ol (13)**: Prepared from **9** (2.64 g, 8.67 mmol) according to the general method B to give **13** (0.886 g, 58%) as a colorless oil. Spectral data were in accord with those previously reported.[32]

**2-(2-(2-(2-Azidoethoxy)ethoxy)ethoxy)ethan-1-ol (14)**: Prepared from **10** (2.16 g, 6.20 mmol) according to the general method B to give **14** (0.966 g, 71%) as a colorless oil. Spectral data were in accord with those previously reported.[32]

**14-Azido-3,6,9,12-tetraoxatetradecan-1-ol (15)**: Prepared from **11** (1.60 g, 4.065 mmol) according to the general method B to give **15** (0.763 g, 71% yield) as a colorless oil. Spectral data were in accord with those previously reported.[50]

**2-(2-Azidoethoxy)ethyl 4-methylbenzenesulfonate (16)**: Prepared from **12** (0.41 g, 3.13 mmol) according to the general method C and purified using automated flash chromatography (SiliCycle 40g $SiO_2$ column, 12-40-80% EtOAc in hexanes)to give **16** (0.490 g, 50%) as a yellow oil, and used in the next step without purification. Spectral data were in accord with those previously reported.[50]

**2-(2-(2-Azidoethoxy)ethoxy)ethyl 4-methylbenzenesulfonate (17)**: Prepared from **13** (0.866 g, 5.1 mmol) according to the general method C and purified using automated flash chromatography (SiliCycle 40g $SiO_2$ column, 12-40-80% EtOAc in hexanes)to give **17** (1.00 g, 60%) as a yellow oil, and used in the next step without purification. Spectral data were in accord with those previously reported.[50]

**2-(2-(2-(2-Azidoethoxy)ethoxy)ethoxy)ethyl 4-methylbenzenesulfonate (18)**: Prepared from **14** (0.966 g, 4.4 mmol) according to the general method C and purified using automated flash chromatography (SiliCycle 40g $SiO_2$ column, 12-55-100% EtOAc in hexanes)to give **18** (1.30 g, 79%) as a yellow oil, and used in the next step without purification. Spectral data were in accord with those previously reported.[50]

**14-Azido-3,6,9,12-tetraoxatetradecyl 4-methylbenzenesulfonate (19)**: Prepared from **15** (0.763 g, 2.90 mmol) according to the general method C and purified using automated flash chromatography (SiliCycle 40g $SiO_2$ column, 0-10% $CH_3OH$ in $CH_2Cl_2$) to give **19** (0.979 g, 90%) as a yellow oil, and used in the next step without purification. Spectral data were in accord with those previously reported.[50]

***S*-(2-(2-Azidoethoxy)ethyl) ethanethioate (20)**: Prepared from **16** (0.490 g, 1.72 mmol) according to the general method D and purified using automated flash chromatography (SiliCycle 40g $SiO_2$ column, 12-100% EtOAc in Hexanes) to give **20** (0.220 g, 66%) as a yellow oil. Spectral data were in accord with those previously reported.[51]

***S*-(2-(2-(2-Azidoethoxy)ethoxy)ethyl) ethanethioate (21)**: Prepared from **17** (1.00 g, 3.0 mmol) according to the general method D and purified using automated flash chromatography (SiliCycle 40g $SiO_2$ column, 12-100% EtOAc in Hexanes) to give **21** (0.419 g, 59%) as a yellow oil. $^1$H NMR (400 MHz, $CDCl_3$) δ 3.67 – 3.64 (m, 2H), 3.63 – 3.61 (m, 4H), 3.59 (t, $J$ = 6.4 Hz, 2H), 3.39 – 3.34 (m, 2H), 3.07 (t, $J$ = 6.4 Hz, 2H), 2.31 (s, 3H); $^{13}C\{^1H\}$ NMR (101 MHz, $CDCl_3$) δ 195.6, 70.7, 70.5, 70.2, 69.9, 50.8, 30.7, 29.0; HRMS (ESI) m/z: $[M + Na]^+$ Calcd for $C_8H_{15}N_3O_3SNa$ 256.0726; Found 256.0728.

***S*-(2-(2-(2-(2-Azidoethoxy)ethoxy)ethoxy)ethyl) ethanethioate (22)**: Prepared from **18** (1.30 g, 3.48 mmol) according to the general method D and purified using automated flash chromatography (SiliCycle 40g $SiO_2$ column, 12-100% EtOAc in Hexanes) to give **22** (0.719 g, 74%) as a yellow oil. $^1$H NMR (400 MHz, $CDCl_3$) δ 3.68 – 3.66 (m, 2H), 3.65 (br s, 4H), 3.64 – 3.60 (m, 4H), 3.59 (t, *J* = 6.4 Hz, 2H), 3.38 (dd, *J* = 5.6, 4.6 Hz, 2H), 3.08 (t, *J* = 6.5 Hz, 2H), 2.32 (s, 3H); $^{13}$C{$^1$H} NMR (101 MHz, $CDCl_3$) δ 195.6, 70.8 (2C), 70.7, 70.4, 70.2, 69.9, 50.8, 30.7, 28.9; HRMS (ESI) m/z: $[M + Na]^+$ Calcd for $C_{10}H_{19}N_3O_4SNa$ 300.0988; Found 300.0994.

***S*-(14-Azido-3,6,9,12-tetraoxatetradecyl) ethanethioate (23)**: Prepared from **19** (0.979 g, 2.35 mmol) according to the general method D and purified using automated flash chromatography (SiliCycle 40g $SiO_2$ column, 20-100% EtOAc/Hexanes) to give **23** (0.483 g, 64%) as a yellow oil. $^1$H NMR (400 MHz, $CDCl_3$) δ 3.68 – 3.66 (m, 2H), 3.66 – 3.64 (m, 8H), 3.64 – 3.61 (m, 4H), 3.59 (t, *J* = 6.5 Hz, 2H), 3.38 (dd, *J* = 5.5, 4.6 Hz, 2H), 3.08 (t, *J* = 6.5 Hz, 2H), 2.32 (s, *J* = 0.6 Hz, 3H); $^{13}$C{$^1$H} NMR (101 MHz, $CDCl_3$) δ 195.6, 70.83, 70.80, 70.77 (2C), 70.6, 70.4, 70.2, 69.9, 50.8, 30.7, 29.0; HRMS (ESI) m/z: $[M + Na]^+$ Calcd for $C_{12}H_{23}N_3O_5SNa$ 344.1250; Found 344.1253.

**(3a*R*,4*R*,5*R*,7*S*,8*S*,9*R*,9a*S*,12*R*)-8-Hydroxy-4,7,9,12-tetramethyl-3-oxo-7-vinyldecahydro-4,9a-propanocyclopenta[8]annulen-5-yl 2-(tosyloxy)acetate (24)**: Synthesis and characterization as previously reported.[18]

**(3a*R*,4*R*,5*R*,7*S*,8*S*,9*R*,9a*S*,12*R*)-8-Hydroxy-4,7,9,12-tetramethyl-3-oxo-7-vinyldecahydro-4,9a-propanocyclopenta[8]annulen-5-yl 2-((2-hydroxyethyl)thio)acetate (25)**: To a $N_2$ sparged, 1.0 M solution of *t*-BuOK in THF (1.00 mL, 1.00 mmol), freshly distilled b-mercaptoethanol (0.132 mL, 1.88 mmol) was added resulting in a white suspension. After stirring for 30 min, a $N_2$ sparged solution of **24** (0.5065 mg, 0.9508 mmol) in methyl ethyl ketone (4.0 mL

+ 0.3 mL rinse) was added. The white suspension was stirred overnight. The mixture was diluted with one third saturated aqueous $Na_2CO_3$ (10 mL) and extracted with $CH_2Cl_2$ (3x20 mL). The combined organic layers were dried with $Na_2SO_4$ and concentrated. The residue was purified using automated flash chromatography (SiliCycle 25g $SiO_2$ column, 22-31% EtOAc in $CH_2Cl_2$) to give **25** (248 mg, 60%) as a colorless oil: $^1$H NMR (500 MHz, $CDCl_3$) δ 6.46 (dd, *J* = 17.4, 11.0 Hz, 1H), 5.75 (d, *J* = 8.5 Hz, 1H), 5.35 (dd, *J* = 11.0, 1.5 Hz, 1H), 5.20 (dd, *J* = 17.4, 1.6 Hz, 1H), 3.76 – 3.72 (m, 2H), 3.35 (dd, *J* = 10.8, 6.6 Hz, 1H), 3.18 (s, 1H), 3.18 (s, 1H), 2.78 (dd, *J* = 6.1, 5.2 Hz, 2H), 2.7 – 2.68 (m, 1H), 2.33 (p, *J* = 6.9 Hz, 1H), 2.30 – 2.14 (m, 2H), 2.12 – 2.05 (m, 2H), 1.79 – 1.73 (m, 1H), 1.69 – 1.61 (m, 2H), 1.58 – 1.51 (m, 1H), 1.49 (dd, *J* = 10.7, 2.3 Hz, 1H), 1.48 – 1.42 (m, 1H), 1.44 (s, 3H), 1.39 – 1.34 (m, 1H), 1.31 (d, *J* = 16.1 Hz, 1H), 1.16 (s, 3H), 1.12 (td, *J* = 14.2, 4.6 Hz, 1H), 0.87 (d, *J* = 7.0 Hz, 3H) , 0.72 (d, *J* = 7.0 Hz, 3H); $^{13}$C{$^1$H} NMR (126 MHz, $CDCl_3$) δ 217.3, 169.8, 139.0, 117.5, 74.7, 69.8, 60.6, 58.2, 45.6, 44.9, 44.0, 41.8, 36.8, 36.4, 36.1, 34.6, 34.4, 30.5, 26.9, 26.4, 24.9, 17.0, 15.0, 11.7; HRMS (ESI) m/z: $[M + Na]^+$ Calcd for $C_{24}H_{38}O_5SNa$ 461.2332; Found 461.2339; $[\alpha]_D^{27}$ = +23.4 (*c* 1.13, $CH_3OH$).

**(3a*R*,4*R*,5*R*,7*S*,8*S*,9*R*,9a*S*,12*R*)-8-Hydroxy-4,7,9,12-tetramethyl-3-oxo-7-vinyldecahydro-4,9a-propanocyclopenta[8]annulen-5-yl 2-((2-azidoethyl)thio)acetate (28)**: To a stirring solution of **25** (0.404 g, 0.922 mmol) and tosyl chloride (0.246 g, 1.29 mmol) in $CH_2Cl_2$ (3.0 mL), triethylamine (0.260 mL, 1.86 mmol) was added. The mixture was stirred overnight. The mixture was diluted with $CH_2Cl_2$ (10 mL), washed sequentially with 0.3 M aqueous $KHSO_4$ (10 mL), saturated aqueous $NaHCO_3$ (10 mL), and brine (10 mL), dried with $Na_2SO_4$, and concentrated to afford **26** as an off-white amorphous solid (451 mg, 82% yield). This solution of **26** (451 mg, 0.760 mmol) and $NaN_3$ (80.2 mg, 1.23 mmol) in acetone (4 mL) and water (1.5 mL) was heated at reflux for 4.5 h. The mixture was cooled and concentrated. The residue was dissolved in EtOAc, washed

with water (2x10 mL) and brine (5 mL), dried over $Na_2SO_4$, and concentrated. The residue was purified using automated flash chromatography (SiliCycle 12 g $SiO_2$ column, 40% EtOAc in hexanes) to give **28** (256 mg, 73%) as a colorless oil (By NMR, compound **28** exists as two rotomeric forms in a 4:1 ratio, believed to be due to favorable orbital interactions of the azide with the alkene.[52] $^1$H NMR peaks have been reported as decimal amounts where peaks are resolvable, and $^{13}$C NMR peaks from the rotomer have been marked with an asterisk): $^1$H NMR (500 MHz, $CDCl_3$) δ 6.50 (dd, *J* = 17.4, 11.0 Hz, 0.8H), 6.49 (dd, *J* = 17.3, 11.0 Hz, 0.2H) 5.78 (d, *J* = 8.4, Hz, 1H), 5.382 (dd, *J* = 11.0, 1.6 Hz, 0.2H) 5.378 (dd, *J* = 11.0, 1.5 Hz, 0.8H), 5.24 (dd, *J* = 17.4, 1.5 Hz, 1H), 3.69 – 3.64 (m, 0.4H), 3.51 (td, *J* = 6.8, 1.3 Hz, 1.6H), 3.38 (d, *J* = 6.6 Hz, 1H), 3.21 (s, 1.6H), 3.20 (s, 0.4H), 2.99 – 2.95 (m, 0.4H), 2.84 – 2.81 (m, 1.6H), 2.37 (m, 1H), 2.32 – 2.17 (m, 2H), 2.15 – 2.09 (m, 2H), 1.80 (dq, *J* = 14.5, 3.2 Hz, 1H), 1.73 – 1.64 (m, 2H), 1.62 – 1.53 (m, 2H), 1.51 – 1.45 (m, 1H), 1.47 (s, 3H), 1.43 – 1.37 (m, 1H), 1.342 (d, *J* = 16.1 Hz, 0.8H), 1.340 (d, *J* = 16.1 Hz, 0.2H), 1.20 (s, 3H), 1.16 (td, *J* = 14.2, 4.5 Hz, 1H), 0.90 (d, *J* = 7.0 Hz, 3H), 0.758 (dd, *J* = 7.0 Hz, 2.4H), 0.753 (dd, *J* = 7.0 Hz, 0.6H); $^{13}$C{$^1$H} NMR (101 MHz, $CDCl_3$) δ 217.0, 168.8, 139.2, 139.1*, 117.5*, 117.4, 74.8, 69.7*, 69.6, 58.3, 50.8, 45.6, 45.0, 44.1, 42.7*, 41.9, 36.9, 36.2, 34.8*, 34.60*, 34.58, 34.5, 31.9, 30.6, 27.0, 26.5, 25.0, 17.0, 15.0, 11.6; HRMS (ESI) m/z: $[M + Na]^+$ Calcd for $C_{24}H_{37}N_3O_4SNa$ 486.2397; Found 486.2390; $[\alpha]_D^{24}$ = +25.6 (*c* 4.28, $CH_3OH$).

**(3a*R*,4*R*,5*R*,7*S*,8*S*,9*R*,9a*S*,12*R*)-8-Hydroxy-4,7,9,12-tetramethyl-3-oxo-7-vinyldecahydro-4,9a-propanocyclopenta[8]annulen-5-yl 2-((2-(2-azidoethoxy)ethyl)thio)acetate (29)**: A solution of **20** (0.209 g, 1.10 mmol) in MeOH (1.0 mL) was sparged with $N_2$ for 15 min and a sparged solution of 10 N NaOH in $H_2O$ (0.11 mL, 1.1 mmol) was added. The mixture was stirred for 40 min, and then added to a stirring, sparged solution of **24** (0.533 g, 1.00 mmol) in methyl

ethyl ketone (4.1 mL). The mixture stirred at 60 °C (oil bath) for 24 h. After cooling, the mixture was concentrated, the residue was taken up in water (15 mL) and EtOAc (15 mL), and the layers were separated. The aqueous layer was extracted with EtOAc (3x15 mL) and the combined organic layers were dried over $Na_2SO_4$ and concentrated. The residue was purified using automated flash chromatography (SiliCycle 12 g $SiO_2$ column, 30% EtOAc in hexanes) to give **29** (447 mg, 88%) as a colorless oil: $^1$H NMR (500 MHz, $CDCl_3$) δ 6.48 (dd, *J* = 17.4, 11.0 Hz, 1H), 5.74 (d, *J* = 8.4 Hz, 1H), 5.34 (dd, *J* = 11.0, 1.6 Hz, 1H), 5.20 (dd, *J* = 17.4, 1.6 Hz, 1H), 3.68 (td, *J* = 6.5, 1.6 Hz, 2H), 3.63 (dd, *J* = 5.5, 4.6 Hz, 2H), 3.38 (dd, *J* = 5.6, 4.5 Hz, 2H), 3.36 – 3.33 (m, 1H), 3.21 (s, 2H), 2.81 (t, *J* = 6.4 Hz, 2H), 2.33 (p, *J* = 7.0 Hz, 1H), 2.30 – 2.14 (m, 2H), 2.11 – 2.05 (m, 2H), 1.76 (dq, *J* = 14.5, 3.1 Hz, 1H), 1.69 – 1.61 (m, 2H), 1.59 – 1.50 (m, 1H), 1.48 (br s, 1H), 1.48 – 1.42 (m, 1H), 1.45 (s, 3H), 1.39 – 1.34 (m, 1H), 1.32 (d, *J* = 16.1 Hz, 1H), 1.16 (s, 3H), 1.16 – 1.08 (m, 1H), 0.87 (d, *J* = 7.0 Hz, 3H), 0.73 (d, *J* = 7.0 Hz, 3H); $^{13}$C{$^1$H} NMR (126 MHz, $CDCl_3$) δ 217.2, 169.0, 139.0, 117.3, 74.6, 70.7, 69.8, 69.2, 58.2, 50.7, 45.5, 44.7, 43.9, 41.8, 36.8, 36.0, 34.7, 34.5, 31.9, 30.4, 26.8, 26.3, 24.8, 16.9, 14.9, 11.6; HRMS (ESI) m/z: $[M + Na]^+$ Calcd for $C_{26}H_{41}N_3O_5SNa$ 530.2659; Found 530.2673; $[\alpha]_D^{24}$ = +23.8 (*c* 2.22, $CH_3OH$).

**(3a*R*,4*R*,5*R*,7*S*,8*S*,9*R*,9a*S*,12*R*)-8-Hydroxy-4,7,9,12-tetramethyl-3-oxo-7-vinyldecahydro-4,9a-propanocyclopenta[8]annulen-5-yl 2-((2-(2-(2-azidoethoxy)ethoxy)ethyl)thio)acetate (30)**: A solution of **21** (0.263 g, 1.13 mmol) in MeOH (1.0 mL) was sparged with $N_2$ for 15 minutes and a sparged solution of 10 N NaOH in $H_2O$ (0.11 mL, 1.1 mmol) was added. The mixture was stirred for 40 min and then added to a stirring, sparged solution of **24** (0.536 g, 1.00 mmol) in methyl ethyl ketone (4.1 mL). The mixture was heated to 60 °C (oil bath) and stirred for 24 h. After cooling, the mixture was concentrated. The residue was taken up in water (15 mL) and EtOAc (15 mL) and the layers were separated. The aqueous layer was extracted with EtOAc (3x15

mL) and the combined organic layers were dried over $Na_2SO_4$ and concentrated. The residue was purified using automated flash chromatography (SiliCycle 12 g $SiO_2$ column, 40% EtOAc in hexanes) to give **30** (477 mg, 86%) as a colorless oil. $^1$H NMR (500 MHz, $CDCl_3$) δ 6.48 (dd, *J* = 17.4, 11.0 Hz, 1H), 5.75 (d, *J* = 8.5 Hz, 1H), 5.34 (dd, *J* = 11.0, 1.4 Hz, 1H), 5.20 (dd, *J* = 17.4, 1.3 Hz, 1H), 3.70 – 3.61 (m, 8H), 3.41 – 3.37 (m, 2H), 3.36 (d, *J* = 6.5 Hz, 1H), 3.21 (s, 2H), 2.82 – 2.79 (m, 2H), 2.34 (p, *J* = 7.0 Hz, 1H), 2.30 – 2.15 (m, 2H), 2.12 – 2.05 (m, 2H), 1.77 (dq, *J* = 14.6, 3.2 Hz, 1H), 1.70 – 1.62 (m, 2H), 1.61 – 1.50 (m, 2H), 1.48 – 1.42 (m, 1H), 1.45 (s, 3H), 1.37 (dq, *J* = 14.1, 3.5 Hz, 1H), 1.33 (d, *J* = 16.1 Hz, 1H), 1.17 (s, 3H), 1.13 (td, *J* = 14.2, 4.4 Hz, 1H), 0.87 (d, *J* = 7.0 Hz, 3H), 0.74 (d, *J* = 7.0, 3H); $^{13}$C{$^1$H} NMR (126 MHz, $CDCl_3$) δ 217.3, 169.1, 139.2, 117.4, 74.7, 70.8 (2C), 70.5, 70.2, 69.3, 58.3, 50.8, 45.6, 44.9, 44.0, 41.9, 36.9, 36.1, 34.8, 34.6, 32.0, 30.5, 27.0, 26.5, 25.0, 17.0, 15.0, 11.6; HRMS (ESI) m/z: $[M + Na]^+$ Calcd for $C_{28}H_{45}N_3O_6SNa$ 574.2921; Found 574.2922; $[\alpha]_D^{23}$ = +22.7 (*c* 1.57, $CH_3OH$).

**(3a*R*,4*R*,5*R*,7*S*,8*S*,9*R*,9a*S*,12*R*)-8-Hydroxy-4,7,9,12-tetramethyl-3-oxo-7-vinyldecahydro-4,9a-propanocyclopenta[8]annulen-5-yl 1-azido-3,6,9-trioxa-12-thiatetradecan-14-oate (31)**: A solution of **22** (0.310 g, 1.12 mmol) in MeOH (0.65 mL) was sparged with $N_2$ for 15 min and a sparged solution of 10 N NaOH in $H_2O$ (0.11 mL, 1.1 mmol) was added. The mixture was stirred for 40 min and then added to a stirring, sparged solution of **24** (0.530 g, 0.995 mmol) in methyl ethyl ketone (4.1 mL). The mixture was heated to 60 °C (oil bath) and stirred for 24 h. After cooling, the mixture was concentrated, the residue was taken up in water (10 mL) and $CH_2Cl_2$ (15 mL), and the layers were separated. The aqueous layer was extracted with $CH_2Cl_2$ (1x15 mL) and EtOAc (15 mL). The combined organic layers were dried over $Na_2SO_4$ and concentrated. The residue was purified using automated flash chromatography (SiliCycle 12 g $SiO_2$ column, 50% EtOAc in hexanes) to give **31** (331 mg, 56%) as a colorless oil. $^1$H NMR (500 MHz, $CDCl_3$) δ

6.48 (dd, *J* = 17.4, 11.0 Hz, 1H), 5.74 (d, *J* = 8.4 Hz, 1H), 5.34 (dd, *J* = 11.0, 1.6 Hz, 1H), 5.20 (dd, *J* = 17.4, 1.6 Hz, 1H), 3.69 – 3.60 (m, 12H), 3.39 (dd, *J* = 5.6, 4.6 Hz, 2H), 3.36 (d, *J* = 6.6 Hz, 1H), 3.21 (s, 2H), 2.80 (t, *J* = 6.5 Hz, 2H), 2.34 (p, *J* = 7.0 Hz, 1H), 2.30 – 2.15 (m, 2H), 2.11 – 2.05 (m, 2H), 1.77 (dq, *J* = 14.5, 3.1 Hz, 1H), 1.70 – 1.63 (m, 2H), 1.62 – 1.50 (m, 2H), 1.48 – 1.42 (m, 1H), 1.45 (s, 3H), 1.40 – 1.35 (m, 1H), 1.33 (d, *J* = 16.0 Hz, 1H), 1.17 (s, 3H), 1.16 – 1.09 (m, 1H), 0.87 (d, *J* = 7.0 Hz, 3H), 0.73 (d, *J* = 7.0 Hz, 3H). $^{13}C\{^{1}H\}$ NMR (126 MHz, $CDCl_3$) δ 217.2, 169.0, 139.0, 117.3, 74.6, 70.71, 70.67, 70.64, 70.56, 70.3, 70.1, 69.2, 58.2, 50.7, 45.5, 44.7, 43.9, 41.8, 36.8, 36.0, 34.7, 34.5, 31.9, 30.4, 26.8, 26.3, 24.8, 16.9, 14.9, 11.6; HRMS (ESI) m/z: $[M + Na]^+$ Calcd for $C_{30}H_{49}N_3O_7SNa$ 618.3183; Found 618.3181; $[\alpha]_D^{23}$ = +21.6 (*c* 1.70, $CH_3OH$).

**(3a*R*,4*R*,5*R*,7*S*,8*S*,9*R*,9a*S*,12*R*)-8-Hydroxy-4,7,9,12-tetramethyl-3-oxo-7-vinyldecahydro-4,9a-propanocyclopenta[8]annulen-5-yl 1-azido-3,6,9,12-tetraoxa-15-thiaheptadecan-17-oate (32)**: A solution of **23** (0.176 g, 0.548 mmol) in MeOH (0.50 mL) was sparged with $N_2$ for 15 minutes and a solution of 2 N NaOH in EtOH (0.27 mL) was added. The mixture was stirred for 40 min, and then the solution was added to a stirring, sparged solution of **24** (0.266 g, 0.499 mmol) in methyl ethyl ketone (2.0 mL). After stirring at rt overnight, the mixture was concentrated, the residue was taken up in water (10 mL) and $CH_2Cl_2$ (10 mL), and the layers were separated. The aqueous layer was extracted with $CH_2Cl_2$ (3x10 mL). The combined organic layers were diluted with EtOAc (5 mL), dried over $Na_2SO_4$, and concentrated. The residue was purified using automated flash chromatography (SiliCycle 12 g $SiO_2$ column, 1%, then 3%, then 5% $CH_3OH$ in $CH_2Cl_2$) to give **32** (157 mg, 49%) as a colorless oil. $^{1}H$ NMR (400 MHz, $CDCl_3$) δ 6.44 (dd, *J* = 17.4, 11.0 Hz, 1H), 5.71 (d, *J* = 8.5 Hz, 1H), 5.31 (dd, *J* = 11.0, 1.6 Hz, 1H), 5.17 (dd, *J* = 17.4, 1.6 Hz, 1H), 3.67 – 3.55 (m, 16H), 3.35 (dd, *J* = 5.6, 4.6 Hz, 2H), 3.37 – 3.31 (m, 1H), 3.17 (s,

2H), 2.76 (t, *J* = 6.6 Hz, 2H), 2.31 (p, *J* = 7.3 Hz, 1H), 2.27 – 2.19 (m, 1H), 2.19 – 2.11 (m, 1H), 2.09 – 2.01 (m, 2H), 1.74 (dq, *J* = 14.3, 3.0 Hz, 1H), 1.68 – 1.58 (m, 2H), 1.57 – 1.47 (m, 1H), 1.46 – 1.38 (m, 1H), 1.45 (br s, 1H), 1.42 (s, 3H), 1.37 – 1.30 (m, 1H), 1.30 (d, *J* = 1.60 Hz, 1H), 1.14 (s, 3H), 1.14 – 1.05 (m, 1H), 0.85 (d, *J* = 7.0 Hz, 3H), 0.70 (d, *J* = 6.9 Hz, 3H). $^{13}C\{^{1}H\}$ NMR (101 MHz, $CDCl_3$) δ 217.1, 169.0, 139.2, 117.3, 74.7, 70.80, 70.77, 70.73 (2C), 70.69, 70.6, 70.4, 70.1, 69.3, 58.3, 50.8, 45.6, 44.9, 44.0, 41.9, 36.9, 36.1, 34.8, 34.6, 32.0, 30.5, 27.0, 26.5, 24.9, 16.9, 15.0, 11.6; HRMS (ESI) m/z: $[M + Na]^+$ Calcd for $C_{32}H_{53}N_3O_8SNa$ 662.3446; Found 662.3451; $[\alpha]_D^{23}$ = +19.8 (*c* 2.91, $CH_3OH$).

**17-Hydroxy-3,6,9,12,15-pentaoxaheptadecyl 4-methylbenzenesulfonate (35)**: Prepared from **33** according to the general method A (1.00 g TsCl, 5.25 mmol) and purified using automated flash chromatography (SiliCycle 40g $SiO_2$ column, 5% $CH_3OH$ in $CH_2Cl_2$) to give **35** (1.84 g, 80%) as a colorless oil: $^{1}H$ NMR (500 MHz, $CDCl_3$) δ 7.80 (d, *J* = 8.3 Hz, 2H), 7.35 (d, *J* = 8.0 Hz, 2H), 4.17 – 4.15 (m, 2H), 3.72 (dd, *J* = 5.6, 4.0 Hz, 2H), 3.70 – 3.60 (m, 16H), 3.59 (br s, 4H), 2.64 (t, *J* = 6.2 Hz, 1H), 2.45 (s, 3H); $^{13}C\{^{1}H\}$ NMR (126 MHz, $CDCl_3$) δ 144.8, 133.0, 129.8, 128.0, 72.5, 70.7, 70.60 (2C), 70.56, 70.55, 70.53, 70.51, 70.3, 69.3, 68.7, 61.7, 21.6; HRMS (ESI) m/z: $[M + Na]^+$ Calcd for $C_{19}H_{32}O_9SNa$ 459.1659; Found 459.1665.

**23-Hydroxy-3,6,9,12,15,18,21-heptaoxatricosyl 4-methylbenzenesulfonate (36)**: Prepared from **34** according to the general method A (0.250 g TsCl, 1.31 mmol) and purified using automated flash chromatography (SiliCycle 40g $SiO_2$ column, 6% $CH_3OH$ in $CH_2Cl_2$) to give **36** (0.474 g, 69%) as a colorless oil: $^{1}H$ NMR (500 MHz, $CDCl_3$) δ 7.79 – 7.76 (m, 2H), 7.34 – 7.30 (m, 2H), 4.15 – 4.11 (m, 2H), 3.71 – 3.68 (m, 2H), 3.67 – 3.57 (m, 24H), 3.56 (s, 4H), 2.65 (t, *J* = 6.2 Hz, 1H), 2.43 (s, 3H); $^{13}C\{^{1}H\}$ NMR (126 MHz, $CDCl_3$) δ 144.9, 133.0, 129.9, 128.0, 72.6,

70.8, 70.7 (2C), 70.63 (7C), 70.58, 70.4, 69.3, 68.7, 61.8, 21.7; HRMS (ESI) m/z: $[M + Na]^+$ Calcd for $C_{19}H_{32}O_9SNa$ 547.2183; Found 547.2186.

***S*-(2-(2-Hydroxyethoxy)ethyl) ethanethioate (37)**: Prepared from **8** according to the general method E and purified using automated flash chromatography (SiliCycle 40g $SiO_2$ column, 50-100% EtOAc in Hexanes) to give **37** (240 mg, 76%) as a yellow oil. $^1H$ NMR (500 MHz, $CDCl_3$) δ 3.72 (q, *J* = 4.8 Hz, 2H), 3.62 (t, *J* = 6.3 Hz, 2H), 3.59 – 3.56 (m, 2H), 3.10 (t, *J* = 6.3 Hz, 2H), 2.34 (s, 3H), 2.34 – 2.32 (m, 1H); $^{13}C\{^1H\}$ NMR (126 MHz, $CDCl_3$) δ 195.7, 72.1, 69.7, 61.7, 30.7, 29.0; HRMS (ESI) m/z: $[M + Na]^+$ Calcd for $C_6H_{12}O_3SNa$ 187.0399; Found 187.0391.

***S*-(2-(2-(2-Hydroxyethoxy)ethoxy)ethyl) ethanethioate (38)**: Prepared from **9** according to the general method E and purified using automated flash chromatography (SiliCycle 40g $SiO_2$ column, 50-100% EtOAc in Hexanes) to give **38** (231 mg, 67%) as a yellow oil. $^1H$ NMR (500 MHz, $CDCl_3$) δ 3.73 (t, *J* = 4.4 Hz, 2H), 3.67 – 3.62 (m, 4H), 3.62 – 3.59 (m, 4H), 3.10 (t, *J* = 6.5 Hz, 2H), 2.57 (s, 1H), 2.34 (s, 3H); $^{13}C\{^1H\}$ NMR (126 MHz, $CDCl_3$) δ 195.7, 72.6, 70.41, 70.37, 69.8, 61.8, 30.6, 28.8; HRMS (ESI) m/z: $[M + Na]^+$ Calcd for $C_8H_{16}O_4SNa$ 231.0661; Found 231.0655.

***S*-(2-(2-(2-(2-Hydroxyethoxy)ethoxy)ethoxy)ethyl) ethanethioate (39)**: Prepared from **10** according to the general method E and purified using automated flash chromatography (SiliCycle 40g $SiO_2$ column, 12-100% acetone in EtOAc) to give **39** (284 mg, 78%) as a yellow oil. $^1H$ NMR (400 MHz, $cdcl_3$) δ 3.75 – 3.70 (m, 2H), 3.70 – 3.61 (m, 10H), 3.60 (t, *J* = 6.5 Hz, 2H), 3.09 (t, *J* = 6.5 Hz, 2H), 2.47 – 2.42 (m, 1H), 2.33 (s, 3H); $^{13}C\{^1H\}$ NMR (101 MHz, $cdcl_3$) δ 195.6, 72.6, 70.8, 70.6, 70.5, 70.4, 69.9, 61.8, 30.6, 28.9; HRMS (ESI) m/z: $[M + Na]^+$ Calcd for $C_{10}H_{20}O_5SNa$ 275.0924; Found 275.0924.

***S*-(14-Hydroxy-3,6,9,12-tetraoxatetradecyl) ethanethioate (40)**: Prepared from **11** according to the general method E and purified using automated flash chromatography (SiliCycle 40g $SiO_2$ column, 12-100% acetone in EtOAc) to give **40** (288 mg, 76%). $^1$H NMR (400 MHz, cdcl$_3$) δ 3.73 – 3.68 (m, 2H), 3.68 – 3.59 (m, 14H), 3.58 (t, *J* = 6.4 Hz, 2H), 3.07 (t, *J* = 6.4 Hz, 2H), 2.62 (t, *J* = 6.2 Hz, 1H), 2.31 (s, 3H); $^{13}$C{$^1$H} NMR (101 MHz, cdcl$_3$) δ 195.7, 72.6, 70.73 (2C), 70.69, 70.62, 70.5, 70.4, 69.9, 61.8, 30.7, 28.9; HRMS (ESI) m/z: $[M + Na]^+$ Calcd for $C_{12}H_{24}O_6SNa$ 319.1186; Found 319.1186.

***S*-(17-Hydroxy-3,6,9,12,15-pentaoxaheptadecyl) ethanethioate (41)**: Prepared from **35** according to the general method E and purified using automated flash chromatography (SiliCycle 40g $SiO_2$ column, 12-100% acetone in EtOAc) to give **41** (293 mg, 74%). $^1$H NMR (400 MHz, cdcl$_3$) δ 3.70 (td, *J* = 6.0, 4.4 Hz, 2H), 3.67 – 3.59 (m, 18H), 3.57 (t, *J* = 6.5 Hz, 2H), 3.07 (t, *J* = 6.5 Hz, 2H), 2.65 (t, *J* = 6.2 Hz, 1H), 2.31 (s, 3H); $^{13}$C{$^1$H} NMR (101 MHz, cdcl$_3$) δ 195.6, 72.6, 70.72, 70.71, 70.67 (2C), 70.65, 70.60, 70.44, 70.39, 69.8, 61.8, 30.6, 28.9; HRMS (ESI) m/z: $[M + H]^+$ Calcd for $C_{14}H_{28}O_7SNa$ 341.1628; Found 341.1629.

***S*-(23-Hydroxy-3,6,9,12,15,18,21-heptaoxatricosyl) ethanethioate (42)**: Prepared from **36** according to the general method E and purified using automated flash chromatography (SiliCycle 40g $SiO_2$ column, 12-100% acetone in EtOAc) to give **42** (195 mg, 53%) $^1$H NMR (400 MHz, $CDCl_3$) δ 3.72 – 3.68 (m, 2H), 3.66 – 3.59 (m, 26H), 3.58 (t, *J* = 6.4 Hz, 2H), 3.07 (t, *J* = 6.4 Hz, 2H), 2.66 (t, *J* = 6.2 Hz, 1H), 2.32 (s, 3H); $^{13}$C{$^1$H} NMR (101 MHz, cdcl$_3$) δ 195.6, 72.6, 70.73 (2C), 70.68 (6C), 70.65, 70.61, 69.9, 61.8, 30.7, 28.9; HRMS (ESI) m/z: $[M + Na]^+$ Calcd for $C_{18}H_{36}O_9SNa$ 451.1972; Found 451.1972.

**(3a*R*,4*R*,5*R*,7*S*,8*S*,9*R*,9a*S*,12*R*)-8-Hydroxy-4,7,9,12-tetramethyl-3-oxo-7-vinyldecahydro-4,9a-propanocyclopenta[8]annulen-5-yl 2-((2-(2-hydroxyethoxy)ethyl)thio)acetate (43)**: A

solution of **37** (86.4 mg, 0.526 mmol) in MeOH (0.5 mL) was sparged with $N_2$ for 15 min and a sparged solution of 10 N NaOH in $H_2O$ (0.05 mL, 0.5 mmol) was added. The mixture was stirred for 1 h, and then added to a stirring, sparged solution of **24** (0.250 g, 0.470 mmol) in methyl ethyl ketone (2.0 mL). The mixture was heated to 60 °C (oil bath) and stirred for 24 h. The mixture was concentrated, the residue was taken up in water (5 mL) and EtOAc (10 mL), and the phases were separated. The aqueous layer was extracted with EtOAc (3x10 mL) and the combined organic layers were dried with $Na_2SO_4$ and concentrated. The residue was purified using automated flash chromatography (SiliCycle 12 g $SiO_2$ column, 50% EtOAc in hexanes) to give **43** (58.9 mg, 25%) as a colorless oil: $^1$H NMR (500 MHz, $CDCl_3$) δ 6.47 (dd, *J* = 17.4, 11.0 Hz, 1H), 5.74 (d, *J* = 8.5 Hz, 1H), 5.34 (dd, *J* = 11.0, 1.6 Hz, 1H), 5.19 (dd, *J* = 17.4, 1.6 Hz, 1H), 3.72 – 3.70 (m, 2H), 3.68 (td, *J* = 6.2, 2.1 Hz, 2H), 3.55 (dd, *J* = 4.8, 3.9 Hz, 2H), 3.35 (dd, *J* = 10.2, 6.5 Hz, 1H), 3.23 (d, *J* = 14.8 Hz, 1H), 3.19 (d, *J* = 14.8 Hz, 1H), 2.79 (td, *J* = 6.2, 1.9 Hz, 2H), 2.37 (br s, 1H), 2.33 (p, *J* = 7.0 Hz, 1H), 2.29 – 2.23 (m, 1H), 2.22 – 2.13 (m, 1H), 2.11 – 2.05 (m, 2H), 1.76 (dq, *J* = 14.5, 3.2 Hz, 1H), 1.69 – 1.60 (m, 2H), 1.59 – 1.48 (m, 2H), 1.47 – 1.41 (m, 1H), 1.44 (s, 3H), 1.36 (dq, *J* = 14.1, 3.4 Hz, 1H), 1.32 (d, *J* = 16.1 Hz, 1H), 1.16 (s, 3H), 1.12 (td, *J* = 14.2, 4.6 Hz, 1H), 0.86 (d, *J* = 7.0 Hz, 3H), 0.72 (d, *J* = 7.0 Hz, 3H); $^{13}$C{$^1$H} NMR (126 MHz, $CDCl_3$) δ 217.3, 169.2, 139.1, 117.4, 74.7, 72.2, 70.5, 69.4, 61.8, 58.3, 45.6, 44.8, 44.0, 41.8, 36.8, 36.1, 34.7, 34.6, 32.1, 30.5, 26.9, 26.4, 24.9, 17.0, 15.0, 11.7; HRMS (ESI) m/z: $[M + Na]^+$ Calcd for $C_{26}H_{42}O_6SNa$ 505.2594; Found 505.2597; $[\alpha]_D^{26}$ = +22.8 (*c* 1.11, $CH_3OH$).

**(3a*R*,4*R*,5*R*,7*S*,8*S*,9*R*,9a*S*,12*R*)-8-Hydroxy-4,7,9,12-tetramethyl-3-oxo-7-vinyldecahydro-4,9a-propanocyclopenta[8]annulen-5-yl 2-((2-(2-(2-hydroxyethoxy)ethoxy)ethyl)thio)acetate (44)**: A solution of **38** (0.111 g, 0.532 mmol) in MeOH (0.50 mL) was sparged with $N_2$ for 15 minutes and a spared solution of 10 N NaOH in $H_2O$ (0.052 mL, 0.52 mmol) was added. The

mixture was stirred for 40 min, and then added to a stirring, sparged solution of **24** (0.254 g, 0.476 mmol) in methyl ethyl ketone (2.0 mL). The mixture was heated to 60 °C (oil bath) and stirred for 48 h. The mixture was concentrated, the residue was taken up in water (5 mL) and EtOAc (10 mL), and the layers were separated. The aqueous layer was extracted with EtOAc (3x10 mL) and the combined organics were dried over $Na_2SO_4$ and concentrated. The residue was purified using automated flash chromatography (SiliCycle 12 g $SiO_2$ column, 75% EtOAc in $CH_2Cl_2$) to give **44** (125.9 mg, 48%) as a colorless oil: $^1$H NMR (500 MHz, $CDCl_3$) δ 6.46 (dd, *J* = 17.3, 11.1 Hz, 1H), 5.73 (d, *J* = 8.4 Hz, 1H), 5.33 (dd, *J* = 10.9, 1.6 Hz, 1H), 5.19 (dd, *J* = 17.4, 1.5 Hz, 1H), 3.73 – 3.70 (m, *J* = 4.9, 3.1, 1.8 Hz, 2H), 3.69 – 3.63 (m, 4H), 3.62 – 3.57 (m, 4H), 3.34 (t, *J* = 8.1 Hz, 1H), 3.21 (s, 2H), 2.79 (t, *J* = 6.5 Hz, 2H), 2.53 (br s, 1H), 2.33 (dt, *J* = 7.0 Hz, 1H), 2.29 – 2.13 (m, 2H), 2.10 – 2.04 (m, 2H), 1.75 (dq, *J* = 14.6, 3.2 Hz, 1H), 1.68 – 1.59 (m, 2H), 1.58 – 1.47 (m, 2H), 1.47 – 1.41 (m, 1H), 1.44 (s, 3H), 1.35 (dq, *J* = 14.2, 3.0 Hz, 1H), 1.31 (d, *J* = 16.1 Hz, 1H), 1.15 (s, 3H), 1.15 – 1.08 (m, 1H), 0.86 (dd, *J* = 7.0 Hz, 3H), 0.72 (dd, *J* = 7.0 Hz, 3H); $^{13}$C{$^1$H} NMR (126 MHz, $CDCl_3$) δ 217.3, 169.1, 139.1, 117.4, 74.7, 72.6, 70.6, 70.41, 70.38, 69.4, 61.8, 58.3, 45.5, 44.8, 44.0, 41.8, 36.8, 36.1, 34.7, 34.6, 31.9, 30.5, 26.9, 26.4, 24.9, 17.0, 15.0, 11.6; HRMS (ESI) m/z: $[M + Na]^+$ Calcd for $C_{28}H_{46}O_7SNa$ 549.2856; Found 549.2855; $[\alpha]_D^{26}$ = +21.8 (*c* 1.31, $CH_3OH$).

**(3a*R*,4*R*,5*R*,7*S*,8*S*,9*R*,9a*S*,12*R*)-8-Hydroxy-4,7,9,12-tetramethyl-3-oxo-7-vinyldecahydro-4,9a-propanocyclopenta[8]annulen-5-yl 1-hydroxy-3,6,9-trioxa-12-thiatetradecan-14-oate (45)**: A solution of **39** (0.1325 g, 0.525 mmol) in MeOH (0.50 mL) was sparged with $N_2$ for 15 minutes and a sparged solution of 10 N NaOH in $H_2O$ (0.095 mL, 0.95 mmol) was added. The mixture was stirred for 15 min and then added to a stirring, sparged solution of **24** (0.253 g, 0.476 mmol) in methyl ethyl ketone (2.0 mL). The mixture was stirred at rt for 18 h, and then at 60 °C

(oil bath) for 24 h. The mixture was concentrated, the residue was taken up in water (5 mL) and EtOAc (10 mL), and the layers were separated. The aqueous layer was extracted with EtOAc (4x10 mL) and the combined organic layers were washed with brine (10 mL), dried over $Na_2SO_4$ and concentrated. The residue was purified using automated flash chromatography (SiliCycle 12 g $SiO_2$ column, 5-10% $CH_3OH$ in $CH_2Cl_2$) to give **45** (105.2 mg, 39%) as a colorless oil: $^1$H NMR (500 MHz, $CDCl_3$) δ 6.46 (dd, *J* = 17.4, 11.0 Hz, 1H), 5.73 (d, *J* = 8.4 Hz, 1H), 5.33 (dd, *J* = 11.0, 1.5 Hz, 1H), 5.19 (dd, *J* = 17.4, 1.6 Hz, 1H), 3.73 – 3.69 (m, 2H), 3.68 – 3.57 (m, 12H), 3.34 (dd, *J* = 10.5, 6.5 Hz, 1H), 3.20 (s, 2H), 2.79 (t, *J* = 6.5 Hz, 2H), 2.75 (br s, 1H), 2.32 (p, *J* = 7.0 Hz, 1H), 2.29 – 2.14 (m, 2H), 2.11 – 2.03 (m, 2H), 1.75 (dq, *J* = 14.5, 3.1 Hz, 1H), 1.68 – 1.59 (m, 2H), 1.58 – 1.47 (m, 2H), 1.47 – 1.42 (m, 1H), 1.44 (s, 3H), 1.37 – 1.32 (m, 1H), 1.31 (d, *J* = 16.0 Hz, 1H), 1.15 (s, 3H), 1.15 – 1.08 (m, 1H), 0.86 (d, *J* = 7.0 Hz, 3H), 0.72 (d, *J* = 7.0 Hz, 3H); $^{13}$C{$^1$H} NMR (126 MHz, $CDCl_3$) δ 217.3, 169.1, 139.1, 117.4, 74.7, 72.6, 70.7, 70.60, 70.57, 70.37, 70.35, 69.3, 61.8, 58.3, 45.5, 44.8, 44.0, 41.8, 36.9, 36.0, 34.7, 34.6, 31.9, 30.5, 26.9, 26.4, 24.9, 17.0, 15.0, 11.6; HRMS (ESI) m/z: $[M + Na]^+$ Calcd for $C_{30}H_{50}O_8SNa$ 593.3119; Found 593.3131; $[\alpha]_D^{26}$ = +21.0 (*c* 1.20, $CH_3OH$).

**(3a*R*,4*R*,5*R*,7*S*,8*S*,9*R*,9a*S*,12*R*)-8-Hydroxy-4,7,9,12-tetramethyl-3-oxo-7-vinyldecahydro-4,9a-propanocyclopenta[8]annulen-5-yl 1-hydroxy-3,6,9,12-tetraoxa-15-thiaheptadecan-17-oate (46)**: A solution of **40** (0.153 g, 0.517 mmol) in THF (0.50 mL) was sparged with $N_2$ for 15 minutes and a sparged solution of 10 N NaOH in $H_2O$ (0.095 mL, 0.95 mmol) was added. The mixture was stirred for 30 min and then added to a stirring, sparged solution of **24** (0.255 g, 0.479 mmol) in methyl ethyl ketone (2.0 mL). A noticeable amount of the sodium salt of deprotected **40** became insoluble in the THF/water mixture and failed to be transferred. The resulting mixture was stirred at 60 °C (oil bath) for 48 h. The mixture was concentrated, the residue was taken up in

water (5 mL) and EtOAc (10 mL), and the layers were separated. The aqueous layer was extracted with EtOAc (4x10 mL) and the combined organics were washed with brine, dried over $Na_2SO_4$, and concentrated. The residue was purified using automated flash chromatography (SiliCycle 12 g $SiO_2$ column, 1-12% (20:1 $CH_3OH$:conc. $NH_4OH_{(aq)}$) in $CH_2Cl_2$) to give **46** (104.6 mg, 36%) as a colorless oil: $^1$H NMR (500 MHz, $CDCl_3$) δ 6.48 (dd, *J* = 17.4, 11.0 Hz, 1H), 5.74 (d, *J* = 8.5 Hz, 1H), 5.34 (dd, *J* = 11.0, 1.5 Hz, 1H), 5.20 (dd, *J* = 17.5, 1.6 Hz, 1H), 3.72 (q, *J* = 4.9 Hz, 2H), 3.69 – 3.60 (m, 16H), 3.35 (dd, *J* = 10.8, 6.6 Hz, 1H), 3.21 (s, 2H), 2.79 (t, *J* = 6.5 Hz, 2H), 2.68 (t, *J* = 6.4 Hz, 1H), 2.37 – 2.31 (m, 1H), 2.30 – 2.15 (m, 2H), 2.11 – 2.05 (m, 2H), 1.77 (dq, *J* = 14.5, 3.2 Hz, 1H), 1.69 – 1.61 (m, 2H), 1.60 – 1.50 (m, 1H), 1.49 – 1.42 (m, 1H), 1.47 (s, 1H), 1.45 (s, 3H), 1.40 – 1.34 (m, 1H), 1.33 (d, *J* = 16.1 Hz, 1H), 1.17 (s, 3H), 1.16 – 1.09 (m, 1H), 0.87 (d, *J* = 7.0 Hz, 3H), 0.73 (d, *J* = 7.0 Hz, 3H); $^{13}$C{$^1$H} NMR (126 MHz, $CDCl_3$) δ 217.3, 169.1, 139.1, 117.4, 74.7, 72.6, 70.72, 70.70, 70.68, 70.65 (2C), 70.4 (2C), 69.3, 61.9, 58.3, 45.6, 44.9, 44.0, 41.9, 36.9, 36.1, 34.8, 34.6, 32.0, 30.6, 27.0, 26.4, 25.0, 17.0, 15.0, 11.7; HRMS (ESI) m/z: $[M + Na]^+$ Calcd for $C_{32}H_{54}O_9SNa$ 637.3381; Found 637.3391; $[\alpha]_D^{26}$ = +22 (*c* 0.40, $CH_3OH$).

**(3a*R*,4*R*,5*R*,7*S*,8*S*,9*R*,9a*S*,12*R*)-8-Hydroxy-4,7,9,12-tetramethyl-3-oxo-7-vinyldecahydro-4,9a-propanocyclopenta[8]annulen-5-yl 1-hydroxy-3,6,9,12,15-pentaoxa-18-thiaicosan-20-oate (47)**: To a solution of **41** (0.0750 g, 0.220 mmol) in $N_2$ sparged MeOH (0.20 mL) was added a sparged solution of 10 N NaOH in $H_2O$ (0.095 mL, 0.95 mmol). The mixture was stirred for 45 min and then a sparged solution of **24** (0.1010 g, 0.1896 mmol) in methyl ethyl ketone (0.8 mL + 0.5 mL wash) was added resulting in a faintly yellow solution that was stirred at rt for 120 h. The mixture was concentrated, the residue was taken up in water (5 mL) and EtOAc (10 mL), and the layers were separated. The aqueous layer was extracted with EtOAc (5x10 mL) and the combined organic layers were washed with brine, dried over $Na_2SO_4$, and concentrated. The residue was

purified using automated flash chromatography (SiliCycle 12 g $SiO_2$ column, 1-12% (20:1 $CH_3OH$:conc. $NH_4OH_{(aq)}$) in $CH_2Cl_2$) to give **47** (63.5 mg, 51%) as a colorless oil: $^1H$ NMR (500 MHz, $CDCl_3$) δ 6.48 (dd, *J* = 17.4, 11.0 Hz, 1H), 5.75 (d, *J* = 8.5 Hz, 1H), 5.35 (dd, *J* = 11.0, 1.6 Hz, 1H), 5.20 (dd, *J* = 17.4, 1.6 Hz, 1H), 3.74 – 3.70 (m, 2H), 3.69 – 3.60 (m, 20H), 3.36 (dd, *J* = 10.9, 6.5 Hz, 1H), 3.21 (s, 2H), 2.80 (t, *J* = 6.6 Hz, 2H), 2.76 (br s, 1H), 2.37 – 2.31 (m, 1H), 2.30 – 2.16 (m, 2H), 2.12 – 2.05 (m, 2H), 1.77 (dq, *J* = 14.4, 2.9 Hz, 1H) 1.69 – 1.61 (m, 2H), 1.55 (qd, *J* = 13.3, 3.5 Hz, 1H), 1.48 – 1.42 (m, 1H), 1.47 (s, 1H), 1.45 (s, 3H) 1.40 – 1.35 (m, 1H), 1.33 (d, *J* = 16.1 Hz, 1H), 1.17 (s, 3H), 1.13 (td, *J* = 14.3, 4.6 Hz, 1H), 0.88 (d, *J* = 7.1 Hz, 3H), 0.73 (d, *J* = 7.0 Hz, 3H); $^{13}C\{^1H\}$ NMR (126 MHz, $CDCl_3$) δ 217.3, 169.1, 139.1, 117.4, 74.7, 72.7, 70.73 (2C), 70.68 (2C), 70.66, 70.65 (2C), 70.4 (2C), 69.3, 61.9, 58.3, 45.6, 44.9, 44.0, 41.9, 36.9, 36.1, 34.8, 34.6, 32.0, 30.6, 27.0, 26.5, 25.0, 17.0, 15.0, 11.7; HRMS (ESI) m/z: $[M + Na]^+$ Calcd for $C_{34}H_{58}O_{10}SNa$ 681.3643; Found 681.3640; $[\alpha]_D^{26}$ = +23 (*c* 0.25, $CH_3OH$).

**(3a*R*,4*R*,5*R*,7*S*,8*S*,9*R*,9a*S*,12*R*)-8-Hydroxy-4,7,9,12-tetramethyl-3-oxo-7-vinyldecahydro-4,9a-propanocyclopenta[8]annulen-5-yl 1-hydroxy-3,6,9,12,15,18,21-heptaoxa-24-thiahexacosan-26-oate (48)**: To a solution of **42** (0.0890 g, 0.208 mmol) in $N_2$ sparged MeOH (0.20 mL) was added a sparged solution of 10 N NaOH in $H_2O$ (0.040 mL, 0.40 mmol). The mixture was stirred for 1.5 h and then a sparged solution of **24** (0.1022 g, 0.1919 mmol) in methyl ethyl ketone (0.8 mL + 0.3 mL wash) was added resulting in a faintly yellow solution that was stirred at rt for 96 h. The mixture was concentrated, the residue was taken up in water (5 mL) and EtOAc (10 mL), and the layers were separated. The aqueous layer was extracted with EtOAc (7x10 mL) and the combined organic layers were washed with brine, dried over $Na_2SO_4$, and concentrated. The residue was purified using automated flash chromatography (SiliCycle 12 g $SiO_2$ column, 1-12% (20:1 $CH_3OH$:conc. $NH_4OH_{(aq)}$) in $CH_2Cl_2$) to give **48** (54.2 mg, 38%) as a

colorless oil: $^{1}$H NMR (500 MHz, $CDCl_3$) δ 6.48 (dd, *J* = 17.4, 11.0 Hz, 1H), 5.75 (d, *J* = 8.5 Hz, 1H), 5.35 (dd, *J* = 11.0, 1.6 Hz, 1H), 5.20 (dd, *J* = 17.4, 1.6 Hz, 1H), 3.74 – 3.70 (m, 2H), 3.68 – 3.59 (m, 28H), 3.36 (dd, *J* = 10.8, 6.5 Hz, 1H), 3.21 (s, 2H), 2.98 (br s, 1H), 2.79 (t, *J* = 6.6 Hz, 2H), 2.37 – 2.31 (m, 1H), 2.30 – 2.15 (m, 2H), 2.12 – 2.05 (m, 2H), 1.77 (dq, *J* = 14.5, 2.9 Hz, 1H), 1.67 – 1.62 (m, 2H), 1.55 (qd, *J* = 13.4, 3.6 Hz, 1H), 1.49 – 1.42 (m, *J* = 14.2 Hz, 2H), 1.45 (s, 3H), 1.40 – 1.35 (m, 1H), 1.33 (d, *J* = 16.1 Hz, 1H), 1.17 (s, 3H), 1.16 – 1.09 (m, 1H), 0.88 (d, *J* = 7.0 Hz, 3H), 0.73 (d, *J* = 7.0 Hz, 3H); $^{13}$C{$^{1}$H} NMR (126 MHz, $CDCl_3$) δ 217.4, 169.1, 139.1, 117.4, 74.7, 72.7, 70.71 (2C), 70.67 (4C), 70.64 (4C), 70.61, 70.43, 70.36, 69.3, 61.8, 58.3, 45.6, 44.9, 44.0, 41.9, 36.9, 36.1, 34.8, 34.6, 32.0, 30.6, 27.0, 26.5, 25.0, 17.0, 15.0, 11.7; HRMS (ESI) m/z: $[M + Na]^+$ Calcd for $C_{38}H_{66}O_{12}SNa$ 769.4167; Found 769.4167; $[\alpha]_D^{27}$ = +29 (*c* 0.13, $CH_3OH$).

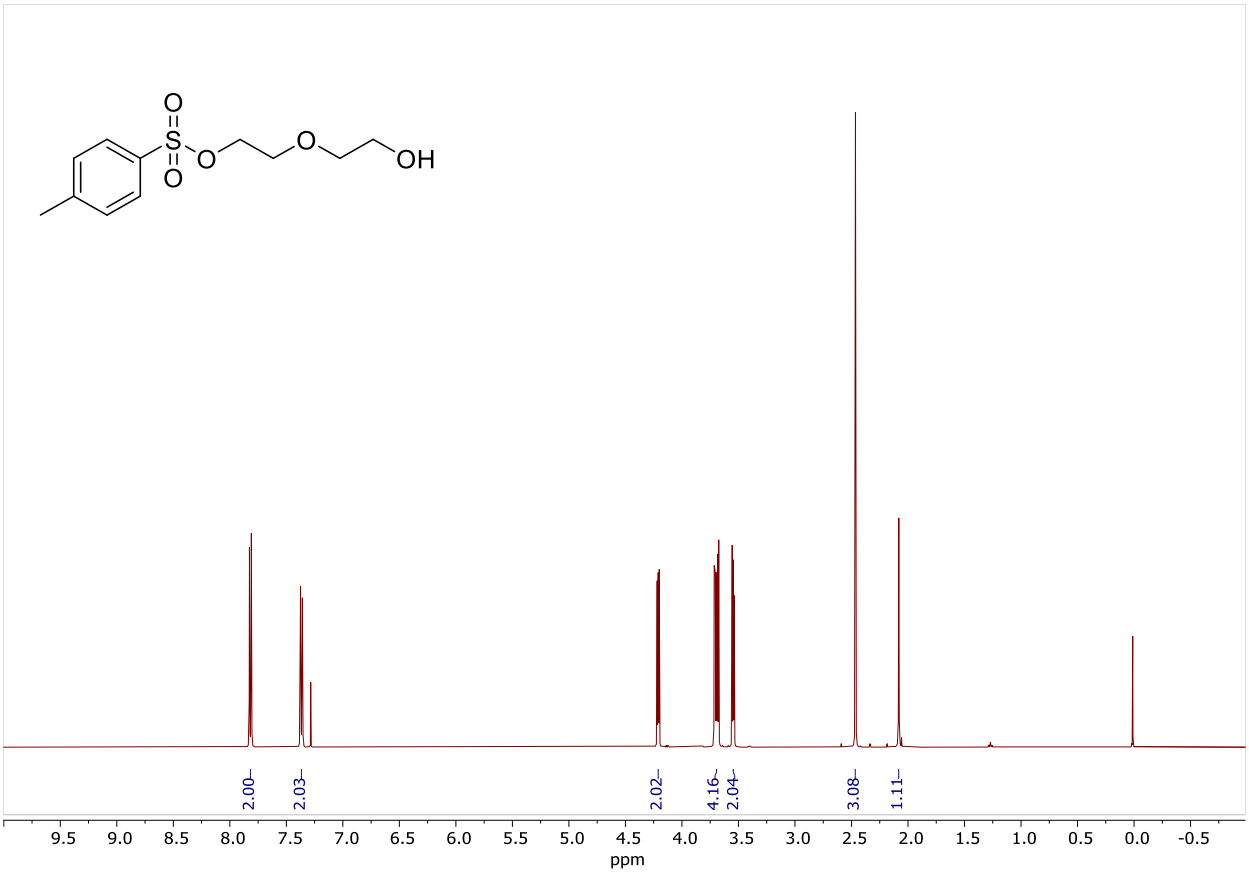


$^{1}$H-NMR (500 MHz, $CDCl_3$) spectrum of **8**

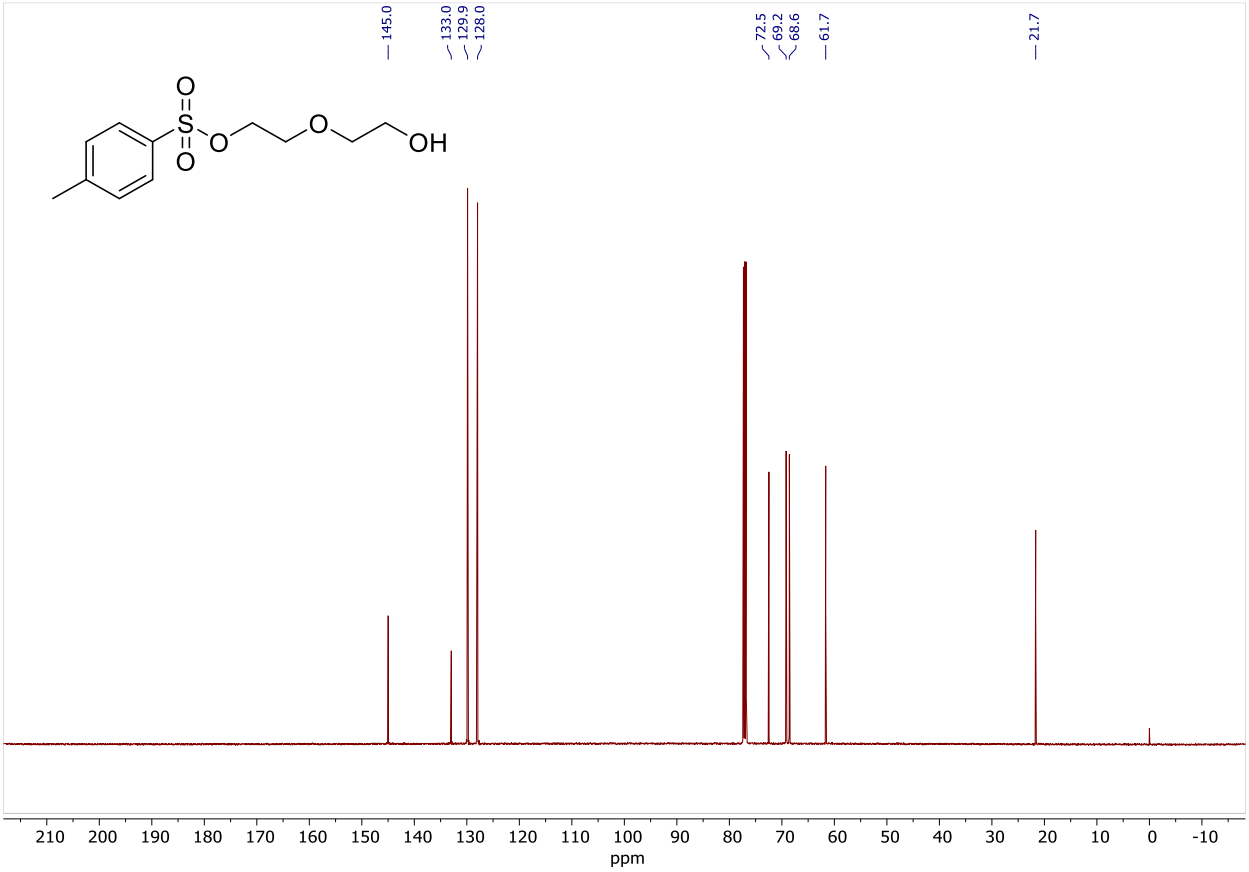

$^{13}C\{^{1}H\}$-NMR (126 MHz, $CDCl_3$) spectrum of **8**

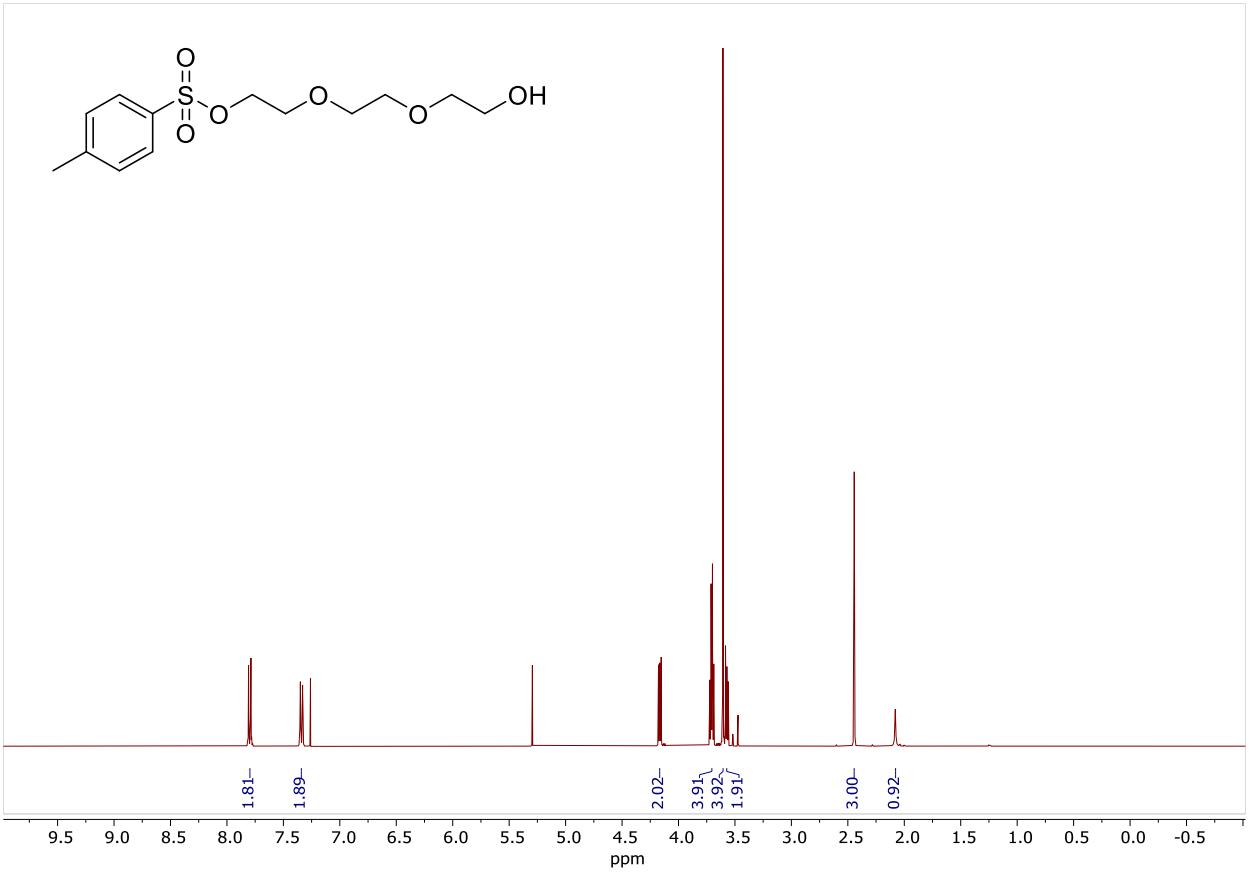


$^{1}H$-NMR (400 MHz, $CDCl_3$) spectrum of **9**

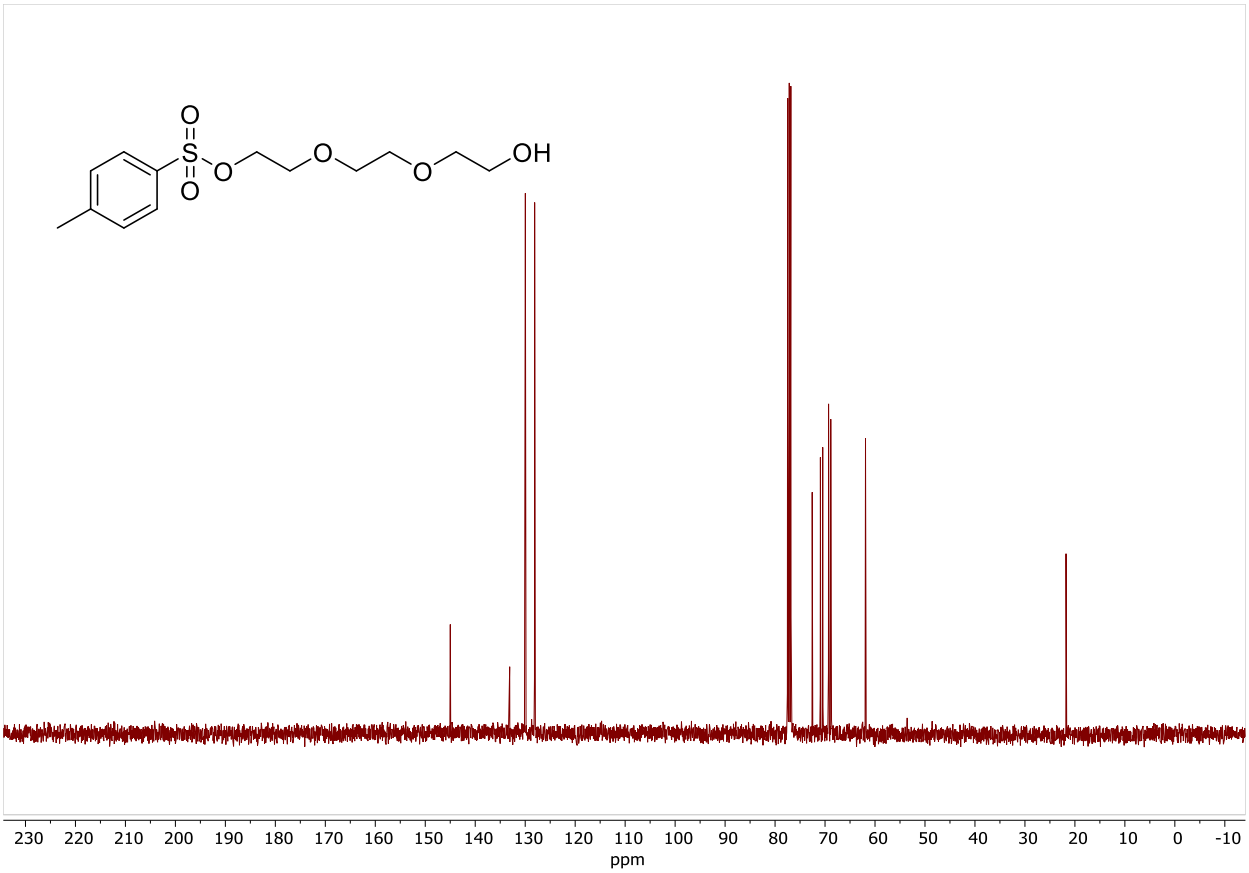


$^{13}C\{^{1}H\}$-NMR (101 MHz, $CDCl_3$) spectrum of **9**

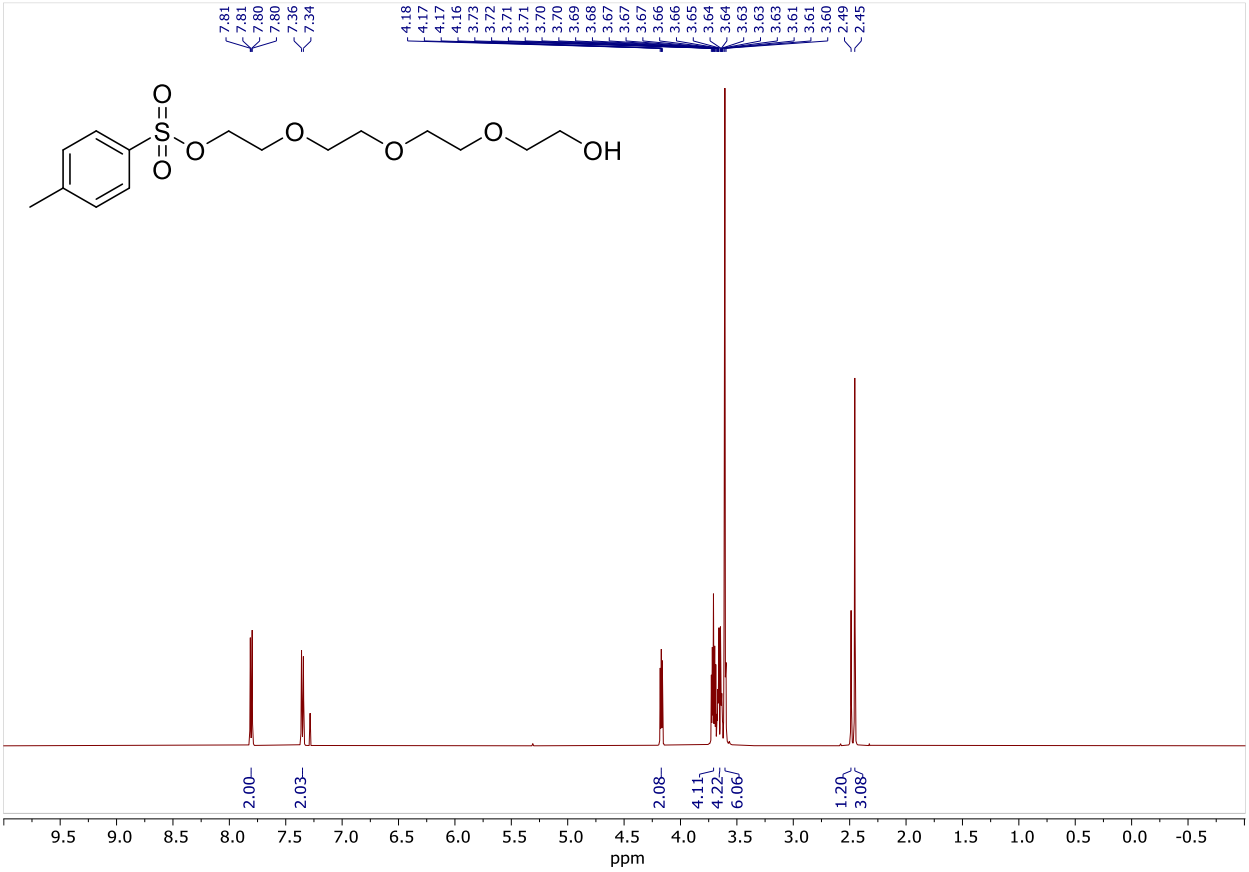

$^{1}$H-NMR (500 MHz, $CDCl_3$) spectrum of **10**

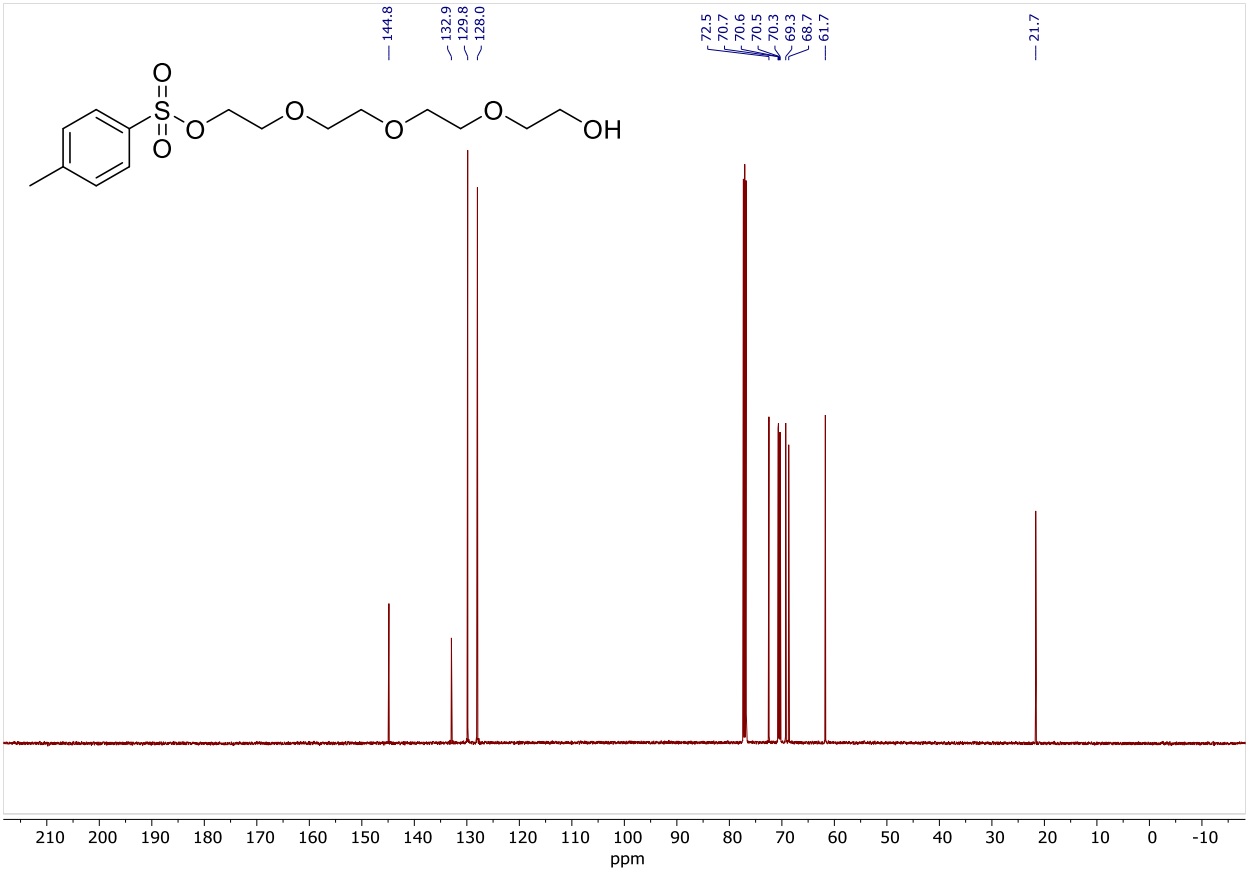


$^{13}$C{$^{1}$H}-NMR (126 MHz, $CDCl_3$) spectrum of **10**

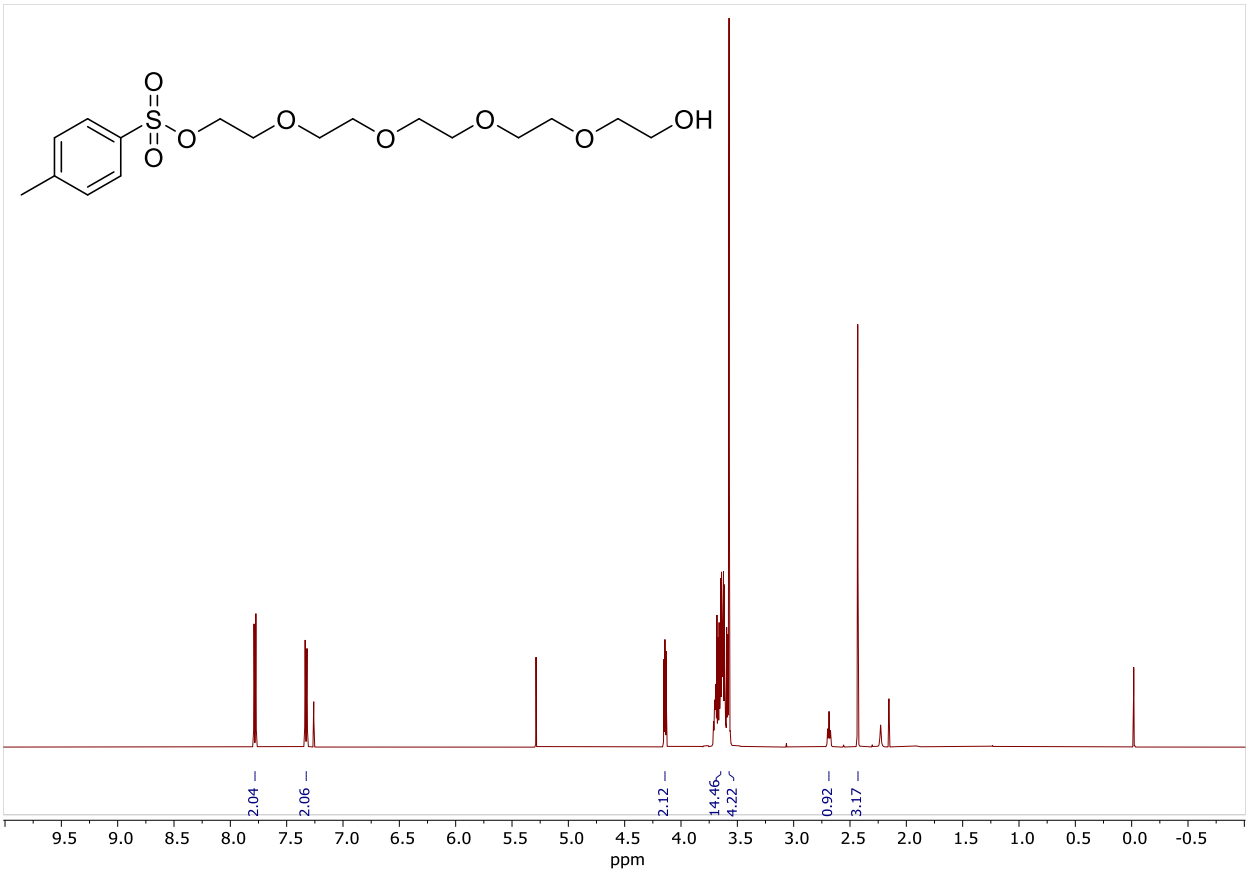


$^{1}$H-NMR (500 MHz, $CDCl_3$) spectrum of **11** (trace $CH_2Cl_2$, acetone)

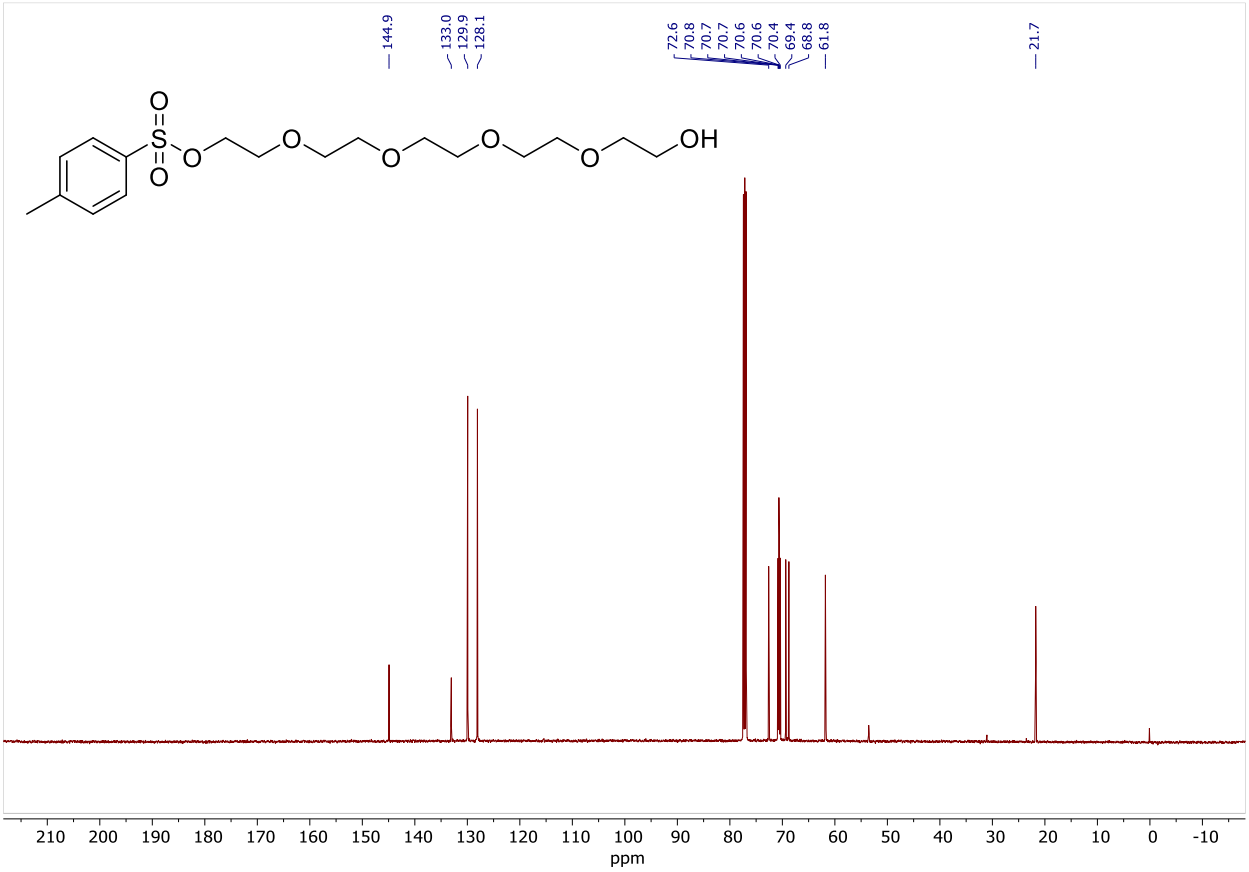

$^{13}C\{^{1}H\}$-NMR (126 MHz, $CDCl_3$) spectrum of **11** (trace $CH_2Cl_2$, acetone)

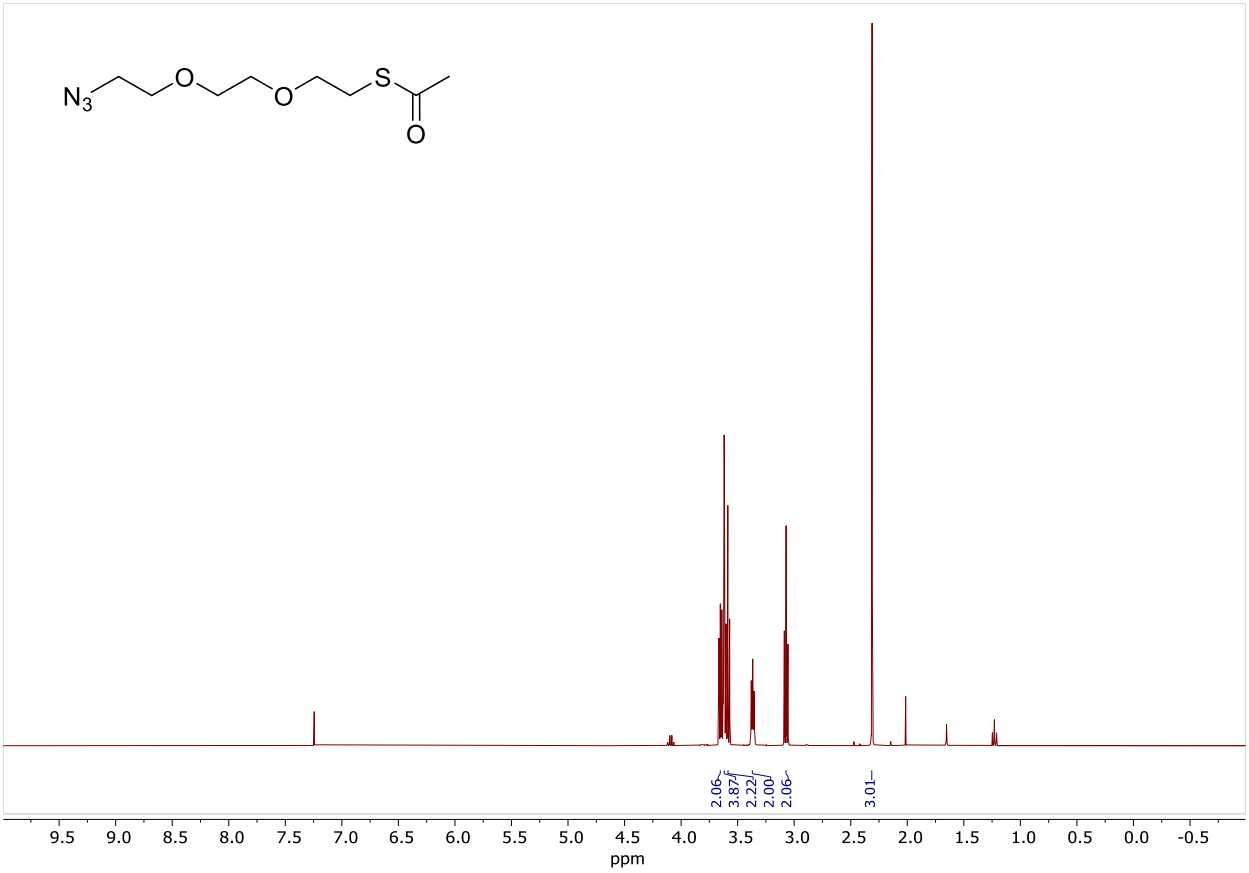


$^{1}H$-NMR (400 MHz, $CDCl_3$) spectrum of **21** (trace EtOAc)

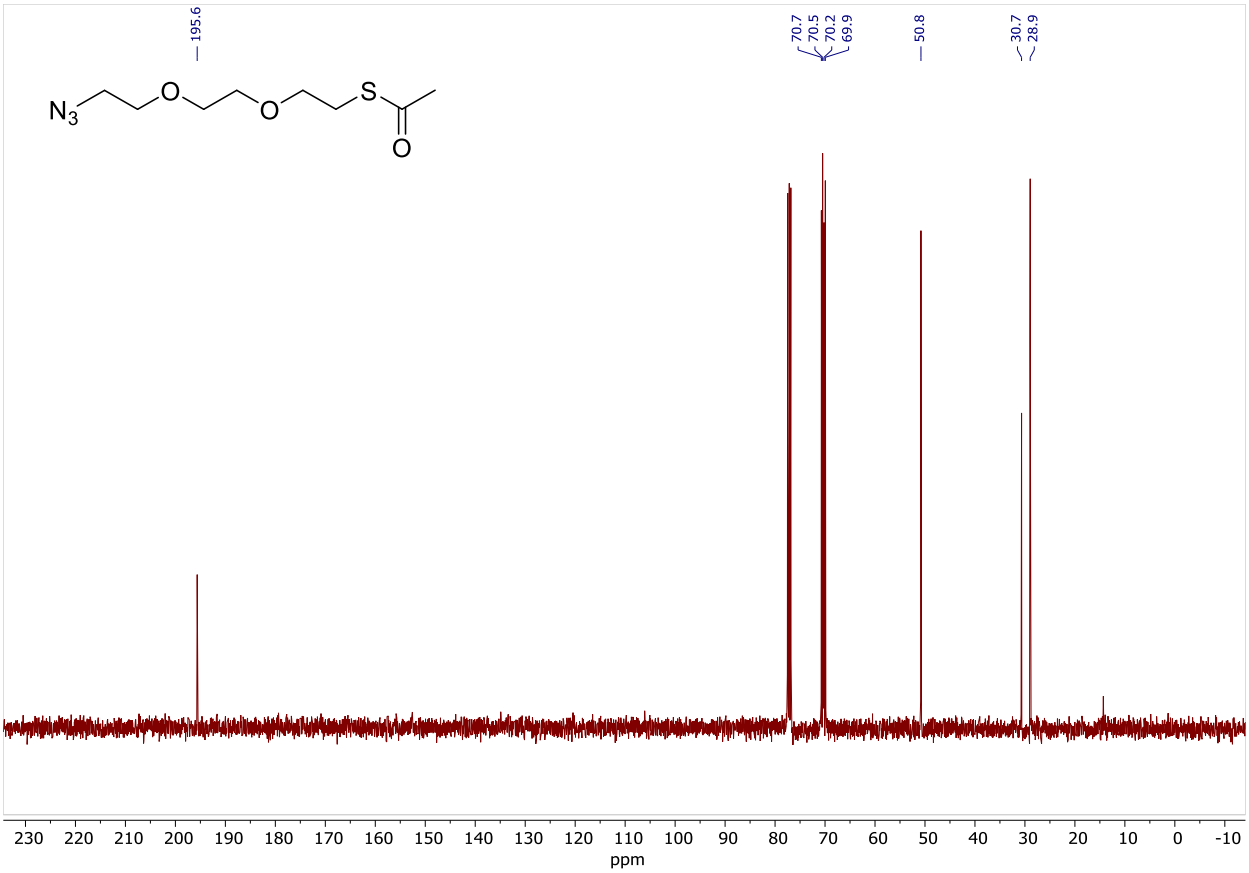


$^{13}C\{^{1}H\}$-NMR (101 MHz, $CDCl_3$) spectrum of **21** (trace EtOAc)

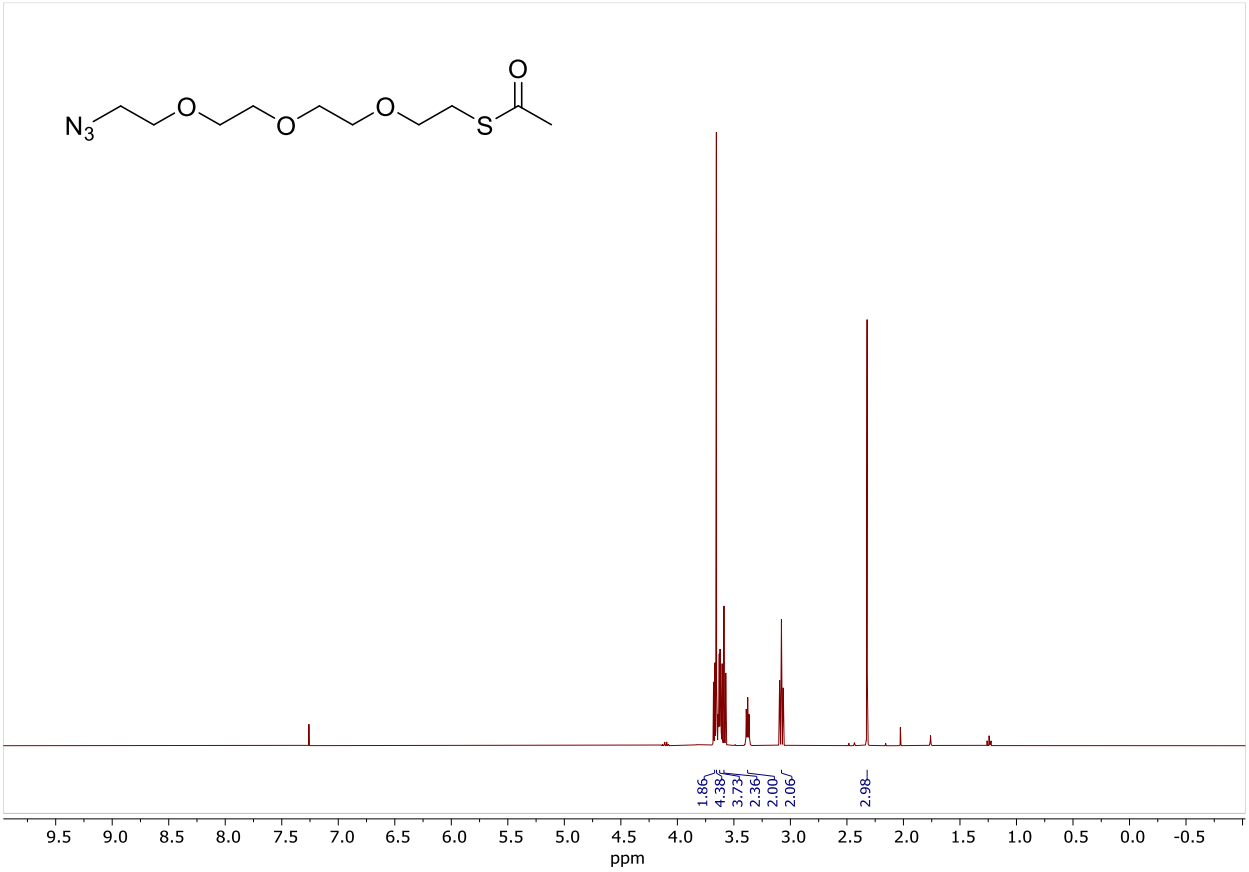

$^{1}$H-NMR (400 MHz, $CDCl_3$) spectrum of **22**

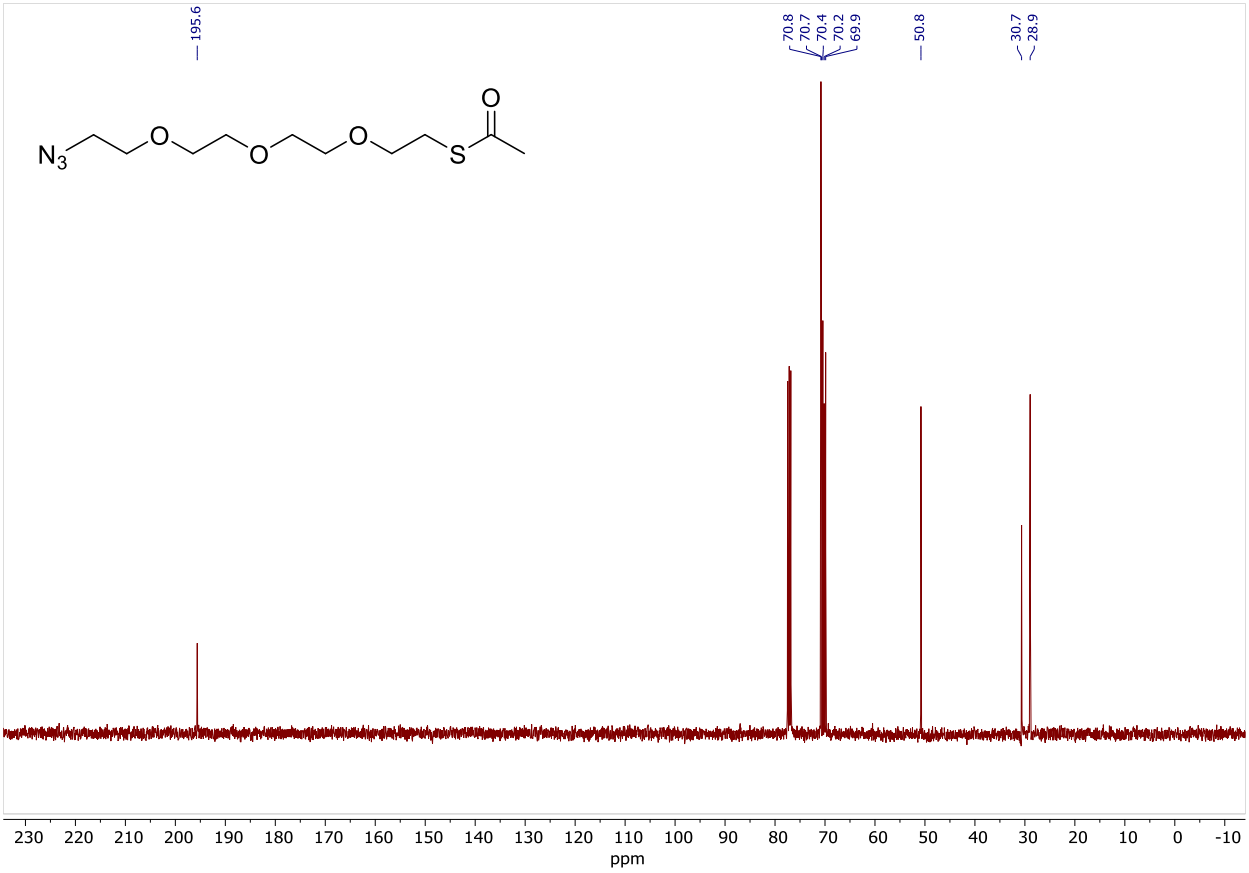


$^{13}$C{$^{1}$H}-NMR (101 MHz, $CDCl_3$) spectrum of **22**

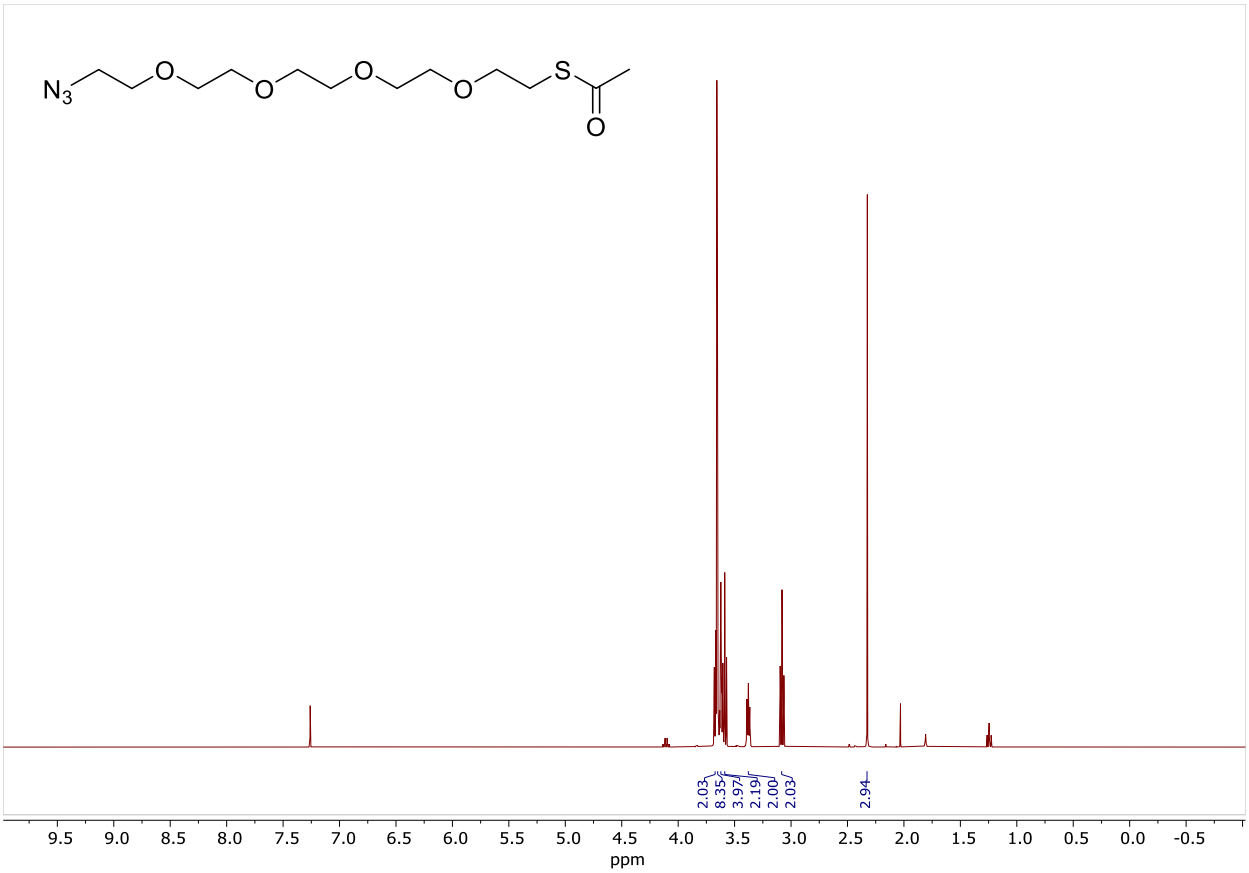


$^{1}$H-NMR (400 MHz, $CDCl_3$) spectrum of **23** (trace EtOAc)

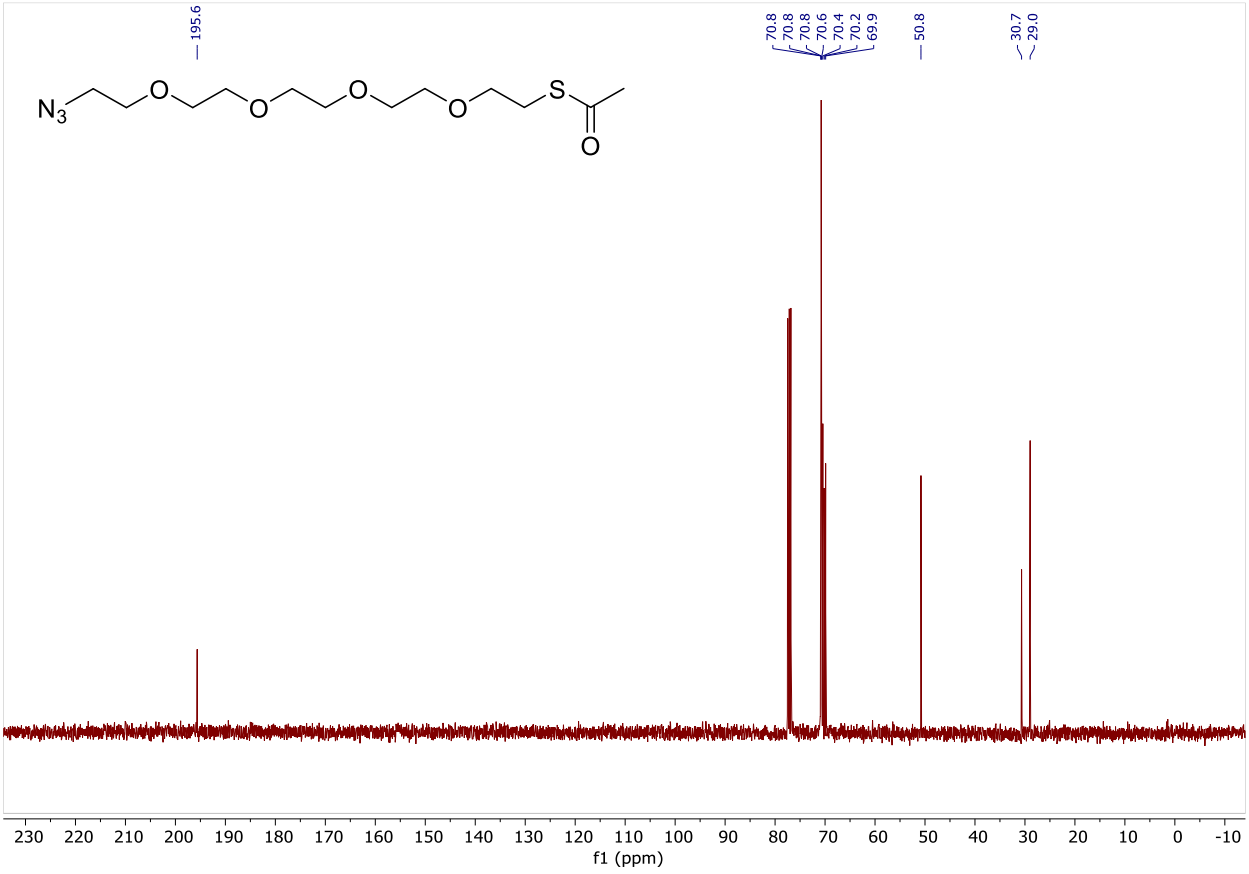

$^{13}C\{^{1}H\}$-NMR (101 MHz, $CDCl_3$) spectrum of **23** (trace EtOAc)

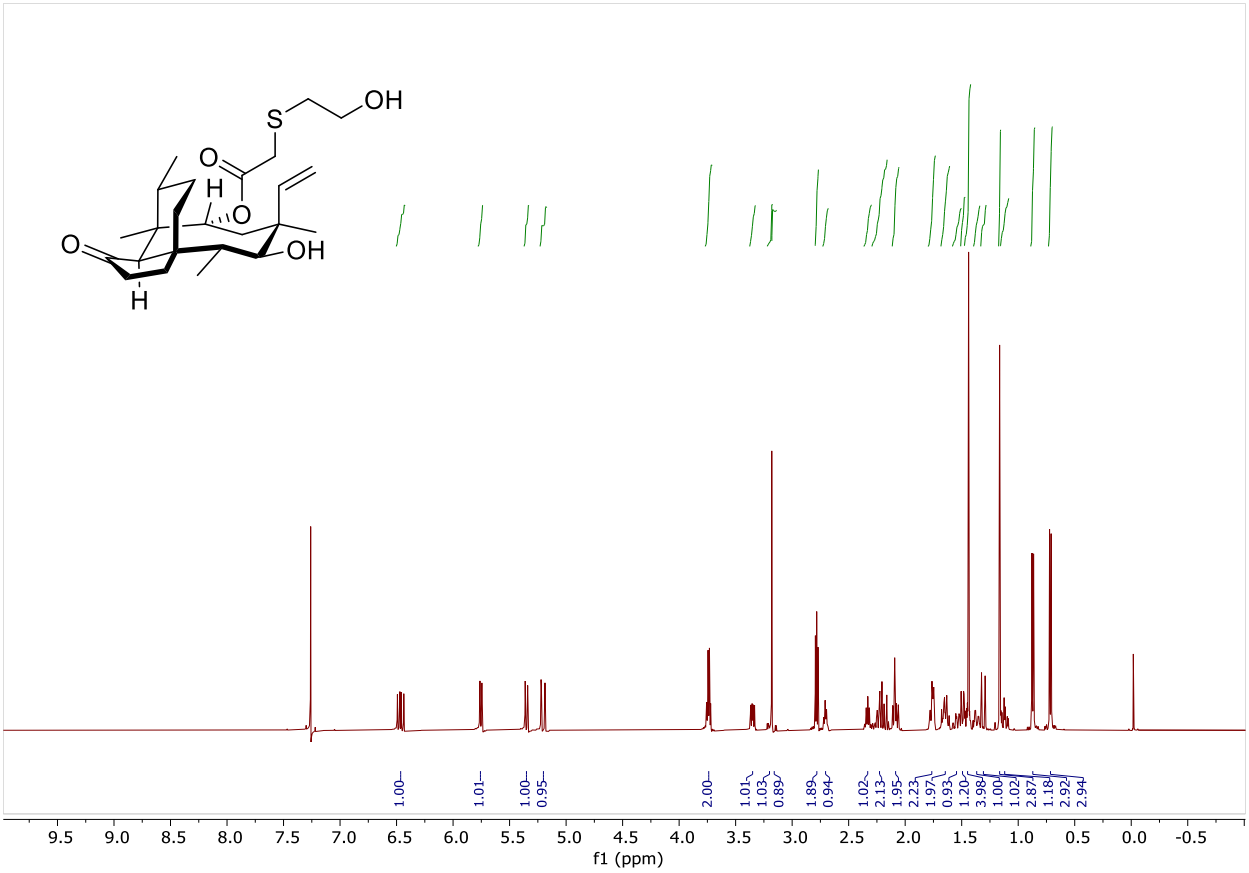


$^{1}H$-NMR (500 MHz, $CDCl_3$) spectrum of **25**

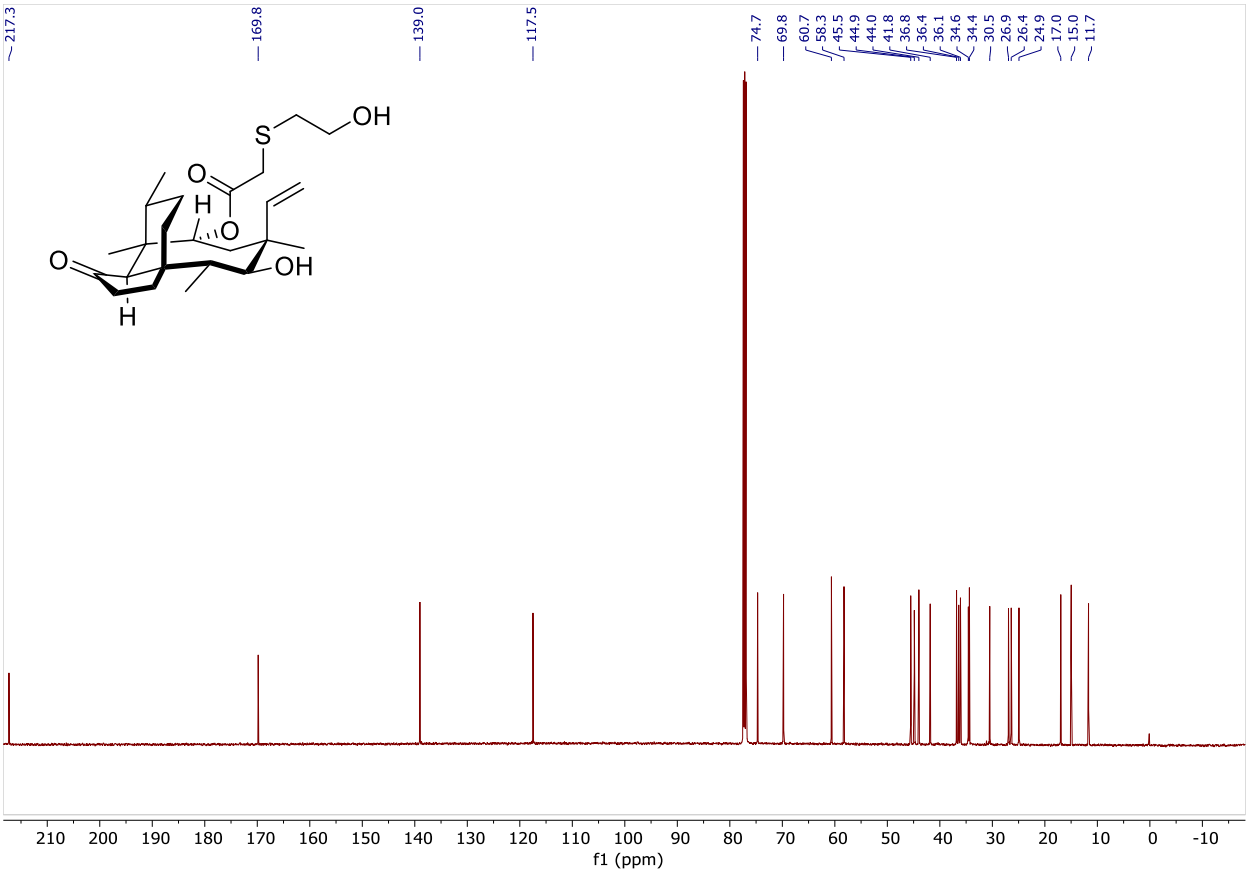


$^{13}C\{^{1}H\}$-NMR (126 MHz, $CDCl_3$) spectrum of **25**

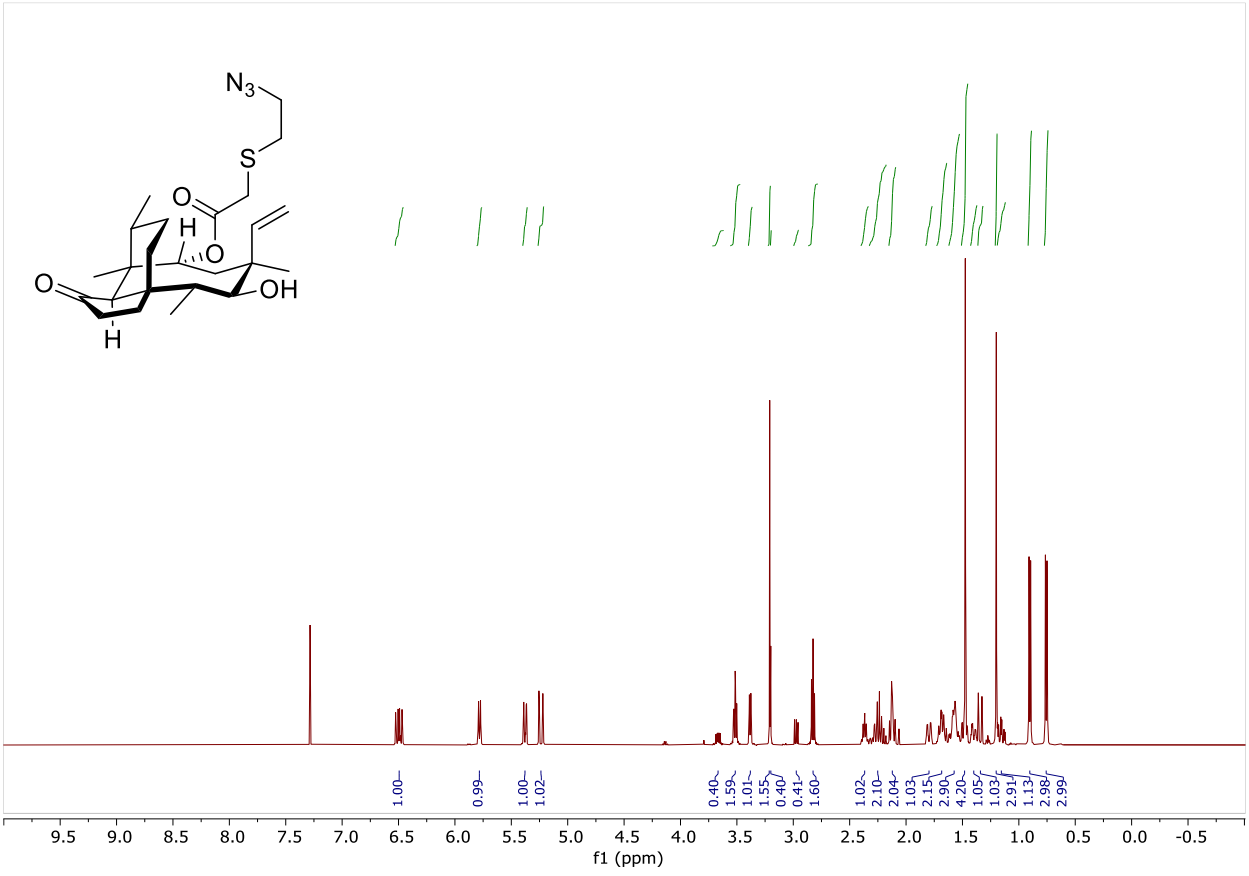

$^{1}$H-NMR (500 MHz, $CDCl_3$) spectrum of **28**

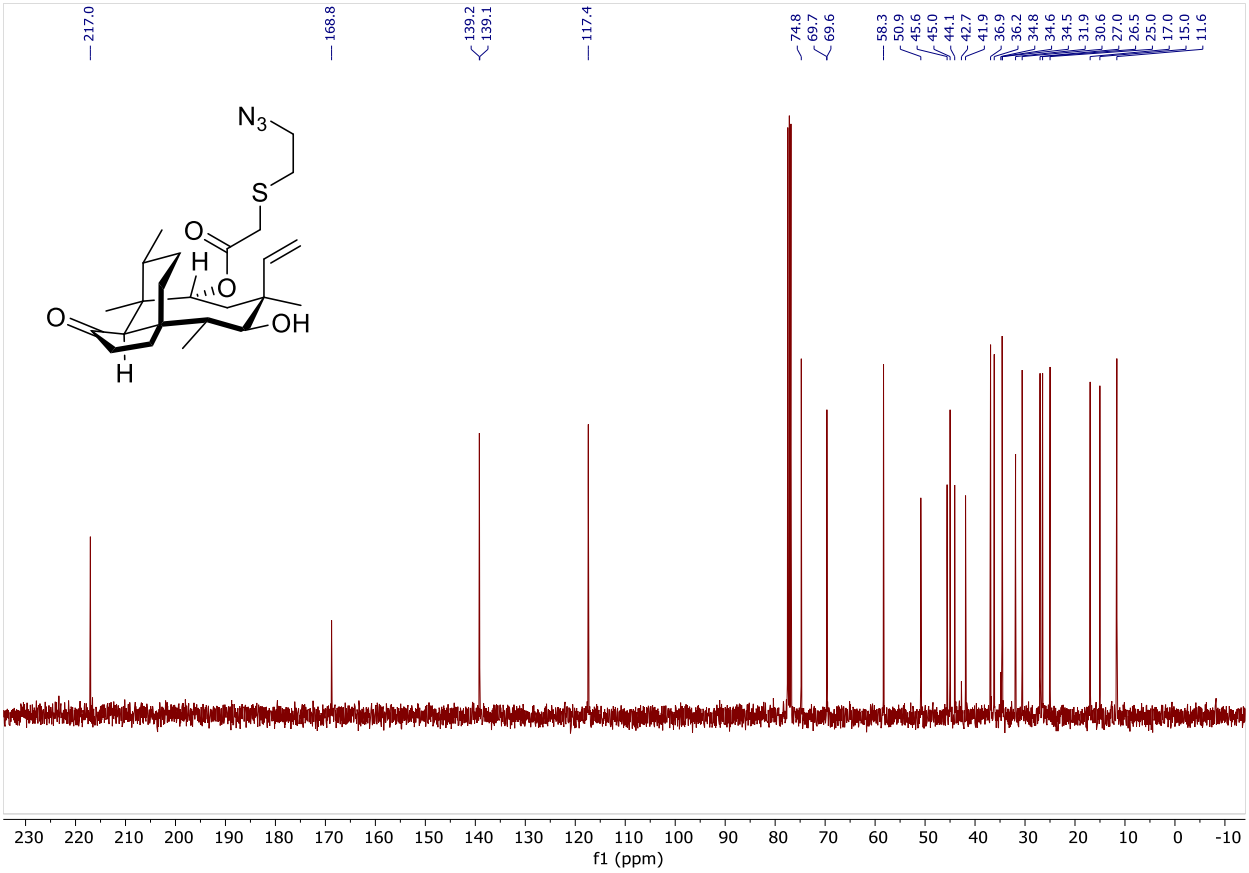


$^{13}$C{$^{1}$H}-NMR (101 MHz, $CDCl_3$) spectrum of **28**

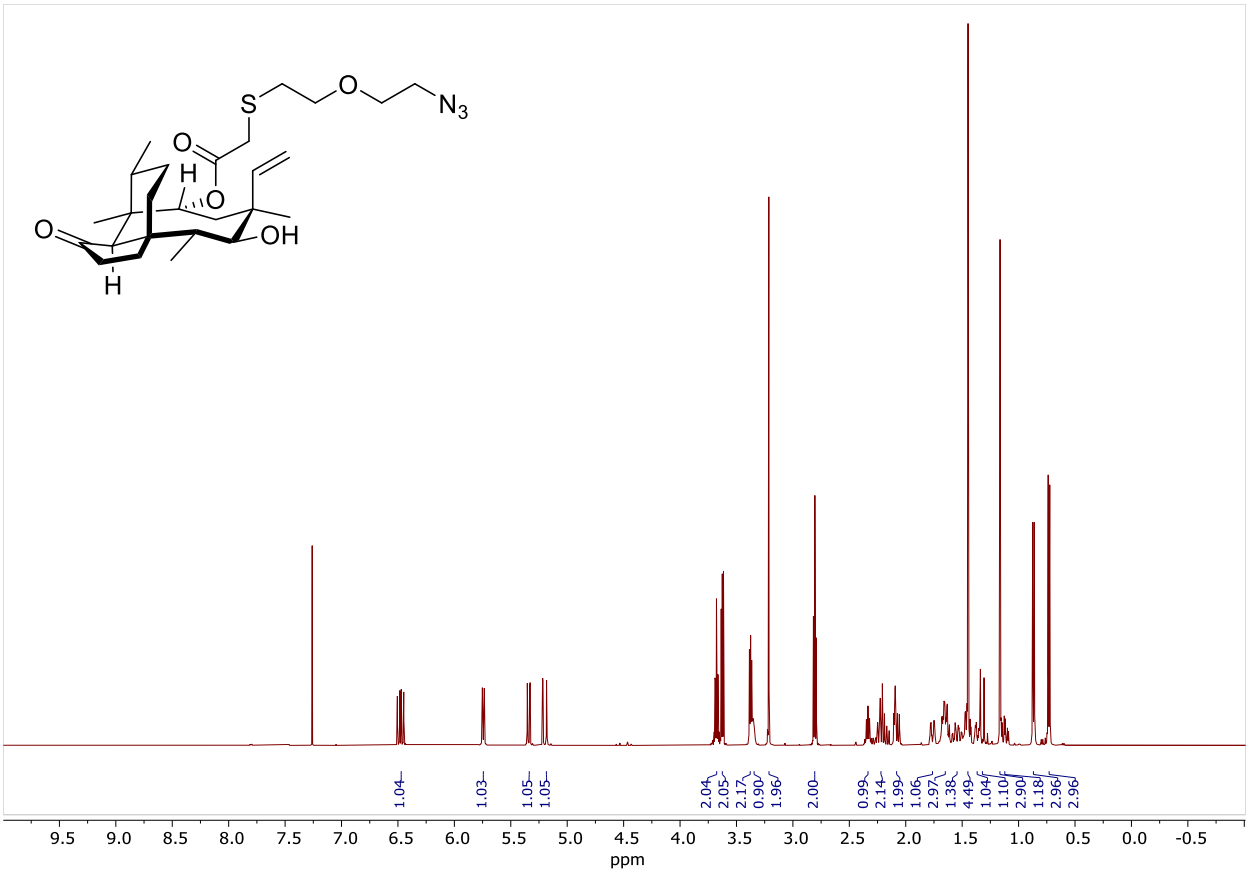


$^{1}$H-NMR (500 MHz, $CDCl_3$) spectrum of **29**

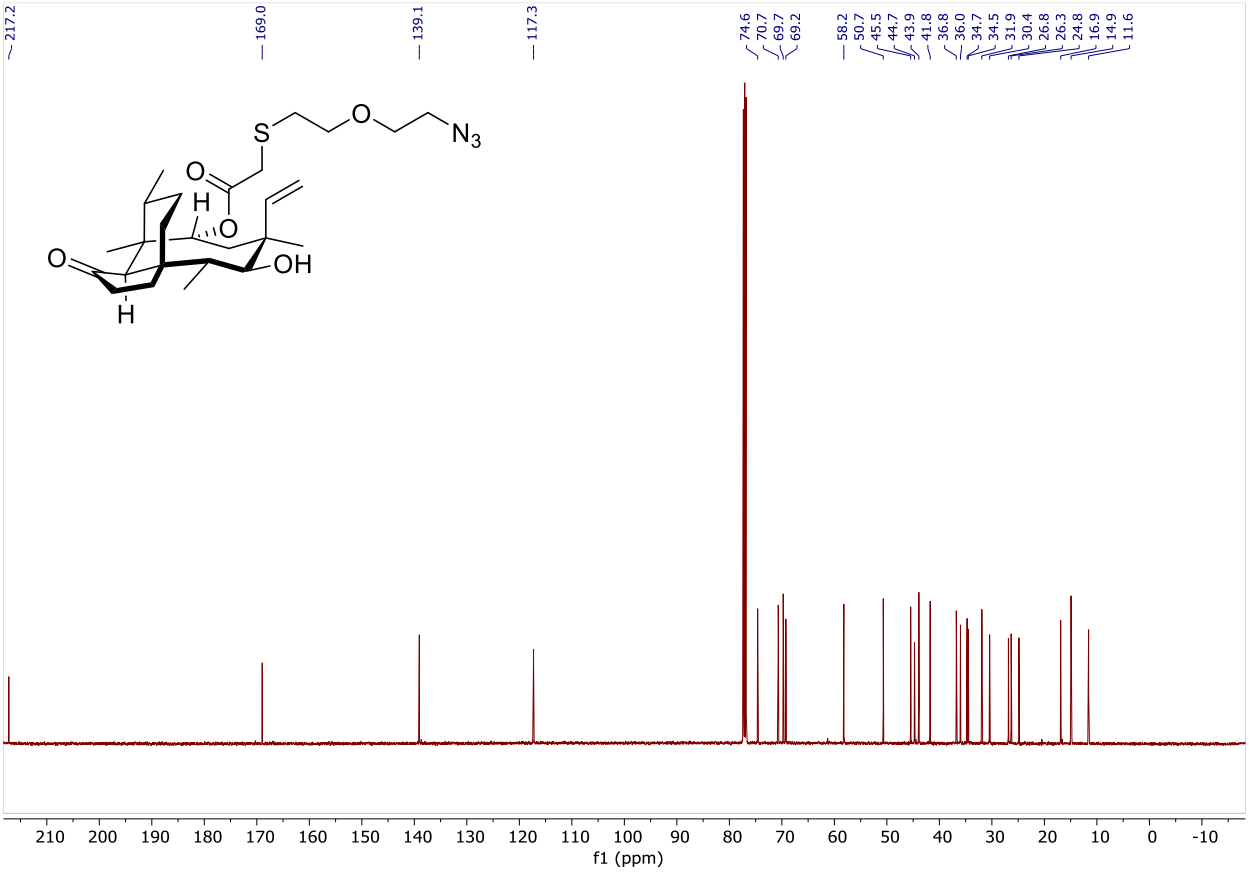

$^{13}C\{^{1}H\}$-NMR (126 MHz, $CDCl_3$) spectrum of **29**

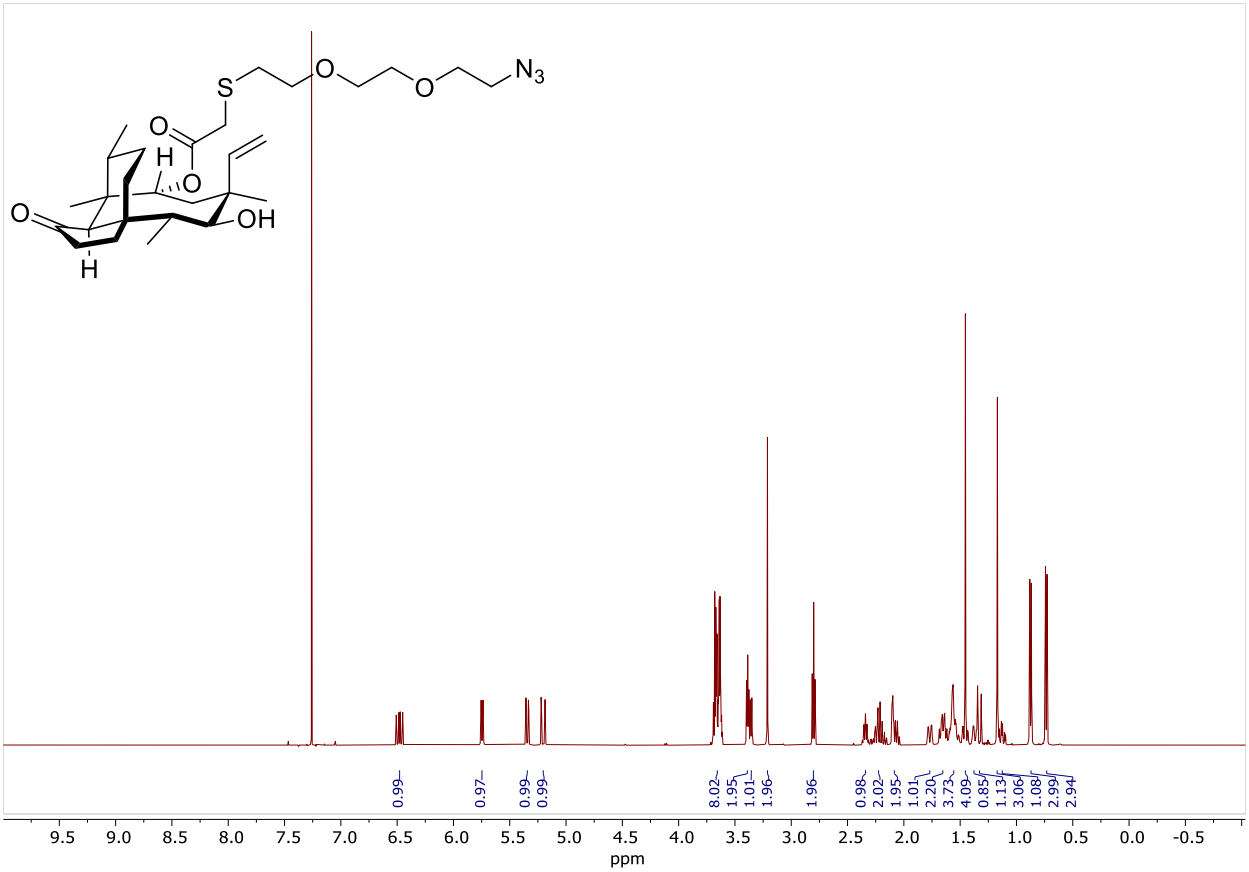


$^{1}H$-NMR (500 MHz, $CDCl_3$) spectrum of **30**

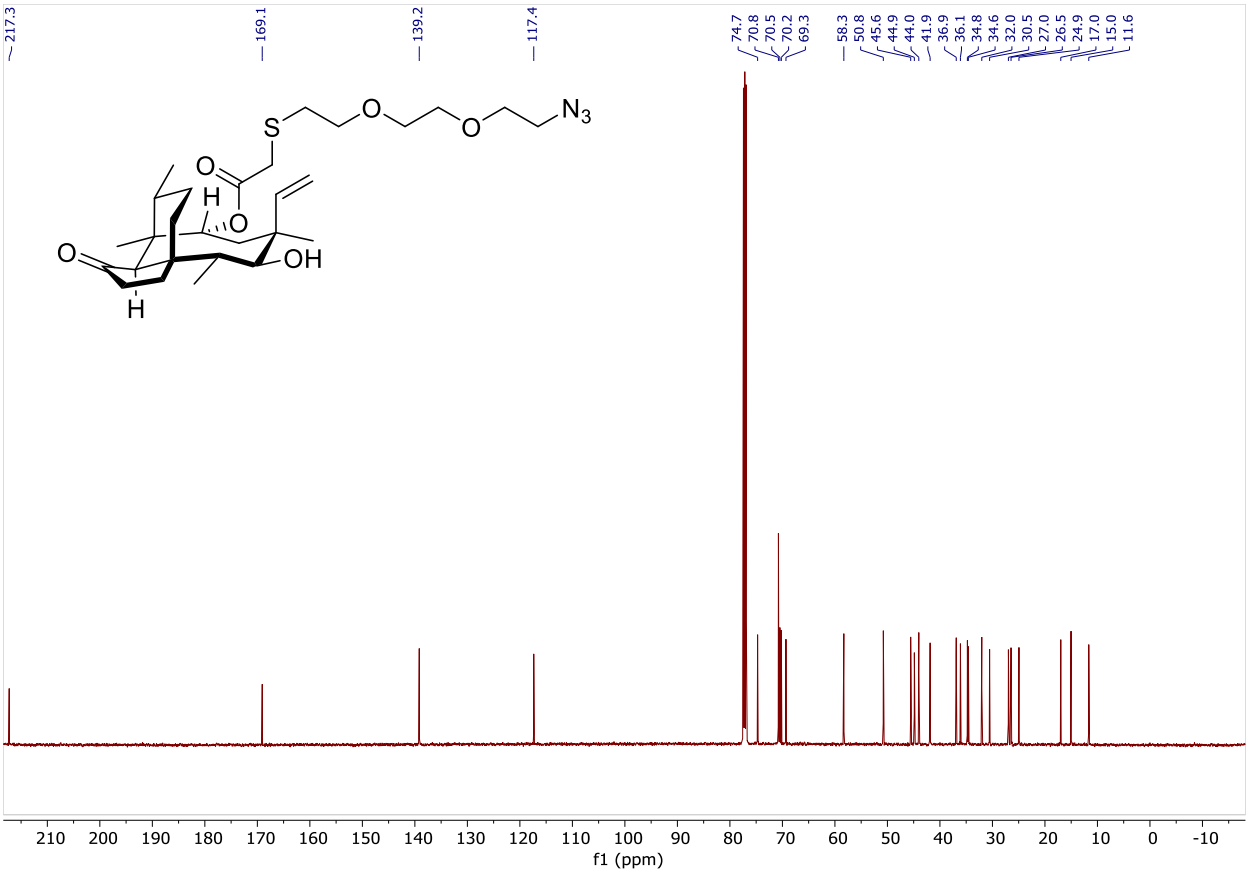


$^{13}C\{^{1}H\}$-NMR (126 MHz, $CDCl_3$) spectrum of **30**

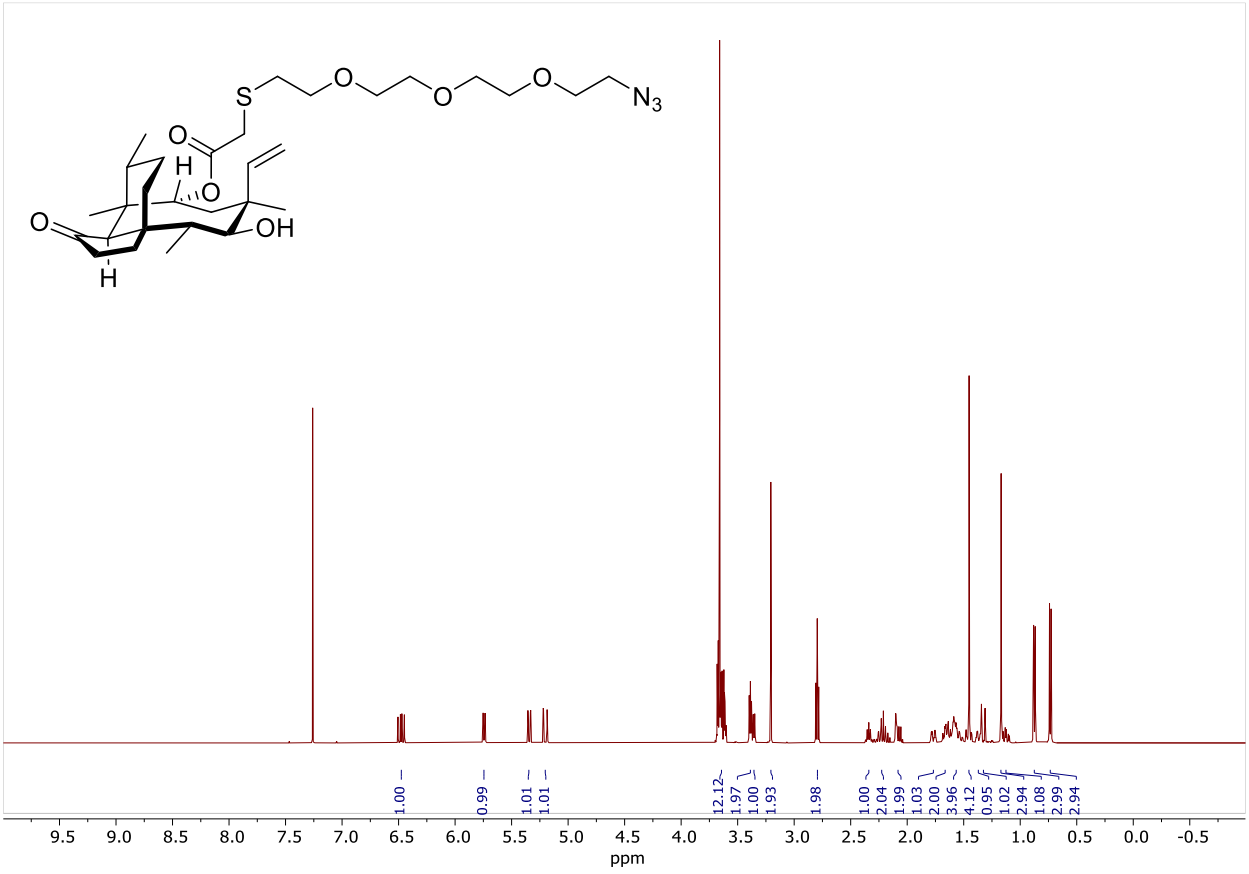

$^{1}$H-NMR (500 MHz, $CDCl_3$) spectrum of **31**

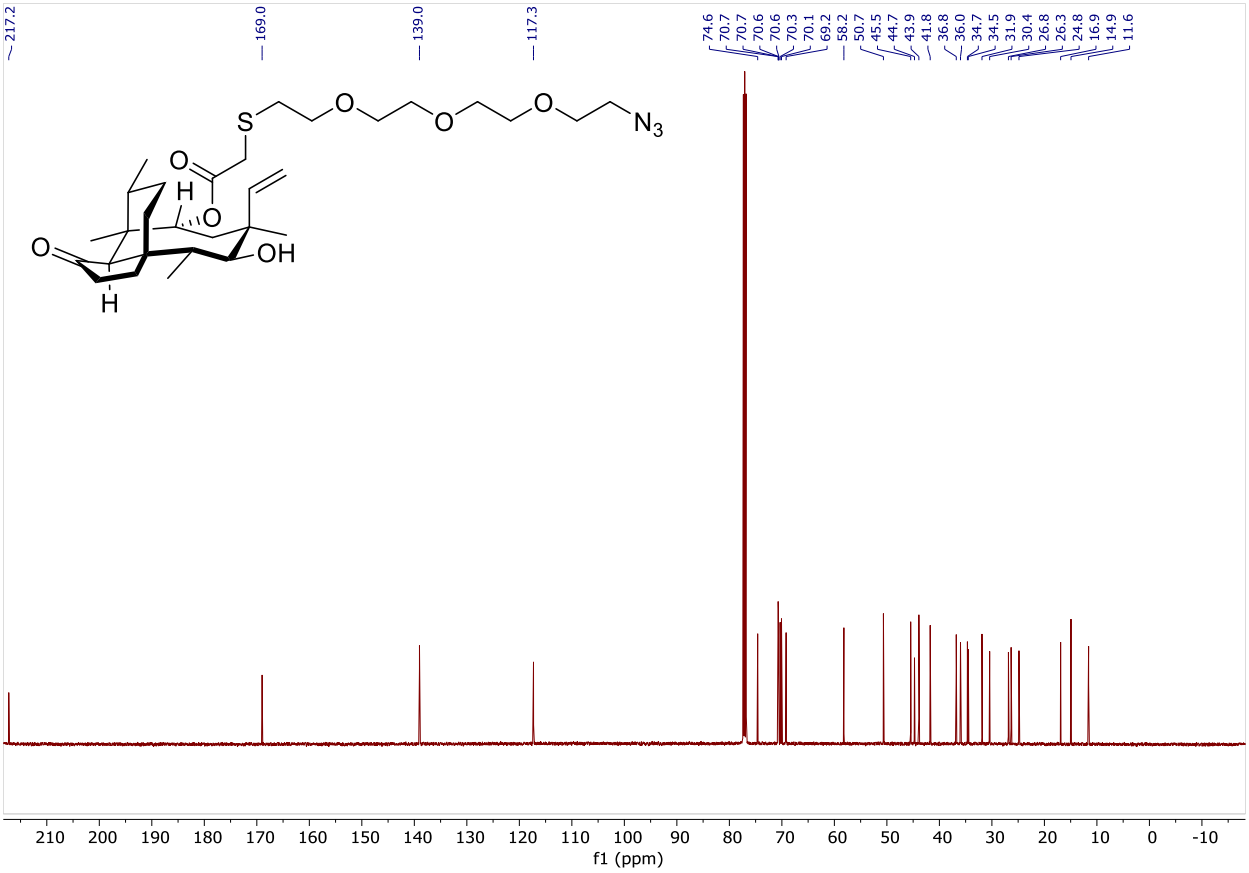


$^{13}$C{$^{1}$H}-NMR (126 MHz, $CDCl_3$) spectrum of **31**

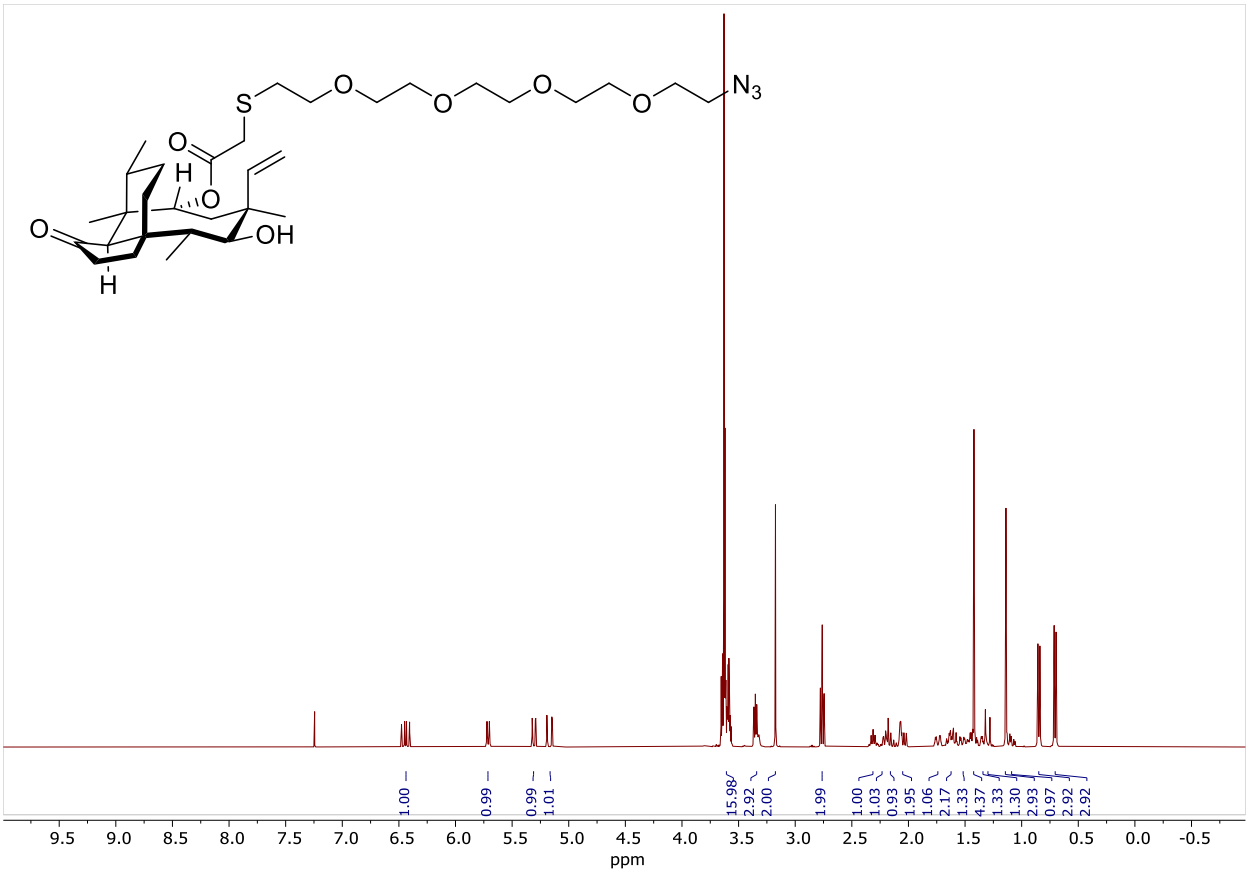


$^{1}$H-NMR (500 MHz, $CDCl_3$) spectrum of **32**

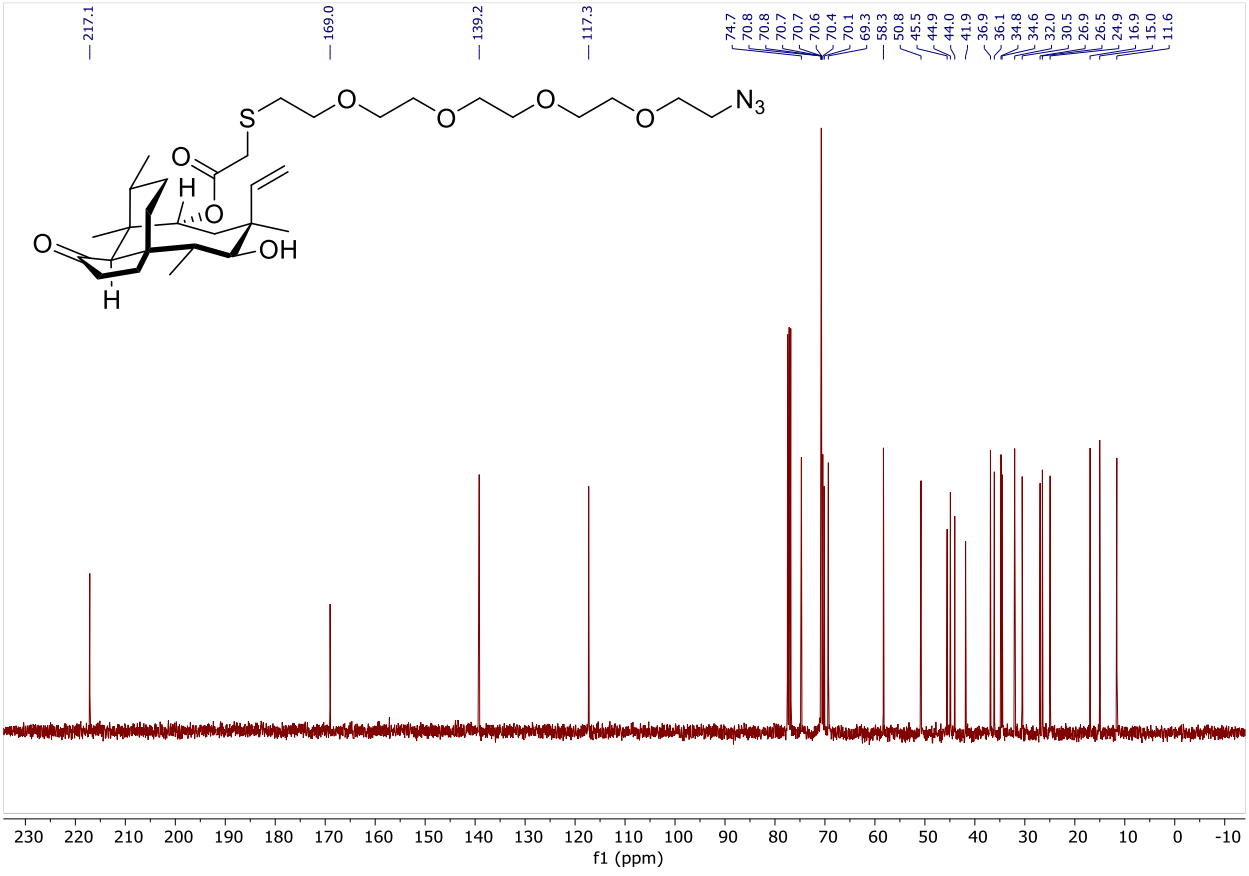

$^{13}C\{^{1}H\}$-NMR (126 MHz, $CDCl_3$) spectrum of **32**

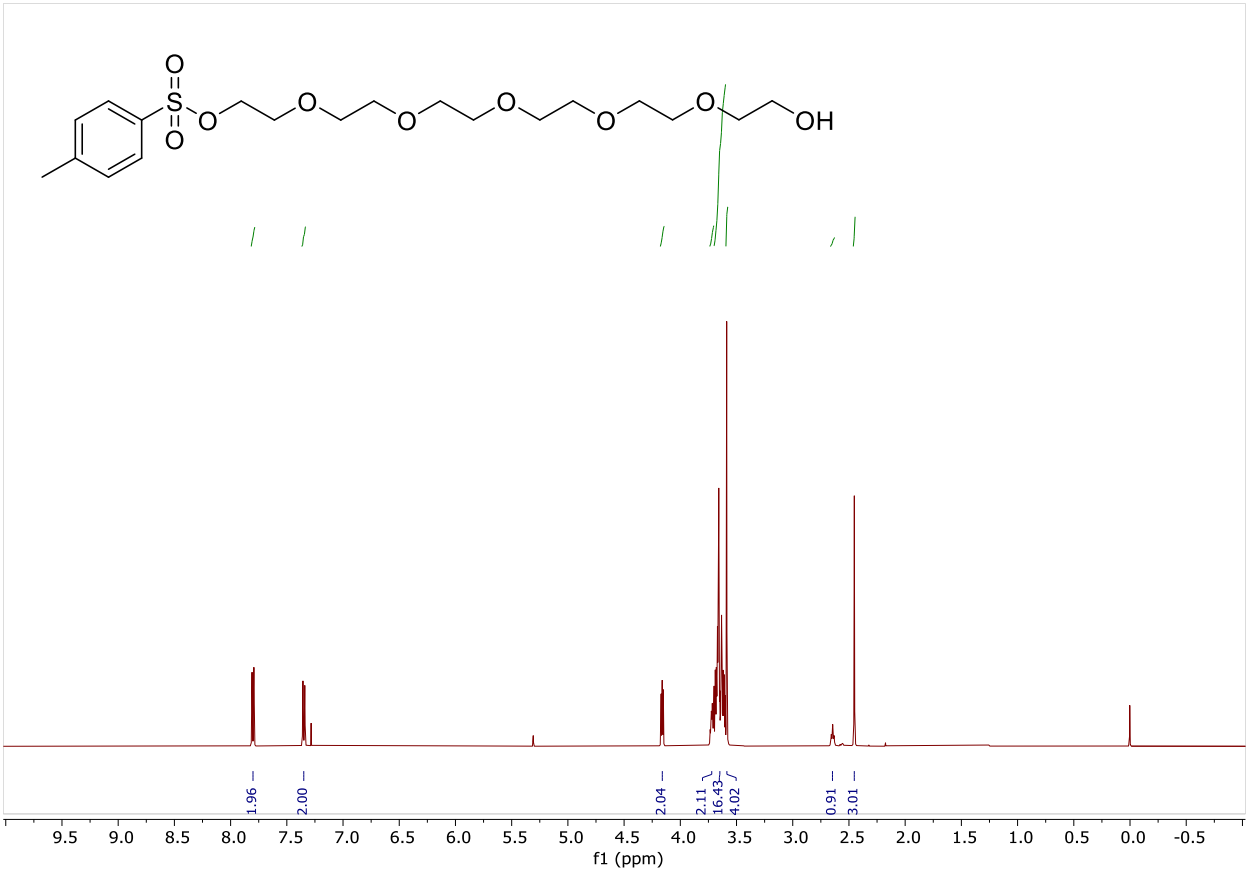


$^{1}H$-NMR (500 MHz, $CDCl_3$) spectrum of **35**

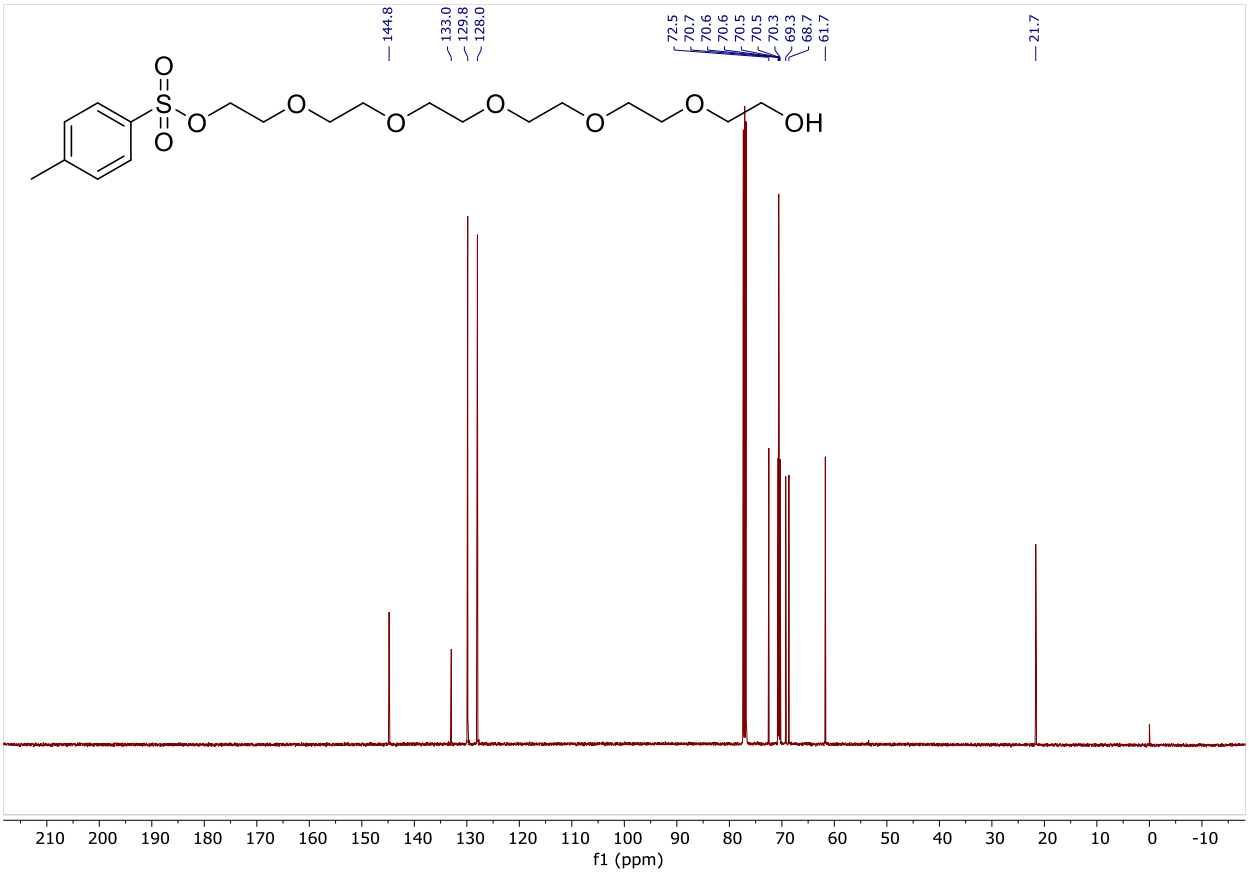


$^{13}C\{^{1}H\}$-NMR (126 MHz, $CDCl_3$) spectrum of **35**

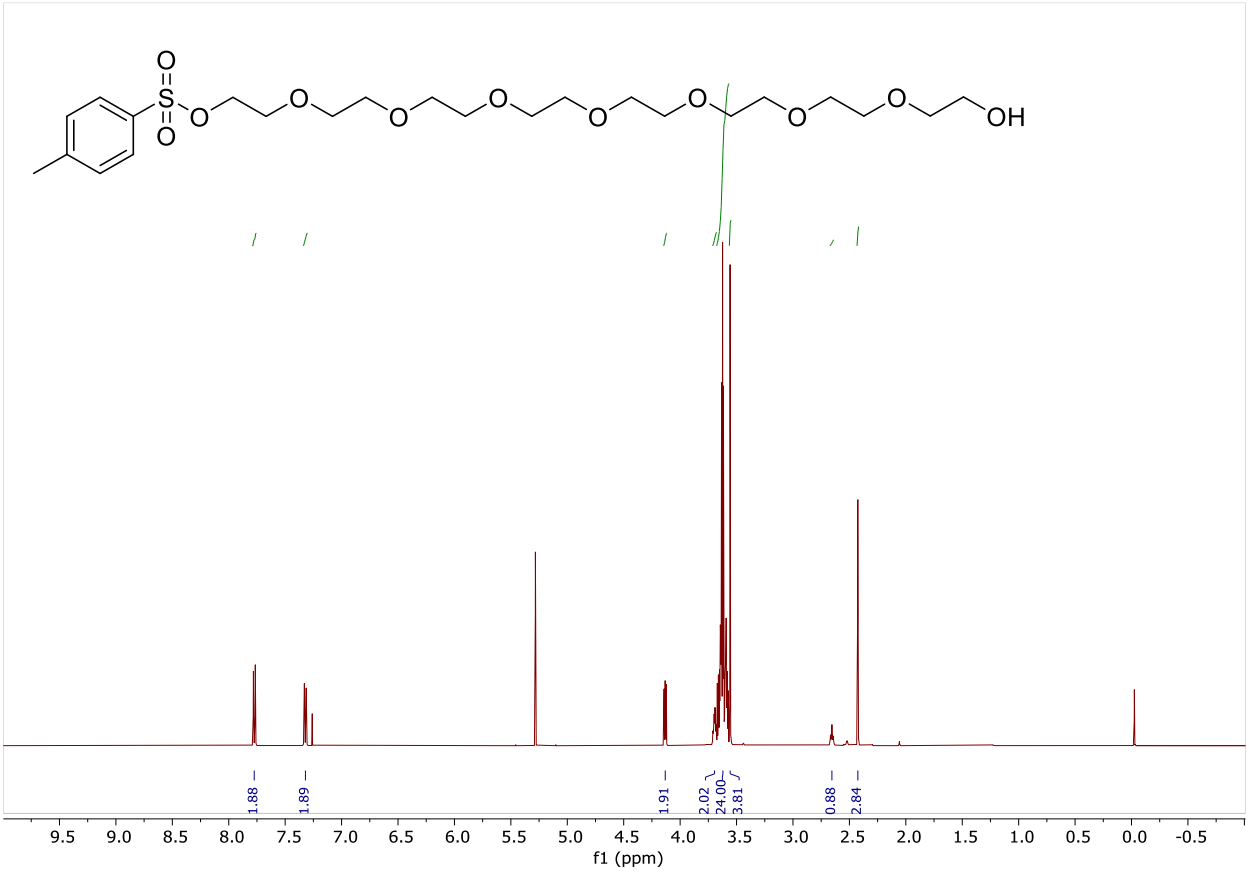

$^{1}$H-NMR (500 MHz, $CDCl_3$) spectrum of **36** (trace $CH_2Cl_2$)

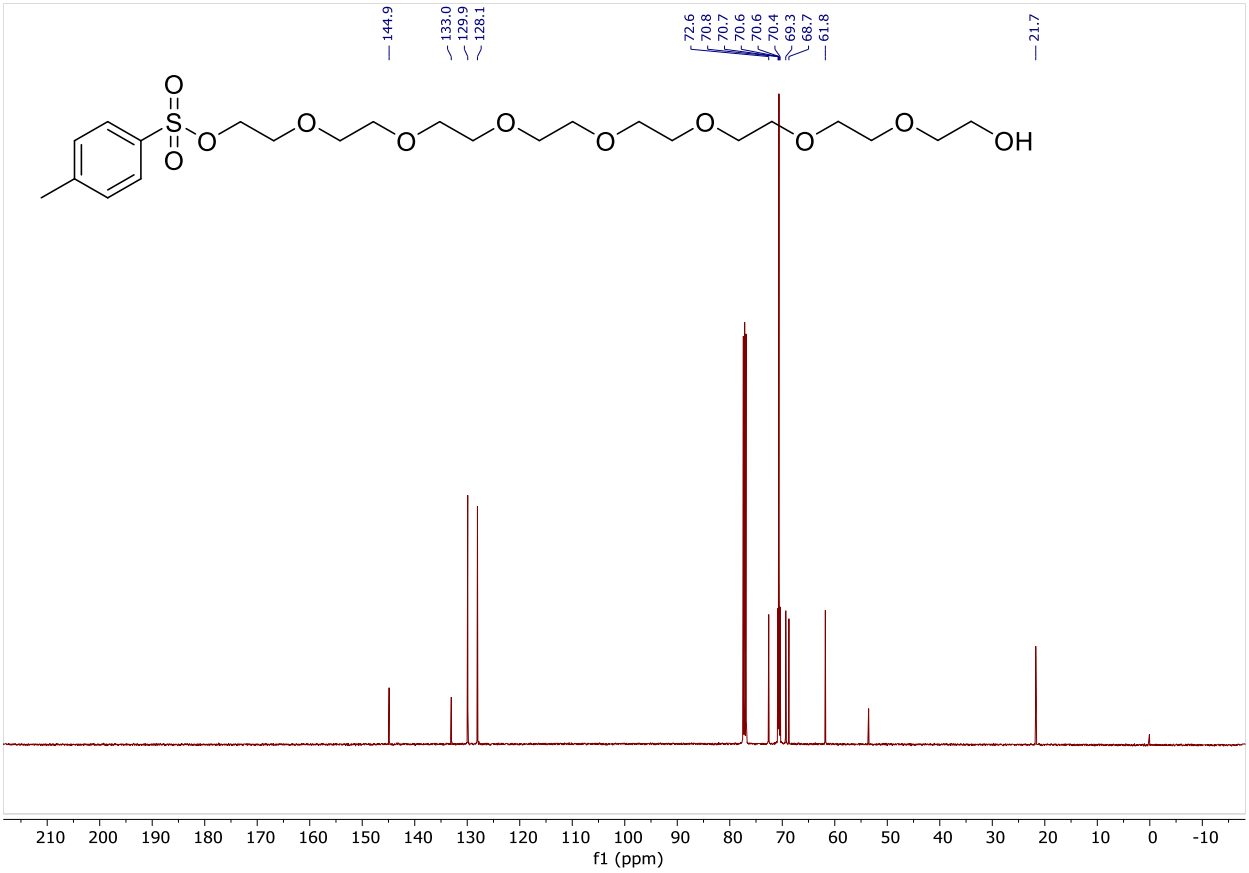


$^{13}$C{$^{1}$H}-NMR (126 MHz, $CDCl_3$) spectrum of **36** (trace $CH_2Cl_2$)

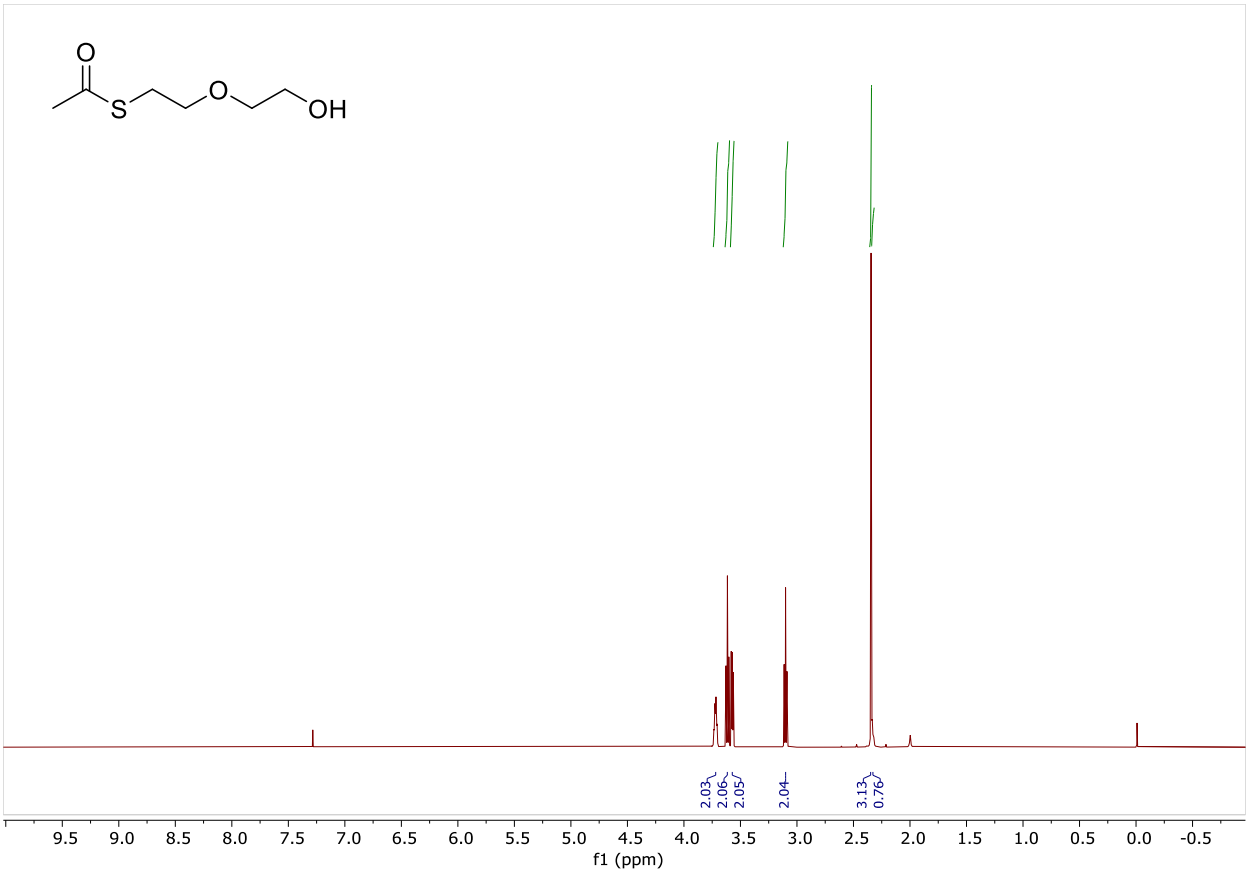


$^{1}$H-NMR (500 MHz, $CDCl_3$) spectrum of **37** (trace acetate)

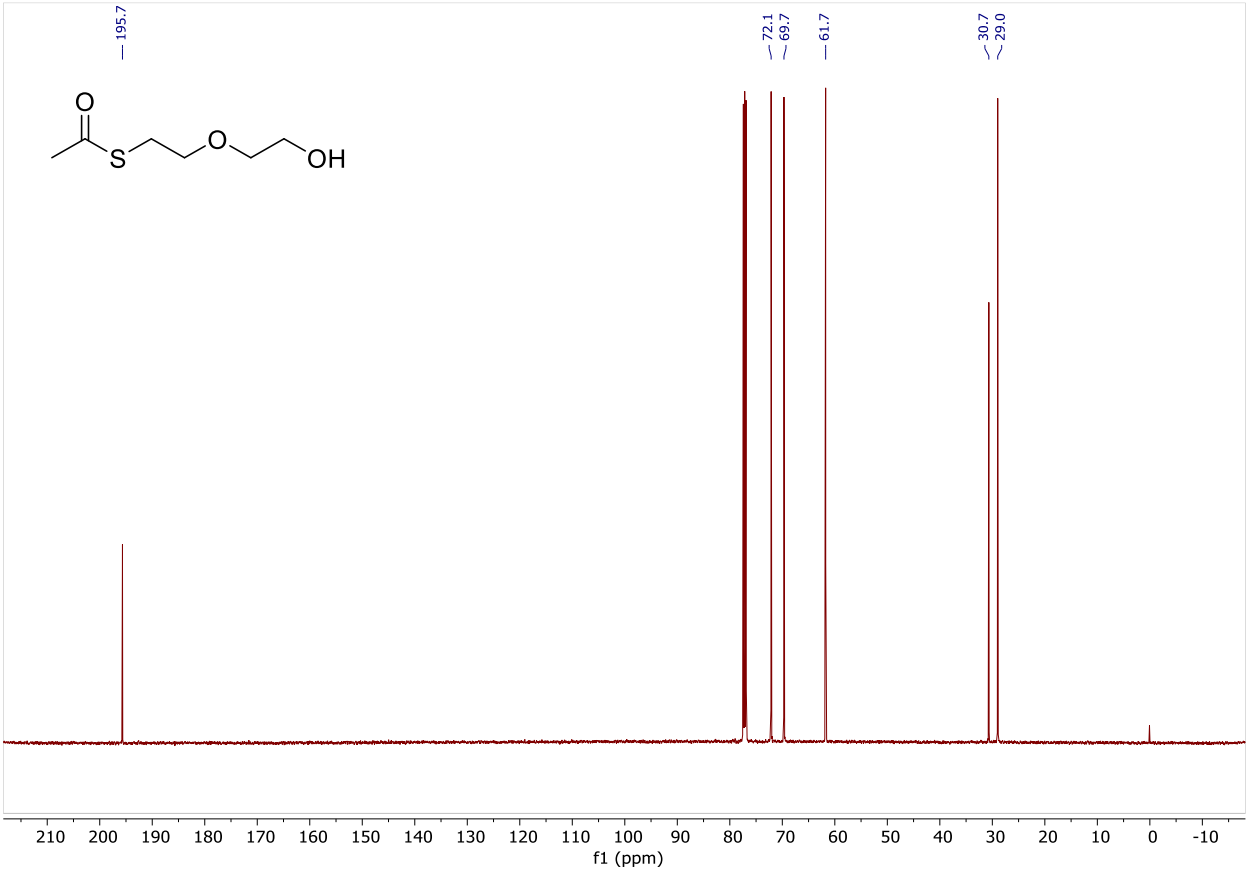

$^{13}C\{^{1}H\}$-NMR (126 MHz, $CDCl_3$) spectrum of **37** (trace acetate)

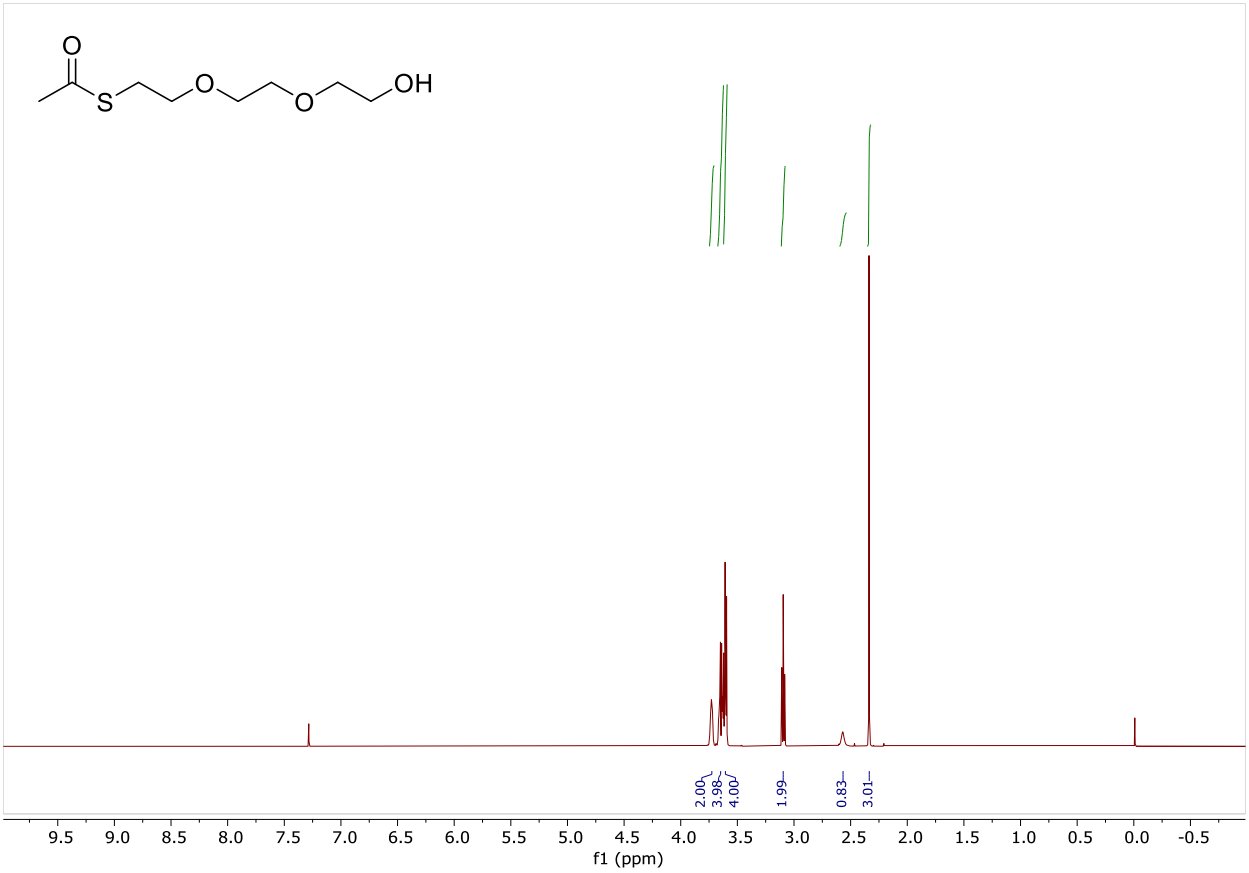


$^{1}H$-NMR (500 MHz, $CDCl_3$) spectrum of **38**

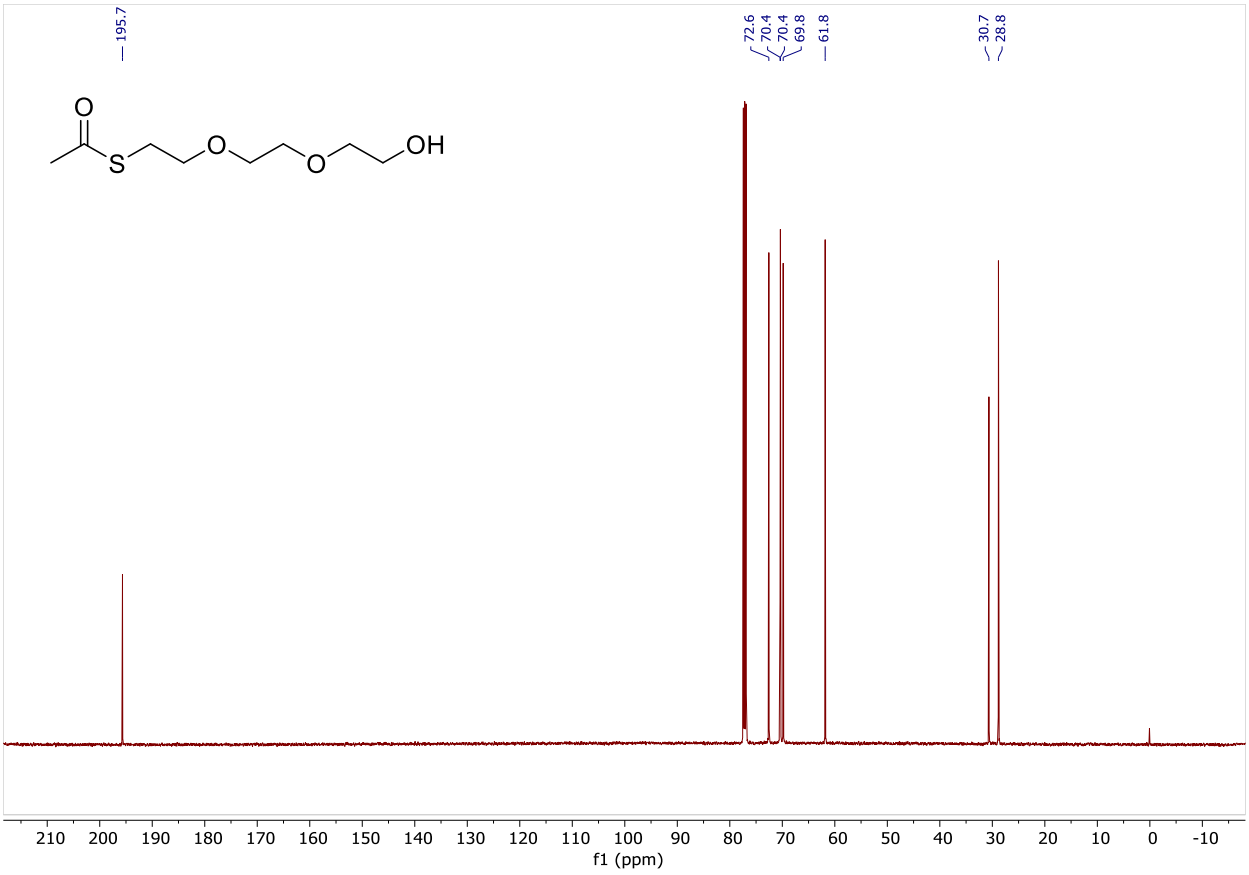


$^{13}C\{^{1}H\}$-NMR (126 MHz, $CDCl_3$) spectrum of **38**

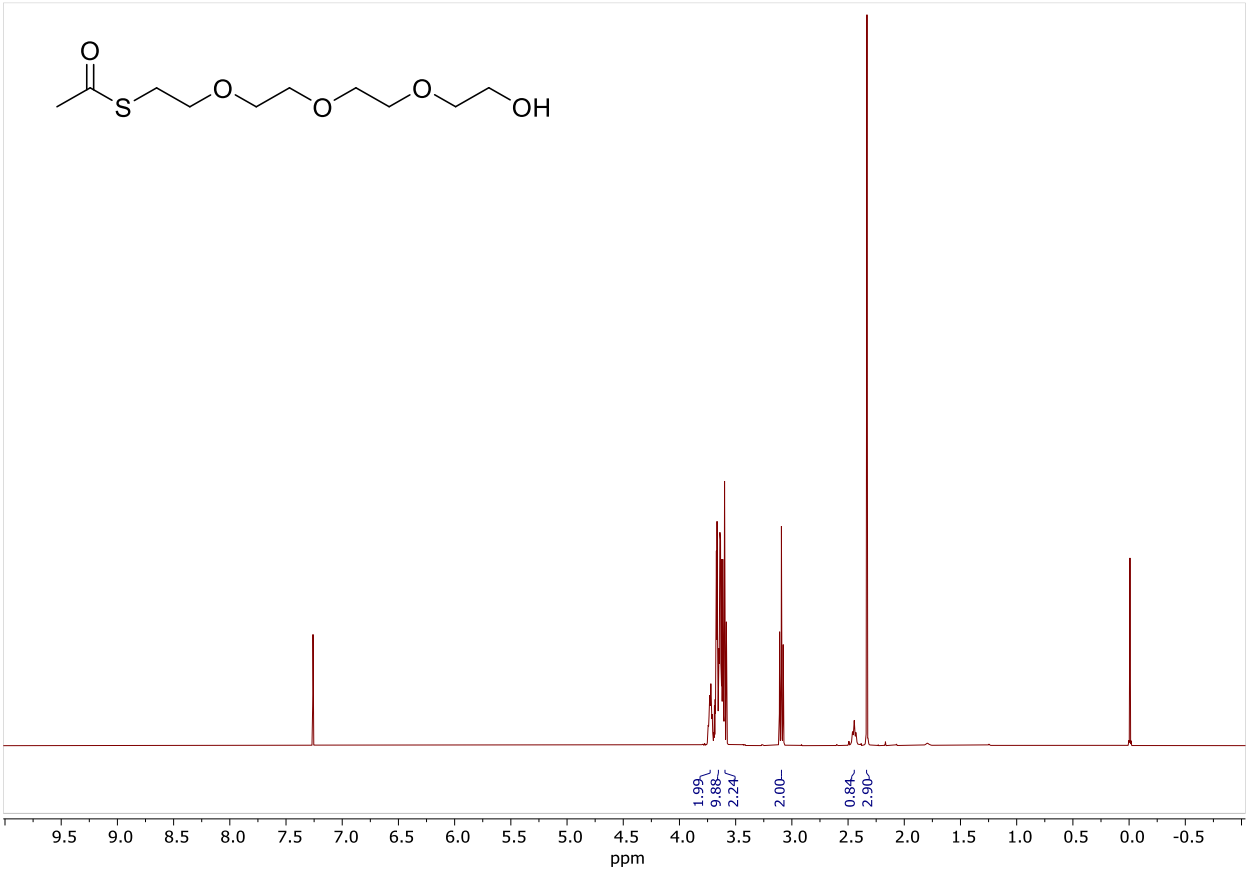

$^{1}$H-NMR (400 MHz, $CDCl_3$) spectrum of **39**

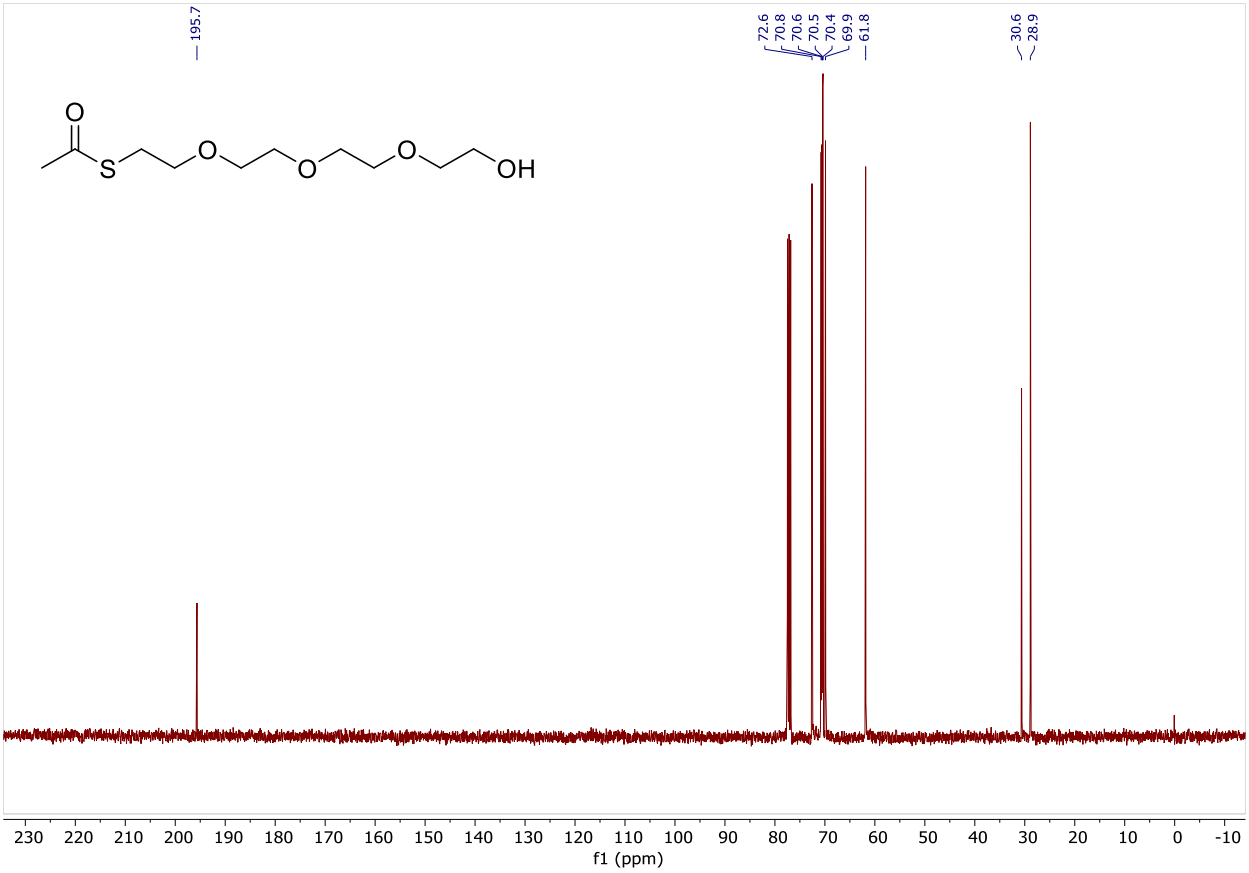


$^{13}$C{$^{1}$H}-NMR (101 MHz, $CDCl_3$) spectrum of **39**

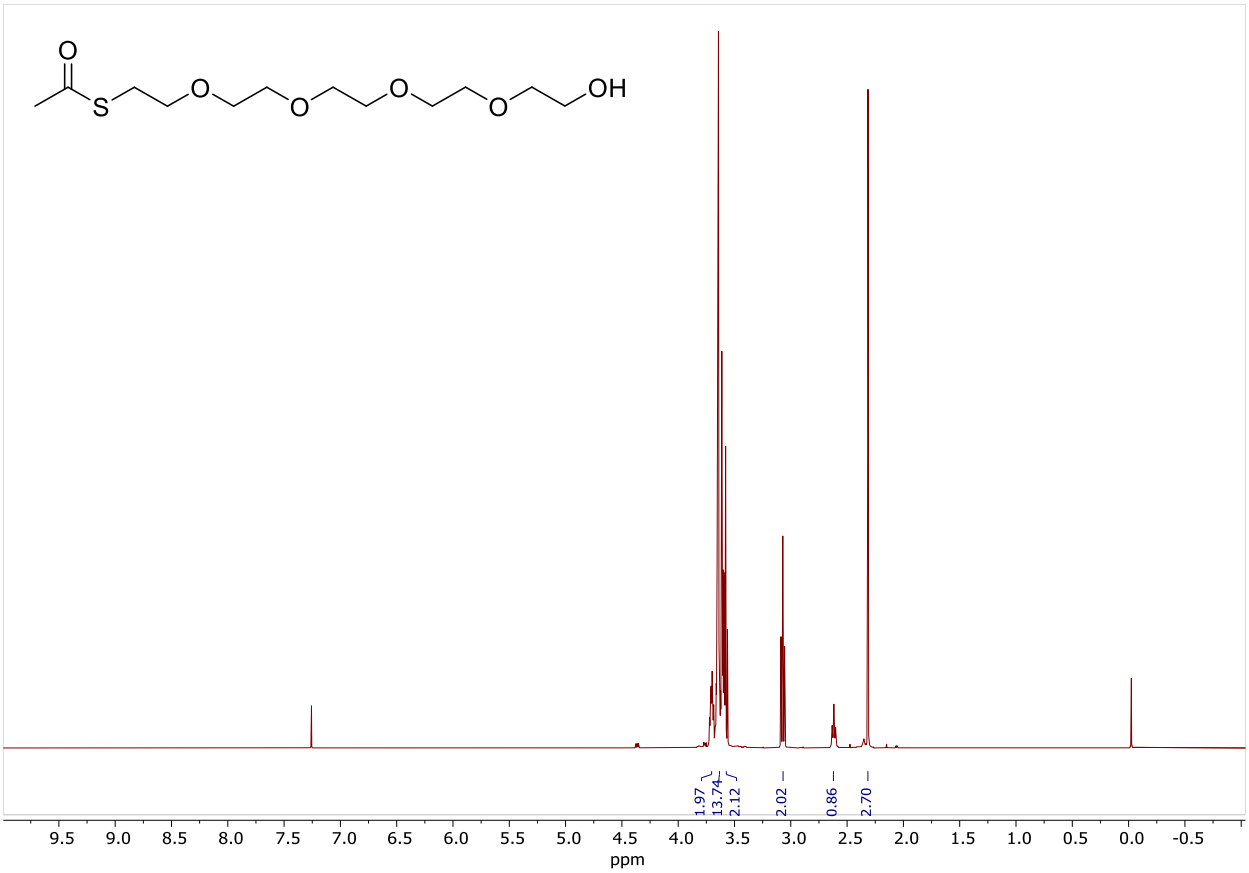


$^{1}$H-NMR (400 MHz, $CDCl_3$) spectrum of **40**

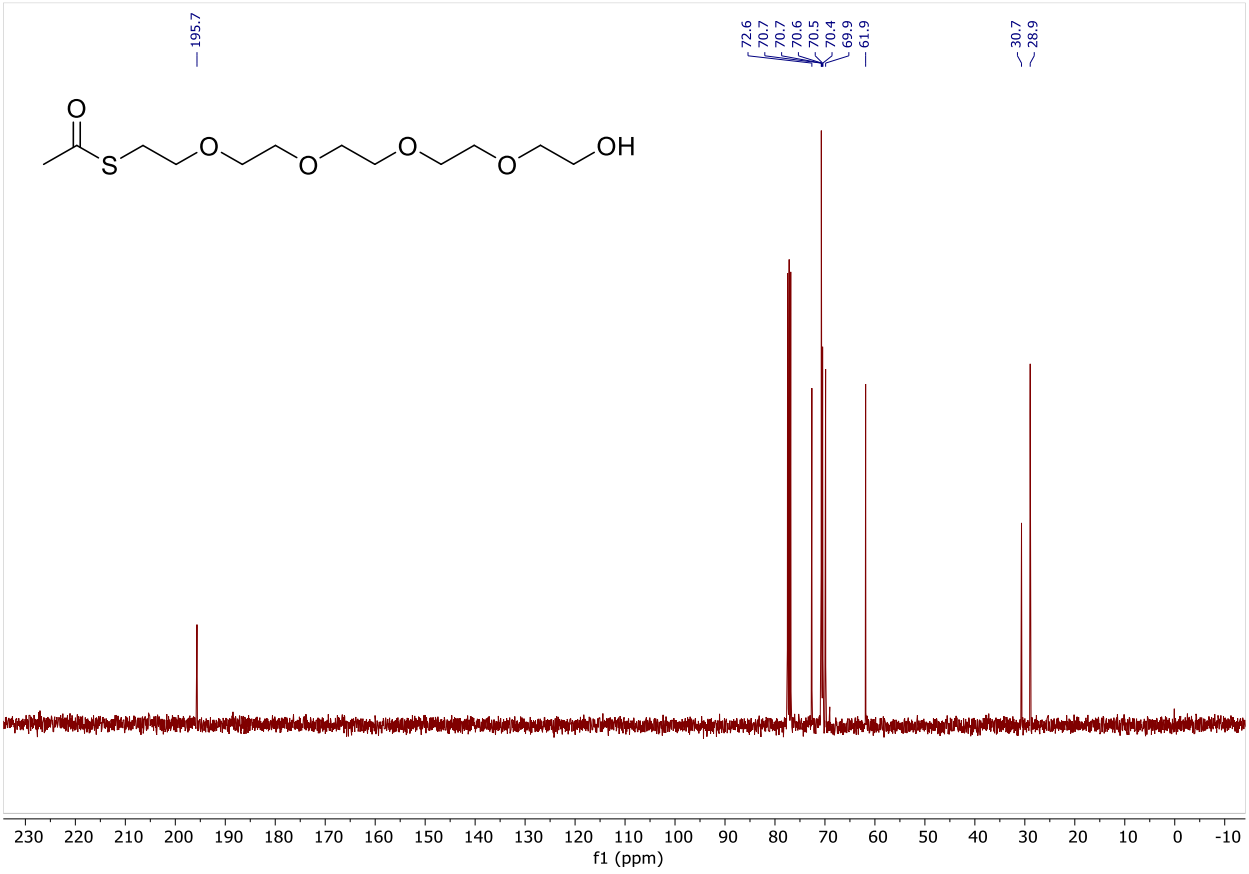

$^{13}C\{^{1}H\}$-NMR (101 MHz, $CDCl_3$) spectrum of **40**

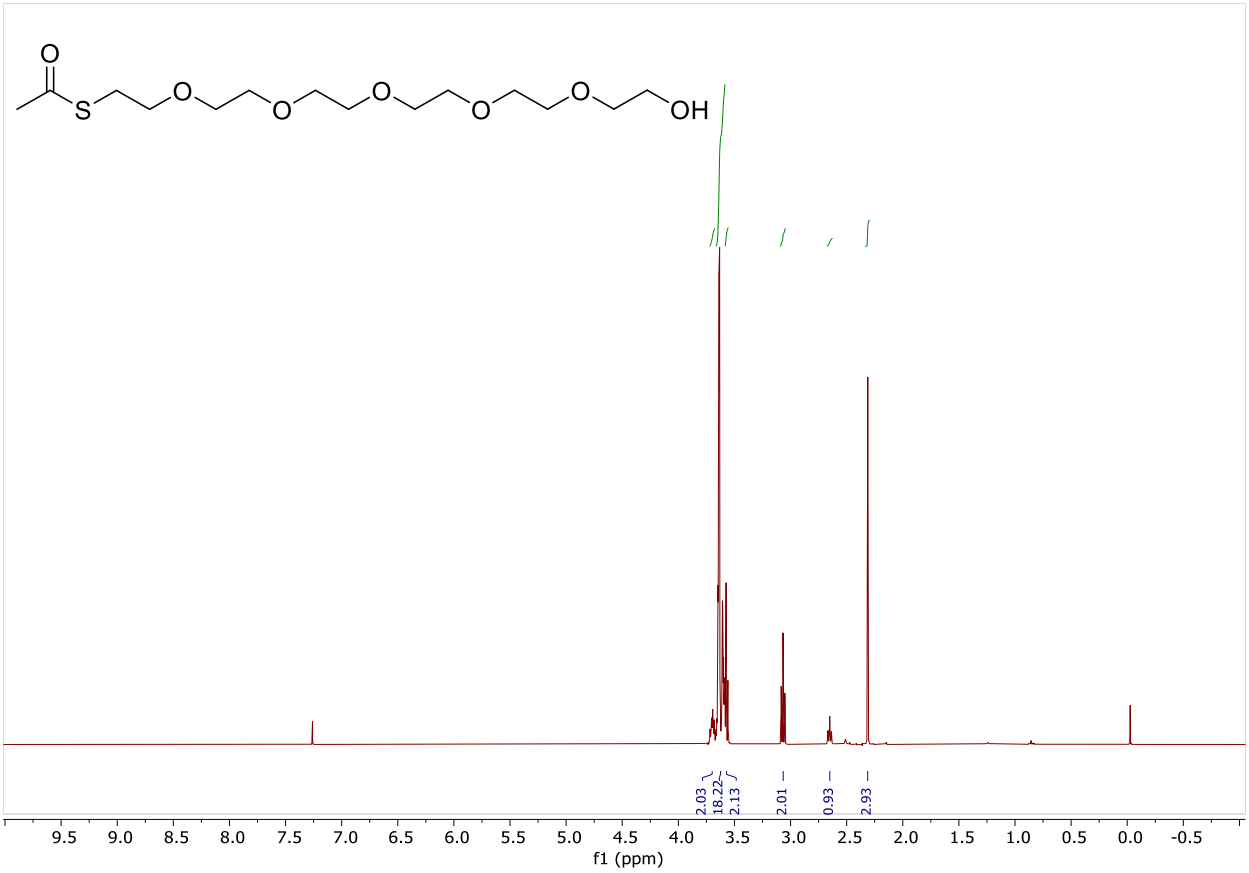


$^{1}H$-NMR (400 MHz, $CDCl_3$) spectrum of **41**

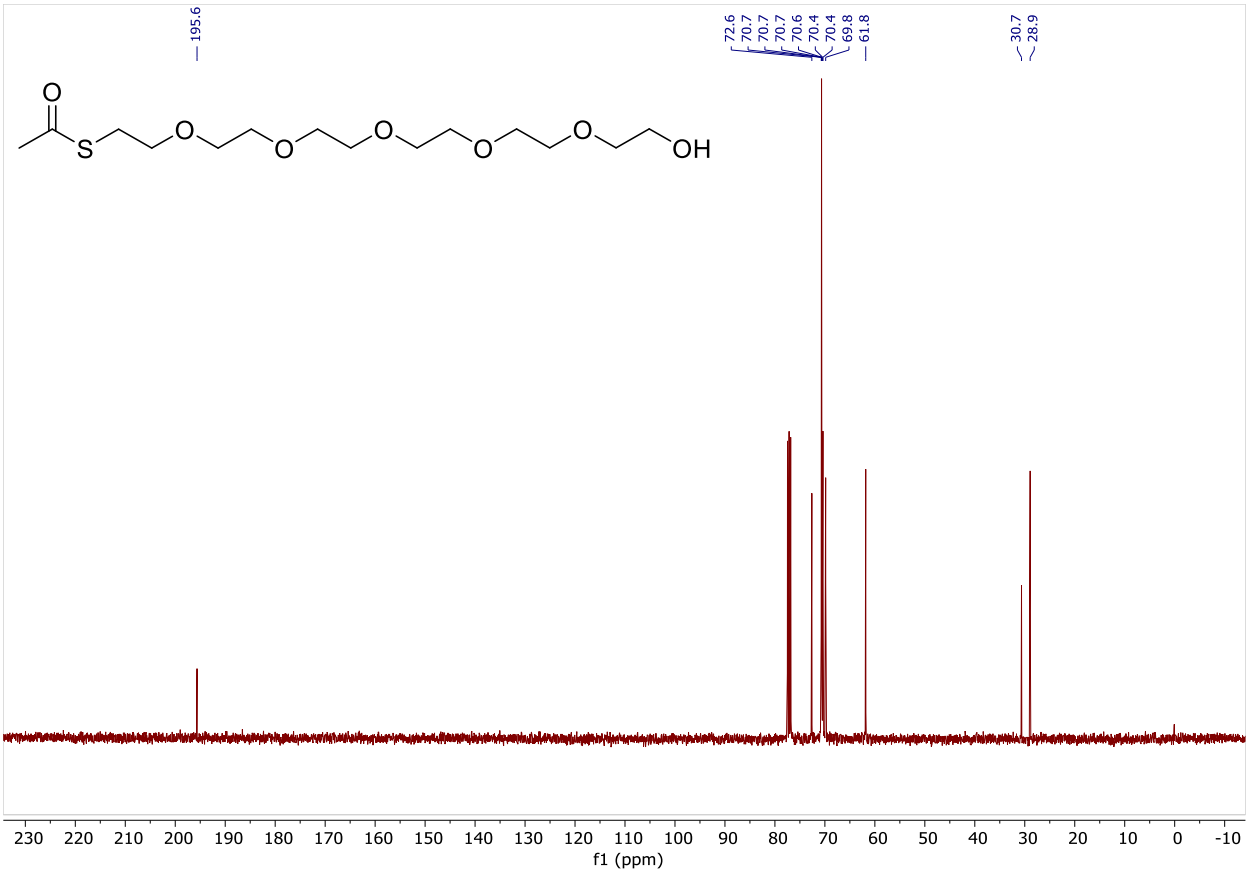


$^{13}C\{^{1}H\}$-NMR (101 MHz, $CDCl_3$) spectrum of **41**

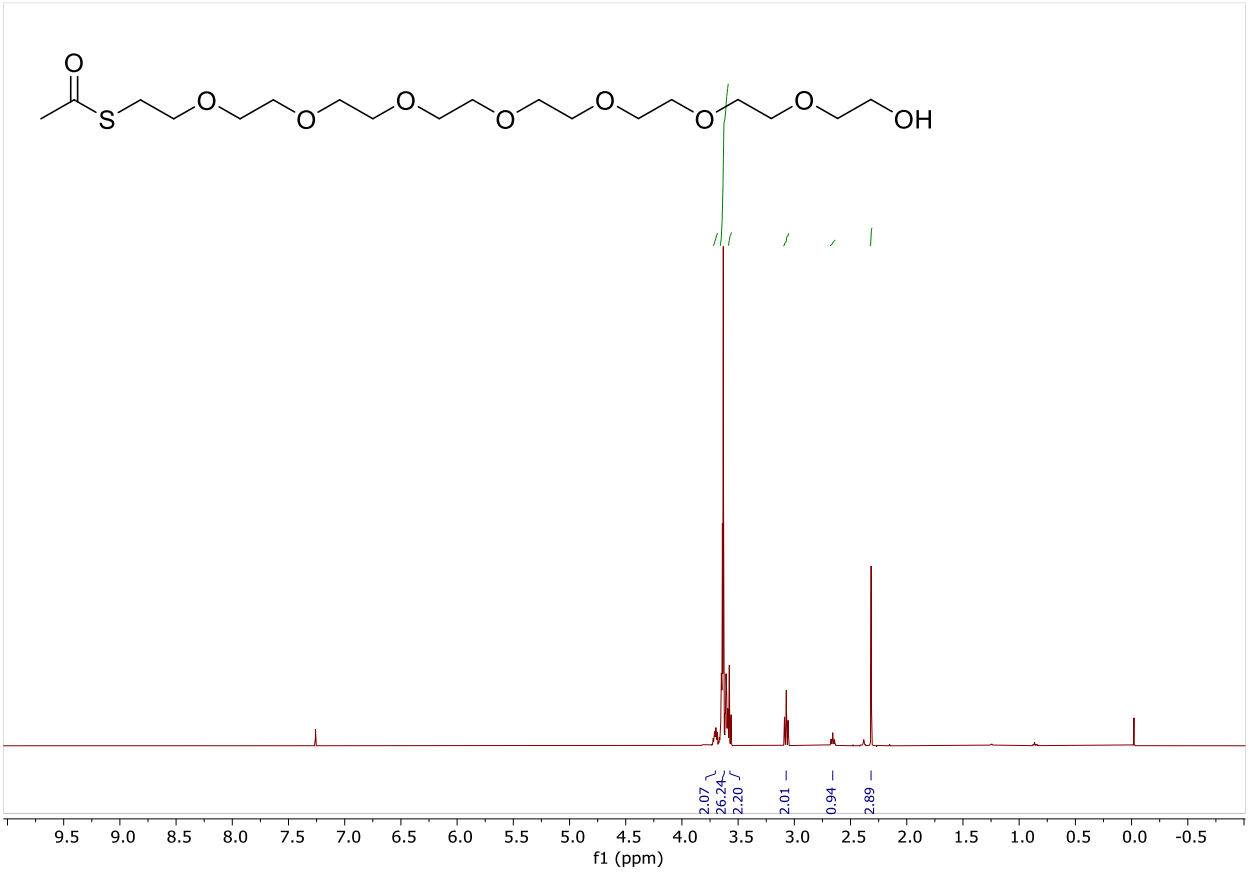

$^{1}$H-NMR (400 MHz, $CDCl_3$) spectrum of **42**

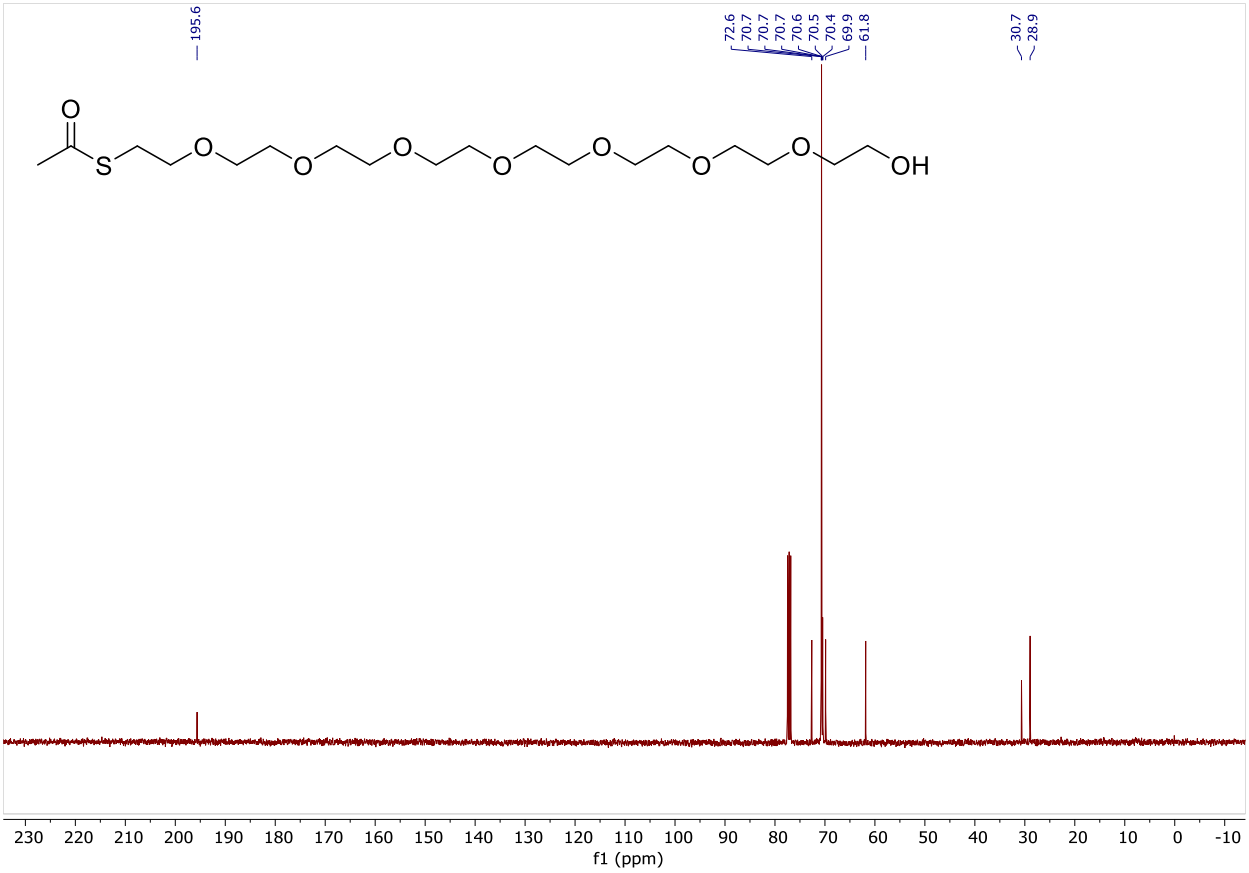


$^{13}$C{$^{1}$H}-NMR (101 MHz, $CDCl_3$) spectrum of **42**

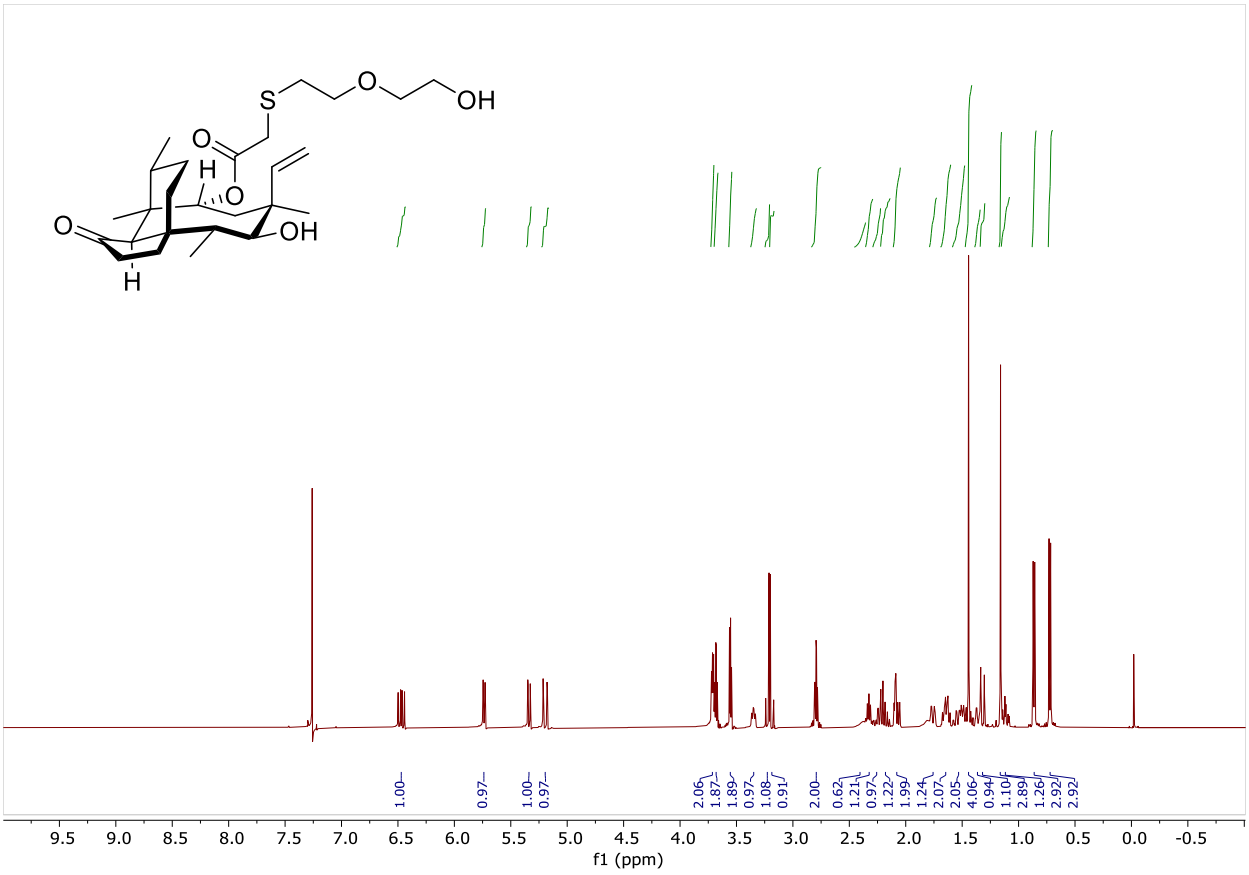


$^{1}$H-NMR (500 MHz, $CDCl_3$) spectrum of **43**

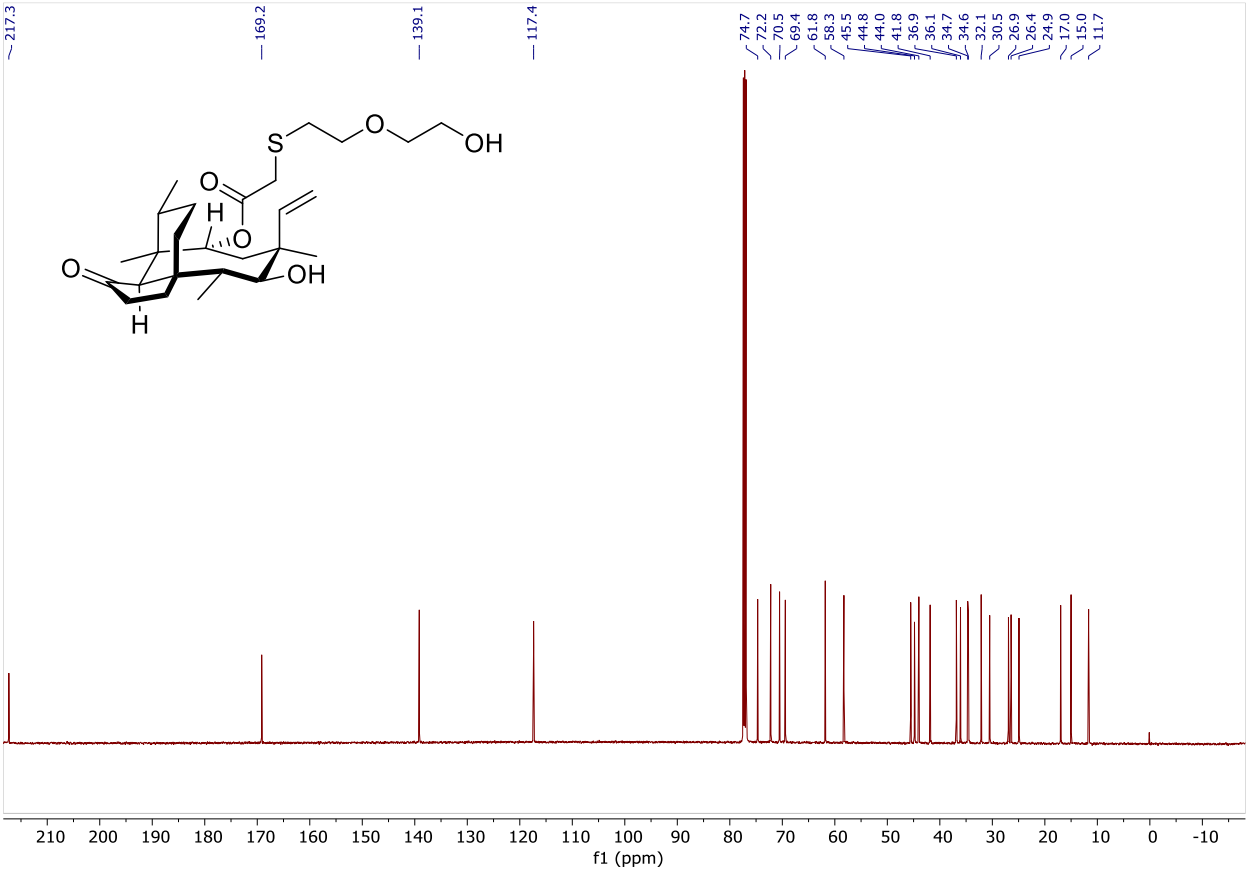

$^{13}C\{^{1}H\}$-NMR (126 MHz, $CDCl_3$) spectrum of **43**

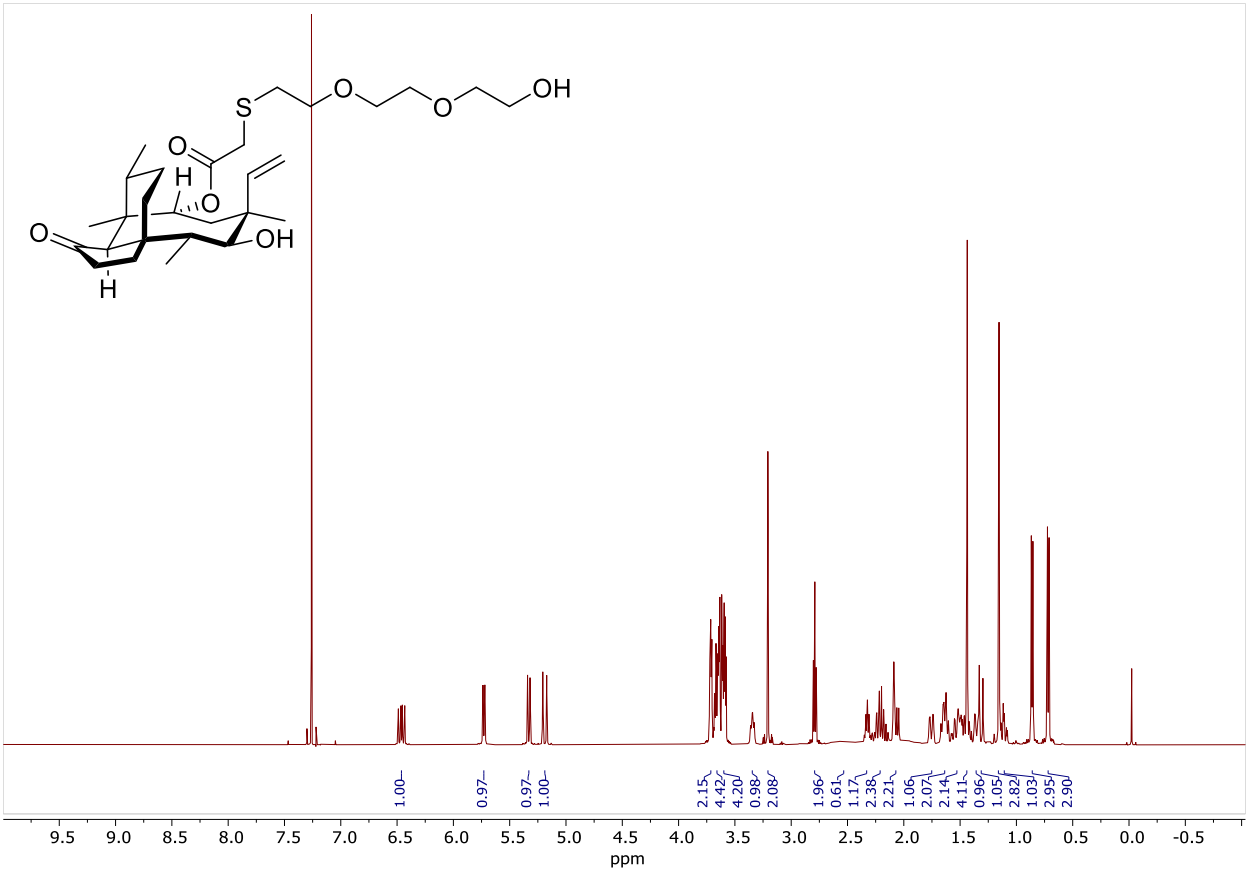


$^{1}H$-NMR (500 MHz, $CDCl_3$) spectrum of **44**

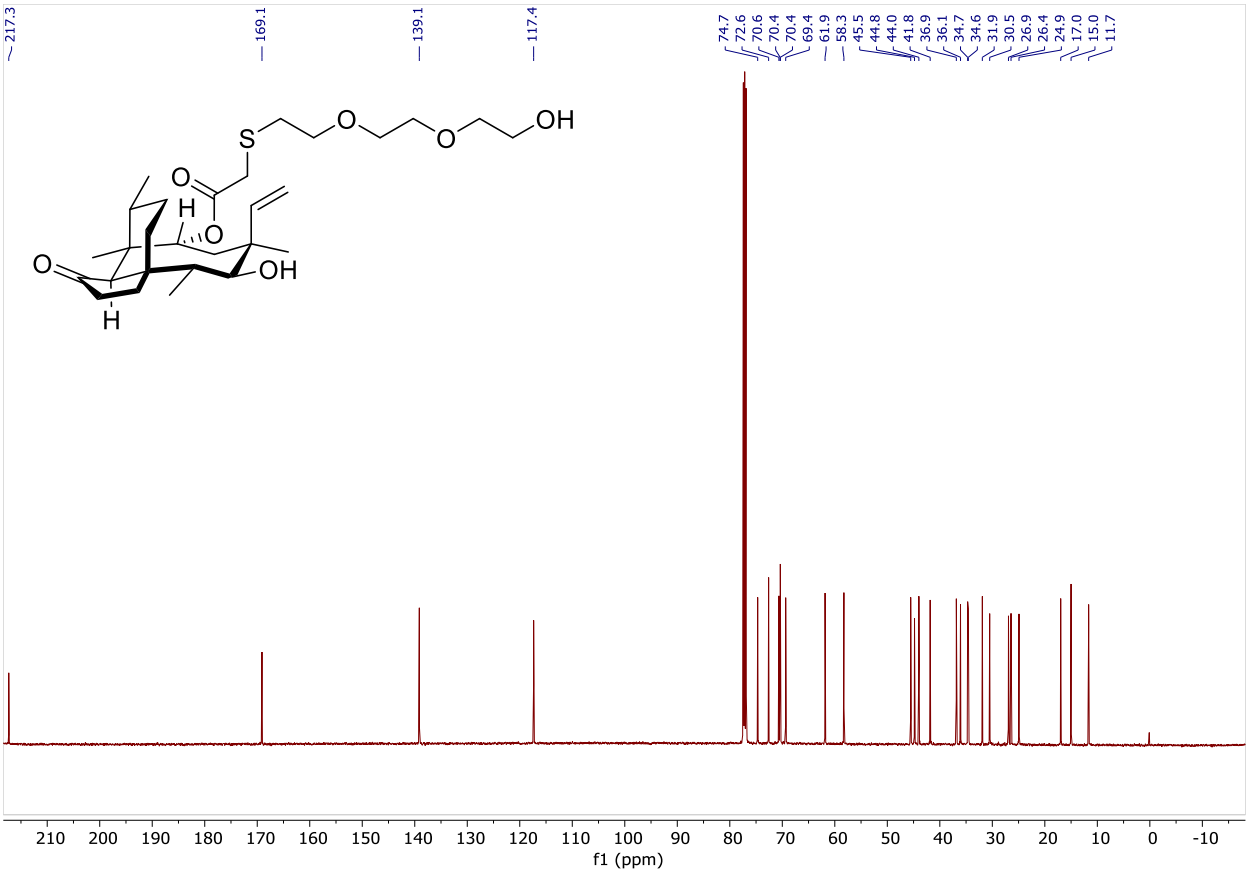


$^{13}C\{^{1}H\}$-NMR (126 MHz, $CDCl_3$) spectrum of **44**

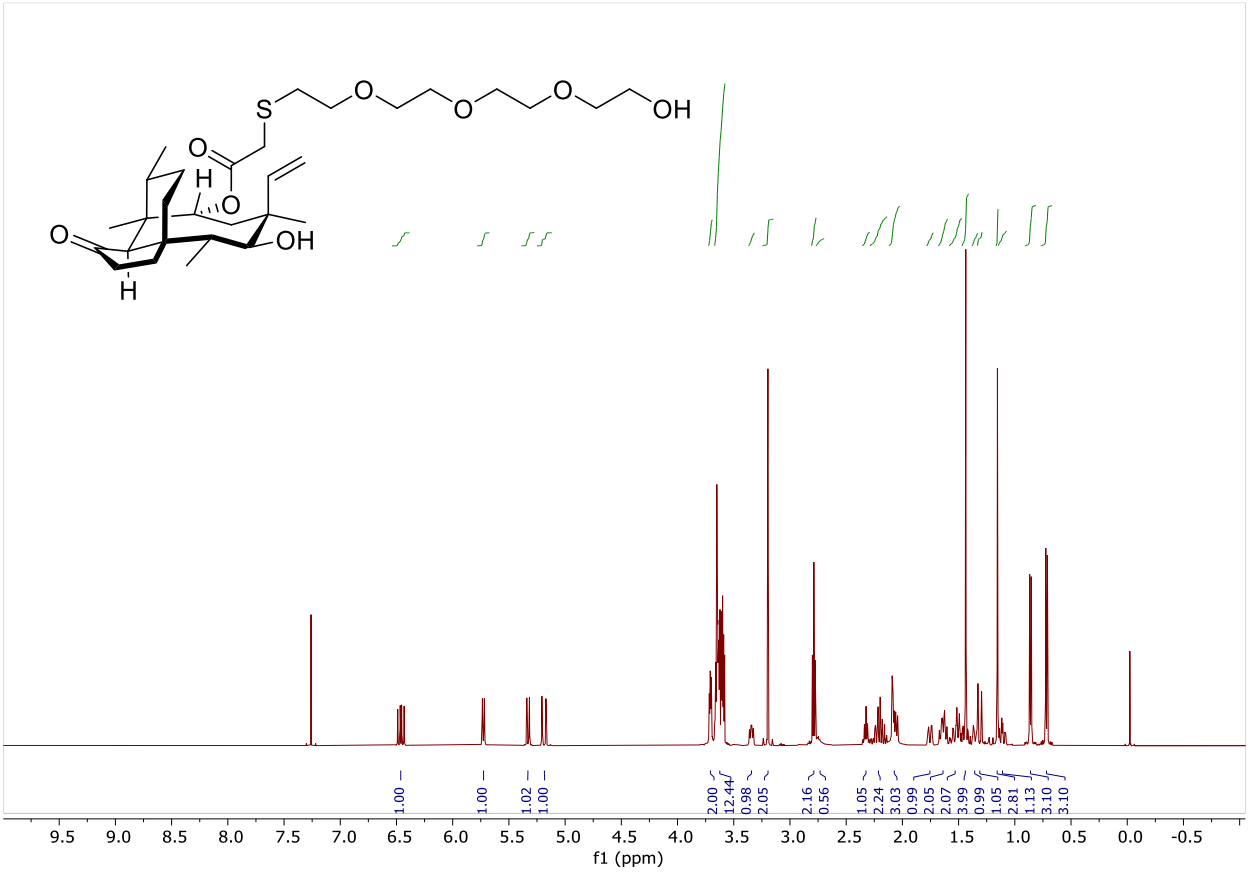

$^{1}$H-NMR (500 MHz, $CDCl_3$) spectrum of **45**

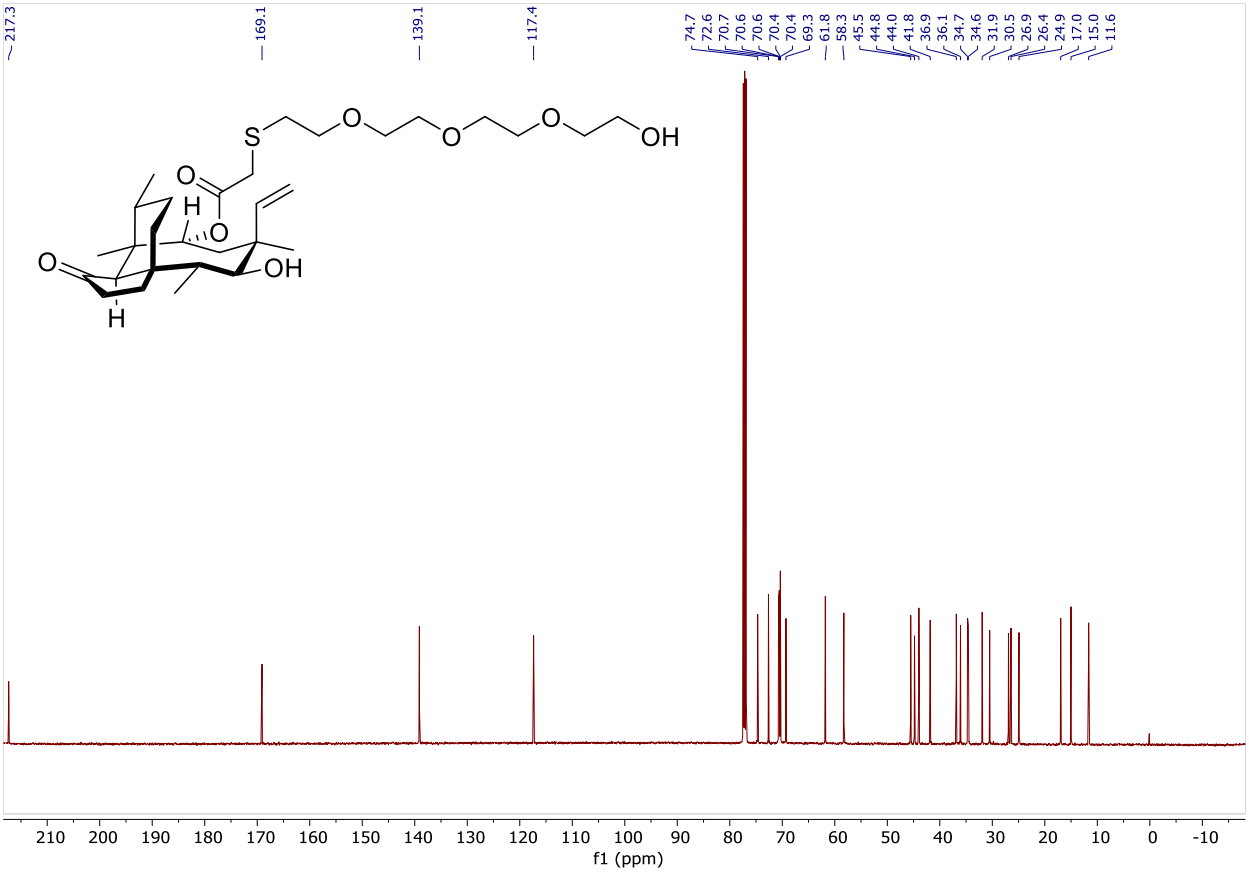


$^{13}$C{$^{1}$H}-NMR (126 MHz, $CDCl_3$) spectrum of **45**

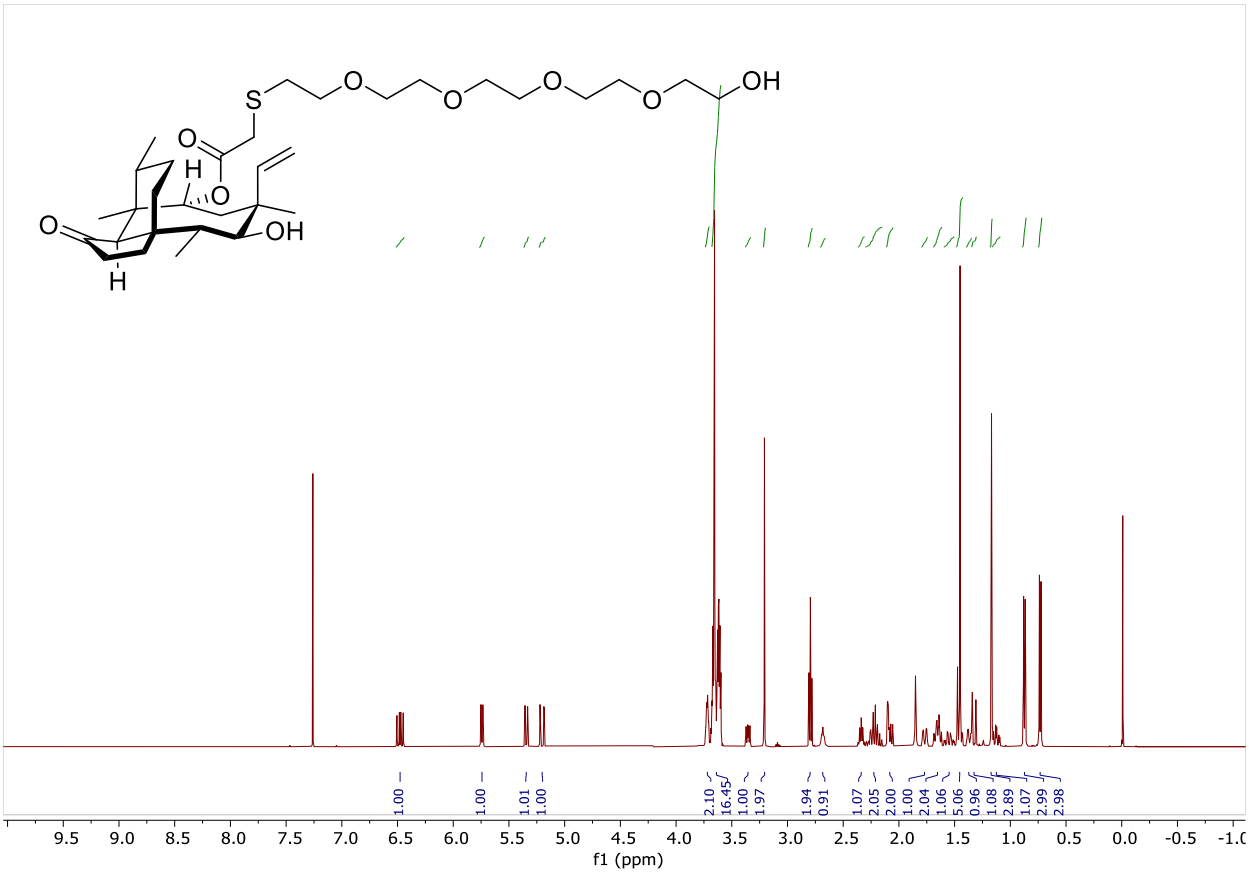


$^{1}$H-NMR (500 MHz, $CDCl_3$) spectrum of **46**

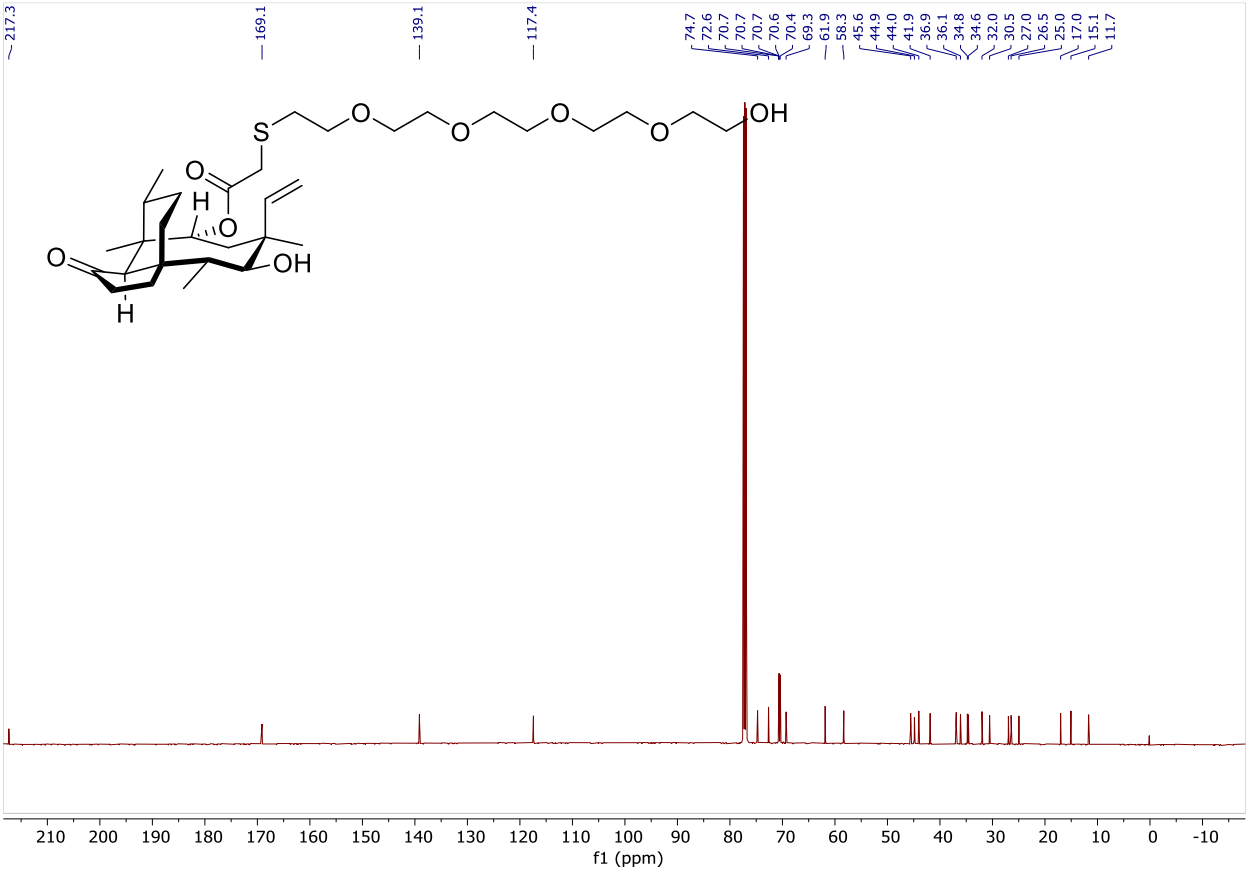

$^{13}C\{^{1}H\}$-NMR (126 MHz, $CDCl_3$) spectrum of **46**

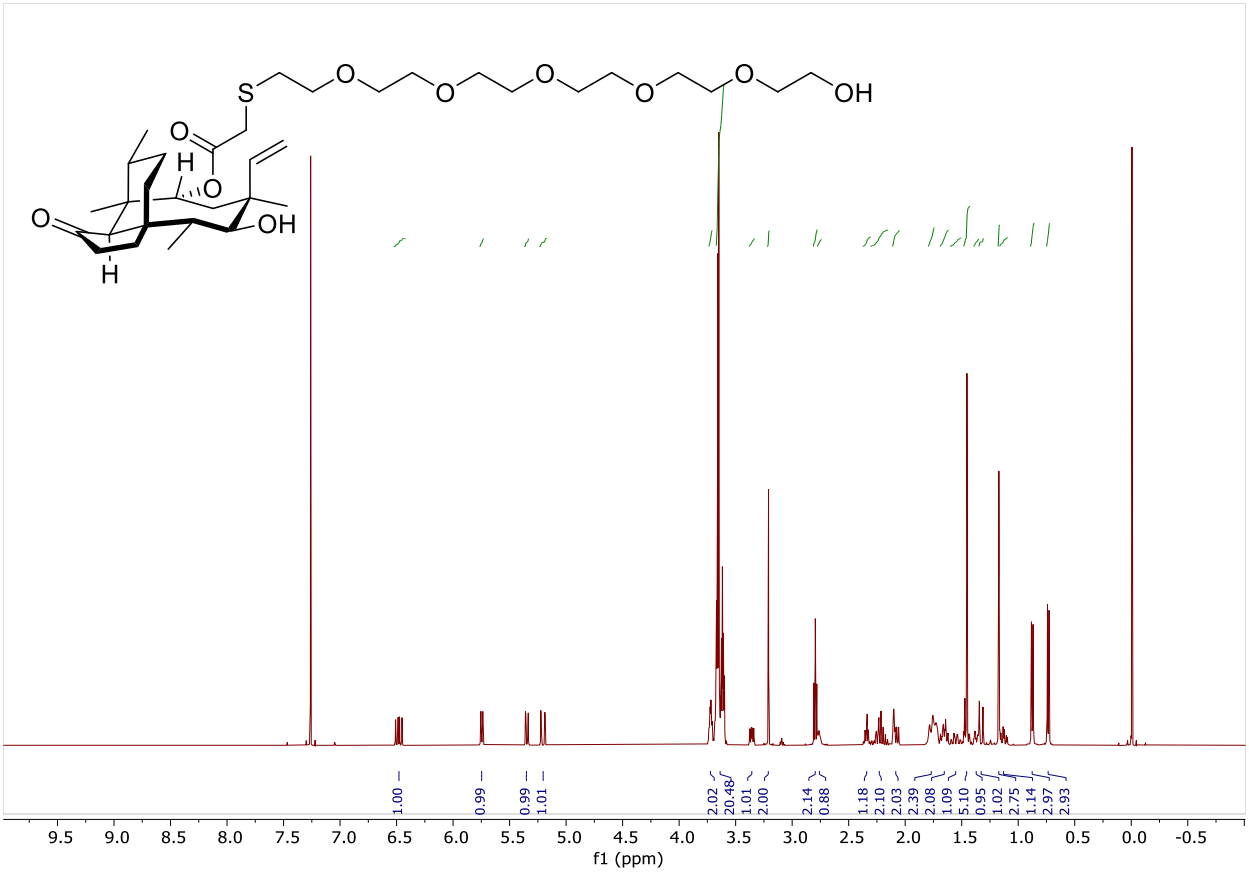


$^{1}H$-NMR (500 MHz, $CDCl_3$) spectrum of **47**

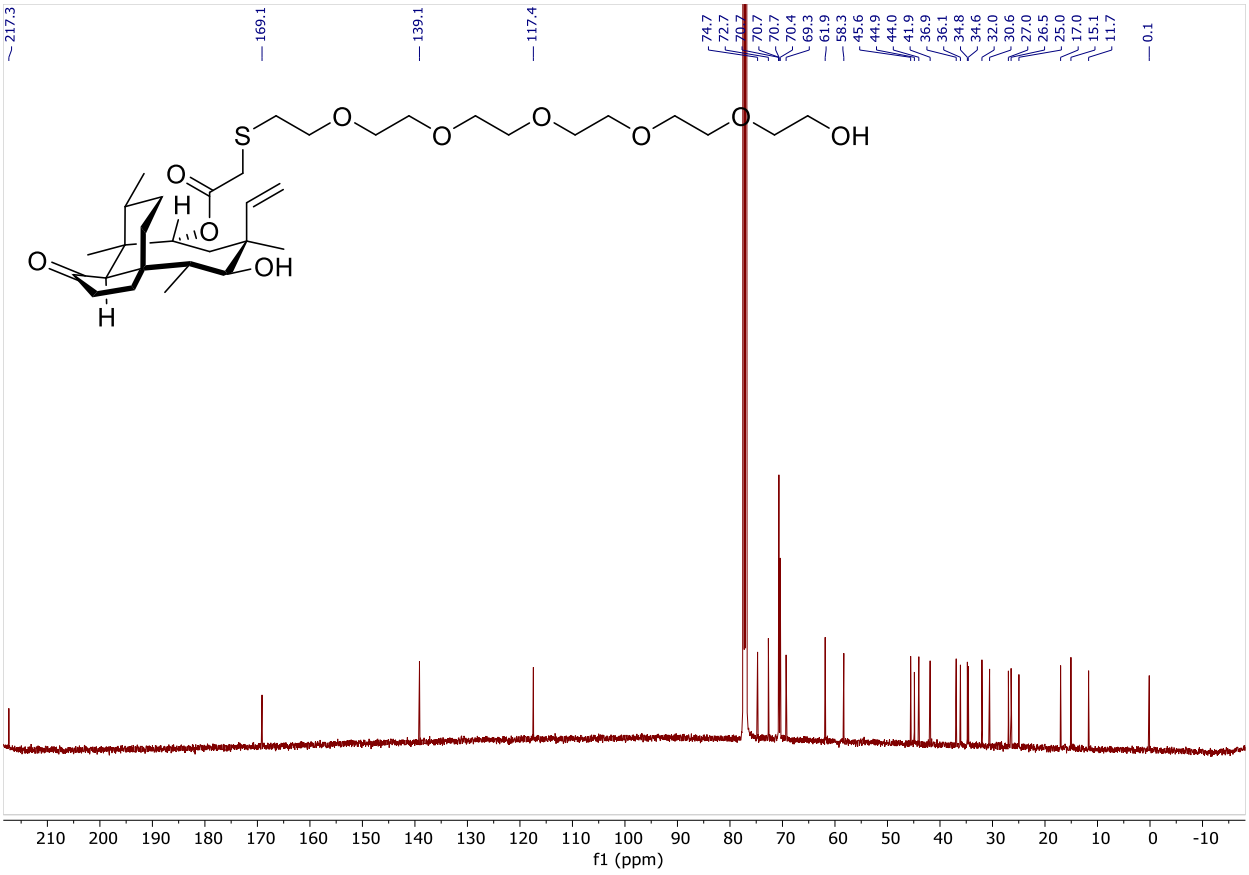


$^{13}C\{^{1}H\}$-NMR (126 MHz, $CDCl_3$) spectrum of **47**

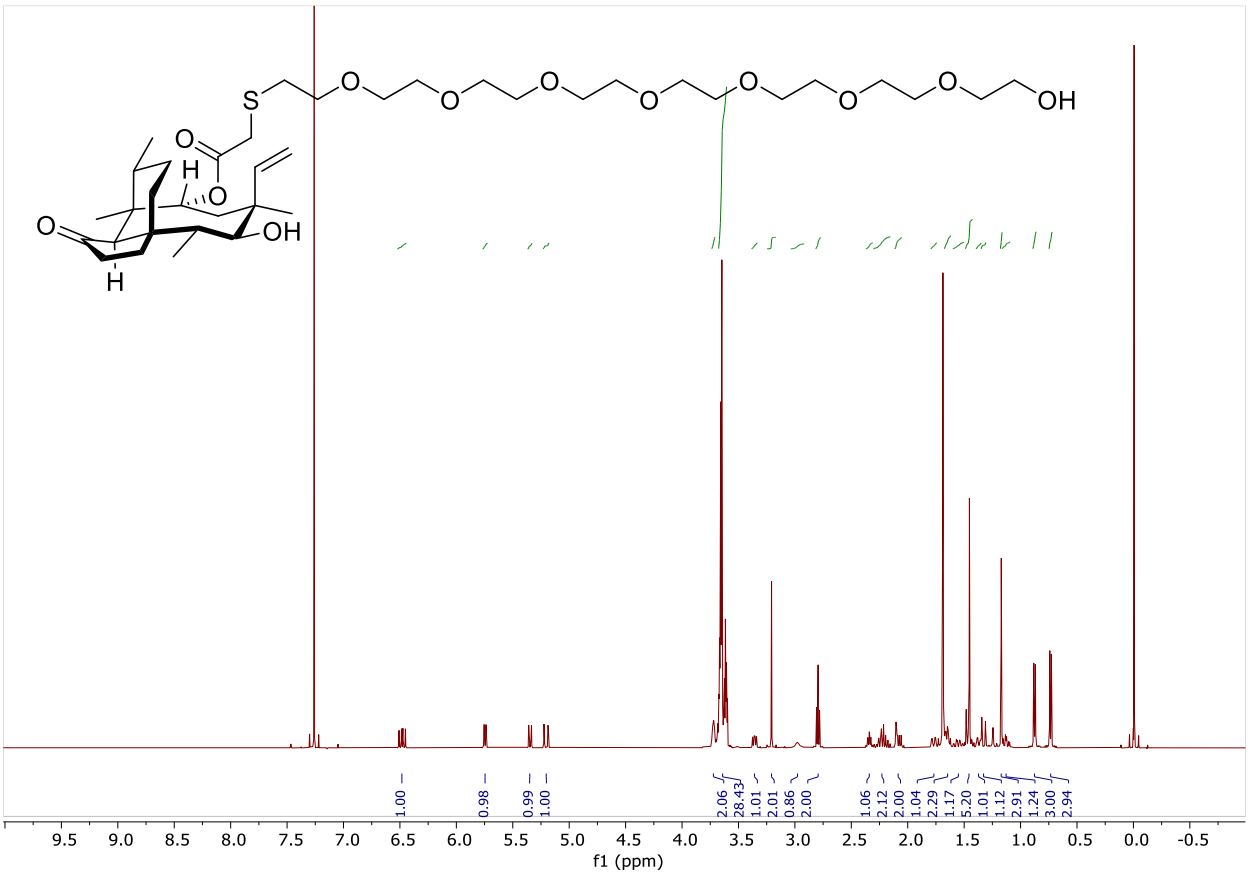

$^{1}$H-NMR (500 MHz, $CDCl_3$) spectrum of **48**

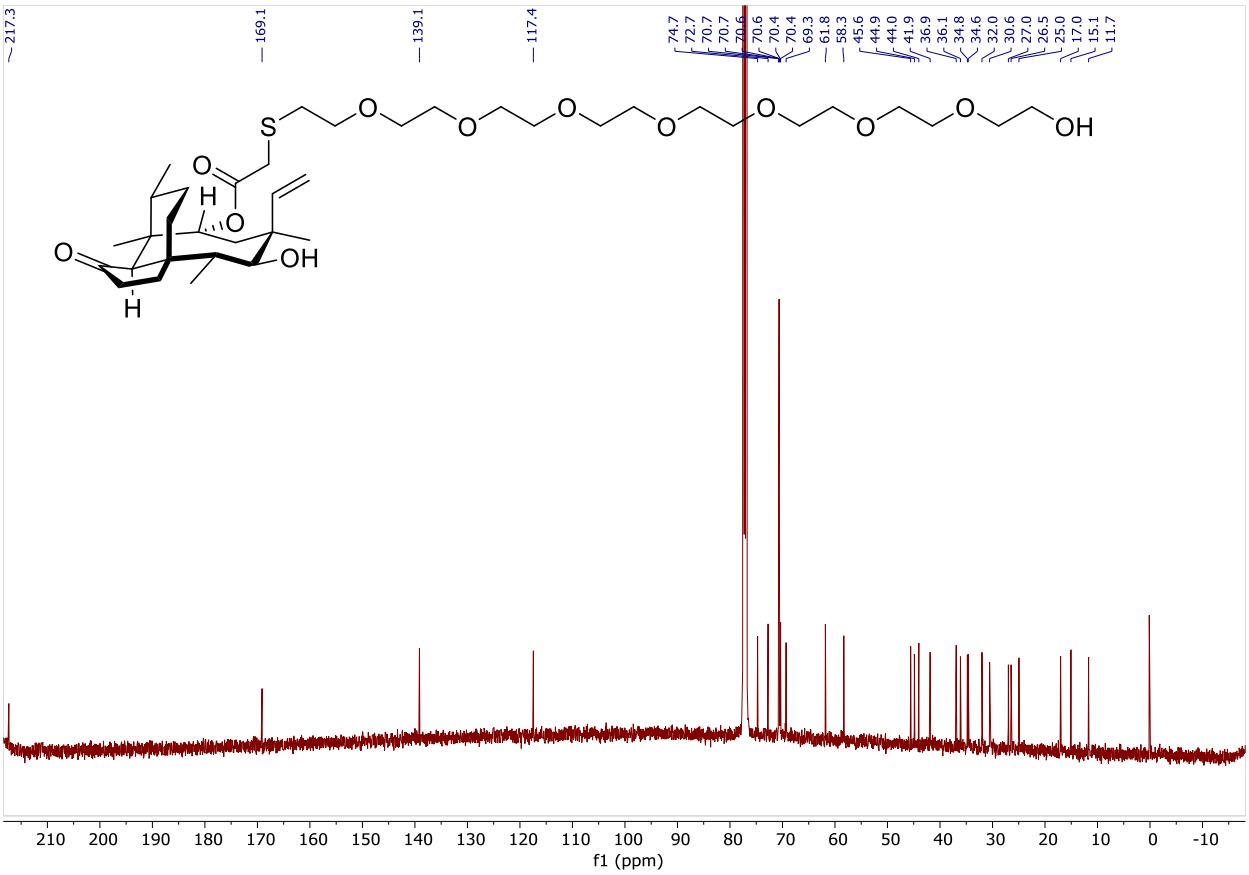


$^{13}$C{$^{1}$H}-NMR (126 MHz, $CDCl_3$) spectrum of **48**

## 5.6 References


1. Lipinski, C. A.; Lombardo, F.; Dominy, B. W.; Feeney, P. J., Experimental and computational approaches to estimate solubility and permeability in drug discovery and development settings. *Adv. Drug Del. Rev.* **2001,** *46* (1), 3-26.
2. Shultz, M. D., Two decades under the influence of the rule of five and the changing properties of approved oral drugs. *J. Med. Chem.* **2019,** *62* (4), 1701-1714.
3. Veber, D. F.; Johnson, S. R.; Cheng, H. Y.; Smith, B. R.; Ward, K. W.; Kopple, K. D., Molecular properties that influence the oral bioavailability of drug candidates. *J. Med. Chem.* **2002,** *45* (12), 2615-23.
4. Rex, J. The Hunt For Oral Antibiotics: Beyond Lipinski's Rule Of Five. https://amr.solutions/2018/10/08/the-hunt-for-oral-antibiotics-beyond-lipinskis-rule-of-five/.
5. Tomišić, Z., The story of azithromycin. *Kem. Ind.* **2011,** *60*, 603-617.
6. Conover, L. H.; Moreland, W. T.; English, A. R.; Stephens, C. R.; Pilgrim, F. J., Terramycin. XI. Tetracycline. *J. Am. Chem. Soc.* **1953,** *75* (18), 4622-4623.
7. Paukner, S.; Sader, H. S.; Ivezic-Schoenfeld, Z.; Jones, R. N., Antimicrobial activity of the pleuromutilin antibiotic BC-3781 against bacterial pathogens isolated in the SENTRY antimicrobial surveillance program in 2010. *Antimicrob. Agents Chemother.* **2013,** *57* (9), 4489-95.
8. Kavanagh, F.; Hervey, A.; Robbins, W. J., Antibiotic substances from Basidiomycetes: VIII. *Pleurotus multilus* (Fr.) Sacc. and *Pleurotus passeckerianus* Pilat. *Proc. Natl. Acad. Sci. U. S. A.* **1951,** *37* (9), 570.
9. Arigoni, D., Structure of a new type of terpene. *Gazz. Chim. Ital* **1962,** *92*, 884-901.
10. Birch, A. J.; Holzapfel, C. W.; Rickards, R. W., The structure and some aspects of the biosynthesis of pleuromutilin. *Tetrahedron* **1966,** *22*, 359-387.
11. Rittenhouse, S.; Biswas, S.; Broskey, J.; McCloskey, L.; Moore, T.; Vasey, S.; West, J.; Zalacain, M.; Zonis, R.; Payne, D., Selection of retapamulin, a novel pleuromutilin for topical use. *Antimicrob. Agents Chemother.* **2006,** *50* (11), 3882-3885.
12. Hunt, A., FDA approves new antibiotic to treat community-acquired bacterial pneumonia. www.fda.gov/news-events/press-announcements, 2019.
13. Czok, R.; Meingassner, J. G.; Mieth, H.; Schutze, E. Antibiotic compositions for treating coccidiosis. US patent 4,148,890, 1979.
14. Paukner, S.; Riedl, R., Pleuromutilins: Potent drugs for resistant bugs—Mode of action and resistance. *Cold Spring Harb. Perspect. Med.* **2017,** *7* (1), a027110.
15. Pleuromutilin; SDS No. 19452 [Online]; Cayman Chemical: Ann Arbor, M., April 30th, 2024.https://www.caymanchem.com/product/19452 (accessed 06/13/2024).
16. Bento, C.; Katz, M.; Santos, M. M. M.; Afonso, C. A. M., Striving for uniformity: A review on advances and challenges to achieve uniform polyethylene glycol. *Org. Process Res. Dev.* **2024,** *28* (4), 860-890.
17. Himo, F.; Lovell, T.; Hilgraf, R.; Rostovtsev, V. V.; Noodleman, L.; Sharpless, K. B.; Fokin, V. V., Copper(I)-Catalyzed Synthesis of Azoles. DFT Study Predicts Unprecedented Reactivity and Intermediates. *J. Am. Chem. Soc.* **2005,** *127* (1), 210-216.
18. Breiner, L. M.; Briganti, A. J.; McCord, J. P.; Heifetz, M. E.; Philbrook, S. Y.; Slebodnick, C.; Brown, A. M.; Lowell, A. N., Synthesis, testing, and computational modeling of pleuromutilin 1,2,3-triazole derivatives in the ribosome. *Tetrahedron Chem* **2022,** *4*, 100034.
19. Ruofeng, S. Y., Li; Yunpeng, Yi; Baocheng, Hao; Zhen, Yang; Jianping, Liang A kind of preparation method of Tiamulin. CN107759502B, 2018.

20. Egger, H.; Reinshagen, H., New pleuromutilin derivatives with enhanced antimicrobial activity. I. Synthesis. *J. Antibiot.* **1976,** *29* (9), 915-922.
21. Kleczkowska, P.; Nowicka, K.; Bujalska-Zadrozny, M.; Hermans, E., Neurokinin-1 receptor-based bivalent drugs in pain management: The journey to nowhere? *Pharmacol. Ther.* **2019,** *196*, 44-58.
22. Dumontet, C.; Reichert, J. M.; Senter, P. D.; Lambert, J. M.; Beck, A., Antibody–drug conjugates come of age in oncology. *Nature Reviews Drug Discovery* **2023,** *22* (8), 641-661.
23. Tsuchikama, K.; Anami, Y.; Ha, S. Y. Y.; Yamazaki, C. M., Exploring the next generation of antibody–drug conjugates. *Nature Reviews Clinical Oncology* **2024,** *21* (3), 203-223.
24. Parkes, A. L.; Yule, I. A., Hybrid antibiotics – clinical progress and novel designs. *Expert Opinion on Drug Discovery* **2016,** *11* (7), 665-680.
25. Klahn, P.; Broenstrup, M., Bifunctional antimicrobial conjugates and hybrid antimicrobials. *Nat. Prod. Rep.* **2017,** *34* (7), 832-885.
26. Batchelder, J. I.; Hare, P. J.; Mok, W. W., Resistance-resistant antibacterial treatment strategies. *Frontiers in antibiotics* **2023,** *2*.
27. Li, J.; Kao, W. J., Synthesis of Polyethylene Glycol (PEG) Derivatives and PEGylated−Peptide Biopolymer Conjugates. *Biomacromolecules* **2003,** *4* (4), 1055-1067.
28. Goswami, L. N.; Houston, Z. H.; Sarma, S. J.; Jalisatgi, S. S.; Hawthorne, M. F., Efficient synthesis of diverse heterobifunctionalized clickable oligo(ethylene glycol) linkers: potential applications in bioconjugation and targeted drug delivery. *Org. Biomol. Chem.* **2013,** *11* (7), 1116-1126.
29. Ursuegui, S.; Schneider, J. P.; Imbs, C.; Lauvoisard, F.; Dudek, M.; Mosser, M.; Wagner, A., Expedient synthesis of trifunctional oligoethyleneglycol-amine linkers and their use in the preparation of PEG-based branched platforms. *Org. Biomol. Chem.* **2018,** *16* (44), 8579-8584.
30. Mikesell, L.; Eriyagama, D. N. A. M.; Yin, Y.; Lu, B.-Y.; Fang, S., Stepwise PEG synthesis featuring deprotection and coupling in one pot. *Beilstein J. Org. Chem.* **2021,** *17*, 2976-2982.
31. Ameijde, J. V.; Liskamp, R. M. J., Synthesis of novel trivalent amino acid glycoconjugates based on the cyclotriveratrylene ('CTV') scaffold. *Org. Biomol. Chem.* **2003,** *1* (15), 2661-2669.
32. Zhang, F.; Wu, Z.; Chen, P.; Zhang, J.; Wang, T.; Zhou, J.; Zhang, H., Discovery of a new class of PROTAC BRD4 degraders based on a dihydroquinazolinone derivative and lenalidomide/pomalidomide. *Biorg. Med. Chem.* **2020,** *28* (1), 115228.
33. Gobbo, P.; Novoa, S.; Biesinger, M. C.; Workentin, M. S., Interfacial strain-promoted alkyne–azide cycloaddition (I-SPAAC) for the synthesis of nanomaterial hybrids. *Chem. Commun.* **2013,** *49* (38), 3982.
34. Hamburger, R.; Azaz, E.; Donbrow, M., Autoxidation of polyoxyethylenic non-ionic surfactants and of polyethylene glycols. *Pharm. Acta Helv.* **1975,** *50* (1-2), 10-7.
35. Bräse, S.; Gil, C.; Knepper, K.; Zimmermann, V., Organic azides: An exploding diversity of a unique class of compounds. *Angew. Chem. Int. Ed.* **2005,** *44* (33), 5188-5240.
36. Aguilella-Arzo, M.; Hoogerheide, D. P.; Doucet, M.; Wang, H.; Aguilella, V. M., Charged biological membranes repel large neutral molecules by surface dielectrophoresis and counterion pressure. *J. Am. Chem. Soc.* **2024,** *146* (4), 2701-2710.
37. Jang, S., AcrAB-TolC, a major efflux pump in Gram negative bacteria: toward understanding its operation mechanism. *BMB Rep.* **2023,** *56* (6), 326-334.
38. Fanani, M. L.; Nocelli, N. E.; Zulueta Díaz, Y. d. l. M., What can we learn about amphiphile-membrane interaction from model lipid membranes? *Biochim. Biophys. Acta* **2022,** *1864* (1), 183781.
39. Janin, J.; Chothia, C., Role of hydrophobicity in the binding of coenzymes. Appendix. Translational and rotational contribution to the free energy of dissociation. *Biochemistry* **1978,** *17* (15), 2943-8.
40. Sharp, K. A.; Nicholls, A.; Friedman, R.; Honig, B., Extracting hydrophobic free energies from experimental data: relationship to protein folding and theoretical models. *Biochemistry* **1991,** *30* (40), 9686-97.

41. Banerjee, S. S.; Aher, N.; Patil, R.; Khandare, J., Poly(ethylene glycol)-Prodrug Conjugates: Concept, Design, and Applications. *J. Drug Deliv.* **2012,** *2012*, 103973.
42. Dong, X.; Shu, X.; Wang, Y.; Niu, Z.; Xu, S.; Zhang, Y.; Zhao, S., Synthesis, characterization and in vitro release performance of the pegylated valnemulin prodrug. *J. Vet. Med. Sci.* **2018,** *80* (1), 173-180.
43. Shi, S.; Yao, C.; Cen, J.; Li, L.; Liu, G.; Hu, J.; Liu, S., High-fidelity end-functionalization of poly(ethylene glycol) using stable and potent carbamate linkages. *Angew. Chem. Int. Ed.* **2020,** *59* (41), 18172-18178.
44. Novak, R., Are pleuromutilin antibiotics finally fit for human use? *Ann. N.Y. Acad. Sci.* **2011,** *1241* (1), 71-81.
45. Engler, A. C.; Wiradharma, N.; Ong, Z. Y.; Coady, D. J.; Hedrick, J. L.; Yang, Y.-Y., Emerging trends in macromolecular antimicrobials to fight multi-drug-resistant infections. *Nano Today* **2012,** *7* (3), 201-222.
46. Veseli, A.; Žakelj, S.; Kristl, A., A review of methods for solubility determination in biopharmaceutical drug characterization. *Drug Dev. Ind. Pharm.* **2019,** *45* (11), 1717-1724.
47. Alsenz, J.; Meister, E.; Haenel, E., Development of a partially automated solubility screening (PASS) assay for early drug development. *J. Pharm. Sci.* **2007,** *96* (7), 1748-62.
48. Wyttenbach, N.; Alsenz, J.; Grassmann, O., Miniaturized assay for solubility and residual solid screening (SORESOS) in early drug development. *Pharm. Res.* **2007,** *24* (5), 888-98.
49. Andrés, A.; Rosés, M.; Ràfols, C.; Bosch, E.; Espinosa, S.; Segarra, V.; Huerta, J. M., Setup and validation of shake-flask procedures for the determination of partition coefficients (logD) from low drug amounts. *Eur. J. Pharm. Sci.* **2015,** *76*, 181-191.
50. Geiger, T. M.; Walz, M.; Meyners, C.; Kuehn, A.; Dreizler, J. K.; Sugiarto, W. O.; Maciel, E. V. S.; Zheng, M.; Lermyte, F.; Hausch, F., Discovery of a Potent Proteolysis Targeting Chimera Enables Targeting the Scaffolding Functions of FK506-Binding Protein 51 (FKBP51). *Angew. Chem. Int. Ed.* **2024,** *63* (3), e202309706.
51. Sulforaphane-derived compounds, production method thereof and the medical, food and cosmetic use of same. EP2842940, 2015.
52. Katz, C. E.; Ribelin, T.; Withrow, D.; Basseri, Y.; Manukyan, A. K.; Bermudez, A.; Nuera, C. G.; Day, V. W.; Powell, D. R.; Poutsma, J. L.; Aubé, J., Nonbonded, Attractive Cation−π Interactions in Azide-Mediated Asymmetric Ring Expansion Reactions. *J. Org. Chem.* **2008,** *73* (9), 3318-3327.

# Chapter 6. Pleuromutilin containing bidentate antibiotics with blasticidin S and azithromycin

Logan M. Breiner,[1,2] Katherine R. Fike,[2,3,6] Somaia Abdelmegeed,[2,4,6] Mohamed N. Seleem,[2,4,6] Michael Klemba,[2,3,5] Andrew N. Lowell[1,2,7]

[1] Department of Chemistry, Virginia Polytechnic Institute and State University (Virginia Tech), Blacksburg, Virginia 24061, USA

[2] Center for Emerging, Zoonotic, and Arthropod-borne Pathogens, Virginia Polytechnic Institute and State University (Virginia Tech), Blacksburg, Virginia 24061, USA

[3] Department of Biochemistry, Virginia Tech, Blacksburg, Virginia 24061, USA

[4] Center for One Health Research, Virginia Tech, Blacksburg, VA, 24061, USA

[5] Virginia Tech Center for Drug Discovery Screening Laboratory, Virginia Tech, Blacksburg, VA 24061, USA

[6] Department of Biomedical Sciences and Pathobiology, Virginia-Maryland College of Veterinary Medicine, Virginia Tech, Blacksburg, Virginia 24061, USA

[7] Faculty of Health Sciences, Virginia Tech, Blacksburg, VA, USA

## 6.1 Abstract

Beyond treatment with individual antibiotics, co-administration of two antibiotics, either as individual drugs or linked together to form a hybrid antibiotic, is an established strategy that we build on in the form of bidentate antibiotics. As previously demonstrated by the many veterinary drugs and two clinical drugs approved by the FDA, pleuromutilin derivatives have enormous potential as antibiotics. Azithromycin is a powerful antibiotic which can treat a selection of Gram-positive and Gram-negative bacteria, as well as some atypical ones. Blasticidin S is a potent antibiotic that is non-selective, and thus toxic to mammalian cells and fungi. All three of these antibiotics target the ribosome, which is responsible for protein production, and all three bind within 15 Å of each other without overlapping each other's binding sites. These characteristics make them ideal candidates for bidentate antibiotics, defined as covalently bound antibiotics that can simultaneously engage their respective target sites. Herein we outline the design factors of bidentate antibiotics and report the efficient synthesis and testing of two types of bidentate libraries: Pleuromutilin-blasticidin S (PLE-BLS) and *epi*-pleuromutilin-azithromycin (*e*PLE-AZI) conjugates using copper-catalyzed azido-alkyne cycloaddition reactions, also known as click chemistry. These commercial natural products or natural product derivatives were activated for CuAAC in 2-4 steps and then cyclized, with cycloaddition yields ranging from 27 to 98%. Testing of the bidentates themselves as well as their precursors, both individually and in combination with their partner antibiotic as controls, showed enhanced activity against *S. aureus* and promising antimalarial activity.

## 6.2 Introduction

### 6.2.1 Combination therapies and hybrid antibiotics

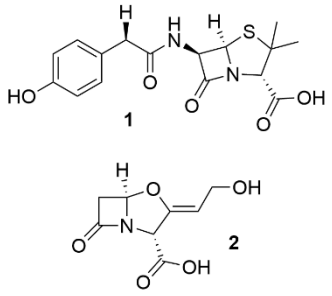


**Figure 1.** Amoxicillin **1** and clavulanic acid **2**, administered as Augmentin where the amoxicillin trihydrate to potassium clavulanate ratio ranges from 4–8 to 1.

In a never-ending effort to improve antibiotics and better treat infectious disease, scientists have continually sought methods to enhance already efficacious treatments. Combination therapies, where two or more antibiotics or adjuvants (compounds that enhance the activity of an antibiotic by suppressing a resistance mechanism but are not antibiotics themselves) are administered simultaneously, are an effective strategy to overcome antimicrobial resistance. The commonly used Augmentin, which is amoxicillin (**1**) (a β-lactam) combined with the β-lactamase inhibitor clavulanic acid (**2**) as an adjuvant, is a prime example of the pharmaceutical success of this strategy. Besides an antibiotic with an adjuvant, the co-administration of multiple antibiotics can also be utilized. This strategy has become common practice for the clinical treatment of sepsis.[1-3] These combinations can have synergistic effects, allowing shorter durations of treatment or lower doses. Co-administration also lowers the development of resistance, as it is statistically unlikely that spontaneous resistance to both compounds will arise during the treatment duration. In addition, an organism resistant to one of the co-administered antibiotics may still be affected by the remaining antibiotic(s).[4]

Despite being recognized as an impactful new strategy, the actual development and implementation of combination therapy has been complex to implement. Many combinations of antibiotics do not demonstrate their synergistic *in vitro* effects *in vivo*. This discrepancy may be due to differing pharmacokinetics of the separate antibiotics.[4] Two compounds with different pharmacokinetic properties (the rate of diffusion across cell membranes, metabolism, and excretion) will achieve peak concentrations in the blood, or other biological fluid, at different times. One drug may peak in its concentration and decline while the other is still increasing, and thus their synergistic effects are underutilized.

Hybrid drugs maintain the beneficial effects of combination therapies while mitigating the detrimental effects, such as differing rates of metabolism, cell penetration and accumulation,[5-7] and toxicity.[8] However, we must properly define what is meant by conjugate and hybrid drugs before we can place them in appropriate context alongside more advanced ideas, such as bidentate antibiotics. In both cases, two or more functional molecules are attached to each other using a covalent linker. Conjugates, or more formally bifunctional antimicrobial conjugates, utilize an antimicrobial agent attached to an agent the promotes cellular penetration or accumulation within a target organism. Hybrid drugs utilize two antimicrobial agents attached to each other, however in some cases one or both of these agents also can have a penetrant or accumulator effect.[9] Hybrid drugs are the focus of this work. By maintaining a covalent linkage between the two antimicrobial agents, beneficial effects of one can be conferred to the other agent. Indeed, the world of medicinal chemistry is no stranger to conjugate and hybrid antibiotics and the improved traits of covalently linked hybrids are well demonstrated in the literature (*vide infra*).

### 6.2.2 Hybrid antibiotics with distinct, remote binding sites

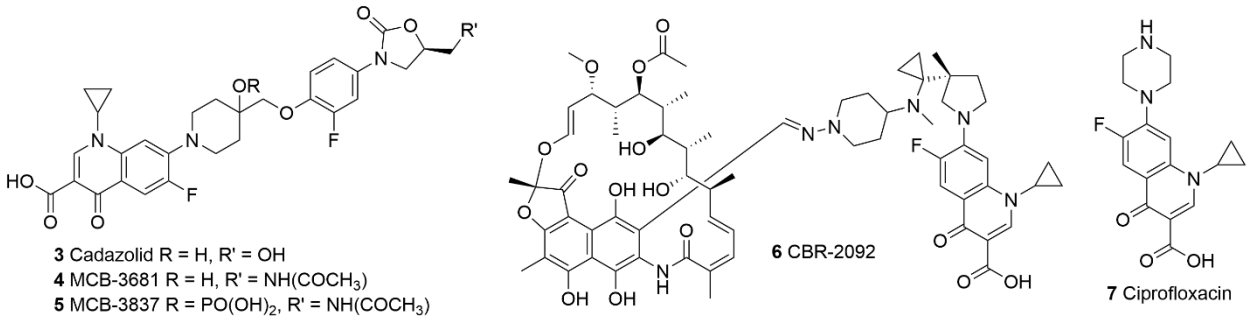


**Figure 2.** Fluoroquinolone-oxazolidinones **3**–**5**, a fluoroquinolone-rifampicin hybrid **6**, and clinical fluoroquinolone ciprofloxacin **7**.

The fluoroquinolones, oxazolidinones, and macrolides have seen the highest amount of development as hybrid antibiotics. Fluoroquinolones have been included with a variety of other antibiotics to create hybrid antibiotics with significantly enhanced potency (Figure 2). Cadazolid (**3**), a fluoroquinolone-oxazolidinone hybrid antibiotic developed by Actelion Pharmaceuticals, passed phase III clinical trials;[10] however, development was halted for financial reasons.[11] This hybrid demonstrated synergy over its components in *C. difficile* strains, including those that were resistant to one or both of its components.[12] Morphochem has also developed two advanced fluoroquinolone-oxazolidinone hybrids, MCB-3681 (**4**) and its phosphorylated prodrug MCB-3837 (**5**). These demonstrated synergistic potency against a range of Gram-positive bacteria and *C. difficile*,[13, 14] passing a Phase I study,[13, 14] and have been fast tracked by the FDA for future clinical development. Cumbre pharmaceuticals developed a fluoroquinolone-rifampicin hybrid, linked by a hydrazide, called CBR-2092 (**6**). Typically, rifamycins suffer from rapid resistance development, and are confined to combination therapies.[15] What makes rifamycins of interest is their ability to attack bacteria that are in a biofilm state.[16] CBR-2092 has demonstrated potent antimicrobial effects against a wide range of Gram-positive pathogens with potency up to several hundred times greater than ciprofloxacin (**7**), a clinical fluoroquinolone.[17, 18] Even in rifamycin

resistant strains, CBR-2092 retained potent activity. Fluoroquinolones have also been hybridized with anilinouracils,[17, 18] tetracyclines,[19] benzyl diamino pyrimidines (e.g. trimethoprim),[20] pyrazinamides,[21] macrolides,[22] and aminoglycosides.[5, 6, 23] In general, exemplary compounds of these series have demonstrated increased potency versus coadministration of the parent antibiotics, activity against strains of bacteria that have resistance to one or both parents, heightened bacterial cell accumulation, diminished toxicity, and lower rates of spontaneous resistance development.

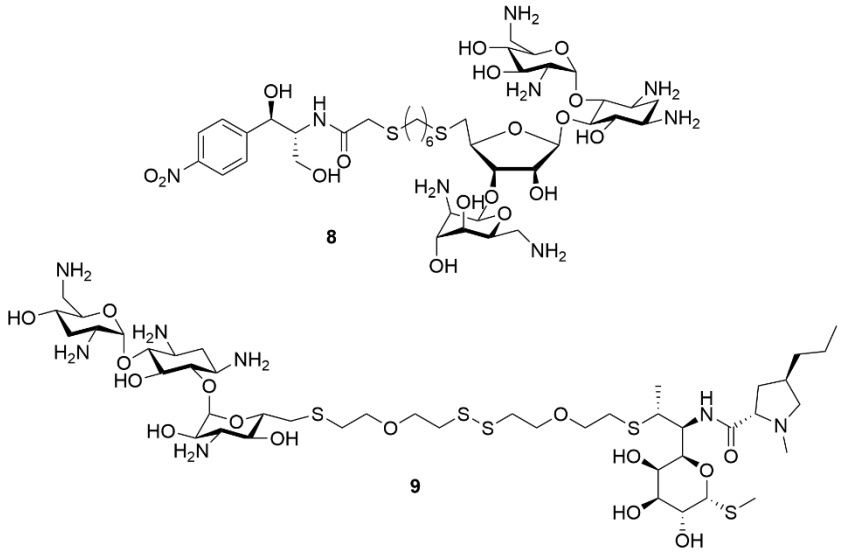

**Figure 3.** Neomycin-chloramphenicol hybrid **8**, tobramycin-clindamycin hybrid **9**.

The aminoglycosides have been hybridized with oxazolidinones and chloramphenicol,[24, 25] triclosan,[26] and clindamycin.[25] Not all hybrid drugs have resulted in enhanced properties. In the efforts of Yu and colleauges[24] with chloramphenicol (**8)**, the linker attachment was through the dichloromethyl moiety, a pharmacophoric position (Figure 3). Activity in these derivatives was lost, demonstrating the necessity of appropriate linker attachment. In the case of Garneau-Tsodlikova et al. with their aminoglycoside-chloramphenicol/clindamycin hybrids (**9**), the attachment was via a disulfide bond, meant to be cleaved within the organism. Additionally,

aminoglycosides have been hybridized among members of their class, and those will be discussed further in a later section.

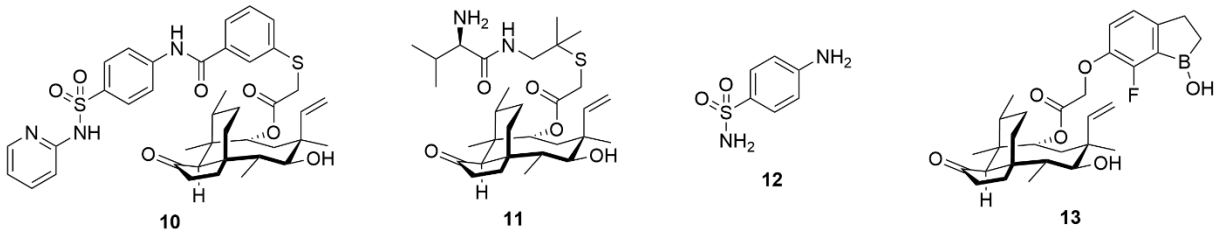


**Figure 4**. Pleuromutilin-sulfonamide hybrid **10**, valnemulin **11**, sulfanilamide **12**, pleuromutilin-benzoxaborole hybrid **13**.

Pleuromutilin, the focus of my work, has been used in the creation of hybrid antibiotics. Chen et al. synthesized sulfonamide-pleuromutilin hybrids (Figure 4, **10**),[27] bound through a thioether at the C22 position of pleuromutilin. C22 thioethers are a common motif among many pleuromutilin derivatives and all derivatives in veterinary or clinical use. The hybrids produced by Chen et al. exhibited activities; generally, between that of valnemulin (**11**) and sulfanilamide (**12**) in Gram-positive and mycobacteria. One derivative, with a pyridinyl sulfonamide, exhibited higher activity (0.016-0.063 μg/mL) than valnemulin (0.016-0.50) μg/mL in all tested Gram-positive bacteria, and comparable activity (0.004 μg/mL) in *Mycoplasma gallisepticum*. However, this hybrid lost activity in *E. coli* (64 μg/mL compared to valnemulin's 16 μg/mL) but was still more potent than sulfanilamide (128 μg/mL). The generally low MICs for this series of compound exemplifies an interesting aspect of pleuromutilin antibiotics: C22 substitution is often well tolerated, and the binding site accommodates large, bulky substituents quite well, as shown by our work in Chapter 5.

Jacobs et al. explored the hybridization of pleuromutilin with benzoxaboroles (Figure 4, **13**) to combat onchocerciasis and lymphatic filariasis.[28] Although these two disease are caused by

parasitic nematode and not bacterial infections, these nematodes (*Brugia malayi*, *Onchocerca volvulus*, and *Wuchereria bancrofti*, of the Filarioidea family) have an obligate symbiotic relationship with bacteria of the *Wolbachia* genus.[29] Thus, if the bacteria could killed, the nematode would also be cleared.

To give some background, treatment of roundworm diseases is a complicated task. The typical line of treatment, ivermectin, only kills juvenile worms and sterilizes the adults but does not kill them.[30] Ivermectin acts as a positive allosteric modulator of glutamate-gated chloride channels, causing paralysis in diverse tissues of nematodes and resulting their rapid death.[31, 32] However, ivermectin treatment can cause nerve damage, coma, and death due to the rapid mass die-off of worms if there is a high juvenile population.[33] Previous studies had shown that targeting the *Wolbachia* of the worms microbiome with doxycycline, an inhibitor of protein synthesis, can cause a reduction of lifespan of the adult worms[34-36] and impairs their ability to replicate.[37] Thus, treatment with tetracycline was shown to avoid the neurological damage associated with ivermectin due to mass nematicide and lower the transmission of juvenile worms through insect vectors. However, treatment with doxycycline requires long periods of administration (more than 4 weeks) and cannot be used in pregnant women or children, limiting its effectiveness as a method of mass treatment of nematode infections.[38]

With inhibition of *Wolbachia* in mind, Jacobs et al. employed a strategy of hybridizing pleuromutilin with benzoxaboroles, a class of compounds with diverse anti-parasitic action.[39] The lead pleuromutilin-benzoxaborole (Figure 4, **13**) demonstrated up to 15-fold or 150-fold increase in activity over lefamulin (the most potent pleuromutilin) in *Wolbachia* infected *Aedes albopictus* (mosquito) or *Drosophila melanogaster* (fruit fly) cell lines, respectively. *In vitro* ADME assays showed this lead had good permeability, low protein binding, and low clearance. In contrast, most

pleuromutilin derivatives have poor permeability, high protein binding, and high clearance. *In vivo* mouse tests of the lead had low clearance and good bioavailability, and outperformed tetracycline and ivermectin in reducing roundworm load.[40]

### 6.2.3 Hybrids with overlapping binding site and indeterminate proximity

There have also been examples of hybrid drugs produced from structure-based drug design, which intend to create new hybrid antibiotics based on the pharmacophores of antibiotics whose binding sites overlap or are in close proximity in the ribosome or other targets. Rib-X pharmaceuticals recognized the overlapping binding orientations of sparsomycin and linezolid.[41] New hybrids were generated where the overlapping portions of both molecules were replaced by a partially unsaturated bridging element. These original compounds demonstrated the correctness of the bridging hypothesis; however, further optimization was necessary to create higher potency drugs. The solution was the utilization of a biaryl scaffold between the two pharmacophores. This strategy allowed the hybrids to use pi stacking interactions of the rings to enhance binding interactions, and this series resulted in compounds which had activity against linezolid resistant enterococci.[42] Radezolid also came from this series, although it has completely replaced the sparsomycin pharmacophore with a triazole, that has completed two phase II clinical trials.[43]

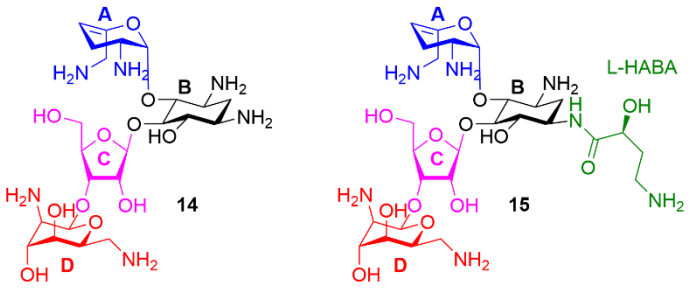


**Figure 5.** A sisomycin-neomycin hybrid **14** and a sisomycin-neomycin-butirosin hybrid **15**. The **A** ring of sisomycin is represented in blue, the conserved central **B** ring in black, the **C** ring

shared by neomycin B and butirosin in magenta, the **D** ring of neomycin in red, and the L-α-hydroxyl-γ-amino butyric acyl side chain of butirosin in green.

Hanessian et al. created two aminoglycoside hybrids based on analysis of the overlapping ribosomal binding sites of the aminoglycosides neomycin B, sisomycin, and butirosin (Figure 5). These compounds share a central aminosugar moiety whose structure, and binding site, is conserved between all three. The first hybrid (**14**) was a combination of the A ring of sisomycin, and the C and D rings of neomycin B, with the central conserved B ring of both.[44] This hybrid was equipotent with neomycin B and sisomycin against susceptible Gram-negative bacteria; however, it was inactive against resistant Gram-negative bacteria. The second hybrid **15** of the series was a neomycin B, sisomycin, and butirosin hybrid, containing the A ring of sisomycin, the D ring of neomycin B, the L-HABA moiety of butirosin, the C ring of both neomycin B and butirosin, and the B ring of all three.[45] This hybrid was equipotent with neomycin B and sisomycin against susceptible Gram-negative bacteria, and up to 32x more potent against all parents in resistant strains.

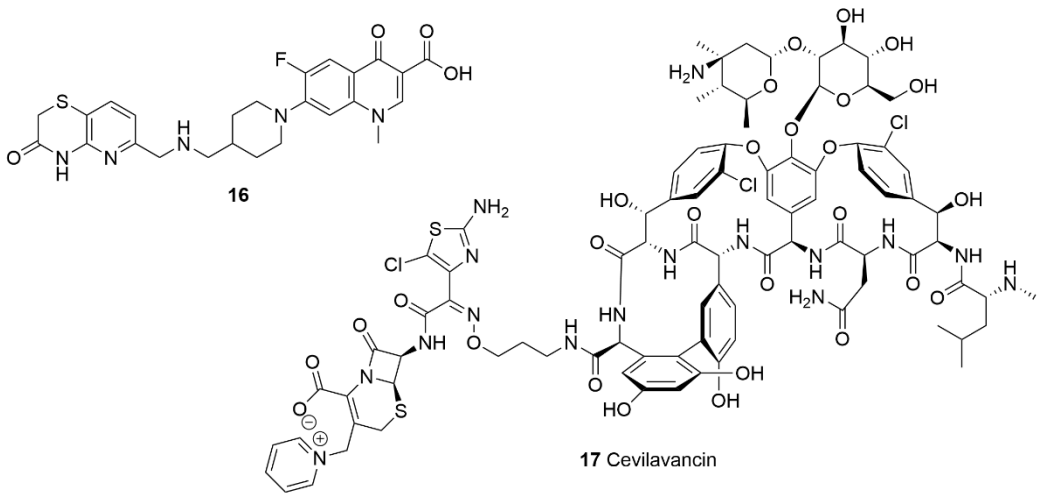

**16**

**17** Cevilavancin

**Figure 6**. Fluoroquinolone-pyridothiazine hybrid **16**, and vancomycin-ceftazidime hybrid (cefilavancin) **17**.

Actelion Pharmaceuticals created fluoroquinolone-pyridothiazine hybrids (Figure 6, **16**).[46] Both fluoroquinolones and pyridothiazines target the DNA gyrase, but bind at different sites. The best hybrid of the series retained its activity against quinolone resistant strains. However, it is unlikely that these hybrids simultaneously engage both binding sites simultaneously due to their short linker length of only three atoms.

Theravance Biopharma created vancomycin-cephalosporin hybrids (Figure 6, **17**). Both parent compounds interfere with cell wall biosynthesis. Multiple different linker points were used on each parent to ensure pharmacophores were not obscured in the resulting hybrids. The best hybrids showed a synergistic antimicrobial effect against all tested strains, including stains with resistance to β-lactams and vancomycin.[47, 48] However the researchers do not believe that these hybrids engage both sites simultaneously, due to the selection of linker site attachment having no significant difference in activity among the hybrids. As of 2020, the best hybrid of this series, cefilavancin (**17**), is in Phase III clinical development.[49]

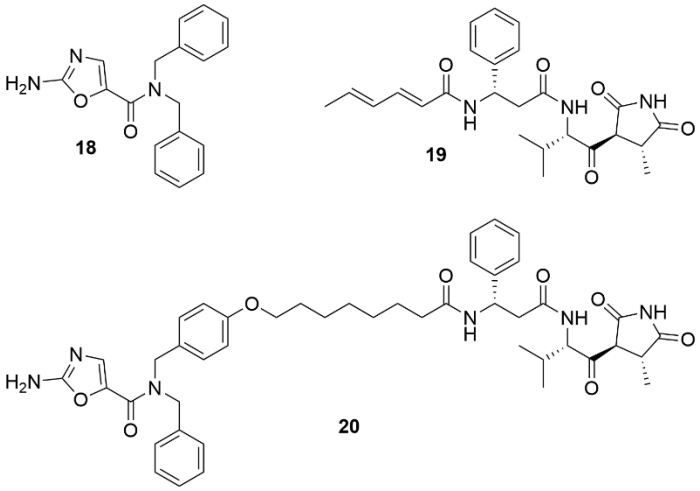

**Figure 7.** Amino oxazole **18** and moiramide B **19** with Waldrop's hybrid **20**.

Beyond classical antibacterial targets, Waldrop et al. targeted acetyl-CoA carboxylase, an enzyme responsible for fatty acid biosynthesis.[50] This process is vital and is highly conserved among bacteria, but not eukaryotes,[51] presenting an attractive selective target. By combining the pharmacophore of moiramide B (Figure 20, **19**), a carboxyl transferase inhibitor, with an amino oxazole (**18**) inhibitor of biotin carboxylase, via a flexible alkyl chain linker to make a hybrid, they intended to create a bivalent, or bidentate, antibiotic (**20**).[52] Both of these compounds target separate subunits of the initial stage of acetyl-CoA carboxylase,[53] and must first complex *in vivo* to function.[54] Unfortunately, it appears that the hybrid compounds were especially prone to efflux, leading to inactivity in Gram-negative organisms. However, the hybrid was only slightly less active than moiramide B in *S. aureus*, and the rate of spontaneous resistance development was greatly decreased. I had the opportunity to speak with Waldrop, and he believed that his compound does not simultaneously engage both binding sites, despite their proximity and the relatively long length of the linker (9 atoms).

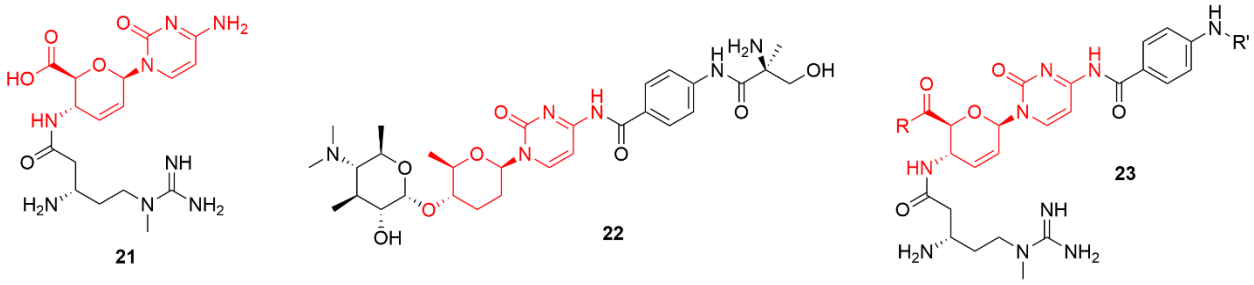


**Figure 8.** Blasticidin S **21** and amicetin **22** with Gannett's hybrid **23**. Note the cytosine/sugar highlighted in red that indicates the overlapping pharmacophore.

Dr. Cole Gannett, a PhD graduate from our lab, created a series of blasticidin S-amicetin hybrids (Figure 8, **23**). Blasticidin S (**21**) exhibits antimicrobial activity, but has poor selectivity

for the bacterial ribosome and is cytotoxic.[55] Amicetin (**22**) is a poor antibiotic, but has high selectivity for the prokaryotic ribosome over the eukaryotic ribosome. Serrano et al. found that the nucleoside portions of blasticidin S and amicetin overlap in the same binding site.[56] Dr. Gannett hypothesized that by including the PABA-amino acid moiety of amicetin onto blasticidin S, it might increase the selectivity of hybrids when compared to blasticidin S. He found that his best hybrids retained the potency of blasticidin (8-16 ug/mL) but were highly selective for bacteria, having a selectivity indices (SI) greater than 100, compared to blasticidin's SI of 0.3.[*unpublished*]

These literature examples demonstrate historic approaches to hybrid antibiotics and the successes of that work in creating potent drugs for fighting AMR. For further reading on the hybrid antibiotics previously mentioned in this section, please see these reviews.[9, 57-60] Currently, there is a plethora of antimicrobial hybrids that have achieved high stages of clinical development, and even more that demonstrate excellent activity against resistant organisms. There has even been structure-based design of hybrids whose parents have overlapping binding sites, and hybrids bound by covalent linkers intending to target their respective binding sites in sequential steps of bacterial metabolism. However, there have been few reports[61, 62] of hybridizing antibiotics who have distinct, yet close proximity, binding sites within the ribosome that allow simultaneous engagement of both pharmacophores.

### 6.2.4 Bidentate Antibiotics

#### 6.2.4.1 The limitation of hybrid and conjugate antibiotics

Despite the high clinical potential of hybrid and conjugate antibiotics, there is one aspect that prevents them from being as exceptional as they could be. Most published work on hybrids

and conjugate antibiotics has focused on compounds which target disparate binding sites. In short, there is no way for a single compound to simultaneously engage both of its targets.

#### 6.2.4.2 Main foundational concepts of bidentate antibiotics

All professional chemists are familiar with the concept of a bidentate ligand in coordination and organometallic chemistry. These compounds bind to a metal ion through two (or more in the case of polydentate ligands) points of interaction. The result of these simultaneous interactions results in a much higher affinity for the metal than by an analogous system of two separate ligands. This stronger affinity is the fundamental idea behind the bidentate antibiotic, a molecule that is one compound that can interact with multiple discrete molecular targets simultaneously. Hypothetically, this would be beneficial to the drug's activity, as it would have an additive — or better — affinity for its target, while also lowering the entropic penalty of binding that the two parent antibiotics have when separated. Bidentate ligands in medicinal chemistry, outside of the field of antibiotics, exist. These are referred to as bivalent ligands and they are often used to target heterodimer receptors. However, bivalent ligands are typically not designed with linkers of discrete length, which is a fundamental aspect of bidentate design.

#### 6.2.4.3 Selection of candidates

The key parameters for bidentate partners are adjacent binding sites in the target, additive or synergistic activity, and ideally compatible mechanisms of action. Binding sites must be within a certain, undetermined range, to physically allow for simultaneous binding of the two pharmacophores of the bidentate. Two candidates, one possessing an action on the ribosome and the other on cell wall synthesis, would not be able to bind both targets while being connected through a linker, due to the distance between the cellular components within the organism.

Additionally, if the two compounds exhibit less potency when co-administered, indicating incompatible mechanisms of action, their pairing should be avoided. When selecting partners for a bidentate, tools such as PyMOL[63] can help visualize the positioning of the compounds in relation to one another while engaging with the target. This method can build a list of potential compounds. Compounds which overlap with each other should be excluded from partnering. After compiling a list of suitable pairings, these should be tested in a synergy assay, such as a checkerboard assay.[64] This assay can determine if these compounds have synergistic, additive, or inhibitory activity. Synergy is ideal, but additive activity can also be utilized. Once a pairing has been selected, their respective pharmacophore and auxophores should be analyzed. First, literature should be consulted to find what modifications have been applied to a molecule historically. Modifications on functional groups that have increased or decreased activity should be noted as pharmacophores and potentially avoided if similar chemistry cannot be reliably used. Auxophores present the most attractive point of modification. These are functional groups on the molecule that are not responsible for the activity of a compound, as they do not interact with the binding site, and thus can be utilized for a linking site. Finally, the positioning of the functional groups in relation to each other on the molecules should be assessed. Ideally, the functional groups should be pointing toward each other, or at the very least be positioned on adjacent hemispheres of the two molecules topologies.

#### 6.2.4.4 Selection of linkers

A standard linker should be composed of a material with some degree of biocompatibility, inertness, and participate as an auxophore in the final conjugate. Additionally, the water-solubility of the linker may be tuned to ensure enhanced solubility in biological systems, as well as to aid in

purification during synthesis. Finally, a linker could be flexible or semi-rigid, depending on the specific needs of the system.

In the case of flexible linkers, three systems may be identified, in increasing degrees of polarity. These three linker types are the non-polar alkanes, the polar oligoethylene glycols, and the potentially ionic polyamines. The decision to choose between alkanes and ethylene glycols comes down to a matter of synthetic workability but also predicted pharmacodynamic properties. Alkanes can make highly water-soluble compounds easier to purify via traditional methods such as liquid-liquid extraction and normal phase flash chromatography. Alkanes can also serve to temper the highly polar nature of certain compounds, to bring them into an acceptable cLogP range (~1.0-5.0),[65] and vice versa with the ethylene glycols.[66] Polyamines can serve to greatly enhance water solubility, as they can be converted into a salt form, but may also enhance potency against Gram-negative organisms.[67] To introduce rigidity, carbocycles or heterocycles could be included.

#### 6.2.4.5 Synthetic design and selection of linking chemistry

When designing a synthetic pathway to bidentates, and indeed all conjugates, reaction order can be thought of as a pyramid of orthogonality. On the bottom we have many possible reactions, but they are nonspecific to the functional groups. At the top, we have a handful of highly specific reactions that do not undergo side reactions with other functional groups. When starting with natural products, we have already greatly narrowed the possible reactions, as it is typical for them to inherently contain a variety of functional groups.

It thus makes sense to make the final connection of the compounds the more orthogonal reaction, especially those that have come to been known as “click chemistry,” such as the thiol-ene and copper-catalyzed azide alkyne cycloaddition (CuAAC) reactions. In the case of CuAAC,

azides and alkynes are compatible with a wide range of other functional groups under various conditions. Installing these functional groups at the earliest stage of the longest reaction pathway is probably ideal.

Regarding which half of the conjugate to start with, we have found that the most facile is the linker portion itself. Often innately simplistic and lacking reactive functional groups, most chemical transformations should take place on the linker material. An "attaching" functional group can then be selected that will connect to the main compounds themselves but not interfere with the final connection functionality. The natural products (or synthetic compounds) are prepared separately to accept these linkers. In this way I have built several bidentate hybrid antibiotics starting from commercially available natural products, and readily available, simple linker materials such as oligoethylene glycols and alkyne alcohols.

### 6.2.5 Potential bidentate antibiotics in the literature

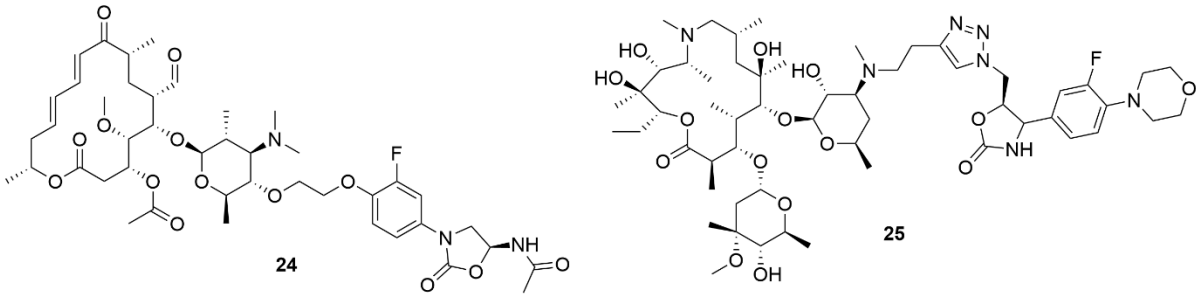


**Figure 9.** Morphochem's deglycosylated spiramycin-oxazolidinone hybrid **24** and Rib-X Pharmaceuticals azithromycin-oxazolidinone hybrid **25**.

Morphochem[61] and Rib-X Pharmaceuticals[62] have reported macrolide-oxazolidinone hybrids. Morphochem's series incorporates a linezolid derived oxazolidinone bound to spiramycin II lacking its forosamine and mycarose groups through the alcohol of the remaining sugar moiety

(Figure 9, **24**). Rib-X has created azithromycin-linezolid hybrids linked via a 1,2,3-triazole directly attached to the C5 position of the oxazolidinone core and linked to the amine of the aminosugar moiety of azithromycin via an alkyl chain (Figure 9, **25**). No antimicrobial data has been reported for these compounds. Other, similar compounds by the same authors are being pursued as antimicrobials, however they lack the linezolid moiety.[68] This lack of continued development of the macrolide-oxazolidinone hybrids as antibiotics may be due to unfavorable conformations of the two classes when combined in the ribosome. However, the work by Rib-X laid the foundation for our modification of azithromycin in the pursuit of bidentate antibiotics.

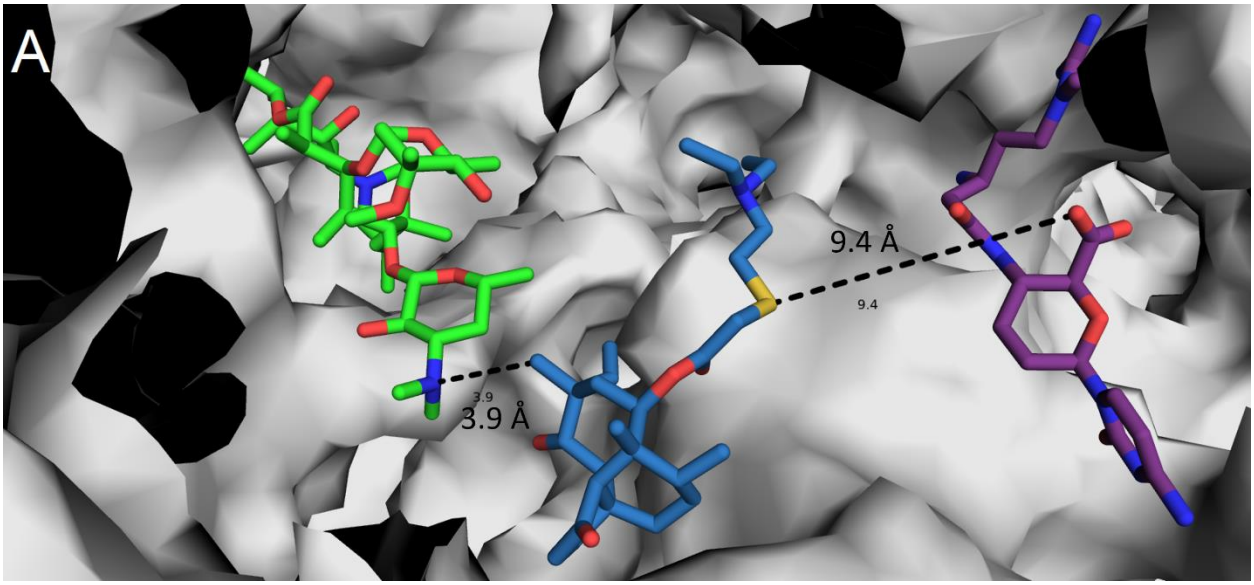


**Figure 10.** A) Overlayed cocrystal structures of azithromycin (8E42, green) and tiamulin (8E42, blue) in *E. coli* ribosome, and blasticidin S (4V9Q,[69] purple) in the ribosome of *T. thermophilus*. The dimethylamino moiety of azithromycin is 3.9 Å from the methyl at C12 of tiamulin, and the C22 thioether of tiamulin is 9.4 Å from the carboxylate of blasticidin S. Note no overlap of the structures.

As I have demonstrated in the previous chapters, pleuromutilin is an ideal candidate for a bidentate antibiotic. The diterpenoid can undergo selective, orthogonal reactions, and has two auxophoric sites which can handle triazole heterocycles and both polar and nonpolar flexible chains without loss of activity. Additionally, it binds the ribosome in close proximity to several other antibiotics. Because of our lab's experience, established protocols in the literature, and available semisynthetic starting materials, out of the available partners the peptidyl nucleoside natural product blasticidin S and the semi-synthetic macrolide azithromycin (Figure 1) were selected. Pleuromutilin-blasticidin S bidentates were designed to incorporate long, PEG-based linkers. In Chapter 5, we demonstrated the attachment of azide-terminated PEG chain bearing-pleuromutilins, and their potency as individual antibiotics.[66] These could then be paired with blasticidin alkynyl amides. For the pleuromutilin-azithromycin bidentates, native pleuromutilin could not be used. In Chapter 2, I showed that triazolyl functionalization of pleuromutilin resulted in inactive antibiotics. However, in Chapter 3, it was demonstrated that epimerization of the C12 position, followed by functionalization with triazoles resulted in highly potent derivatives. Thus, it was decided that 12-*epi*-pleuromutilins would function as the partner with azithromycin in their bidentate derivatives, bound covalently through a via a triazole linkage. The azido portion would arise from our previously synthesized 20-azido-12-*epi*-pleuromutilin (see Chapter 3), and alkyne from nor-azithromycin with 2-5 carbon spacers (*vide infra*).

## 6.3 Results and discussion

### 6.3.1 Pleuromutilin-blasticidin S hybrid synthesis

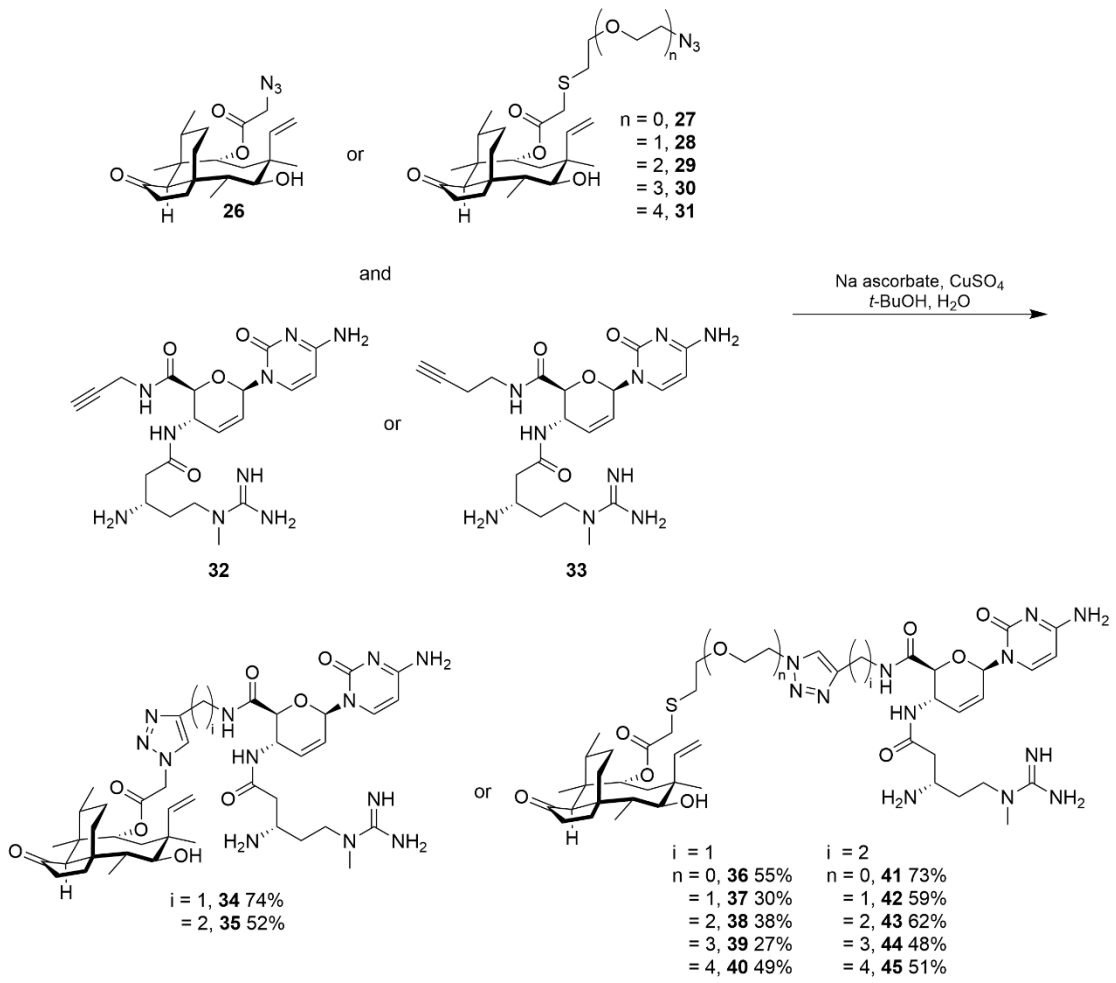


**Figure 11.** Synthesis of pleuromutilin-blasticidin S conjugates.

Previously, I generated azide-terminated C22 PEG pleuromutilins (Figure 11, **27**–**31**, see Chapter 5).[66] These derivatives demonstrated high activity in their own right. As part of a series of blasticidin amide derivatives,[55] Dr. Cole Gannett created propargyl and butynyl blasticidin S amides, **32** and **33** respectively. These blasticidin S amides were 2–4 fold more potent than blasticidin S in *S. aureus*. To construct the bidentate library, these azides and alkynes underwent copper-catalyzed azide alkyne cycloadditions, generating the triazoles. The series derived from the propargyl amide (**34**, **36**–**40**) were achieved in moderate yields (27-74%). For the butynyl amide series **35**, **41**–**45**, the yields were typically better, 48-73%. The discrepancy in yields may be

attributed to a difference of reaction temperature, 70 °C for **34**, **36**–**40** and 50 °C for **35**, **41**–**45**, indicating that degradation may occur at higher temperatures. Nevertheless, enough of each compound was recovered to conduct full characterization and antimicrobial testing, demonstrating the utility of proper synthetic path design when making semisynthetic natural product hybrids.

### 6.3.2 Pleuromutilin-Blasticidin S antimicrobial testing

Table 1a. MRSA

| Hybrid | MIC | Coadmin. | MIC | BLS comp. | MIC | PLE comp. | MIC |
|---|---|---|---|---|---|---|---|
| **34** | 12.5 | **26**+**32** | 1.56 | **32** | 50 | **26** | 1.56 |
| **36** | 3.12 | **27**+**32** | 0.391 | ---- | ---- | **27** | 0.391 |
| **37** | 3.12 | **28**+**32** | 0.391 | ---- | ---- | **28** | 0.391 |
| **38** | 1.56 | **29**+**32** | 0.391 | ---- | ---- | **29** | 0.781 |
| **39** | 6.25 | **30**+**32** | 0.781 | ---- | ---- | **30** | 0.781 |
| **40** | 3.12 | **31**+**32** | 0.781 | ---- | ---- | **31** | 0.781 |
| **35** | 25 | **26**+**33** | 1.56 | **33** | 50 | ---- | ---- |
| **41** | 6.25 | **27**+**33** | 0.391 | ---- | ---- | ---- | ---- |
| **42** | 3.12 | **28**+**33** | 0.391 | ---- | ---- | ---- | ---- |
| **43** | 6.25 | **29**+**33** | 0.391 | ---- | ---- | ---- | ---- |
| **44** | 3.12 | **30**+**33** | 0.781 | ---- | ---- | ---- | ---- |
| **45** | 3.12 | **31**+**33** | 0.781 | ---- | ---- | ---- | ---- |
| ---- | ---- | BLS+PLE | 3.12 | BLS | >200 | PLE | 3.12 |

Table 2b. *S. aureus* 8810

| Hybrid | MIC | Coadmin. | MIC | BLS comp. | MIC | PLE comp. | MIC |
|---|---|---|---|---|---|---|---|
| **34** | 12.5 | **26**+**32** | 1.56 | **32** | 50 | **26** | 1.56 |
| **36** | 3.12 | **27**+**32** | 0.781 | ---- | ---- | **27** | 0.391 |
| **37** | 1.56 | **28**+**32** | 0.781 | ---- | ---- | **28** | 0.781 |
| **38** | 1.56 | **29**+**32** | 0.781 | ---- | ---- | **29** | 0.781 |
| **39** | 1.56 | **30**+**32** | 0.781 | ---- | ---- | **30** | 0.781 |
| **40** | 1.56 | **31**+**32** | 0.781 | ---- | ---- | **31** | 0.781 |
| **35** | 12.5 | **26**+**33** | 1.56 | **33** | 50 | ---- | ---- |
| **41** | 6.25 | **27**+**33** | 0.781 | ---- | ---- | ---- | ---- |
| **42** | 1.56 | **28**+**33** | 0.781 | ---- | ---- | ---- | ---- |
| **43** | 3.12 | **29**+**33** | 0.781 | ---- | ---- | ---- | ---- |
| **44** | 1.56 | **30**+**33** | 0.781 | ---- | ---- | ---- | ---- |
| **45** | 1.56 | **31**+**33** | 0.781 | ---- | ---- | ---- | ---- |
| ---- | ----- | BLS+PLE | 3.12 | BLS | 200 | PLE | 3.12 |

| Table 1c. *E. coli* 1061 | | | | | | | |
|---|---|---|---|---|---|---|---|
| Hybrid | MIC | Coadmin. | MIC | BLS comp. | MIC | PLE comp. | MIC |
| **34** | 100 | **26+32** | 6.25 | **32** | 100 | **26** | 12.5 |
| **36** | 25 | **27+32** | 6.25 | ---- | ---- | **27** | 12.5 |
| **37** | 50 | **28+32** | 25 | ---- | ---- | **28** | 25 |
| **38** | 25 | **29+32** | 12.5 | ---- | ---- | **29** | 25 |
| **39** | 25 | **30+32** | 12.5 | ---- | ---- | **30** | 50 |
| **40** | 50 | **31+32** | 12.5 | ---- | ---- | **31** | 25 |
| **35** | 200 | **26+33** | 12.5 | **33** | 100 | ---- | ---- |
| **41** | 50 | **27+33** | 6.25 | ---- | ---- | ---- | ---- |
| **42** | 25 | **28+33** | 12.5 | ---- | ---- | ---- | ---- |
| **43** | 50 | **29+33** | 12.5 | ---- | ---- | ---- | ---- |
| **44** | 50 | **30+33** | 12.5 | ---- | ---- | ---- | ---- |
| **45** | 50 | **31+33** | 12.5 | ---- | ---- | ---- | ---- |
| ---- | ---- | BLS+PLE | 3.12 | BLS | 50 | PLE | 6.25 |

| Table 1d. *E. coli* ΔTolC | | | | | | | |
|---|---|---|---|---|---|---|---|
| Hybrid | MIC | Coadmin. | MIC | BLS comp. | MIC | PLE comp. | MIC |
| **34** | 12.5 | **26+32** | 1.56 | **32** | 50 | **26** | 1.56 |
| **36** | 1.56 | **27+32** | 0.391 | ---- | ---- | **27** | 0.195 |
| **37** | 1.56 | **28+32** | 0.391 | ---- | ---- | **28** | 0.391 |
| **38** | 0.781 | **29+32** | 0.391 | ---- | ---- | **29** | 0.391 |
| **39** | 0.781 | **30+32** | 0.781 | ---- | ---- | **30** | 0.391 |
| **40** | 0.781 | **31+32** | 0.781 | ---- | ---- | **31** | 0.391 |
| **35** | 12.5 | **26+33** | 1.56 | **33** | 50 | ---- | ---- |
| **41** | 1.56 | **27+33** | 0.391 | ---- | ---- | ---- | ---- |
| **42** | 0.781 | **28+33** | 0.391 | ---- | ---- | ---- | ---- |
| **43** | 0.781 | **29+33** | 0.781 | ---- | ---- | ---- | ---- |
| **44** | 0.781 | **30+33** | 0.781 | ---- | ---- | ---- | ---- |
| **45** | 0.781 | **31+33** | 0.781 | ---- | ---- | ---- | ---- |
| ---- | ---- | BLS+PLE | 3.12 | BLS | 100 | PLE | 3.12 |

| Table 1e. VRE | | | | | | | |
|---|---|---|---|---|---|---|---|
| Hybrid | MIC | Coadmin. | MIC | BLS comp. | MIC | PLE comp. | MIC |
| **34** | >100 | **26+32** | 6.25 | **32** | 100 | **26** | 12.5 |
| **36** | 50 | **27+32** | 1.56 | ---- | ---- | **27** | 1.56 |
| **37** | 50 | **28+32** | 3.12 | ---- | ---- | **28** | 3.12 |
| **38** | 12.5 | **29+32** | 3.12 | ---- | ---- | **29** | 3.12 |
| **39** | 25 | **30+32** | 3.12 | ---- | ---- | **30** | 3.12 |
| **40** | 25 | **31+32** | 3.12 | ---- | ---- | **31** | 3.12 |
| **35** | >100 | **26+33** | 6.25 | **33** | 100 | ---- | ---- |
| **41** | 50 | **27+33** | 1.56 | ---- | ---- | ---- | ---- |
| **42** | 25 | **28+33** | 3.12 | ---- | ---- | ---- | ---- |
| **43** | 25 | **29+33** | 3.12 | ---- | ---- | ---- | ---- |
| **44** | 12.5 | **30+33** | 3.12 | ---- | ---- | ---- | ---- |
| **45** | 6.25 | **31+33** | 3.12 | ---- | ---- | ---- | ---- |
| ---- | ---- | BLS+PLE | 12.5 | BLS | >100 | PLE | 12.5 |

| Table 1f. *E. faecalis* | | | | | | | |
|---|---|---|---|---|---|---|---|
| Hybrid | MIC | Coadmin. | MIC | BLS comp. | MIC | PLE comp. | MIC |
| **34** | >100 | **26+32** | 12.5 | **32** | 25 | **26** | >100 |
| **36** | >100 | **27+32** | 12.5 | ---- | ---- | **27** | >100 |
| **37** | >100 | **28+32** | 12.5 | ---- | ---- | **28** | >100 |
| **38** | >100 | **29+32** | 25 | ---- | ---- | **29** | >100 |
| **39** | >100 | **30+32** | 25 | ---- | ---- | **30** | >100 |
| **40** | >100 | **31+32** | 25 | ---- | ---- | **31** | >100 |
| **35** | >100 | **26+33** | 12.5 | **33** | 50 | ---- | ---- |
| **41** | >100 | **27+33** | 12.5 | ---- | ---- | ---- | ---- |
| **42** | >100 | **28+33** | 12.5 | ---- | ---- | ---- | ---- |
| **43** | 100 | **29+33** | 12.5 | ---- | ---- | ---- | ---- |
| **44** | >100 | **30+33** | 12.5 | ---- | ---- | ---- | ---- |
| **45** | >100 | **31+33** | 12.5 | ---- | ---- | ---- | ---- |
| ---- | ---- | BLS+PLE | 50 | BLS | 100 | PLE | >25 |

**Table 1a-f.** $MIC_{90}$ in µM of pleuromutilin-blasticidin S hybrids against 6 strains of bacteria: methicillin-resistant *S. aureus*, methicillin-susceptible *S. aureus*, *E. coli* MC1061, *E. coli* ΔTolC, Vancomycin-resistant Enterococcus, and *E. faecalis*. The column labelled Hybrid is the covalently bound pleuromutilin-blasticidin hybrids. Coadmin. is an equimolar dose of the two advanced intermediates prior to CuAAC as well as blasticidin S + pleuromutilin. BLS comp. or PLE-comp. are the advanced intermediates that led to the specific hybrid of that row, either blasticidin S or

pleuromutilin based, as well as blasticidin S or pleuromutilin. Green highlights indicate hybrids that exceed the potency of a coadministration of pleuromutilin and blasticidin S. Blue highlights indicate synergistic effects, with the solo administration of the parents in red highlights.

The testing data for the pleuromutilin-blasticidin S hybrids is shown in Table 1. In *S. aureus* (**Tables 1a** and **1b**) there were several hybrids that were 2-fold more potent than a coadministration of pleuromutilin and blasticidin, with around half of the hybrids out-performing coadministration in methicillin-susceptible *S. aureus*. Interestingly, no hybrid outperformed a coadministration of its advanced intermediates. Additionally, it appears that all activity in coadministrations came from the pleuromutilin advanced intermediates. Blasticidin S itself was essentially inactive in these organisms, with the advanced blasticidin S intermediates (**32** and **33**) being 4-fold more potent than blasticidin S. The activity of the hybrids tends to increase as linker length increases, and this makes sense as the distance between the linker attachment sites of pleuromutilin and blasticidin is 9.4 Å, as the microscopic crow flies. The maximum linker lengths contributed by the pleuromutilin PEG tails measuring from the thioether to the proximal nitrogen (N1) of the triazole is 4.0 Å, 7.6 Å, 11.2 Å, 14.8 Å and 18.4 Å for **36**–**40** or **41**–**45**, respectively, with the blasticidin S linker from the amide nitrogen to N1 of the triazole contributing 3.8 Å angstroms for the propargyl series and 4.7 Å angstroms for the butynyl series. However, the attachment site of blasticidin S is the carboxylate, and in the overlayed crystal structures, this functional group is orientated nearly 180° away from the C22 of pleuromutilin. Due to this unideal orientation, for both functionalized ends of the hybrid to bind simultaneously, any linker would have to wrap around the blasticidin S portion of the molecule. This unideal situation could interfere with blasticidin S's binding contacts in the ribosome, potentially preventing optimal binding or even totally reorienting blasticidin S so it cannot bind. However, interference of the PEG linker with blasticidin S's binding contacts may

not be occurring, and we must look to the hybrids' activity in *E. coli* to elucidate the impact of the covalent linkage between pleuromutilin and blasticidin S.

In *E. coli* MC1061 (**Table 1c**), a strain containing an intact TolC efflux pump, all hybrids (**34**–**45**) were far less potent than coadministration of parents pleuromutilin and blasticidin S, and even the coadministration of advanced intermediates (**26**–**31** with **32**–**33**) had less potency than parent coadministration, however less so than the hybrids. Additionally, the azido PEG pleuromutilins were less active than pleuromutilin, a reversal of the activity trend found in *S. aureus* (**Tables 1a**–**1b**). *E. coli* ΔTolC (**Table 1d**) showed a correction of that trend, with the 22-azido-pleuromuromutilin **26** and azido PEG pleuromutilins **27**–**31** once again more potent than pleuromutilin. The hybrids of longer lengths had activity comparable to a coadministration of the advanced intermediates, indicating that linker length is indeed important. The juxtaposition of the hybrids' activity in MC1061 and *E. coli* indicate that these compounds are prone to efflux via TolC pumps. Even the azido PEG pleuromutilins appear to be prone to efflux. The ability of TolC to efflux PEG containing molecules is a known phenomenon,[66, 70] which suggests that PEG based linkers may not be an ideal material for certain types of hybrids, and especially not in Gram negative organisms.

In *E. faecalis* (**Table 1f**), the hybrids (**34**–**35**) completely lost activity; however, coadministration of the advanced intermediates (**26**–**31** with **33**) appears to be synergistic as demonstrated by their increase in activity over administration of the pleuromutilin PEG derivatives (**26**–**31**) or blasticidin S butynyl amide (**33**) alone. In VRE (**Table 1e**), all hybrids (**34**–**45**) were significantly worse than the coadministration of the advanced intermediates (**26**–**31** with **32** and **33**), except for with the longest of the linkers (**45**). This trend indicates that long linkers are especially important in VRE.

Overall, it may be seen that linker length is an important factor in pleuromutilin-blasticidin S bidentate hybrids. Shorter linkers hamper the activity of the bidentate, which may be due to blasticidin S disrupting the pleuromutilin binding contacts, as activity of these hybrids seems to stem solely from pleuromutilin. The bidentates of longer linker length showed good activity, when not exposed to TolC efflux pumps. For future iterations of these hybrids the composition of the linker must be of a material which resists efflux, or incorporates efflux resistant scaffolds.[71, 72] Future hybrids of this type should be composed of an alkyl linker or perhaps a polyamine, to take advantage of the high cellular penetration of polyamines into Gram-negative organisms.[67]

#### 6.3.2.1 High anti-malarial potency of 41

In addition to antibacterial assays, these pleuromutilin-blasticidin S hybrids were submitted to the Klemba lab at Virginia Tech for anti-malarial testing. Only one, **41**, showed sub-micromolar activity. Compound **41** has an $EC_{50}$ in *P. falciparum* between 310-420 nM, determined between two rounds of testing. The coadministration of **27** and **33**, the two advanced intermediate parents of **41**, have an $EC_{50}$ of over 10 μM, and thus the synergistic potency of **41** is two orders of magnitude higher than its co-administered parents. What is especially intriguing about this compound, and can be inferred from Figure 10, is that simultaneous binding of both antibiotics in the hybrid is doubtful as was outlined in the discussion of the necessity of long linkers between pleuromutilin and blasticidin S. Further studies are in progress to determine if **41** is targeting the ribosome, or if it may have other targets.

### 6.3.3 12-*epi*-Pleuromutilin-azithromycin hybrid synthesis

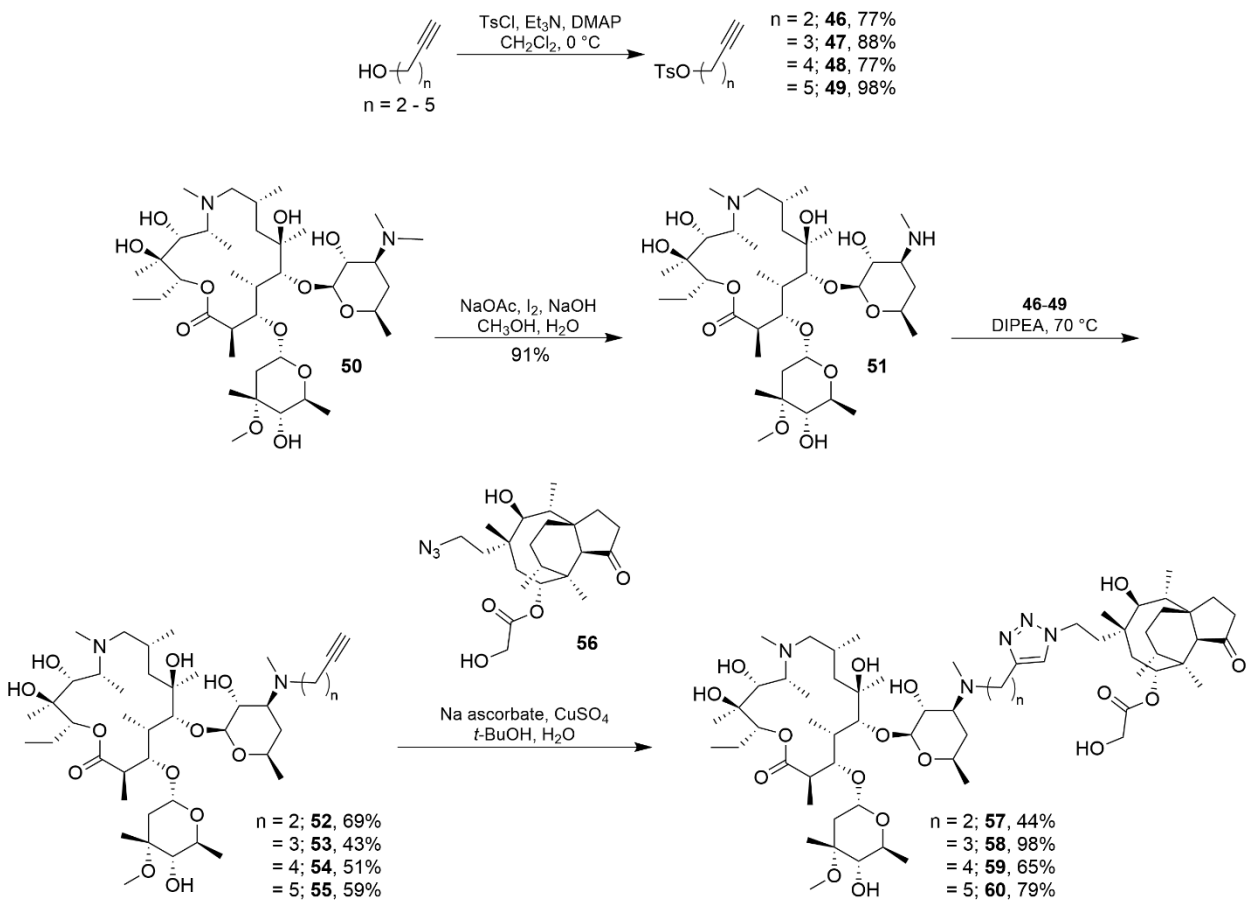


**Figure 12.** Synthesis of 12-*epi*-pleuromutilin-azithromycin conjugates.

To generate the alkynyl azithromycin partners **52**–**55**, alkynylating agents (**46**–**49**) and nor-azithromycin (**51**) had to be prepared. The alkynylating agents **46**–**49** were prepared by activating the corresponding alkynl alcohols with a tosylate group, in high yields. Nor-azithromycin **51** had literature precedent for its synthesis,[73] and two different routes were pursued. An initial experiment utilizing diethyl azodicarboxylate (DEAD) oxidation of a methyl group on the dimethyl amino moiety of azithromycin **50** appeared successful, however the desired product was contaminated with a large amount of diethyl hydrazine dicarbamate, the reduced form of DEAD. This mixture proved difficult to purify. Alternatively, iodine-mediated demethylation proved successful, and nor-azithromycin **51** was isolated in an excellent yield of 91%. Compound **51** was then alkynylated

using the alkynyl tosylates **46**–**49** to obtain alkynyl azithromycins **52**–**55** in moderate yield, following a literature procedure.[73] Long reaction times and an excess of alkynylating reagents proved to be necessary. Finally, **52**–**55** could be combined with **56** to give the 12-*epi*-pleuromutilin-azithromycin hybrids (**57**-**60)** in moderate to excellent yields, the highest being **58** at a 98% yield. CuAAC once again demonstrated its utility in combining highly functionalized natural products selectively.

### 6.3.4 12-*epi*-Pleuromutilin-azithromycin antimicrobial testing

| Compound | *E. faecium* NR-31909 | *E. faecalis* NR31972 | MRSA USA300 | WT *E. coli* Bw 25113 | *E. coli* ΔTol C Jw 55031 |
|---|---|---|---|---|---|
| **57** | 2 | >64 | 8 | >64 | 4 |
| **58** | 1-2 | >64 | 8 | >64 | 4 |
| **59** | 1 | >64 | 2 | >64 | 2 |
| **60** | 1 | >64 | 2 | >64 | 2 |
| **52** | >64 | >64 | >64 | 32 | <0.5 |
| **53** | >64 | >64 | >64 | 32 | <0.5 |
| **54** | >64 | >64 | >64 | 16 | <0.5 |
| **55** | >64 | >64 | >64 | 64 | <0.5 |
| **56** | 2 | >64 | 4 | >64 | <0.5 |
| **52+56** | 2 | 64 | 2 | 32 | <0.5 |
| **53+56** | 2 | >64 | 2 | 32 | <0.5 |
| **54+56** | 2 | >64 | 4 | 32 | <0.5 |
| **55+56** | 1 | >64 | 1-2 | >64 | <0.5 |
| AZI | >64 | >64 | >64 | 2 | <0.5 |
| PLE | 1-2 | >64 | 2 | >64 | 1 |
| AZI+PLE | 1-2 | 32 | 2 | 1 | <0.5 |
| Linezolid | 0.5 | 1 | 1 | - | - |
| Amikacin | - | - | - | 4 | 0.5-1 |

**Table 2.** MIC values (μM) of 12-*epi*-pleuromutilin-azithromycin against five strains of bacteria. The color codes are as follows: Hybrids **57**–**60** (green), alkynyl azithromycins **52**–**55**(yellow),

20-azido-12-*epi*-pleuromutilin **56** (blue), coadministrations of alkynyl azithromycin and 20-azido-12-*epi*-pleuromutilin **52**–**56** (red).

Somaia Abdelmegeed, a graduate student in the Seleem lab, tested our 12-*epi*-pleuromutilin-azithromycin hybrids **57**–**60** against an array of Gram positive and Gram negative strains (Table 2). Alongside the hybrids, coadministrations **52**–**56** of the advanced synthetic intermediates were tested, along with azithromycin, pleuromutilin, and a coadministration of azithromycin and pleuromutilin. An overall trend in the Gram positive strains is readily apparent. In pathogens which are susceptible to pleuromutilin but not to azithromycin (*E. faecium*, MRSA), the hybrids retained the activity of pleuromutilin. In *E. faecium*, all linker lengths preserved activity, however in MRSA only the longer linker lengths (**59**–**60**) maintained activity. These results are comparable to the coadministration MIC values of both the advanced intermediates and of pleuromutilin and azithromycin. In *E. faecalis*, which is a Gram positive but is not susceptible to pleuromutilin or azithromycin, the hybrids were inactive. In the WT *E. coli*, which is susceptible to azithromycin but inactive to pleuromutilin, the activity of the hybrids compared to azithromycin was lost. Interestingly, the alkynyl azithromycins **52-55** by themselves substantially lost activity compared to azithromycin in the WT *E. coli* and compared to their high activity in *E. coli* ΔTolC, this loss of potency suggests recognition of the alkynyl azithromycins for efflux. In the *E. coli* ΔTolC all synthetic intermediates, azithromycin, pleuromutilin, and their coadministrations were highly active. However, the hybrids had comparably lower activities.

Based on our interpretation of the results, it appears that the 12-*epi*-pleuromutilin-azithromycin hybrids are prone to efflux, as are pleuromutilin species and the alkynyl azithromycins. The difference in activity between the hybrids and their coadministrations in *E. coli* ΔTolC, but not in the Gram positive strains (at longer linker lengths) suggests that hybrids are

additionally hampered by low penetration into the Gram negative cell. These results indicate that the hybrids may be good antibiotic agents against azithromycin resistant Gram positive strains, but have little utility against Gram negative strains. More testing will be required against Gram positive strains which are susceptible to both pleuromutilin and azithromycin to determine if the hybrids have enhanced activity over their components.

Some discussion of the disparate actions of pleuromutilin, blasticidin S, and azithromycin are necessary. Pleuromutilins bind to the A- and P-site of the peptidyl transferase center (PTC) of the 50s ribosomal subunit. The diterpenoid core is positioned in the A-site, and the C14 side chain in the P-site. This mode of binding inhibits the transfer of the 3'-end tRNA from the A-site to the P-site, preventing peptide bond formation.[74, 75] Blasticidin S's mechanism of action is primarily via preventing the termination of translation through distorting the P-site tRNA and promoting enhanced binding the tRNA's binding while blocking releasing factors, but to a lesser extent it also inhibits peptide bond formation.[69, 76] Azithromycin functions blocks the nascent peptide exit tunnel and impedes the assembly of the 50s ribosomal subunit.[77] The inhibition of these mechanisms of protein synthesis, while not antagonistic, do not necessarily imply a synergistic activity by simultaneous inhibition, save for pleuromutilin and blasticidin's minor mode of actions. For synergistic bidentates, other antibiotics that prevent tRNA binding or movement, but bind in discrete binding pockets, should be considered in the future.

### 6.4 Conclusion

In this chapter, we have discussed the literature precedence for hybrid and bidentate antibiotics and explored the synthesis and testing of pleuromutilin-blasticidin S and 12-*epi*-pleuromutilin-azithromycin bidentate hybrids. Select pleuromutilin-blasticidin S hybrids (**34**–**45**) demonstrated enhanced activity over their parent antibiotics in Gram positive pathogens; however,

they were especially prone to efflux. The 12-*epi*-pleuromutilin-azithromycin hybrids (**57**–**60**) retained their activity in azithromycin resistant Gram positive pathogens but were prone to poor penetration into and efflux from Gram negative strains. Further experiments by our collaborators in the Polikanov lab will elucidate whether these hybrids are acting as true bidentates by co-crystallizing them with the ribosome and determining their structural conformation.

## 6.5 Experimental

### 6.5.1 General synthetic

Unless otherwise noted, chemical reagents and solvents were purchased from EMD Millipore, Oakwood Chemical, Sigma-Aldrich, and Thermo Fisher Scientific. Unless otherwise specified, all reactions were carried out under an atmosphere of dry nitrogen in dried glassware. Commercially available starting materials and reagents were used as received or purified prior to use if necessary. Diisopropylethylamine was distilled from calcium hydride. Pleuromutilin was purchased as a commercial compound from TRC Canada. Azithromycin was ordered from Indofine Chemical Company. Analytical thin layer chromatography was performed using Supelco 0.25 mm silica gel 60 $F_{254}$ plates. Visualization was accomplished by irradiation with a 254 nm UV lamp or by staining with an aqueous solution of ceric ammonium molybdate, an acidified ethanolic solution of *p*-anisaldehyde, or a basified solution of potassium permanganate. Chromatography was performed using a forced flow of the indicated solvent system on SiliCycle SiliaFlash P60 silica gel (40-63 μm) or via automated flash chromatography using a Biotage Selekt system with SiliCycle SiliaSep or Teledyne RediSepRf gold chromatography columns. Deionized water was obtained from the house deionized water system.

$^{1}$H NMR spectra were recorded on a Bruker Avance II 500 MHz spectrometer or an Agilent U4-DD2 400 MHz spectrometer. Chemical shifts are reported in parts per million from tetramethylsilane (0 ppm) using the solvent resonance as an internal standard ($CDCl_3$ 7.26 ppm). Data are reported as follows: chemical shift, multiplicity (s=singlet, d=doublet, t=triplet, q=quartet, m=multiplet, br=broad), coupling constants, and number of protons. Proton decoupled $^{13}$C NMR were recorded on a Bruker Avance II 500 MHz (126 MHz) spectrometer or an Agilent U4-DD2 400 MHz (101 MHz) spectrometer. Chemical shifts are reported in ppm from tetramethylsilane (0 ppm) using the solvent resonance as an internal standard ($CDCl_3$ 7.26 ppm). High resolution mass spectra were obtained on an Agilent Technologies 6220 TOF LC/MS or a Waters Synapt Q-TOF G2 or Thermo Exploris 120 HESI Orbitrap MS in the Department of Chemistry and the VT-Mass Spectrometry Incubator at the Virginia Polytechnic Institute and State University. Specific rotations were obtained on a Jasco P-2000 polarimeter.

### 6.5.2 Broth microdilution Assays – Blasticidin S and pleuromutilin

Media and solutions were autoclaved or sterile filtered prior to use and manipulations were carried out in a laminar flow hood. Antibacterial testing was performed in polypropylene 96-well flat bottom plates in triplicate. The minimal inhibitory concentration (MIC) of derivatives **26**–**45** was assessed against *Staphylococcus aureus* DHS 8810, methicillin-resistant *S. aureus* (MRSA) ATCC 43300, *Enterococcus faecalis* ATCC 29212, vancomycin-resistant *Enterococcus*, *Escherichia coli* ΔTolC, *E. coli* MC1061, *Klebsiella pneumoniae* ATCC 29665, and *Acinetobacter baumannii* ATCC 17978, using serial dilutions. Pleuromutilin and Blasticidin S were used as positive controls and the vehicle (DMSO) as a negative control. Stock solutions of each compound were prepared at 8 mM in DMSO and serially diluted in DMSO to create master plates. For the co-administered antibiotics, they were prepared at 8 mM in DMSO each (a combined 16 mM concentration), and

serially diluted in DMSO to create master plates. From the master plates, 5 μL of each dilution was applied to test plates using a Bravo automated liquid transfer system (Agilent). Bacteria previously grown overnight (37 °C, 120 – 200 RPM), in LB broth were diluted to an OD600 of 0.05 in cation-adjusted Mueller-Hinton broth, grown to an OD600 of ~0.5, and diluted to an OD600 of 0.004 in cation-adjusted Mueller-Hinton broth. These diluted cultures were applied to the test plates (195 μL per test well) resulting in final concentrations of the test compounds of 200-0.0977 μM. The plates were incubated at 37 °C for 16–18 h, except for VRE and *E. faecalis*, which were incubated at 37 °C for 24 h. Inhibition was determined by measuring the optical density at 600 nm (OD600) with a Cytation 3 plate reader (BioTek). The optical density measurements were normalized to the positive and negative controls. The MIC was the lowest concentration that inhibited >90% of growth.

### 6.5.4 Syntheses and characterizations of compounds

**General Method A for Alkynyl Tosylate Formation (46–49):** A specific alkynyl alcohol (3-butynol–6-heptynol) (21.0 mmol) and $CH_2Cl_2$ (20 mL) were added. The solution was cooled to 0 °C (ice-water bath), and triethylamine (3.5 mL, 25 mmol) and 4-dimethylaminepyridine (25 mg, 0.21 mmol) were added. With stirring, tosyl chloride (4.0 g, 21 mmol) was added. The mixture was stirred for 18 hours and allowed to come to room temperature. The reaction was then quenched with $H_2O$ (20 ml), the layers separated, and the aqueous layer was extracted with $CH_2Cl_2$ (2x10 mL). The combined organics were dried over $Na_2SO_4$, and concentrated. The residue was purified using flash column chromatography ($SiO_2$) with the indicated mobile phase.

**General Method B for Alkynyl nor-Azithromycin Formation (52–55):** Following the procedure of Wang et al.,[73] Nor-azithromycin (0.065-0.070 mmol), Hunig's base (0.3 mL) and a specific alkynyl toxylate **46**–**49** (2.0 equiv.) were added. The mixture was heated to 70 °C, (started

20250120-1400) and stirred for 18 h. The reaction mixture was evaporated under nitrogen and the residue was purified using flash column chromatography ($SiO_2$) with the indicated mobile phase.

**General Method C for Triazole Formation (34, 36–40):** Following the conditions of Sharpless,[78] 22-azidopleuromutilin (**26**) or a 22-azidoOEG-pleuromutilin (**27**–**31**) (1.2 equiv.) and propargyl blasticidin (0.0300 mmol, 1.0 equiv.), sodium ascorbate (0.25 equiv.), 10.8 mM CuSO4 (5 mol %), and *t*-BuOH (0.20-0.40 mL) were combined and heated to 70 °C (oil bath) for 3-18 h with stirring. The *t*-BuOH was stripped under vacuum and the aqueous solution was purified using reverse-phase flash column chromatography (C18) with the indicated mobile phase.

**General Method D for Triazole Formation (35, 41–45):** Following the conditions of Sharpless,[78] 22-azidopleuromutilin (**26**) or a 22-azidoOEG-pleuromutilin (**27**–**31**) (1.2 equiv.) and butynyl blasticidin (0.0300 mmol, 1.0 equiv.), sodium ascorbate (0.25 equiv.), 10.8 mM CuSO4 (5 mol %), and *t*-BuOH (0.20-0.40 mL) were combined and heated to 50 °C (oil bath) for 3-18 h with stirring. The *t*-BuOH was stripped under vacuum and the aqueous solution was purified using reverse-phase flash column chromatography (C18) with the indicated mobile phase.

**General Method E for Triazole Formation (57–60):** Following the conditions of Sharpless,[78] 20-azido-12-*epi*-pleuromutilin (**56**) (1.5 equiv.), a specific alkynyl azithromycin (**52**–**55**) (0.0120-0.0130 mmol, 1.0 equiv.), sodium ascorbate (0.25 equiv.), 10.8 mM CuSO4 (5 mol %), and *t*-BuOH (0.20 mL) were combined and stirred at room temperature for 3-18 h. After cooling, the solvent was evaporated under a stream of nitrogen gas, and the residue was purified using flash column chromatography ($SiO_2$) with the indicated mobile phase.

**(3a*R*,4*R*,5*R*,7*S*,8*S*,9*R*,9a*S*,12*R*)-8-Hydroxy-4,7,9,12-tetramethyl-3-oxo-7-vinyldecahydro-4,9a-propanocyclopenta[8]annulen-5-yl 2-(4-(((2*S*,3*S*,6*R*)-6-(4-amino-2-oxopyrimidin-**

**1(2*H*)-yl)-3-((*S*)-3-amino-5-(1-methylguanidino)pentanamido)-3,6-dihydro-2*H*-pyran-2-carboxamido)methyl)-1*H*-1,2,3-triazol-1-yl)acetate (34).** Synthesized according to general method C using **26** and **32**. Residue purified via flash chromatography (C18, 10-100% $CH_3CN$ in $H_2O$, 0.1% formic acid), dissolved in 0.3% methanolic HCl and concentrated to give **34** (as the tri HCl salt) as a white powder (22.7 mg, 74%): $^1$H NMR (500 MHz, MeOD) δ 7.98 (s, 1H), 7.90 (d, *J* = 7.8 Hz, 1H), 6.62 (dt, *J* = 3.5, 1.8 Hz, 1H), 6.26 (dd, *J* = 17.6, 11.2 Hz, 1H), 6.17 (dd, *J* = 9.1, 7.3 Hz, 2H), 5.91 (ddd, *J* = 10.2, 2.7, 1.5 Hz, 1H), 5.73 (d, *J* = 8.3 Hz, 1H), 5.28 (d, *J* = 17.6 Hz, 1H), 5.22 (d, *J* = 17.5 Hz, 1H), 5.19 – 5.12 (m, 2H), 4.90 – 4.88 (m, 1H), 4.48 (s, 2H), 4.33 (d, *J* = 9.3 Hz, 1H), 3.66 (p, *J* = 7.1 Hz, 1H), 3.54 (q, *J* = 7.8 Hz, 1H), 3.50 (d, *J* = 6.0 Hz, 1H), 3.08 (s, 3H), 2.73 (dd, *J* = 17.0, 5.6 Hz, 1H), 2.64 (dd, *J* = 15.7, 7.7 Hz, 1H), 2.36 (s, 1H), 2.32 – 2.23 (m, 2H), 2.19 – 2.05 (m, 4H), 1.82 – 1.76 (m, 1H), 1.73 – 1.65 (m, 1H), 1.59 (ddd, *J* = 12.4, 7.1, 3.3 Hz, 1H), 1.54 – 1.30 (m, 5H), 1.29 (s, 3H), 1.15 (s, 3H), 1.14 – 1.10 (m, 1H), 0.92 (d, *J* = 7.0 Hz, 3H), 0.68 (d, *J* = 7.0 Hz, 3H). $^{13}$C NMR (126 MHz, MeOD) δ 219.6, 171.4, 170.3, 166.8, 161.5, 158.3, 148.6, 147.0, 141.1, 135.8, 126.2, 116.7, 95.9, 80.9, 77.6, 75.3, 72.5, 59.1, 52.7, 48.1, 46.8, 46.6, 45.7, 45.4, 43.2, 38.2, 38.0, 37.8, 36.7, 35.3, 35.3, 31.4, 30.7, 28.3, 28.0, 25.8, 17.1, 15.3, 11.8. HR-MS (ESI): Calcd for $C_{42}H_{63}N_{12}O_8$ $[M+H]^+$: 863.4886; Found 863.4886.

**(3a*R*,4*R*,5*R*,7*S*,8*S*,9*R*,9a*S*,12*R*)-8-Hydroxy-4,7,9,12-tetramethyl-3-oxo-7-vinyldecahydro-4,9a-propanocyclopenta[8]annulen-5-yl 2-(4-(2-((2*S*,3*S*,6*R*)-6-(4-amino-2-oxopyrimidin-1(2*H*)-yl)-3-((*S*)-3-amino-5-(1-methylguanidino)pentanamido)-3,6-dihydro-2*H*-pyran-2-carboxamido)ethyl)-1*H*-1,2,3-triazol-1-yl)acetate (35).** Synthesized according to general method D using **26** and **33**. Residue purified via flash chromatography (C18, 10-100% $CH_3CN$ in $H_2O$, 0.1% formic acid), dissolved in 0.3% methanolic HCl and concentrated to give **35** (as the tri HCl salt) as a white powder (11.5 mg, 52%): $^1$H NMR (500 MHz, MeOD) δ 7.90 (s, 1H), 7.75

(d, *J* = 7.7 Hz, 1H), 6.63 (s, 1H), 6.29 (dd, *J* = 17.6, 11.2 Hz, 1H), 6.14 (dt, *J* = 10.1, 2.0 Hz, 1H), 6.10 (d, *J* = 7.6 Hz, 1H), 5.91 (ddd, *J* = 10.2, 2.7, 1.5 Hz, 1H), 5.77 (d, *J* = 8.4 Hz, 1H), 5.31 (d, *J* = 17.6 Hz, 1H), 5.24 (d, *J* = 17.6 Hz, 1H), 5.19 (dd, *J* = 17.6, 1.3 Hz, 1H), 5.16 (dd, *J* = 11.2, 1.3 Hz, 1H), 4.27 (d, *J* = 9.4 Hz, 1H), 3.67 (td, *J* = 7.9, 3.3 Hz, 1H), 3.64 – 3.49 (m, 4H), 3.45 (dt, *J* = 13.5, 7.1 Hz, 1H), 3.11 (s, 3H), 2.96 (t, *J* = 7.1 Hz, 2H), 2.79 – 2.71 (m, 1H), 2.66 (dd, *J* = 15.6, 7.7 Hz, 1H), 2.39 (s, 1H), 2.33 – 2.25 (m, 2H), 2.21 – 2.08 (m, 4H), 1.81 (dq, *J* = 14.6, 3.1 Hz, 1H), 1.74 – 1.67 (m, 1H), 1.65 – 1.60 (m, 1H), 1.57 – 1.34 (m, 4H), 1.33 (s, 3H), 1.17 (s, 3H), 1.16 – 1.12 (m, 1H), 0.94 (d, *J* = 7.0 Hz, 3H), 0.72 (d, *J* = 7.0 Hz, 3H). $^{13}$C NMR (126 MHz, MeOD) δ 219.5, 171.4, 170.5, 167.1, 164.7, 164.5, 158.3, 153.6, 146.2, 145.1, 141.1, 135.2, 126.9, 125.6, 116.7, 96.7, 81.1, 77.7, 75.3, 72.5, 59.1, 52.7, 48.1, 46.8 (2C), 45.6, 45.4, 43.2, 39.8, 38.2, 38.0, 37.8, 36.8, 35.3, 31.4, 30.7, 28.4, 28.0, 26.0, 25.8, 17.1, 15.2, 11.8. HR-MS (ESI): Calcd for $C_{43}H_{65}N_{12}O_8$ $[M+H]^+$: 877.5043; Found 877.5062.

**(3a*R*,4*R*,5*R*,7*S*,8*S*,9*R*,9a*S*,12*R*)-8-Hydroxy-4,7,9,12-tetramethyl-3-oxo-7-vinyldecahydro-4,9a-propanocyclopenta[8]annulen-5-yl 2-((2-(4-(((2*S*,3*S*,6*R*)-6-(4-amino-2-oxopyrimidin-1(2*H*)-yl)-3-((*S*)-3-amino-5-(1-methylguanidino)pentanamido)-3,6-dihydro-2*H*-pyran-2-carboxamido)methyl)-1*H*-1,2,3-triazol-1-yl)ethyl)thio)acetate (36).** Synthesized according to general method C using **27** and **32**. Residue purified via flash chromatography (C18, 10-100% $CH_3CN$ in $H_2O$, 0.1% formic acid), dissolved in 0.3% methanolic HCl and concentrated to give **36** (as the tri HCl salt) as a white powder (17.1 mg, 55%): $^1$H NMR (500 MHz, MeOD) δ 7.95 (s, 1H), 7.56 (d, *J* = 7.5 Hz, 1H), 6.61 (s, 1H), 6.31 (dd, *J* = 17.1, 11.5 Hz, 1H), 6.07 (d, *J* = 10.2 Hz, 1H), 5.95 (d, *J* = 7.4 Hz, 1H), 5.87 (d, *J* = 10.2 Hz, 1H), 5.74 (d, *J* = 8.3 Hz, 1H), 5.16 – 5.10 (m, 2H), 4.86 (d, *J* = 10.5 Hz, 1H), 4.61 (t, *J* = 6.8 Hz, 2H), 4.44 (q, *J* = 15.3 Hz, 2H), 4.29 (d, *J* = 9.3 Hz, 1H), 3.60 (s, 1H), 3.55 – 3.49 (m, 3H), 3.23 (d, *J* = 3.2 Hz, 2H), 3.13 (t, *J* = 6.7 Hz, 2H),

3.07 (s, 3H), 2.65 (s, 2H), 2.37 (s, 1H), 2.33 (p, *J* = 6.8 Hz, 1H), 2.27 (dd, *J* = 19.4, 10.6 Hz, 1H), 2.20 – 2.11 (m, 2H), 2.06 (s, 2H), 1.82 (dq, *J* = 14.3, 3.0 Hz, 1H), 1.74 – 1.52 (m, 3H), 1.47 (dd, *J* = 10.4, 2.8 Hz, 1H), 1.44 (s, 3H), 1.38 – 1.32 (m, 2H), 1.19 – 1.15 (m, 1H), 1.15 (s, 3H), 0.93 (d, *J* = 7.0 Hz, 3H), 0.72 (d, *J* = 6.7 Hz, 3H). $^{13}$C NMR (126 MHz, MeOD) δ 219.6, 171.5, 170.7, 170.3, 167.7, 158.4, 158.1, 146.0, 143.3, 141.3, 134.6, 127.8, 124.8, 116.6, 97.2, 81.3, 77.7, 75.4, 71.4, 59.3, 50.5, 48.5, 48.1, 46.80, 46.76, 46.0, 45.3, 43.1, 39.1, 38.2, 37.7, 36.6, 35.4, 35.3, 34.7, 33.3, 31.5, 31.0, 28.3, 28.1, 25.8, 17.1, 15.4, 11.8. Calcd for $C_{44}H_{67}N_{12}O_8S_1$ $[M+H]^+$: 923.4920; Found 923.4933.

**(3a*R*,4*R*,5*R*,7*S*,8*S*,9*R*,9a*S*,12*R*)-8-Hydroxy-4,7,9,12-tetramethyl-3-oxo-7-vinyldecahydro-4,9a-propanocyclopenta[8]annulen-5-yl 2-((2-(2-(4-(((2*S*,3*S*,6*R*)-6-(4-amino-2-oxopyrimidin-1(2*H*)-yl)-3-((*S*)-3-amino-5-(1-methylguanidino)pentanamido)-3,6-dihydro-2*H*-pyran-2-carboxamido)methyl)-1*H*-1,2,3-triazol-1-yl)ethoxy)ethyl)thio)acetate (37).** Synthesized according to general method C using **28** and **32**. Residue purified via flash chromatography (C18, 10-100% $CH_3CN$ in $H_2O$, 0.1% formic acid), dissolved in 0.3% methanolic HCl and concentrated to give **37** (as the tri HCl salt) as a white powder (9.8 mg, 30%): $^1$H NMR (500 MHz, MeOD) δ 8.17 (s, 1H), 7.92 (d, *J* = 7.2 Hz, 1H), 6.62 (s, 1H), 6.31 (dd, *J* = 18.1, 10.6 Hz, 1H), 6.20 – 6.15 (m, 2H), 5.90 (d, *J* = 10.4 Hz, 1H), 5.72 (d, *J* = 8.2 Hz, 1H), 5.18 – 5.12 (m, 2H), 4.86 – 4.78 (m, 1H), 4.64 (t, *J* = 4.7 Hz, 2H), 4.52 (q, *J* = 13.0 Hz, 2H), 4.35 (dd, *J* = 17.4, 9.2 Hz, 1H), 3.91 (t, *J* = 4.8 Hz, 2H), 3.66 (t, *J* = 6.1 Hz, 3H), 3.59 – 3.49 (m, 2H), 3.23 (d, *J* = 14.9 Hz, 1H), 3.18 (d, *J* = 14.8 Hz, 1H), 3.09 (s, 2H), 2.79 – 2.71 (m, 3H), 2.67 – 2.58 (m, 1H), 2.38 (s, 1H), 2.35 – 2.24 (m, 2H), 2.19 – 2.12 (m, 2H), 2.11 – 2.06 (m, 2H), 1.81 (dq, *J* = 14.6, 3.0 Hz, 1H), 1.74 – 1.66 (m, 1H), 1.65 – 1.51 (m, 2H), 1.48 – 1.45 (m, 1H), 1.44 (s, 3H), 1.37 – 1.33 (m, 2H), 1.19 – 1.11 (m, 1H), 1.15 (s, 3H), 0.93 (d, *J* = 7.1 Hz,

3H), 0.72 (d, *J* = 6.8 Hz, 3H). $^{13}$C NMR (126 MHz, MeOD) δ 219.7, 171.4, 170.7, 170.4, 161.4, 158.3, 148.5, 147.2, 141.4, 135.9, 130.0, 126.9, 126.2, 116.5, 95.9, 80.9, 77.7, 75.4, 71.4, 71.2, 69.8, 59.3, 52.2, 48.5, 48.1, 46.8, 46.6, 46.0, 45.3, 43.1, 38.2, 38.1, 37.7, 36.8, 35.3, 35.3, 35.0, 32.9, 31.5, 30.7, 28.3, 28.1, 25.8, 17.2, 15.4, 11.8. Calcd for $C_{46}H_{71}N_{12}O_9S_1$ $[M+H]^+$: 967.5182; Found 967.5175.

**(3a*R*,4*R*,5*R*,7*S*,8*S*,9*R*,9a*S*,12*R*)-8-Hydroxy-4,7,9,12-tetramethyl-3-oxo-7-vinyldecahydro-4,9a-propanocyclopenta[8]annulen-5-yl 2-((2-(2-(2-(4-(((2*S*,3*S*,6*R*)-6-(4-amino-2-oxopyrimidin-1(2*H*)-yl)-3-((*S*)-3-amino-5-(1-methylguanidino)pentanamido)-3,6-dihydro-2*H*-pyran-2-carboxamido)methyl)-1*H*-1,2,3-triazol-1-yl)ethoxy)ethoxy)ethyl)thio)acetate** plePEG3-probls **(38).** Synthesized according to general method C using **29** and **32**. Residue purified via flash chromatography (C18, 10-100% $CH_3CN$ in $H_2O$, 0.1% formic acid), dissolved in 0.3% methanolic HCl and concentrated to give **38** (as the tri HCl salt) as a white powder (12.6 mg, 38%): $^1$H NMR (500 MHz, MeOD) δ 8.17 (s, 1H), 7.93 (d, *J* = 7.9 Hz, 1H), 6.62 (dt, *J* = 3.3, 1.8 Hz, 1H), 6.35 – 6.28 (m, 1H), 6.20 – 6.16 (m, 2H), 5.91 (ddd, *J* = 10.2, 2.6, 1.5 Hz, 1H), 5.72 (d, *J* = 8.2 Hz, 1H), 5.18 – 5.13 (m, 2H), 4.90 – 4.81 (m, 1H), 4.64 (t, *J* = 5.0 Hz, 2H), 4.55 – 4.46 (m, 2H), 4.34 (d, *J* = 9.4 Hz, 1H), 3.94 (t, *J* = 5.0 Hz, 2H), 3.69 – 3.61 (m, 5H), 3.61 – 3.53 (m, 4H), 3.51 (d, *J* = 6.1 Hz, 1H), 3.28 (d, *J* = 14.8 Hz, 1H), 3.24 (d, *J* = 15.0 Hz, 1H), 3.09 (s, 3H), 2.79 (t, *J* = 6.3 Hz, 2H), 2.77 – 2.72 (m, 1H), 2.67 – 2.57 (m, 1H), 2.40 – 2.38 (m, 1H), 2.36 – 2.27 (m, 2H), 2.19 – 2.11 (m, 2H), 2.08 (q, *J* = 7.7 Hz, 2H), 1.82 (dq, *J* = 14.2, 2.9 Hz, 1H), 1.70 (ddd, *J* = 13.1, 11.1, 9.0 Hz, 1H), 1.65 – 1.51 (m, 2H), 1.48 – 1.42 (m, 1H), 1.45 (s, 3H), 1.39 – 1.32 (m, 2H), 1.19 – 1.11 (m, 1H), 1.15 (s, 3H), 0.93 (d, *J* = 7.1 Hz, 3H), 0.73 (d, *J* = 6.8 Hz, 3H). $^{13}$C NMR (126 MHz, MeOD) δ 219.7, 171.4, 170.7, 170.4, 161.4, 158.3, 148.5, 147.2, 141.3 (2C), 135.8, 126.1 (2C), 116.5, 95.9, 80.9, 77.7, 75.4, 71.7, 71.3, 71.2 (4C), 70.0, 59.3,

57.46, 52.2, 49.8, 48.4, 48.1, 46.8, 46.6, 46.0, 45.3, 43.1, 38.2, 38.0, 37.8, 36.8, 35.4, 35.3, 35.0, 33.0, 31.5, 30.7, 28.3, 28.1, 25.8, 17.1, 15.4, 11.8. Calcd for $C_{48}H_{75}N_{12}O_{10}S_1$ $[M+H]^+$: 1011.5444; Found 1011.5458.

**(3a*R*,4*R*,5*R*,7*S*,8*S*,9*R*,9a*S*,12*R*)-8-Hydroxy-4,7,9,12-tetramethyl-3-oxo-7-vinyldecahydro-4,9a-propanocyclopenta[8]annulen-5-yl 1-(4-(((2*S*,3*S*,6*R*)-6-(4-amino-2-oxopyrimidin-1(2*H*)-yl)-3-((*S*)-3-amino-5-(1-methylguanidino)pentanamido)-3,6-dihydro-2*H*-pyran-2-carboxamido)methyl)-1*H*-1,2,3-triazol-1-yl)-3,6,9-trioxa-12-thiatetradecan-14-oate (39).** Synthesized according to general method C **30** and **32**. Residue purified via flash chromatography (C18, 10-100% $CH_3CN$ in $H_2O$, 0.1% formic acid), dissolved in 0.3% methanolic HCl and concentrated to give **39** (as the tri HCl salt) as a white powder (9.7 mg, 27%): $^1$H NMR (500 MHz, MeOD) δ 8.30 (s, 1H), 7.95 (d, *J* = 7.8 Hz, 1H), 6.65 – 6.62 (m, 1H), 6.36 – 6.29 (m, 1H), 6.23 – 6.18 (m, 2H), 5.93 (dt, *J* = 9.9, 2.0 Hz, 1H), 5.74 (d, *J* = 8.3 Hz, 1H), 5.21 – 5.15 (m, 2H), 4.92 – 4.82 (m, 1H), 4.70 (t, *J* = 5.0 Hz, 2H), 4.55 (q, *J* = 15.4 Hz, 2H), 4.36 (d, *J* = 9.2 Hz, 1H), 3.98 (t, *J* = 5.0 Hz, 2H), 3.73 – 3.63 (m, 9H), 3.62 (s, 4H), 3.57 (dd, *J* = 9.6, 6.6 Hz, 2H), 3.53 (d, *J* = 6.1 Hz, 1H), 3.30 (d, *J* = 15.0 Hz, 1H), 3.27 (d, *J* = 14.8 Hz, 1H), 3.11 (s, 2H), 2.82 (t, *J* = 6.3 Hz, 2H), 2.79 – 2.74 (m, 1H), 2.66 (dd, *J* = 15.9, 7.7 Hz, 1H), 2.42 – 2.39 (m, 1H), 2.38 – 2.26 (m, 2H), 2.21 – 2.14 (m, 2H), 2.13 – 2.07 (m, 2H), 1.84 (dq, *J* = 14.1, 2.9 Hz, 1H), 1.77 – 1.69 (m, 1H), 1.67 – 1.53 (m, 2H), 1.50 – 1.44 (m, 1H), 1.47 (s, 3H), 1.41 – 1.34 (m, 2H), 1.19 – 1.14 (m, 1H), 1.17 (s, 3H), 0.95 (d, *J* = 7.1 Hz, 3H), 0.75 (d, *J* = 6.7 Hz, 3H). $^{13}$C NMR (126 MHz, MeOD) δ 219.7, 171.5, 170.7, 170.5, 161.4, 158.3, 148.5, 147.2, 142.0, 141.3, 135.8, 126.1, 118.6, 116.5, 95.9, 80.9, 77.7, 75.4, 71.7, 71.45, 71.41, 71.3, 71.23, 71.18, 69.9, 59.3, 52.6, 48.4, 48.1, 46.8, 46.6, 46.0, 45.3, 43.1, 38.2, 38.0, 37.8, 36.8, 35.4, 35.3, 34.8, 32.9,

31.5, 30.7, 28.3, 28.1, 25.8, 17.1, 15.4, 11.8. Calcd for $C_{50}H_{79}N_{12}O_{11}S_1$ $[M+H]^+$: 1055.5706; Found 1055.5725.

**(3a*R*,4*R*,5*R*,7*S*,8*S*,9*R*,9a*S*,12*R*)-8-Hydroxy-4,7,9,12-tetramethyl-3-oxo-7-vinyldecahydro-4,9a-propanocyclopenta[8]annulen-5-yl 1-(4-(((2*S*,3*S*,6*R*)-6-(4-amino-2-oxopyrimidin-1(2*H*)-yl)-3-((*S*)-3-amino-5-(1-methylguanidino)pentanamido)-3,6-dihydro-2*H*-pyran-2-carboxamido)methyl)-1*H*-1,2,3-triazol-1-yl)-3,6,9,12-tetraoxa-15-thiaheptadecan-17-oate (40).** Synthesized according to general method C using **31** and **32**. Residue purified via flash chromatography (C18, 10-100% $CH_3CN$ in $H_2O$, 0.1% formic acid), dissolved in 0.3% methanolic HCl and concentrated to give **40** (as the tri HCl salt) as a white powder (15.5 mg, 49%): $^1$H NMR (600 MHz, MeOD) δ 7.95 (s, 1H), 7.60 – 7.55 (m, 1H), 6.59 (s, 1H), 6.31 (dd, *J* = 17.4, 11.3 Hz, 1H), 6.08 (dd, *J* = 10.2, 2.2 Hz, 1H), 5.95 (s, 1H), 5.84 (dd, *J* = 10.1, 2.3 Hz, 1H), 5.73 (d, *J* = 8.4 Hz, 1H), 5.19 – 5.14 (m, 2H), 4.79 (d, *J* = 9.2 Hz, 1H), 4.56 (t, *J* = 5.1 Hz, 2H), 4.44 (s, 2H), 4.26 (s, 1H), 3.90 (t, *J* = 4.9 Hz, 2H), 3.84 (s, 1H), 3.66 (td, *J* = 6.4, 1.2 Hz, 2H), 3.63 – 3.55 (m, 12H), 3.50 (d, *J* = 6.2 Hz, 1H), 3.48 – 3.41 (m, 1H), 3.37 – 3.33 (m, 1H), 3.28 (d, *J* = 14.9 Hz, 1H), 3.24 (d, *J* = 14.9 Hz, 1H), 3.02 (s, 3H), 2.79 (t, *J* = 6.4 Hz, 2H), 2.48 (dd, *J* = 13.8, 5.0 Hz, 1H), 2.39 – 2.36 (m, 1H), 2.33 (p, *J* = 6.9 Hz, 2H), 2.30 – 2.24 (m, 1H), 2.19 – 2.12 (m, 2H), 1.93 (s, 1H), 1.82 (dq, *J* = 14.4, 3.1 Hz, 1H), 1.78 – 1.66 (m, 2H), 1.65 – 1.53 (m, 2H), 1.50 – 1.47 (m, 1H), 1.45 (s, 3H), 1.38 (d, *J* = 16.0 Hz, 1H), 1.36 – 1.31 (m, 1H), 1.18 – 1.12 (m, 1H), 1.15 (s, 3H), 0.93 (d, *J* = 7.1 Hz, 3H), 0.73 (d, *J* = 6.8 Hz, 3H). $^{13}$C NMR (126 MHz, $CDCl_3$) δ 219.7, 172.6, 170.7, 170.3, 167.8, 158.2, 158.1, 157.9, 143.3, 141.3, 135.0, 127.3, 125.2, 116.6, 81.2, 80.5, 78.0, 75.4, 71.8, 71.6, 71.51, 71.5, 71.48 (2C), 71.3, 71.1, 70.3, 59.3, 51.4, 47.6, 46.8, 46.6, 46.0, 45.3, 43.1, 42.8, 38.2, 37.8, 36.6, 35.6, 35.4, 35.3, 32.9, 32.2,

31.5, 28.8, 28.3, 28.0, 25.9, 17.1, 15.5, 11.8. Calcd for $C_{50}H_{79}N_{12}O_{11}S_1$ $[M+H]^+$: 1099.5969; Found 1099.6003.

**(3a*R*,4*R*,5*R*,7*S*,8*S*,9*R*,9a*S*,12*R*)-8-Hydroxy-4,7,9,12-tetramethyl-3-oxo-7-vinyldecahydro-4,9a-propanocyclopenta[8]annulen-5-yl 2-((2-(4-(2-((2*S*,3*S*,6*R*)-6-(4-amino-2-oxopyrimidin-1(2*H*)-yl)-3-((*S*)-3-amino-5-(1-methylguanidino)pentanamido)-3,6-dihydro-2*H*-pyran-2-carboxamido)ethyl)-1*H*-1,2,3-triazol-1-yl)ethyl)thio)acetate (41).** Synthesized according to general method D using **27** and **33**. Residue purified via flash chromatography (C18, 10-100% $CH_3CN$ in $H_2O$, 0.1% formic acid), dissolved in 0.3% methanolic HCl and concentrated to give **41** (as the tri HCl salt) as a white powder (18.9 mg, 73%): $^1$H NMR (500 MHz, MeOD) δ 8.41 (s, 1H), 7.96 (dd, *J* = 7.7, 2.6 Hz, 1H), 6.59 (s, 1H), 6.36 – 6.28 (m, 1H), 6.22 – 6.14 (m, 2H), 5.91 (d, *J* = 9.5 Hz, 1H), 5.74 (d, *J* = 8.3 Hz, 1H), 5.19 – 5.11 (m, 2H), 4.88 – 4.80 (m, 3H), 4.26 (dd, *J* = 9.3, 2.5 Hz, 1H), 3.71 – 3.55 (m, 4H), 3.52 (dd, *J* = 6.2, 2.5 Hz, 1H), 3.47 (q, *J* = 6.2 Hz, 1H), 3.35 (d, *J* = 17.3 Hz, 1H), 3.30 (d, *J* = 17.3 Hz, 1H), 3.25 – 3.21 (m, 2H), 3.11 (s, 3H), 3.09 – 3.05 (m, 2H), 2.75 (dt, *J* = 16.1, 3.3 Hz, 1H), 2.64 (ddd, *J* = 15.7, 8.1, 2.4 Hz, 1H), 2.39 (s, 1H), 2.36 – 2.24 (m, 2H), 2.21 – 2.07 (m, 4H), 1.82 (dt, *J* = 14.3, 2.9 Hz, 1H), 1.75 – 1.67 (m, 1H), 1.66 – 1.52 (m, 2H), 1.46 (m, 1H), 1.45 (s, 3H), 1.40 – 1.33 (m, 2H), 1.20 – 1.11 (m, 1H), 1.16 (s, 3H), 0.94 (d, *J* = 7.1 Hz, 3H), 0.73 (d, *J* = 6.8 Hz, 3H). $^{13}$C NMR (126 MHz, MeOD) δ 219.6, 171.4, 170.6, 170.3, 161.4, 158.3, 148.5, 147.3, 144.4, 141.4, 135.8, 127.6, 126.2, 116.5, 95.9, 81.0, 77.8, 75.3, 71.5, 59.2, 52.2, 48.6, 48.2, 46.8, 46.7, 46.0, 45.3, 43.1, 39.0, 38.3, 38.1, 37.7, 36.8, 35.3, 34.8, 33.0, 31.5, 30.7, 28.3, 28.1, 25.8, 25.0, 17.2, 15.4, 11.8. Calcd for $C_{45}H_{69}N_{12}O_8S_1$ $[M+H]^+$: 937.5076; Found 937.5054.

**(3a*R*,4*R*,5*R*,7*S*,8*S*,9*R*,9a*S*,12*R*)-8-Hydroxy-4,7,9,12-tetramethyl-3-oxo-7-vinyldecahydro-4,9a-propanocyclopenta[8]annulen-5-yl 2-((2-(2-(4-(2-((2*S*,3*S*,6*R*)-6-(4-amino-2-**

**oxopyrimidin-1(2*H*)-yl)-3-((*S*)-3-amino-5-(1-methylguanidino)pentanamido)-3,6-dihydro-2*H*-pyran-2-carboxamido)ethyl)-1*H*-1,2,3-triazol-1-yl)ethoxy)ethyl)thio)acetate (42).**

Synthesized according to general method D using **28** and **33**. Residue purified via flash chromatography (C18, 10-100% $CH_3CN$ in $H_2O$, 0.1% formic acid), dissolved in 0.3% methanolic HCl and concentrated to give **42** (as the tri HCl salt) as a white powder (16.2 mg, 59%): $^1$H NMR (600 MHz, MeOD) δ 7.90 (s, 1H), 7.86 (d, *J* = 7.8 Hz, 1H), 6.64 (s, 1H), 6.35 – 6.29 (m, 1H), 6.20 – 6.14 (m, 2H), 5.92 (ddd, *J* = 10.2, 2.7, 1.5 Hz, 1H), 5.73 (d, *J* = 8.3 Hz, 1H), 5.19 – 5.13 (m, 2H), 4.88 (dq, *J* = 9.3, 2.6 Hz, 1H), 4.58 (t, *J* = 4.9 Hz, 2H), 4.30 (d, *J* = 9.4 Hz, 1H), 3.88 (t, *J* = 5.0 Hz, 2H), 3.71 – 3.65 (m, 1H), 3.67 (t, *J* = 6.3 Hz, 2H), 3.61 – 3.49 (m, 4H), 3.48 – 3.42 (m, 1H), 3.23 (d, *J* = 14.8 Hz, 1H), 3.19 (d, *J* = 14.8 Hz, 1H), 3.12 (s, 3H), 2.93 (t, *J* = 7.2 Hz, 2H), 2.78 (t, *J* = 6.2 Hz, 2H), 2.77 – 2.73 (m, 1H), 2.68 (dd, *J* = 15.6, 7.9 Hz, 1H), 2.40 (s, 1H), 2.36 – 2.26 (m, 2H), 2.20 – 2.08 (m, 4H), 1.83 (dq, *J* = 14.4, 3.0 Hz, 1H), 1.72 (ddd, *J* = 13.2, 11.1, 9.0 Hz, 1H), 1.66 – 1.53 (m, 2H), 1.50 – 1.46 (m, 1H), 1.45 (s, 3H), 1.39 – 1.33 (m, 2H), 1.19 – 1.13 (m, 1H), 1.16 (s, 3H), 0.95 (d, *J* = 7.0 Hz, 3H), 0.73 (d, *J* = 6.8 Hz, 3H). $^{13}$C NMR (126 MHz, MeOD) δ 218.3, 170.0, 169.2, 169.0, 163.1, 156.9, 149.7, 144.7, 144.5, 139.9, 134.2, 125.1, 123.3, 115.1, 95.0, 79.6, 76.2, 74.0, 70.1, 69.8, 68.7, 57.9, 50.0, 47.2, 46.7, 45.4, 45.3, 44.6, 43.9, 41.7, 38.5, 36.83, 36.77, 36.4, 35.4, 33.9, 31.6, 30.1, 29.4, 26.9, 26.7, 24.8, 24.5, 17.0, 15.8, 14.1, 10.5. Calcd for $C_{47}H_{73}N_{12}O_9S_1$ $[M+H]^+$: 981.5339; Found 981.5330.

**(3a*R*,4*R*,5*R*,7*S*,8*S*,9*R*,9a*S*,12*R*)-8-Hydroxy-4,7,9,12-tetramethyl-3-oxo-7-vinyldecahydro-4,9a-propanocyclopenta[8]annulen-5-yl 2-((2-(2-(2-(4-(2-((2*S*,3*S*,6*R*)-6-(4-amino-2-oxopyrimidin-1(2*H*)-yl)-3-((*S*)-3-amino-5-(1-methylguanidino)pentanamido)-3,6-dihydro-2*H*-pyran-2-carboxamido)ethyl)-1*H*-1,2,3-triazol-1-yl)ethoxy)ethoxy)ethyl)thio)acetate (43).**

Synthesized according to general method D using **29** and **33**. Residue purified via flash

chromatography (C18, 10-100% $CH_3CN$ in $H_2O$, 0.1% formic acid), dissolved in 0.3% methanolic HCl and concentrated to give **43** (as the tri HCl salt) as a white powder (17.7 mg, 62%): $^1$H NMR (500 MHz, MeOD) δ 7.90 (s, 1H), 7.88 (d, *J* = 8.0 Hz, 1H), 6.64 (s, 1H), 6.36 – 6.28 (m, 1H), 6.20 (d, *J* = 7.8 Hz, 1H), 6.17 (d, *J* = 10.9 Hz, 1H), 5.94 – 5.90 (m, 1H), 5.74 (d, *J* = 8.3 Hz, 1H), 5.20 – 5.14 (m, 2H), 4.90 – 4.83 (m, 1H), 4.58 (t, *J* = 5.0 Hz, 2H), 4.31 (d, *J* = 9.3 Hz, 1H), 3.91 (t, *J* = 5.0 Hz, 2H), 3.71 – 3.50 (m, 11H), 3.49 – 3.42 (m, 1H), 3.30 (d, *J* = 14.8 Hz, 1H), 3.25 (d, *J* = 14.9 Hz, 1H), 3.12 (s, 3H), 2.93 (t, *J* = 7.2 Hz, 2H), 2.80 (t, *J* = 6.3 Hz, 2H), 2.78 – 2.65 (m, 2H), 2.40 (s, 1H), 2.37 – 2.26 (m, 2H), 2.22 – 2.08 (m, 4H), 1.83 (dq, *J* = 14.3, 2.9 Hz, 1H), 1.72 (ddd, *J* = 13.3, 11.2, 9.0 Hz, 1H), 1.66 – 1.53 (m, 2H), 1.50 – 1.47 (m, 1H), 1.46 (s, 3H), 1.41 – 1.33 (m, 2H), 1.19 – 1.12 (m, 1H), 1.16 (s, 3H), 0.95 (d, *J* = 7.0 Hz, 3H), 0.74 (d, *J* = 6.7 Hz, 3H). $^{13}$C NMR (126 MHz, MeOD) δ 219.7, 171.4, 170.7, 170.3, 164.4, 162.4, 158.3, 150.2, 146.4, 145.9, 141.3, 135.7, 126.4, 124.7, 116.5, 96.2, 81.0, 77.6, 75.4, 71.7, 71.4, 71.21, 71.15, 70.4, 59.3, 51.4, 48.5, 48.1, 46.8, 46.6, 46.0, 45.3, 43.1, 39.9, 38.2, 37.7, 36.8, 35.4, 35.3, 33.0, 31.5, 30.7, 28.3, 28.0, 26.2, 25.8, 17.1, 15.5, 11.8. Calcd for $C_{49}H_{77}N_{12}O_{10}S_1$ $[M+H]^+$: 1025.5601; Found 1025.5576.

**(3a*R*,4*R*,5*R*,7*S*,8*S*,9*R*,9a*S*,12*R*)-8-Hydroxy-4,7,9,12-tetramethyl-3-oxo-7-vinyldecahydro-4,9a-propanocyclopenta[8]annulen-5-yl 1-(4-(2-((2*S*,3*S*,6*R*)-6-(4-amino-2-oxopyrimidin-1(2*H*)-yl)-3-((*S*)-3-amino-5-(1-methylguanidino)pentanamido)-3,6-dihydro-2*H*-pyran-2-carboxamido)ethyl)-1*H*-1,2,3-triazol-1-yl)-3,6,9-trioxa-12-thiatetradecan-14-oate (44).** Synthesized according to general method D using **30** and **33**. Residue purified via flash chromatography (C18, 10-100% $CH_3CN$ in $H_2O$, 0.1% formic acid), dissolved in 0.3% methanolic HCl and concentrated to give **44** (as the tri HCl salt) as a white powder (14.2 mg, 48%): $^1$H NMR (500 MHz, MeOD) δ 7.88 (s, 1H), 7.72 (d, *J* = 7.6 Hz, 1H), 6.65 – 6.62 (m, 1H),

6.36 – 6.29 (m, 1H), 6.13 (d, *J* = 9.7 Hz, 1H), 6.09 (d, *J* = 7.6 Hz, 1H), 5.92 – 5.89 (m, 1H), 5.74 (d, *J* = 8.3 Hz, 1H), 5.20 – 5.15 (m, 2H), 4.89 – 4.85 (m, 1H), 4.58 (t, *J* = 5.0 Hz, 2H), 4.28 (d, *J* = 9.4 Hz, 1H), 3.91 (t, *J* = 5.1 Hz, 2H), 3.69 (t, *J* = 6.4 Hz, 2H), 3.69 – 3.49 (m, 15H), 3.48 – 3.41 (m, 1H), 3.31 (d, *J* = 14.9 Hz, 1H), 3.26 (d, *J* = 14.8 Hz, 1H), 3.11 (s, 3H), 2.92 (t, *J* = 7.1 Hz, 2H), 2.81 (t, *J* = 6.3 Hz, 2H), 2.79 – 2.65 (m, 2H), 2.40 (s, 1H), 2.37 – 2.31 (m, 1H), 2.31 – 2.26 (m, 1H), 2.21 – 2.08 (m, 4H), 1.83 (dq, *J* = 14.2, 2.9 Hz, 1H), 1.72 (ddd, *J* = 13.1, 11.1, 9.0 Hz, 1H), 1.66 – 1.53 (m, 2H), 1.50 – 1.44 (m, 1H), 1.46 (s, 3H), 1.41 – 1.33 (m, 2H), 1.19 – 1.13 (m, 1H), 1.17 (s, 3H), 0.95 (d, *J* = 7.0 Hz, 3H), 0.74 (d, *J* = 6.7 Hz, 3H). $^{13}$C NMR (126 MHz, MeOD) δ 219.7, 171.4, 170.7, 170.5, 165.5, 164.6, 158.3, 154.9, 145.9, 144.6, 141.3, 135.1, 127.1, 124.7, 116.6, 96.9, 81.2, 77.7, 75.4, 71.8, 71.5 (2C), 71.4, 71.3, 71.1, 70.4, 59.3, 51.4, 48.6, 48.1, 46.8, 46.7, 46.0, 45.3, 43.1, 39.8, 38.2, 37.8, 36.8, 35.4, 35.3, 32.9, 31.5, 30.7, 28.3, 28.1, 26.2, 25.9, 17.1, 15.5, 11.8. Calcd for $C_{51}H_{81}N_{12}O_{11}S_1$ $[M+H]^+$: 1069.5863; Found 1069.5863.

**(3a*R*,4*R*,5*R*,7*S*,8*S*,9*R*,9a*S*,12*R*)-8-Hydroxy-4,7,9,12-tetramethyl-3-oxo-7-vinyldecahydro-4,9a-propanocyclopenta[8]annulen-5-yl 1-(4-(2-((2*S*,3*S*,6*R*)-6-(4-amino-2-oxopyrimidin-1(2*H*)-yl)-3-((*S*)-3-amino-5-(1-methylguanidino)pentanamido)-3,6-dihydro-2*H*-pyran-2-carboxamido)ethyl)-1*H*-1,2,3-triazol-1-yl)-3,6,9,12-tetraoxa-15-thiaheptadecan-17-oate (45).** Synthesized according to general method D using **31** and **33**. Residue purified via flash chromatography (C18, 10-100% $CH_3CN$ in $H_2O$, 0.1% formic acid), dissolved in 0.3% methanolic HCl and concentrated to give **45** (as the tri HCl salt) as a white powder (14.4 mg, 51%): $^1$H NMR (500 MHz, MeOD) δ 8.49 (s, 1H), 7.98 (d, *J* = 7.8 Hz, 1H), 6.61 (dt, *J* = 3.2, 1.8 Hz, 1H), 6.37 – 6.29 (m, 1H), 6.23 (d, *J* = 7.8 Hz, 1H), 6.18 (dt, *J* = 10.4, 2.1 Hz, 1H), 5.93 (ddd, *J* = 10.2, 2.7, 1.5 Hz, 1H), 5.75 (d, *J* = 8.3 Hz, 1H), 5.20 – 5.15 (m, 2H), 4.87 (dq, *J* = 9.2, 2.6

Hz, 1H), 4.82 (dq, *J* = 4.9, 2.6 Hz, 2H), 4.28 (d, *J* = 9.4 Hz, 1H), 4.02 (t, *J* = 4.7 Hz, 2H), 3.71 – 3.67 (m, 5H), 3.67 – 3.62 (m, 11H), 3.60 – 3.56 (m, 2H), 3.53 (d, *J* = 6.2 Hz, 1H), 3.52 – 3.46 (m, 1H), 3.32 (d, *J* = 14.9 Hz, 1H), 3.26 (d, *J* = 14.9 Hz, 1H), 3.15 – 3.11 (m, 2H), 3.12 (s, 3H), 2.82 (t, *J* = 6.4 Hz, 2H), 2.77 (dd, *J* = 15.8, 4.3 Hz, 1H), 2.66 (dd, *J* = 15.8, 8.0 Hz, 1H), 2.41 (s, 1H), 2.37 – 2.26 (m, 2H), 2.21 – 2.08 (m, 4H), 1.84 (dq, *J* = 14.3, 3.0 Hz, 1H), 1.72 (ddd, *J* = 13.2, 11.1, 9.0 Hz, 1H), 1.67 – 1.54 (m, 2H), 1.51 – 1.43 (m, 1H), 1.47 (s, 3H), 1.41 – 1.35 (m, 2H), 1.20 – 1.13 (m, 1H), 1.17 (s, 3H), 0.95 (d, *J* = 7.1 Hz, 3H), 0.75 (d, *J* = 6.7 Hz, 3H). $^{13}$C NMR (126 MHz, MeOD) δ 219.7, 171.4, 170.7, 161.4, 158.3, 148.5, 147.3, 143.4, 141.3, 135.8, 128.4, 126.2, 116.5, 95.9, 81.0, 77.8, 75.4, 71.7, 71.49, 71.46, 71.40, 71.37, 71.34, 71.25, 71.2, 69.5, 59.3, 53.8, 49.8, 48.5, 48.1, 46.8, 46.7, 46.0, 45.3, 43.1, 38.8, 38.2, 38.1, 37.8, 36.8, 35.4, 35.3, 32.9, 31.5, 30.7, 28.3, 28.1, 25.8, 24.7, 17.1, 15.4, 11.8. Calcd for $C_{53}H_{85}N_{12}O_{12}S_1$ $[M+H]^+$: 1113.6125; Found 1113.6095.

**But-3-yn-1-yl 4-methylbenzenesulfonate (46).** Synthesized according to general method A using 3-butynol. Residue purified via flash chromatography ($SiO_2$, 5-40% EtOAC/Hexanes) to give **46** as clear oil (3.605 g, 77%): Spectral data were in accordance with those previously reported.[79]

**Pent-4-yn-1-yl 4-methylbenzenesulfonate (47).** Synthesized according to general method A using 4-pentynol. Residue purified via flash chromatography ($SiO_2$, 5-40% EtOAC/Hexanes) to give **47** as clear oil (4.393 g, 88%): Spectral data were in accordance with those previously reported.[80]

**Hex-5-yn-1-yl 4-methylbenzenesulfonate (48).** Synthesized according to general method A using 5-hexynol. Residue purified via flash chromatography ($SiO_2$, 5-40% EtOAC/Hexanes) to

give **48** as clear oil (4.084 g, 77%): Spectral data were in accordance with those previously reported.[81]

**Hept-6-yn-1-yl 4-methylbenzenesulfonate (49).** Synthesized according to general method A using 6-hexynol. Residue purified via flash chromatography ($SiO_2$, 5-40% EtOAC/Hexanes) to give **49** as clear oil (5.4515 g, 98%): Spectral data were in accordance with those previously reported.[82]

**(2*R*,3*S*,4*R*,5*R*,8*R*,10*R*,11*R*,12*S*,13*S*,14*R*)-2-Ethyl-3,4,10-trihydroxy-13-(((2*R*,4*R*,5*S*,6*S*)-5-hydroxy-4-methoxy-4,6-dimethyltetrahydro-2*H*-pyran-2-yl)oxy)-11-(((2*S*,3*R*,4*S*,6*R*)-3-hydroxy-6-methyl-4-(methylamino)tetrahydro-2*H*-pyran-2-yl)oxy)-3,5,6,8,10,12,14-heptamethyl-1-oxa-6-azacyclopentadecan-15-one (51).** The reaction was carried out according to a literature procedure.[73] To a stirring solution of azithromycin (**50**) (800 mg, 1.07 mmol), sodium acetate (702 mg, 2.33 mmol) and 80 % aqueous MeOH (25 mL), was added $I_2$ (290 mg, 1.14 mmol) in two portions over one minute, turning the solution a deep brown. At 10, 45, 75, and 120 minutes 1 M NaOH (0.5 mL each) was added, keeping the pH between 8-9. During this time the reaction gradually became colorless (at 2.5 hours). Reaction was allowed to proceed for a total of 3 hours. The reaction contents were poured into a separatory funnel containing aqueous ammonia (75 mL $H_2O$, 3 mL conc. $NH_4OH$), immediately becoming opaque white, and was extracted with $CHCl_3$ (30 mL) and ethyl acetate (5x30 mL), during the extractions additional ammonia was added to maintain a pH of >11. The combined organics were washed with brine made basic with ammonia (20 mL brine, 3 mL conc. $NH_4OH$), dried over $Na_2SO_4$, and concentrated to afford a snowy white powder. The residue was purified using flash chromatography ($SiO_2$, 11% (10:1 $CH_3OH$:$NH_4OH$) in $CH_2Cl_2$) to give **51** (716 mg, 91%) as a white powder: Spectral data were in accordance with those previously reported.[83]

**(2*R*,3*S*,4*R*,5*R*,8*R*,10*R*,11*R*,12*S*,13*S*,14*R*)-11-(((2*S*,3*R*,4*S*,6*R*)-4-(But-3-yn-1-yl(methyl)amino)-3-hydroxy-6-methyltetrahydro-2*H*-pyran-2-yl)oxy)-2-ethyl-3,4,10-trihydroxy-13-(((2*R*,4*R*,5*S*,6*S*)-5-hydroxy-4-methoxy-4,6-dimethyltetrahydro-2*H*-pyran-2-yl)oxy)-3,5,6,8,10,12,14-heptamethyl-1-oxa-6-azacyclopentadecan-15-one (52).** Synthesized according to general method B from **46** and **51**. Residue purified via flash chromatography ($SiO_2$, 6% (10:1 $CH_3OH$:$NH_4OH$) in $CH_2Cl_2$) to give **52** as white powder (35.3 mg, 69%): Spectral data were in accordance with those previously reported.[73]

**(2*R*,3*S*,4*R*,5*R*,8*R*,10*R*,11*R*,12*S*,13*S*,14*R*)-2-Ethyl-3,4,10-trihydroxy-13-(((2*R*,4*R*,5*S*,6*S*)-5-hydroxy-4-methoxy-4,6-dimethyltetrahydro-2*H*-pyran-2-yl)oxy)-11-(((2*S*,3*R*,4*S*,6*R*)-3-hydroxy-6-methyl-4-(methyl(pent-4-yn-1-yl)amino)tetrahydro-2*H*-pyran-2-yl)oxy)-3,5,6,8,10,12,14-heptamethyl-1-oxa-6-azacyclopentadecan-15-one (53).** Synthesized according to general method B from **47** and **51**. Residue purified via flash chromatography ($SiO_2$, 7% (10:1 $CH_3OH$:$NH_4OH$) in $CH_2Cl_2$) to give **53** as white powder (22.8 mg, 43%): Spectral data were in accordance with those previously reported.[73]

**(2*R*,3*S*,4*R*,5*R*,8*R*,10*R*,11*R*,12*S*,13*S*,14*R*)-2-Ethyl-11-(((2*S*,3*R*,4*S*,6*R*)-4-(hex-5-yn-1-yl(methyl)amino)-3-hydroxy-6-methyltetrahydro-2*H*-pyran-2-yl)oxy)-3,4,10-trihydroxy-13-(((2*R*,4*R*,5*S*,6*S*)-5-hydroxy-4-methoxy-4,6-dimethyltetrahydro-2*H*-pyran-2-yl)oxy)-3,5,6,8,10,12,14-heptamethyl-1-oxa-6-azacyclopentadecan-15-one (54).** Synthesized according to general method B from **48** and **51**. Residue purified via flash chromatography ($SiO_2$, 7% (10:1 $CH_3OH$:$NH_4OH$) in $CH_2Cl_2$) to give **54** as white powder (27.1 mg, 51%): Spectral data were in accordance with those previously reported.[73]

**(2*R*,3*S*,4*R*,5*R*,8*R*,10*R*,11*R*,12*S*,13*S*,14*R*)-2-Ethyl-11-(((2*S*,3*R*,4*S*,6*R*)-4-(hept-6-yn-1-yl(methyl)amino)-3-hydroxy-6-methyltetrahydro-2*H*-pyran-2-yl)oxy)-3,4,10-trihydroxy-13-

**(((2*R*,4*R*,5*S*,6*S*)-5-hydroxy-4-methoxy-4,6-dimethyltetrahydro-2*H*-pyran-2-yl)oxy)-3,5,6,8,10,12,14-heptamethyl-1-oxa-6-azacyclopentadecan-15-one (55).** Synthesized according to general method B from **49** and **51**. Residue purified via flash chromatography ($SiO_2$, 7% (10:1 $CH_3OH$:$NH_4OH$) in $CH_2Cl_2$) to give **55** as white powder (32.2 mg, 59%): $^1$H NMR (500 MHz, MeOD) δ 5.05 (d, *J* = 4.8 Hz, 1H), 4.87 – 4.84 (m, 1H), 4.55 (d, *J* = 7.3 Hz, 1H), 4.25 (dd, *J* = 4.7, 2.0 Hz, 1H), 4.24 – 4.18 (m, 1H), 3.75 (dqd, *J* = 12.1, 5.9, 2.0 Hz, 1H), 3.68 (d, *J* = 6.9 Hz, 1H), 3.62 (d, *J* = 1.7 Hz, 1H), 3.37 (s, 3H), 3.23 (dd, *J* = 10.3, 7.3 Hz, 1H), 3.04 (d, *J* = 9.5 Hz, 1H), 2.84 – 2.76 (m, 2H), 2.73 (ddd, *J* = 12.1, 10.3, 3.9 Hz, 1H), 2.60 (ddd, *J* = 12.4, 8.7, 6.1 Hz, 1H), 2.54 (dd, *J* = 12.1, 2.6 Hz, 1H), 2.49 – 2.43 (m, 1H), 2.43 (d, *J* = 15.1 Hz, 1H), 2.30 (s, 3H), 2.29 (s, 3H), 2.20 – 2.13 (m, 4H), 2.01 (pd, *J* = 7.4, 3.9 Hz, 2H), 1.91 – 1.83 (m, 1H), 1.77 (d, *J* = 14.7 Hz, 1H), 1.72 (ddd, *J* = 12.5, 4.0, 2.1 Hz, 1H), 1.58 (dd, *J* = 15.2, 5.1 Hz, 1H), 1.56 – 1.41 (m, 7H), 1.37 (dd, *J* = 15.0, 8.4 Hz, 1H), 1.33 (s, 3H), 1.28 (d, *J* = 6.2 Hz, 3H), 1.26 (s, 3H), 1.21 (d, *J* = 7.5 Hz, 3H), 1.22 – 1.19 (m, 1H), 1.18 (d, *J* = 6.0 Hz, 3H), 1.10 (s, 3H), 1.08 (d, *J* = 7.1 Hz, 3H), 1.06 (d, *J* = 7.6 Hz, 3H), 0.93 (d, *J* = 7.0 Hz, 3H), 0.90 (t, *J* = 7.5 Hz, 3H). $^{13}$C NMR (126 MHz, MeOD) δ 179.7, 104.0, 96.4, 84.6, 79.7, 79.5, 78.2, 75.7, 75.6, 75.1, 74.5, 72.4, 70.9, 69.5, 69.2, 66.4, 65.3, 63.7, 54.7, 50.1, 46.8, 43.5, 43.4, 37.4, 36.7, 36.1, 31.9, 29.6, 28.6, 28.0, 27.8, 27.5, 22.4, 22.3, 22.0, 21.7, 19.1, 19.00, 18.97, 17.3, 15.6, 11.6, 9.9, 7.6. Calcd for $C_{44}H_{81}N_2O_{12}$ $[M+H]^+$: 829.5784; Found 829.5806.

**(3a*R*,4*R*,5*R*,7*S*,8*S*,9*R*,9a*S*,12*R*)-7-(2-(4-(2-(((2*S*,3*R*,4*S*,6*R*)-2-(((2*R*,3*S*,4*R*,5*R*,8*R*,10*R*,11*R*,12*S*,13*S*,14*R*)-2-Ethyl-3,4,10-trihydroxy-13-(((2*R*,4*R*,5*S*,6*S*)-5-hydroxy-4-methoxy-4,6-dimethyltetrahydro-2*H*-pyran-2-yl)oxy)-3,5,6,8,10,12,14-heptamethyl-15-oxo-1-oxa-6-azacyclopentadecan-11-yl)oxy)-3-hydroxy-6-methyltetrahydro-2*H*-pyran-4-yl)(methyl)amino)ethyl)-1*H*-1,2,3-triazol-1-yl)ethyl)-8-**

**hydroxy-4,7,9,12-tetramethyl-3-oxodecahydro-4,9a-propanocyclopenta[8]annulen-5-yl 2-hydroxyacetate (57).** Synthesized according to general method E from **52** and **56**. Residue purified via flash chromatography ($SiO_2$, 9% (10:1 $CH_3OH$:$NH_4OH$) in $CH_2Cl_2$) to give **57** as white powder (6.7 mg, 44%): $^1$H NMR (500 MHz, MeOD) δ 7.83 (s, 1H), 5.69 (d, *J* = 8.3 Hz, 1H), 5.04 (d, *J* = 4.8 Hz, 1H), 4.88 – 4.84 (m, 1H), 4.58 (ddd, *J* = 13.6, 9.9, 6.5 Hz, 1H), 4.53 (d, *J* = 7.3 Hz, 1H), 4.45 (ddd, *J* = 13.7, 10.1, 5.3 Hz, 1H), 4.24 (dd, *J* = 4.7, 2.0 Hz, 1H), 4.20 (dd, *J* = 9.5, 6.2 Hz, 1H), 4.04 (d, *J* = 17.0 Hz, 1H), 3.98 (d, *J* = 17.1 Hz, 1H), 3.78 – 3.72 (m, 1H), 3.65 (dd, *J* = 6.6, 5.0 Hz, 2H), 3.61 (d, *J* = 1.7 Hz, 1H), 3.34 (s, 3H), 3.20 (dd, *J* = 10.3, 7.3 Hz, 1H), 3.04 (d, *J* = 9.5 Hz, 1H), 2.91 – 2.85 (m, 3H), 2.85 – 2.79 (m, 2H), 2.71 (ddd, *J* = 22.4, 11.3, 4.9 Hz, 2H), 2.57 (s, 1H), 2.43 (d, *J* = 15.2 Hz, 1H), 2.37 – 2.31 (m, 4H), 2.33 (s, 3H), 2.29 (d, *J* = 11.4 Hz, 1H), 2.26 (d, *J* = 2.5 Hz, 1H), 2.23 – 2.12 (m, 2H), 2.08 (ddd, *J* = 13.6, 10.0, 5.3 Hz, 1H), 2.04 – 1.96 (m, 3H), 1.90 – 1.80 (m, 3H), 1.78 – 1.70 (m, 3H), 1.65 – 1.53 (m, 3H), 1.53 – 1.44 (m, 2H), 1.40 (s, 3H), 1.40 – 1.34 (m, 2H), 1.33 (s, 3H), 1.28 (d, *J* = 6.1 Hz, 3H), 1.25 (s, 3H), 1.23 – 1.16 (m, 2H), 1.21 (d, *J* = 7.5 Hz, 3H), 1.18 (d, *J* = 6.0 Hz, 3H), 1.12 (s, 3H), 1.11 (s, 3H), 1.14 – 1.08 (m, 3H), 1.05 (d, *J* = 15.4 Hz, 1H), 1.04 (d, *J* = 7.6 Hz, 3H), 0.97 (d, *J* = 7.1 Hz, 3H), 0.93 (d, *J* = 7.0 Hz, 3H), 0.92 (d, *J* = 7.5 Hz, 3H), 0.72 (d, *J* = 6.8 Hz, 3H). $^{13}$C NMR (126 MHz, MeOD) δ 219.2, 179.8, 173.2, 147.6, 123.7, 104.0, 96.5, 84.6, 79.8, 79.5, 78.2, 75.6, 75.2, 74.4, 72.49, 72.46, 70.7, 70.4, 69.2, 66.5, 65.8, 61.9, 59.0, 54.5, 50.1, 47.8, 46.8, 46.7, 44.2, 43.8, 43.6, 43.3, 43.0, 41.6, 38.1, 36.8, 36.7, 36.6, 36.1, 35.3, 31.9, 31.6, 28.1, 27.94, 27.93, 27.7, 25.9, 25.3, 22.34, 22.31, 22.05, 22.01, 21.7, 19.1, 18.5, 17.3, 17.1, 15.6, 15.4, 11.6 (2C), 10.1, 7.7. Calcd for $C_{63}H_{110}N_5O_{17}$ $[M+H]^+$: 1208.7891; Found 1208.7897.

**(3a*R*,4*R*,5*R*,7*S*,8*S*,9*R*,9a*S*,12*R*)-7-(2-(4-(3-(((2*S*,3*R*,4*S*,6*R*)-2-(((2*R*,3*S*,4*R*,5*R*,8*R*,10*R*,11*R*,12*S*,13*S*,14*R*)-2-Ethyl-3,4,10-trihydroxy-13-(((2*R*,4*R*,5*S*,6*S*)-5-**

**hydroxy-4-methoxy-4,6-dimethyltetrahydro-2*H*-pyran-2-yl)oxy)-3,5,6,8,10,12,14-heptamethyl-15-oxo-1-oxa-6-azacyclopentadecan-11-yl)oxy)-3-hydroxy-6-methyltetrahydro-2*H*-pyran-4-yl)(methyl)amino)propyl)-1*H*-1,2,3-triazol-1-yl)ethyl)-8-hydroxy-4,7,9,12-tetramethyl-3-oxodecahydro-4,9a-propanocyclopenta[8]annulen-5-yl 2-hydroxyacetate (58).** Synthesized according to general method E from **53** and **56**. Residue purified via flash chromatography ($SiO_2$, 9% (10:1 $CH_3OH$:$NH_4OH$) in $CH_2Cl_2$) to give **58** as white powder (15.0mg, 98%): $^1$H NMR (500 MHz, MeOD) δ 7.67 (s, 1H), 5.58 (d, *J* = 8.3 Hz, 1H), 4.95 (d, *J* = 4.9 Hz, 1H), 4.78 – 4.76 (m, 1H), 4.50 – 4.46 (m, 1H), 4.44 (d, *J* = 7.3 Hz, 1H), 4.34 (ddd, *J* = 13.6, 9.8, 5.2 Hz, 1H), 4.15 (dd, *J* = 4.7, 2.0 Hz, 1H), 4.13 – 4.08 (m, 1H), 3.94 (d, *J* = 17.1 Hz, 1H), 3.87 (d, *J* = 17.1 Hz, 1H), 3.64 (ddt, *J* = 13.2, 7.1, 3.5 Hz, 1H), 3.57 (d, *J* = 7.0 Hz, 1H), 3.55 (d, *J* = 6.3 Hz, 1H), 3.52 (d, *J* = 1.6 Hz, 1H), 3.25 (s, 3H), 3.13 (dd, *J* = 10.3, 7.3 Hz, 1H), 2.94 (d, *J* = 9.4 Hz, 1H), 2.71 (td, *J* = 7.5, 4.4 Hz, 2H), 2.67 – 2.59 (m, 3H), 2.59 – 2.52 (m, 1H), 2.48 – 2.43 (m, 1H), 2.40 (dt, *J* = 12.8, 7.1 Hz, 1H), 2.33 (d, *J* = 15.2 Hz, 1H), 2.28 – 2.17 (m, 2H), 2.21 (s, 3H), 2.19 (s, 3H), 2.15 (s, 1H), 2.11 – 2.03 (m, 2H), 2.03 – 1.97 (m, 1H), 1.95 – 1.85 (m, 3H), 1.84 (s, 2H), 1.81 – 1.69 (m, 5H), 1.69 – 1.59 (m, 3H), 1.55 – 1.43 (m, 3H), 1.42 – 1.34 (m, 2H), 1.29 (s, 3H), 1.28 – 1.24 (m, 2H), 1.23 (s, 3H), 1.18 (d, *J* = 6.2 Hz, 3H), 1.15 (s, 3H), 1.14 – 1.04 (m, 2H), 1.11 (d, *J* = 7.5 Hz, 3H), 1.08 (d, *J* = 6.1 Hz, 3H), 1.03 – 0.97 (m, 3H), 1.02 (s, 3H), 1.00 (s, 3H), 0.96 (d, *J* = 7.7 Hz, 3H), 0.87 (d, *J* = 7.1 Hz, 3H), 0.83 (d, *J* = 6.9 Hz, 3H), 0.80 (t, *J* = 7.5 Hz, 3H), 0.62 (d, *J* = 6.8 Hz, 3H). $^{13}$C NMR (126 MHz, MeOD) δ 219.3, 179.7, 173.2, 149.3, 123.1, 104.0, 96.4, 84.6, 79.8, 79.5, 78.2, 75.7, 75.6, 75.1, 74.5, 72.5, 72.4, 70.8, 70.4, 69.2, 66.5, 65.5, 63.7, 61.9, 59.0, 54.1, 50.1, 47.7, 46.8, 46.7, 44.1, 43.7, 43.6, 43.4, 43.0, 41.6, 38.0, 37.3, 36.7, 36.6, 36.1, 35.3, 32.0, 31.6, 28.9, 28.1, 28.0, 27.8, 25.9, 24.0,

22.3 (2C), 22.0, 21.7, 19.1, 18.6, 17.3, 17.1, 15.6 (2C), 15.4, 11.6, 9.9, 7.6. Calcd for $C_{64}H_{112}N_5O_{17}$ $[M+H]^+$: 1222.8048; Found 1222.8036.

**(3a*R*,4*R*,5*R*,7*S*,8*S*,9*R*,9a*S*,12*R*)-7-(2-(4-(4-(((2*S*,3*R*,4*S*,6*R*)-2-(((2*R*,3*S*,4*R*,5*R*,8*R*,10*R*,11*R*,12*S*,13*S*,14*R*)-2-Ethyl-3,4,10-trihydroxy-13-(((2*R*,4*R*,5*S*,6*S*)-5-hydroxy-4-methoxy-4,6-dimethyltetrahydro-2*H*-pyran-2-yl)oxy)-3,5,6,8,10,12,14-heptamethyl-15-oxo-1-oxa-6-azacyclopentadecan-11-yl)oxy)-3-hydroxy-6-methyltetrahydro-2*H*-pyran-4-yl)(methyl)amino)butyl)-1*H*-1,2,3-triazol-1-yl)ethyl)-8-hydroxy-4,7,9,12-tetramethyl-3-oxodecahydro-4,9a-propanocyclopenta[8]annulen-5-yl 2-hydroxyacetate (59).** Synthesized according to general method E from **54** and **56**. Residue purified via flash chromatography ($SiO_2$, 8% (10:1 $CH_3OH$:$NH_4OH$) in $CH_2Cl_2$) to give **59** as white powder (9.8 mg, 65%): $^1$H NMR (500 MHz, MeOD) δ 7.75 (s, 1H), 5.68 (d, *J* = 8.3 Hz, 1H), 5.05 (d, *J* = 4.9 Hz, 1H), 4.87 – 4.83 (m, 1H), 4.61 – 4.56 (m, 1H), 4.55 (d, *J* = 7.3 Hz, 1H), 4.44 (ddd, *J* = 13.7, 9.7, 5.3 Hz, 1H), 4.25 (dd, *J* = 4.7, 2.0 Hz, 1H), 4.23 – 4.18 (m, 1H), 4.04 (d, *J* = 17.0 Hz, 1H), 3.97 (d, *J* = 17.1 Hz, 1H), 3.74 (dtd, *J* = 12.1, 6.0, 1.9 Hz, 1H), 3.67 (dd, *J* = 9.8, 6.5 Hz, 2H), 3.62 (d, *J* = 1.7 Hz, 1H), 3.35 (s, 3H), 3.23 (dd, *J* = 10.3, 7.3 Hz, 1H), 3.04 (d, *J* = 9.5 Hz, 1H), 2.84 – 2.78 (m, 2H), 2.76 – 2.68 (m, 1H), 2.71 (t, *J* = 7.5 Hz, 2H), 2.63 (dt, *J* = 14.0, 7.6 Hz, 1H), 2.55 (d, *J* = 11.8 Hz, 1H), 2.49 (q, *J* = 6.6 Hz, 1H), 2.43 (d, *J* = 15.1 Hz, 1H), 2.37 – 2.33 (m, 1H), 2.31 (s, 3H), 2.29 (s, 3H), 2.25 (s, 1H), 2.21 – 2.07 (m, 3H), 2.05 – 1.94 (m, 3H), 1.94 (s, 2H), 1.90 – 1.82 (m, 2H), 1.82 – 1.66 (m, 6H), 1.65 – 1.53 (m, 5H), 1.52 – 1.44 (m, 2H), 1.39 (s, 3H), 1.38 – 1.35 (m, 2H), 1.33 (s, 3H), 1.28 (d, *J* = 6.3 Hz, 3H), 1.25 (s, 3H), 1.21 (d, *J* = 7.5 Hz, 3H), 1.20 – 1.15 (m, 2H), 1.18 (d, *J* = 6.1 Hz, 3H), 1.13 – 1.08 (m, 3H), 1.12 (s, 3H), 1.10 (s, 3H), 1.06 (d, *J* = 7.6 Hz, 3H), 0.97 (d, *J* = 7.1 Hz, 3H), 0.92 (d, *J* = 7.4 Hz, 3H), 0.89 (t, *J* = 7.5 Hz, 3H), 0.72 (d, *J* = 6.8 Hz, 3H). $^{13}$C NMR (126 MHz, MeOD) δ 219.3, 179.7,

173.2, 149.4, 123.1, 104.0, 96.4, 84.6, 79.7, 79.5, 78.2, 75.7, 75.6, 75.1, 74.5, 72.4, 72.4, 70.8, 70.4, 69.2, 66.5, 65.5, 63.7, 61.9, 59.0, 54.2, 50.1, 47.7, 46.8, 46.7, 44.0, 43.7, 43.6, 43.4, 43.0, 41.6, 38.0, 37.5, 36.7, 36.6, 36.1, 35.3, 31.9, 31.6, 28.5, 28.3, 28.1, 28.0, 27.8, 26.2, 25.9, 22.4, 22.3, 22.0, 21.7, 19.1, 18.6, 17.3, 17.1, 15.6, 15.4, 11.6 (2C), 9.9, 7.6. Calcd for $C_{65}H_{114}N_5O_{17}$ $[M+H]^+$: 1236.8204; Found 1236.8190.

**(3a*R*,4*R*,5*R*,7*S*,8*S*,9*R*,9a*S*,12*R*)-7-(2-(4-(5-(((2*S*,3*R*,4*S*,6*R*)-2-(((2*R*,3*S*,4*R*,5*R*,8*R*,10*R*,11*R*,12*S*,13*S*,14*R*)-2-Ethyl-3,4,10-trihydroxy-13-(((2*R*,4*R*,5*S*,6*S*)-5-hydroxy-4-methoxy-4,6-dimethyltetrahydro-2*H*-pyran-2-yl)oxy)-3,5,6,8,10,12,14-heptamethyl-15-oxo-1-oxa-6-azacyclopentadecan-11-yl)oxy)-3-hydroxy-6-methyltetrahydro-2*H*-pyran-4-yl)(methyl)amino)pentyl)-1*H*-1,2,3-triazol-1-yl)ethyl)-8-hydroxy-4,7,9,12-tetramethyl-3-oxodecahydro-4,9a-propanocyclopenta[8]annulen-5-yl 2-hydroxyacetate (60).** Synthesized according to general method E from **55** and **56**. Residue purified via flash chromatography ($SiO_2$, 9% (10:1 $CH_3OH$:$NH_4OH$) in $CH_2Cl_2$) to give **60** as white powder (12.5 mg, 79%): $^1$H NMR (500 MHz, MeOD) δ 7.74 (s, 1H), 5.68 (d, *J* = 8.3 Hz, 1H), 5.05 (d, *J* = 4.9 Hz, 1H), 4.87 – 4.84 (m, 1H), 4.60 – 4.56 (m, 1H), 4.55 (d, *J* = 7.3 Hz, 1H), 4.44 (ddd, *J* = 13.6, 9.6, 5.3 Hz, 1H), 4.25 (dd, *J* = 4.6, 2.0 Hz, 1H), 4.23 – 4.18 (m, 1H), 4.04 (d, *J* = 17.1 Hz, 1H), 3.97 (d, *J* = 17.1 Hz, 1H), 3.75 (ddd, *J* = 10.8, 6.0, 2.0 Hz, 1H), 3.67 (t, *J* = 6.5 Hz, 2H), 3.62 (d, *J* = 1.8 Hz, 1H), 3.35 (s, 3H), 3.23 (dd, *J* = 10.3, 7.3 Hz, 1H), 3.04 (d, *J* = 9.5 Hz, 1H), 2.84 – 2.77 (m, 2H), 2.76 – 2.72 (m, 1H), 2.69 (t, *J* = 7.5 Hz, 2H), 2.63 – 2.52 (m, 2H), 2.49 – 2.43 (m, 1H), 2.43 (d, *J* = 15.2 Hz, 1H), 2.35 (p, *J* = 7.3 Hz, 2H), 2.31 (s, 3H), 2.29 (s, 3H), 2.25 (d, *J* = 2.6 Hz, 1H), 2.21 – 2.08 (m, 3H), 2.06 – 1.94 (m, 3H), 1.94 (s, 1H), 1.90 – 1.80 (m, 3H), 1.79 – 1.65 (m, 5H), 1.65 – 1.44 (m, 7H), 1.42 – 1.34 (m, 4H), 1.39 (s, 3H), 1.33 (s, 3H), 1.28 (d, *J* = 6.2 Hz, 3H), 1.25 (s, 3H), 1.21 (d, *J* = 7.5 Hz, 3H), 1.22 – 1.17 (m, 1H), 1.18 (d,

*J* = 6.0 Hz, 3H), 1.12 (s, 3H), 1.10 (s, 3H), 1.09 (d, *J* = 7.4 Hz, 3H), 1.06 (d, *J* = 7.6 Hz, 3H), 1.02 (d, *J* = 15.8 Hz, 1H), 0.97 (d, *J* = 7.1 Hz, 3H), 0.93 (d, *J* = 7.0 Hz, 3H), 0.90 (t, *J* = 7.4 Hz, 3H), 0.72 (d, *J* = 6.9 Hz, 3H). $^{13}$C NMR (126 MHz, MeOD) δ 219.2, 179.7, 173.2, 149.4, 123.1, 104.0, 96.4, 84.6, 79.7, 79.5, 78.2, 75.7, 75.6, 75.1, 74.5, 72.4, 72.3, 70.9, 70.4, 69.2, 66.5, 65.3, 63.7, 61.9, 59.0, 54.6, 50.1, 47.7, 46.8, 46.7, 44.0, 43.6, 43.6, 43.4, 43.0, 41.6, 38.0, 37.5, 36.7, 36.6, 36.1, 35.3, 31.8, 31.6, 30.5, 28.8, 28.1, 28.0, 27.9, 27.8, 26.3, 25.9, 22.4, 22.3, 22.0, 21.7, 19.1, 18.7, 17.3, 17.1, 15.6, 15.4, 11.6 (2C), 9.9, 7.6. Calcd for $C_{66}H_{116}N_5O_{17}$ $[M+H]^+$: 1250.8361; Found 1250.8383.

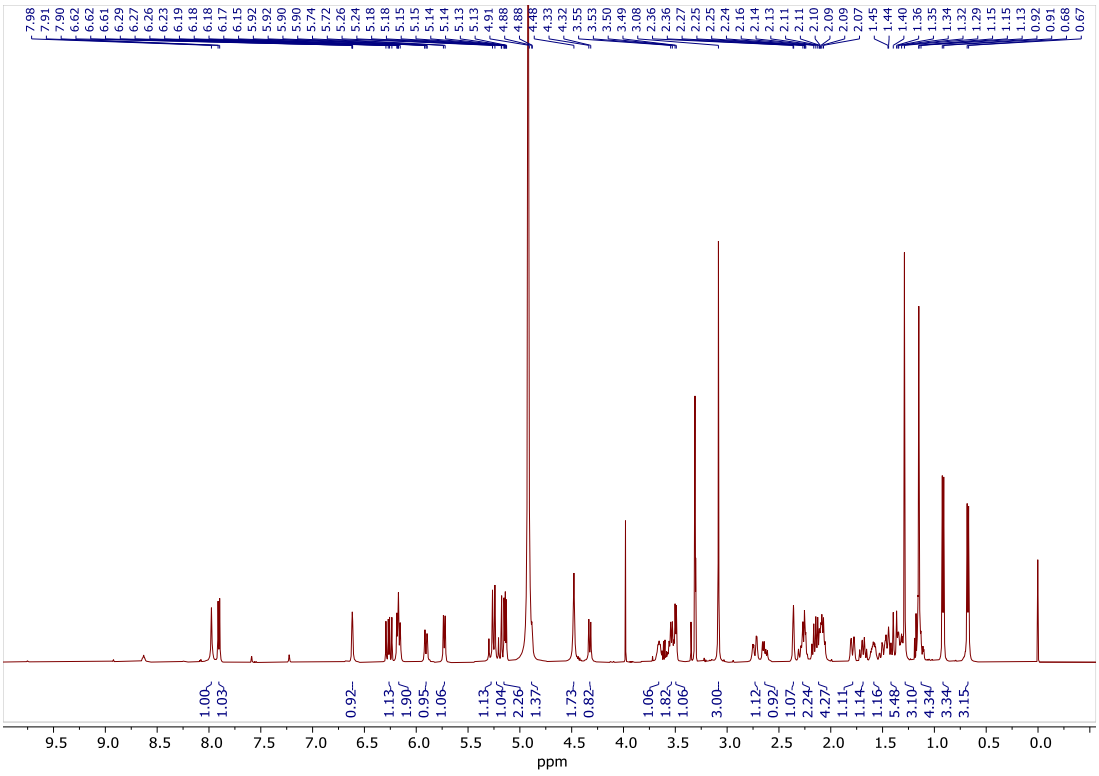

**Figure S1.** $^{1}$H-NMR (500 MHz, $CDCl_3$) of **34**.

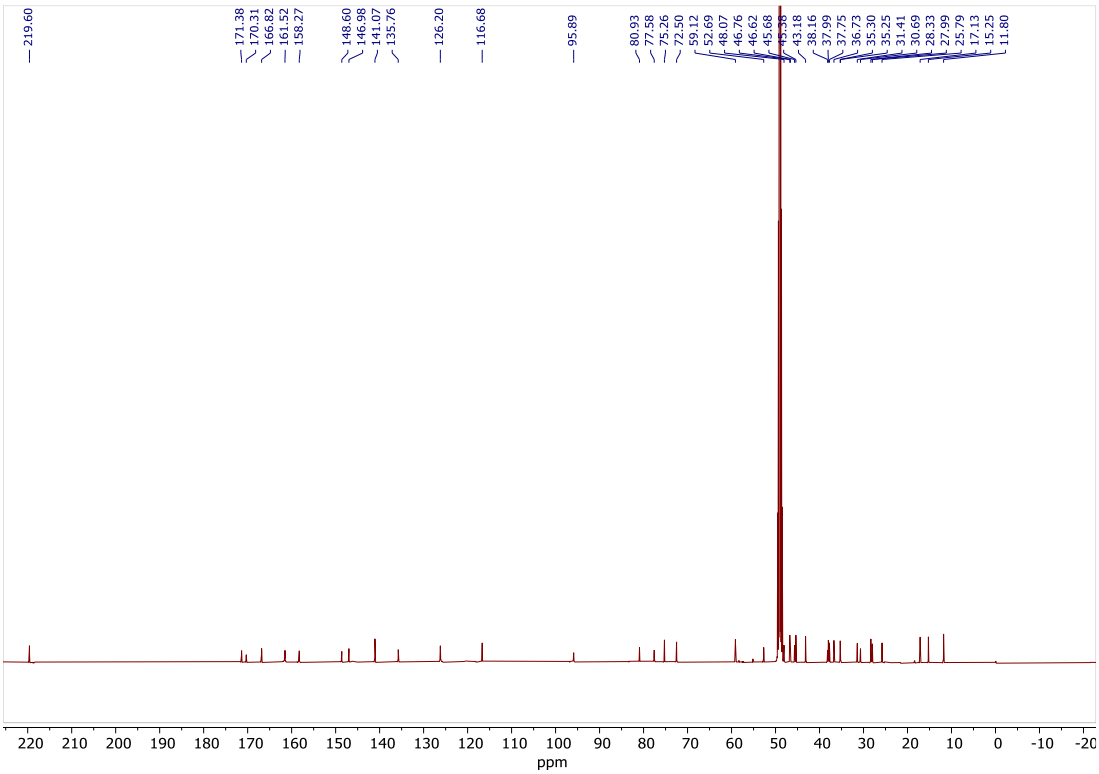

**Figure S2.** $^{13}$C-NMR (125 MHz, $CDCl_3$) of **34**.

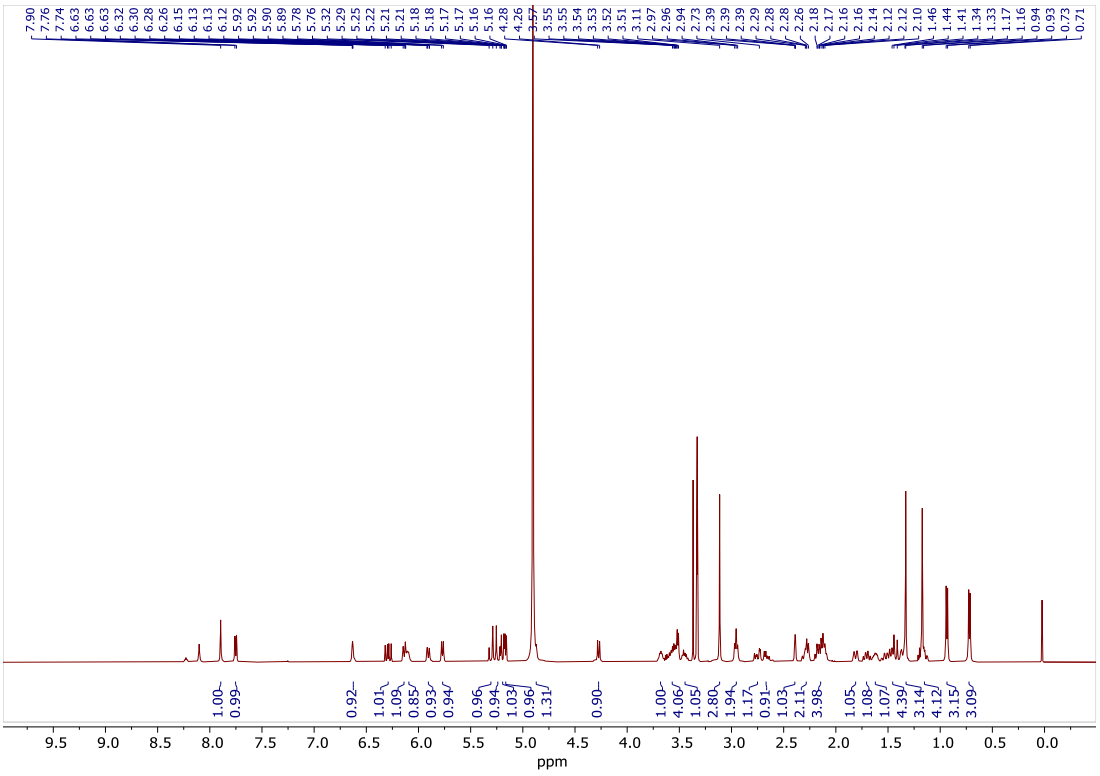


**Figure S3.** $^{1}$H-NMR (500 MHz, $CDCl_3$) of **35**.

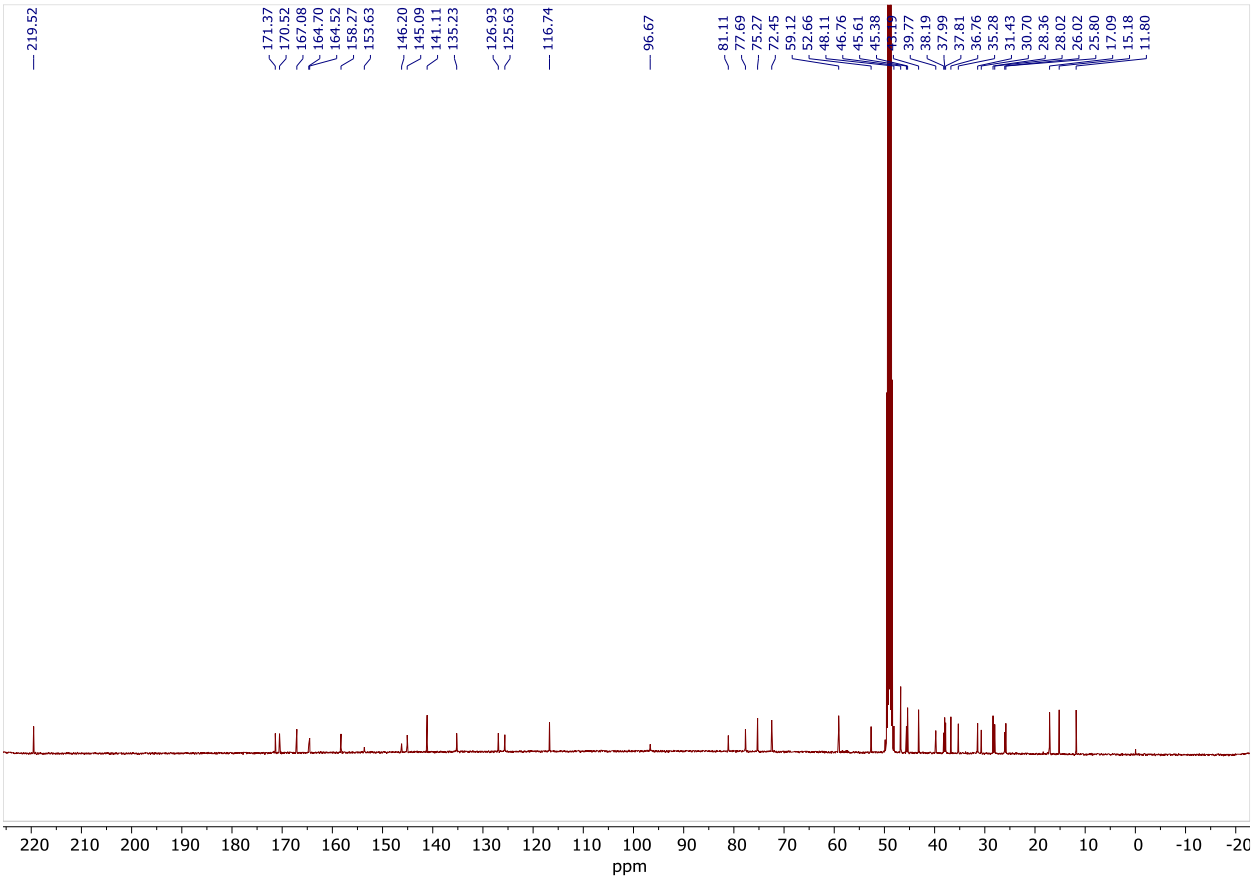

**Figure S4.** $^{13}$C-NMR (125 MHz, $CDCl_3$) of **35**.

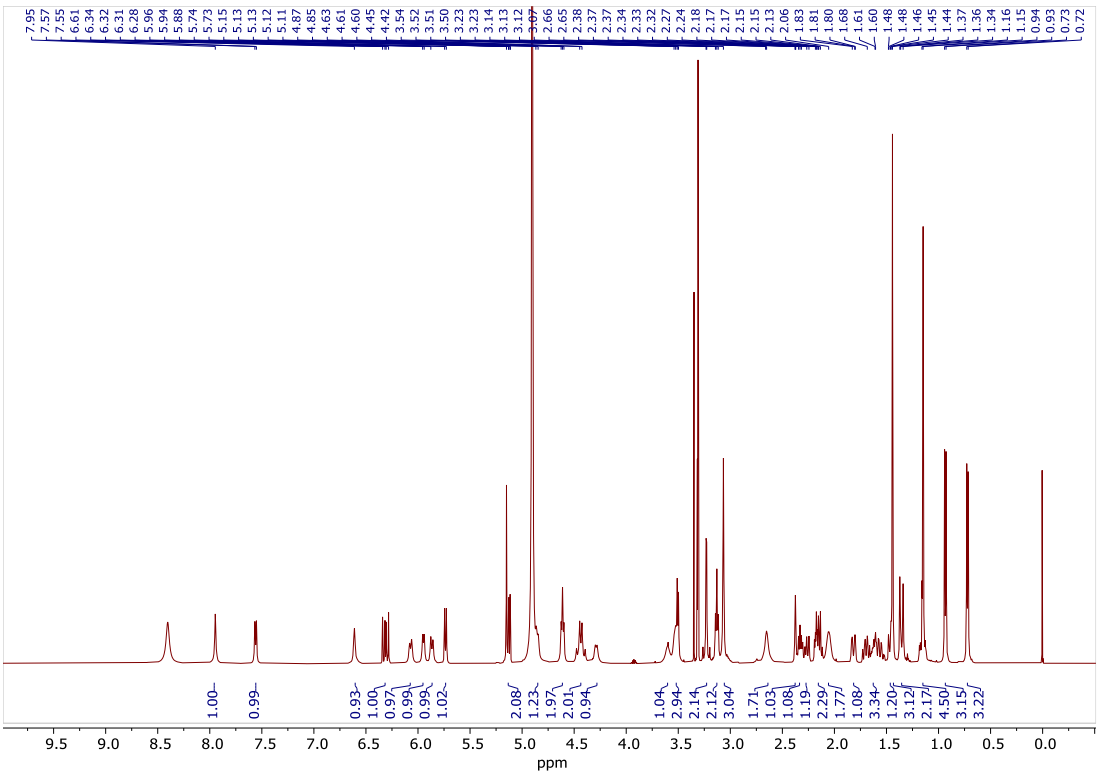

**Figure S5.** $^{1}$H-NMR (500 MHz, $CDCl_3$) of **36**.

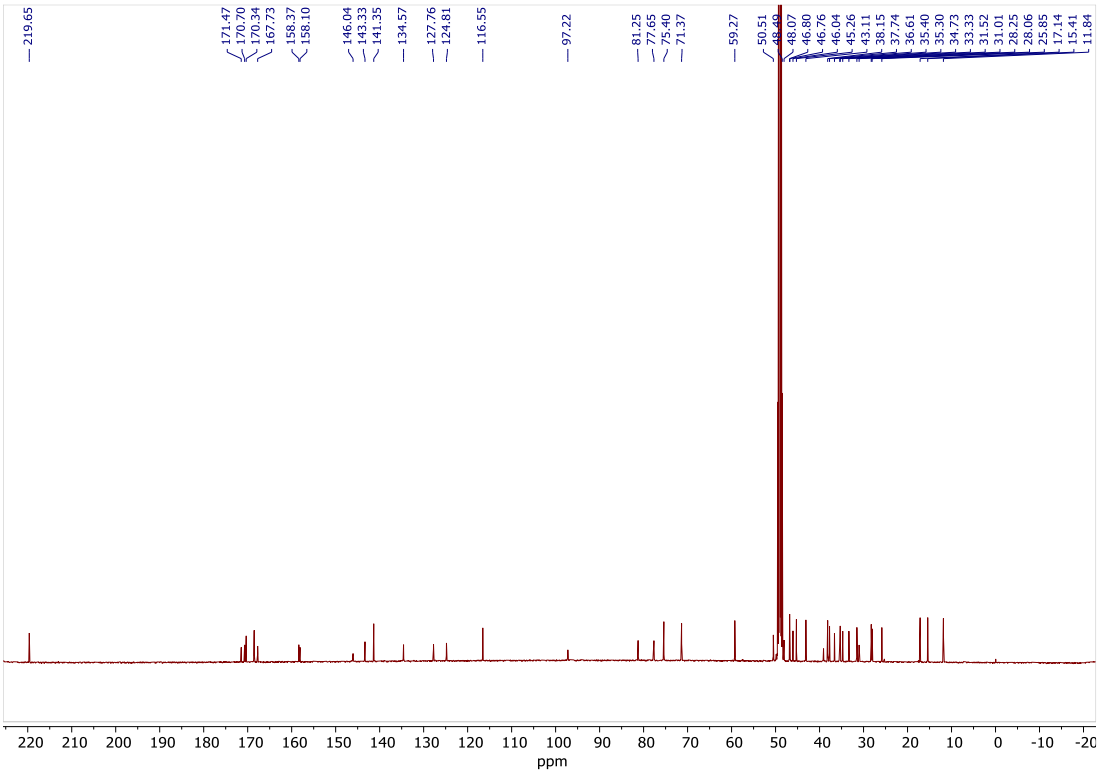

**Figure S6.** $^{13}$C-NMR (125 MHz, $CDCl_3$) of **36**.

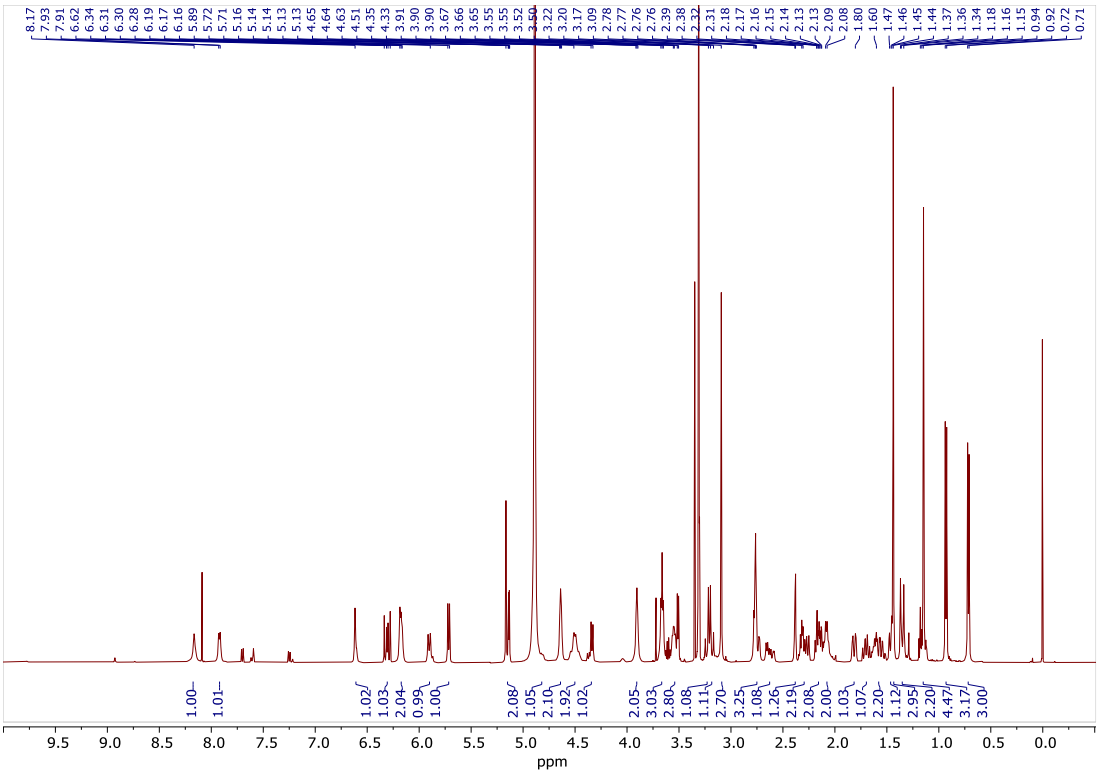

**Figure S7.** $^{1}$H-NMR (500 MHz, $CDCl_3$) of **37**.

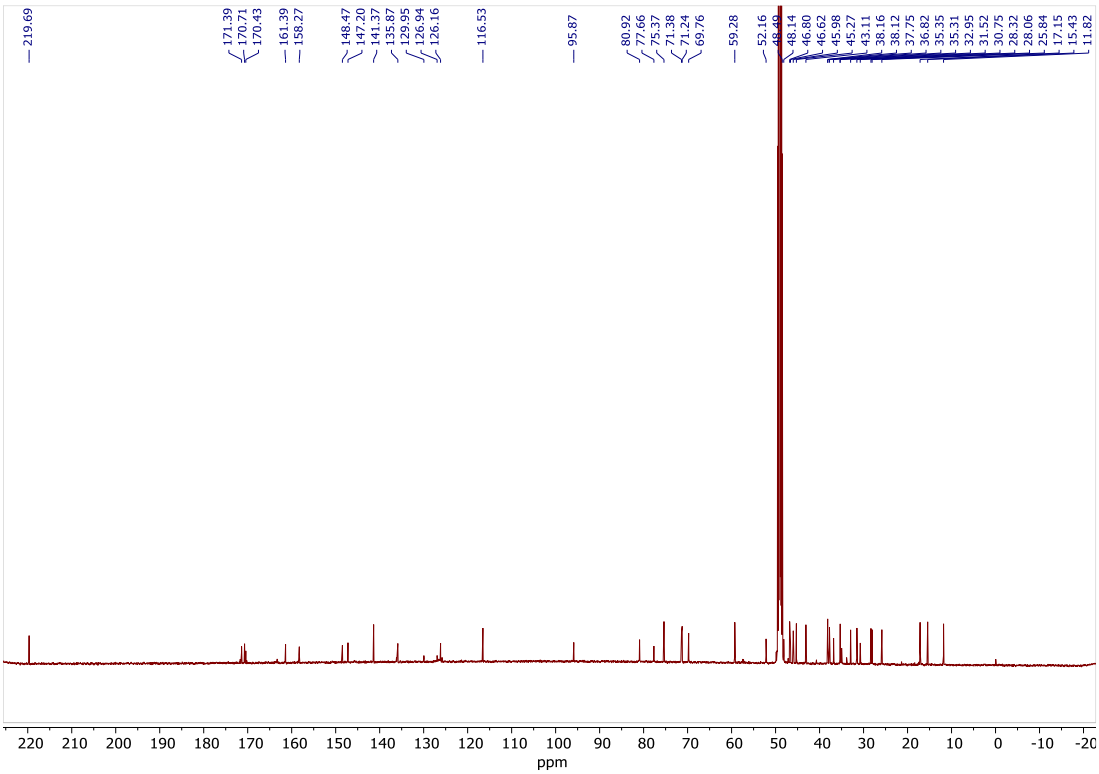

**Figure S8.** $^{13}$C-NMR (125 MHz, $CDCl_3$) of **37**.

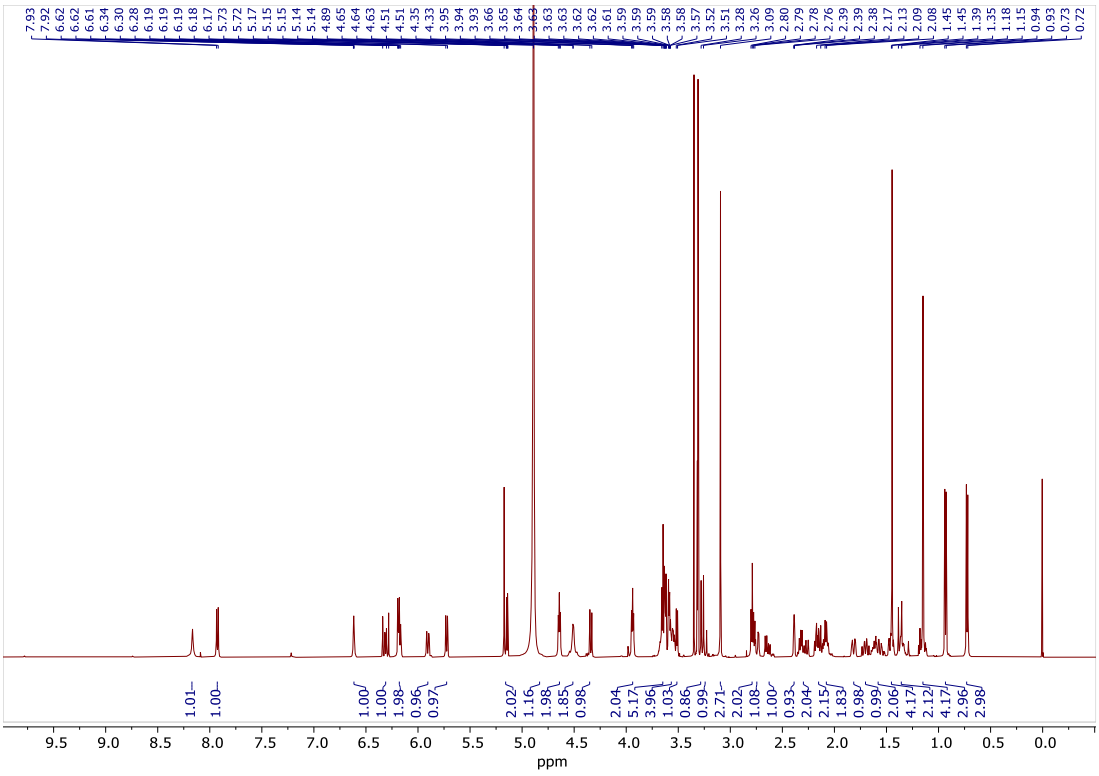

**Figure S9.** $^{1}$H-NMR (500 MHz, $CDCl_3$) of **38**.

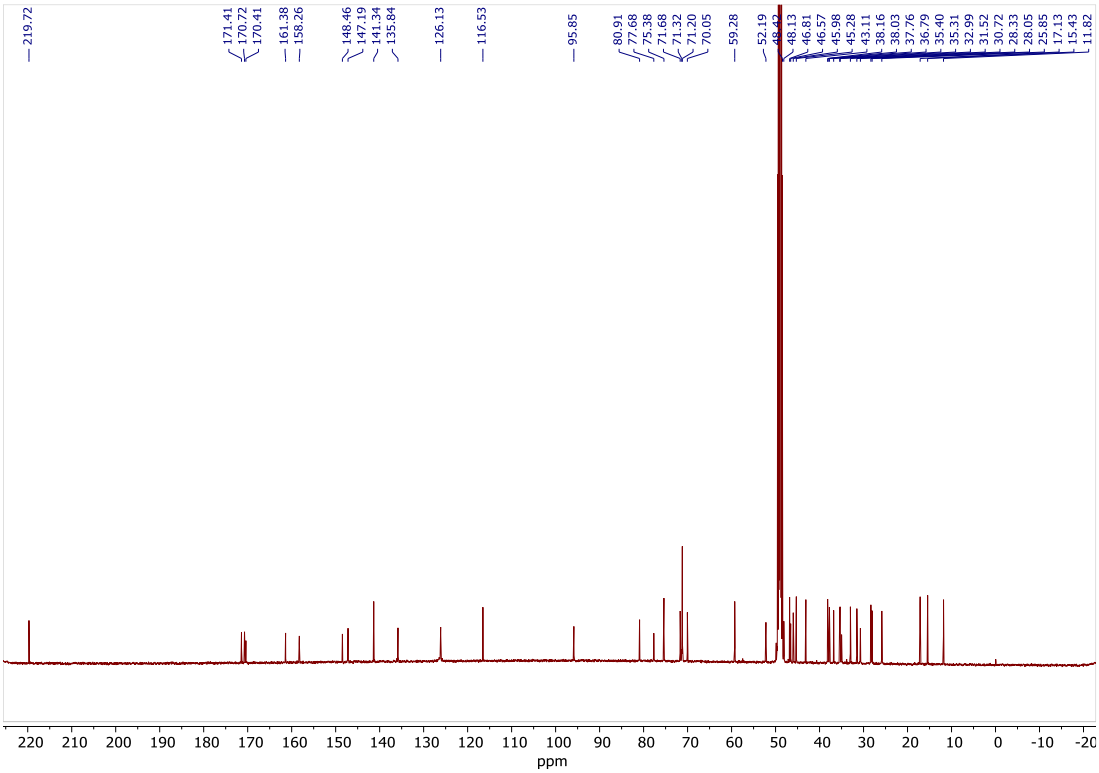

**Figure S10.** $^{13}$C-NMR (125 MHz, $CDCl_3$) of **38**.

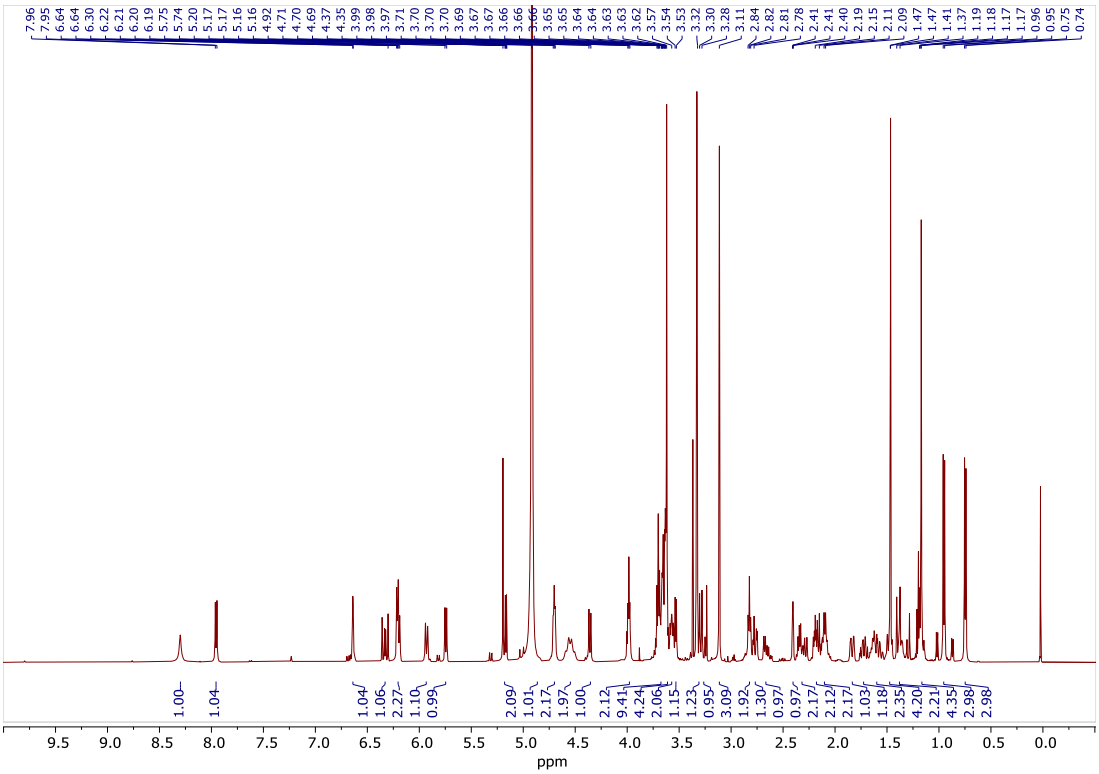


**Figure S11.** $^{1}$H-NMR (500 MHz, $CDCl_3$) of **39**.

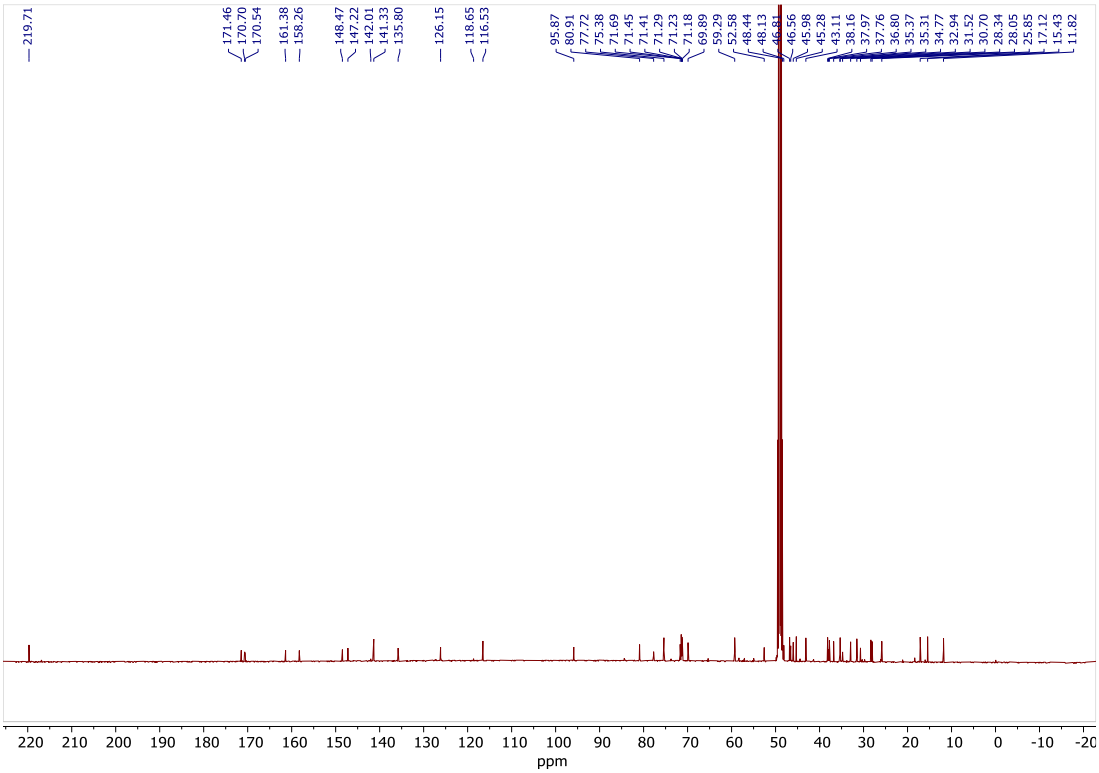


**Figure S12.** $^{13}$C-NMR (125 MHz, $CDCl_3$) of **39**.

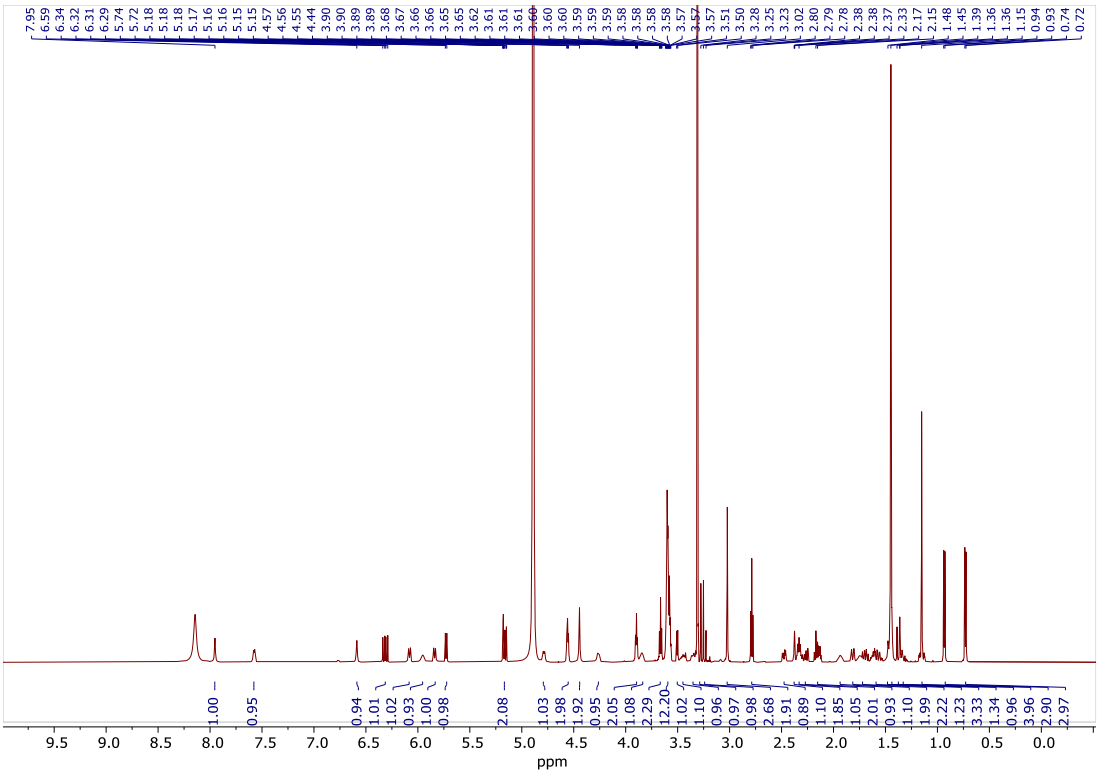

**Figure S13.** $^{1}$H-NMR (500 MHz, $CDCl_3$) of **40**.

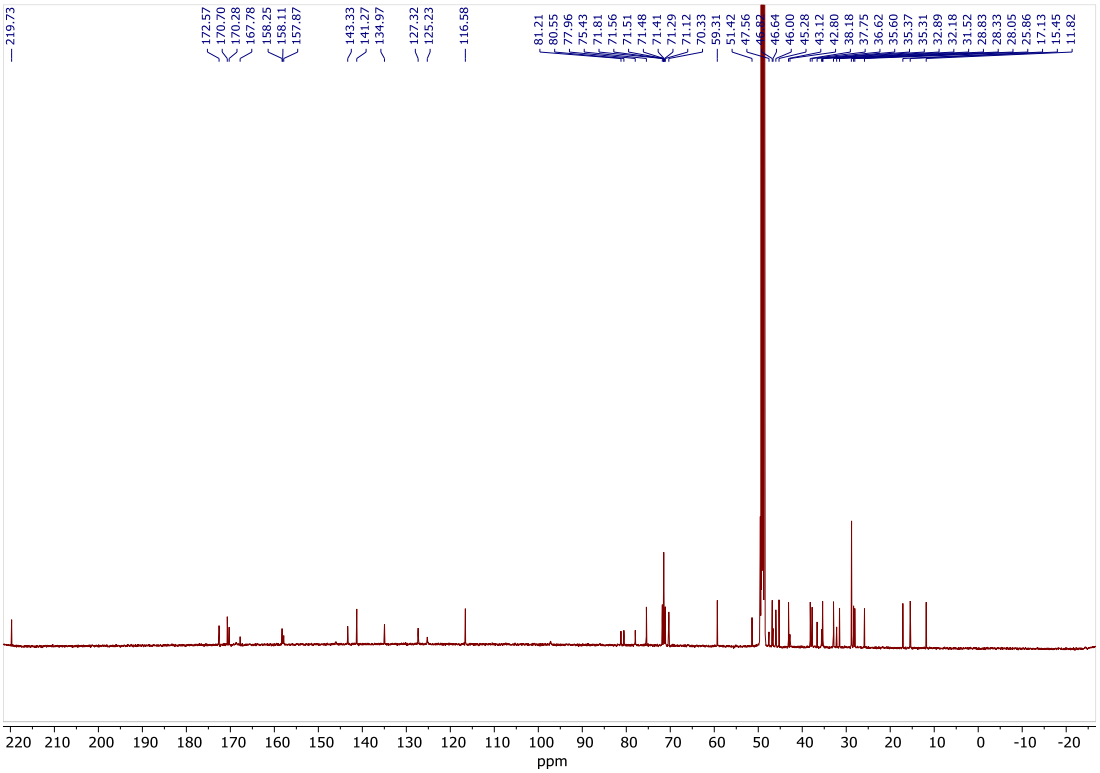

**Figure S14.** $^{13}$C-NMR (125 MHz, $CDCl_3$) of **40**.

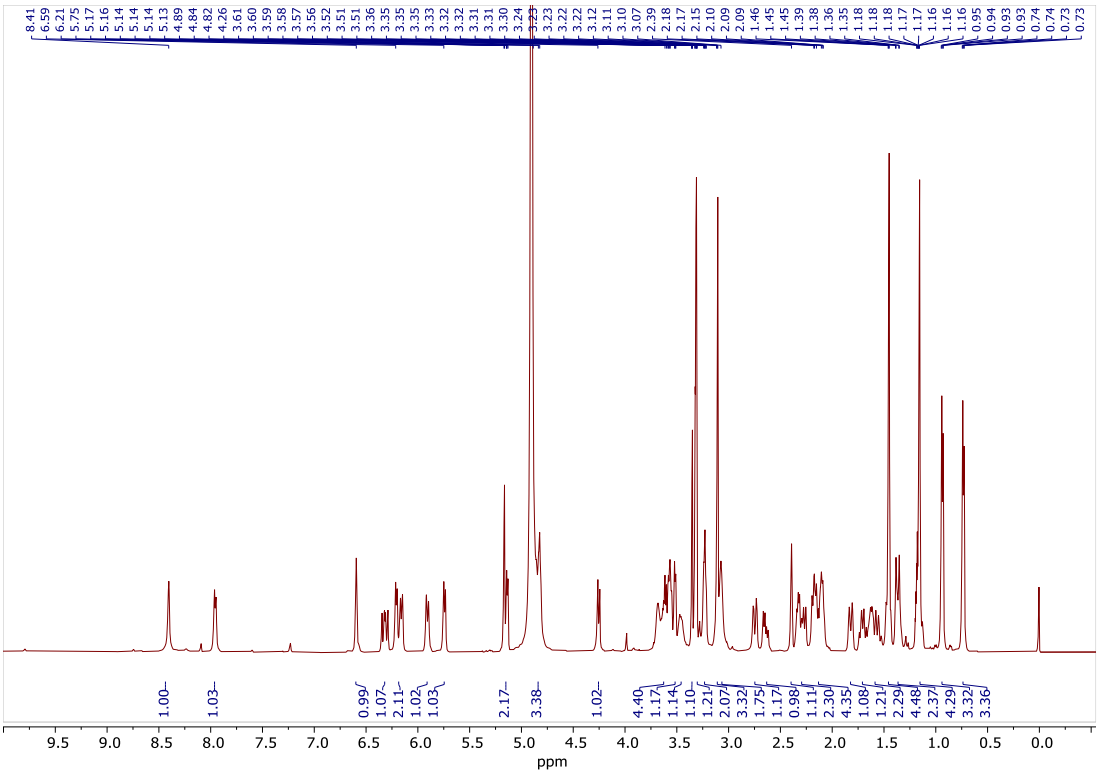

**Figure S15.** $^{1}$H-NMR (500 MHz, $CDCl_3$) of **41**.

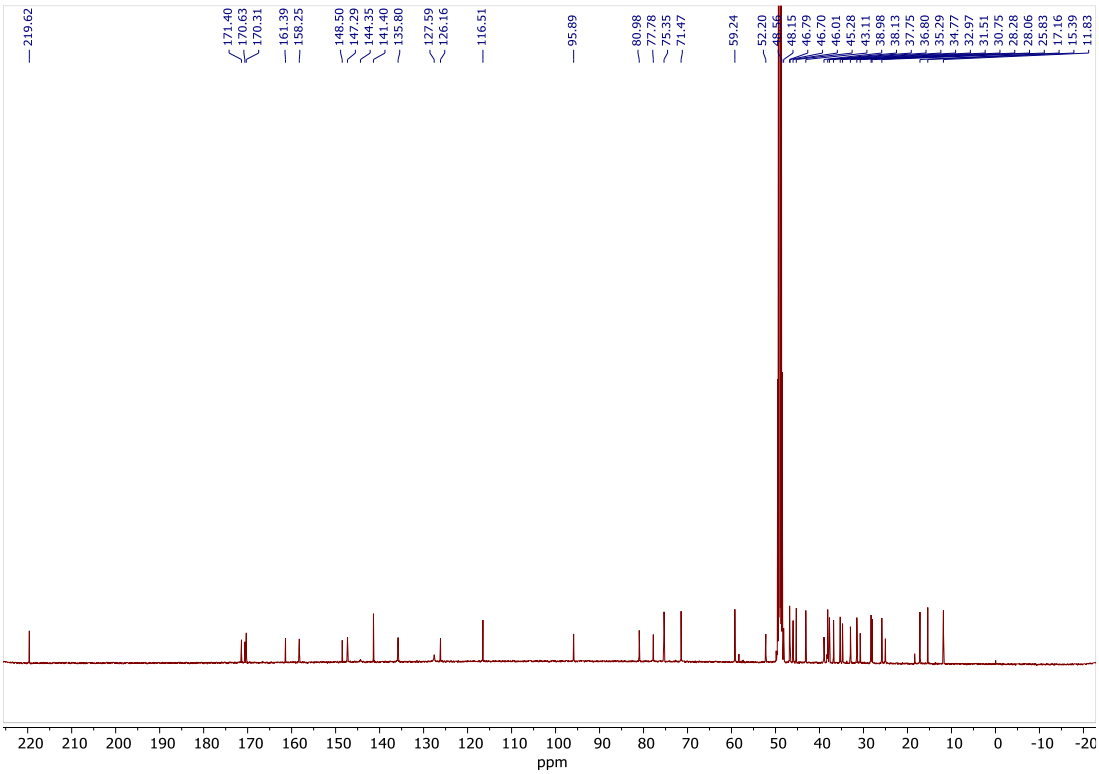

**Figure S16.** $^{13}$C-NMR (125 MHz, $CDCl_3$) of **41**.

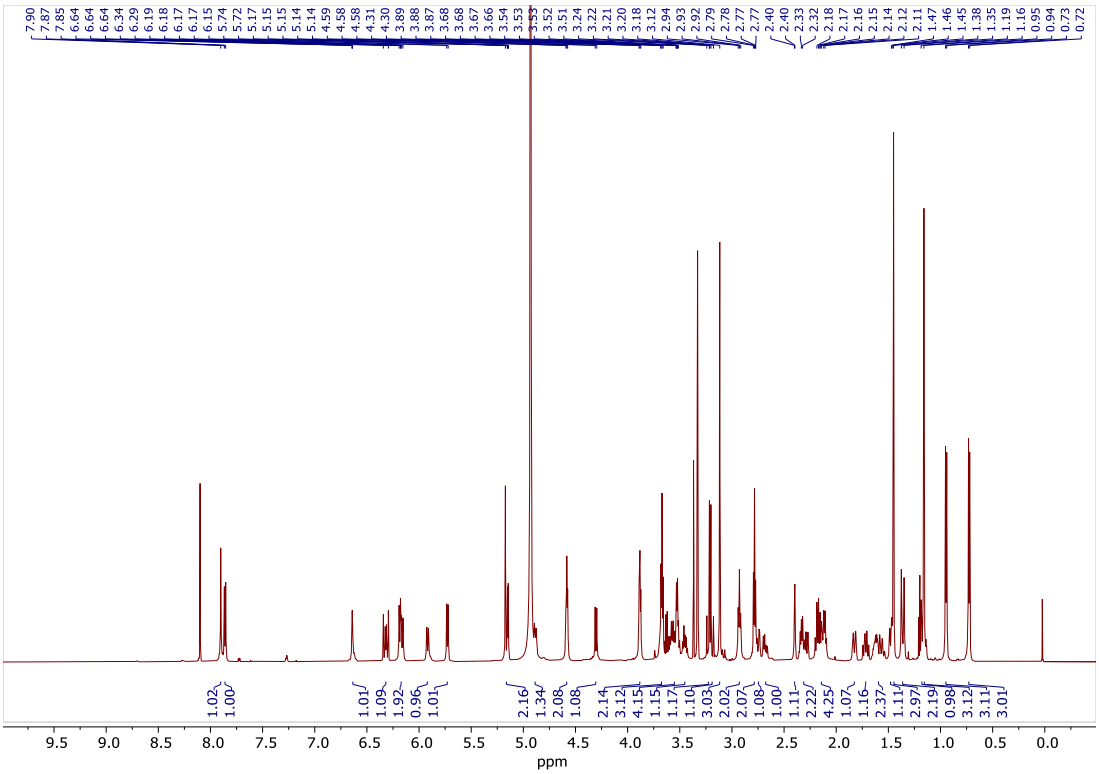

**Figure S17.** $^{1}$H-NMR (500 MHz, $CDCl_3$) of **42**.

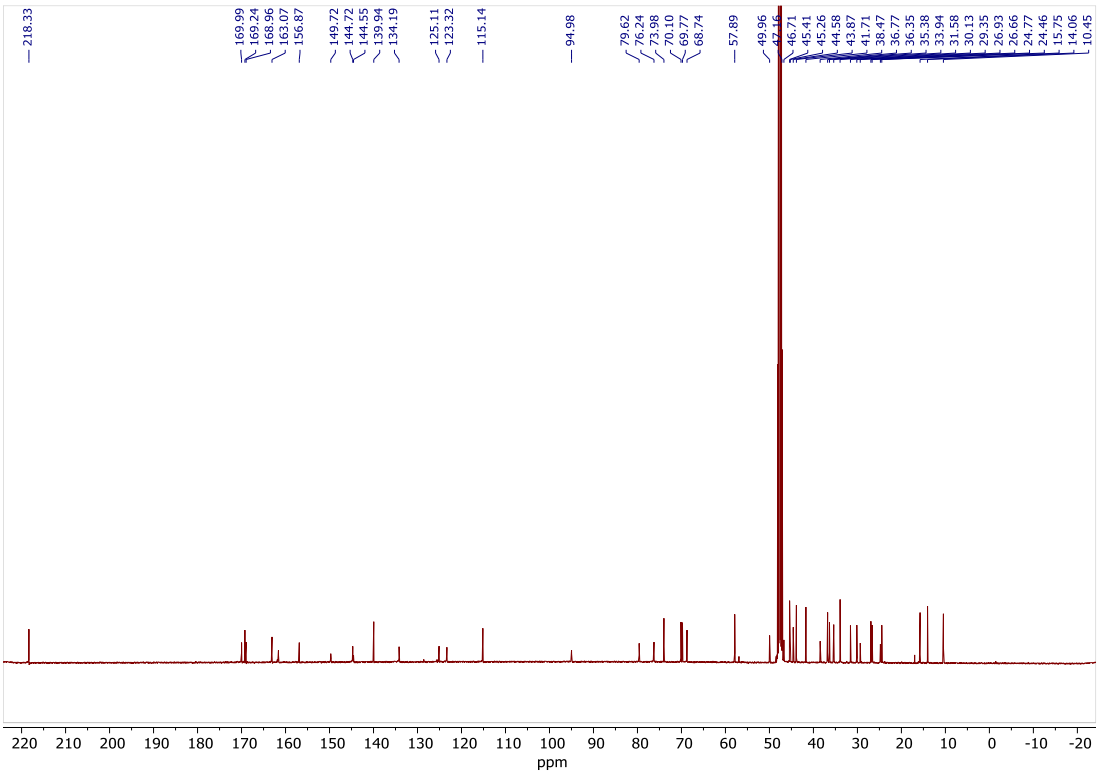

**Figure S18.** $^{13}$C-NMR (125 MHz, $CDCl_3$) of **42**.

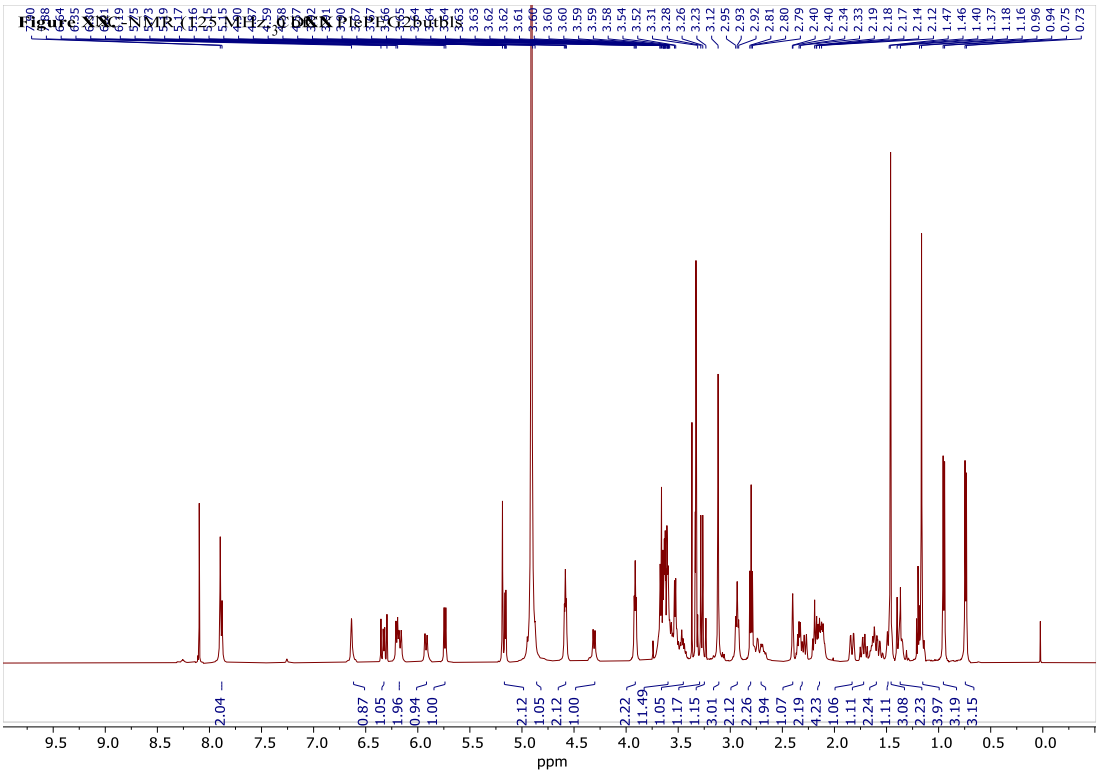

**Figure S19.** $^{1}$H-NMR (500 MHz, $CDCl_3$) of **43**.

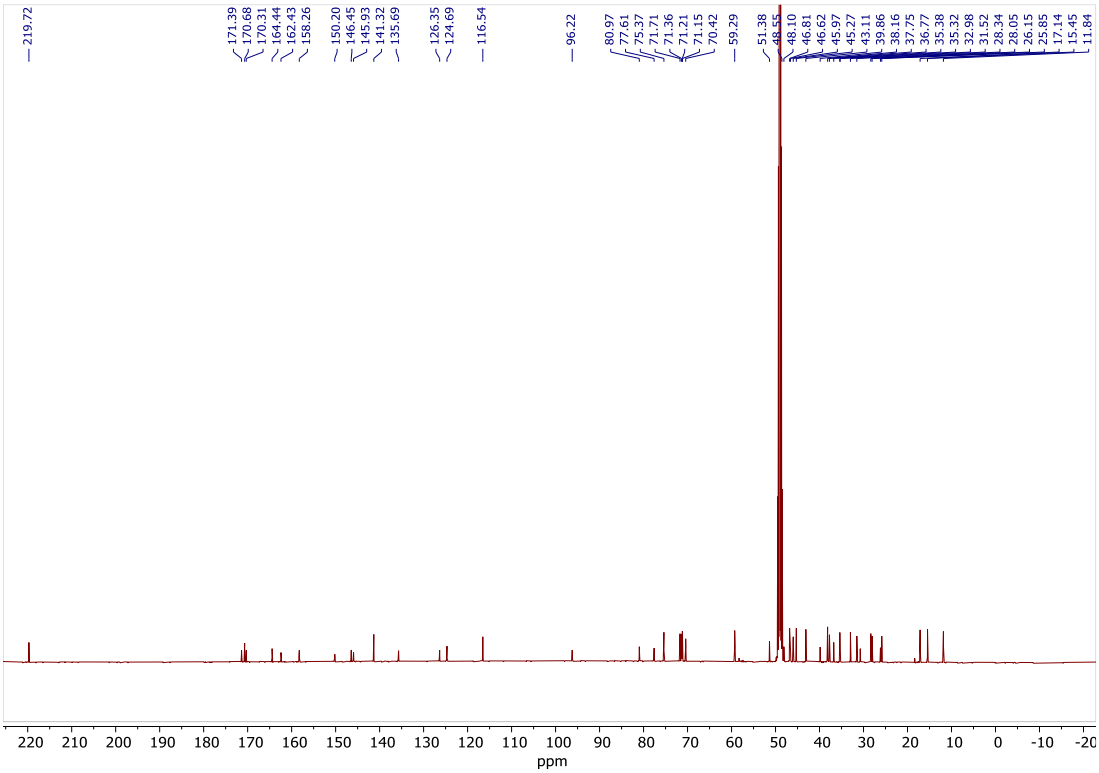

**Figure S20.** $^{13}$C-NMR (125 MHz, $CDCl_3$) of **43**.

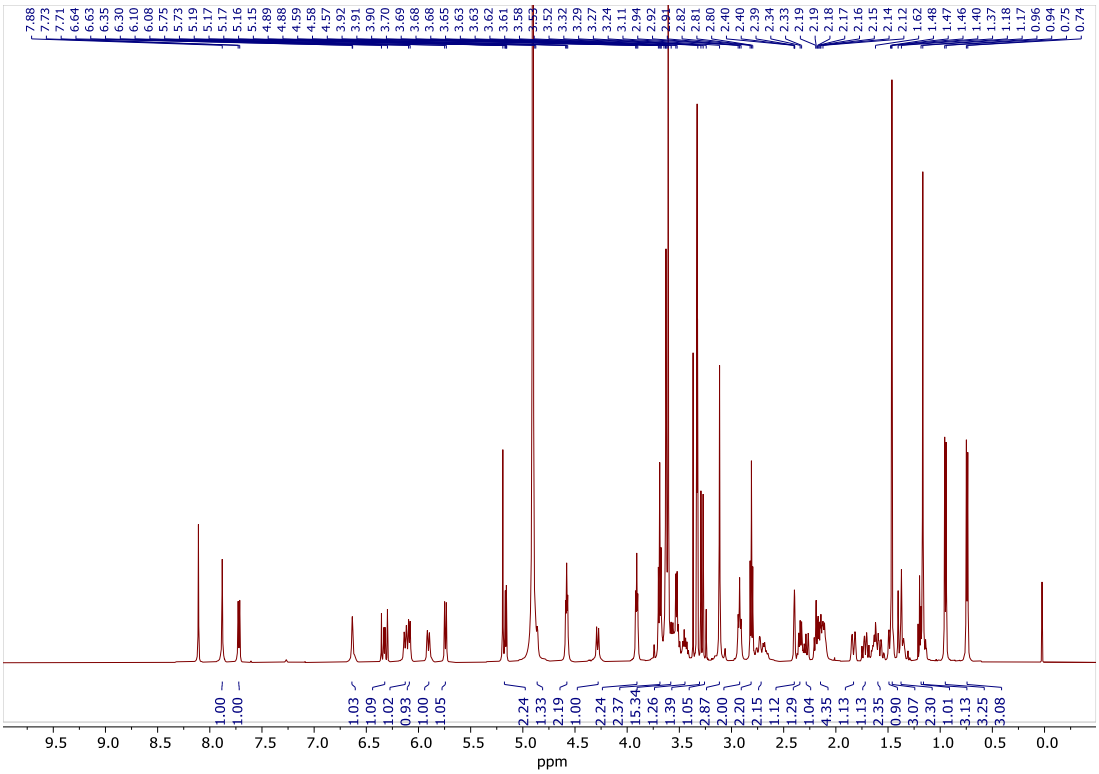

**Figure S21.** $^{1}$H-NMR (500 MHz, $CDCl_3$) of **44**.

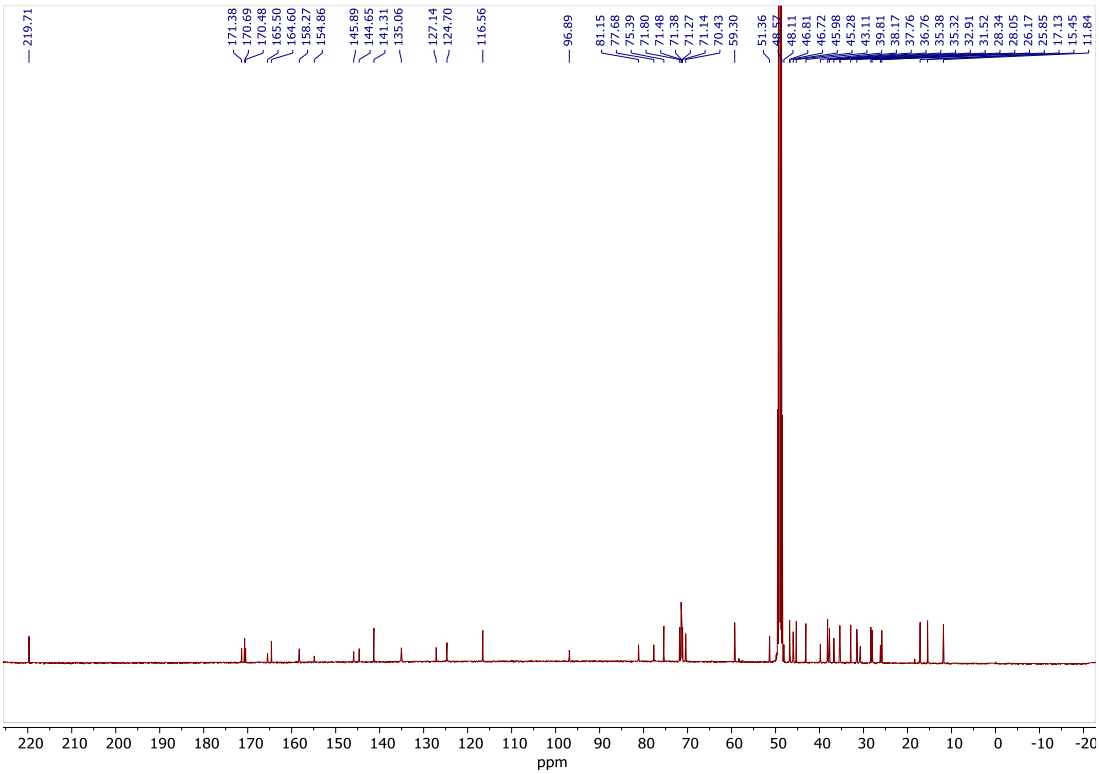

**Figure S22.** $^{13}$C-NMR (125 MHz, $CDCl_3$) of **44**.

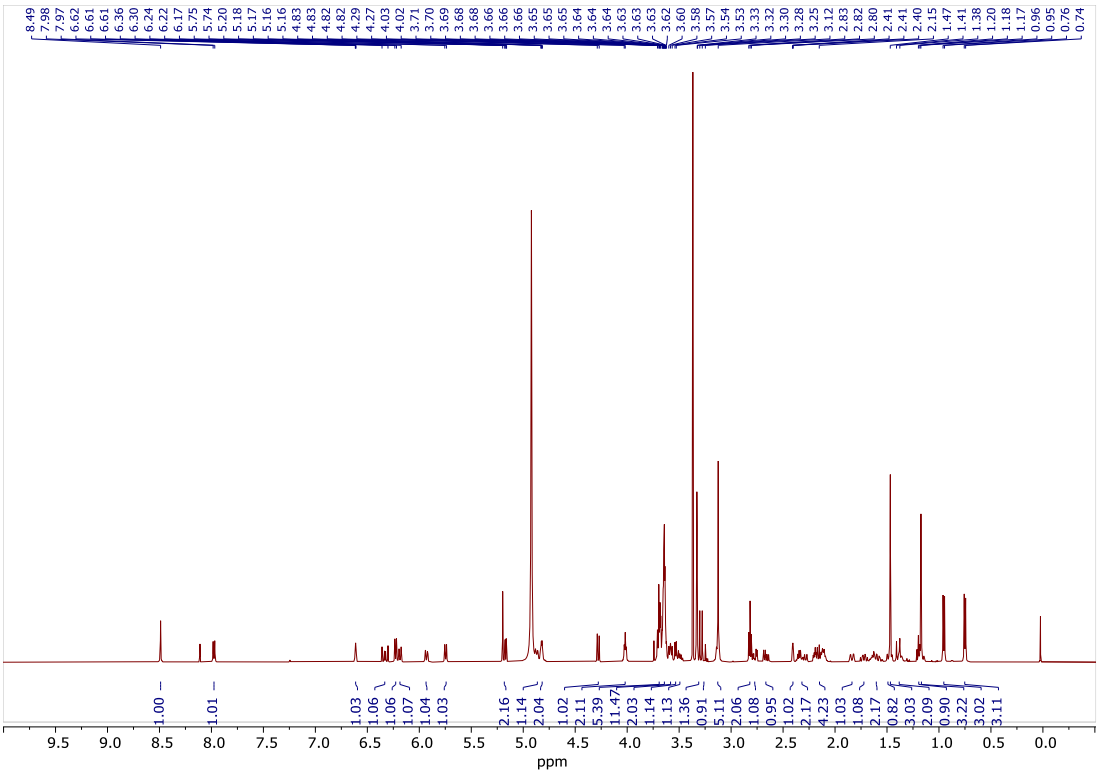


**Figure S23.** $^{1}$H-NMR (500 MHz, $CDCl_3$) of **45**.

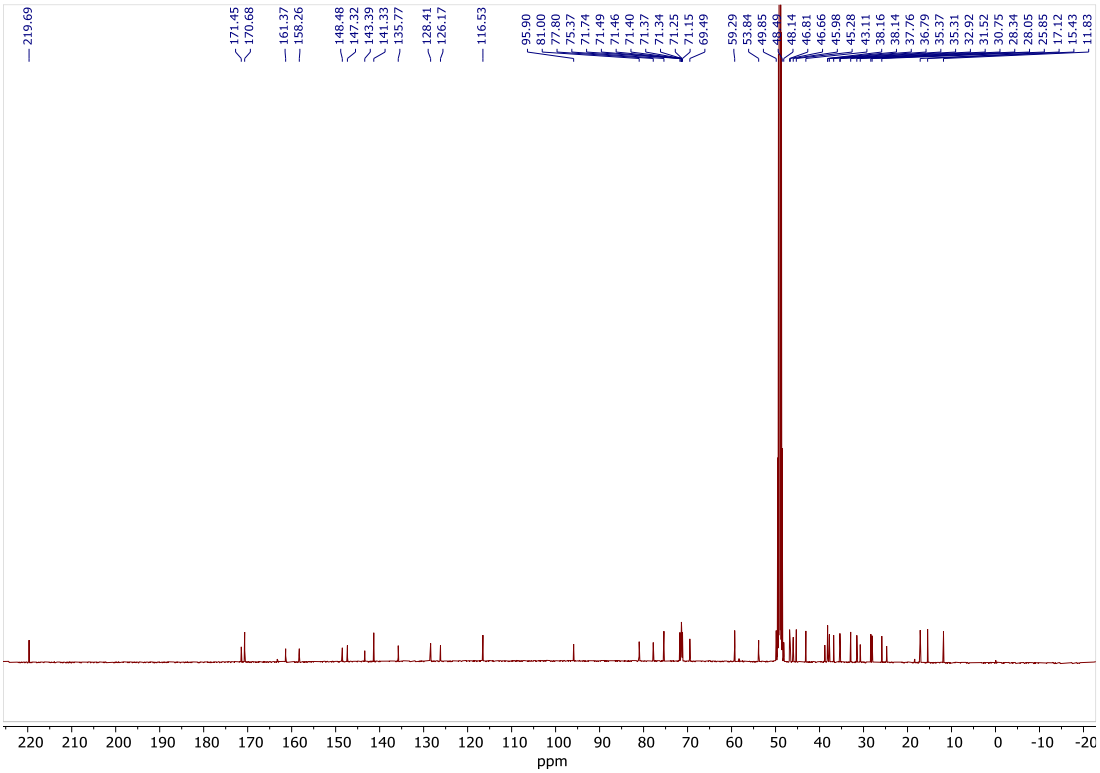


**Figure S24.** $^{13}$C-NMR (125 MHz, $CDCl_3$) of **45**.

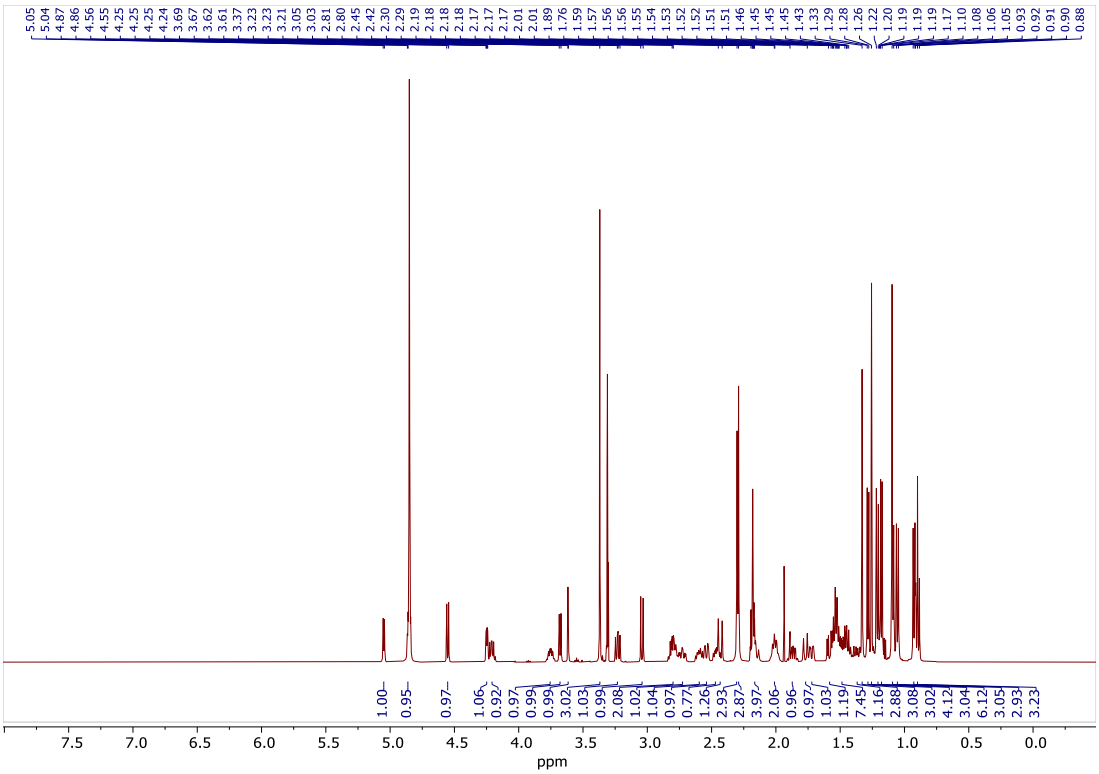

**Figure S25.** $^{1}$H-NMR (500 MHz, $CDCl_3$) of **55**.

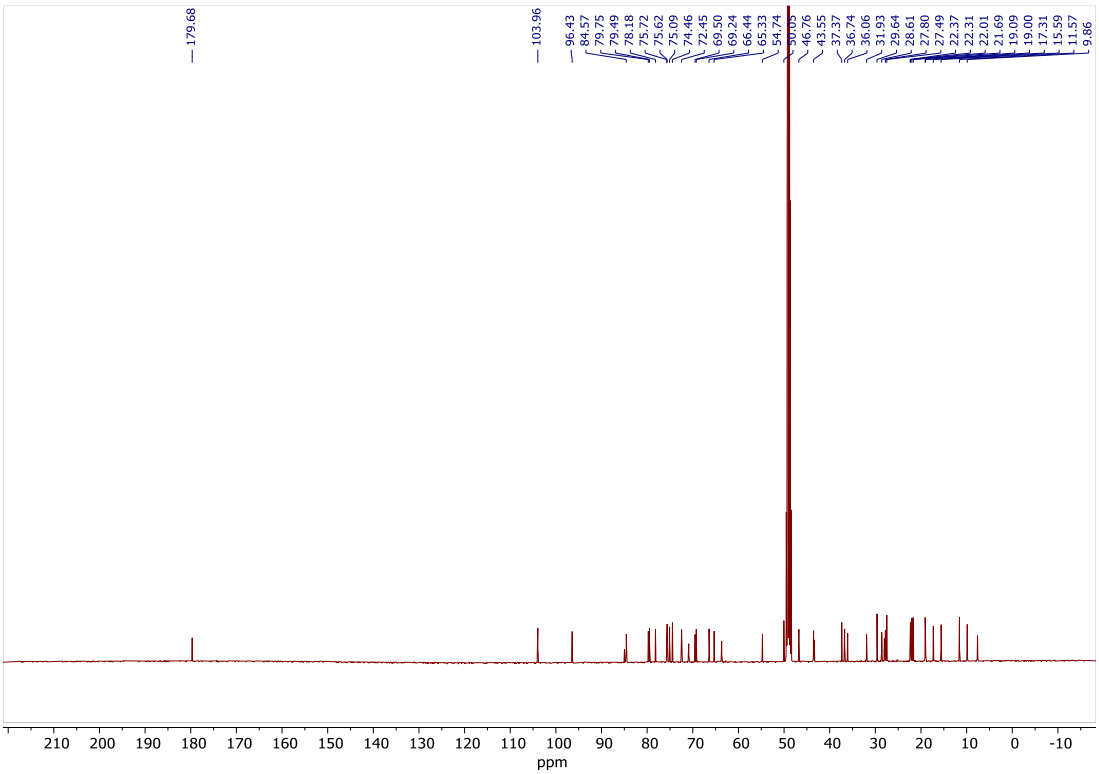

**Figure S26.** $^{13}$C-NMR (125 MHz, $CDCl_3$) of **55**.

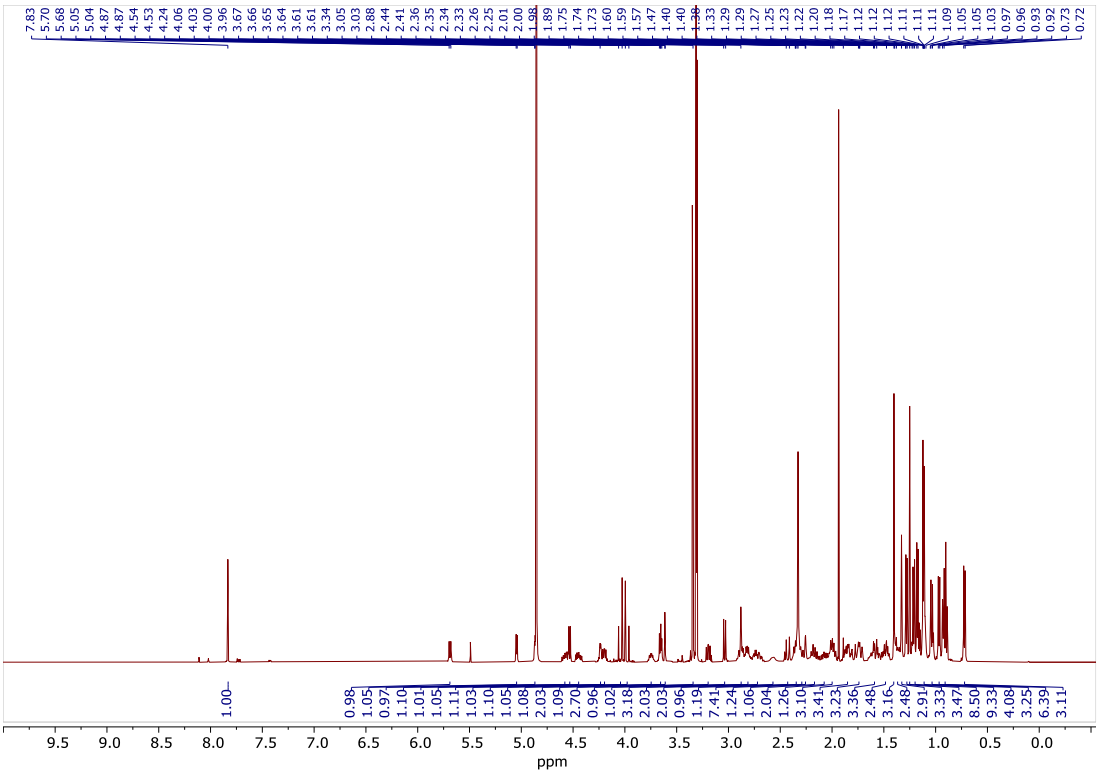

**Figure S27.** $^{1}$H-NMR (500 MHz, $CDCl_3$) of **57**.

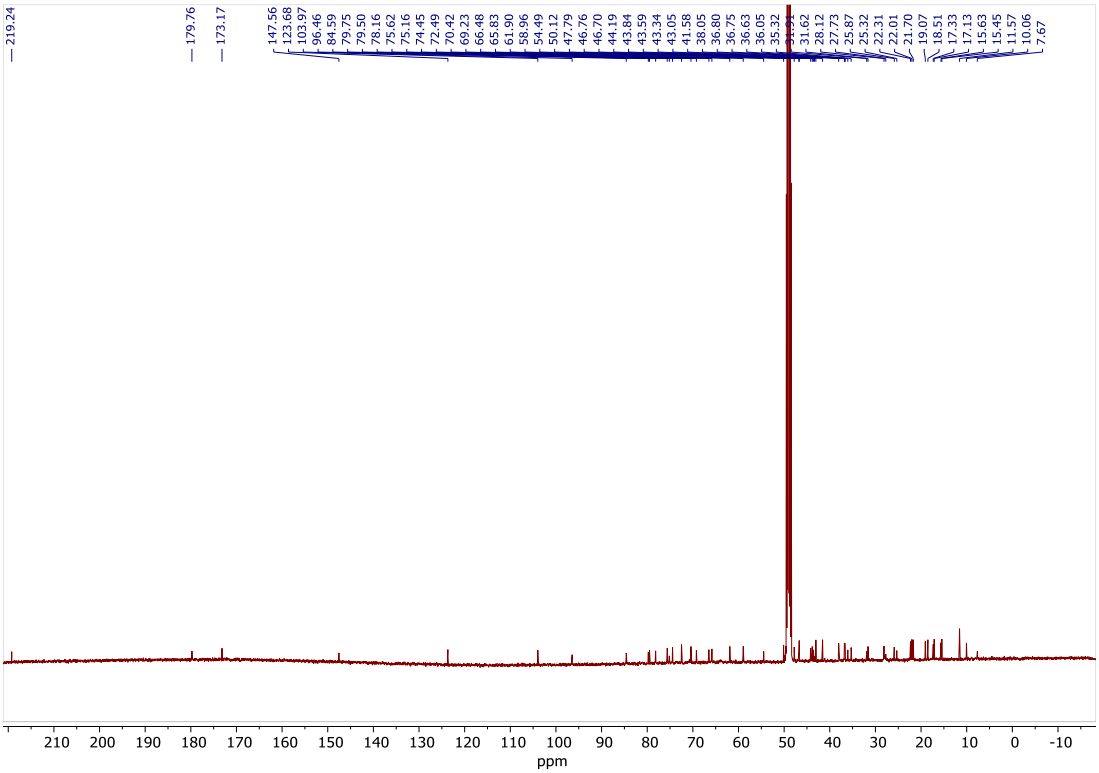

**Figure S28.** $^{13}$C-NMR (125 MHz, $CDCl_3$) of **57**.

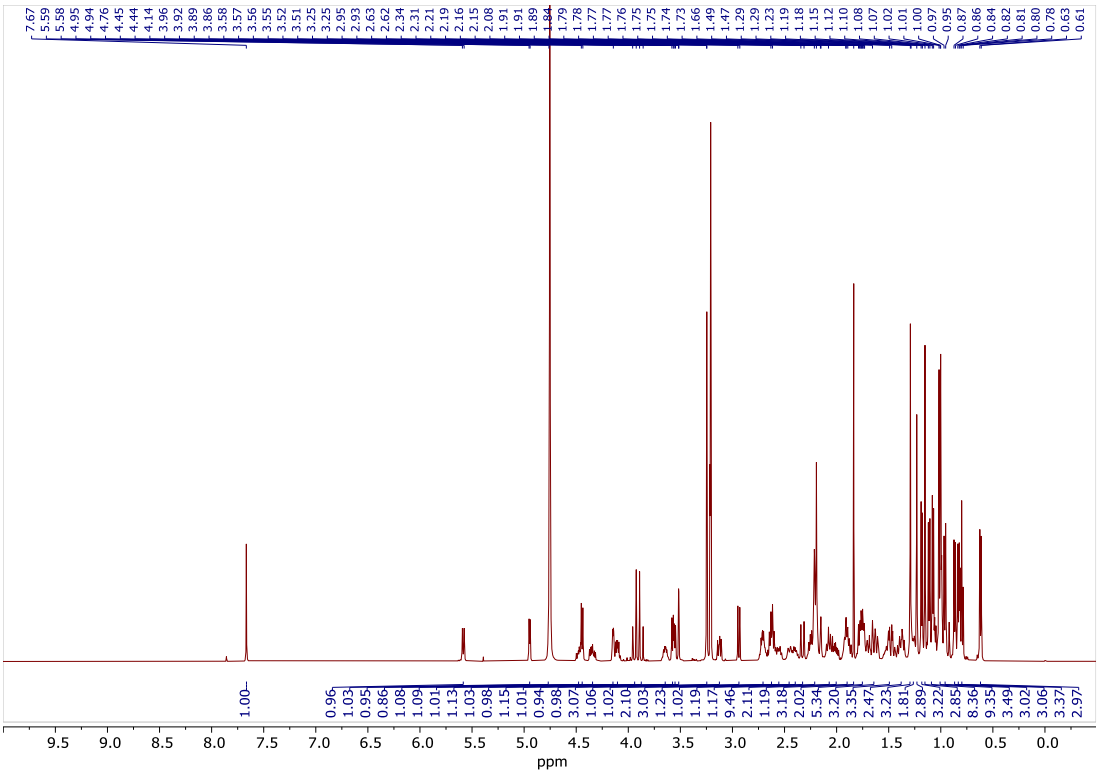

**Figure S29.** $^{1}$H-NMR (500 MHz, $CDCl_3$) of **58**.

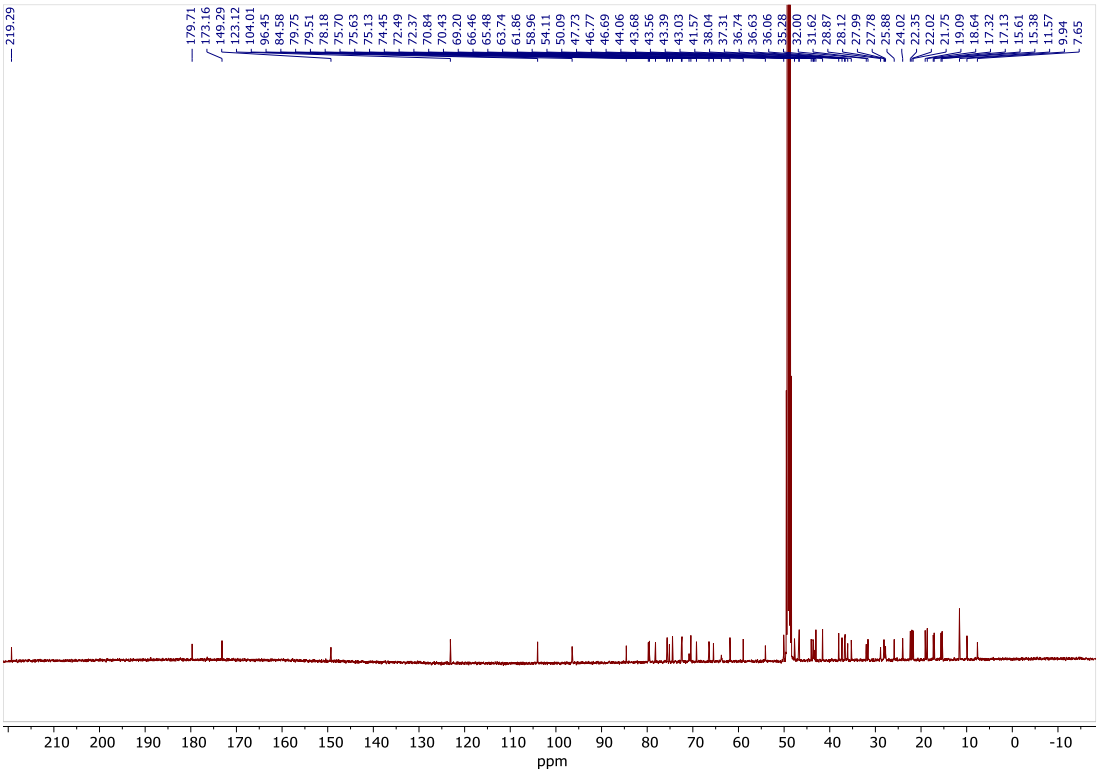

**Figure S30.** $^{13}$C-NMR (125 MHz, $CDCl_3$) of **58**.

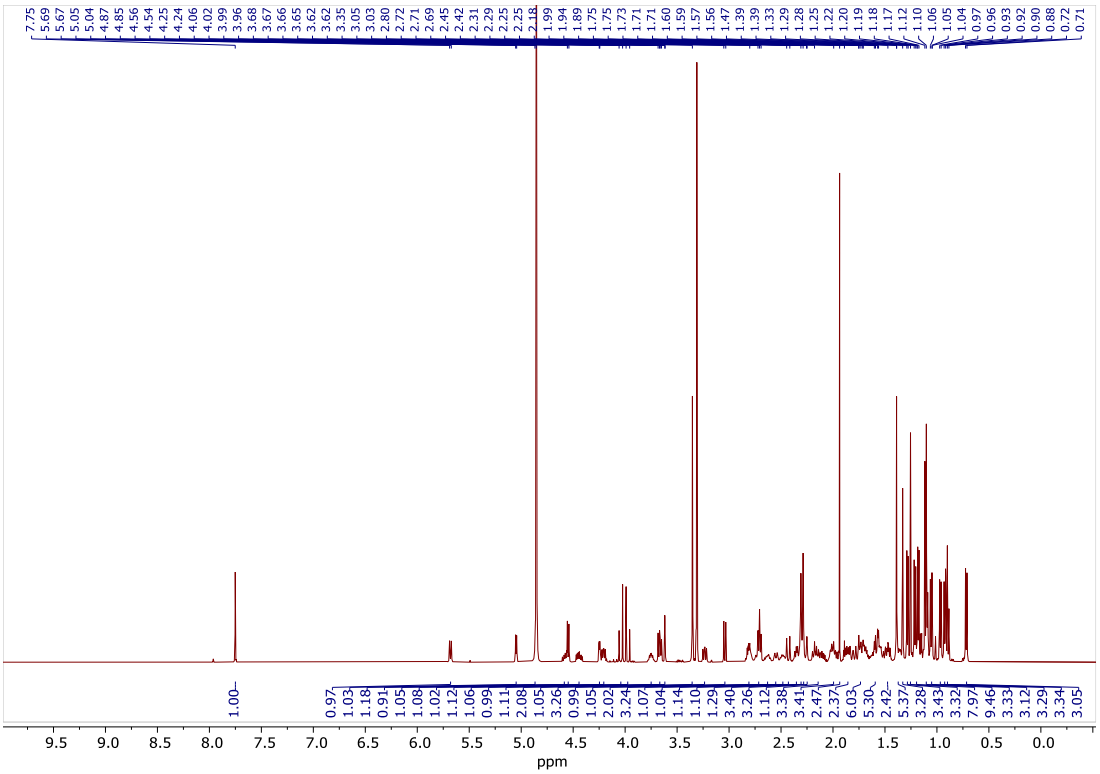

**Figure S31.** $^{1}$H-NMR (500 MHz, $CDCl_3$) of **59**.

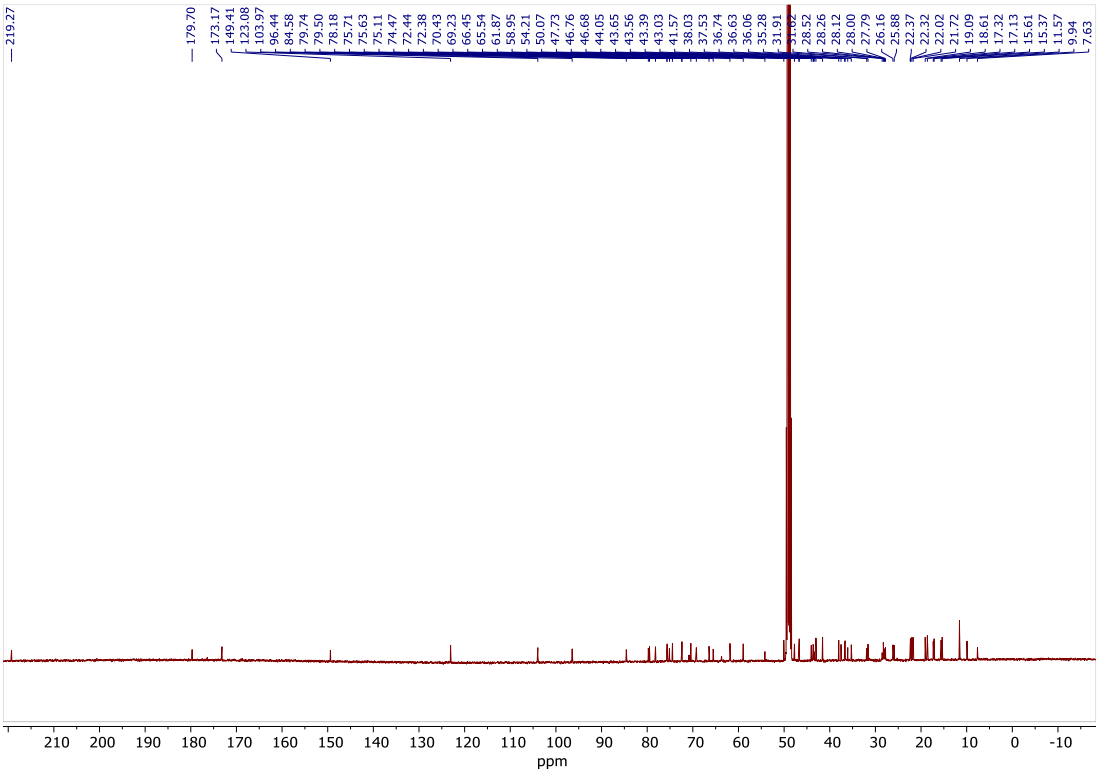

**Figure S32.** $^{13}$C-NMR (125 MHz, $CDCl_3$) of **59**.

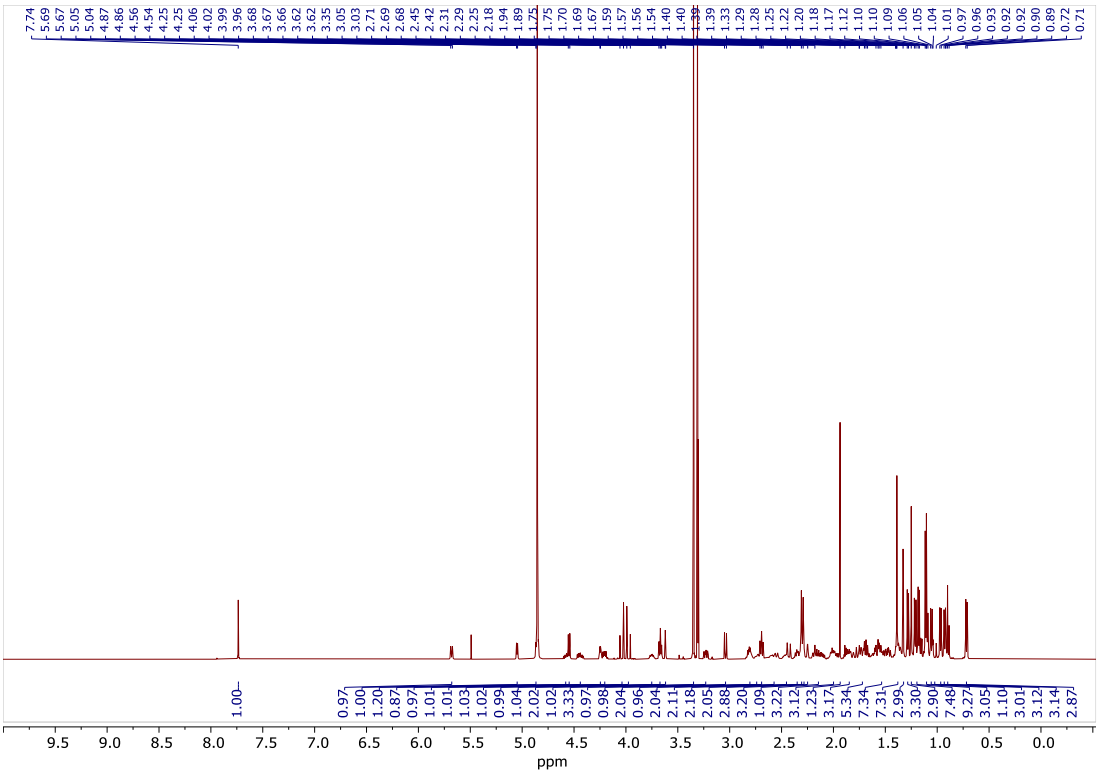

**Figure S33.** $^{1}$H-NMR (500 MHz, $CDCl_3$) of **60**.

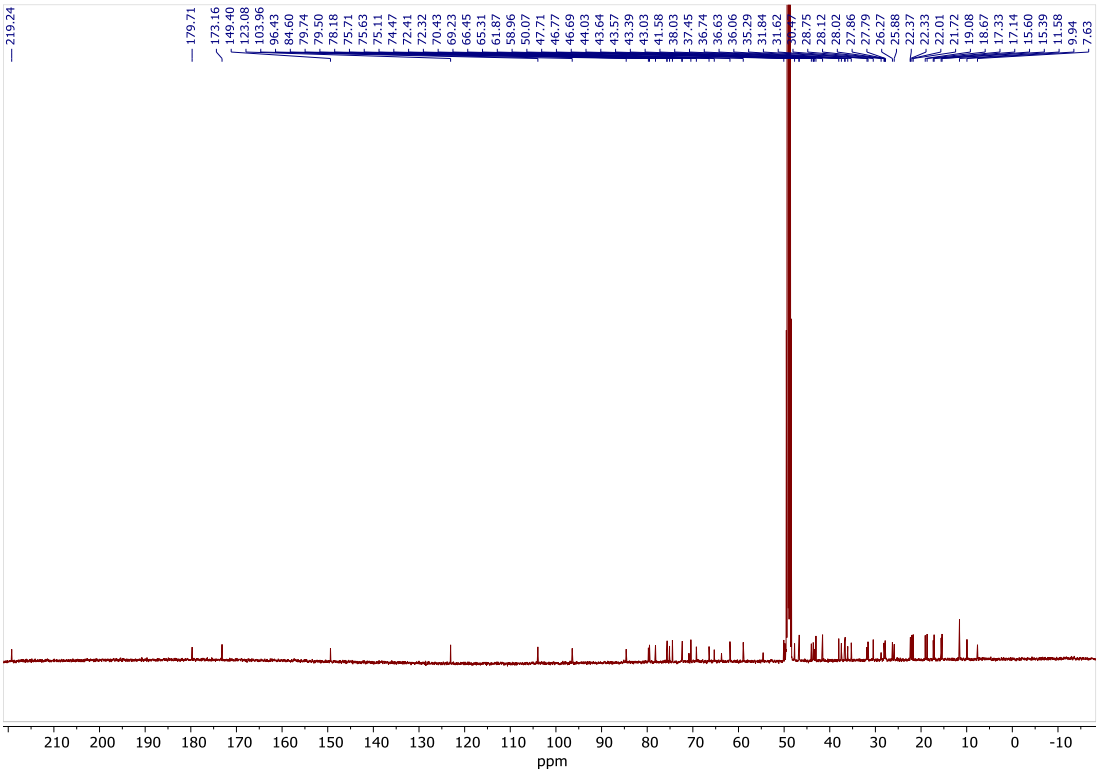

**Figure 34.** $^{13}$C-NMR (125 MHz, $CDCl_3$) of **60**.

## 6.6 References


1. Ahmed, A.; Azim, A.; Gurjar, M.; Baronia, A. K., Current concepts in combination antibiotic therapy for critically ill patients. *Indian J Crit Care Med* **2014,** *18* (5), 310-4.
2. Tamma, P. D.; Cosgrove, S. E.; Maragakis, L. L., Combination therapy for treatment of infections with gram-negative bacteria. *Clin. Microbiol. Rev.* **2012,** *25* (3), 450-70.
3. Bassetti, M.; Righi, E., New antibiotics and antimicrobial combination therapy for the treatment of Gram-negative bacterial infections. *Curr Opin Crit Care* **2015,** *21* (5), 402-11.
4. Morales-Durán, N.; León-Buitimea, A.; Morones-Ramírez, J. R., Unraveling resistance mechanisms in combination therapy: A comprehensive review of recent advances and future directions. *Heliyon* **2024,** *10* (6), e27984.
5. Gorityala, B. K.; Guchhait, G.; Goswami, S.; Fernando, D. M.; Kumar, A.; Zhanel, G. G.; Schweizer, F., Hybrid antibiotic overcomes resistance in *P. aeruginosa* by enhancing outer membrane penetration and reducing efflux. *J. Med. Chem.* **2016,** *59* (18), 8441-55.
6. Wang, K. K.; Stone, L. K.; Lieberman, T. D.; Shavit, M.; Baasov, T.; Kishony, R., A hybrid drug limits resistance by evading the action of the multiple antibiotic resistance pathway. *Mol. Biol. Evol.* **2016,** *33* (2), 492-500.
7. Locher, H. H.; Caspers, P.; Bruyère, T.; Schroeder, S.; Pfaff, P.; Knezevic, A.; Keck, W.; Ritz, D., Investigations of the mode of action and resistance development of cadazolid, a new antibiotic for treatment of *Clostridium difficile* infections. *Antimicrob. Agents Chemother.* **2014,** *58* (2), 901-8.
8. Grapsas, I.; Lerner, S. A.; Mobashery, S., Conjoint molecules of cephalosporins and aminoglycosides. *Arch Pharm (Weinheim)* **2001,** *334* (8-9), 295-301.
9. Klahn, P.; Broenstrup, M., Bifunctional antimicrobial conjugates and hybrid antimicrobials. *Nat. Prod. Rep.* **2017,** *34* (7), 832-885.
10. Boschert, S., Promising *C. difficile* antibiotic in pipeline. *Internal Medicine News* **2012**.
11. Idorsia, Idorsia announces financial results for the first quarter 2018. 2018.
12. Gilbert, D. N.; Kohlhepp, S. J.; Slama, K. A.; Grunkemeier, G.; Lewis, G.; Dworkin, R. J.; Slaughter, S. E.; Leggett, J. E., Phenotypic resistance of *Staphylococcus aureus*, selected Enterobacteriaceae, and *Pseudomonas aeruginosa* after single and multiple in vitro exposures to ciprofloxacin, levofloxacin, and trovafloxacin. *Antimicrob. Agents Chemother.* **2001,** *45* (3), 883-92.
13. Dalhoff, A.; Rashid, M. U.; Kapsner, T.; Panagiotidis, G.; Weintraub, A.; Nord, C. E., Analysis of effects of MCB3681, the antibacterially active substance of prodrug MCB3837, on human resident microflora as proof of principle. *Clin. Microbiol. Infect.* **2015,** *21* (8), 767.e1-767.e4.
14. Rashid, M.-U.; Dalhoff, A.; Bäckström, T.; Björkhem-Bergman, L.; Panagiotidis, G.; Weintraub, A.; Nord, C. E., Ecological impact of MCB3837 on the normal human microbiota. *Int. J. Antimicrob. Agents* **2014,** *44* (2), 125-130.
15. Floss, H. G.; Yu, T. W., Rifamycin-mode of action, resistance, and biosynthesis. *Chem. Rev.* **2005,** *105* (2), 621-32.
16. Robertson, G. T.; Bonventre, E. J.; Doyle, T. B.; Du, Q.; Duncan, L.; Morris, T. W.; Roche, E. D.; Yan, D.; Lynch, A. S., In vitro evaluation of CBR-2092, a novel rifamycin-quinolone hybrid antibiotic: microbiology profiling studies with Staphylococci and Streptococci. *Antimicrob. Agents Chemother.* **2008,** *52* (7), 2324-34.
17. Butler Michelle, M.; LaMarr William, A.; Foster Kimberly, A.; Barnes Marjorie, H.; Skow Donna, J.; Lyden Patrick, T.; Kustigian Lauren, M.; Zhi, C.; Brown Neal, C.; Wright George, E.; Bowlin Terry, L., Antibacterial activity and mechanism of action of a novel anilinouracil-fluoroquinolone hybrid compound. *Antimicrob. Agents Chemother.* **2007,** *51* (1), 119-127.

18. Zhi, C.; Long, Z.-y.; Manikowski, A.; Comstock, J.; Xu, W.-C.; Brown, N. C.; Tarantino, P. M.; Holm, K. A.; Dix, E. J.; Wright, G. E.; Barnes, M. H.; Butler, M. M.; Foster, K. A.; LaMarr, W. A.; Bachand, B.; Bethell, R.; Cadilhac, C.; Charron, S.; Lamothe, S.; Motorina, I.; Storer, R., Hybrid antibacterials. DNA polymerase−topoisomerase inhibitors. *J. Med. Chem.* **2006,** *49* (4), 1455-1465.
19. Sriram, D.; Yogeeswari, P.; Senchani, G.; Banerjee, D., Newer tetracycline derivatives: Synthesis, anti-HIV, antimycobacterial activities and inhibition of HIV-1 integrase. *Bioorg. Med. Chem. Lett.* **2007,** *17* (8), 2372-2375.
20. Labischinski, H.; Cerian, J.; Calanasan, C.; Boyce, R. S. Hybrid antimicrobial compounds and their use. WO2010025906A3, 2010.
21. Markad, S. D.; Kaur, P.; Kishore Reddy, B. K.; Chinnapattu, M.; Raichurkar, A.; Nandishaiah, R.; Panda, M.; Iyer, P. S., Novel lead generation of an anti-tuberculosis agent active against non-replicating mycobacteria: exploring hybridization of pyrazinamide with multiple fragments. *Med. Chem. Res.* **2015,** *24* (7), 2986-2992.
22. Pavlović, D.; Mutak, S., Discovery of 4''-ether linked azithromycin-quinolone hybrid series: Influence of the central linker on the antibacterial activity. *ACS Medicinal Chemistry Letters* **2011,** *2* (5), 331-336.
23. Pokrovskaya, V.; Belakhov, V.; Hainrichson, M.; Yaron, S.; Baasov, T., Design, synthesis, and evaluation of novel fluoroquinolone-aminoglycoside hybrid antibiotics. *J. Med. Chem.* **2009,** *52* (8), 2243-54.
24. Lee, J.; Kwon, M.; Lee, K. H.; Jeong, S.; Hyun, S.; Shin, K. J.; Yu, J., An approach To enhance specificity against RNA targets using heteroconjugates of aminoglycosides and chloramphenicol (or linezolid). *J. Am. Chem. Soc.* **2004,** *126* (7), 1956-1957.
25. Berkov-Zrihen, Y.; Green, K. D.; Labby, K. J.; Feldman, M.; Garneau-Tsodikova, S.; Fridman, M., Synthesis and evaluation of hetero- and homodimers of ribosome-targeting antibiotics: Antimicrobial activity, in vitro inhibition of translation, and drug resistance. *J. Med. Chem.* **2013,** *56* (13), 5613-5625.
26. Findlay, B.; Zhanel, G. G.; Schweizer, F., Neomycin-phenolic conjugates: polycationic amphiphiles with broad-spectrum antibacterial activity, low hemolytic activity and weak serum protein binding. *Bioorg. Med. Chem. Lett.* **2012,** *22* (4), 1499-503.
27. Chen, L.; Yang, D.; Pan, Z.; Lai, L.; Liu, J.; Fang, B.; Shi, S., Synthesis and antimicrobial activity of the hybrid molecules between sulfonamides and active antimicrobial pleuromutilin derivative. *Chemical Biology & Drug Design* **2015,** *86* (2), 239-245.
28. Jacobs, R. T.; Lunde, C. S.; Freund, Y. R.; Hernandez, V.; Li, X.; Xia, Y.; Carter, D. S.; Berry, P. W.; Halladay, J.; Rock, F.; Stefanakis, R.; Easom, E.; Plattner, J. J.; Ford, L.; Johnston, K. L.; Cook, D. A. N.; Clare, R.; Cassidy, A.; Myhill, L.; Tyrer, H.; Gamble, J.; Guimaraes, A. F.; Steven, A.; Lenz, F.; Ehrens, A.; Frohberger, S. J.; Koschel, M.; Hoerauf, A.; Hubner, M. P.; McNamara, C. W.; Bakowski, M. A.; Turner, J. D.; Taylor, M. J.; Ward, S. A., Boron-pleuromutilins as anti-Wolbachia agents with potential for treatment of Onchocerciasis and lymphatic filariasis. *J. Med. Chem.* **2019,** *62* (5), 2521-2540.
29. Slatko, B. E.; Taylor, M. J.; Foster, J. M., The Wolbachia endosymbiont as an anti-filarial nematode target. *Symbiosis* **2010,** *51* (1), 55-65.
30. Geary, T. G., Ivermectin 20 years on: maturation of a wonder drug. *Trends Parasitol.* **2005,** *21* (11), 530-2.
31. Campbell, W. C., *Ivermectin and abamectin*. Springer Science & Business Media: 2012.
32. Vercruysse, J.; Rew, R. S., *Macrocyclic lactones in antiparasitic therapy*. CAB International: 2002.
33. Gardon, J.; Gardon-Wendel, N.; Demanga, N.; Kamgno, J.; Chippaux, J. P.; Boussinesq, M., Serious reactions after mass treatment of onchocerciasis with ivermectin in an area endemic for *Loa loa* infection. *Lancet* **1997,** *350* (9070), 18-22.
34. Hoerauf, A.; Mand, S.; Volkmann, L.; Büttner, M.; Marfo-Debrekyei, Y.; Taylor, M.; Adjei, O.; Büttner, D. W., Doxycycline in the treatment of human onchocerciasis: Kinetics of Wolbachia endobacteria

reduction and of inhibition of embryogenesis in female Onchocerca worms. *Microbes Infect* **2003,** *5* (4), 261-73.
35. Hoerauf, A.; Mand, S.; Fischer, K.; Kruppa, T.; Marfo-Debrekyei, Y.; Debrah, A. Y.; Pfarr, K. M.; Adjei, O.; Büttner, D. W., Doxycycline as a novel strategy against bancroftian filariasis-depletion of Wolbachia endosymbionts from *Wuchereria bancrofti* and stop of microfilaria production. *Med. Microbiol. Immunol.* **2003,** *192* (4), 211-6.
36. Hoerauf, A.; Mand, S.; Adjei, O.; Fleischer, B.; Büttner, D. W., Depletion of Wolbachia endobacteria in *Onchocerca volvulus* by doxycycline and microfilaridermia after ivermectin treatment. *Lancet* **2001,** *357* (9266), 1415-6.
37. Albers, A.; Esum, M. E.; Tendongfor, N.; Enyong, P.; Klarmann, U.; Wanji, S.; Hoerauf, A.; Pfarr, K., Retarded *Onchocerca volvulus* L1 to L3 larval development in the *Simulium damnosum* vector after anti-wolbachial treatment of the human host. *Parasit Vectors* **2012,** *5*, 12.
38. Goetze, S.; Hiernickel, C.; Elsner, P., Phototoxicity of doxycycline: A systematic review on clinical manifestations, frequency, cofactors, and prevention. *Skin Pharmacol Physiol* **2017,** *30* (2), 76-80.
39. Zoltner, M.; Horn, D.; Field, M. C., Pass the boron: benzoxaboroles as antiparasite drugs. *Trends Parasitol.* **2024,** *40* (9), 820-828.
40. Ehrens, A.; Lunde, C. S.; Jacobs, R. T.; Struever, D.; Koschel, M.; Frohberger, S. J.; Lenz, F.; Fendler, M.; Turner, J. D.; Ward, S. A.; Taylor, M. J.; Freund, Y. R.; Stefanakis, R.; Easom, E.; Li, X.; Plattner, J. J.; Hoerauf, A.; Huebner, M. P., In vivo efficacy of the boron-pleuromutilin AN11251 against Wolbachia of the rodent filarial nematode *Litomosoides sigmodontis*. *PLoS Neglected Trop. Dis.* **2020,** *14* (1), e0007957/1-e0007957/17.
41. Ippolito, J.; Kanyo, Z.; Wimberly, B.; Wang, D.; Skripkin, E.; Devito, J. In *Structural basis for the binding Rx-01, a novel oxazolidinone class, to bacterial ribosomes*, Proceedings of the 45th Interscience Conference on Antimicrobial Agents and Chemotherapy, Abstract A-3445., Washington, DC, Washington, DC, 2005.
42. Skripkin, E.; McConnell, T.; King, B.; Devito, J.; Franceschi, F.; Sutcliffe, J. In *Designer oxazolidinones bind to the 50S peptidyl-transferase region and can overcome ribosome based linezolid resistance*, Proceedings of the 45th Interscience Conference on Antimicrobial Agents and Chemotherapy, Abstract A-3440, Washington, DC, Washington, DC, 2005.
43. Skripkin, E.; McConnell, T. S.; DeVito, J.; Lawrence, L.; Ippolito, J. A.; Duffy, E. M.; Sutcliffe, J.; Franceschi, F., R chi-01, a new family of oxazolidinones that overcome ribosome-based linezolid resistance. *Antimicrob. Agents Chemother.* **2008,** *52* (10), 3550-7.
44. Hanessian, S.; Maianti, J. P.; Matias, R. D.; Feeney, L. A.; Armstrong, E. S., Hybrid aminoglycoside antibiotics via Tsuji palladium-catalyzed allylic deoxygenation. *Org. Lett.* **2011,** *13* (24), 6476-6479.
45. Maianti, J. P.; Hanessian, S., Structural hybridization of three aminoglycoside antibiotics yields a potent broad-spectrum bactericide that eludes bacterial resistance enzymes. *MedChemComm* **2016,** *7* (1), 170-176.
46. Dougherty Thomas, J.; Nayar, A.; Newman Joseph, V.; Hopkins, S.; Stone Gregory, G.; Johnstone, M.; Shapiro Adam, B.; Cronin, M.; Reck, F.; Ehmann David, E., NBTI 5463 is a novel bacterial type II topoisomerase inhibitor with activity against Gram-negative bacteria and In vivo efficacy. *Antimicrob. Agents Chemother.* **2014,** *58* (5), 2657-2664.
47. Long, D. D.; Aggen, J. B.; Christensen, B. G.; Judice, J. K.; Hegde, S. S.; Kaniga, K.; Krause, K. M.; Linsell, M. S.; Moran, E. J.; Pace, J. L., A multivalent approach to drug discovery for novel antibiotics. *J. Antibiot.* **2008,** *61* (10), 595-602.
48. Long, D. D.; Aggen, J. B.; Chinn, J.; Choi, S.-K.; Christensen, B. G.; Fatheree, P. R.; Green, D.; Hegde, S. S.; Judice, J. K.; Kaniga, K.; Krause, K. M.; Leadbetter, M.; Linsell, M. S.; Marquess, D. G.; Moran, E. J.; Nodwell, M. B.; Pace, J. L.; Trapp, S. G.; Turne, S. D., Exploring the positional attachment of glycopeptide/β-lactam heterodimers. *J. Antibiot.* **2008,** *61* (10), 603-614.

49. Al-Tawfiq, J. A.; Momattin, H.; Al-Ali, A. Y.; Eljaaly, K.; Tirupathi, R.; Haradwala, M. B.; Areti, S.; Alhumaid, S.; Rabaan, A. A.; Al Mutair, A.; Schlagenhauf, P., Antibiotics in the pipeline: a literature review (2017-2020). *Infection* **2022,** *50* (3), 553-564.
50. Cronan, J. E.; Waldrop, G. L., Multi-subunit acetyl-CoA carboxylases. *Prog. Lipid Res.* **2002,** *41* (5), 407-435.
51. Campbell, J. W.; Cronan, J. E., Bacterial fatty acid biosynthesis: Targets for antibacterial drug discovery. *Annu. Rev. Microbiol.* **2001,** *55* (Volume 55, 2001), 305-332.
52. Silvers, M. A.; Robertson, G. T.; Taylor, C. M.; Waldrop, G. L., Design, synthesis, and antibacterial properties of dual-ligand inhibitors of acetyl-CoA carboxylase. *J. Med. Chem.* **2014,** *57* (21), 8947-8959.
53. Freiberg, C.; Brunner, N. A.; Schiffer, G.; Lampe, T.; Pohlmann, J.; Brands, M.; Raabe, M.; Häbich, D.; Ziegelbauer, K., Identification and characterization of the first class of potent bacterial acetyl-CoA carboxylase inhibitors with antibacterial activity. *J. Biol. Chem.* **2004,** *279* (25), 26066-26073.
54. Broussard, T. C.; Price, A. E.; Laborde, S. M.; Waldrop, G. L., Complex formation and regulation of *Escherichia coli* acetyl-CoA carboxylase. *Biochemistry* **2013,** *52* (19), 3346-57.
55. Gannett, C.; Tiller, K.; Briganti, A. J.; Brown, A. M.; Weger-Lucarelli, J.; Lowell, A. N., Forgotten natural products: Semisynthetic development of blasticidin S as an antibiotic lead. *ACS Medicinal Chemistry Letters* **2024,** *15* (3), 362-368.
56. Serrano, C. M.; Kanna Reddy, H. R.; Eiler, D.; Koch, M.; Tresco, B. I. C.; Barrows, L. R.; VanderLinden, R. T.; Testa, C. A.; Sebahar, P. R.; Looper, R. E., Unifying the aminohexopyranose- and peptidyl-nucleoside antibiotics: Implications for antibiotic design. *Angew. Chem. Int. Ed. Engl.* **2020,** *59* (28), 11330-11333.
57. Franceschi, F.; Duffy, E. M., Structure-based drug design meets the ribosome. *Biochem. Pharmacol.* **2006,** *71* (7), 1016-1025.
58. Long, D. D.; Marquess, D. G., Novel heterodimer antibiotics: a review of recent patent literature. *Future Med Chem* **2009,** *1* (6), 1037-50.
59. Chellat, M. F.; Raguž, L.; Riedl, R., Targeting antibiotic resistance. *Angew. Chem. Int. Ed.* **2016,** *55* (23), 6600-6626.
60. Parkes, A. L.; Yule, I. A., Hybrid antibiotics - clinical progress and novel designs. *Expert Opin. Drug Discovery* **2016,** *11* (7), 665-680.
61. Hubschwerlen, C.; Wyss, P. New macrolide oxazolidinone derivatives useful for treating bacterial infections. DE10342292A1, 2005.
62. Wang, D.; Sutcliffe, J. A.; Oyelere, A. K.; McConnell, T. S.; Ippolito, J. A.; Abelson, J. N.; Springer, D. M.; Salvino, J. M.; Lou, R.; Goldberg, J. A.; Farmer, J. J.; Duffy, E. M.; Bhattacharjee, A. Bifunctional heterocyclic compounds and methods of making and using same. US7091196B2, 2006.
63. Schrodinger, L. *The PyMOL Molecular Graphics System, Version 8*, 2021.
64. Black, C.; Al Mahmud, H.; Howle, V.; Wilson, S.; Smith, A. C.; Wakeman, C. A., Development of a polymicrobial checkerboard assay as a tool for determining combinatorial antibiotic effectiveness in polymicrobial communities. *Antibiotics (Basel)* **2023,** *12* (7).
65. Lipinski, C. A., Lead- and drug-like compounds: the rule-of-five revolution. *Drug Discovery Today: Technologies* **2004,** *1* (4), 337-341.
66. Breiner, L. M.; Slowinski, R. P.; Lowell, A. N., Highly active oligoethylene glycol pleuromutilins via systematic linker synthesis/one-pot attachment and a microscale solubility method. *The Journal of Organic Chemistry* **2025,** *90* (1), 919-924.
67. Kwon, D. H.; Lu, C. D., Polyamine effects on antibiotic susceptibility in bacteria. *Antimicrob. Agents Chemother.* **2007,** *51* (6), 2070-7.
68. Washington, A. Z.; Tapadar, S.; George, A.; Oyelere, A. K., Exploiting translational stalling peptides in an effort to extend azithromycin interaction within the prokaryotic ribosome nascent peptide exit tunnel. *Biorg. Med. Chem.* **2015,** *23* (16), 5198-5209.

69. Svidritskiy, E.; Ling, C.; Ermolenko, D. N.; Korostelev, A. A., Blasticidin S inhibits translation by trapping deformed tRNA on the ribosome. *Proc. Natl. Acad. Sci. U. S. A.* **2013,** *110* (30), 12283-12288.
70. Jang, S., AcrAB-TolC, a major efflux pump in Gram negative bacteria: toward understanding its operation mechanism. *BMB Rep.* **2023,** *56* (6), 326-334.
71. Hu, Z.; Leus, I. V.; Chandar, B.; Sherborne, B. S.; Avila, Q. P.; Rybenkov, V. V.; Zgurskaya, H. I.; Duerfeldt, A. S., Structure–uptake relationship studies of oxazolidinones in Gram-negative ESKAPE pathogens. *J. Med. Chem.* **2022,** *65* (20), 14144-14179.
72. Stoorza, A. M.; Duerfeldt, A. S., Guiding the way: Traditional medicinal chemistry inspiration for rational Gram-negative drug design. *J. Med. Chem.* **2024,** *67* (1), 65-80.
73. Wang, D.; Ippolito, J. A.; Abelson, J. N.; McConnell, T. S.; Sutcliffe, J. A.; Oyelere, A. K. Bifunctional heterocyclic compounds and methods of making and using same. WO2004/29066A2, 2004.
74. Poulsen, S. M.; Karlsson, M.; Johansson, L. B.; Vester, B., The pleuromutilin drugs tiamulin and valnemulin bind to the RNA at the peptidyl transferase centre on the ribosome. *Mol. Microbiol.* **2001,** *41* (5), 1091-1099.
75. Schlünzen, F.; Pyetan, E.; Fucini, P.; Yonath, A.; Harms, J. M., Inhibition of peptide bond formation by pleuromutilins: the structure of the 50S ribosomal subunit from *Deinococcus radiodurans* in complex with tiamulin. *Mol. Microbiol.* **2004,** *54* (5), 1287-1294.
76. Svidritskiy, E.; Korostelev, A. A., Mechanism of inhibition of translation termination by blasticidin S. *J. Mol. Biol.* **2018,** *430* (5), 591-593.
77. Hansen, J. L.; Ippolito, J. A.; Ban, N.; Nissen, P.; Moore, P. B.; Steitz, T. A., The structures of four macrolide antibiotics bound to the large ribosomal subunit. *Mol. Cell* **2002,** *10* (1), 117-128.
78. Himo, F.; Lovell, T.; Hilgraf, R.; Rostovtsev, V. V.; Noodleman, L.; Sharpless, K. B.; Fokin, V. V., Copper(I)-catalyzed synthesis of azoles. DFT study predicts unprecedented reactivity and intermediates. *J. Am. Chem. Soc.* **2005,** *127* (1), 210-216.
79. Santhoshkumar, P.; Kanagaraj, T.; Suresh, P., Iron-catalysed synthesis of sulfonamides and sulfonic esters: Greener sulfonation of amines and alcohols under mechanical grinding conditions. *Tetrahedron* **2025,** *171*, 134410.
80. Murugesan, V.; Muralidharan, A.; Anantharaj, G. V.; Chinnusamy, T.; Rasappan, R., Photoredox–Ni dual catalysis: Chelation-free hydroacylation of terminal alkynes. *Org. Lett.* **2022,** *24* (45), 8435-8440.
81. Borsato, G.; Carnio, F.; Lunardon, S.; Moletta, M.; Pavan, G.; Terrin, F.; Scarso, A.; Plotegher, N.; Fabris, F., A β-glucosyl sterol probe for in situ fluorescent labelling in neuronal cells to investigate neurodegenerative diseases. *Chemistry – A European Journal* **2024,** *30* (41), e202400778.
82. Bucher, J.; Wurm, T.; Nalivela, K. S.; Rudolph, M.; Rominger, F.; Hashmi, A. S. K., Cyclization of gold acetylides: Synthesis of vinyl sulfonates via gold vinylidene complexes. *Angew. Chem. Int. Ed.* **2014,** *53* (15), 3854-3858.
83. Starčević, K.; Pešić, D.; Toplak, A.; Landek, G.; Alihodžić, S.; Herreros, E.; Ferrer, S.; Spaventi, R.; Perić, M., Novel hybrid molecules based on 15-membered azalide as potential antimalarial agents. *European Journal of Medicinal Chemistry* **2012,** *49*, 365-378.

# Chapter 7. Conclusions and future directions

## 7.1 Summary conclusion

As I have shown herein, the natural product pleuromutilin can serve as the basis for a diversity of substituted, semi-synthetic antibiotics. The C22 position lends itself to functionalization with 1,4-disubstituted 1,2,3-triazoles, oligoethylene glycol chains, and halogens. The C20 position of native pleuromutilin is unfavorable for derivatization with triazoles, presumably because of poor directionality as assessed by computational and structural analysis; however, the C12 epimer lends itself well to this endeavor. Finally, pleuromutilin has demonstrated its potential as a partner in bidentate hybrid antibiotics with blasticidin S and azithromycin, and compounds of this and previous classes have shown themselves to be potent antimalarials as well as antibiotics.

## 7.2 Future directions for C22-triazolyl pleuromutilins (Chapter 2)

The C22-triazolyl pleuromutilins (Chapter 2) demonstrated comparable activity to pleuromutilin in antibiotic assays. Due to the auxophoric nature of this position on the molecule, direct attachment through a triazole linkage at this position may be pursued in the future for hybrid antibiotics. The high activity of C22-oligoethylene glycol pleuromutilins (Chapter 5) makes them a higher priority candidate for hybridization, however. The C20-triazolyl pleuromutilins (Chapter 2) are not worth further investigation, as even the smallest of modifications tested at this position (C20 azido) resulted in inactive antibiotics.

## 7.3 Future directions for C20-triazolyl-12-*epi*-mutilins (Chapter 3)

The 20-triazolyl-12-*epi*-mutilins, either with a C22 hydroxyl (analogous to pleuromutilin) or a C22 diethylaminoethylenethioether (analogous to tiamulin) were potent antibiotics. From

these series, the 20-phenyltriazolyl-12-*epi*-mutlins proved to be the most active, with the pleuromutilin analog slightly outperforming the tiamulin analog. As of the time of this writing, we have submitted a provisional patent application on this material as a lead for the development of further derivatives. Future work on compounds of this class will be focused on structure-activity relationship (SAR) studies to determine the effects of ring substitution on antibiotic potency, as well as testing different C22 sidechain compositions. Future studies will also test if resistance mechanisms to C22 thioether mutilins can be bypassed by the C20 phenyltriazole group, as these provide new binding contacts within the ribosome that are previously unsampled.

### 7.4 Future directions for pleuromutilin electrophiles (Chapter 4)

Future work on the C22 electrophile pleuromutilins will focus on their co-crystallization with the ribosome, in collaboration with Yuri Polikanov's group at the University of Illinois, Chicago. These studies will finally demonstrate whether this class has the potential to act as covalent inhibitors of the ribosome. Additionally, the serendipitous discovery of this class's antimalarial activity has spun off a new project, which will be conducted by Toheeb Ajasa, a 2$^{nd}$ year graduate student in our lab, in collaboration with Michael Klemba's group at Virginia Tech. These studies will focus on increasing their potency and lowering their toxicity.

### 7.5 Future directions for oligoethylene glycol pleuromutilins (Chapter 5)

Due to the unexpectedly high activities of the oligoethylene glycol functionalized pleuromutilins, these are worthy of further exploration. There are two main questions I would like to see explored: 1. Can their propensity to be removed from the bacterial cell via efflux be reduced, and 2. Can the use of a terminal amine or guanidine increase their effectiveness against Gram-negative pathogens. To extend this further point, how would two sites of oligoethylene glycol

functionalization, say the C22 and C20 of *epi*-pleuromutilin, change the antimicrobial properties? Conceivably, the azido thiol bifunction OEGs could be used in both sites of functionalization, from the demonstrated nucleophilic displacement at an electrophilic site, and through a thiol-ene reaction at the vinyl. The azido could then be reduced to the amine to provide the polycationic, diOEG chain pleuromutilins. Additionally, the effectiveness of mammalian cell penetration of these compounds should be studied, for their use in the treatment of intracellular bacterial pathogens.

### 7.6 Future directions of pleuromutilin-based bidentate hybrid antibiotics (Chapter 6)

I have great hopes for the continuation of this project. Although pleuromutilin-blasticidin S hybrids only demonstrated marginal improvement in bacterial activity over the co-administered parents, one compound in particular, the hybrid of pleuromutilin-monoEG-azido and butynyl blasticidin S demonstrated potent activity against *P. falciparum* which was at least one order of magnitude greater than a coadministration of the unattached parents. There is room for improvement in this area, as the positioning of the triazole and the composition and length of the linker need to be studied, but I believe there is great potential in this compound. The 12-*epi*-pleuromutilin-azithromycins show good potential against azithromycin resistant Gram positives, however more testing is required to see if they have an increased effect over their co-administered parents in dually susceptible strains.

Both series of hybrids require structural conformation in the ribosome to determine if they are acting as true bidentates, or just separately acting hybrids. Additionally, both hybrid series are prone to efflux, and the 12-*epi*- pleuromutilin-azithromycins suffer from poor penetration. More work will be required to overcome these issues. Potential avenues for investigation are the composition of the linker material, and one possibility is the use of polyamine linkers to take

advantage of polycation penetration into Gram negative cells. Another method of improving their activity may be to incorporate an efflux pump inhibitor into their design. Both methods would transform these bidentate hybrids into bidentate bifunctional conjugates (see definitions in Chapter 6). While these are not the proverbial "nuclear bomb" against bacteria as we had dreamed, I see great potential in their future, not just with pleuromutilin, but with other pairs whose mechanisms of action in the ribosome have been carefully considered and paired.

### 7.7 A Note on the Politics and Economics of Antibiotics

The need for effective antibiotics has been well established previously in this work. The tried-and-true method to furnish these is the iterative creation of derivatives that bypass resistance, or the discovery of new classes of antibiotics. Indeed, the former is our approach, and hybrid antibiotics are especially promising to avoid further resistance development. However, these methods are akin to a biological arms race, an inherently reactionary process in which we are constantly on our back foot.

If instead, the strategy of combatting AMR focused on prevention, we may negate the worst of its effects in the future. Monitoring of AMR genes and administrative control of the use of antibiotic classes is most likely the ideal way to limit the impact of AMR before it becomes an issue. The abolition of the use of antibiotics in agriculture as growth promoters would slow the proliferation of AMR genes in the wild and preserve the integrity of our most useful classes of antibiotics. The cycling of antibiotic classes in clinical settings would allow for pathogens with developed AMR to lose their resistance genes through evolution, as these AMR genes are a fitness cost for the organism, and in the absence of the selective pressure of an antibiotic these resistance mechanisms would fade away.

Unfortunately, despite the necessity of treatments for AMR pathogens, funding lags, and we lack the political will to establish proper administrative controls. We will indeed always need new classes of antibiotics, but we must be promoting preventative measures as well. However, within our current mode of economic and political production, these measures do not serve the profit motive. Antibiotics are not profitable, save for their usage in agriculture. Until society can agree on the existential risk of AMR, the best we can do is try to develop new therapies. However, the day will come when this will be insufficient. The question we must ask ourselves is how many more are we willing to let die before we demand more from our political leaders? The answer is as many as is still profitable.